CHALMERS

Analysis of High Strength Stainless Steel in Road Bridges

Parametric study and Scripted Finite Element Method Fatigue Assessment

Master of Science Thesis in the Master's Programme Structural Engineering and Building Technology

MATTIAS RENSTRÖM, OSKAR RYDH

Department of Civil and Environmental Engineering
Division of Structural Engineering
Steel Structures
CHALMERS UNIVERSITY OF TECHNOLOGY
Gothenburg, Sweden 2014:118

Master's Thesis 2014:118

MASTER'S THESIS 2014:118

Analysis of High Strength Stainless Steel in Road Bridges

Parametric study and Scripted Finite Element Method Fatigue Assessment

Master of Science Thesis in the Master's Programme Structural Engineering and Building Technology

MATTIAS RENSTRÖM, OSKAR RYDH

Department of Civil and Environmental Engineering
Division of Structural Engineering
Steel Structures
CHALMERS UNIVERSITY OF TECHNOLOGY
Gothenburg, Sweden 2014:118

Analysis of High Strength Stainless Steel in Road Bridges
Parametric study and Scripted Finite Element Method Fatigue Assessment

Master of Science Thesis in the Master's Programme Structural Engineering and Building Technology

MATTIAS RENSTRÖM, OSKAR RYDH

Examensarbete / Institutionen för bygg- och miljöteknik,
Chalmers tekniska högskola 2014:118

Department of Civil and Environmental Engineering
Division of Structural Engineering
Steel Structures
Chalmers University of Technology
SE-412 96 Göteborg
Sweden
Telephone: + 46 (0)31-772 1000

Cover:
Photograph of one of the earliest stainless steel road bridges in Sweden, more information can be found in chapter 2.5 - *Analysis of existing structures*. Photograph by Magnus Alfredsson 2012.

Chalmers Reproservice / Department of Civil and Environmental Engineering
Göteborg, Sweden 2014:118

Analysis of High Strength Stainless Steel in Road Bridges
Parametric study and Scripted Finite Element Method Fatigue Assessment

Master of Science Thesis in the Master's Programme Structural Engineering and Building Technology

MATTIAS RENSTRÖM, OSKAR RYDH
Department of Civil and Environmental Engineering
Division of Structural Engineering
Steel Structures
Chalmers University of Technology

Abstract

Carbon steel structures, especially bridges, are subjected to corrosion in outdoor environments. Needless to say, this is undesirable and limits the overall durability of the bridge. It does this both directly, by decreasing the cross section, and indirectly, by acting as a stress raiser for fatigue damage. However, this does not have to be the case. The central question this thesis attempts to answer is; *What if stainless steel was used instead of carbon steel?*

In the moment of writing, there are virtually no stainless steel road bridges in existence across the world, less than ten in total wherein two of these are road bridges located in Sweden. In other words, the knowledge of stainless steel is scarce and dispersed.

In short, this thesis studies the viability of stainless steel as an alternate option for carbon steel in road bridges. This thesis is split into two sections. The first part is a literature study of some size, whilst the second part is a parametric study. The review is intended to give a comprehensive overview of the current knowledge within academia and the field of structural engineering about the use of stainless steel in structures. As mentioned, the second part is a parametric study, which numerically assesses the impact of implementing stainless steel in a composite bridge.

The results of this thesis are quite a lot of different observations, which are justified from both the literature study as well as the parametric study. Stainless steel is indeed a very promising option, especially when considering long service life or corrosive environments. Particularly noteworthy is that there are indications that stainless steel might have considerably higher fatigue strength in comparison to carbon steel. It is also indicated that instability phenomena are more critical for stainless steel and that Eurocode does not cover this adequately.

In the light of the many observations and discoveries of this thesis there is also a discussion under what circumstances stainless steel is most suitable. In addition, what weaknesses stainless steel has and recommendations for further research.

Keywords: Stainless steel, Finite Element Method, Python Script, Eurocode, Parametric study, Fatigue Assessment, Palmgren-Miner Cumulative Damage method.

Analys av höghållfast rostfritt stål i vägbroar
Parameterstudie och skriptad finita element metods utmattnings beräkning
Examensarbete inom Structural Engineering and Building Technology
MATTIAS RENSTRÖM, OSKAR RYDH
Institutionen för bygg- och miljöteknik
Avdelningen för Konstruktionsteknik
Stål- och Träkonstruktioner
Chalmers tekniska högskola

Sammanfattning

Broar I kolstål, det vill säga vanligt konstruktionsstål, är ofta utsatt för korrosion. Trots rostskyddsmålning och andra åtgärder är det fortfarande ett problem. Dels tär korrosion på materials bärförmåga men kan även ge upphov till spänningskoncentration i sammanhanget av metallutmattning. Detta leder osökt till frågan ifall det finns ett bättre alternativ. I detta fall, huruvida rostfritt stål lämpar sig som alternativ till det mer konventionella kolstålet som konstruktionsstål? Detta är den centrala frågeställningen denna rapport ämnar bearbeta.

I skrivande stund finns det endas ett ytterst fåtal vägbroar utförda i rostfritt stål. Det finns sammanlagt kring tio vägbroar i rostfritt stål världen över, varav 2 av dessa befinner sig i Sverige. Med andra ord, erfarenheten av rostfria broar är väldigt begränsad och därtill spridd.

I enkelhet, denna rapport undersöker möjligheterna att använda rostfritt stål istället för kolstål i vägbroar. Rapporten i fråga består av två stycken delar. Den första delen är en omfattande litteraturstudie medan den andra delen är en numerisk parameterstudie. Litteraturstudien har som mål att sammanställa den befintliga kunskapen inom den akademiska sektorn och den kommersiella sektorn om användingen av rostfritt stål inom konstruktion. Parameterstudien undersöker numeriskt, via beräkningar i enlighet med befintlig Eurocode standard, vilken inverkan rostfritt stål har på olika parametrar, exempelvis totalkostnad och materialåtgång.

Litteraturstudien i samband med parameterstudien ger många intressanta och nämnvärda observationer. En av de mer centrala observationerna är att rostfritt stål ter sig vara ett mer fördelaktigt alternativ än kolstål under vissa förutsättningar. Framförallt lämpar sig rostfritt stål under mer korrosiva omständigheter eller där lång livslängd är eftertraktat. Ytterligare så finns det indikationer att utmattningskapaciteten hos rostfritt är betydligt högre än hos kolstål. Även nackdelar diskuteras och undersöks, exempelvis det faktum att rostfritt tenderar att vara mer utsatt av instabilitetsfenomen än kolstål.

För att avsluta, så hittas i slutet av rapporten rekommendationer för fortsatt forskning. I diskussionskapitlet innefattas också en diskussion om under vilka omständigheter rostfritt stål lämpar sig bäst och svagheterna hos rosfritt stål.

Nyckelord: Rostfritt stål, Finite Element Method, Python Skript, Eurocode, Parameterstudie, Uttmattningsanalys, Palmgren-Miner delskademetod

CONTENTS

Also included:

- Appendix A – Result Data from the Parametric Study
- Appendix B – About the FEM-script and Flow Chart
- Appendix C – Convergence Study and Model Validation
- Appendix D – Matlab Functions for the Parametric Study
- Appendix E – Matlab Functions for the Fatigue Calculations
- Appendix F – Calculations for the Parametric Study

Preface

This master thesis was carried out at the Division of Structural Engineering at Chalmers University of Technology during the period of January to June of 2014. In addition, the thesis was carried out in cooperation with NCC Teknik. However, we wish to acknowledge all the other people who have contributed to this thesis and made it possible.

First and foremost, we wish to extend our utmost gratitude to our examiner and supervisor Associate Professor Mohammad Al-Emrani at Chalmers University of Technology. We can say with perfect honesty that we have seldom met a more knowledgeable person within his field. It has been nothing short of a privilege to have had him as a supervisor and we can truly say that we could never have had hoped for a better supervisor.

We also wish to extend our full gratitude to our supervisors at NCC Teknik Gothenburg; Alexandre Mathern and Tobias Larson. Without their knowledge, feedback and valuable insight this master thesis would not have been possible. Once again, we are thankful for having such excellent supervisors.

In addition, we wish to thank our opponents David Tarazona and Luis Santiago. Not only have their feedback and opposition been of great help, but also the cooperation between our master theses has enabled both of our works to obtain greater value than they otherwise would have done alone.

Moreover, special thanks to Anders Finnås and Anders Olsson at Outokumpu Stainless AB. Of whom both have shared their extensive knowledge about stainless steel which has been of great help.

At Chalmers University of Technology we also wish to give a special thanks to Reza Haghani, who took the time when it was in short supply to help us with matters of finite element method modelling when we needed it the most.

We would also like to express our gratitude to Clara Nyman, whose extensive aid in matters of language and writing has been of great help. Not to mention the many thorough proof readings during the making of this thesis.

Last but not least, we wish to extend our gratitude to our families who consists of: AnnaLena, Gun, Johan, Kurt, Markus and Ofelia. Despite the fact that the making of this master thesis has been a marvellous experience it has also been trying at times. We are thankful for the understanding and support during many a late evenings and occupied weekends alike.

Göteborg, June 2014

Mattias Renström and Oskar Rydh

Nomenclature

Abbreviations

CCR	Crevice corrosion resistance
CPT	Critical pitting temperature
FCAW	Flux-cored arc welding
FEM	Finite element method
FRC	Fibre reinforced concrete
FZ	Fused zone
GMAW	Gas metal arc welding
GTAW	Gas tungsten arc welding
HAZ	Heat affected zone
LBW	Laser beam welding
LB-GMAW	Laser beam gas metal arc welding
LCA	Life cycle analysis
LCC	Life cycle cost
LCCA	Life cycle cost analysis
PREN	Pitting resistance equivalent number
SAW	Submerged arc welding
SCC	Stress corrosion cracking
SMAW	Shielded metal arc welding

1 Introduction

As the title suggests, this thesis looks into the matter of using high strength stainless steel for bridge constructions. The first aspect of stainless steel is that it is a new material in the construction sector. Consequently, there is not much information available about the structural use of stainless steel. This holds true for both the commercial sector and the academic sector. More on this can be read in the background section of this chapter.

In short, due to the scarcity of information together with the apparent benefits of stainless steel in construction a literature study has been conducted. The literature study is included in full within this report and can be found in chapter 2 - *Literature Study*.

This chapter is the introduction chapter for both this report and the thesis in general. Herein the following is included: background, problem description, aim, method and scope. To sum up, this chapter is dedicated to relay all the information this thesis is based upon.

1.1 Background

For bridges constructed from conventional carbon steel, the durability of load bearing steel members is of great importance and concern. This is due to the fact that maintenance constitutes a substantial part of the overall cost of the bridge, see chapter 3 - *Parametric Study*.

However, it should be noted that the maintenance cost has not always been taken into full consideration when comparing different bridge alternatives. In later years, more emphasis has been put on the cost that takes place during the service life of the bridge.

With this in mind, there is an increased demand for materials and solutions that require less maintenance than ordinary carbon steel. One option for reducing the requirement and so the cost of maintenance is implementing stainless steel instead of the conventional carbon steel. Up to the moment of writing, stainless steel has generally not been used for load bearing structures due to the higher initial cost of stainless steel. In addition, the construction industry is unfamiliar with stainless steel as a building material.

To elaborate, stainless steel does not require surface treatment. For example, there is no requisite to paint stainless steel to obtain a passive corrosion resistance, more on this in chapter *2.1.3 - Corrosion resistance*. The fact that paint can be omitted when implementing stainless steel results in a substantial reduction in maintenance cost.

Painting of carbon steel bridges and also carbon steel structures in general is otherwise required to be done on a regular basis. This adds to the overall cost. Note however, that the maintenance cost varies a lot, this cost can in some instances surmount to about half of the total material cost, see chapter *5.3 - Comparison of carbon steel and stainless steel* for more details.

Furthermore, paint and the residues of paint can be hazardous in certain environments. For instance, paint residues can be especially harmful in environments that include water and ground water. Consequently, it is preferable, if possible, to avoid using

harmful contaminants all together in a sensitive environment. Something that is achievable to a better extent when using stainless steel compared against carbon steel.

As discussed in chapter *2.1.2 - Microstructures*, there are several types of stainless steel with different types of microstructures. Of these microstructures, the most relevant for future bridge constructions is the combination of austenite and ferrite, called duplex structure. The word *duplex* roughly translates to *double system*. More on the reasons of why duplex is the most relevant microstructure is discussed in *2.5 - Analysis of existing structures*. Though in short, duplex stainless steel has a proof strength, or *effective yield strength*, of approximately 460MPa. This can be compared to the 355MPa of conventional structural carbon steel. A result of the increased strength of stainless steel is that it enables more slender cross sections, and in turn, more slender bridges.

However, a downside to more slender cross section is the increased stress amplitudes when road bridges are subjected to loading, especially traffic load. Of course, this also hold true for railway bridges as well as road bridges. A consequence of the increased stress amplitudes is increased cumulative fatigue damage, since it depends very much of the stress amplitude as well as frequency.

To conclude, stainless steel has many benefits that make it a potentially superior material for many bridges. Adjacent to the fact that the high strength of stainless steel enables the ability to build more slender bridges, there is also the prospect of reduced cost through less maintenance. There are more benefits of stainless steel, many of them discussed in the following chapters. Of course, the drawbacks of stainless steel are of equal importance if not of an even higher interest in this thesis.

1.2 Problem description

In the moment of writing, there are very few bridges built with stainless steel for major load bearing members. In addition, current norms and codes do not consider the specific properties of stainless steels to a sufficient degree, see chapter 2.4 - *Eurocode in relation to stainless steel* for more details.

Moreover, this causes problems where the capacity of stainless steel can be either overestimated or underestimated, occasionally to a substantial degree. Thus the uncertainties in design may lead to either unsafe or overly conservatively designed bridges, which in turn render stainless steel bridges a less viable option for all the wrong reasons.

A subject that is of particular interest is the fatigue strength of welded connections. For instance, some test data suggests that welded connections with duplex stainless steel have a fatigue strength that is at least on the same level as carbon steel, more on this in subchapter *2.3 - Fatigue of stainless steel*. However, the test data also sometimes the strength is substantially higher, near twice as much as for carbon steel connections. Of course, this is a benefit to stainless steel that should be utilized.

Another area where research about the different properties of stainless steel leaves much to be desired is on the topic of instability. This is due to the fact that duplex stainless steel does not have a distinct yield point, which is a fundamental assumption for many instability phenomena when designing carbon steel structures.

To conclude, stainless steel has a lot of potential both from an economical point of view as well as structural. However, current research ranges from adequate to little, even sometimes as non-existent. Consequently, if to utilise stainless steel to its fullest, it is important to know what research exists, what is missing and what requires improvement. This is the main topic this thesis works with. Also, to better understand the impact of different aspects of stainless steel, there is also a parametric study.

1.3 Aim

The aim of this thesis is split into two major aims; first one being a literature study and second being a parametric study. Both of these parts have their own separate goals and achievements.

As stated, the first part is a literature study which looks into the topic of available current research. In short, it aims to give an overview of the total knowledge in academia about the structural use of stainless steel. In addition, the aim of the literature study is to analyse the viability of implementing stainless steel in bridge constructions.

For convenience and clarity, the literature study has been broken down into the following questions:

- *What are the important properties of stainless steel?*
- *What is currently known in both the commercial field and scientific community about stainless steel?*
- *What are the known problems when using stainless steel in constructions and especially bridge constructions?*
- *What are the benefits of using stainless steel in bridge constructions?*
- *Under what conditions is it suitable to use stainless steel?*
- *Are there any problems that are currently not being considered adequately when using stainless steel?*

Lastly, an additional aim, which somewhat transcends the scope of this master thesis, pertaining to the literature study is to give a foundation for further research within this topic. In other words, this thesis aims to shed some light on research topics for stainless steel that requires more research in the future. In addition, highlight promising aspects as well as the less desirable properties within stainless steel in the construction industry.

For the second part of the thesis the aim is to assess how stainless steel bridges can be optimised in design. An additional objective pertaining to this aim is to show if and when stainless steel bridges are a better option than carbon steel bridges.

1.4 Method

During the initial phase of the master thesis a literature study was carried out. In this study the current knowledge about stainless steel and bridges made from stainless steel was researched in all available literature. Also, some specialists and companies were consulted about their knowledge about stainless steel. Finally, case studies of existing structures have been conducted. The findings from this literature study can be found in Chapter 2 - *Literature Study*.

For the second part of the thesis a parametric study was conducted. The study looks into, among other things, on how different aspects affect dimensions, material consumption and cost of the bridge. In short, the topic of the parametric study is to research how much of an impact stainless steel has on a steel bridge.

The parametric study was conducted via hand calculations, FEM model and script as well as Matlab calculations. The supporting documents, such as calculations, can be found in their respective appendixes. Needless to say, the results of the parametric study can be found in the result chapter.

Note that all hand calculations are in accordance with the most recent edition of Eurocode.

1.5 Scope and limitation

The focus of this thesis lies on the use of stainless steel in load bearing bridge constructions. Note that with regard to stainless steel, the focus will be on duplex stainless steel and austenitic stainless steel, albeit to a lesser extent.

Also, another limitation is that this thesis mainly focuses on road bridges. In other words, railway and pedestrian bridges are basically omitted. However, to some extent the results presented in this thesis may be applicable to other bridge types as well. For instance, stainless steel has a higher proof strength than conventional carbon steel, regardless of whether it is a railway bridge or a road bridge.

Effort has been put into selecting the most important and relevant parts for the final thesis. However, not everything can be included in this thesis, which already of a considerable size. Consequently, the most important aspects have been selected. The selection is based upon relevance, impact, importance and whether they can be hazardous for the structural integrity.

Below follows a list of what is not considered in this thesis:

- *Aesthetic aspects; focus lies instead purely on the structural load bearing capacity.*
- *Laboratory and experimental work has not been performed due to shortage of resources and time. Instead there has been an emphasis on numerical analysis.*
- *Life cycle analysis (LCA) has not been conducted, see previous motivation.M*

2 Literature Study

If stainless steel is to become a viable alternative for structural engineering, it is necessary to have an understanding of the material itself and its behaviour. Thus, a literature study has been conducted and this chapter aims to present important aspects of stainless steel pertaining to bridge construction in a condensed form. This is to create a solid foundation of the current knowledge about stainless steel as a construction material.

2.1 About stainless steel

The first aspects of stainless steel to recognise are that it is an alloy and it is not a new material per se. There are many examples of corrosion resistant alloys throughout history. A classic historical example of corrosion resistant alloys is the ancient *Iron Pillar of Delhi,* which obtains its resistivity through a phosphor-iron alloy (Balasubramaniam, 2000).

However, the modern type of stainless steel is defined by a chromium-iron alloy (Finnås, 2012). An example of this modern stainless steel put to use is the cladding on top of the Chrysler Building in New York, United States of America. As Finnås points out;

> *"Built in 1930 it is still as new after more than 80 years [of service]". – Finnås, 2012*

Though, despite the fact that stainless steel has been available for many decades, it is only in recent years that stainless steel has once again emerged into consideration in the field of structural engineering. The earliest bridge with major load carrying components in stainless steel is the Waldeck-Rousseau Bridge. This bridge was erected in France in 1998 (ArcelorMittal, 2009). This bridge, was erected a little more than 15 years ago, which is not a very long time span when considering bridges. The fact that this bridge was the first stainless steel road bridge and that it was built so recently justifies the fact that stainless steel in structural engineering is a rather new material.

As will be clear in this report, stainless steel has many desirable aspects in comparison with structural carbon steel. However, since stainless steel has seen very limited use as a construction material, the full potential of stainless steel still remains largely unexplored. To elaborate, compared to other more established materials, such as concrete and carbon steel, the construction sector is somewhat unfamiliar with stainless steel and how to best use it.

In addition, practical guidance in codes and guidelines for the proper use of stainless steel is limited and dispersed.

2.1.1 Basic mechanical properties

This chapter presents some of the most basic mechanical properties of stainless steel. In general, the metallic properties of stainless steel, ranging from density to electrical properties, are quite well known and documented. As a clarification, this thesis does not go in depth about the material properties of stainless steel within the field of metallurgy, but rather how well suited stainless steel is for construction purposes. As such, a thorough analysis of the material properties of stainless steel is not of particular interest for this thesis.

For further information about metallurgical properties of stainless steel, the following sources can be of help:

- Machinery's Handbook, 2009, by Horton et al.
- EN Standard 10088, part 1-5
- *Rostfria Stål Handbok 4 utgåva 6* (Handbook of Stainless Steel 6, 4th edition), 2000, Swedish Material and Mechanical Standard.

If to briefly discuss the mechanical properties of stainless steel, it can be said that stainless steel is generally stronger than ordinary carbon steel, see table 2.1. For instance, duplex stainless steel is usually compared with the carbon steel class of S460 as a reference grade. Note that the most common carbon steel grade is S355 and that S460 is considered to be *high strength steel*.

***Table 2.1**: This table displays proof strength, ultimate strength and elongation for some of the more common stainless steels used in construction. Note that the duplex stainless steel is generally stronger than S355 carbon steel and is in fact on par with S460 carbon steel. All values are obtained from the EN 1993-1-4:* Supplementary rules for stainless steel *standard and the EN 10088-4 standard. (Finnås, 2012).*

Type	EN Steel Grade	Proof Strength [MPa]	Ultimate Strength [MPa]	Elongation at ultimate strength [%]
Austenitic	1.4301	210	600	40
	1.4401	220	520	45
Duplex	1.4162	450	650	30
	1.4362	400	630	25
	1.4662	480	680	25
	1.4462	460	640	25
	1.4410	530	730	20

Regarding the strength of stainless steels it should be emphasised that both austenitic and duplex stainless steel do not have a pronounced yield limit (Abidelah et al., 2008). The implication of this is that it is not possible to easily measure yield strength of the material. To explain in short, the yield strength is defined as the stress at which the yield point is reached. Thus, without a yield point it is not possible to measure the yield strength in the same fashion as for carbon steel.

However, since it is somewhat difficult to measure yield strength when there is no pronounced yield limit, a proof strength is used instead. The proof strength can be used since it is not dependent on a yield point; instead the proof strength considers the remaining plastic strain after a given total strain. For an illustration of how the proof-strength is defined see figure *2*.1.

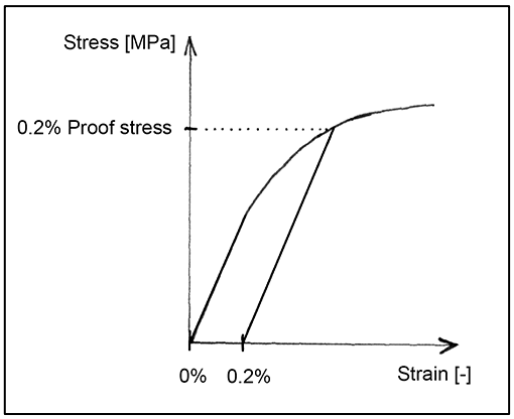

Figure 2.1: *Illustration of how the proof strength is defined and measured. Note that the proof strength can be measured for materials that have a yield point as well.*

The amount of strain used for the proof strength can be chosen freely, although a strain of 0.2% is the most common and established choice. As a matter of fact, in Eurocode the 0.2% proof strength can be used instead of the yield strength in most calculations, when no yield strength can be measured.

Concerning the proof strengths of stainless steels the values themselves is by some considered overly conservative (Fanica et al., 2008). When the proof strength was examined it was shown that the plastic deformation actually was between 0.09% and 0.15% at most. As mentioned previously the proof strength, with the full name of 0.2% proof strength, should result in a plastic strain of 0.2%. The values are supposed to be conservative, but the low amount of strain indicates that the values are overly conservative according to some test data. In conclusion, the proof strength of stainless steel can arguably be much higher than what it is today with current tolerances of safety.

Further information about the nonlinear behaviour of stainless steel can be found in *Stainless Steel Plasticity - Material Modelling and Structural Applications* which is written by Anders Olsson.

2.1.2 Microstructures

To understand stainless steel, it is imperative to comprehend the governing microstructures. In this thesis there are three main microstructures that are of interest: austenite, ferrite and austenite-ferrite. Note that austenite-ferrite is usually referred to as *duplex* and this thesis uses this convention. Lastly, even though it is not one of the three aforementioned structures, a fourth microstructure known as *martensite* is also included, albeit briefly. Martensite is included since it is sometimes an unintended by-product during manufacturing and welding of stainless steel and thus is a relevant usually undesired by-product.

To exemplify how the microstructures affect the properties of stainless steel one needs only to look at the stress-strain curves. Representative stress-strain curves can be found in figure 2.2. Note however that they can vary widely depending on what alloys are used and how the specific steel has been manufactured and treated. Consequently, the accuracy of these characteristic stress-strain curves is not overwhelming. However, they will suffice as a representation of how the different microstructures behave under typical circumstances.

As can be seen in figure 2.2, martensite has the highest ultimate strength. However, the ductility of martensite is far too low for constructional purposes. Therefore, it is mostly used for details and specific applications were ductility is not a concern.

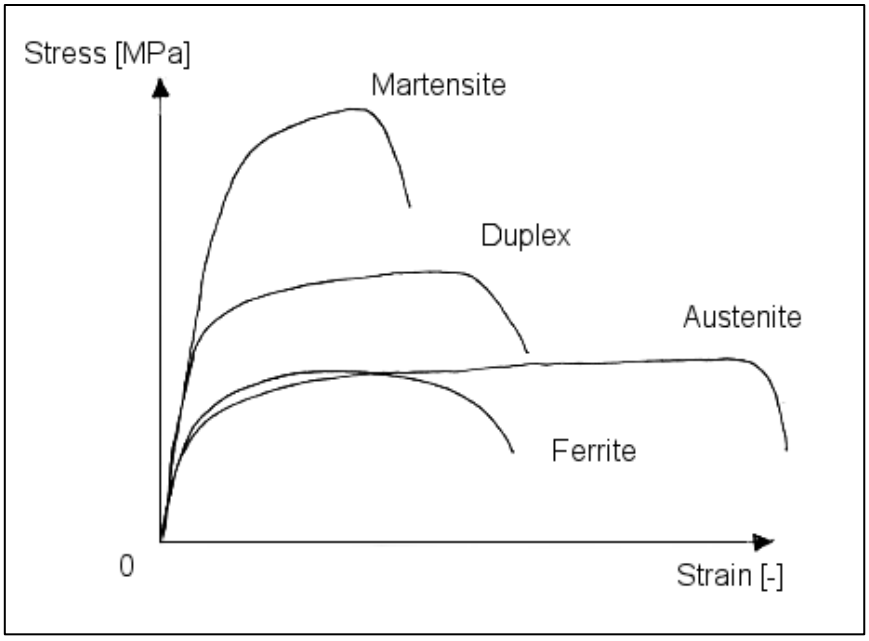

Figure 2.2: *Typical work curves for the steel microstructures considered. Note that martensite is very hard and brittle. Conversely, austenitic steel grade have the highest ductility (SMS, 2000).*

Whilst on the topic of ductility, in figure 2.2 it is also possible to see that austenite generally have a high amount of ductility, which is also exemplified in table 2.2. This ductility is one of the two major advantages of austenite, the other being relatively high corrosion resistance even when compared to other stainless steel microstructures.

There are two noteworthy observations pertaining to duplex stainless steel. First, duplex stainless steel does not have a pronounced yield limit (Abidelah et al., 2008). Moreover, besides lacking a well-defined yield limit, there is also no well-defined plastic plateau that follows the yield point. Secondly, duplex stainless steel does not have a constant Young's modulus of elasticity. This is also an important aspect that affects much of the material response in structures. Great consideration should be shown for these two aspects, since stainless steel does not have the same structural response as that of carbon steel.

***Table 2.2**: This table shows typical proof strengths and maximum elongation. Note that the values are only representative values. All values are obtained from the EN 10088-4 standard, in particular, from table 7 and 9 in the standard.*

Grade	***Proof strength [MPA]***	***Elongation [%]***
Ferritic steel	*220-320*	*18-25*
Austenitic steel	*200-420*	*30-45*
Duplex steel	*400-650*	*20-30*

Austenite

Of all the microstructures presented in this chapter, austenitic steel have the highest corrosion resistance (Vélon, 1996). However, when considering the mechanical properties, such as proof strength and ultimate strength, austenitic steel generally performs less than other microstructures (Finnås & Olsson, 2002). Notwithstanding, there is one aspect where austenitic steel excels, which is the ductility. This can be seen in figure 2.2, even though the figure shows only a typical stress-strain relationship. An example of an austenitic microstructure can be seen below in figure 2.3.

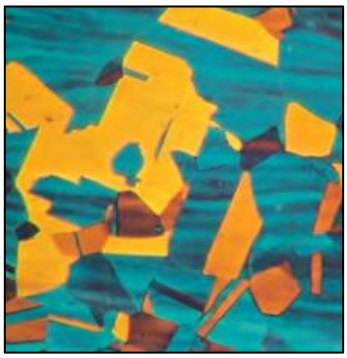

Figure 2.3: *Austenitic microstructure from a polished and etched sample, enlarged under a light microscope (IMOA, 2009). To obtain this microstructure alloying is required. In particular nitrogen and nickel is used to form austenite.*

However, as previously mentioned, austenitic steels have higher ductility than the other microstructures considered in this thesis. This in turn infers that austenitic steels can withstand considerably more deformations than would be feasible for other steels. Consequently, austenitic steel enables the ability to form complicated cross sections with small bend radii.

Also worth noting about austenite is that it is not a naturally stable structure at room temperature (Johansson & Liljas, 2002). This means that the austenite is prone to transform into other microstructures, especially martensite, during manufacturing. At a glance, the higher mechanical strength of martensite might appear to be beneficial. However, as explained in the beginning of this subchapter, martensite entails a far too low ductility to be a viable option for construction. Thus, to avoid martensite and obtain austenite or ferrite measures must be taken. This usually is in the form of alloys; however there are other alternatives in production that can help promote an austenitic structure. But that goes beyond the scope of this paper.

Nevertheless, austenite has the benefit of being insensitive to brittle fracture when treated with solution annealing (CEN, 2009). Moreover, austenite has the benefit of not having a distinct transition temperature. This is despite the fact that distinct transition temperature is characteristic for most other steel.

As a final remark, the austenitic grade is considered non-magnetic by default (Horton et al., 2008). However, the austenite is cold worked which means some amount of magnetic properties can be obtained, although small. Usually, this is of no concern for most applications. Still, it is an aspect that should be considered in applications where austenitic steel is involved.

Ferrite

Compared to austenite, ferrite entails a much lower corrosion resistance than that of austenite (Vélon, 1996). This is especially the case in more acidic environments, where ferrite is significantly weaker than austenite. However, ferrite in general has better mechanical properties. An example of a ferritic structure can be found in figure 2.4.

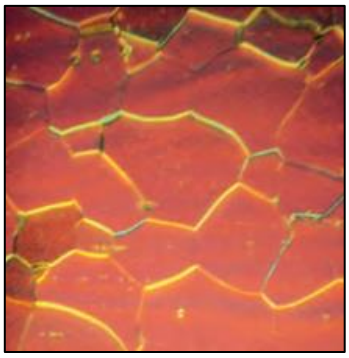

Figure 2.4: *Ferritic microstructure from a polished and etched sample, enlarged under a light microscope (IMOA, 2009). This is a stable structure without contamination of other phases.*

Unlike austenite, ferrite is a stable microstructure at room temperature (Evertsson, 1993). Furthermore, due to the fact that iron has a ferritic microstructure at room temperature the ferritic structure is in turn often referred to as "pure iron".

Similarly to *pure iron*, ferritic stainless steel grades have a more pronounced yield limit. Moreover, the mechanical properties of ferrite are higher than that of austenite, though not as high as duplex or martensitic steels.

As for the chemical composition of ferritic stainless steel, it contains between 11-27% chromium by weight to achieve the stainless status (Evertsson, 1993). Note however that the percentages are only the approximate numbers since the passivation of the steel in question is dependent on several factors.

Ferrite, much like austenite, cannot be worked with heat treatment, as this degrades the crystalline structure (Horton et al., 2008). Also, ferrite has magnetic properties by default. Much like earlier, the magnetic properties are usually not of great concern in most applications, but should be noted.

To conclude, ferritic stainless steels are iron-chromium alloys. However, they can also contain other alloying elements. For instance, titanium and niobium can be implemented to act as stabilisers during welding (Brown et al., 2012). Though, the most important properties of ferrite are that it contributes with exceptional mechanical properties, such as significantly improved ductility.

Duplex (Austenite-Ferrite)

As the title of this section suggests, duplex is a combination between two metallic phases or microstructures. Of course, it is possible to have many other metallic phases. Still, when speaking of duplex steels it exclusively refers to the austenite-ferrite combination. For the sake of convenience, this thesis sticks to the convention of duplex.

As explained in subchapter *2.5 - Analysis of existing structures*, duplex is the most relevant microstructure for future construction with stainless steel. Though in short, the most beneficial property of duplex stainless steels are that they have a superior strength compared to both austenitic and ferritic steels. Also worth mentioning is that the most common duplex grade is EN 1.4462, also referred to as UR45MNo (Johansson & Liljas, 2002).

Note however, that there are alternatives to EN 1.4462 that should be mentioned since 1.4462 is an expensive highly alloyed stainless steel. The cheaper alternatives are in the category of lean-duplex steels.

The high strength of duplex steel rivals that of martensitic grades and also, duplex steel have a better ductility and toughness compared to that of martensite. Though, unlike martensitic steel which gains its strength directly from the small grains in the microstructure, duplex obtain its properties from the fact that there are two phases present (IMOA, 2009). In addition, the large content of nitrogen in duplex steel also has a positive impact on the strength properties.

Much like austenite, or because of the austenite, duplex steel has no clear yield point and plastic plateau (Sobrino, 2006). Instead it is common practise to utilise 0.2% elongation strength as *proof strength*. Note that it is difficult to measure where plastic strains start and where elastic strain ends.

Lastly, duplex stainless steel does not polish as easily as austenitic grades, which makes them more expensive if a certain finish is desired. (Brown et al., 2012)

Martensite

In general, martensite is very stiff and quite strong compared to ferrite and austenite. However, it is also brittle in comparison, making it perform rather poorly when it comes to ductility and fatigue. These are the major reasons for why martensite is unsuitable for construction purposes.

Martensitic crystalline structures are formed by tempering the steel followed by letting it cool quickly, or by deliberately quenching the steel. Generally, martensite is not a desired crystalline structure for constructions. However, when welding steel martensite might form as a by-product of the rapid heating and sometimes rapid cooling (IMOA, 2009).

2.1.3 Corrosion resistance

First and foremost, stainless steel has an outstanding natural corrosion resistance in comparison with carbon steel (Fanica et al., 2008). Available test data supports the claim that properly designed and executed structures in stainless steel will at most suffer only miniscule and negligible corrosion damage. Thus, stainless steel truly earns its name when used in the right way. However, a word of caution is that even stainless steel can corrode if implemented incorrectly. If the stainless steel starts to corrode the structural integrity is at risk just as it would be for carbon steel.

In fact, if stainless steels begin to corrode for some given reason, the whole point of utilising stainless steel then becomes superfluous. Thus, this subchapter is dedicated to further investigation on corrosion and how it relates to stainless steel. Also included in this thesis are different corrosion modes and how they originate, more on this in subchapter *2.1.4 - Corrosion modes*.

First and foremost, corrosion is one of the major problems when it comes to carbon steel structures. Still, contrary to what the name *stainless steel* implies, it is not stainless in the true sense of the word. To elaborate, even stainless steel corrodes, although at a much slower rate than conventional carbon steel does. The intention of stainless steel is that the corrosion rate is so miniscule that it is negligible for all intents and purposes that the steel might just as well be truly stainless.

Before delving into the matter of different and specific corrosion modes applicable to stainless steel, it is best to understand how stainless steel works in general with regard to corrosion. Also included before corrosion modes are how stainless steel is selected and what the pitting resistance equivalent number (PREN) is.

The first question to answer is; how does stainless steel obtain a natural resistance towards corrosion?

To put it simply, stainless steel gains a natural resistance towards corrosion by forming a thin layer, only 2.5nm thick, of chromium oxide (Finnås & Olsson, 2002). An illustration of this passive film can be seen in figure 2.5. This thin layer of chromium oxide halts further corrosion from taking place by preventing oxygen to reach the steel. Regarding terminology, this type of corrosion protection is referred to as *passivation*. In addition, if the thin film of chromium oxide were to be scratched or damages, it would almost instantly reform and regaining its protective abilities.

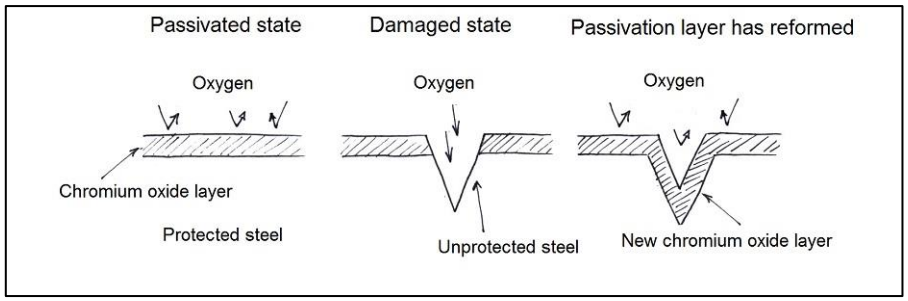

***Figure 2.5**: An illustration of how the chromium oxide forms a thin film that passivate the stainless steel. Note that the chromium oxide reforms after the original film has been damaged, possibly by a scratch. The reforming of the film is referred to as the* self-healing *properties of stainless steel.*

On the subject of alloying steel with chromium, note that stainless steel is always alloyed with more elements. For instance, nickel is used to stabilize the austenitic or duplex microstructure. More on the alloying elements can be found in chapter *2.1.5 - Alloying elements*.

Moving on to the next topic of corrosion, which is environmental classification and how to accordingly select the right type of stainless steel.

Unfortunately, the alloying elements in stainless steel are expensive, especially nickel[1]. Thus, the alloying elements present in stainless steel are one of the major reasons for why the steel is more expensive by weight than carbon steel. Consequently, in the interest of keeping the cost of the raw material down it is desirable to select a stainless steel without an excessive amount of alloying elements for the given circumstances.

With regard to this, the stainless steel type is selected as to correspond to the environmental class. In other words, the environmental class determines how corrosion resistant the steel has to be. When the corrosion resistance is determined, the type of stainless steel is also determined. Or to be more precise, the family of stainless steel is decided. From that point onward it is other factors that determine the selection of a specific stainless steel.

Moving on to discuss a bit about the classes themselves, a summary of the classes can be found in table 2.3. A highlight of the table and the classes therein, is that *normal* indoor climate is omitted in the C-classes. The reason is partially explained in EN 1993-1-4 Annex A.1, which reads as following:

> *"Although stainless steel can be subjected to discolouration and staining (often due to carbon steel contamination), they are extremely durable in buildings."* – EN 1993-1-4. A.1-(9*)*

What is also implied is that stainless steel is extremely durable in building and indoor climate. Of course, this statement does not cover unusual or industrial application of stainless steel.

[1] Anders Finnås (Segment Business Manager on Stainless Steel, Outokumpu) interviewed by the authors, 2014-02-11

***Table 2.3**: Guidelines for duplex stainless steel selection. Also, gives example of what the different C-classes correspond to (Baddoo & Kosmac, 2011).*

ISO 9223 Atmospheric Corrosion Class	**Typical outdoor environment**	**Suitable duplex grade**
C1	Deserts and arctic areas (rural)	1.4162
C2	Arid and low pollution (rural).	1.4162, 1.4362
C3	Coastal areas with low deposits of salt. Urban or industrialised areas with moderate pollution.	1.4162, 1.4362, (1.4462)
C4	Polluted urban and industrialised atmosphere. Coastal areas with moderate deposits. Road environments with de-icing agents.	1.4462, (1.4362), other higher alloyed duplexes.
C5	Severely polluted industrial atmospheres with high humidity. Marine atmospheres with high degree of salt deposits and splashes.	1.4462, other higher alloyed duplexes.
Grades suitable for a higher class may be used for lower classes but might not be cost-effective. Grades within brackets denote use/need in special cases.		

As previously mentioned, in contrast to traditional carbon steel, which is selected by its mechanical properties, stainless steel is selected by its corrosion resistance. Moreover, it is the alloying elements that constitute the increased material cost of stainless steel. Note that it is the alloying elements that give stainless steel its corrosion resistance. Thus, the more resistant the steel has to be the more alloys are required and the cost increases with the alloys. Consequently, to keep the price down, stainless steel is selected by its desired corrosion resistance and preferably not much more as not to have overcapacity with regard to corrosion resistance.

Of course, stainless steel has been tested in both laboratories and with field testing. There is also a noteworthy example of a full scale test of duplex stainless steel bridges. This test, conducted by Fanica et al. and commissioned by the European Commission of Research, is one of the few where duplex stainless steel in a bridge construction was tested in full scale. Among many results from this research, they concluded that stainless steel is indeed as corrosion resistant as advertised. As a matter of fact, the test data yielded that the stainless steel is likely more corrosion resistant than expected.

To elaborate further, the result tells that duplex stainless steel, grade EN 1.4462 in the test, withstand all the C-classes without succumbing to anything more than superficial corrosion (Fanica et al., 2008). Though the superficial corrosion is questionable whether it is from the stainless steel or some other contaminant on the steel surface.

As a comparison, in the C5 category carbon steel is expected to corrode within the interval of 80 to 200µm/year (Fanica et al., 2008). Whilst duplex stainless steel, grade

EN 1.4462 tested in synthetic sea water, corrodes at a rate less than 0.5µm/year. Needless to say, stainless steel corrodes at a considerably lower rate than carbon steel. To conclude, the corrosion rate of stainless steel can be kept negligible when the correct steel grade is chosen. In addition this implies that there will be no notable reduction of the cross section caused by corrosion.

In light of the aforementioned statements it is possible to draw a conclusion that stainless steel has more capacity in the aspect of corrosion than what is currently utilised. Furthermore, this may allow for lesser steel grades with lower corrosion resistance to be used, effectively rendering the stainless steel less expensive to use. However, the corrosion rate is not a one dimensional problem, and using less corrosive resistant steel grades might cause unexpected problems.

As a closing statement for this subchapter, there is no *true* stainless steel. The best that can be done is to slow down the corrosion progress. There are too many ways of preventing corrosion damage to list or discuss comprehensively within this thesis. However, the intent of stainless steel is always to slow the corrosion progress until the rate is sufficiently low that it can be considered negligible for the given application and environment.

Pitting Corrosion Equivalence number

It is generally acknowledged that stainless steel is not particularly sensitive towards general corrosion. However, when the environment of application becomes too severe some localised corrosion phenomena, like pitting- and crevice corrosion, usually occurs (Comer, 2003). Furthermore, at marine environments where chlorides are in abundance, it is usually crevice corrosion that occurs as the first mode of corrosion, more on this can be found in subchapter *2.1.4 - Corrosion modes*.

However, pitting corrosion bears a special significance for stainless steel compared to other types of corrosion modes. For this reason the corrosion resistance of different steel grades are usually compared by means of the pitting corrosion resistance. This makes it possible to compare the corrosion resistance of different stainless steel types. Note however, that the comparison of pitting corrosion resistance is mostly relevant when comparing stainless steel of similar alloy composition.

As previously mentioned, different stainless steel types offer different amounts of corrosion resistance. For instance, there are some grades that handle crevice- and pitting corrosion better than others. Note however, that the specific resistance towards corrosion is determined by many interrelated factors. Consequently, corrosion resistance can only be reliably determined on a case-by-case basis.

With that in mind and to simplify, it is possible to say that corrosion resistance is largely determined by the alloy composition of the steel in question, which in turn affects the price. Of course, the microstructure also affects the corrosion resistance in combination with the alloy composition since the microstructure determines what amount of alloys that can be used and the effect of said alloys.

Consequently, in the interest of not overcompensating the corrosion resistance of a stainless steel a tool by the abbreviation PREN is often put to use (EuroInox & Stålbyggnadsinstitutet, 2006). The abbreviation PREN stands for *Pitting Resistance Equivalence Number*. The number is calculated according to equation (2.1) and equation (2.2), see (Comer, 2003). Note that the equation differs somewhat depending on whether it is an austenitic or a duplex stainless steel.

$$\mathrm{PREN}_{\mathrm{duplex}} = (\%\mathrm{Cr}) + 3.3 * (\%\mathrm{Mo}) + 16 * (\%\mathrm{N}) \qquad (2.1)$$

$$\mathrm{PREN}_{\mathrm{austenitic}} = (\%\mathrm{Cr}) + 3.3 * (\%\mathrm{Mo}) + 30 * (\%\mathrm{N}) \qquad (2.2)$$

Where

%Cr = Percentage chromium content by weight
%Mo is the molybdenum content
%N is the nitrogen content

However, for duplex grades containing both nitrogen and tungsten there is a modified version for the pitting resistance equivalence number, see equation (2.3).

$$\mathrm{PREN}_{\mathrm{duplex}} = (\%\mathrm{Cr}) + 3.3 * (\%\mathrm{Mo} + 0.5 * \%\mathrm{W}) + 16 * (\%\mathrm{N}) \qquad (2.3)$$

Where

%W = Percentage tungsten content by weight

In short, this number is a scalar to give an approximation of how a given stainless steel performs against pitting corrosion based on the alloy composition of said steel. Note however, that PREN only gives an approximation. The true pitting corrosion resistance needs to be measured by more sophisticated means. For instance, it can be done in accordance with the ASTM-G-150 standard.

In table 2.4, for the sake of comparison some common stainless steels and corresponding PREN are listed. In general, when the number reaches about 40 it indicates that there is no more than a minimal risk of pitting corrosion (Comer, 2003). However, this varies somewhat and in some instances literature advocates that a PREN of 30 or more is satisfactory.

Note that duplex grades generally tend to have a better pitting corrosion resistance than that of austenitic grades. Though, in the end it is largely dependent upon the specific steel in question and also in what environment the steel is implemented in.

***Table 2.4**: This table exemplifies some values of the PREN for the more common stainless steel grades. Note that the pitting resistance equivalence number (PREN) increases with duplex and the more alloyed the steel is (ESAB, 2012).*

Type	EN Steel Grade	PREN
Austenitic	1.4307	18
	1.4401	24
Lean Duplex	1.4482	23
	1.4162	26
	1.4062	26
	1.4362	26
	1.4655	26
Duplex	1.4362	26
	1.4462	35
Super Duplex	1.4507	39
	1.4410	42
	1.4501	42

As an additional note pertaining to the PREN, it is claimed that there is a good correlation between the PREN and fatigue limit of stainless steel in seawater (Comer, 2003). However, a more in-depth analysis of this correlation is not included in this thesis.

On the other hand, care must be taken as not to overly rely on the PREN. As stated earlier, the PREN is fairly accurate in predicting corrosion resistance of a given stainless steel. However, the number in question omits several aspects that play a vital role in the corrosion resistance of a given stainless steel. For instance, the PREN assumes perfectly treated material and without any alloy discrepancies. Or for that matter, how alloys interact with other alloying elements. In the end, the PREN is a good estimate of corrosion resistance, though only an estimate and should not be taken for true corrosion resistance in any circumstance.

As a final remark about the measuring of corrosion resistance, despite focusing on the PREN, there are many other options available for determining corrosion resistance. For instance, it is possible to look into the resistance of *stress corrosion cracking (SCC)* or *crevice corrosion resistance (CCR)* (IMOA, 2009). There is also a *chromium equivalence number* and a *nickel equivalence number*. However, they are not as important or widely used when estimating the corrosion resistance of stainless steel.

2.1.4 Corrosion modes

Even though corrosion might appear to be *just corrosion*, there are actually many different kinds of corrosion modes. In addition, these corrosion modes have different appearances and they also operate differently from each other. Consequently, it is important to understand how the different corrosion modes operate and what causes them to appropriately thwart corrosion from taking place.

For this thesis, corrosion has been divided into the following categories:

- General corrosion
- Intergranular corrosion
- Pitting corrosion
- Crevice corrosion
- Stress corrosion cracking
- Bimetallic corrosion
- Corrosion with heat

General corrosion

General corrosion, in a word, occurs over the whole metal surface. This type of corrosion affects the metal surface uniformly. As far as stainless steel is concerned, in outdoor and indoor environments, this is not an issue for stainless steel (Finnås, 2012). Of course, this statement is only valid for normal environments. For instance, certain industrial applications involving intense heat and very acidic environments give cause for corrosion even for stainless steel. Lastly, the statement is only valid if the stainless steel is correctly implemented. If incorrectly implemented, even stainless steel can corrode.

General corrosion is a minor issue when considering stainless steel. Usually, to avoid the problem of general corrosion altogether when alloys are utilised. The most important alloy in respect to general corrosion is chromium (Comer, 2003). The reason is that chromium forms the passive layer that prevents general corrosion from taking place. An illustration of this passive layer can be found in figure 2.5.

On the other hand, it is still possible for stainless steel to succumb to general corrosion. If this happens, there are two likely explanations. The first one being that the steel might contain too little alloying as to properly form a passive layer or that the passive layer is simply insufficient in strength. The other reason, being similar to the first, is that the environment is too extreme or contains unforeseen difficulties. For instance, if the environment contains too strong acids or entailing a considerably higher temperature than specified during the selection of stainless steel type.

However, general corrosion is in almost all cases not an issue for stainless steel in bridges and buildings. Industrial usage of stainless steel is another matter that brings other challenges and conditions, but those considerations are not included in this thesis.

Intergranular corrosion

Intergranular corrosion is a particular mode of corrosion that appears between the grain boundaries on a microscopic level. It is a mode of corrosion that is relevant for all stainless steel (Comer, 2003). As a matter of fact, it is one of the corrosion modes that stainless steel is somewhat more susceptible to compared to other corrosion modes, especially with welded stainless steel members.

Intergranular corrosion occurs after alloyed steel has been heated and the grain boundaries are depleted of chromium. For the sake of comparison, austenitic steel has to be heated, and then kept, within the temperature interval of 450 to 850°C (EuroInox & Stålbyggnadsinstitutet, 2006). There is no critical time for chromium depletion to occur, though it ranges from a few minutes to about half an hour. The reason why there is no critical time is due to the fact that there are several factors that affect the phenomena of chromium depletion. An example of a possible cause for chromium depletion is when welding stainless steel and then letting the metal slowly cool through the critical temperature interval.

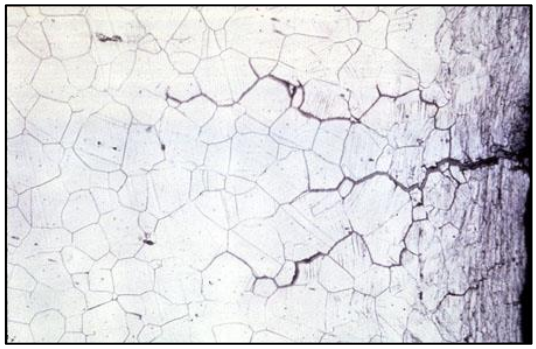

***Figure 2.6**: Example of intergranular corrosion. Note that the corrosion forms on the grain boundaries. Of course, the corrosion product reduces the strength of the steel. This in turn increases the risk of cracking due to tensile stresses (Groth & Johansson, 1991).*

When the steel has reached a given temperature, carbon diffuses to the grain boundaries. At these boundaries chromium carbides form due to the high affinity of chromium to form compounds with carbon. A micrograph showing the formation of chromium carbides can be found in figure 2.7. The carbides themselves are not problematic. However, these carbides tend to deplete the chromium content at the grain boundaries which leaves no chromium left to form a passive film of chromium oxide. Needless to say, without the passive film there is nothing preventing corrosion from taking place, especially at the grain boundaries. It is from this intergranular corrosion originates. An example of how intergranular corrosion can cause cracking can be found in figure 2.6.

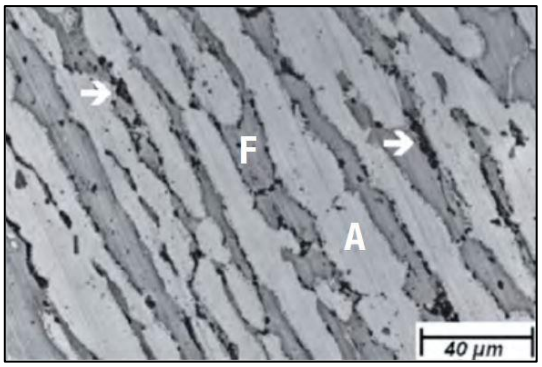

***Figure 2.7**: A micrograph showing the formation of carbides. Note that these carbides indicate that there is a depletion of chromium on the grain borders. This in turn implies an increased risk of intergranular corrosion.*

The problem of intergranular corrosion was particularly relevant for the earlier stainless steels due to the fact that these types of steels contained a lot more carbon than the modern stainless steel does. To elaborate, modern stainless steel usually contains less than 0.03% carbon content by weight. This effectively reduces the formation of carbon carbides due to the fact that there is insufficient carbon to form carbides with.

However, modern stainless steel is effectively saturated with nitrogen. Chromium also has an affinity with nitrogen. Nitrogen can similarly to carbon form compounds with chromium, which are then called chromium nitrides (Muthupandi et al., 2003). The formation of chromium nitrides can also cause chromium depletion. A more elaborate analysis of the formation process and also preventative measurements can be found in subchapter *2.2 - Welding of stainless steel*.

Lastly, duplex stainless steel has a particularly good resistance towards intergranular corrosion. This is due to the combination of microstructure together with low carbon content (Outokumpu, 2013). However, even duplex stainless steel is not immune towards intergranular corrosion.

Pitting corrosion

Pitting corrosion is in some ways the opposite of general corrosion. For instance, pitting affects a very local region on the steel surface instead of being spread across the whole of the surface, see figure 2.8 (SMS, 2000). In addition, it is harder to determine the actual corrosion rate of pitting corrosion. Consequently, it makes it more difficult to determine life expectancy of a given construction member in the case of active pitting corrosion.

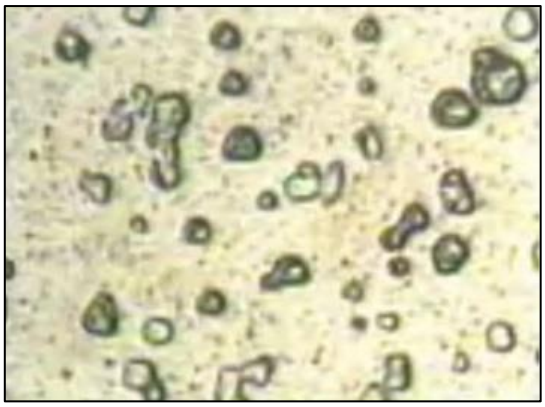

***Figure 2.8**: Example of pitting corrosion on a stainless steel sample. Note that the pitting corrosion is a localized corrosion phenomenon, whereas the intermittent surfaces remain largely intact. The sample metal is of the type Zeron 100. The sample is synthetically corroded in a lab environment (Comer, 2003).*

Though pitting and crevice corrosion bear many similarities, pitting corrosion is not the same as crevice corrosion. It is especially the initiation processes that differ between pitting- and crevice corrosion. Though, a relatively easy way to tell them apart is that pitting corrosion does not require a tight gap which crevice corrosion does. As mentioned earlier, pitting corrosion can occur on a flat and open surface.

The classic method of illustrating pitting corrosion is by a droplet of water on a flat steel surface, see figure 2.9. To put it simply, there is a scarcity of oxygen supply in the middle of the droplet whilst at the borders of the droplet the oxygen supply is much larger due to oxygen diffusion through the water. This difference gives cause to a galvanic cell and renders the central part anodic (Comer, 2003). From this point on, pitting corrosion can occur.

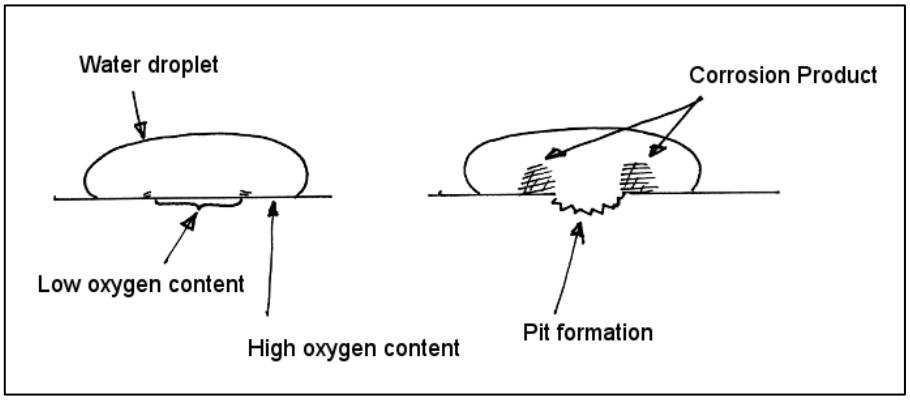

***Figure 2.9**: An illustration of how pitting corrosion is initiated, in this case, via a drop of water. Note that pitting corrosion is a localized phenomenon that occurs in the middle of the water droplet.*

For steel bridges, which are only exposed to atmospheric conditions, the most important types of corrosion to consider are pitting corrosion and crevice corrosion (Finnås, 2012). The reason is that stainless steel, as mentioned earlier, have a more than adequate resistance towards general corrosion. Consequently, general corrosion is typically not of great concern.

However, a higher concentration of more aggressive substances in combination with a sufficiently high oxidising electrochemical potential can initiate pitting corrosion. An example of a highly aggressive substance is chloride ions, which are prevalent in both de-icing agents for roads and in marine environments.

Also worth mentioning is that the rate of pitting corrosion, as well as many other corrosion phenomena, is influenced by temperature (Fanica et al., 2008). In normal circumstances, an increase in temperature entails an increase in corrosion rate and sometimes by quite much. For instance, an increase in temperature from 20 to 60°C entailed an increase in pitting corrosion rate by a factor of 50.

To give a few words on the preventative measures against pitting corrosion. Firstly, there is a possibility of increasing the chromium content, which leads to a stronger passive layer of chromium oxide. As the strength of the chromium oxide layer increases so does the corrosion resistance. In other words, due to the fact that pitting corrosion is caused by a localised concentration of more aggressive reactants, like chloride ions, the passive film prevents pitting corrosion to some extent.

In addition to chromium, there is also the possibility of alloying with molybdenum. This alloy is considerably more effective towards pitting corrosion than chromium (IMOA, 2009).

By the same token, nitrogen is also a more effective alloy than chromium in increasing the pitting corrosion resistance. An added benefit for nitrogen compared to molybdenum and chromium is that it can be extracted from the air and thus is much more inexpensive. Consequently, the nitrogen content of modern stainless steels is kept high, in some cases the content is close to saturation. Note however, that there are additional benefits to alloying with nitrogen besides increasing the pitting corrosion resistance. More on nitrogen and other alloys can be read in subchapter *2.1.5 - Alloying elements*.

There are numerous tests conducted on pitting corrosion. They are far too many to list, though one in particular is worth highlighting, a test on pitting corrosion on duplex stainless steel type EN 1.4462, though called UR45Mo in the test. This specific grade was tested in synthetic sea-water by Fanica et al. The test data shows that pitting corrosion on the tested steel could not be observed. Thus, it is shown that duplex stainless steel exhibit an exceptionally good pitting resistance. Especially since any other steel is expected to show little to severe pitting corrosion. Part of the test data obtained by Fanica et al. can be seen in figure 2.10. For more information, the reader is referred to the report by Fanica et al.

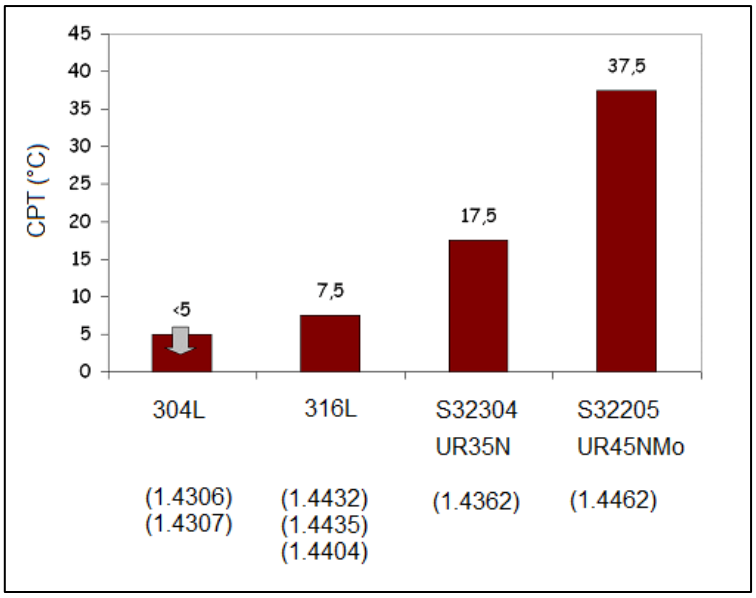

***Figure 2.10**: Laboratory results showing Critical Pitting Temperature (CPT) in degrees of Celsius according to the ASTM G48-03 method-E standard (Fanica et al., 2008). Note that the authors of this thesis took the liberty of including an approximate translation of the metal classes according to the EN10080 standard, see parentheses. Also note that the duplex grade UR45MNo shows an exceptional pitting corrosion resistance.*

Crevice corrosion

Crevice corrosion is in many ways related to pitting corrosion. For instance, they both appear as localised forms of corrosion. Though, pitting and crevice corrosion are caused by different processes. Lastly, in marine environments where duplex stainless steels are used crevice corrosion is the most common corrosion mode (Finnås, 2012).

For crevice corrosion to appear, there are a few requirements that needs to be fulfilled. First and foremost, some kind of crevice is required for this corrosion mode to be able to initiate. Note that it is not the crevice itself that is harmful, but the fact that there is a lower supply of oxygen and at the same time an increase in chloride ions (SMS, 2000). Of course, there are other particles beside chloride ions that can initiate crevice corrosion. However, chloride ions from both de-icing agents on roads and from saltwater are well acknowledged for being the most predominant cause of crevice corrosion (Comer, 2003).

To shed some light on the electrochemical process that is crevice corrosion, the reader is referred to figure 2.11. In a simplified manner, crevice corrosion is caused by a concentration of chloride ions within a crevice (Comer, 2003). As these ions accumulate, the protective passive film breaks down. In short, the crevice allows for chloride ions and similarly aggressive substances to accumulate. Due to the high concentration of aggressive substances the local environment within the crevice becomes much more severe than the surrounding environment. Of course, this is only a simplified explanation. For more information the reader is referred to *Corrosion Fatigue of Duplex Stainless Steel Weldments in Aggressive Environments* by Anthony Comer.

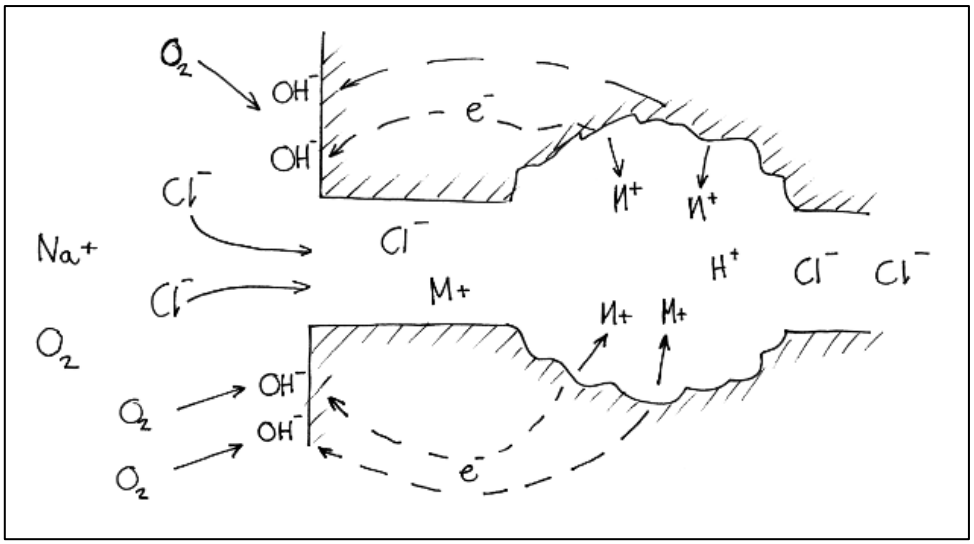

***Figure 2.11**: An illustration of how crevice corrosion propagates. Note that crevice corrosion does not require two metals, but rather two separate environments and only one metal (Comer, 2003)*

A quite important trait for crevice corrosion is the fact that it does not require two metal surfaces. Instead, any crevice will do, as can be seen in figure 2.11. Some examples of crevices can be under rust deposits, rubber, sand, under weld spatter, flanged joints and so on (SMS, 2000). That is to say, there are a lot of unintentional crevices that can cause crevice corrosion. Lastly, the tighter the gap, the more likely it is that crevice corrosion will occur.

Stress corrosion cracking

Stress corrosion cracking is a terminology referring to cracks that are formed through a combination of tensile stresses and corrosion. That is to say, tensile stresses and corrosion have a synergic effect that helps create cracks. In other words, tensile stresses or corrosion alone would not be sufficient to create a given crack, but when the two phenomena work in tandem they have the ability to create cracks.

In general, it is only austenitic stainless steels that are susceptible to stress corrosion cracking. Conversely, both duplex and ferritic grades exhibit a considerable resistance towards this particular mode of corrosion (Baddoo & Kosmac, 2011).

For reason explained in chapter *2.1.2 - Microstructures*, austenitic steel is only of peripheral interest in this thesis. The most relevant material to analyse for bridges is the duplex grades. Also note that stress corrosion cracking is a problem that is mostly, or only, relevant for the austenitic stainless steels. Consequently, besides briefly mentioning stress corrosion cracking, this paper will not further elaborate on this particular corrosion mode.

Bimetallic corrosion

Bimetallic corrosion shares some similarities with crevice corrosion. However, instead of it being one metal that is connected with two environments, bimetallic corrosion requires two metals and only one environment. In short, when two metals come into contact, the most active, or less noble, of the metals is consumed whilst the more noble metal remains intact during the corrosion process, see figure 2.12 for example. Also see anode-cathode reactions for further details.

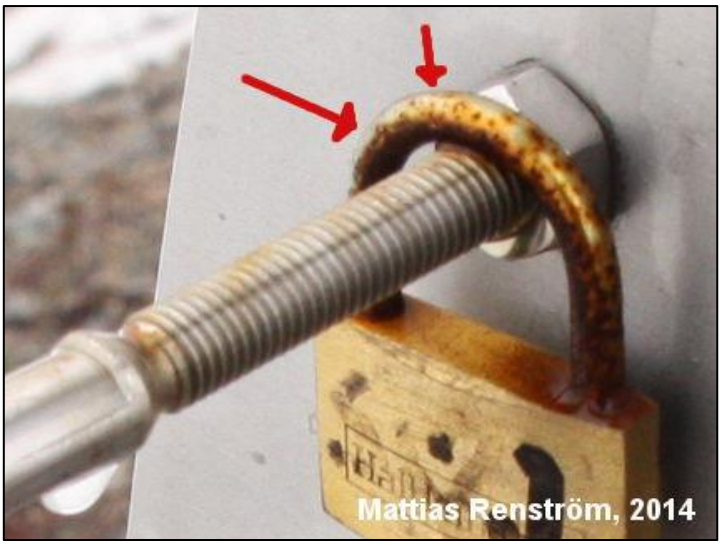

***Figure 2.12**: Example of bimetallic corrosion. Note that the stainless bolt remains bereft of corrosion whilst the padlock is severely corroded. The small amounts of rust that can be found on the bolt are most likely superficial rust from surface contaminants or rust deposit from the padlock.*

Between carbon steel and stainless steel, it is the carbon steel that is the more active of the two. In other words, carbon steel that is in contact with stainless steel corrodes at a much higher rate than it would otherwise (SMS, 2000). An example of a practical application where bimetallic corrosion needs to be considered, is in fasteners and details. To elaborate, it is disadvantageous to use carbon steel details and bolts on an otherwise stainless steel bridge, since the smaller carbon steel details would corrode at a considerably higher rate than otherwise.

Note however, that bimetallic corrosion can also be utilised as a measure to circumvent active corrosion damage on a structural steel member. For instance, it is possible to protect a metal part from corrosion by connecting it to a more active metal. Thus, the active metal would be *sacrificed* whilst the nobler would remain intact. This method of *active protection* is applicable to stainless steel (Outokumpu, 2013). However, it is usually considered under given circumstances. Though, a by far more effective protection is to rely on the natural passivation of stainless steel, given that it is correctly implemented.

If to avoid bimetallic corrosion, especially since stainless steel is relatively noble in this aspect, the method of *isolation* is usually put to practise. Example of this can be found in figure 2.13.

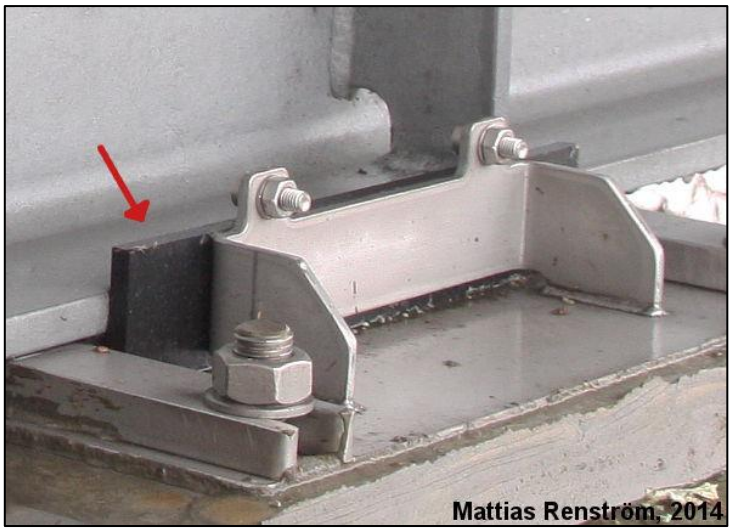

***Figure 2.13**: Example of rubber isolation to avoid unintentional bimetallic corrosion, the rubber is arrowed. The role of thumb to avoid bimetallic corrosion is to break electric contact between the two metals in question. Note that this extra step in construction entails extra risk, cost and work. Moreover, it also slightly complicates the detail itself.*

Corrosion with heat

Needless to say, corrosion and the rate of corrosion are affected by many interrelated factors. One worth mentioning is the impact of temperature, especially higher temperatures.

For instance, test data shows that the electrochemical potential of stainless steel is significantly reduced when the temperature is increased from 20 to 80°C (Comer, 2003). To clarify, when the electrochemical potential is decreased the resistance towards pitting corrosion, as well as other types of corrosion, is also decreased. As a matter of fact, it is commonplace to measure the pitting corrosion resistance through a concept of *critical temperature*. An example of this can be seen in figure 2.10.

In figure 2.14 partial results is presented from a research conducted by Fanica et al. In this figure it is possible to see that in a given solution, synthetic brine to be specific, even a small temperature increase of 10°C can make the difference between no corrosion occurring and initiated pitting corrosion.

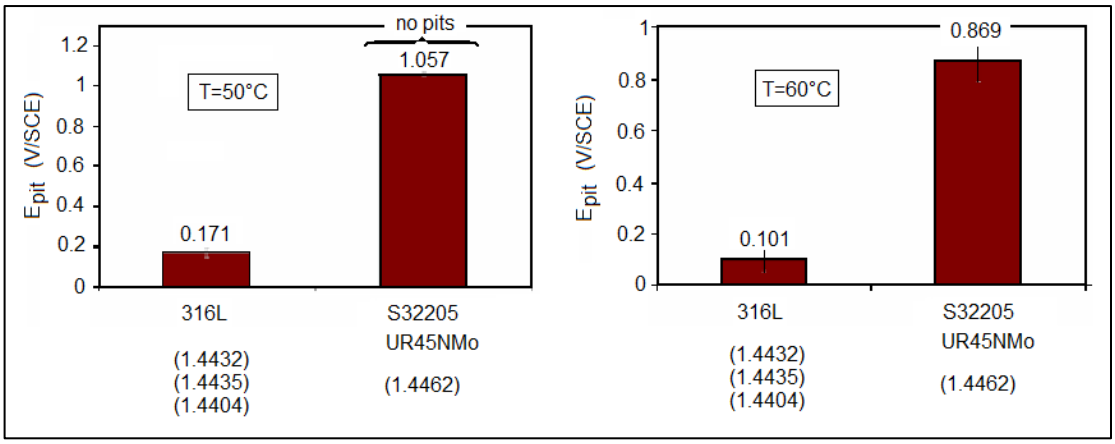

Figure 2.14: *Laboratory results showing electrochemical potential for two duplex stainless steels in accordance with the ASTM G48-03 method-F standard (Fanica et al., 2008). Note that the authors of this thesis took the liberty of including an approximate translation of the metal classes to the EN 10088 standard, see parentheses. Also note that the duplex grade UR45MNo has an exceptional pitting resistance. In addition, the diagrams have been modified to increase readability. Lastly, the importance of this figure is the decrease of electrochemical potential with increased temperature.*

However, the relationship between temperature increase and the increased likelihood of corrosion or the rate of corrosion is very complex. Generally it has to be determined on a case by case basis. The impact of temperature with regard to corrosion goes outside the scope of this thesis.

2.1.5 Alloying elements

Alloyed steel, or simply *alloys*, play a vital role in both mechanical and the chemical behaviour of stainless steel. To a large extent, stainless steel is defined by the involved alloys and their composition. Consequently, this subchapter is dedicated to give a rudimentary overview of the different alloys and their most important properties.

Of course, this chapter will only mention the most important alloys for stainless steel that are used in constructions. That is to say, alloys that are used in stainless steel intended for industrial purposes are omitted. In addition, to further narrow down the scope of alloys, residual elements that are not intended or accounted for is not considered in this chapter.

Lastly, some alloys are omitted even though they are used for stainless steel. These are the following:

- **Aluminium** enhances corrosion resistance. However, only if added in substantial amounts.
- **Copper,** which is used to promote austenitic microstructure and enhance corrosion resistance. Is mainly used for industrial application.
- **Carbon,** which significantly increases mechanical properties. Though most modern stainless steel use less than 0.030% carbon by weight to increase weldability (Brown et al., 2012).
- **Cobalt** almost exclusively in martensitic steels to increase strength and tampering abilities at high temperatures.
- **Tungsten** is sometimes used for improving pitting corrosion. Also, usually exists as an impurity
- **Vanadium** forms carbides and nitrides at lower temperatures and is used for steels that can be hardened.

Of course, there are more uncommon alloys that are not at all included, cerium for instance. That is to say, there are more alloys and no real limit to the amount of possible combinations. Below are some of the more important alloys and their properties, which are discussed in a somewhat more elaborate manner.

Chromium

As stated in the beginning of this chapter, chromium is one of the most important and frequently used alloys for stainless steel in construction. It is chromium that gives stainless steel its passivation film of chromium oxide.

For stainless steel to be able to form a passivation film the steel must have a chromium content of at least 10-11% by weight (Brown et al., 2012). Note that there is no absolute lower limit of chromium content, as it depends on a lot of other factors. Similarly, there is also no clearly defined upper limit for the chromium content. However, for the sake of comparison the maximum chromium content is in the vicinity of about chromium content 30% by weight.

Another important aspect of chromium is that it promotes the formation of a ferritic microstructure (IMOA, 2009). Consequently, chromium might require to be balanced with an alloy that promotes an austenitic structure, as not to overcompensate with ferrite in the manufacturing of duplex stainless steel.

Molybdenum

As can be read in subchapter *2.1.4 - Corrosion modes*, pitting corrosion is considered to be one of the more likely corrosion modes for stainless steel. To counter pitting corrosion it is possible to alloy with molybdenum. This alloy increases the resistance towards pitting corrosion considerably. In addition, molybdenum also slows down the corrosion rate when pitting corrosion is in an active state.

Moreover, molybdenum is particularly effective when the chromium content exceeds 18% by weight (IMOA, 2009). However, due to the accumulative detrimental effects of molybdenum, such as promoting formation of unfavourable intermetallic phases, there is usually a limitation of maximum allowed molybdenum content. For instance, the content is limited to about 7% by weight for austenitic steels and 4% for duplex grades.

Nickel

As can be read in subchapter *2.1.2 - Microstructures*, the formation of austenitic microstructures requires a stabilizing alloy. A particularly adept alloy for this purpose is nickel.

Besides the aspect of promoting an austenitic microstructure nickel also have the benefit of decreasing the corrosion rate in the active corrosion state. In addition, it also reduces the sensitivity towards stress corrosion cracking (CEN, 2006).

However, nickel has some disadvantages to consider. One of the major disadvantages of nickel is the cost. When considering the alloys typically required for stainless steel, nickel is by far the most expensive by weight (Johansson & Liljas, 2002). As a matter of fact, the price fluctuation of nickel causes problematic price fluctuations for stainless steel as a whole. Consequently, it is often desired to keep the nickel content as low as possible as to obtain a more stable market price for stainless steel.

A method of decreasing the nickel content is by substituting some of the alloy with manganese and nitrogen (Johansson & Liljas, 2002). By lowering the nickel content, the goal of also lowering the price fluctuations of stainless steel is also achieved.

However, the downside to reduced nickel content, among other things, is that the steel obtains a reduced impact toughness and workability. (Johansson & Liljas, 2002)

Nitrogen

Much like nickel, nitrogen is a strong austenite former. However, nitrogen comes at a much cheaper price than nickel. An additional benefit of nitrogen is that it substantially increases strength properties of the stainless steel (IMOA, 2009). Moreover, nitrogen has the added benefit of delaying the formation of detrimental intermetallic phases. This simplifies, and to some extent enables, the manufacturing of duplex grade steels.

The downside of nitrogen is that it reduces impact toughness as well as corrosion resistance in the ferritic microstructures (Outokumpu, 2013).

Titanium

Titanium is used for stabilising austenitic structure during welding (Brown et al., 2012). Titanium entails a much greater affinity for carbon than chromium. As such, carbides and nitrides are much more readily formed with titanium rather than chromium. Thus, with titanium it is possible to circumventing the problem of chromium depletion in welds. More on chromium depletion can be read in subchapter *2.2.3 - Chromium depletion*.

Titanium, unfortunately, lends a certain hue to the material finish. In addition, the titanium gives certain aesthetical discrepancies when polished. As such it is not generally used for decorative purposes or when aesthetics are of concern. Thus, the titanium alloys are in this case replaced in favour of low-carbon stainless steel. This is almost as weldable, though with much greater results when it comes to polishing. (Brown et al., 2012).

2.2 Welding of stainless steel

To begin, most of the common welding techniques available for carbon steel can also be successfully applied for welding of stainless steel (EuroInox & Stålbyggnadsinstitutet, 2006). An exception to this rule is laser beam welding (LBW) which as of now have proved inappropriate for use on stainless steel. However, even if the welding technique is possible to use there remain certain considerations specific to welding of stainless steels. This chapter will highlight both the benefits and problems that should be considered when welding stainless steel.

It should be noted that welds are an important and yet vulnerable part of the structure, for this reason certain aspects pertaining to welds are also covered in chapter *2.1.3 - Corrosion resistance* and in chapter *2.3 - Fatigue of stainless steel.*

A benefit pertaining to the welding of stainless steel is that for most weld techniques no preheating of the parent metal is required (Fanica et al., 2008). Note that laser beam welding once again is an exception to this rule since it requires excessive amount of preheating, further on laser beam welding can be found in subchapter 2.2.5 - Limitations. Nonetheless, it is very beneficial not to need preheating of the structure since preheating requires additional time, work and equipment. Also, substantial amounts of energy can be saved during assembly due to the fact that no preheating is needed.

One of the main reasons why preheating is not required for both duplex and austenitic stainless steel is that hydrogen is highly soluble in the austenitic phase. This stands in contrast to ferritic steels and carbon steels where the presence of hydrogen may lead to cracking in the weld. In order to prevent said cracking in carbon steel preheating is used for these steels.

The preheating is used to dissipate the hydrogen present in the parent material and thus decrease the risk of hydrogen induced cracking. Since both duplex and austenitic stainless steel is not susceptible to this kind of cracking the need of preheating is significantly reduced.

However, note that preheating is also used to achieve other desirable properties for the welding. An example is that the cooling speed is slower when preheating is used. In the case of laser welding this is a very important property since slower cooling speed helps to reduce the residual stresses in the weld. Additionally, preheating can also be utilized in order to improve mechanical properties of the weld. Examples of such mechanical properties are ductility and notch toughness.

Furthermore, regarding multi-pass welding, there have been no problems that are specific to the use of stainless steel (Liljas & Ericsson, 2002). Although to preserve the correct microstructure the inter-pass temperature should be kept below 150°C. Of course, still remaining are the all too common problems with welding, such as lack of fusing.

2.2.1 Cleaning of welds

To begin, a concern that is specifically tied to the use of stainless steel is that without any treatment the corrosion resistance of the weld is lowered (CEN, 2006). Due to this fact all welds in stainless steel have to be cleaned and treated after the welding process is completed. This implies that all welds have to remain accessible after welding, something that has to be considered in design (Finnås, 2012).

The chief reason for the lower corrosion resistance lies in that chromium easily oxidise and that during welding chromium is drawn to the surface (Euro Inox, 2004). This phenomenon is visible as a tint around the weld due to a thickening of the passivation layer, see figure 2.15. While the passivation layer is thickened it also implies that the surface layer underneath is depleted of chromium. In conclusion, unless this chromium depleted layer is removed the weld remains prone to future corrosion.

***Figure 2.15**: Visible weld tint of stainless steel weld. The tint indicates that chromium has reacted and subsequently is depleted at the surface (Euro Inox, 2004).*

Further, the removal of the chromium depleted layer is often chemical. (Euro Inox, 2004). Chemical cleaning is done through pickling, which works by dissolving the surface layer with acids. After this procedure is carried out the corrosion resistance is restored and a new passivation layer is formed, see figure 2.16.

***Figure 2.16**: Weld after pickling, the tint of has been removed and the corrosion resistance has been restored (Euro Inox, 2004).*

In addition, when welding is performed there is also risk of spatter, slag and other irregularities which have to be removed (CEN, 2006). The spatter may otherwise induce both pitting corrosion and fatigue crack initiation, for an example of spatter see figure 2.17 (Fanica et al., 2008). Stainless steel is generally more sensitive to the

induced pitting corrosion since no additional layer will be applied later to protect the steel from corrosion.

With regard to the cleaning, it should be noted that rotating grind tools may cause crack initiation and therefore should be used sparingly and with caution. Finally, note that certain welding techniques cause no spatter, and thus making mechanical cleaning unnecessary. An example of such a welding technique is the laser beam gas metal arc welding (LB-GMAW).

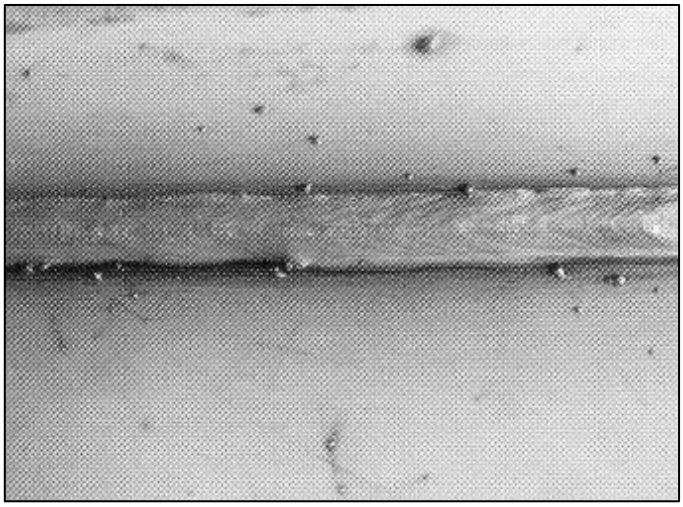

***Figure 2.17**: Photo of weld spatter. If left untreated, weld spatter may induce both pitting corrosion and fatigue crack initiation (Outokumpu, 2010).*

Finally, any contamination from carbon steel should be avoided, as to not induce corrosion in the stainless steel. One way to avoid contamination is to use tools that are devoted solely for stainless steel use. In addition, steel brushes and other tools that are used on the steel have to be made from stainless steel as well.

2.2.2 Alloy and microstructure composition in the weld

For duplex stainless steel, which is composed of the two microstructures austenite and ferrite, the ratio between these two phases is of utmost importance. To clarify, an imbalance in the phase distribution will affect both mechanical properties and the corrosion resistance of the steel negatively. This becomes of special concern in welding due to a limited control of heating, cooling and the alloy composition of the weld. The distribution and grains may also differ; see figure 2.18 for a micrograph of the difference in microstructure.

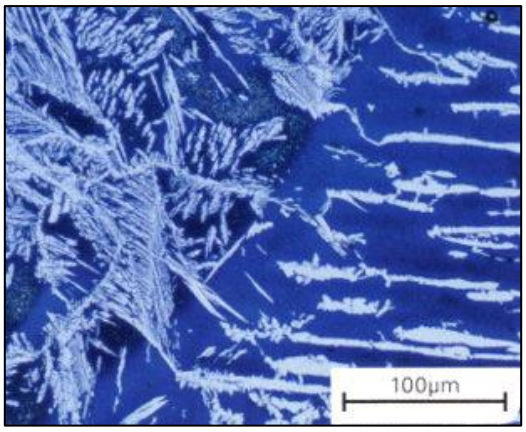

***Figure 2.18**: Micrograph of the parent metal, lower right, and weld metal, upper left, showing the difference in microstructures (Outokumpu, 2010).*

What is important to emphasise in this subchapter is that two different kinds of compositions are discussed. They are the alloy composition and the composition of microstructures respectively and they should not be confused. As mentioned, the composition of microstructures determines both mechanical properties and corrosion resistance of the weld. However, the alloy composition in combination with heating and cooling conditions determine the composition of the microstructure. On the other hand, the ferrite is providing the high strength of duplex stainless steel which stands in contrast to austenitic steel.

For duplex stainless steel it is the presence and distribution of types of microstructures that provides the many beneficial properties. The high strength is for example mostly attributed to the smaller grain size that is formed. In addition, the ferrite also generally has a lower corrosion resistance and may therefore render the stainless steel more prone to corrosion when the ferrite content increases.

In addition, the property of the grain of a certain microstructure is also very much dependent on the specific alloy composition in the grain. To further complicate matters, it is not possible to determine the alloy composition of the different microstructures independently; rather they are dependent on the overall alloy composition of the metal.

Ideally the ratio of austenite and ferrite should be kept the same in the weld as in the parent metal (Fersini et al., 2010). However, this is rarely possible to achieve and a certain imbalance can be accepted as long as sufficient properties of the weld are obtained. Usually, the austenitic content is lower than the ferrite content. Generally, austenite content below 30% is discouraged, since beyond this point the detrimental effects of low austenite content becomes more pronounced.

For this reason the aim when welding is to achieve as high an austenitic content as possible, as long as it does not exceed that of the parent metal (Fersini et al., 2010). For the weld there are two zones to especially consider, the fused zone (FZ) and the heat affected zone (HAZ) respectively, see figure 2.19 as well as figure 2.20.

For the heat affected zone it is not possible to specifically control the alloy composition, and the heat generally causes more ferrite to form. On the other hand the resulting phase composition in the fused zone can be controlled with the choice of weld consumables. Finally, it should be noted that a lack of fusion in the fused zone may lead to corrosion (Fanica et al., 2008).

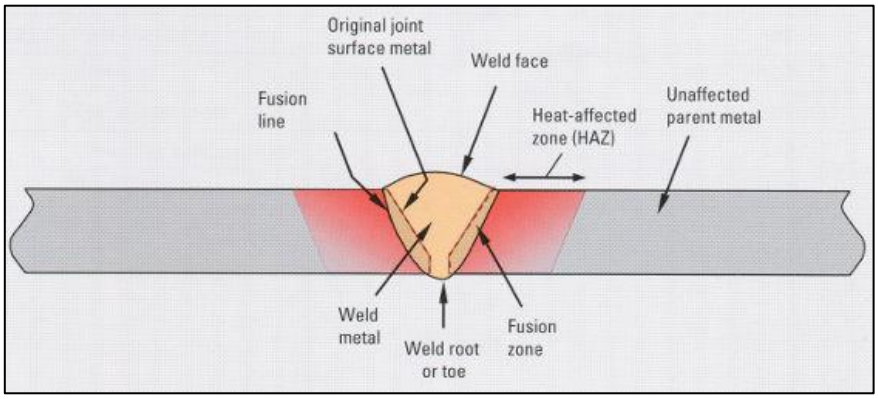

***Figure 2.19**: Illustration of the weld with nomenclature. Note the heat affected zone (HAZ) and the fused zone (FZ) (Outokumpu, 2010).*

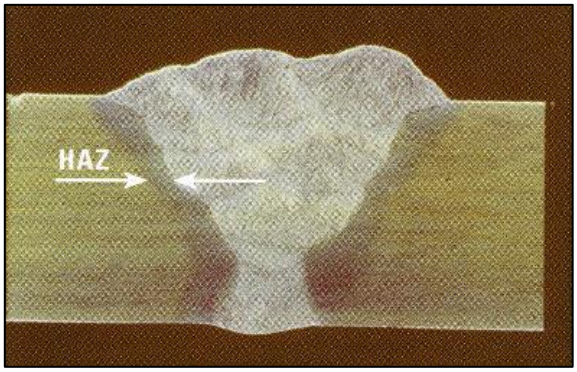

***Figure 2.20**: Photo of the cross-section of a weld. The heat affected zone (HAZ) is marked with arrows (Outokumpu, 2010).*

As mentioned, consumables can be used to improve the austenite content of the weld when arc welding. This can be achieved by using a consumable that contains alloys promoting the forming of austenite (Fersini et al., 2010). Another way is to use highly alloyed super duplex as a consumable, which will often yield austenitic contents of 30-35% in the weld. Furthermore, using super duplex as a consumable will also provide a higher pitting resistance due to the high alloy content.

However, when it is not possible to sufficiently control the alloy content of the weld the austenite content may become too low. To go into further detail, the aforementioned problem is especially distinct for laser beam welding (LBW) where the alloy composition of the weld becomes very similar to that of the parent metal, even if consumables are used (Fersini et al., 2010). This is due to the fact that in laser welding the parent metal dilutes the metal in the fusing zone. In effect, the fused zone has practically the same alloy composition as the parent metal.

To elaborate, for laser welding there is little to no benefit of using high alloy consumables since it will be diluted by the parent metal, which means the beneficial effect of the consumable will be lost. As a result the austenite content can fall between 15-20%, which is deemed to be too low. For such low austenite content the weld loses both ductility and corrosion resistance.

However, this does not imply that laser hybrid welding techniques cannot be used. For example, laser beam gas metal arc welding (LB-GMAW) has shown to have many beneficial aspects. When using laser beam gas metal arc welding slightly lower austenite content has been observed, however, unlike for laser beam welding, the content is within the limits of what can be accepted.

2.2.3 Chromium depletion

Chromium is, as described in chapter *2.1.3 - Corrosion resistance*, what primarily provides the corrosion resistance of stainless steel. Thus it is of importance to have sufficient levels of chromium present in the steel. However, chromium can react with other elements and consequently the chromium can be depleted, particularly during welding. This phenomenon of chromium depletion is also referred to as sensitisation of the stainless steel.

There are several ways this chromium depletion may occur. An example of this can be seen in figure 2.21. For duplex stainless steel, one of the more common elements that chromium reacts with is nitrogen (Muthupandi et al., 2003). This leads not only to depletion of the chromium, but also to the forming of chromium nitride, see figure 2.22.

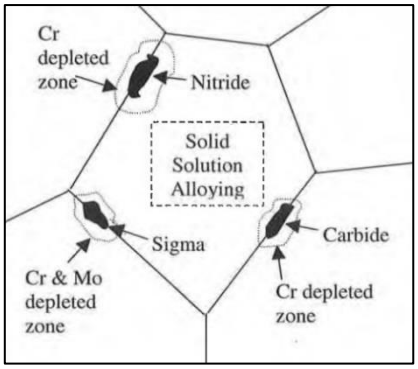

***Figure 2.21**: Illustration of chromium depletion with three of the common reactions. (Comer, 2003).*

There are reasons why chromium nitride can form during welding of duplex stainless steel. Firstly, very high nitrogen content is desired in the weld since this yield a high PREN. Further information on this can be found in chapter *2.1.3 - Corrosion resistance*. Secondly, the solubility of nitrogen in ferrite decreases rapidly with falling temperature. Consequently, the ferrite may become oversaturated with nitrogen when the weld cools.

In addition, oversaturation at rapid cooling may also cause entrapment of small gas bubbles inside the weld. This phenomena has been observed for laser beam welding and, to some extent, laser beam gas metal arc welding where the fused zone have a certain porosity (Fersini et al., 2010). The phenomenon was more severe in the laser beam welding due to a faster cooling rate for this technique.

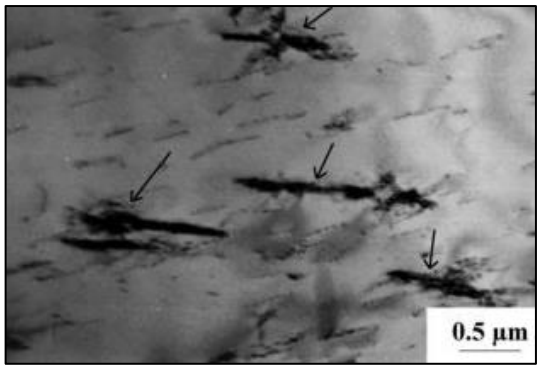

***Figure 2.22**: Electron micrograph of weld where chromium nitride has formed. The nitride is marked with arrows in the figure (Muthupandi et al., 2003).*

However, the austenite can hold significant amounts of nitrogen, thus preventing the formation of chromium nitride. To elaborate, the nitrogen that can no longer be contained within the ferrite will instead be absorbed in the austenitic phase (Muthupandi et al., 2003). Nonetheless, when the austenitic content is low, in combination with rapid cooling, the nitrogen cannot dissipate to the austenite fast enough. To conclude, the forming of chromium nitride becomes more problematic both when the austenite content is low and when the cooling of the weld is rapid.

However, it is not only in the weld that chromium nitride can form. It can also form in the heat affected zone (HAZ), which also experience heating and cooling (International Molybdenum Association, 2009). In the heat affected zone the chromium nitride may form at the borders between grains. As one might suspect it is not an issue of austenite-austenite boundaries, due to the good solvability of nitrogen in austenite. On the other hand the nitride may form at ferrite-ferrite and ferrite-austenite boundaries.

In addition, an issue that is related to the oversaturation of nitrogen is that it may form gas pores inside the weld. Though not directly tied to chromium depletion, it still remains very relevant. An example of this occurrence occurs with laser beam gas metal arc welding (LB-GMAW) which has been shown to contain small trapped pores (Fersini et al., 2010). The pores in question are about 0.1 to 0.4mm in size. A critical aspect of these pores is that they may cause fatigue crack initiation. Initiation inside the weld, where it is hard to detect, is of special concern.

To continue, chromium depletion may also occur when chromium reacts with the carbon in the steel (EuroInox & Stålbyggnadsinstitutet, 2006). In further detail, the carbides are formed during thermal fluctuations and deposited at the grain boundaries. The thermal fluctuation may be caused by multi-pass welding and the grains are then depleted of chromium.

Although, it should be noted that the forming of chromium carbide is rarely a concern for duplex stainless steel since duplex contains very low amounts of carbon which makes the forming of chromium carbides unlikely. (International Molybdenum Association, 2009). For further information of alloy composition see chapter *2.1.5 - Alloying elements*.

Yet another way that chromium may be depleted is by the formation of secondary austenite (Shin et al., 2012). Here the secondary austenite refers to austenite that forms from ferrite due to heat input when welding. The secondary austenite in question has high alloy content and is in itself not susceptible to corrosion; instead it is the surrounding ferrite that is depleted of chromium, molybdenum and nitrogen. In turn the depleted ferrite will render the weld prone to pitting corrosion.

2.2.4 Distortion and residual stresses

All metal, to some extent, suffers from distortion and shrinkage when welded. With regard to duplex stainless steel this effect is not notably worse compared to carbon steel. However, for austenitic stainless steel the distortions are a more pronounced problem. This chapter will clarify why this is the case, and why it is not severe for duplex stainless steel.

The explanation for this is related to the thermal expansion and conductivity of different kinds of steel. To be more specific, large thermal expansion naturally causes larger movements and distortions when welding. In conjunction with the thermal conductivity of the material, this affects how the material behaves when rapidly heated and cooled.

Thus, as can be seen in table 2.5 the difference between carbon and duplex steel is much lower compared to that of austenitic stainless steel and carbon steel. Comparing the thermal expansion coefficient of duplex stainless steel with that of carbon steel, the duplex stainless steel is about 4% higher. Note however, when comparing austenitic stainless steel with carbon steel, austenitic is about 33% higher than that of carbon steel. Furthermore, austenitic steel also have a lower thermal conductivity than duplex steel in relation to carbon steel, at 47% and 67% respectively.

In conclusion, duplex stainless steel should show slightly higher distortion than carbon steel. However, distortion of duplex stainless steel is not a pronounced issue.

***Table 2.5**: Thermal conductivity and coefficient of thermal expansion for carbon and stainless steels (SMS, 2000)*

Steel type	**Carbon steel**	**Austenitic steel**	**Duplex steel**
Thermal conductivity [W m^{-1} K^{-1}]	~30	~14	~20
Coefficient of thermal expansion [10^{-6}/C]	~12	~16	~12.5

In fact, certain welding techniques, LB-GMAW and SAW, have been noted to provide both small fused zone (FZ) and almost negligible heat affected zone (HAZ) (Fersini et al., 2010). This in turn means that both residual stresses and distortion are reduced for the weld.

Nonetheless, there have also been reports of angular distortions that have been greater for duplex stainless steel (Fanica et al., 2008). Though not crucial, it implies that additional care has to be applied when choosing the shrink angle, especially for butt welds and complex geometries.

2.2.5 Limitations

Although welding in stainless steel is achievable as long as proper procedure and considerations are followed, there are still certain limitations. A selection of these limitations are presented in this chapter.

One of these limitations is that laser beam welding (LBW) cannot be recommended for duplex stainless steel. Firstly, as previously mentioned, laser beam welding results in low austenite content in the fused zone (FZ) which leads to both inferior mechanical properties and lowered corrosion resistance. Secondly, there is a need for an excessive amount of preheating, in the range of 250°C (Fersini et al., 2010). Achieving this level of preheating is deemed impractical for welding of bridge structures and in combination with inferior properties renders laser beam welding a poor alternative.

A further limitation related to the use of duplex steel is that annealing, which is heat treatment at high temperatures, should be used with caution. The reason for this is twofold; firstly, depending on the alloying of the steel the ferrite content may increase at these temperatures. Secondly, the ferrite in the steel may become brittle when exposed to temperatures close to 475°C. The latter phenomenon is usually referred to as 475°C embrittlement. For further reading on the subject, see *Plastic Deformation of Duplex stainless Steel* written by M. Nyström.

2.3 Fatigue of stainless steel

When regarding the fatigue strength of stainless steel, in particular duplex stainless steel, it is important to be aware that there is a limited amount of testing that has been performed. For such a complicated and sensitive phenomenon as fatigue, empirical data is crucial and the current level of research leaves much to be desired. Nevertheless, this chapter aims to highlight what is known and what requires further investigation.

To begin, when it comes to fatigue and fatigue testing it is important to note there are different stages of fatigue. The first phase, which is crack initiation, amounts for a vast part of the fatigue life. Nonetheless, the crack initiation phase is not applicable in bridge constructions, since there are always imperfections present which induce fatigue cracks.

Furthermore, there are indications that the chromium layer of stainless steel increases the fatigue strength (Groth & Johansson, 1991). While this may at a first glance seem favourable; the positive effect is only obtained in the crack initiation phase, which as mentioned is not applicable for steel constructions. The chromium layer is only a few nanometres thick, in comparison to imperfections that are several hundred micrometres. In a word, the effect of the chromium layer is negligible in relation to the imperfections that are present.

Also noteworthy is the effect of two different phases within duplex stainless steel, austenite and ferrite, is indicated to retard fatigue crack initiation in duplex stainless steel (Liljas & Ericsson, 2002). However, this phenomenon does not likely affect the fatigue life in the propagation phase: It is still an important difference compared to both ferritic and austenitic steel.

However, even though the research regarding fatigue in stainless steel at the moment of writing is both scattered and scarce, some relevant research still exists. Regarding fatigue, most research shows that duplex steel has a superior fatigue strength compared to conventional carbon steel (Liljas & Ericsson, 2002). In fact, the superior fatigue strength was not only observed for the parent metal, but also for the welds in these steels.

For example, when submerged arc welding (SAW) was used on duplex, the fatigue strength measured for the weld was higher than for the parent metal (Liljas & Ericsson, 2002). However, a word of caution as many factors can affect the fatigue life substantially. A prominent factor is imperfections, which are always present to a varying degree in structural welds. Nonetheless, it is a noteworthy observation that requires some attention. This since it indicates that duplex stainless steel may have good fatigue properties.

Concerning the fatigue limit of the parent metal of duplex stainless steel, it can be noted that it is at the same magnitude as the tensile yield strength of the material. In fact, there is some amount of correlation between the fatigue strength and tensile strength. An approximation of this correlation is that the fatigue strength is two thirds of the tensile strength (Groth & Johansson, 1991).

By the same token, a sign of this correlation might have been observed for gas tungsten arc welding (GTAW) of duplex stainless steel (Liljas & Ericsson, 2002). In the experiment it was shown that the fatigue strength of the weld was improved with increased strength of the material. In addition, the duplex weld was compared to a corresponding austenitic weld, which showed lower fatigue strength due to a lower tensile strength.

Going into further specifics, multi-pass welds are also at least on par with the parent material when tested (Liljas & Ericsson, 2002). However, this is not valid for all types of welding techniques. For instance, welding of thinner material, about 3mm, with gas tungsten arc welding or gas metal arc welding (GMAW) results in lower fatigue strength than that of the parent material.

Furthermore, a series of tests has been carried out specifically on structural joints in bridges. The test in question showed that duplex stainless steel had a fatigue strength that was either on par or better than the values used for carbon steel in Eurocode (Fanica et al., 2008). For certain weld details the fatigue strength of duplex stainless steel was substantially higher, see table 2.6 for a breakdown of the test results.

Moreover, as can be seen in table 2.6, for certain details there are two values of the fatigue strength. The reason for this is due to the nonlinear behaviour and varying elastic modulus of the duplex steel in combination with a stress range that can be measured by either load or strain. To elaborate, the corresponding stress range that is calculated from strain measurements should use the real modulus of elasticity at the current stress level (Fanica et al., 2008).

***Table 2.6**: Fatigue strength of duplex stainless steel details in comparison with corresponding values for carbon steel (Fanica et al., 2008)[Modified].*

Detail	Carbon steel	Duplex steel			
	95% Fatigue strength [MPa]	Derived from load measurements, $\Delta P/A$		Derived from strain measurements, $\Delta\varepsilon\ \alpha E$	
		95% Fatigue strength [MPa]	Increase over carbon steel	95% Fatigue strength [MPa]	Increase over carbon steel
A1	56	72	29%	88	57%
A2	87	85	-2%	103	18%
A3	80	88	10%	107	34%
A4	71	162	127%	159	124%
A5	71	73	3%	86	21%
A6	80	122	53%	-	-
B2	71	98	38%	-	-

Regardless of the potential of duplex stainless steel, without sufficient data supporting the claims, the high fatigue strength cannot be taken into account. For further information on how fatigue of stainless steel is currently considered in design, see chapter *2.4 - Eurocode in relation to stainless steel*. On the whole, it is currently recommended to use the fatigue classes given in Eurocode, even though they are most likely overly conservative for duplex stainless steel (Fanica et al., 2008).

Thus, when designing bridges, the fact that duplex stainless steel as well as austenitic stainless steel has stronger fatigue strength is disregarded in favour of safety (Fanica et al., 2008). On the other hand, if the superior fatigue strength were to be implemented in bridge design, it opens up for the possibility of saving material. As shown in the results of the parametric study, quite a bit of material can be saved. This in turn is beneficial for both the material cost and also decreases the self-weight of the bridge, further on this is to be found in chapter *2.5.2 - Benefits of stainless steel in bridges*.

In the same way as for carbon steel, the fatigue strength of duplex stainless steel connections is dependent on the type of weld technique that is used, see subchapter *2.2 - Welding of stainless steel*. Note that in figure 2.23 the fatigue strength is well above the corresponding class of C100 given in Eurocode for the corresponding carbon steel detail. On the other hand, as can be seen in figure 2.24, the fatigue strength of automatic welds is superior to that of manual welds. This is similar to the case of carbon steel where the fatigue strength is improved by automatic welding in comparison to manual welding. Note that in the latter case it is the reduction of imperfections which leads to the increase in fatigue strength.

Furthermore, something that is of great interest is the use of post-weld treatment to improve the fatigue strength. These post-weld treatments are not to be confused with other types of post-weld treatments like annealing or pickling. It should however be noted that these treatments might have some effect on the fatigue strength, though it is usually not their main purpose. An example of a fatigue improving post-weld techniques is ultrasonic impact treatment.

Unfortunately, at the moment of writing, there is no known data available about fatigue improving post-weld treatment of stainless steel. However, it should be noted that post-weld treatment has proved very beneficial for carbon steel bridges (Kostakakis & Mosiello, 2013). For this reason it would not be farfetched to assume that stainless steel bridges may benefit from fatigue improving post-weld treatments as well. Consequently, a recommendation for further research is the fatigue properties of stainless steel, more on this in chapter 7 - *Discussion and Recommendations*.

Assuming that post-weld treatment could have similar beneficial effects on stainless steel it is certainly a field that deserves further research. Coupled with the prior knowledge of the outstanding properties of duplex stainless steel with regard to crack initiation, it would not be farfetched to assume that there is great potential in this field.

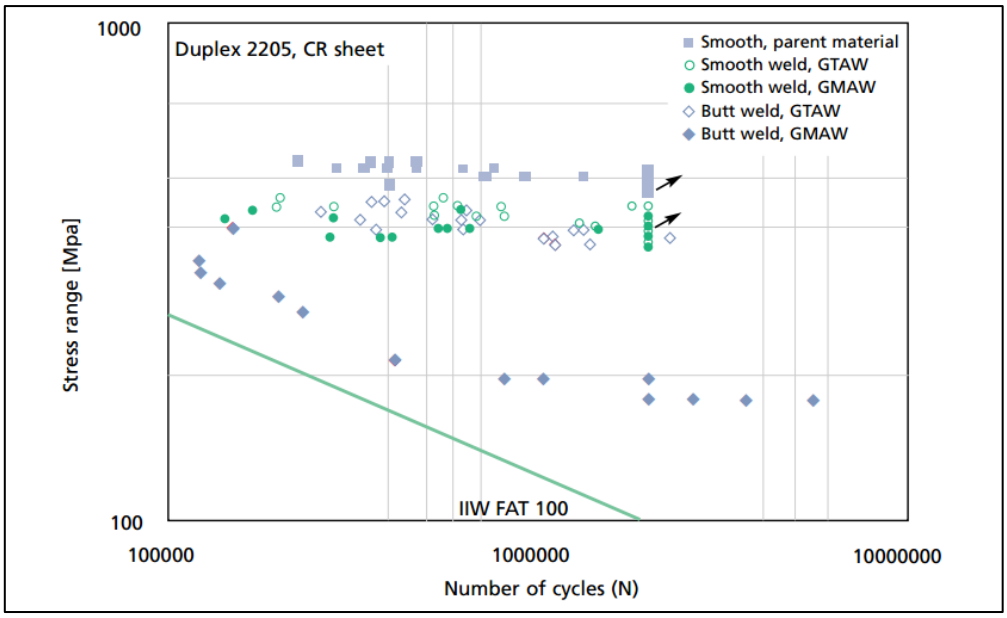

***Figure 2.23**: S-N curves for both the parent metal and welds in EN 1.4462 (Liljas & Ericsson, 2002)*

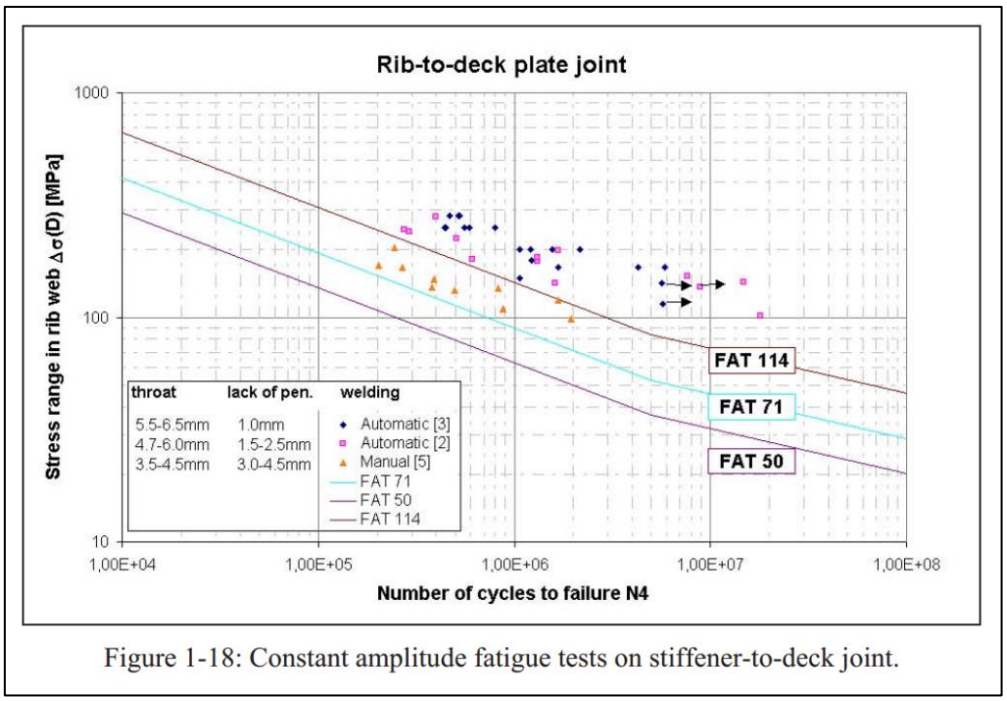

Figure 1-18: Constant amplitude fatigue tests on stiffener-to-deck joint.

***Figure 2.24**: S-N curves for the stiffener-to-deck joint, which also is referred to as detail A4. Note the difference in the fatigue strength between automatic and manual weld methods (Fanica et al., 2008).*

Another specific area is corrosion fatigue, which takes into account the combined effect of fatigue and corrosion, see *Stress Corrosion Cracking* in chapter *2.1.4 - Corrosion modes*. This is relevant for bridges that can be exposed to seawater or other corrosive environments. In order to observe the difference in fatigue strength, the same fatigue test is performed both in air and in a corrosive environment, which for example can be synthetic seawater.

The result from this test showed that both duplex and austenitic steel exhibited lowered fatigue strength when submerged in seawater (Liljas & Ericsson, 2002). To be more precise, for duplex the fatigue strength was decreased with about 10%, while for the austenite the decrease was up to about 25%.

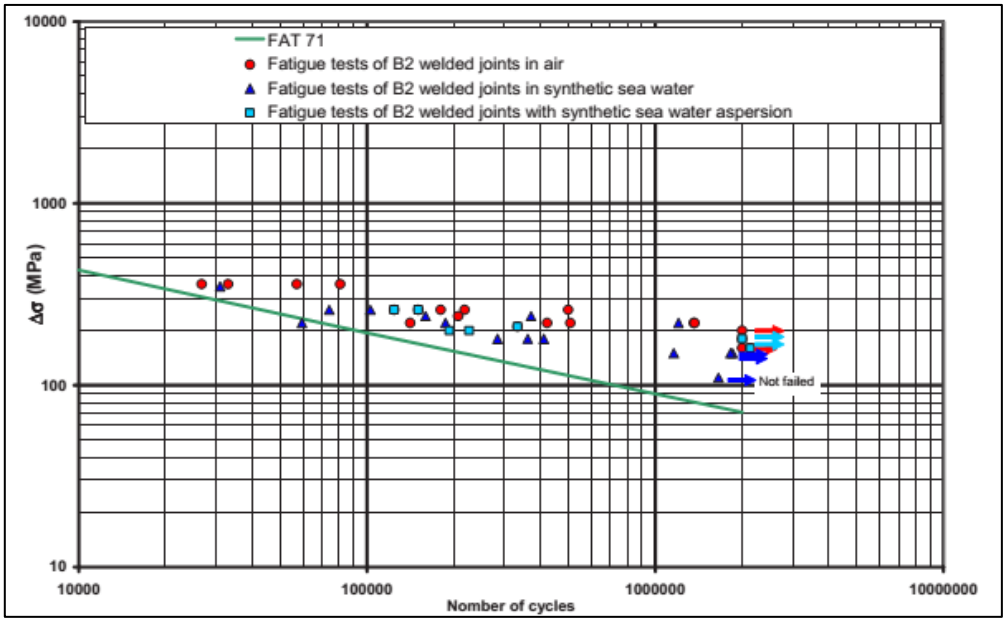

***Figure 2.25**: S-N curves for B2 detail in different exposure to synthetic seawater. Note that the fatigue strength is slightly higher in air than in seawater. (Fanica et al., 2008).*

As a final conclusion there are three things to take special note of concerning fatigue strength of stainless steel. Firstly, there are only a few fatigue tests on structural weld connections in existence. Secondly, a common element in the fatigue test that has been performed is that the strength of duplex stainless steel is either at the same level or higher than that of carbon steel. As a final remark; further investigation and testing is needed for both structural connections and effects of fatigue post-weld treatment.

2.4 Eurocode in relation to stainless steel

Eurocode is a standard for structural design of structures within the field of engineering. Since 2010 the guidelines and rules of Eurocode are mandatory for all public construction in Sweden (Akhlaghi, 2009). There are also plans to make Eurocode a de facto standard for both the private sector as well as the public sector in the construction industry.

That being said, there is actually a part of Eurocode that specifically pertains to construction with stainless steel, namely: *EN 1993-1-4:2006 – Supplementary Rules for Stainless Steel*.

This subchapter aims to give a brief overview on how the standard treats stainless steel. To elaborate, the chapter will discuss briefly what aspects are covered and also parts poorly covered.

2.4.1 Covered by the standard

Stainless steel, in particular duplex stainless steel, lacks a well-defined yield point. To circumvent this issue the strength at 0.2% plastic deformation is utilized instead. This strength is generally referred to as the *proof strength* or more specifically the *0.2% proof strength*.

With this in mind, Eurocode utilises a proof strength for the stainless steel materials. There is both an explanation on how the proof strength is defined as well as common values for all the standard steel defined according to the EN 10088. Note that the values for specific steels can be found in EN 10088 and not in EN 1993-1-4.

As previously stated, stainless steel exhibits a nonlinear behaviour with regard to the stress-strain relationship. Consequently, the nonlinear behaviour means that the modulus of elasticity will vary depending on the stress level. This behaviour is present both above and below the proof strength. As a comparison, carbon steel that is used in construction generally has a distinct yield point which allows for a simpler material model.

In the standard, nonlinear behaviour is considered in two different ways. Firstly, a simplified approach incorporating a fix modulus of elasticity can be used for global analysis. The value of this fix modulus of elasticity is then chosen with regard to the steel grade that is used, see table 2.7.

Table 2.7: *This table illustrates the Young's modulus of elasticity that may be used in global analysis of stainless steel structures. Of course, these values are only viable for certain steel grades, these can be found in EN 1993-1-4:2006 - table2:1 (European Committee for standardization, 2006).*

Steel grade	**Modulus of elasticity [GPa]**
Austenitic and Duplex grades	200
Austenitic grades 1.4539, 1.4529 and 1.4547	195
Ferritic steel grades	220

Note however, that the simplified values for the modulus of elasticity are only valid for the global analysis. When local analysis is considered in design, or deflection, the modulus of elasticity should be taken for the more precise values in calculations. For this purpose the secant modulus of elasticity is used. To elaborate, the secant modulus gives a more accurate approximation.

However, it should be noted that the secant modulus of elasticity is calculated by means of the Ramberg-Osgood equation. As is discussed in further detail in the following subchapter, a more accurate model might be more suitable when designing with stainless steel.

Furthermore, for beams in bending the nonlinear behaviour implies that the modulus of elasticity varies along the cross-section. In order to simplify calculations a mean value for the modulus of elasticity is used. The mean value is taken for the stress level in the compression flange and in the tension flange.

In addition, the corrosion resistance of stainless steel is considered to be "very good" according to Eurocode. It is also stated in the standard that even in aggressive industrial or marine environments the corrosion resistance remains satisfactory. Furthermore, it is mentioned that any crucial corrosion will, in most cases, occur within the first three years of the service life.

However, the standard also speaks of a risk of rust stains appearing on the steel surface. The stains, which could be caused by contamination from carbon steel, can still be deemed as unacceptable by the owner.

Another subject that is covered by the standard is cold working of stainless steel. More specifically, cold working may be used to increase the strength of austenitic stainless steel. There are however some restrictions for the use of ultimate strengths exceeding 700MPa. For these high strengths a full scale test has to be performed, as to ascertain that the strength requirements are fulfilled. When the test is performed, ultimate strength up to 1000MPa may be used in design. In conclusion this allows for significantly higher strength than is ordinarily achievable with austenitic stainless steel.

Nonetheless, some areas that are treated in the standard, specifically for stainless steel, may still remain overly conservative. For example, the ultimate shear resistance has been adjusted to better suit the properties of stainless steel (Fanica et al., 2008). In fact it is less conservative, by about 15%, compared to the rules for carbon steel yield. Unfortunately, despite the adjustments, the standard still remain overly conservative.

Lastly, a final subject that is aptly covered in the standard is buckling. For buckling there are specific partial factors pertaining to calculations for stainless steel (Fanica et al., 2008). When the rules for carbon steel are applied on stainless steel, the obtained results are on the unsafe side. On the other hand, when using the values given in the standard specific to stainless steel, the values are neither unsafe nor overly conservative. Furthermore, this holds true both when designing buildings and bridges.

2.4.2 Not covered in the standard

In the current revision of Eurocode there are unfortunately quite a few subjects that are either treated insufficiently or not at all. The consequence of this is twofold. Firstly, and most critical, the design may become unsafe, putting both life and property at risk.

Secondly, structures designed in accordance with the standard can end up overly conservative. While conservative designs naturally are on the safe side, they will instead lead to unnecessarily high material consumption and cost for the bridge. In either case, it is required of the Eurocode standard to be both accurate and dependable.

The purpose of this chapter is therefore to illuminate a few of the issues with the current revision of Eurocode. More specifically, consideration is taken to the part of Eurocode that is pertaining to stainless steel structures.

First of all, a major drawback in the current standard is that no special consideration is taken to the fatigue properties of stainless steel. As can be seen in *EN 1993-1-4 chapter 8*, the standard says that all stainless steel should be treated as if it has the same fatigue properties as carbon steel.

However, as can be seen in chapter *2.3 - Fatigue of stainless steel*, there are strong support to assume that duplex stainless steel has higher fatigue strength than carbon steel. In conclusion, the standard is very likely overly conservative in its current state. As mentioned, by being overly conservative the design will be kept on the safe side. However, it will also lead to an excessive material consumption, increased cost and also an increased environmental impact.

Furthermore, there is no consideration taken to the use of post-weld treatment for the purpose of improving fatigue life of stainless steel. This can in large be attributed to the lack of tests performed on this subject. Regardless, if post-weld treatment were to be included in the standard it could lead to major saving in material. Further on post-weld treatment can be found in chapter *2.3 - Fatigue of stainless steel*.

Another area where stainless steel is assumed to have the same properties as carbon steel is in fire resistance. However, austenitic stainless steel actually maintains its mechanical properties much better than carbon steel at high temperatures (EuroInox & Stålbyggnadsinstitutet, 2006).

In further detail, the strength of austenitic steel is preserved much better at temperatures exceeding 550°C, when compared to carbon steel. Moreover, the stiffness of austenitic steel is also retained much better, at any temperature, compared to carbon steel. To conclude, in the current state, none of these favourable properties of austenitic stainless steel is utilised in the design of structures.

Additionally, research conducted on high strength steel welds in bridge constructions suggests that Eurocode is overly conservative in many regards (Günther H.-P., 2008). Note that this is pertaining not exclusively to stainless steel, but is true for high strength steels in general. In particular it was concluded that the current standard yield welds that are excessive in size.

Another subject that could be further improved is the nonlinear modelling of stainless steel. The model currently used in the standard is the Ramberg-Osgood equation in conjunction with the 0.2% proof strength of stainless steel. These curves are rather simplistic and a more accurate model should preferably be utilised (Lukezic, 2013).

In fact, there are at least two suggestions given for more accurate models. One of these is the Ramberg-Osgood-Rasmussen model, which has the advantage of taking into account a non-fix proof strength (Fanica et al., 2008). Another suggestion is the Sigmoid-model. The latter model can describe the non-linearity of the yield point, just as the former. However, the Sigmoid-model has the additional advantage of being able to describe anomalies in a more accurate way (Lukezic, 2013).

Furthermore, the strain hardening of stainless steel is only considered for austenitic steel grades. Thus the substantial strain hardening of duplex stainless steel is neglected in its entirety. The strain hardening becomes of interest when the proof strength is exceeded and the member is subject to large deformations. More information about strain hardening and mechanical properties of the different steel grades can be found in chapter *2.1.2 - Microstructures*.

Finally, a subject that needs further investigation is how stainless steel performs with regard to instability. The concern is that the current models of instability might not be applicable on stainless steel. The cause of this concern is the nonlinear behaviour of stainless steel, which differs significantly from that of carbon steel. To elaborate, a common assumption in instability models is that stresses can be sufficiently redistributed. Due to the difference in stress-strain behaviour this may not necessarily hold true for stainless steel. To conclude, stainless steel might behave differently with regard to instability. If such is the case, a revision of the current models will be needed.

In conclusion, there are definitely areas in the current revision of Eurocode that require improvement. However, as can be seen in this chapter, most of the standard appears to be overly conservative rather than unsafe. However, that does not mean that further research should be neglected, since there are still many uncertainties. And to repeat once more, these uncertainties may lead to both excessive dimensions and increased risk of failure.

2.5 Analysis of existing structures

This chapter consists of three major parts. The parts are the following: a study of existing structures, a description of the benefits of stainless steel in construction and, finally, a description of the considerations that has to be made.

In the moment of writing, only a handful of bridges that incorporate stainless steel in the load bearing structure exist. The majority of these bridges are foot-bridges, at least 15 footbridges have been built in stainless steel around the world. Other examples of bridges built in stainless steel include about seven road bridges and only one known railway bridge.

The long term durability and maintenance of the stainless steel bridges is not well known, since all the bridges studied found in this review are from 1998 or later. Even so, there have been no reports about problems related to the stainless steel bridges.

The load bearing structures of the bridges are made from either austenitic or duplex stainless steel (ArcelorMittal, 2009). It should be noted that austenitic steel is also frequently used in non-load bearing details, for example guardrails. Nevertheless, in recent years the use of austenitic steel for load bearing members has subsided. Instead it has been superseded by duplex stainless steel.

The prominence of duplex stainless steel can foremost be attributed to the significantly higher strength compared to austenitic stainless steel. Furthermore, the content of expensive alloys, such as nickel, can generally be kept lower in duplex grades than in corresponding austenitic grades. In conclusion, the higher strength implies that duplex stainless steel requires less material, which in turn can be kept less expensive. For this reason it is understandable that duplex stainless steel has become the preferred alternative.

2.5.1 Noteworthy examples

As mentioned, there are only a handful stainless steel bridges in the world. For some of these bridges the available information is quite scarce. To describe the currently existing road bridges, two bridges have been selected as representatives. The chosen bridges are comparatively well documented.

The first bridge that has been selected is the Cala Galdana Bridge in Spain. This is a road bridge with a structure made from duplex stainless steel. In fact, it is the earliest known example of a duplex stainless steel road bridge (Sobrino, 2006). Furthermore, this bridge is built in a highly corrosive marine environment, which should ensure that the corrosion resistance of the steel has been put to the test.

Even though the Cala Galdana Bridge was built as early as 2005, it is still built in accordance with the same standards that are used in the moment of writing. The standard in question is Eurocode, and more information about it can be found in chapter *2.4 - Eurocode in relation to stainless steel.*

The second bridge that has been chosen is built in Nynäshamn, which is situated in Sweden. This bridge is also a road bridge built from duplex stainless steel. However, it has quite a different structure compared to the Cala Galdana Bridge. In addition, this bridge is situated in a far less corrosive environment, and is therefore made from a leaner duplex grade.

The bridge in Nynäshamn was also selected for other reasons. The thesis is written in Sweden in collaboration with NCC, the company that built the bridge. This collaboration allowed access to data and information about the bridge which is not publically available. Thus, with more information available, a more extensive and deeper analysis could be made.

Cala Galdana Bridge

This bridge was built in Menorca, which is an island situated in Spain. The bridge is the first road bridge in Europe constructed from duplex stainless steel (Sobrino, 2006). The bridge was finished in 2005 and has a total span of 45m. The structure has two arches made from stainless steel, see figure 2.26 below.

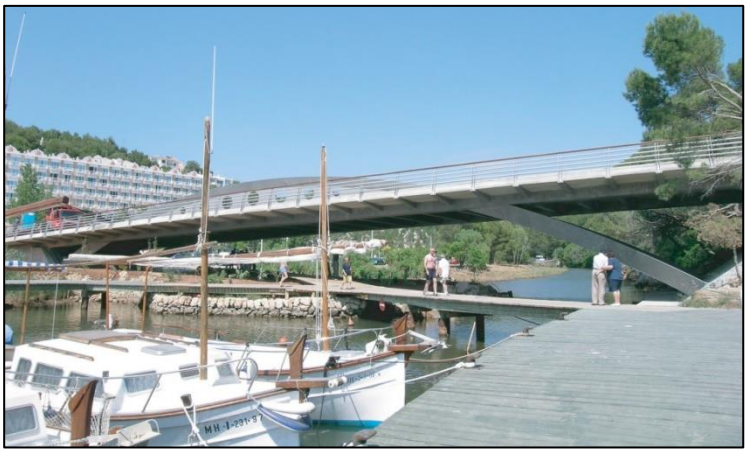

***Figure 2.26**: Cala Galdana Bridge in Menorca, Spain. The structure consists of two arches which support the reinforced concrete deck.*

The stainless steel used in the Cala Galdana Bridge was of the type EN 1.4462 duplex stainless steel (Sobrino, 2006). The reason for this choice was the demand caused by the highly corrosive environment in addition to the high strength of the duplex. As can be observed in table 2.8, the measured strength of the steel greatly surpassed the minimum values that are specified in the standard.

Table 2.8 *Properties of the hot rolled duplex stainless steel plate used in Cala Galdana Bridge compared to other steel types (Sobrino, 2006).*

Mechanical property	**Stainless steel Duplex 1.4462 (Minimum specified values)**	**Stainless steel 1.4404 (ASTM-316L)**	**Carbon steel S-355**	**Stainless steel Duplex 1.4462 (used in Cala Galdana Bridge)**
Tensile Strength [MPa]	640	530	510	767
Conventional yield stress $f_{0.2}$ [MPa]	460	220	355	535
Elongation [%]	25	40	>15	35

The bridge was designed in accordance with *Eurocode 1993-1-4:2005* (Sobrino, 2006). This part of the code contains supplementary rules for design of stainless steel structures and is previously described in chapter *2.4 - Eurocode in relation to stainless steel*. Note that the standard that was used in the bridge is an earlier version of Eurocode since the bridge was finished in 2005 and the current version was released in 2006.

It should also be mentioned that the structure showed smaller deflections than was expected. This is an indication that the steel has a higher stiffness compared to what was assumed. The average modulus of elasticity used was 200GPa. This value is taken according to the standard, further information can be found in chapter *2.4.1 - Covered by the standard*.

In fact, the measured deflections were only about 80% of the calculated values. Based on this, it can be concluded that the steel had an elastic modulus 16% higher than what had been assumed in the calculations. Note that this was an older standard, and that account is also taken for the nonlinear behaviour of stainless steel in the current standard, see chapter *2.4.1 - Covered by the standard*.

Furthermore, the deflections from the static load recovered almost entirely. This is of interest since duplex stainless steel show no clear limit between elastic and plastic responses, as has been previously mentioned in chapter *2.1.1 - Basic mechanical properties*. The concern is that plastic deformations can occur even at small load levels. If these deformations are larger than estimated, it follows that the final deflection of the bridge may become too large.

When constructing the bridge, several welding techniques were used. These welding techniques included the following: shielded metal arc welding (SMAW), gas metal arc welding (GMAW), flux-cored arc welding (FCAW) and submerged arc welding

(SAW) (Sobrino, 2006). There were no problems reported with any of the welding techniques, so in lack of further data it can be assumed that the results were satisfactory. Also, all welds were treated after welding, which is required for stainless steel in order to obtain full corrosion resistance. In short, the welds were treated by a pickling paste in order to remove contaminations and oxides. By doing so it is ensured that the protecting chromium oxide layer is reformed. Further on the subject can be found in chapter *2.2.1 - Cleaning of welds*.

Road Bridge in Nynäshamn, Sweden

As suggested by the title, this chapter will describe the road bridge situated in Nynäshamn, Sweden. In fact, in the moment of writing, this bridge is one out of two stainless steel road bridges that has been built in Sweden. The other bridge, which is of similar design, was built in Orrehammar, Sweden. Furthermore, the bridge in Orrehammar was constructed in 2009. The bridge in Nynäshamn on the other hand was built two years later, in 2011.

Both bridges were built by the company NCC. As previously mentioned, this thesis was written in cooperation with the company NCC. Due to this collaboration a deeper and more thorough analysis of the bridge will be possible as the authors had access to additional information through the cooperation with NCC.

The bridge in Nynäshamn is maintenance free, like all stainless steel bridges are, further information can be found in chapter *2.5.2 - Benefits of stainless steel in bridges*. Not to mention, there are no indications that maintenance should become a problem, at least not within the foreseeable future.

Furthermore, a reason to why this bridge alternative was chosen is because the owner did not want any disruption of the road traffic (Säll & Tiderman, 2013). The maintenance free bridge fulfilled this specific requirement.

However, it is time to go into detail about the bridge itself. The bridge is a composite structure consisting of two I-girders in conjunction with a reinforced concrete deck (Finnås, 2012). For clarity, see figure 2.27. Moreover, as seen in the figure, the bridge only has one single span. The length of the span is 42m.

***Figure 2.27**: Road bridge in Nynäshamn, Sweden. The composite bridge structure consists of two stainless steel I-girders and a reinforced concrete deck (Finnås, 2012).*

Furthermore, the stainless steel used in the girders was manufactured by Outokumpu and has the trade name of *LDX2101* (Finnås, 2012). In addition, this steel is a duplex stainless steel that is classified as *EN 1.4162* in accordance with the standard *EN10088*. Also, this is the same steel grade that was used in the bridge in Orrehammar.

This grade is a leaner type of duplex when compared to the grade that was used in Cala Galdana Bridge. The motivation for using this leaner grade is because the environment in Nynäshamn is not as corrosive. On the other hand, the Cala Galdana Bridge is exposed to chlorides from the nearby sea. Consequently, in Nynäshamn the conditions are different and thus a less expensive grade could be used. For further information about the choice of steel grades see chapter *2.5.3 - Considerations pertaining to construction in stainless steel*.

Owing to the choice of stainless steel the building cost of the bridge will be higher, in comparison to a carbon steel alternative (Finnås, 2012). This remains true even if a leaner steel grade is used. However, the higher initial cost can be compensated by a much lower maintenance cost during the service life. This is once again in comparison to a carbon steel alternative.

For the bridge in Nynäshamn a life cycle cost (LCC) analysis was performed and used to motivate the higher initial cost. The argument being that the overall cost of the bridge would become lower for the stainless steel alternative. For this particular bridge the length of the service life for the bridge was chosen as 80 years. If a longer service life would have been chosen, the stainless steel alternative would potentially have become even more favourable.

To continue, the design of the two bridges in Nynäshamn and Orrehammar is as mentioned quite similar. This is of course not a coincidence, but a deliberate choice. The designs are made similar in order to make the design process more efficient. To elaborate, since the design is not started from scratch each time, additional time can be spent on optimising the structure. This in turn yields more well designed, efficient and reliable bridges.

Furthermore, with only minor changes in the design the bridge can be made to span different lengths. The bridge in question is for example 42m long (Finnås, 2012). However, while still using the same concept with I-girders, the bridge should be able to span up to 70m. On the other hand, if the I-girder is exchanged for a box girder, the span can be made up to 100m long. Thus certain flexibility is provided in the design. This since it is possibility to choose the most suitable solution with regard to the current location.

It should be noted that the current design only allows for a single span. However, with the possibility of spans of up to 100m long, this should still be sufficient for most situations. Conversely, there is a certain advantage of a bridge without any additional support. To elaborate, the foundation for additional supports can be both expensive and disruptive, especially when situated in water.

To continue, a key element of the bridge design is that the abutments are integrated into the loadbearing structure. In practise, this means that the bridge forms a stiff frame together with the abutments. This brings a few advantages, with the most striking one being that there are no bearings needed at the supports. This reinforces the maintenance free nature of the bridge, since bearings otherwise is a vulnerable part of the structure.

Moreover, the bridge was designed in accordance with Eurocode. For more information about the standard see chapter *2.4 - Eurocode in relation to stainless steel*. As is noted in the aforementioned chapter, there are some shortcomings in the current revision of Eurocode. However, this does not mean that the design becomes more complicated to carry out. What it means instead, is that the resulting design may become overly conservative in some areas and unsafe in others.

However, as of the moment of writing, there have been no reported problems with the bridge. In fact there have not been any notable problems, or at least that has been detected, in any of the building phases; not in manufacturing, assembly nor erection. By the same token, no defects or problems have been detected during the service life of the bridge.

In a final conclusion, the bridge works just as intended and has proven that there is great potential in stainless steel bridges. This is supported in everything from the life cycle cost analysis to the final performance of the bridge.

2.5.2 Benefits of stainless steel in bridges

The single most important aspect of stainless steel, compared to conventional carbon steel, is the fact that stainless steel require negligible maintenance (Hechler & Collin, 2008). In fact, the only maintenance needed is washing and routine inspections (Fanica et al., 2008). Moreover, it should be noted that carbon steel bridges also require this fundamental maintenance. In fact, carbon steel bridges require washing and routine inspections at a higher frequency than stainless steel bridges.

The explanation for the maintenance free nature of stainless steel lies in that it is corrosion resistant, further details can be found in chapter *2.1.3 - Corrosion resistance*. To elaborate, with an inherent corrosion resistance there is no need for an additional protective layer to prevent corrosion. Consequently, since no protective layer is needed, no maintenance of said layer is needed either.

As a matter of fact, the largest part of the maintenance cost for carbon steel bridges is associated with the maintenance and renewing of the protective layer (Hechler & Collin, 2008). Thus, with the help of life cycle cost (LCC) analysis, it can be assessed that the higher initial cost of a stainless steel bridge is counterbalanced by the decreased cost of maintenance. Also, the additional benefit of stainless steel is that the cost of the bridge becomes both stable and predictable for the bridge owner.

In addition to the lower maintenance, stainless steel gains an advantage over carbon steel already in the production phase. This is caused by the fact that carbon steel requires several layers of paint before delivery. Each layer of paint requires time to dry before the next layer can be applied. Thus stainless steel bridges can generally be manufactured faster compared to an equivalent carbon steel bridge.

Furthermore, since there is no protective layer on the structural members, the assembly of the structure on site becomes faster (Paulsson-Tralla, 2012). This applies to both welds and bolted connections. Part of the reason is that there is no need to repair the protective layer after the connection is performed. Paint, for example, requires good weather- and temperature conditions in order to dry. Such external events, which are hard to predict and control, is not a problem in stainless steel structures.

In addition, an advantage for stainless steel structures is that bolted connections can be drilled on site, since the connection is not required to be painted prior to assembly (Paulsson-Tralla, 2012). In fact, since the protective layer reforms, other planned or unplanned work can also more easily and reliably be performed on site. Examples of such activities are cutting and drilling of members.

Another aspect related to the erection phase of the bridge is the advantage of not needing to weather proof the structure and structural elements before the final assembly (Paulsson-Tralla, 2012). Carbon steel structures may have surfaces that are left unprotected to allow for welding on-site.

Apart from the high corrosion resistance, duplex steel also have a high inherent mechanical strength compared to commonly used carbon steel, see chapter *2.1.1 - Basic mechanical properties*. In fact, duplex grades are often compared to the high strength carbon steel S460, which has approximately the same mechanical strength.

The high mechanical strength, in combination with high fatigue strength, results in a lesser need for material to carry the same amount of load. Thus, there is the possibility to design more lightweight structures. Moreover, lightweight structures yields a lower self-weight which renders the *dead* load smaller and thus allows for further savings in material. However, this is exempting the possibility where fatigue acts as a determining factor or *bottle neck* if you will.

In addition to the material saving, lightweight structures are also easier to lift, handle and assemble (Finnås, 2012). The effect of this is that savings can be made in both time and expenses for the assembly and erection of the bridge. A shorter building time is especially desirable for roads, railways and waterways with high traffic flows.

The high strength of duplex also results in that fewer supports can be used to span the same distance, since the individual spans can be made longer. The benefit of this is that construction of supports can be expensive, especially when they require foundation in water.

Problems pertaining to maintenance of carbon steel

As mentioned, one of the main advantages of stainless steel is that it does not require maintenance. To fully understand the benefit of a maintenance free bridge, it is necessary to first know what maintenance is typically required. Thus the aim of this subchapter is to give a brief description of maintenance of carbon steel.

To begin, during the service life of the bridge the state of the protection has to be assessed periodically. Whenever maintenance related deterioration arise these problems have to be corrected. Also, the inspections are carried out in addition to a chosen combination of partial and full renewal of the protective layer, occurring several times during the service life. However, it should be noted that at the moment there is no unifying standard as to how often or which type of maintenance should be performed (Fanica et al., 2008).

In further detail, the renewal of the protective layer involves a few aspects and costs in and of itself. Firstly, it involves the removal of the old layer before applying the new protective layer. This is a costly procedure that may require temporary scaffolding and closure of the bridge.

It is worth mentioning that for severely corrosive environments, such as marine environments, the required maintenance will have to be more recurring and also more comprehensive. Albeit, this can be put in comparison to the stainless steel that requires more corrosive resistant grades in corrosive environments. To conclude, both carbon and stainless steel becomes more expensive as the corrosiveness of the environment increases.

The closing of a bridge in turn leads to redirection of traffic flows, which usually cause indirect costs due to loss of economic income (Säll & Tiderman, 2013). For example, in certain cases, like with the Stonecutters Bridge in Hong Kong, closure of the bridge is deemed unacceptable due to the overwhelming economical loss it would cause.

In addition to an economic loss, painted bridges also cause a negative environmental impact (Säll & Tiderman, 2013). Generally, this mostly affects the local environment when both paint and residues are spread. The paint residues are emitted through spillage, peeling, blasting and removal of old paint layers. The damage could be assessed through the help of life cycle analysis (LCA) of the bridge.

Furthermore, the example of Stonecutters Bridge illustrates another benefit of stainless steel in construction. To elaborate, maintenance is sometimes very hard to perform if not outright unfeasible. For instance, the pylons of the Stonecutters Bridge are approximately 300m high. Consequently, to perform substantial maintenance at such a height imposes severe difficulties. In addition, the difficulties in maintenance generally entail a high cost as well. To conclude, sometimes stainless steel is the preferred option in situations where maintenance proves too great a challenge.

2.5.3 Considerations pertaining to construction in stainless steel

The aim of this chapter is to summarise important aspects that should be considered when building a stainless steel bridge. However, note that many of the aspects mentioned in this chapter have been covered in more detail in other subchapters within the literature study. To aid the reader there are references to the appropriate subchapters where more information can be found.

To begin, one of the more prominent concerns for stainless steel bridges is the higher initial cost compared to a carbon steel alternative. This initial cost is partly or fully offset by reduced costs during the service life. Nonetheless, the fact remains that the higher initial cost can be a crucial consideration for the buyer of the bridge.

There are two main factors that contribute to the higher cost. These factors are the cost of the steel material and the cost of assembly in the workshop.

Firstly, the cost of stainless steel is governed by the alloy composition. For more information about the alloys that are used in stainless steel, see chapter *2.1.5 - Alloying elements*. To elaborate, the price of certain alloys, like for example nickel, is much higher than the price of iron. Thus, if high amounts of alloys are used, the stainless steel will become more expensive. On the other hand, it should be noted that some of the alloying elements, like nitrogen, are comparably inexpensive. Nonetheless, to save cost, it is preferred to use as little of the expensive alloys as possible.

In fact, the choice of stainless steel is primarily determined by the required corrosion resistance. The reason being that the corrosion resistance of stainless steel is determined by the alloy composition, see chapter *2.1.3 - Corrosion resistance*. In short, to achieve higher corrosion resistance the alloy content has to be increased.

Furthermore, the assembly of the bridge is another area that is more expensive for stainless steel than for carbon steel (Fanica et al., 2008). The increased costs are partially caused by more expensive welding consumables and faster wear of cutting tools. In addition, the tools that come into contact with stainless steel should not be made from or used on carbon steel. The reason for this is that the stainless steel otherwise can become contaminated by the carbon steel. Finally, a rough estimation is that the workshop cost is approximately 30% higher for stainless steel than for carbon steel. However, the actual workshop cost will of course fluctuate and is dependent on many other factors.

Another area that requires careful consideration is the welds of the structure. For the welds two of the most important aspects are corrosion resistance and fatigue strength. A common element for all welds in stainless steel, regardless of welding technique, is they have to be treated after welding. This is done in order to achieve full corrosion resistance of the weld, for further information see chapter *2.2.1 - Cleaning of welds*.

However, all the other aspects pertaining to welding are too numerous to reiterate on in this chapter. Thus, for more details about welds and welding in general see chapter *2.2 - Welding of stainless steel*. Also, information related to the fatigue strength of welds can be found in chapter *2.3 - Fatigue of stainless steel*.

Of less importance, but still worthy of mention, is that the surface appearance of stainless steel can be determined by different surface treatments. Examples of such treatments are coating, blasting and peening. They can be used to obtain everything from mirror polish to more subtle mate finish. The latter has been used where highly reflective surfaces may otherwise blind nearby traffic.

Another consideration is that the internal components of a stainless steel structure can be made with carbon steel or a stainless steel grade with lower corrosion resistance. Such is the case of the Waldeck-Rousseau Bridge where two different austenitic grades were used (ArcelorMittal, 2009). More specifically, the higher alloy grade with higher corrosion resistance was used on the outside while the lower alloy was used for the internal structure.

In this way a less expensive material can be used for parts of the structure without sacrificing the overall durability of the bridge. The premise which has to be fulfilled is of course that the internal structure is not exposed to the corrosive environment. In addition, it should go without saying that the internal steel is not allowed to corrode.

Concerning the use of two different metals in the same structure there is the risk of bimetallic corrosion. Bimetallic corrosion is described in further detail in chapter *2.1.4 - Corrosion modes*. Although the corrosion rate may be substantially increased due to bimetallic corrosion it rarely becomes an issue unless there is a risk of corrosion to begin with.

This is the reason for why different types of stainless steel can be used in the same structure, like in the aforementioned Waldeck-Rousseau Bridge. In this case neither the exterior nor the internal structure was exposed to an environment that would cause corrosion to the respective steel. To summarise, the internal structure need only to resist the mild internal environment. As long as the steel can fully resist the environment that it exposed to the detrimental effect of bimetallic corrosion is negligible.

On the other hand, bimetallic corrosion can become critical when the less noble metal is exposed to an environment in which it corrodes. An example of this is when carbon steel girders are used in conjunction with stainless steel girders in an open structure. In short, bimetallic corrosion occurs when two metals such as stainless steel and carbon steel is in contact with each other. When they are in contact the more noble metal, the stainless steel, will increase the corrosion rate of the less noble metal, namely the carbon steel.

The solution to the issue of bimetallic corrosion is to separate the different metals in the structure. Without the connection the electric current cannot travel between the metals and the bimetallic corrosion cannot take place. Separation can be ensured with the help of spacers made from material that breaks the electric current. If the bimetallic corrosion is not prevented the structural integrity may be put at risk due to the accelerated corrosion.

Finally, an issue worth considering when building and handling stainless steel is that there is little to no possibility of covering up any cosmetic damage (Finnås, 2012). The reason for this is that stainless steel is rarely painted, as described in chapter *2.5.2 - Benefits of stainless steel in bridges*. To elaborate, minor damage in carbon steel bridges can be repaired, and the repairs can then be hidden by the paint layer. However, for stainless steel this is not possible and damage to the bridge should therefore be avoided. Thus, additional care is required during production and erection. This in turn may require longer construction time, which often leads to an increased cost.

3 Parametric Study

The parametric study is carried out in order to observe the behaviour of stainless steel. In more detail, the parametric study has been used to investigate both the strong and weak points of stainless steel in bridge structures. Both the structural behaviour of the stainless steel and the economic aspect of using stainless steel instead of carbon steel have been examined.

The three parameters which are considered as the most important are the fatigue strength, fatigue assessment method and steel grade. The fatigue strength and fatigue assessment is important since in most cases they have a significant influence on the design of the bridge. Just as important, the comparison of the steel grades is of interest since carbon steel is the main alternative to stainless steel. For further information about these and other parameters see subchapter *3.3 - About the parameters and their relevance*.

The calculations for the parametric study consist of analytical hand calculations in Mathcad and fatigue calculations in Matlab and Octave. The fatigue calculations also utilise data which is obtained from the finite element model which is scripted in Abaqus/Brigade. The hand calculations, which are performed in accordance with Eurocode, are described further in subchapter *3.2 - Hand calculations*. The fatigue assessment on the other hand is described in chapter 4 - *Fatigue Assessment*.

Finally, each case in the parametric study has been optimised with regard to the utilisation ratios and steel consumption. Nevertheless, although the cross-section has been optimised, some features of the original design have been retained. Example of features that has been retained is the location of the splices in the web and flanges. The original design has been partially preserved in order to not yield too extreme solutions and also limit the workload for each step in the study.

3.1 Structural behaviour of the Nynäshamn Bridge

In this chapter the structural behaviour of the Nynäshamn Bridge will be described. In addition, further information about the bridge can be found in chapter *2.5.1 - Noteworthy examples*.

When describing the structural behaviour it is important to note that the self-weight is carried by the steel main I-girders alone. Additionally, the imposed loads are instead carried by the entire composite cross-section. This owes to the fact that the main I-girders carry the entire self-weight of the structure when the concrete deck is cast. When the concrete achieves sufficient strength to contribute to the load bearing the self-weight will still be carried by the steel girders.

Note that in this study no regard is taken to shrinkage or creep of the concrete. These effects may otherwise lead to a redistribution of stresses.

Moreover, the main I-girders are simply supported in both ends at casting and the moment from the self-weight is therefore distributed accordingly, see figure 3.1. The effect of this is that the self-weight cause no moment at support. Instead, it leads to a more significant negative bending moment at the middle of the span. In comparison, for the composite action the bridge has fixed supports at both ends, which lead to large positive moments at the supports.

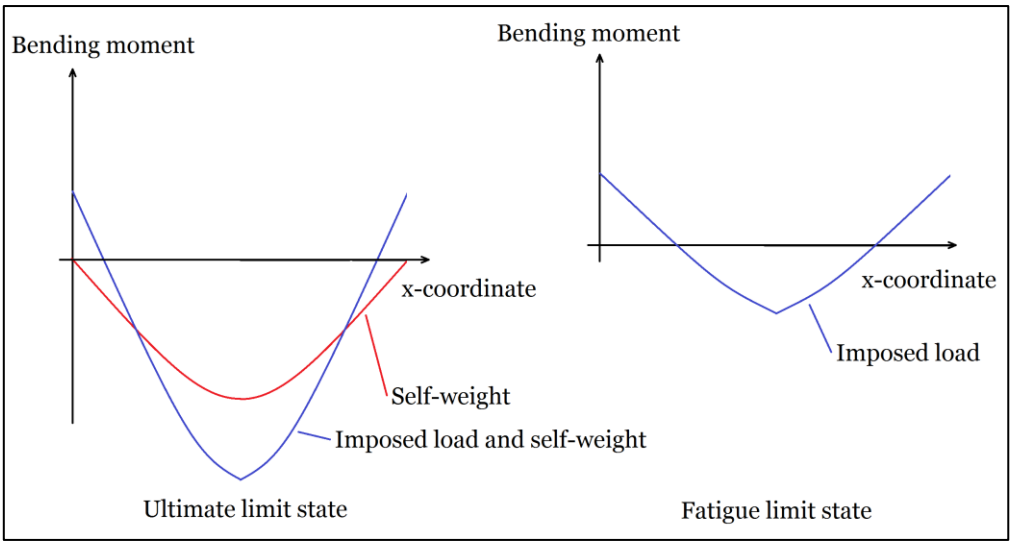

***Figure 3.1**: Figure illustrating the bending moment in the ultimate and fatigue limit state. The self-weight is distributed according to a simply supported case while the imposed loads take into account fixed supports.*

In addition, the positive moments at the support region will cause tension in the concrete. When the reinforced concrete is subjected to tension the contribution from the concrete is neglected. Instead only the reinforcement is considered for the bending resistance. The implication is that the bending resistance is noticeably reduced at the support region for the current design.

In conclusion, the bending moment from the self-weight dominates in the middle of the span and the bending moment from the imposed loads dominates at the support region. Consequently, in the middle of the span the utilisation in the ultimate limit state will often be more critical than the utilisation in the fatigue limit state. In the same manner the fatigue limit state, which depends on the imposed loads, will tend to have the highest utilisation at the support region.

3.2 Hand calculations

The majority of the parametric study is based on hand calculations carried out in accordance with the rules and recommendations given in the current Eurocode. The hand calculations has been performed and written in the software Mathcad, for a full review of the hand calculations see Appendix F.

Note that the hand calculations in Mathcad have been used in conjunction with Matlab functions. In short, the Matlab functions can be divided into two categories. First, there is a set of functions that is used to extract and store the data obtained in the hand calculations. Second, another set of functions are used to calculate the fatigue life of the main I-girders. The functions in question can be found in Appendix D and E respectively.

The hand calculations are structured in to three major parts which are: Input data and parametric study, calculations and results. Each part is briefly described below, in this subchapter.

Input data and Parametric study

In the chapters *Input data* and *Parametric study* all the variables and constants used in the calculations are initialised and declared. In more detail, the input data which is changed in the parametric study will supersede the data given for the original design. To clarify, the data which is not changed in the parametric study will remain intact.

Furthermore, the values given specifically for the parametric study are imported from an Excel document. Keeping the data external allows for fast editing and easier storage of the input data. For an example on how the input data in the excel document is structured see Appendix A.

Calculations

The by far largest part of the hand calculations consists of the actual calculations. Due to the length of the calculations this part is divided into distinct subchapters.

Here is given a list of the subchapters included in the calculations part. Note that the description only includes the most notable content and that each subchapter may include additional calculations.

- *Cross-sectional constants*. This subchapter contains the calculation of cross-sectional constants in each section. Examples of such constants are; area, first and second moment of area and global and local z-coordinates.
- *Loads*. In this subchapter the loads on the bridge structure is calculated for the section along the span. Loads which are included are self-weight, traffic load, fatigue load and wind load.
- *Bending moment resistance*. In this subchapter the various bending resistances and corresponding utilisation of the cross-sections is calculated.
- *Shear resistance*. The shear resistance subchapter contains the calculation of the shear and shear bending resistance of the main I-girders.
- *Interaction between shear force and bending moment*. This subchapter contains a check of the combined effect of shear force and bending moment.
- *Fatigue assessment*. Here the fatigue life of the main I-girders is calculated with the damage equivalent method.

Results

The purpose of the final chapter is twofold. Firstly, in this chapter all the results obtained in the calculations are collected for a better overview. Secondly, some of the data obtained in the hand calculations is exported in this document. Data which is exported includes the results which are of interest in the parametric study in addition to all the data which is required for the external fatigue calculations.

3.3 About the parameters and their relevance

In this chapter the parameters and their corresponding values are described. Furthermore, note that the measurements of the cross-section are not considered as parameters in this study *per se*. Nonetheless, they are important since they determine the capacity and are the means with which the bridge is optimised.

Fatigue design

The fatigue limit state is assessed and designed according to the results obtained with either the damage equivalent method or the more advanced Palmgren-Miner cumulative damage method. Further information about the fatigue assessment methods can be found in chapter 4 - *Fatigue Assessment*.

Span length

The span length has a major influence on many parts of the bridge and is of course strongly dependent on the bridge site. In the parametric study there are three different sets of span lengths which are used in the different studies, see the list below.

- 10-80m in steps of 10m
- 10, 40 and 70m
- 40m

The span length of 40m serves as a reference point since the original bridge was 40m long.

Increased fatigue strength

The fatigue strength is increased in the calculations so that the influence on the bridge design can be observed. The increased fatigue strength which is considered is the inherently higher fatigue strength of stainless steel and the benefit of fatigue improving post-weld treatment.

For the inherently higher fatigue strength the strength is increased for fatigue cracking mode C and D. In the case of post-weld treatment the fatigue strength of all the fatigue cracking modes are increased by two and three classes. Further information about the fatigue cracking modes and the increased fatigue strength is given in chapter *4.2 - Fatigue cracking modes*.

Design life

The design life of the bridge is chosen in conjunction with the fatigue load which is applied to the bridge alternatives. The design life of the bridge is taken as 80, 100 or 120 years which corresponds to low, medium and high fatigue load.

Fatigue loads

The influence of fatigue load caused by traffic is studied by considering three levels of traffic load. The load levels are chosen to be representative for the extreme cases of minimum and maximum fatigue load in addition to a case of medium fatigue load.

The fatigue load is decided by the traffic category, traffic type and the design life of the bridge. The combination which is used for each fatigue load level is shown in table 3.1.

Table 3.1 *Traffic category, traffic type and design life which corresponds to the chosen fatigue load levels used in the parametric study.*

Fatigue load level	Traffic category	Traffic type	Design life
Low fatigue load	Category 4	Local	80 years
Medium fatigue load	Category 2	Medium range	100 years
High fatigue load	Category 1	Long range	120 years

Steel grades

In this parametric study three steel grades are considered. The steel grades in question are the duplex stainless steel grade EN1.4162 and the two carbon steel grades S355 and S460.

EN1.4162, which also is known under the trade name of LDX2101, is chosen since it is used in the original bridge and is also representative for duplex stainless steel. The carbon steel S355 and S460 is representative for ordinary structural steel and high strength structural steel. Furthermore, the high strength steel grade S460 has mechanical properties which are similar to that of the stainless steel EN1.4162.

Cost and interest rate

The costs, both the initial cost of the steel and the cost of maintenance, are included in the parametric study. A high and a low estimate of the cost have been included to account for the uncertainty related to the costs.

Furthermore, the interest rate has also been considered and is also taken as a high and low estimate. The interest rate is used in conjunction with the maintenance costs so that a present value can be calculated. The high interest rate is taken as 3.5% and the low value as 1.5%.

For all the values and calculations considered for the cost of the bridge alternatives see Appendix A.

3.4 Limitations

Due to limitations of time and resources it is not possible to take everything into account in the parametric study. Here is outlined the most prominent limitations to the parametric study.

Firstly, the influence of creep and shrinkage of the reinforced concrete deck is neglected. Furthermore, for the concrete deck the geometry, concrete class and reinforcement has not been changed in the parametric study. In the case of a real bridge it may be of interest to change the concrete deck to further optimise the structure.

Secondly, there is no fatigue assessment performed for the concrete, reinforcement or the shear studs connecting the deck to the steel main I-girders.

Thirdly, in the serviceability limit state only the deflection is checked. It could be of interest to also include a check of stresses and dynamic behaviour for a more detailed study.

Finally, the optimisation of the bridge has been limited to involving just the measurements of the cross-section. In a more advanced study the design could be changed even further. Examples of additional things to consider in the design is the placement and number of splices in the web and flanges as well as the use of stiffeners for the web.

4 Fatigue Assessment

In this thesis there has been a focus on the fatigue strength, fatigue life and fatigue assessment methods which are applicable to stainless steel in particular. This chapter will clarify which methods and assumptions are used and why they were chosen.

With regard to the fatigue assessment methods there are three different methods that have been implemented, utilised and compared in the parametric study. Out of these three methods the first two have been utilised in the design of the bridge.

The first and most basic fatigue assessment method is the damage equivalent method in combination with analytical hand calculations. For this method the fatigue load model 3 was used.

The second method is also based on analytical hand calculations but instead uses the more advanced Palmgren-Miner cumulative damage method. For this method the fatigue load model 4 was used, however fatigue load model 5 could also be applied.

Finally, the third method uses the Palmgren-Miner method in conjunction with a finite element model which is used to derive the stress spectra. As for the analytical counterpart fatigue load model 4 was used in the parametric study and the calculations permit the implementation of fatigue load model 5.

The fatigue assessment methods are described in more detail in subchapter *4.3 - The damage equivalent factor method* and subchapter *4.4 - The Palmgren-Miner cumulative damage method*. The fatigue load models which are used for the fatigue assessment methods are described in subchapter *4.1.1 - Fatigue load model 3* and subchapter *4.1.2 - Fatigue load model 4*.

Finally, the fatigue strength has been considered with different values. The basic values are taken according to recommendations in Eurocode for both stainless steel and carbon steel. However, for the stainless steel higher fatigue strength through inherent properties or post-weld treatment has also been considered. More about the fatigue strength can be found in subchapter *4.2 - Fatigue cracking modes*.

4.1 Fatigue Load Models

The fatigue load models are used to assess the fatigue life of the bridge. They are used in conjunction with fatigue assessment methods such as the damage equivalent method and the damage cumulative Palmgren-Miner method. The fatigue load models that are given by the current Eurocode can be found in *EN 1991-2. Section 4.6*.

In total there are five different fatigue load models given in Eurocode, which are simply referred to by number. In this parametric study fatigue load model 3 and 4 is utilised. These fatigue load models will therefore be described in more detail in subchapter *4.1.1 - Fatigue load model 3* respectively subchapter *4.1.2 - Fatigue load model 4*.

To begin, the three first fatigue load models are primarily used to find the difference between the highest and lowest value of stress. For this reason they are suitable for use with the damage equivalent method, since the damage equivalent method requires only a largest value of the stress range.

By the same token the three first load models are not recommended to be used with the Palmgren-Miner method. This since the Palmgren-Miner method in contrast to the damage equivalent method takes into account all the stress ranges and the corresponding load cycles which can be derived from the stress spectrum. To reiterate, the Palmgren-Miner method should not be used in conjunction with fatigue load model 1, 2 or 3.

In more detail, fatigue load model 1 and 2 is intended to be used when the fatigue life is assumed to be infinite. Load model 3 on the other hand does not assume infinite fatigue life and is therefore more suitable to be used with the damage equivalent method in the parametric study.

In contrast to the three first models the fatigue load models 4 and 5 are intended to produce stress spectra rather than just a difference between highest and lowest stress. Therefore these two models are suitable to use with the Palmgren-Miner method. Consequently they also become less suitable to use with the damage equivalent method.

Load model 4 is based upon a set of characteristic vehicles while load model 5 should be based upon real vehicles and traffic data. It should go without saying that load model 5 is more accurate when it is possible to determine the real traffic. For fatigue load model 4 the estimation of the traffic loads are based upon the traffic category and type.

Note that the there is no measured traffic data available for the original bridge in question. Furthermore, the traffic and fatigue load should be varied in the parametric study. Therefore fatigue load model 4 has been chosen to be used with the Palmgren-Miner method in the parametric study.

4.1.1 Fatigue load model 3

In the parametric study fatigue load model 3 is used with the damage equivalent method. This since fatigue load model 3 is recommended to be used with the damage equivalent method. Additionally, fatigue load model 3 takes into account a fatigue life which is not infinite, in contrast to fatigue load model 1 and 2.

Fatigue load model 3 uses a single vehicle model. The vehicle model is illustrated in figure 4.1. Each axle in the model has a load of 120kN, bringing the total weight of the vehicle to 480kN.

Furthermore, an additional vehicle can be considered in the same lane for bridges that has a length of 40m or longer. The second vehicle is placed at a distance of 40m behind the first vehicle. Additionally, the second vehicle has a markedly lower axle load of just 36kN compared to the axle load of 120kN for the first vehicle.

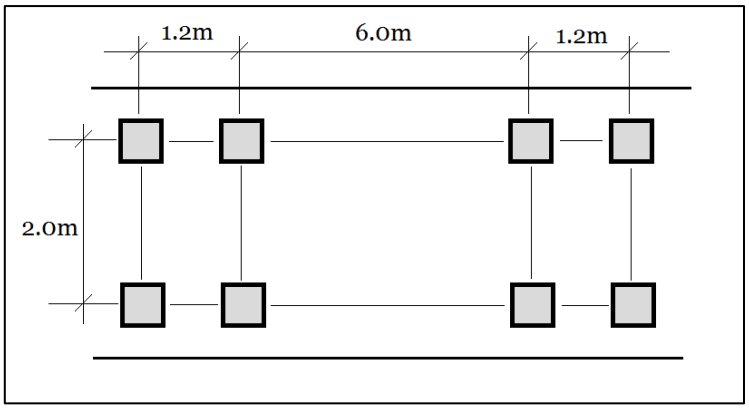

***Figure 4.1**: Illustration of the vehicle model in fatigue load model 3.*

4.1.2 Fatigue load model 4

Fatigue load model 4 is used with the Palmgren-Miner method in the parametric study. The fatigue load model 4 is similar to fatigue load model 5, but doesn't require measured or estimated data of the real traffic. As such it can be used to estimate the fatigue life where the traffic data is not available or incomplete.

The fatigue load model takes into account a set of five vehicles which are defined in EN 1991-2: Table 4.7. Additionally, in the model are defined three types of axles which are used for the different vehicles. Alas, in the parametric study the axles and wheels are simplified as point loads for both the analytical calculations and the finite element model.

Moreover, based on the road category the fatigue load model 4 allows for an estimation of the amount of heavy traffic. The estimation gives a value of the total number of heavy vehicles that will pass the bridge in each slow lane per year. Moreover, the composition of the vehicle types is decided by distance which the heavy traffic is presumed to travel. For long range transports the vehicle mix contains mostly of heavy vehicles while for local transports the vehicle mix is dominated by light vehicles.

Finally, fatigue load model 4 may take into account the occurrence of multiple vehicles passing the bridge at the same time. This is however not included in the model as standard, instead it may be taken into account by modifying the load model when needed. In the parametric study performed in this thesis the effect is assumed to be negligible in order to simplify the calculations. Further details about how to modify the load model are given in *Background to fatigue load models for Eurocode 1: Part 2 Traffic Loads* written by Croce P.

4.2 Fatigue cracking modes

For the fatigue assessment of the bridge only the main I-girders will be considered. To clarify, no fatigue assessment will be carried out for the reinforced concrete or the shear studs connecting the concrete deck to the main I-girders. Nonetheless, for the main I-girders there are six fatigue cracking modes which are considered in the calculations.

In addition to fatigue strength given by Eurocode the fatigue strength has also been increased in parts of the parametric study. The fatigue strength is increased in order to take into account both the benefit of the inherently higher fatigue strength of stainless steel and the effect of fatigue improving post-weld treatment. Further information and background for the higher fatigue strength of stainless steel can be found in chapter *2.3 - Fatigue of stainless steel*.

In this chapter the fatigue cracking modes will be described briefly. For further information about the fatigue cracking modes and the related calculations see Appendix F.

Here is given a brief explanation of the fatigue cracking modes which are used in the parametric study. Please note that the mode names are taken arbitrarily and bear no significance outside the use in this thesis.

Fatigue cracking mode A

Fatigue cracking mode A takes into account the fatigue cracking that starts from the longitudinal welds between the web and the flanges. The fatigue cracking is caused by both the direct stress and shear stress in the web. Here the effect of each stress is considered individually and then added together.

The fatigue strength of the detail with regard to direct stress is based upon detail 3 in EN 1993-1-9: table 8.2. Note that detail 3 is selected since the weld is a continuous but contains stop/start positions. For the shear stress the fatigue strength is based on detail 6 in EN 1993-1-9: table 8.1. For an illustration of the fatigue cracking mode see figure 4.2.

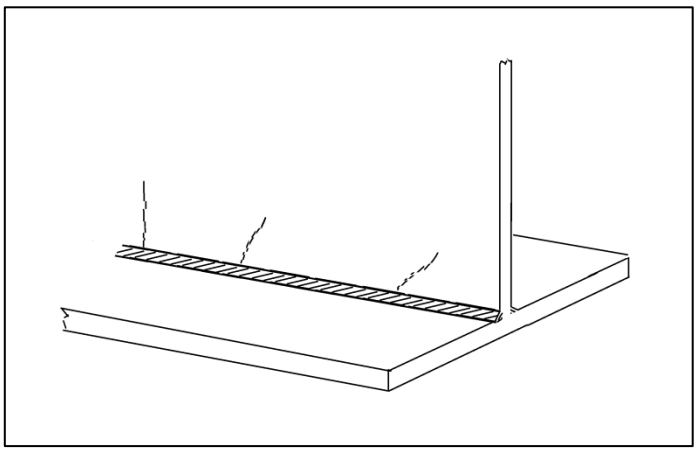

***Figure 4.2**: Illustration of fatigue cracking mode A, which is initiated from the longitudinal weld between web and flanges. Note that this mode takes into account both the direct and shear stress in the web.*

Fatigue cracking mode B

Fatigue cracking mode B takes into account the cracking that starts from the welded splices in the flanges. The stress which is considered is direct stress in the relevant flange. The fatigue strength of this detail is reduced when the thickness of the flange is increased above 25mm.

The fatigue strength and the associated reduction factor for size effect can be found in EN 1993-1-9: table 8.3 for detail 2 and 4. For an illustration of the fatigue cracking mode see figure 4.3.

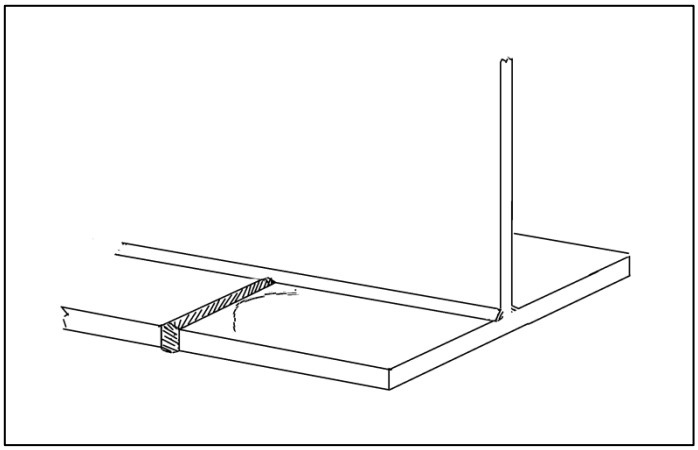

***Figure 4.3**: Illustration of fatigue cracking mode B, which is initiated from the splices in the flanges of the main I-girders.*

Fatigue cracking mode C

Fatigue cracking mode C takes into account the fatigue cracking that starts in the weld between the vertical stiffener and the web at the support. For this detail the principal stress should be used in calculations. The fatigue cracking mode is illustrated in figure 4.4.

The fatigue strength is taken for detail 7 in EN 1993-1-9: table 8.4. Note that the fatigue strength of this detail is increased when the inherently higher fatigue strength of stainless is considered. For more information about the higher fatigue strength of this detail and stainless steel see chapter *2.3 - Fatigue of stainless steel.*

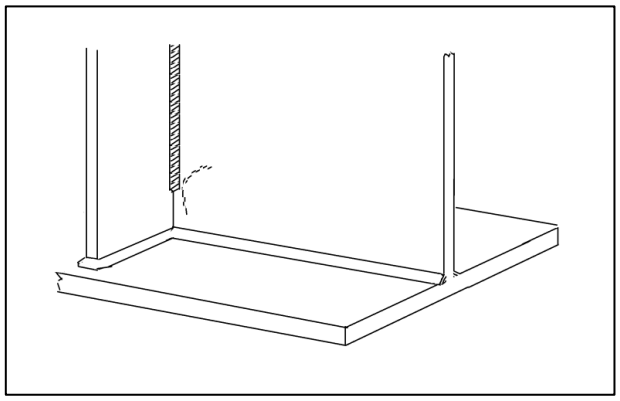

***Figure 4.4**: Illustration of fatigue cracking mode C, which is initiated from weld between the vertical stiffener and the web. Note that this mode takes into account the principal stress in the web.*

Fatigue cracking mode D

Fatigue cracking mode D originates form the vertical stiffener just like mode C but instead considers the fatigue cracks which start from the weld between the stiffener and the flanges. The stress which is considered here is the direct stress in the surfaces of the flanges at which the stiffener is welded to. To clarify, for the upper flange this is the lower surface and for the lower flange this is the upper surface. The fatigue cracking mode is also illustrated in figure 4.5.

The fatigue strength is taken for detail 7 in EN 1993-1-9: table 8.4. Note that the fatigue strength of this detail is increased when the inherently higher fatigue strength of stainless is considered. For more information about the higher fatigue strength of this detail and stainless steel see chapter *2.3 - Fatigue of stainless steel.*

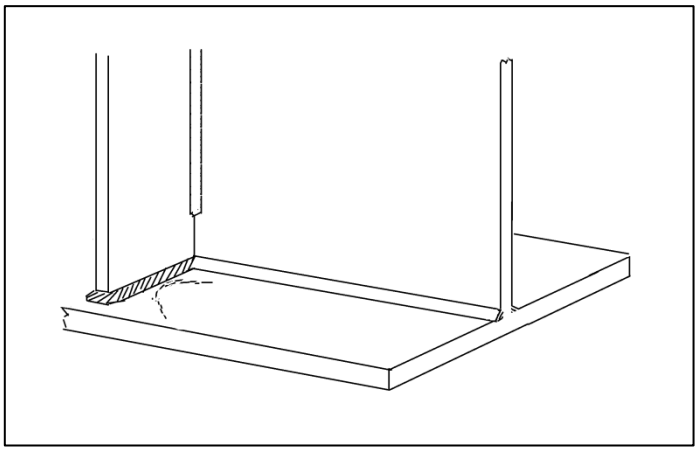

***Figure 4.5**: Illustration of fatigue cracking mode D, which is initiated from weld between the vertical stiffener and the flanges.*

Fatigue cracking mode E

Fatigue cracking mode E takes into account fatigue crack in the longitudinal welds between web and flanges, see figure 4.6. Here it is the shear stress in the weld which is considered. The fatigue strength for the weld is taken for detail 8 in EN 1993-1-9: table 8.5.

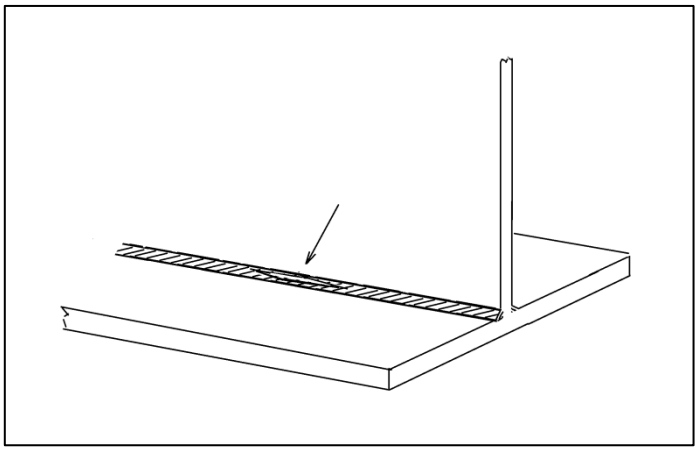

***Figure 4.6**: Illustration of fatigue cracking mode E, which is initiated in the longitudinal weld between the web and the flanges.*

Fatigue cracking mode F

Fatigue cracking mode B takes into account the cracking that starts from the welded splices in the web. The stress which is considered is the direct stress in the web. The fatigue strength of this detail is reduced when the thickness is increased above 25mm.

The fatigue strength and the associated reduction factor for size effect can be found in EN 1993-1-9: table 8.3 for detail 2 and 4. For an illustration of the fatigue cracking mode see figure 4.7

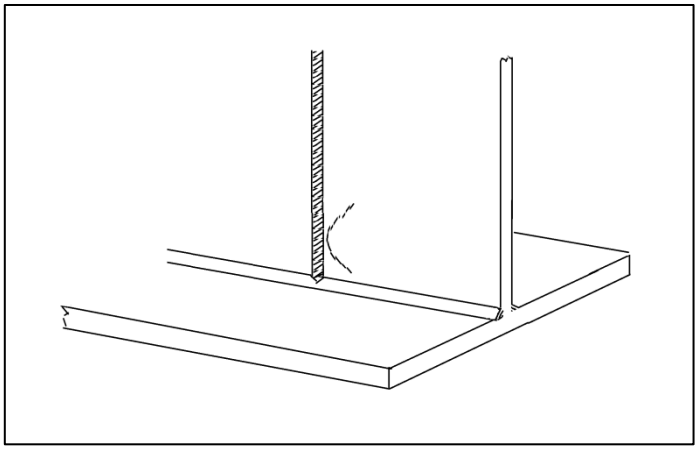

***Figure 4.7**: Illustration of fatigue cracking mode F, which is initiated from the splices in the web of the main I-girders.*

4.3 The damage equivalent factor method

The damage equivalent factor method is a method that uses several factors to estimate the damage that is sustained in the fatigue limit state. The method is alternatively referred to as the λ-factor or lambda-factor method. Note however that in this thesis it is referred to as the damage equivalent method.

The method is taking into account the complex fatigue calculations into one single factor, which is called the damage equivalent factor. The value of the damage equivalent factor is obtained in Eurocode through the use of four factors.

The aspects which are considered in the damage equivalent factor are:

- The length of the span. The span length determines the influence line and the amount of damage that each vehicle causes.
- The amount of traffic on the bridge. The weight and amount of passing vehicles is a major factor in determining the amount of damage that is caused.
- The design life of the bridge. The longer the design life of the bridge, the more vehicles will pass the bridge in total. The number of load cycles naturally has an effect on the damage which is sustained.
- The number of lanes with heavy traffic. If there are multiple lanes on the bridge there will be additional damage sustained when more vehicles pass over the bridge. In addition, the presence of multiple vehicles on the bridge simultaneously should be taken into account since they further increase the stress range.

Finally it should be noted that the damage equivalent factor is limited so that it may not exceed a certain value that is determined by the span length.

For further information about the damage equivalent method see the calculations pertaining to fatigue assessment in Appendix F. In the calculations reference is given to the relevant sections in Eurocode which applies for this method.

4.4 The Palmgren-Miner cumulative damage method

The Palmgren-Miner method is a cumulative damage method and is used to calculate the damage which is sustained due to fatigue loading. The damage should be kept below 1. The damage can therefore in many regards be treated as an utilisation ratio. However note that damage in most regards has a non-linear behaviour and that a small change in stress range may cause a large change in damage.

In brief the Palmgren-Miner method calculates the damage for each stress range with regard to the amount of cycles for the current stress range. In this way the damage is accumulated for all the stress ranges that the detail is subjected to, hence the name cumulative damage method.

In more detail, the damage is calculated with the help of S-N curves which describes the amount of load cycles that may be applied until failure at a given stress range. For steel there is also a cut-off limit for which failure will not occur no matter how many load cycles are applied. The calculations which are carried out in the parametric study and the related references to Eurocode can be found in Appendix E.

Furthermore, in order to obtain the stress ranges and corresponding load cycles a cycle-counting algorithm has to be utilised. Common algorithms for fatigue calculations are the rainflow counting algorithm and the reservoir counting algorithm. In this thesis it is the rainflow counting algorithm which has been utilised for the fatigue calculations.

In short, the cycle-counting algorithm is used to analyse the stress spectra which is caused by the vehicles in the fatigue load model. More information about fatigue load model 4 which is used with the Palmgren-Miner method can be found in subchapter *4.1.2 - Fatigue load model 4*.

4.4.1 Stress spectra obtained from analytical solution and finite element model

The stress spectra that are used to calculate the fatigue damage can be obtained through analytical calculations or by finite element modelling. In this thesis both approaches have been utilised and compared. The results from this comparison can be found in chapter *5.2.2 - Comparison of fatigue assessment with finite element method and analytical method*.

For both approaches the stress spectra for the vehicles in the load model are assembled from an influence line. The influence line can be for stress in a selected node or bending moment and shear force in a section.

The influence line is obtained for a reference axle load and later scaled and assembled to correspond to a vehicle in the load model. The influence line is obtained for a given node or section by moving the axle load along the bridge. The value of interest is observed for each position of the load.

For the analytical solution the bending moment and shear force is obtained for the reference axle load. The bending moment and shear force is then assembled into influence lines which correspond to each vehicle in the fatigue load model. Finally the stress spectra can be calculated for the influence lines with regard to the capacity of the cross-section.

For the finite element model the stresses are instead obtained directly from the model. The implication of this approach is that the superposition principle is utilised for the assembly to be applicable. A drawback which stems from the use of the superposition principle is that the principle only holds true for linear systems. In conclusion, for the approach with reference axles in the finite element model the material models and behaviour of the model must be kept linear.

In comparison, for the analytical approach consideration can be taken to non-linear response. For example the difference in the second moment of area for sections where concrete is in tension respectively compression. This is possible since the analytical solution calculates an influence line for bending moment and shear force for each vehicle independent of the cross-sectional properties. There is therefore no need to use superposition for the stress which is instead calculated directly for each vehicle.

However, it is important to note that non-linear models can be utilised when complete vehicle models are used instead of reference axle loads. When the vehicle model is used there is no longer a need for superposition of stresses, which prevented non-linear models. To summarise, when whole vehicle models are implemented in the finite element model the behaviour is allowed to be non-linear.

Nonetheless, the advantage of using a reference load is that the number of calculations in the finite element model can be reduced. Therefore this simplified method can be used to make a less accurate but faster estimate of the damage which will be sustained in the fatigue limit state.

Finally, the full calculations of the stress spectra for the vehicle loads can be found in Appendix E. In addition, the analytical approach is relying on data which is calculated in accordance with Eurocode. The calculations based on Eurocode can be found in Appendix F.

Moreover, the finite element model which is used to obtain the stress spectra for the reference load is created by scripts in Abaqus/Brigade. A description of the script which was written and utilised in this thesis can be found in Appendix B. Additionally, a convergence study of the model which is used in the parametric study can be found in Appendix C.

5 Results

In this chapter all the significant results obtained from the parametric study are presented. For the full set of results and data see Appendix A. In the appendix all the data obtained from the parametric study is presented in tables and a few additional diagrams. The diagrams presented in the appendix may be of interest but that did not fit into the report.

The results are divided into subchapters that focus on the different aspects of the parametric study. Results included in the study are the influence of span length, grade, fatigue assessment methods and improved fatigue strength. Note that there may be some minor overlap between these subchapters.

For additional information about the parametric study and the parameters which are studied see chapter 3 - *Parametric Study* and subchapter *3.3 - About the parameters and their relevance*.

5.1 Influence of the span length

The span length is one of the most critical parameters to consider for the bridge.

As such the influence of the bridge's span lengths has been investigated specifically in two studies. In the first and more comprehensive study of the span length the span ranges from 10 to 80m in steps of 10m. In the second study only three span lengths are selected. Those span lengths are chosen to be representative for a short, medium and long bridge at 10m, 40m and 70m respectively.

In further detail, in the first study the bridge alternatives are designed with regard to the lowest fatigue load and shortest design life of 80 years. Furthermore the design is verified with the damage equivalent method.

In contrast, in the second study the more advanced Palmgren-Miner method is utilised for the design with regard to the fatigue limit state. In addition, the fatigue load is increased to medium fatigue load for a design life of 100 years.

Moreover, in both studies the fatigue life will be assessed by both the damage equivalent method and the Palmgren-Miner method. In this way a comparison of the two methods can be made in addition to the studies given in subchapter *5.2 – Comparison of different fatigue assessment methods*.

5.1.1 Influence of span length, damage equivalent method

This study will investigate the influence the span length has on the design, utilisation ratios and material consumption of the bridge. This study will be based on the bridge subjected to low fatigue load. Moreover, the design is based on the damage equivalent fatigue assessment method.

First, as can be seen in figure 5.1, the limit states that determines the design in this study are the ultimate limit state in combination with the fatigue limit state. In more detail, for this case of very low fatigue load the fatigue limit state is only determining the design for span lengths of up to 50m.

Here it should be noted that the utilisation of the capacity in the ultimate limit state is maximised in the middle of the span. On the other hand the utilisation in the fatigue limit state is instead maximised at the support region. Further on the structural behaviour can be found in *chapter 3.1- Structural behaviour of the Nynäshamn Bridge*.

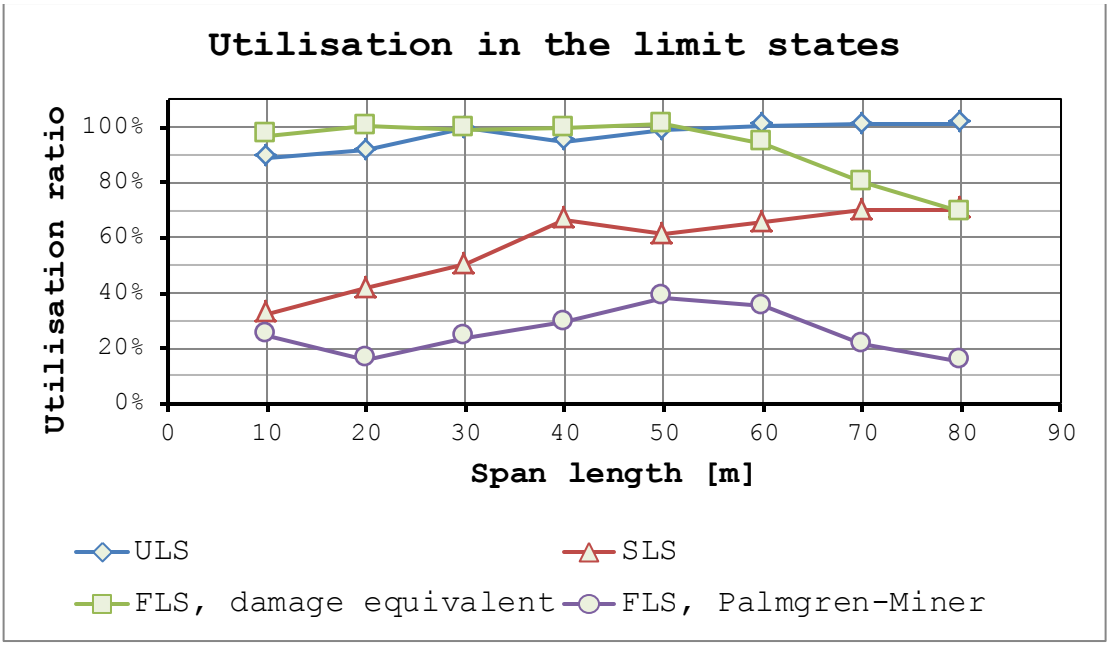

Figure 5.1: *This diagram shows how the utilisation ratio in the different limit states varies with regard to the span length of the bridge. The design is performed with regard to the damage equivalent method for low fatigue load.*

Moreover, as can be seen in figure 5.1 the utilisation ratio with regard to the Palmgren-Miner method is substantially lower than that of the damage equivalent damage method for all of the investigated span lengths. Note that the damage sustained according to the Palmgren-Miner method clearly start to decline at the same point, for spans over 50m, as the utilisation with regard to the damage equivalent method decline. Thus, while the two methods are not of the same magnitude the methods still exhibit good levels of correlation.

Additionally, from the span length of 20m to 40m it appears as the damage equivalent and Palmgren-Miner method are converging for longer span lengths.

When examining the individual utilisation ratios in the ultimate limit state it becomes apparent that it is the bending of the composite cross-section that is the governing mode. The utilisation in the ultimate limit state can be found in figure 5.2.

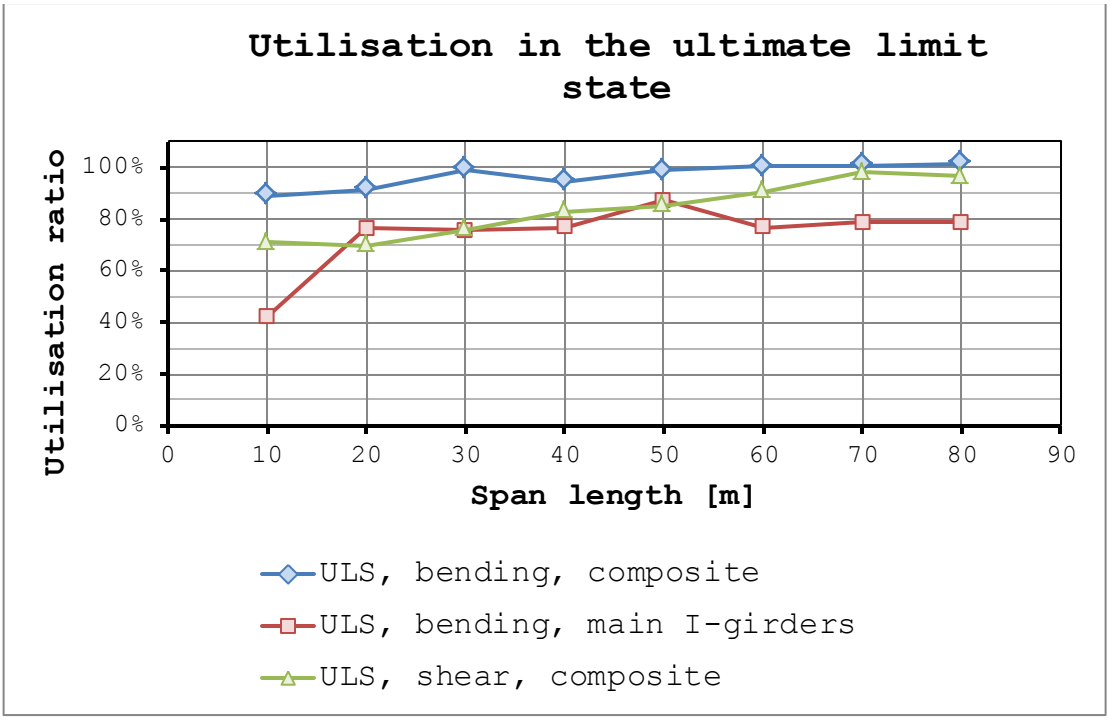

Figure 5.2: *This diagram shows how the utilisation ratio in the ultimate limit state varies with regard to the span length of the bridge. The design is performed with regard to the damage equivalent method for low fatigue load.*

As a matter of fact, the utilisation of the main I-girders at casting is expected to remain lower than the utilisation of the composite cross-section. This since the self-weight which for most span lengths, especially longer spans, is the dominating load remains mostly the same at casting and in the service life. Thus, the addition of imposed loads that is carried by the composite cross-section with composite action will require additional capacity and renders the composite cross-section the limiting factor with regard to the ultimate limit state.

Nonetheless, it should be observed that the shear capacity of the bridge is hard to optimise. The shear capacity is largely dependent on the thickness and height of the web. Due to the small thickness of the web even a small increase in thickness will lead to a steep increase in capacity. Finally, it should be noted that the thickness of the web also affects the bending resistance to a certain degree.

Taking a closer look at the utilisation ratios for the different fatigue cracking modes it is mode C and D that are the most important. See figure 5.3 for a diagram of the fatigue cracking modes assessed with the damage equivalent method for which the current set of bridges are designed after. In fact, mode C and D are both caused by the transversal stiffeners at the supports. Mode C takes into account the principal stress in the web while mode D takes into account the direct stress in the upper and lower flanges.

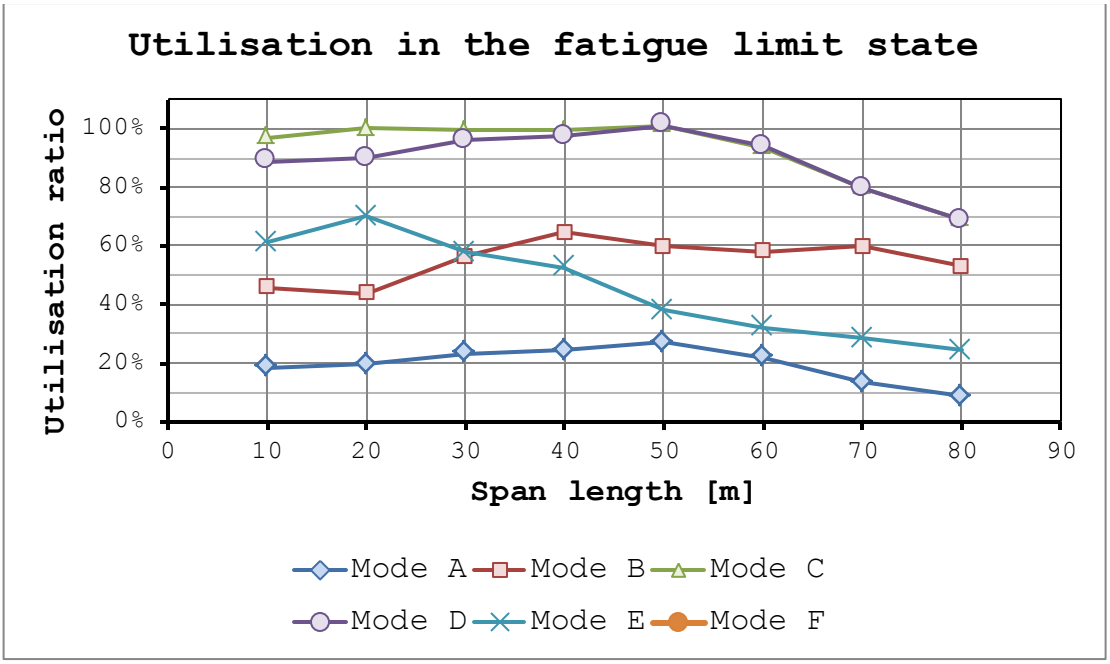

Figure 5.3: *This diagram shows the utilisation ratio in the fatigue limit state according to the damage equivalent method for the various fatigue cracking modes. The design is performed with regard to the damage equivalent method for low fatigue load.*

As mentioned previously the bending moment caused by imposed loads, such as traffic loads, are high at the support region. The high moment is coupled by a moment resistance that is generally lower at the section close to the supports. Finally, the transversal stiffener at the support has one of the lower fatigue strengths of the details considered in the bridge. In conclusion, these three circumstances are the major factors that renders mode C and D to be the critical modes in most cases.

In contrast, for this case with low fatigue load the utilisation design obtained with the damage equivalent method becomes very conservative when compared to the damage that is sustained according to the Palmgren-Miner method. However, note that this is the case for the lowest traffic load and shortest design life, and does not generally hold true for all cases. For further comparison between the two fatigue assessment methods see subchapter *5.2.1 - Comparison of the design obtained through the damage equivalent method and the Palmgren-Miner method*.

Although, as can be seen in figure 5.4, while the damage sustained according to the Palmgren-Miner method is significantly smaller the pattern remains similar. In fact, mode C and D which are the most critical modes with regard to the damage equivalent method still remains the two most critical modes. Alas, there is a difference in that for Palmgren-Miner the damage is persistently lower for mode C than for mode D. This stands in contrast to the case for the damage equivalent method where mode C tends to be more critical or on the same level as mode D.

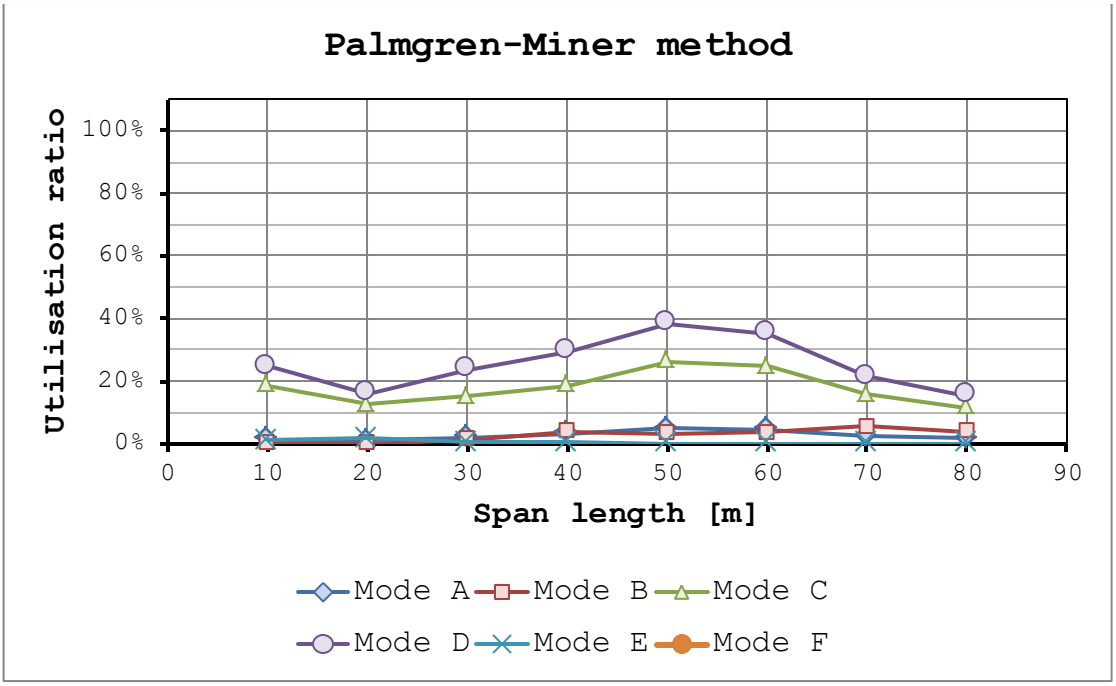

Figure 5.4: *This diagram shows the utilisation ratio in the fatigue limit state according to the Palmgren-Miner method for the various fatigue cracking modes. The design is performed with regard to the damage equivalent method for low fatigue load.*

In addition, it is of interest to know how the exposed steel area and the weight of the steel in the bridge vary with the span length. As can be seen in figure 5.5 both the steel area and steel consumption increases almost exponentially with regard to the span length.

The steel area is of importance when comparing the stainless steel bridges to the carbon steel alternatives. This since the exposed steel area has to be painted for carbon bridges. As such it determines both the initial cost and a major part of the maintenance cost for carbon steel bridges. More comparisons of carbon steel and stainless steel in this parametric study can be found in chapter *5.3 - Comparison of carbon steel and stainless steel*.

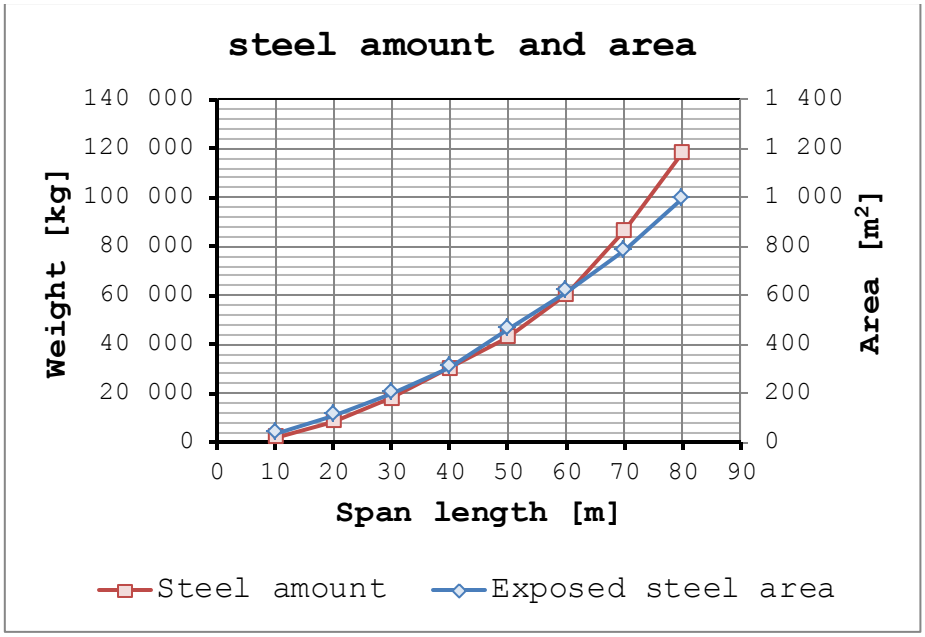

Figure 5.5: *This diagram shows how the steel amount and exposed steel area varies with the length of bridge. The steel amount is given as the weight for all of the structural steel in the bridge. The design is performed with regard to the damage equivalent method for low fatigue load.*

Finally, the ratio between area and weight, which can be seen in figure 5.6, is useful when comparing the stainless steel bridges to the carbon steel alternatives. The current set of stainless steel bridges is used in order to obtain an indication of how the ratio between exposed steel area and steel weight correlates with the span length. As can be seen in figure 5.6 the steel area increase for shorter spans and decrease for longer bridge spans.

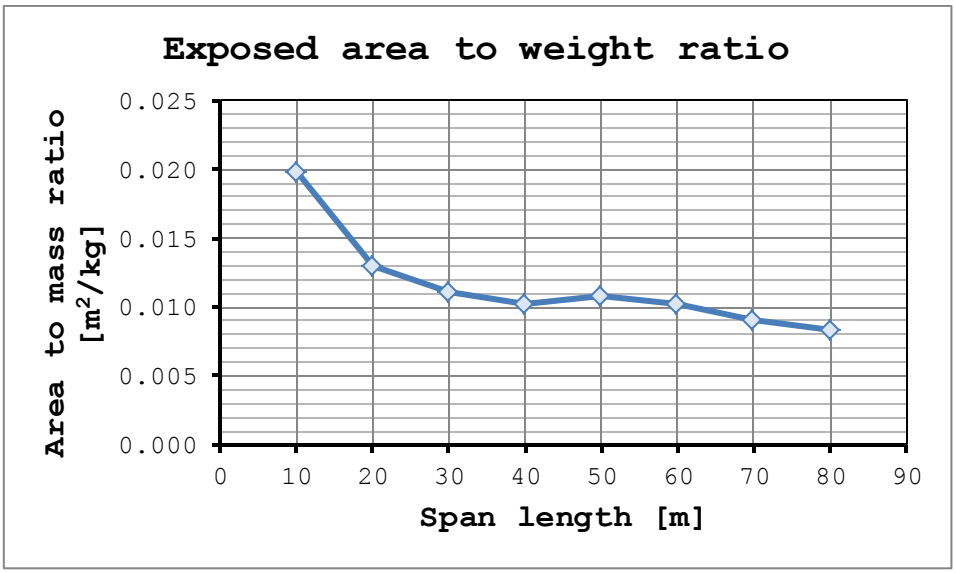

Figure 5.6: *This diagram that shows the ratio between exposed surface area and weight of the steel at different span lengths. The design is performed with regard to the damage equivalent method for low fatigue load.*

5.1.2 Influence of span length, Palmgren-Miner method

This study will investigate the influence that the span length has on the design, utilisation ratios and material consumption of the bridge. In comparison to the study in the previous subchapter this study will consider the bridge when subjected to medium fatigue load rather than low fatigue load. Moreover, the design is assessed with the Palmgren-Miner method in the fatigue limit state, instead of the more simplistic damage equivalent method.

As can be seen in figure 5.7 the fatigue limit state determines the design for span lengths between 10 and 70m. Note that this behaviour is quite different when compared to the result obtained for low fatigue load and design by the damage equivalent method which is described in subchapter *5.1.1 - Influence of span length, damage equivalent method*. In addition, for the short span length of 10m the utilisation in the ultimate limit state is no longer critical for the design.

Furthermore, the damage equivalent method yields consistently higher utilisation ratios than the Palmgren-Miner method. This is especially pronounced for shorter span lengths while for 70m span length the two methods yield almost the same result. At 70m the utilisation ratio with regard to the damage equivalent method is 106%, this in comparison to 248% for the span length of 10m.

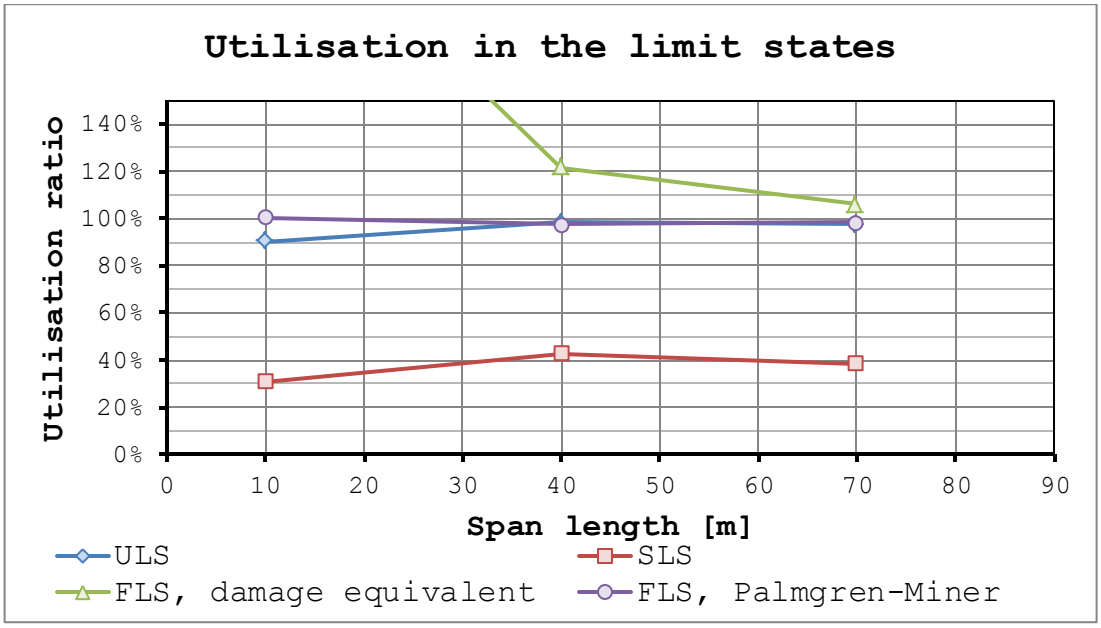

Figure 5.7: *This diagram shows how the utilisation ratio in the different limit states varies with regard to the span length of the bridge. The design is performed with regard to the Palmgren-Miner method for medium fatigue load.*

The deflection, which is measured in the serviceability limit state, remains sufficiently low for all the span lengths. Furthermore it doesn't show any signs to increase excessively.

When observing the individual utilisation ratios in the ultimate limit state the result is similar to the result obtained for the lambda method. The result in question can be seen in figure 5.8. To clarify, for the utilisation of bending resistance the composite section is always higher compared to the bending of the main I-girders at casting. Further, the utilisation of the shear capacity is as previously mentioned fluctuating and remains mostly independent of the utilisation in bending.

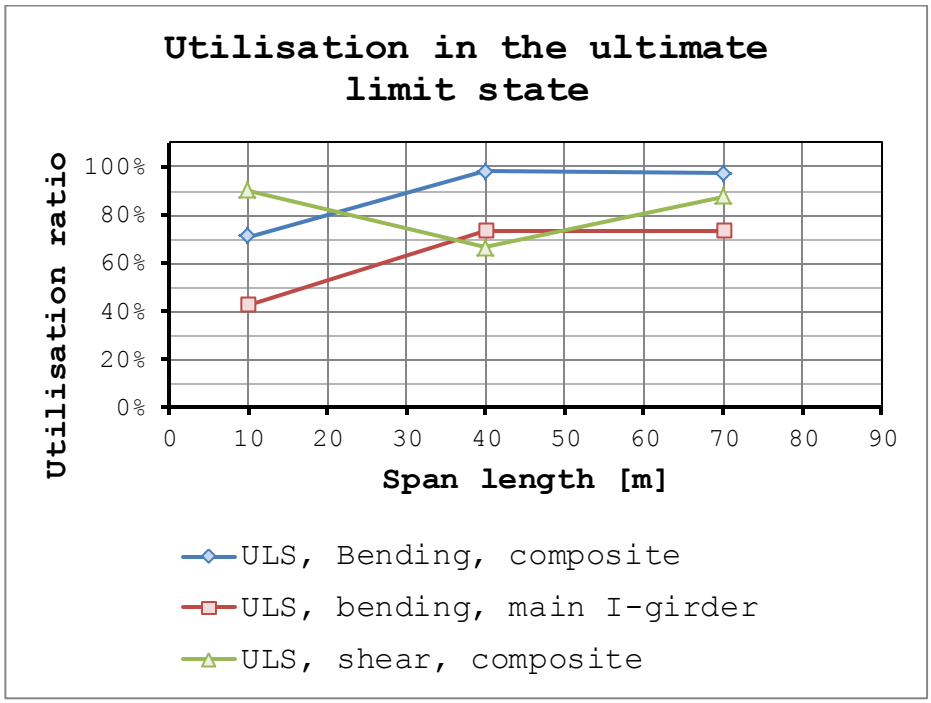

Figure 5.8: *This diagram shows how the utilisation ratio in the different limit states varies with regard to the span length of the bridge. The design is performed with regard to the Palmgren-Miner method for medium fatigue load.*

For the Palmgren-Miner method the critical fatigue cracking mode is mode D. Recall that in a previous chapter, chapter *5.1.1 - Influence of span length, damage equivalent method*, mode C in conjunction with mode D was critical. Both fatigue cracking modes originate from the vertical stiffener located at the supports. What is noteworthy is that the critical mode has shifted from mode C to D.

As previously mentioned the shift from mode C to mode D is due to the fact that in the damage equivalent method the maximum direct stress and shear stress is assumed to coincide. This is not the case, and thus the maximum stress which mode C is based upon will become a lower value. In conclusion, since the stress range is lower the damage that is sustained from cracking mode C is also lowered.

Another interesting observation is that mode E, which depends on the shear stress in the welds, will become critical at short span lengths. This is to a large extent due to the fact that the second moment of area for the cross-section is decreased more than the first moment of area for the flanges. The calculations can be found in Appendix F.

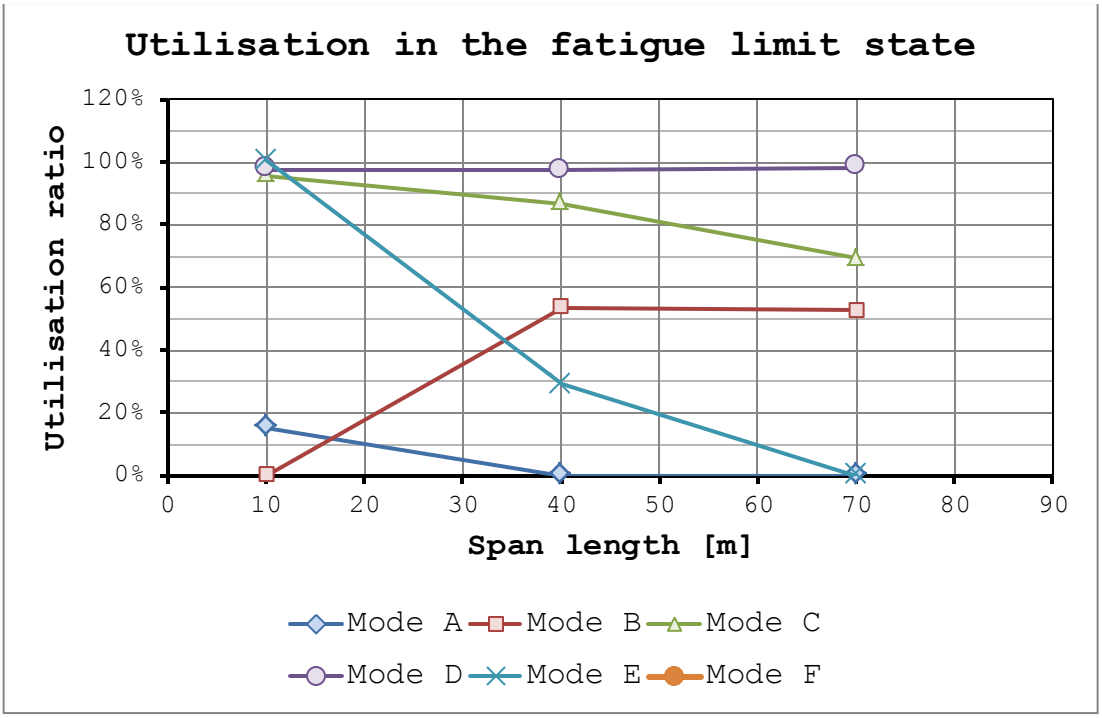

Figure 5.9: *This diagram shows how the utilisation ratio in the different limit states varies with regard to the span length of the bridge. The design is performed with regard to the Palmgren-Miner method for medium fatigue load.*

Furthermore, mode B also becomes more important for longer span lengths since this mode is dependent on the thickness of the flanges. For longer spans the dimensions are increased and consequently the fatigue strength of mode B is decreased.

The values for the damage equivalent method are presented in Appendix A.

5.2 Comparison of different fatigue assessment methods

This chapter is composed of two studies of the fatigue assessment methods. The first study investigates the difference between designs made with regard to the damage equivalent method and the Palmgren-Miner method respectively. The second study primarily investigates the difference between using an analytical or finite element method for obtaining the stress spectra used in the Palmgren-Miner method.

As can be observed in the results presented in chapter *5.1 - Influence of the span length*, the different fatigue assessment methods yields results that can differ substantially depending of the combination of span lengths and fatigue load. Thus it is of interest to investigate the result obtained for the two methods in further detail.

5.2.1 Comparison of the design obtained through the damage equivalent method and the Palmgren-Miner method

In this chapter a brief comparison will be made between the damage equivalent method and the Palmgren-Miner method. The comparison will be performed for a span length of 40m and three different levels of fatigue load.

The utilisation ratios for respective fatigue assessment method can be seen in figure 5.10 and figure 5.11. First and foremost, the damage equivalent method yields a more conservative design for low fatigue load while for high fatigue load the Palmgren-Miner method yields a more conservative design.

When comparing the two methods it is important to note that the Palmgren-Miner scales almost exponentially with the applied stress range while the damage equivalent method have a linear response.

Furthermore, note that in figure 5.10 the Palmgren-Miner method yields a damage of 120%. This is, of course, not acceptable in a real case but is used here to show that the design is optimised and close to the fatigue cut-off limit. The smallest increase to the cross-section will result in zero damage according to the calculations by the Palmgren-Miner method.

To elaborate, for the high fatigue load the most severe vehicle in fatigue load model 4 is vehicle number 3. Vehicle 3 also corresponds to half of the vehicles passing the bridge, which are 2 million vehicles per year and lane in this case. This leads to at least a total amount of 120 million load cycles caused by vehicle 3. Since the fatigue cut-off limit corresponds to 100 million load cycles the lowest damage is 120 million divided by 100 million, which is 120%. To reiterate, the damage of 120% is unacceptable, therefore the damage has to be decreased to 0% by keeping the stress range below the fatigue cut-off limit.

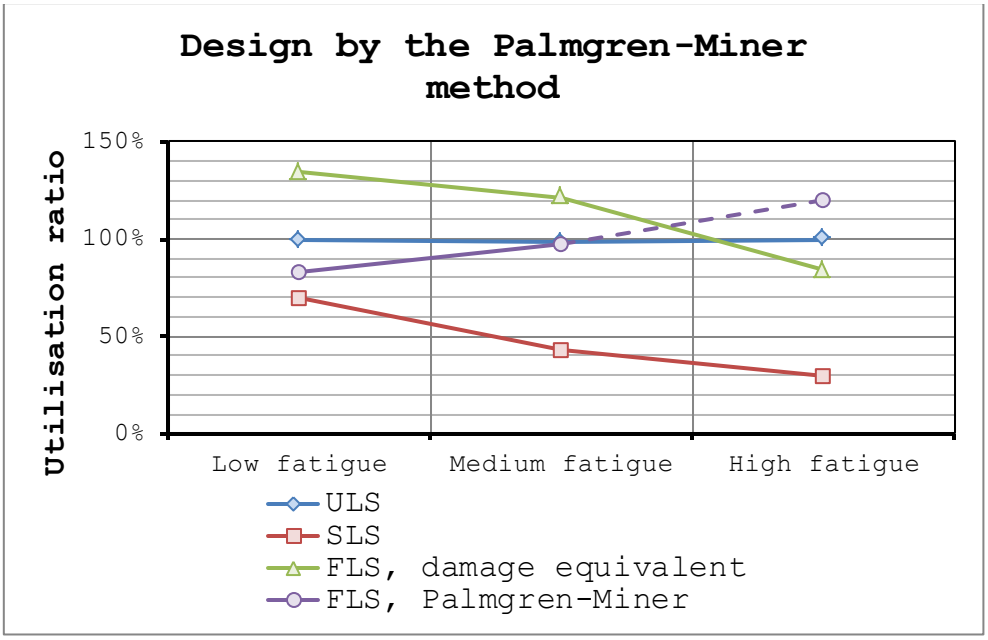

Figure 5.10: *This diagram shows how the utilisation ratio for the different limit states obtained for the design based on the Palmgren-Miner fatigue assessment method. The span length is 40m long. See chapter 3.3 for explanation of the levels of fatigue load.*

As can be seen from the design by damage equivalent method the small difference in stress range yields a very large difference in the damage sustained according to the Palmgren-Miner method. For the case of high fatigue load and a 40m long span the damage according to Palmgren-Miner is 540%. Such a high value corresponds to the bridge only lasting about 22 years of the intended design life of 120 years.

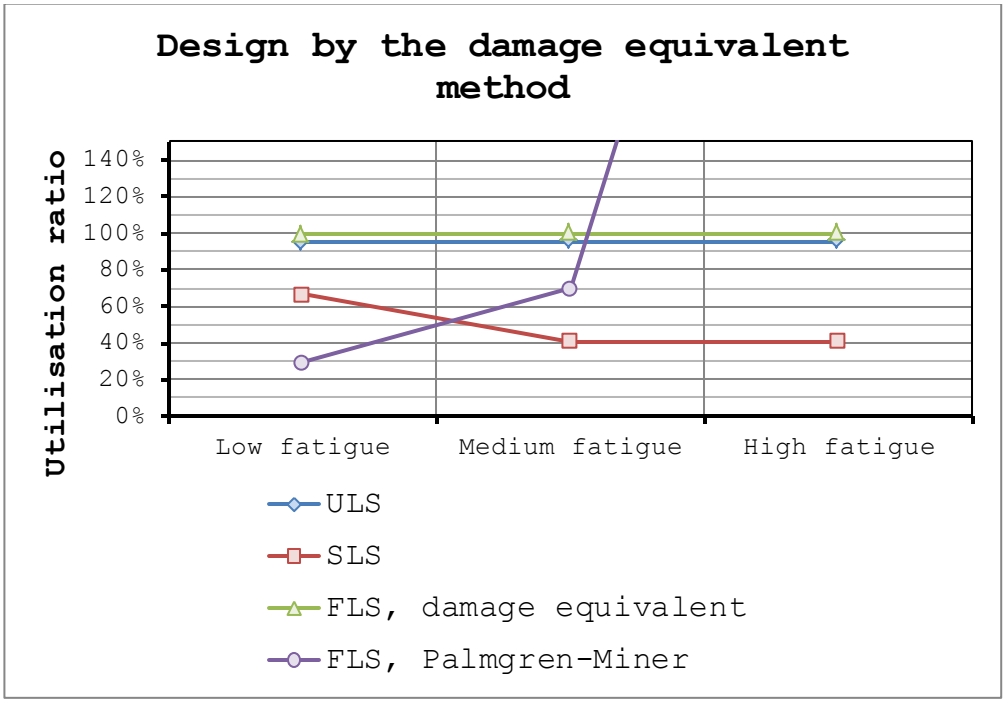

Figure 5.11: *This diagram shows how the utilisation ratio for the different limit states obtained from the design based on the damage equivalent fatigue assessment method. The span length is 40m long. See chapter 3.3 for explanation of the levels of fatigue load.*

Finally, note that the results from the two different methods are also presented in the other studies presented in this main chapter, chapter 5 - *Results*.

5.2.2 Comparison of fatigue assessment with finite element method and analytical method

The fatigue assessment with the help of finite element model created in Abaqus/Brigade Plus is compared to the results obtained for the analytical model. For more information about this fatigue assessment method see chapter *4.4 - The Palmgren-Miner cumulative damage method*.

In figure 5.12 the difference in result for the different fatigue assessment methods are shown. Note that for the damage equivalent method fatigue cracking mode B, C, D and F are investigated. On the other hand, for the Palmgren-Miner method fatigue cracking mode A, B, C and D are investigated instead. Finally, note that for the Palmgren-Miner method in conjunction with the finite element method mode A and B sustains miniscule amount damage, see Appendix A for exact values.

Note that fatigue cracking mode A is not implemented for the damage equivalent method when used in conjunction with the finite element model. Therefore it is not included diagram. The damage equivalent method has not been implemented since it is not intended to be used with the finite element method in this parametric study. Nonetheless, the other fatigue cracking modes is partly implemented and is used here as a reference since the damage equivalent method has a linear behaviour in contrast to the Palmgren-Miner method.

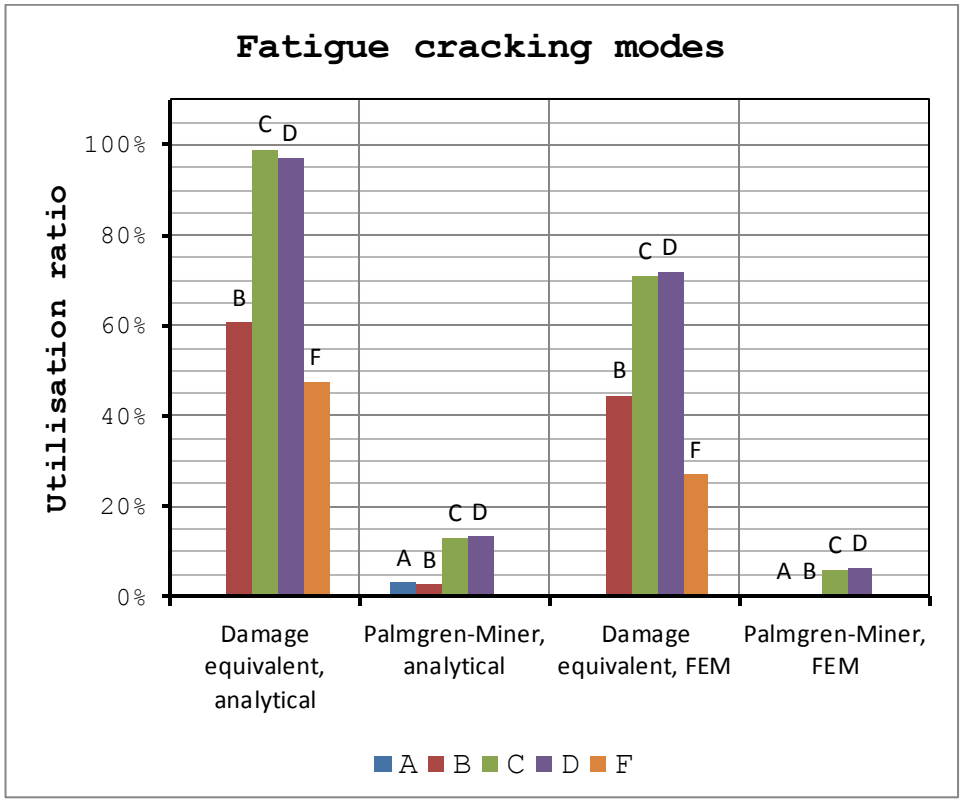

Figure 5.12: *This diagram shows the utilisation ratio for the different fatigue cracking modes which are obtained through different fatigue assessment methods. This is the original design with 40m span and low fatigue load.*

For the damage equivalent method the finite element method yields values that are between 70-74% of the values obtained by the analytical solution. In a similar way the damage that is given by the finite element method and Palmgren-Miner method is also lower than for the corresponding values of the analytical solution.

For the exact values, please see Appendix A.

5.3 Comparison of carbon steel and stainless steel

One of the major competitors to stainless steel bridges is without a doubt the carbon steel alternatives. Thus it is of great interest to compare the performance of the different materials. The performance is compared with regard to mechanical behaviour and with regard to economic viability.

The economical parameters are both uncertain and fluctuate with time and conditions. Therefore the study of the economic cost includes both high and low estimates of the cost in order to take the uncertainty into account.

Furthermore, note the costs which are considered in this study are the costs directly tied to the steel grade. In more detail, only the cost of the steel, paint and maintenance are considered. Also, observe that the maintenance cost which occurs during the service life is discounted to a present value. This is done using simple economical models that depends on a fixed interest rate. This is done in order to obtain more realistic and reliable results.

There are two studies performed for the stainless steel. In the first study the original design is compared to corresponding carbon steel alternatives of grade S355 and S460. Since the comparison is made to the original design the carbon steel alternatives are designed with a regard to a low fatigue load and a design life of only 80 years. In addition the fatigue limit state is assessed with the damage equivalent method for the design.

In the second study the span length is kept at 40m, but the fatigue load is increased to medium and the design life is taken as 100 years. Furthermore, the fatigue limit state is designed with regard to the more advanced Palmgren-Miner method for the fatigue limit state.

Finally, the second study also incorporates the stainless steel design with higher fatigue strength. Further information about the potential of inherently higher fatigue strength of stainless steel compared to carbon steels is discussed in chapter *2.3 - Fatigue of stainless steel*.

The aim is to give clear indications of the difference between stainless steel designs in comparison to alternative carbon steel designs.

5.3.1 Comparison of steel grades for 40m span and low fatigue load

In this comparison the two carbon steel grades S355 and S460 are considered and compared with the stainless steel alternative of grade EN1.4162. The bridges are chosen with a span length of 40m, a low fatigue load and short design life of 80 years. Finally, the fatigue limit state is assessed with the damage equivalent method.

The utilisation ratios for the respective limit state can be found in figure 5.13. As can be seen in the diagram the utilisation ratios for the EN1.4162 and S460 alternatives are very similar. This result is expected since the steel grades in most regards have the same properties.

Worth mentioning is that the stainless steel alternative has a larger deflection than the corresponding S460 alternative. The increased deflection is an inherent property of the stainless steel since it has a lower modulus of elasticity. Further information about the modulus of elasticity for stainless steel can be found in chapter *2.1.1 - Basic mechanical properties* as well as in chapter *2.4.1 - Covered by the standard*. Alas, even with a simplified and conservative calculation of the deflection it remains low for all the considered steel grades.

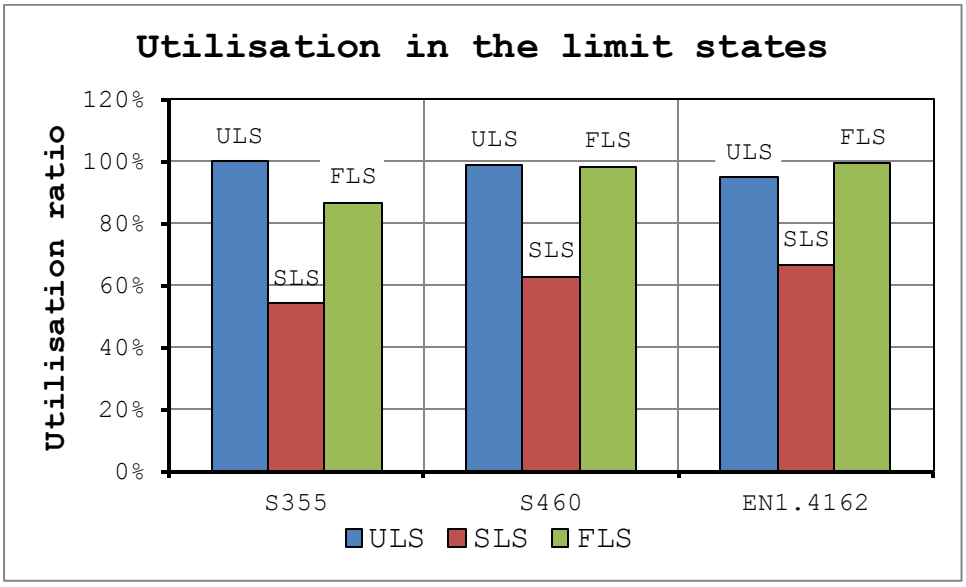

Figure 5.13: *This diagram shows how the utilisation ratio for the different limit states for each steel grade that is considered in this thesis. The design is performed with regard to the damage equivalent method for low fatigue load and 40m span.*

When comparing with the more common S355 carbon steel alternative it becomes apparent that the fatigue limit state is not the governing mode. This could potentially be changed in the design by optimising the structure further. However, this would imply large changes to the original design which is undesirable for the purpose of this study. Therefore the ultimate limit state is limiting the design both at the mid span and at support region for the S355 alternative. For further data about the individual utilisation ratios see Appendix A.

As mentioned there are three main factors that determine the final cost of the bridge. The first, which is investigated here, is the steel grade. The two other factors are the amount of steel needed and, for carbon steel, the exposed surface area of the bridge. Since stainless steel doesn't require any painting the size of the surface area becomes of little to no concern.

The surface area and the amount of steel needed for each alternative can be found in figure 5.14 and figure 5.15 respectively. The pattern that can be observed in the two diagrams is that the S355 alternative requires the most steel in addition to having the largest exposed steel area. On the other hand, the S460 alternative performs slightly better than the stainless steel alternative.

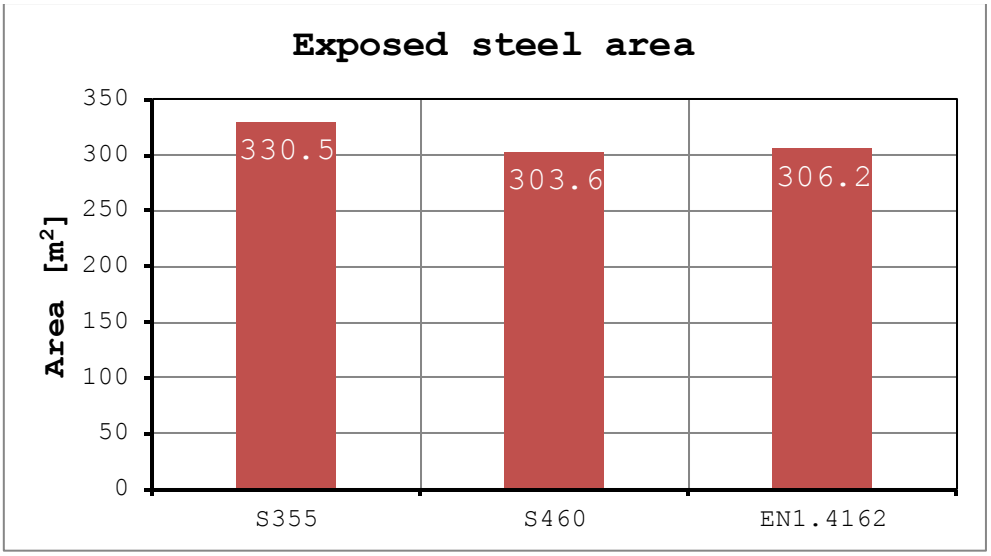

Figure 5.14: *This diagram shows the amount of exposed surface area of the steel with regard to the chosen steel grade. The design is performed with regard to the damage equivalent method for low fatigue load and 40m span.*

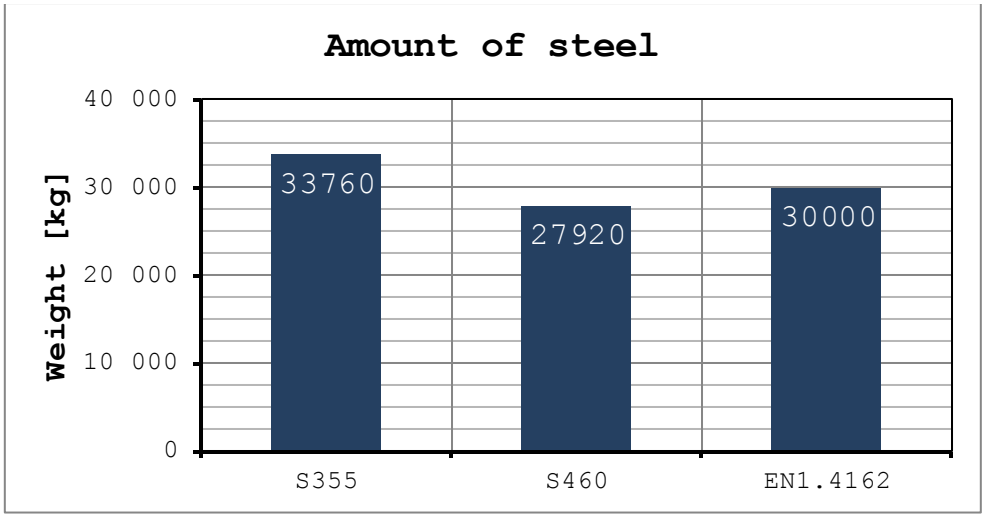

Figure 5.15: *This diagram shows the amount of steel, by weight that is required with regard to the chosen steel grade. The design is performed with regard to the damage equivalent method for low fatigue load and 40m span.*

The importance of both the amount of steel and the exposed steel area can be seen in the cost of each bridge alternative. A high and low estimate of the costs can be found in figure 5.16 and figure 5.17 respectively.

As can be seen the higher cost of stainless steel is partially or fully offset by the high maintenance cost for the carbon steel alternatives. Note that the maintenance included for the stainless steel alternative will only consist of a fraction of the total cost. This stands in contrast to the carbon steel which will require maintenance that cost on the magnitude 50-75% of the initial cost of the steel.

The maintenance cost is related to both the maintenance and renewal of the paint as well as the need for in-depth inspections of the structure. As can be seen in further detail in the data found in Appendix A the major part of the maintenance cost is pertaining to the painting. Consequently the inspections constitute a smaller, but yet significant part of the maintenance cost.

For the low estimates of both the initial cost and maintenance cost the bridge alternatives perform relatively evenly. Note that the S460 alternative in total has the lowest cost due to lower material consumption and smaller surface area. The stainless steel also performs quite well despite the higher initial cost of the steel. Compared to the S460 the alternative the cost of the stainless steel is 3% higher while the cost of the S355 alternative is 12% higher.

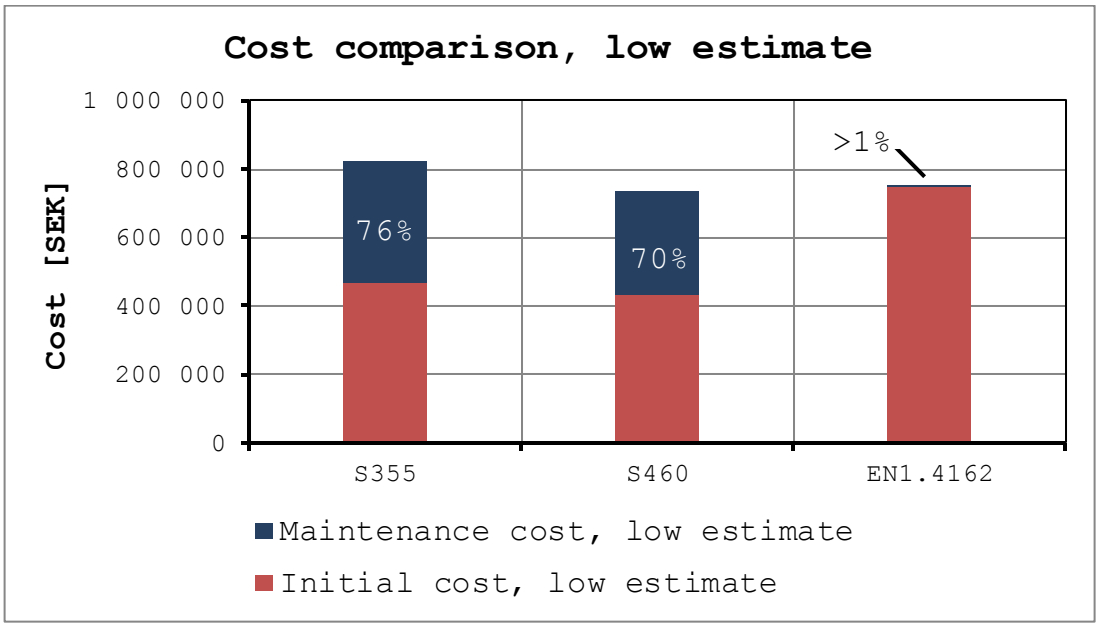

Figure 5.16: *This diagram shows how the estimated cost pertaining to the chosen steel grade. The maintenance cost is also shown as percentage of the initial cost. The design is performed with regard to the damage equivalent method for low fatigue load and 40m span.*

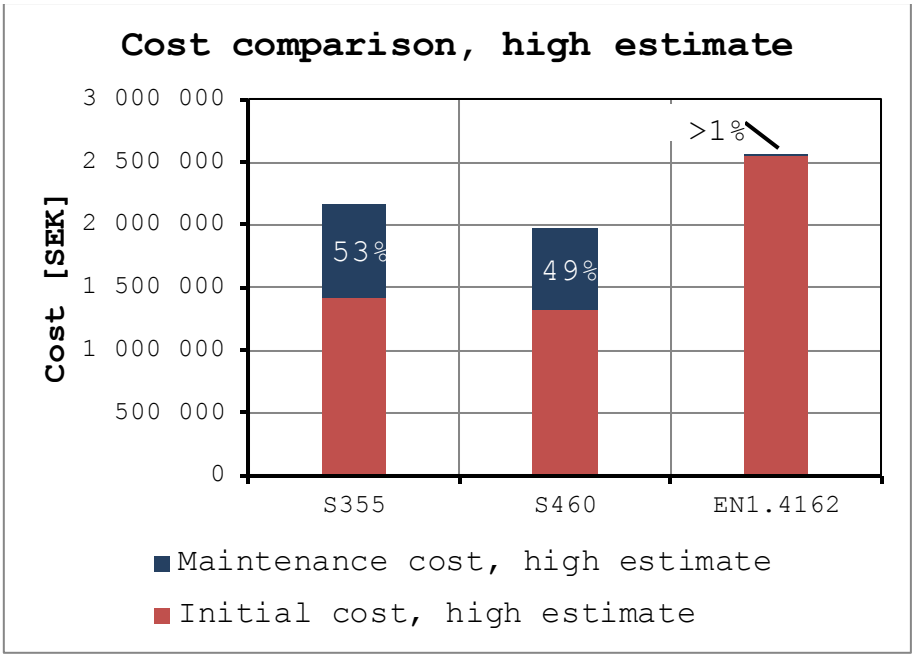

Figure 5.17: *This diagram shows how the estimated cost pertaining to the chosen steel grade. The maintenance cost is also shown as percentage of the initial cost. The design is performed with regard to the damage equivalent method for low fatigue load and 40m span.*

For the high estimates of both the initial cost and maintenance cost the disparity is larger between the alternatives. However, the S460 alternative still remains the alternative with lowest cost. The S355 grade also remains more expensive, but the S355 alternative now has only a 9% higher cost. The major difference is that the higher initial cost has made the stainless steel about 29% more expensive than the S460 alternative.

Further information and data on the comparison of the steel grades can be found in Appendix A.

5.3.2 Comparison for 40m span and medium fatigue load

In this study the three steel grades S355, S460 and EN1.4162 are once again compared. However, now the fatigue load has been increased to medium load and the design life is increased to 100 years. In addition, the more advanced Palmgren-Miner method is used for the fatigue assessment.

Moreover, for the stainless steel there are additional alternatives added with higher fatigue strength than prescribed for the carbon steel and standard stainless steel alternatives. The included additions are a case with improved fatigue strength of mode C and D which assumes that the stainless steel has inherently higher fatigue strength. Two more cases have improved fatigue strength for all of the fatigue cracking modes and are used to investigate the potential benefit of post-weld treatment.

Note that the benefits of fatigue improving post-weld treatment of the carbon steel grades are not considered within this study.

The utilisation ratios of the different methods can be found in further detail in Appendix A. For all of the alternatives both the ultimate and fatigue limit state are kept very close to full utilisation. The deflections on the other hand are not critical for any alternative and are kept between approximately 40 and 60%.

When it concerns the exposed steel area the difference between the steel grades are negligible at less than 1%. The comparison can be seen in figure 5.18. Note that the stainless steel alternative is included only as a reference since the exposed steel area is of little to no concern for the stainless steel. By the same token none of the stainless alternatives with improved fatigue strength is included in this comparison.

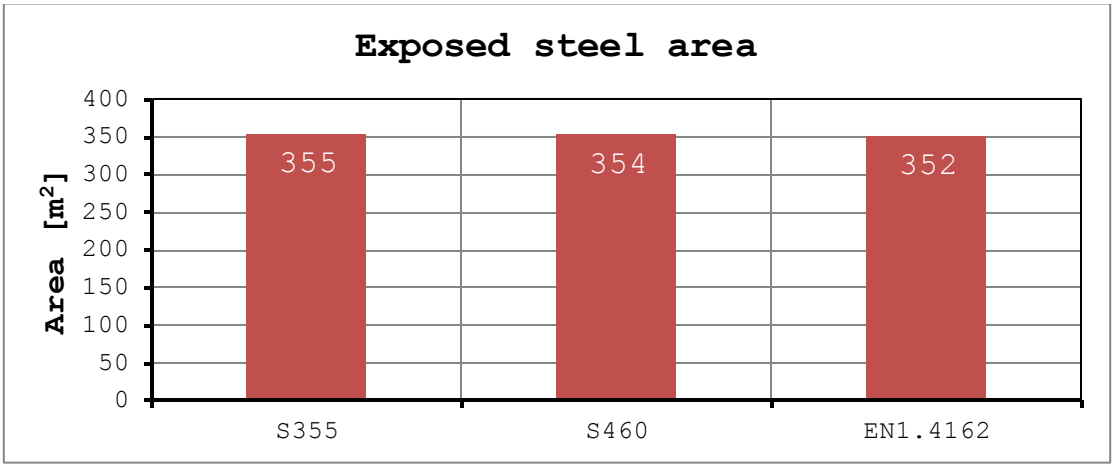

Figure 5.18: *This diagram shows the amount of exposed surface area of the steel with regard to the chosen steel grade. The design is performed with regard to the Palmgren-Miner method for medium fatigue load and 40m span.*

For the steel consumption the difference is more pronounced, see figure 5.19. The higher strength of both S460 and EN1.4162 results in a lower steel consumption for these grades. However, the carbon steel S460, which have a higher stiffness and less buckling, performs better than the stainless steel without higher fatigue strength.

Nonetheless, when higher fatigue strength of the stainless steel is considered, the material consumption decreases drastically. Even for the smallest increase in fatigue strength, which assumes inherently higher fatigue strength of stainless steel renders the stainless steel structure lighter than the S460 alternative. The pattern is repeated for the case of improved fatigue strength classes.

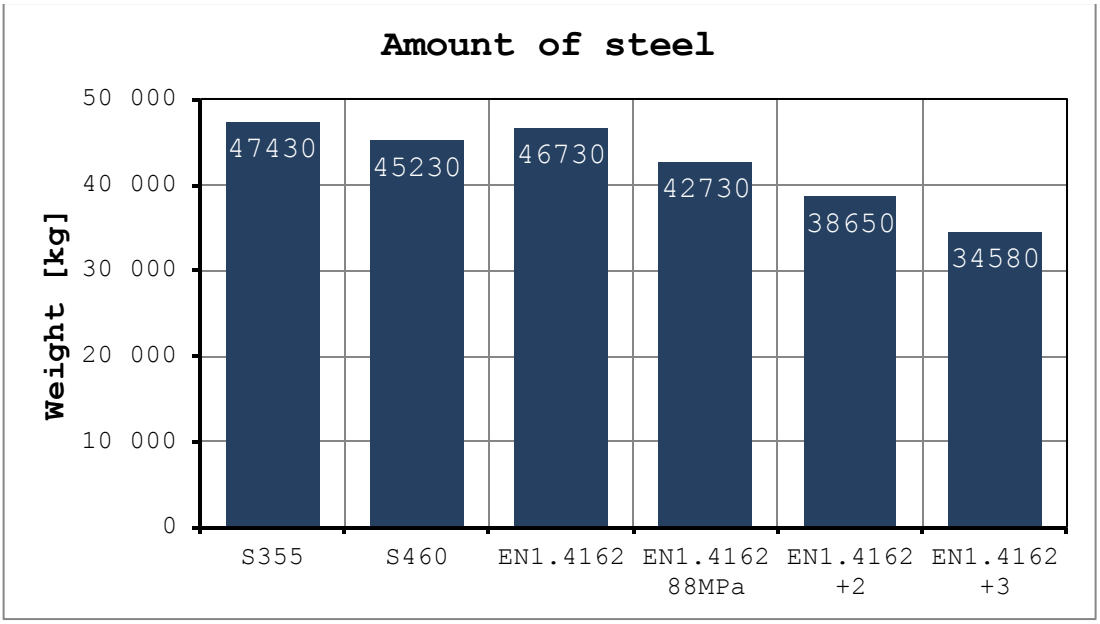

Figure 5.19: *This diagram shows the amount of steel, by weight, which is required with regard to the chosen steel grade and fatigue strength. The design is performed with regard to the Palmgren-Miner method for medium fatigue load and 40m span.*

In more detail, for the stainless steel the material consumption is decreased by 8.6%, 17.3% and 26% for each increase in the fatigue strength. Since the stainless steel doesn't require any substantial maintenance or any additional protective layer this should equate in a proportional decrease in cost.

The low estimate of the initial cost and maintenance cost for the different alternatives can be found in figure 5.20. Notable here is that the carbon steel performs similarly with the S460 alternative being a miniscule 0.5% more expensive than the S355 alternative. The stainless steel is on the contrary more expensive by 12% for the case with standard fatigue strength.

When inherently higher fatigue strength is considered the stainless steel remains more expensive, but only with 2% compared with the S355 alternative. For the post-weld treatment the cost becomes lower than for the carbon steel with 8% and 17% respectively. However, keep in mind that the cost of the post-weld treatment itself is not included in the analysis.

Furthermore, as can be seen in chapter *2.3 - Fatigue of stainless steel* there is no experimental tests to support higher fatigue strength through post-weld treatment. As such the result pertaining to increased fatigue classes serves only as an indication of the potential which post-weld treatment may have. Finally, it should be observed that carbon steels may be improved through post-weld treatment as well.

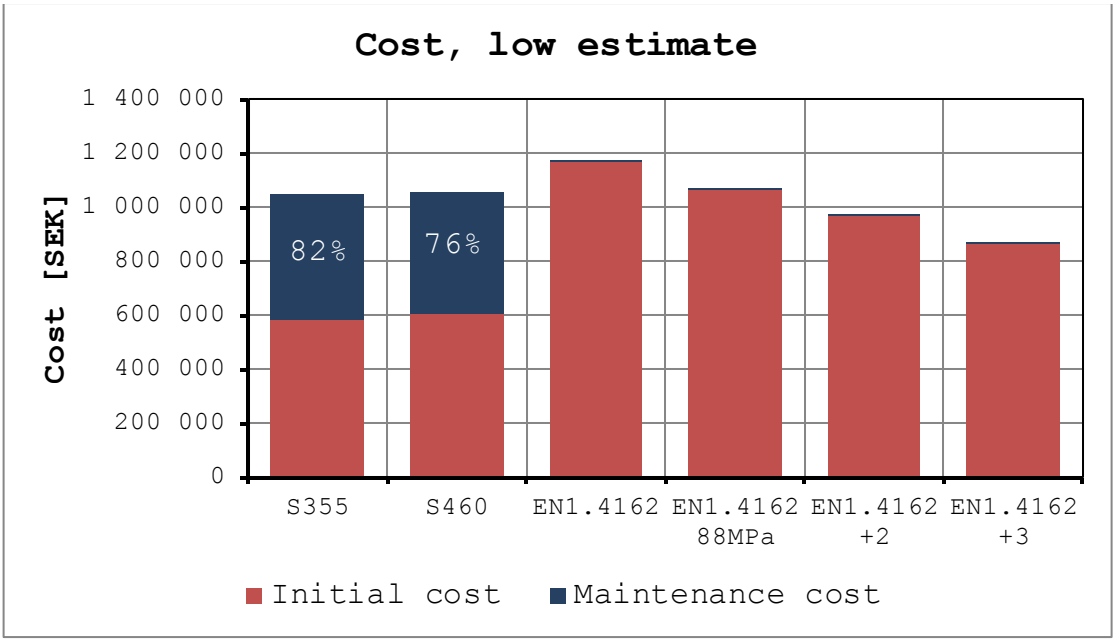

Figure 5.20: *This diagram shows how the estimated cost pertaining to the chosen steel grade and fatigue strength. The maintenance cost is also shown as percentage of the initial cost for the carbon steel. The design is performed with regard to the Palmgren-Miner method for medium fatigue load and 40m span.*

With regard to the high estimate of the cost, which can be seen in figure 5.21, the carbon steel perform persistently better than the stainless steel alternatives. For the stainless steel with standard fatigue strength the cost is 36% higher than for the S355 alternative. The difference decreases with higher fatigue strength, and for the highest fatigue strength the difference is almost negligible at 0.3%.

Furthermore, note that the maintenance cost of the carbon steel is approximately between 50% and 80% of the initial cost of the steel. In contrast, for all of the stainless steel the maintenance is kept below 1% of the initial cost.

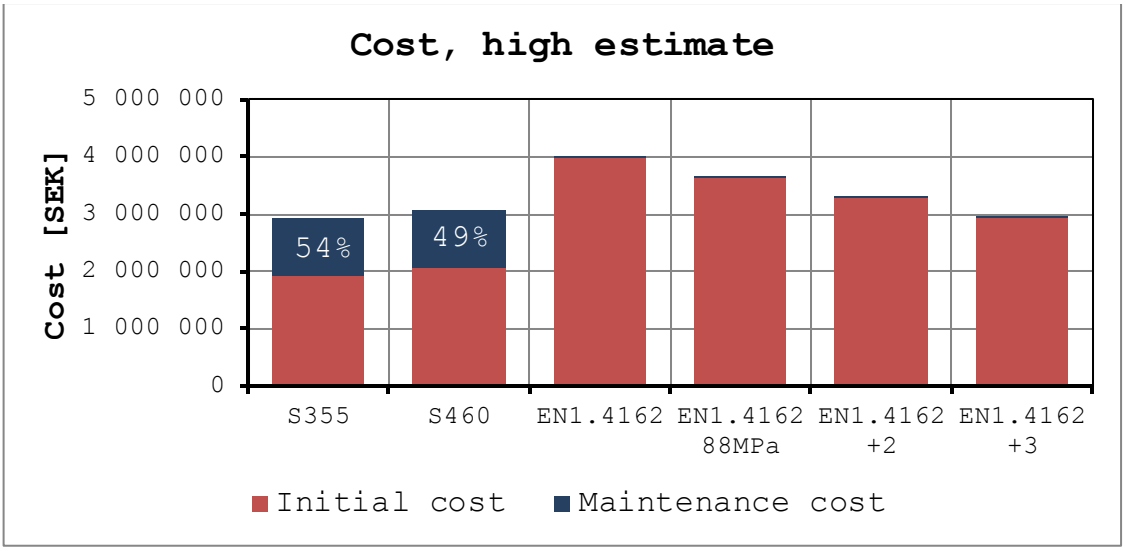

Figure 5.21: *This diagram shows how the estimated cost pertaining to the chosen steel grade and fatigue strength. The maintenance cost is also shown as percentage of the initial cost for the carbon steel. The design is performed with regard to the Palmgren-Miner method for medium fatigue load and 40m span.*

Further information and data on the comparison of the steel grades can be found in Appendix A.

5.4 Influence of improved fatigue strength of stainless steel

In this thesis there are two different ways in which higher fatigue strength can be used for stainless steel in design that has been considered.

The first option is to assume that stainless steel has inherently higher fatigue strength. This assumption is supported by experimental results which are described in more detail in chapter *2.3 - Fatigue of stainless steel*.

The second option is to assume that the fatigue strength can be improved through fatigue improving post-weld treatment. The fatigue improving post-weld treatment has been shown to be beneficial for carbon steel. In this parametric study it is assumed that post-weld treatment can be applied successfully to stainless steel as well.

The study is composed of two parts where the inherently higher strength is investigated for different fatigue loads and different span lengths respectively. In the study of the influence of different fatigue load a span length of 40m is used. For the study of the influence of different span lengths medium fatigue load is applied.

Further investigation of both the inherently higher fatigue strength and the improved fatigue strength through post-weld treatment is treated in chapter *5.3.2 - Comparison for 40m span and medium fatigue load*. Additional data can also be found in Appendix A.

5.4.1 Improved fatigue strength through inherent properties, 40m span and different fatigue loads

In this study the increased fatigue strength of stainless steel is considered. The fatigue strength is assumed to be inherently higher for the stainless steel and applies to the vertical stiffener at the support. Thus fatigue cracking mode C and D has been increased from Eurocode's recommended value of 80MPa to 88MPa. Further information about the fatigue strength can be found in chapter *2.3 - Fatigue of stainless steel.*

Here is considered a span length of 40m and three levels of fatigue load and corresponding design life. The design is performed with the Palmgren-Miner fatigue assessment method.

The utilisation ratios for the different limit states can be seen in figure 5.22. Note that for high fatigue load the utilisation ratio is displayed as 120%. This is done since the design is very close to the fatigue cut-off limit which will cause no damage and yield an utilisation ratio of 0%. Otherwise there are no major differences between the case of increased fatigue strength and the standard case.

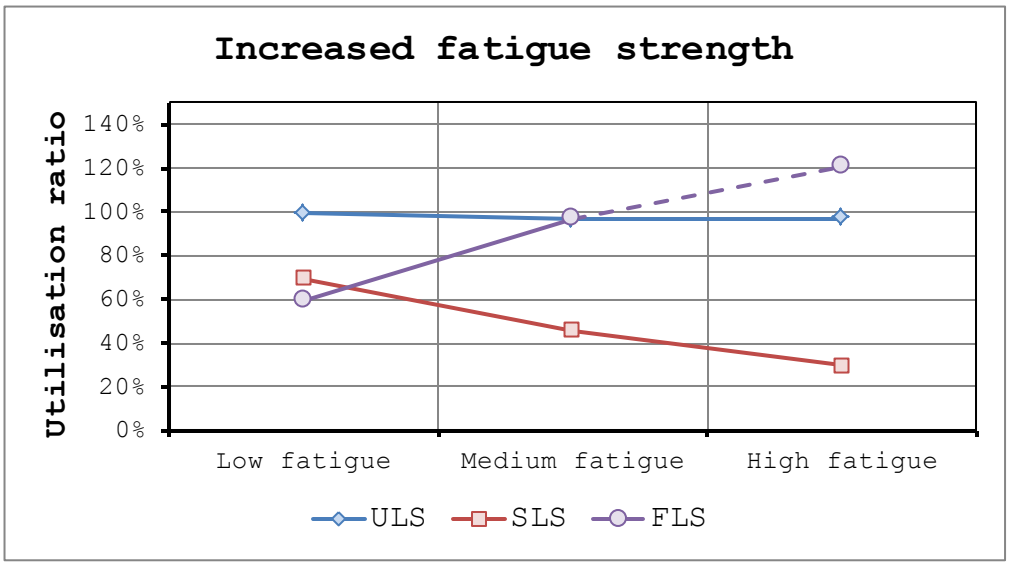

Figure 5.22: *This diagram shows the utilisation ratio in the different limit states for the alternative with higher fatigue strength. The design is performed with regard to the Palmgren-Miner method and a span length of 40m. See chapter 3.3 for explanation of the levels of fatigue load.*

In figure 5.23 the utilisation ratio for each individual fatigue cracking mode is displayed. Note that for all cases the capacity of fatigue cracking mode D remain fully utilised. However, for the case of high fatigue load mode B also has full utilisation and therefore this mode will affect the design partly for the case of higher fatigue strength.

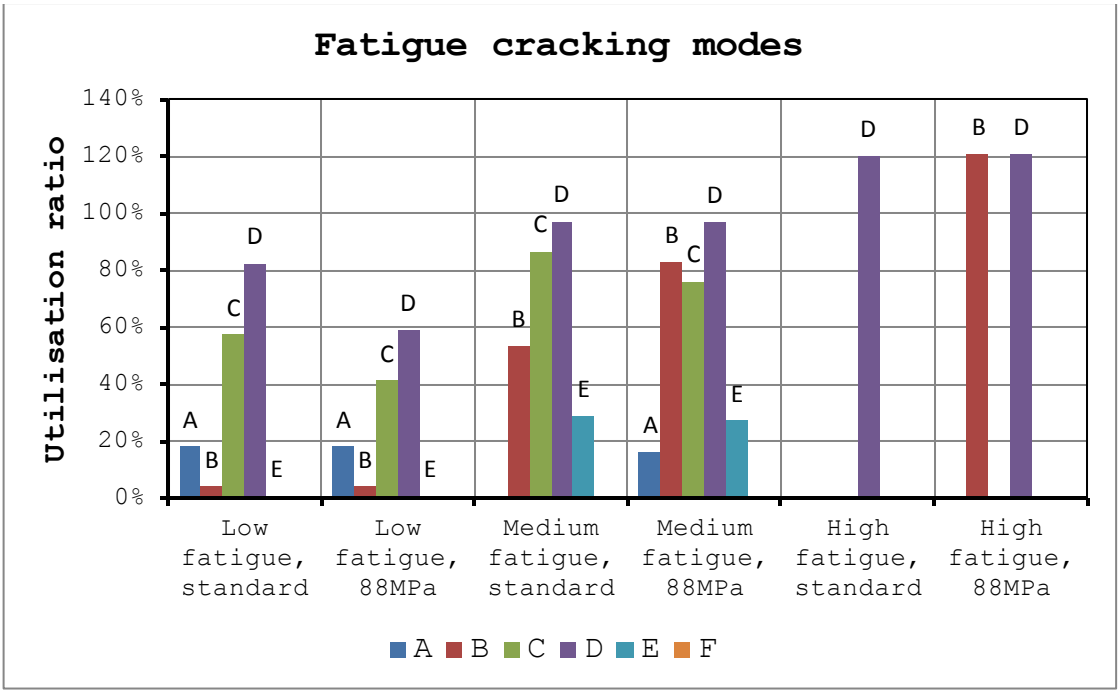

Figure 5.23: *This diagram shows the difference in damage sustained for each fatigue cracking mode for the case of standard and increased fatigue strength respectively. The design is performed with regard to the Palmgren-Miner method and a span length of 40m.*

Finally, the influence of the higher fatigue strength on the material consumption is of great interest. The difference between the original case and the case with higher fatigue strength can be found in figure 5.24. As can be seen, for fatigue loads there will be no difference in the design. Furthermore, there is a larger difference for the medium fatigue load than it is for the high fatigue load.

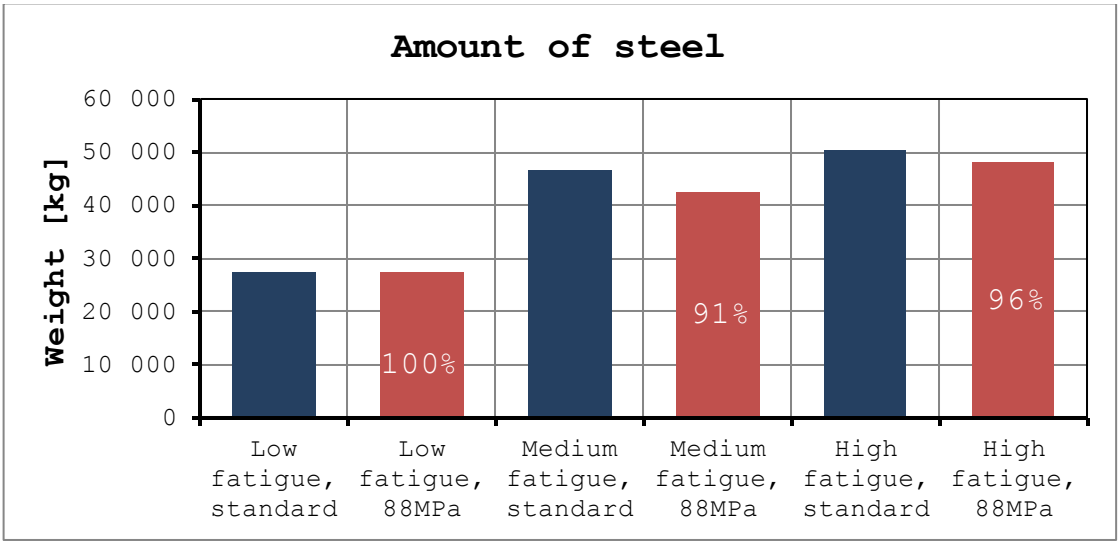

Figure 5.24: *This diagram shows how difference in steel consumption for the case of standard and increased fatigue strength respectively. The design is performed with regard to the Palmgren-Miner method and a span length of 40m.*

For additional data relating to this study, see Appendix A.

5.4.2 Improved fatigue strength through inherent properties, 10 to 70m span and medium fatigue load

Similar to the study in the previous subchapter, this study also consider the increased fatigue strength of stainless steel. The main difference is that here the span length is varied instead of the fatigue load. The fatigue load is taken as a medium load and a design life of 100 years for span lengths of 10m, 40m and 70m. The design is once again performed with the Palmgren-Miner fatigue assessment method.

For the case of medium fatigue load the utilisation in the fatigue limit state is kept at 100% for all the chosen span lengths. See figure 5.25 for the utilisation ratios in each limit state and span length. Note that the ultimate limit state is not fully utilised for the shorter span length of 10m and that the serviceability limit state is never critical. Also note that this pattern is similar to the case of standard fatigue strength investigated in subchapter *5.1.2 - Influence of span length, Palmgren-Miner method*.

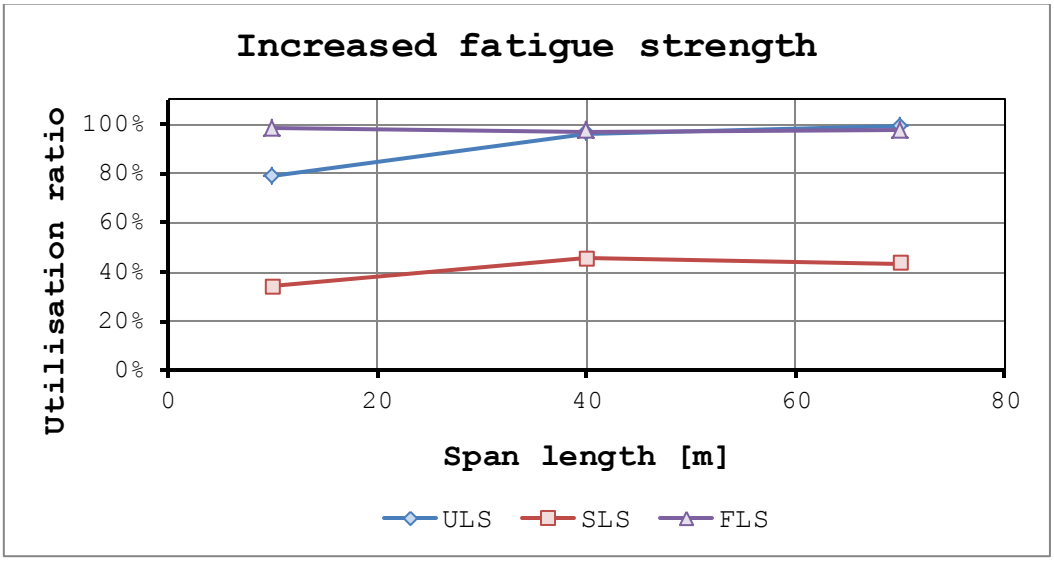

Figure 5.25: *This diagram shows the utilisation ratio in the different limit states for the alternative with higher fatigue strength. The design is performed with regard to the Palmgren-Miner method and medium fatigue load.*

Investigating the individual fatigue cracking modes, it is clear that mode D remains a critical mode in all of the cases, see figure 5.26. Note that for the short span length the fatigue cracking mode E is also critical. However, mode E is limiting the design in the middle of the span while mode D is limiting the design close to the supports.

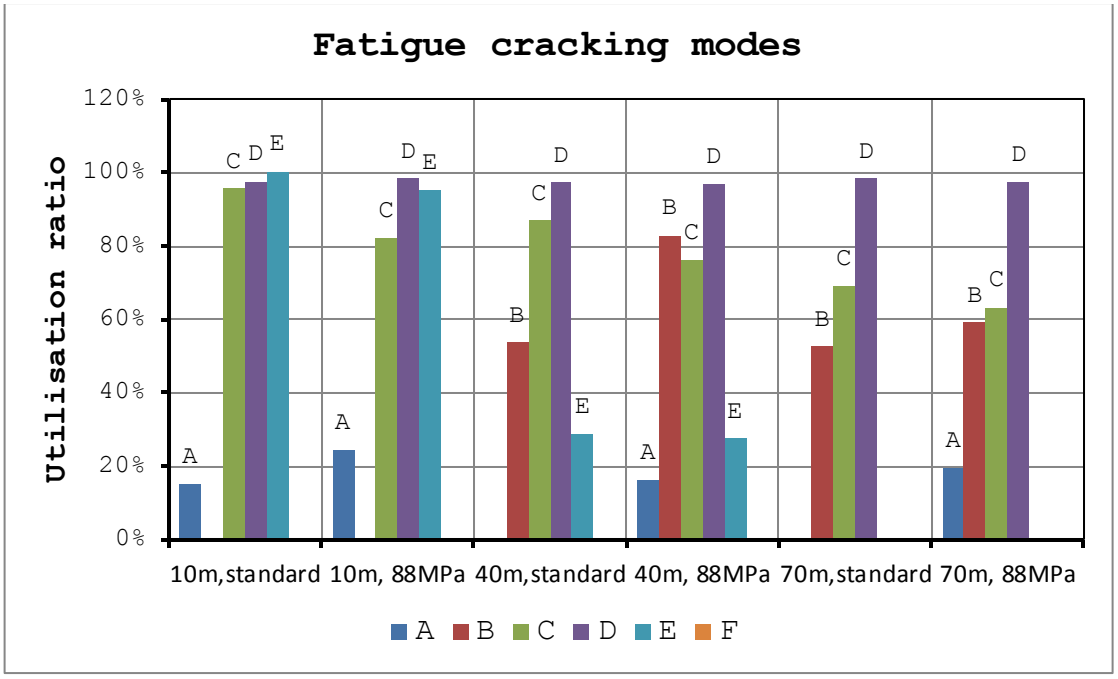

Figure 5.26: *This diagram shows the difference in damage sustained for each fatigue cracking mode for the case of standard and increased fatigue strength respectively. The design is performed with regard to the Palmgren-Miner method and medium fatigue load.*

As usual, it is of interest to see how much the steel consumption can be reduced by assuming higher fatigue strength. The reduction for the current study can be found in figure 5.27. Note that the greatest reduction is achieved for the span length of 40m and declines slightly for longer spans. The short span on the other hand has a markedly lower reduction.

Further results and diagrams pertaining to this study can be found in Appendix A.

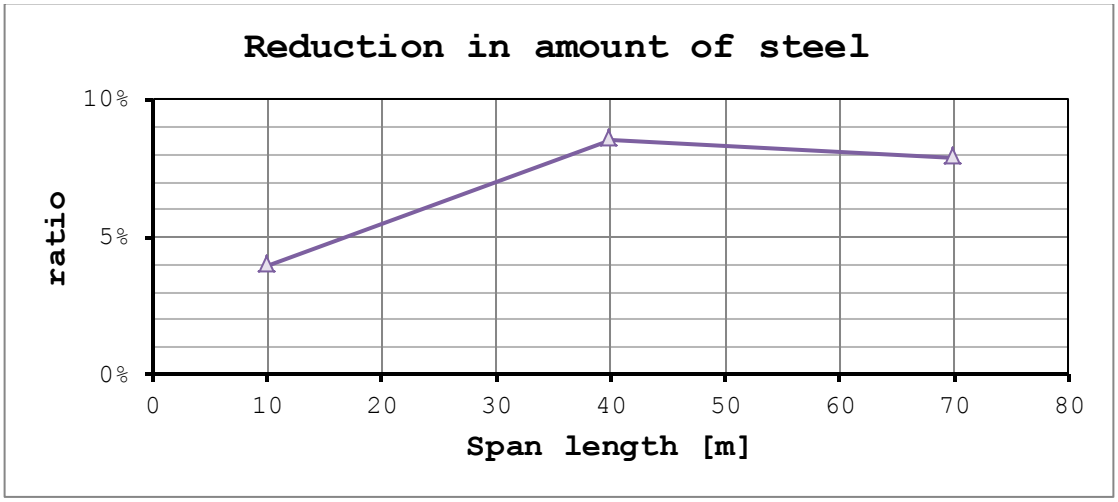

Figure 5.27: *This diagram shows the reduction in the amount of steel for the case of increased fatigue strength in comparison to the case of standard fatigue strength. The design is performed with regard to the Palmgren-Miner method and medium fatigue load.*

6 Conclusions

There are several conclusions which have been drawn from both the literature study and observations made in the parametric study. In this chapter a selection of the most important and interesting conclusions will be presented. As in the previous parts of the report the stainless steel alternative has been compared to the well-established carbon steel alternatives.

In more detail, the parts which are presented pertain to three major subjects; the structural behaviour, the fatigue life and fatigue assessment and, finally, the maintenance and initial cost. A list of the conclusions for respective subject can be found here below.

Conclusions pertaining to the structural behaviour:

- The increased deflection for stainless steel is negligible in this specific parametric study.
- Stainless steel appears to be more prone to buckling, which is supported by both calculations and literature.
- Vertical stiffener at support determines fatigue life in the specific bridge design considered in the parametric study.

Conclusions pertaining to the fatigue life and fatigue assessment:

- For very high fatigue load stresses has to be kept below the fatigue cut-off limit.
- Fatigue improvement has considerable effect. This holds true both when higher fatigue strength is assumed according to test results and for the assumed effect of post-weld treatment.

Conclusions pertaining to the maintenance and initial cost:

- Protective layer affects the initial cost of carbon steel, a cost which is not present for stainless steel.
- Maintenance and maintenance cost for stainless steel is negligible.
- Maintenance cost for carbon steel is significant. In combination with the low maintenance cost of stainless steel it offset the higher initial cost of stainless steel.
- Maintenance cost is highly dependent on the chosen interest rate.

6.1 Motivation for the conclusions

Here is given the underlying motivation behind the conclusions which is presented previously in this chapter. The motivation of the conclusions is intended as a complement to chapter *5 - Results* and *7.1 - Discussion* which presents the result respectively discusses the implications of the results.

Increased deflection for stainless steel is negligible in the parametric study

As described in the literature study the stainless steel has a lower stiffness and modulus of elasticity than common carbon steel. This affects many aspects of the bridge, especially deflections.

However, in the parametric study carried out in this thesis the deflection for stainless steel has not been an issue. In fact it has not been noticeably higher than for the corresponding carbon steel. In effect, when comparing the stainless steel to the high strength S460 alternative the deflection is only a minuscule amount smaller for the stainless steel, see chapter *5.3.2 - Comparison for 40m span and medium fatigue load* as well as the results in Appendix A.

Nonetheless, it should be kept in mind that the stainless steel also requires more material than the S460 alternative, which will result in a larger second moment of area and therefore reduced deflection. In addition, when considering the more common S355 carbon steel, with lower strength and higher material consumption, the deflection was approximately 9% higher for the high strength alternatives.

When comparing the stiffer carbon steel with the stainless steel it is worth mentioning that the contribution from the reinforced concrete deck will become more pronounced when the stiffness of the steel decrease. This is based on the assumption that the concrete deck's design remains unchanged. When the stiffness of the steel is decreased the reinforced concrete will carry more of the load and give a larger contribution to the second moment of area.

Moreover, the deflection remains low for all the cases which have been investigated in the parametric study. In brief this is due to the choice of fixed supports at both ends of the span in combination with pre cambering of the beams. The pre cambering is a simple but effective way to neglect the deflections from the self-weight of the structure. The self-weight may otherwise lead to substantial deflections before the imposed loads are even applied.

To elaborate, the fact that the supports are fixed implies that no rotation can take place at said supports. Since large rotations lead to increased deflection this explains part of how deflections are decreased. Furthermore, the cross-section is also subjected to bending moment of less magnitude since part of the moment is carried by supports. Less bending moment leads to smaller rotation and consequently, less deflection.

Although the supports are considered as rigid in the calculations, the supports are of course not fully fixated in reality. Therefore, a more accurate assumption is that the supports act as partial restraints. This can be modelled with springs. The consequence of the supports being less rigid is that the deflections will increase, since both rotation at the support region and bending moment at middle of the span increase.

An example of a simplification that has been made is that the resistance of the cross-section is taken as a minimum value rather than the actual resistance corresponding to each section, for more details see the calculations in Appendix F. Moreover, for the stainless steel the second moment of area is not recalculated to take into account the decreased stiffness of the steel. Note that these simplifications are conservative, in contrast to the assumption of fully restrained supports.

Alas, while the deflections are kept consistently low in the parametric study, it is important to point out that this should not be assumed to be the general case. As mentioned the special design with fixed supports and composite cross-section leads to smaller deflections for the bridge. Nonetheless, the deflections were not exceedingly higher for the stainless steel, which otherwise could prove to be a drawback.

Stainless steel appears to be more prone to buckling

A distinct difference between the otherwise similar steel grades S460 and EN1.4162 is the inclination to buckling. The stainless steel exhibits a notably higher inclination to buckling in the calculations. The buckling leads to lower cross-section classes and higher reduction factor for the same cross-section. In addition, the calculations which are based on Eurocode can be assumed to be quite accurate and not overly conservative, see chapter *2.4.1 - Covered by the standard*.

The web buckling implies that the web may need to be made less slender by increasing thickness or decreasing height. Alternatively, the web may also be stiffened in order to avoid excessive reduction due to the plate buckling.

Note that the original design considered in the parametric study did not incorporate any stiffener, except at the support. Therefore the web was not stiffened in the parametric study, but was instead allowed to be partially reduced due to plate buckling. The consequence is a slight decrease of the bending resistance, when compared to the carbon steel alternative.

In addition to the web, the slenderness of the flanges is also governed to a certain degree by the plate buckling. However, for the flanges it is easier to allow for thicker and less slender design so that the plate buckling may be avoided. The effect is presumed to be negligible.

To summarise, buckling is an area where the stainless steel have inferior performance when compared to the corresponding carbon steel.

Vertical stiffener at support determines fatigue life

In the current design and for almost all the cases in the parametric study the vertical stiffeners at the supports give cause to the critical fatigue cracking modes. The modes in question are mode C and D, further information about fatigue cracking modes can be found in chapter *4.2 - Fatigue cracking modes*.

These two modes tend to be either the only critical modes or combined with other cracking modes. An exception is when the fatigue is not critical at all, which is the case for very moderate fatigue loads. However the two modes still tend to have the highest utilisation ratio even in these cases.

As explained in chapter *3.1 - Structural behaviour of the Nynäshamn Bridge* the moment at the support in the ultimate limit state is only caused by imposed loads. The fatigue cracking modes C and D have relatively low fatigue strength. The result of this combination is that the stresses caused by the traffic are usually more critical in the fatigue limit state than the ultimate limit state. The exception is when the fatigue load is particularly low.

This is also a reason why the height of the web is increased at the support in the design. The higher web is required to increase resistance of the cross-section at the support region.

However, when comparing the two modes with the damage equivalent method and the Palmgren-Miner method respectively, the results differ slightly. To elaborate, in the damage equivalent method it is mode C that tends to be more critical. On the other hand, for the Palmgren-Miner method it is mode D that tends to be more critical. As previously stated, mode C is caused by principal stress in the web while mode D is caused by direct stress in the flange, see chapter *4.2 - Fatigue cracking modes*.

In fact, this is due to a simplification which is made when using the damage equivalent method. The stress range for mode C is obtained by combining the direct and shear stress into principal stress. However in the simplification for the damage equivalent method the maximum direct and maximum shear is assumed to coincide. This is not the case and thus the real maximum principal stress will be lower than what is assumed in calculations. In contrast, for the Palmgren-Miner method the principal stress is calculated accurately for each position of the load.

Since the real stress spectra is considered in the Palmgren-Miner method the utilisation for fatigue cracking mode D will generally be higher than for mode C. When designing with regard to the Palmgren-Miner method the difference between the modes can often be limited by changing the thickness of the web, which determines the shear stress to a large degree.

To conclude, the design at the support region is highly dependent on the fatigue cracking modes initiated from the vertical stiffener. Additionally, for the more accurate calculation it is the direct stress in the flanges which is tends to be governing.

For very high fatigue load stresses has to be kept below the fatigue cut-off limit

As can be observed in the parametric study, when the highest fatigue load is applied the bridge has to be designed so that the maximum stress for the fatigue cracking modes is kept below the fatigue cut-off limit.

To reiterate, the most severe case of traffic which is considered in this study is traffic category 1 with long distance transports and a design life of 120 years. This traffic category corresponds to 2 million heavy vehicles per slow lane and year. For the long distance traffic the vehicle mix is composed of 50% of vehicle type 3. Vehicle type 3 is also the heaviest of the reference vehicles and therefore tends to cause the largest stress amplitude.

When considering 1 million vehicles per year, half of the total 2 million vehicles per year, during the design life of 120 years it adds up to a total of 120 million load cycles. This is a considerable amount of load cycles. Especially so when put into the context that the cut-off limit for fatigue damage corresponds to 100 million load cycles. Thus, for any stress range which exceeds the fatigue cut-off limit the damage which is caused will be at least 120%. In conclusion, when designing for the worst case scenario the stresses have to be kept under the fatigue cut-off limit.

For shorter span lengths this issue may become more pressing even for less traffic if each vehicle causes multiple stress ranges with similar amplitude. Note that this is partly accounted for in the damage equivalent method by increasing the limit for the damage equivalent factor from 2.0 to 2.5.

To elaborate, the fatigue strength cut-off limit is approximately 40% of the constant amplitude nominal fatigue strength. When the damage equivalent factor is 2.4 it will effectively cause the maximum stress range to be kept under the fatigue cut off-limit. This since the constant amplitude nominal fatigue strength used in calculations will be divided by 2.5 and become 40% of the original value. In conclusion the value will be kept very close to the fatigue strength cut-off limit.

Nevertheless, the fact remains that for very high fatigue load the damage equivalent method underestimates the damage in comparison to the Palmgren-Miner method. Furthermore when the Palmgren-Miner method is applied, only the largest stress range is of importance due to the extremely high number of load cycles.

Fatigue improvement has considerable effect

In the parametric study two cases of increasing the fatigue strength is considered. The increase is attributed to either the inherent properties of stainless steel or by the beneficial effect of fatigue improving post-weld treatment.

When considering the higher fatigue strength of stainless steel the stainless alternative will perform better than the corresponding carbon steel grade S460. In comparison, when the standard fatigue strength is considered the S460 alternative performs better, for the results see chapter *5.3 - Comparison of carbon steel and stainless steel*.

In a bit more detail, the inherently higher fatigue strength will yield a design which requires less material than both the original design and that of the S460 carbon steel grade. When the fatigue is improved further, which is done to indicate the effect of post weld treatment, the amount of steel can be reduced even further. For each step the fatigue strength was increased the steel consumption was reduced by approximately 10% in each consecutive step.

The significant decrease in material consumption proves that improved fatigue strength post-weld treatment is very beneficial. Since the initial cost of stainless steel is relatively high any saving in material would lead to substantial savings in cost.

Moreover, for the case of inherently higher fatigue strength the influence was also investigated for different span lengths and different fatigue loads. Here the effect was most pronounced for medium to long spans and medium amount of fatigue load. It should be noted that for low fatigue load the fatigue is never critical, thus the improved strength has no beneficial effect.

Not to mention, for very high fatigue load and high amount of load cycles the design has to be close to the fatigue cut-off limit. In this case the improved strength is definitely beneficial, however not as distinct as in the case with more moderate amounts of fatigue load.

To summarise, both the post-weld treatment and the inherently higher fatigue strength has proven to be beneficial by reducing the material consumption for stainless steel. Unfortunately, for post-weld treatment there is no data or testing that indicates the magnitude with which the fatigue strength may be improved. On the other hand, the inherently higher fatigue strength is of special interest since it would not require additional cost or work to be utilised in any design.

Nevertheless, the higher fatigue strength of stainless steel is currently not accounted for in Eurocode, see chapter *2.4.2 - Not covered in the standard*. The tests made support the assumption of higher fatigue strength. However, while showing promising results the amount of testing is not sufficient to allow the increased fatigue strength to be accounted for. Therefore more extensive testing has to be performed before the increased fatigue strength may be utilised in calculations and implemented in the code.

Protective layer affects the initial cost of carbon steel

For carbon steel the initial painting constitute an important part of the initial cost of the steel girders, see Appendix A. For the low estimate of the cost of the steel the initial paint will correspond to almost half of the initial cost. If the high estimate is used instead the cost will surmount to a more modest 20% of the total initial cost of the girders.

In conclusion, already at the manufacturing level of the bridge, stainless steel shows clear advantages. This allows for at least partial off-set of the otherwise higher cost of stainless steel.

Maintenance and maintenance cost for stainless steel is negligible.

As described in the literature study, one of the main advantages of stainless steel is that it doesn't require any major maintenance, see chapter *2.5.2 - Benefits of stainless steel in bridges*. In fact, only routine inspections are considered to be needed in the parametric study. Therefore the maintenance cost becomes negligible since the inspections are relatively inexpensive and infrequent. As a result, for all the cases where the maintenance cost was investigated the cost fell below 1% of the initial cost of the steel.

To be fair, the estimate is quite rough and also yields what presumably are unrealistically low values for bridges with short spans. Notwithstanding, the maintenance cost of stainless steel should remain negligible in most cases.

Maintenance cost for carbon steel is significant

For carbon steel, in contrast to stainless steel, the maintenance constitutes a substantial part of the total cost of the bridge, see chapter *5.3 - Comparison of carbon steel and stainless steel*. The cost of maintenance for stainless steel is generally estimated at 50-80% of the initial cost of the steel girders. Note that the high strength steel grade S460 tend to have lower maintenance cost and higher initial cost compared to the S355 grade.

Nevertheless, in the case of a low initial cost estimate the high estimate of maintenance cost may become up to 177% higher than the initial cost. While this may be an extreme case it still indicates the importance the maintenance cost has for carbon steel alternatives.

For carbon steel the main maintenance cost originates from the maintenance of the protective layer in combination with inspections. The maintenance of the protective layer, for example paint, brings a large but infrequent cost. On the other hand, the carbon steel also requires more relatively expensive in-depth inspections. The in depth inspections will unlike routine inspections lead to significant costs. The inspections, which are required more regularly than repainting, constitute approximately 25-45% of the total maintenance cost.

The cost of maintaining the protective layer is presumed to be proportional to the exposed area of the steel. Thus, the size of the exposed steel area naturally becomes of importance. Note that with lower material consumption the area tends to decrease, though not as much. However, the exposed steel area to the amount of steel is shown to increase for shorter span length, see chapter *5.1 - Influence of the span length*.

All things considered, the maintenance cost constitutes a notable part of the total cost of the carbon steel. However, due to variation and uncertainties it is hard to give an accurate estimate of the exact magnitude. In addition, for the S460 grade the importance of maintenance is lessened compared to the S355 grade. However, both grades have a much higher maintenance cost than that of stainless steel.

Maintenance cost is highly dependent on the chosen interest rate

Finally, the cost of maintenance is very much dependent on which interest rate is used. If a high interest rate is used the importance of future costs will be diminished. Since the higher initial cost of stainless steel is offset by the higher maintenance cost of carbon steel, the interest rate which is chosen is of great importance.

For maintenance costs the present value of the costs should be considered. The present value of the cost takes into account the interest rate. In addition to the present value of each individual cost there is a theoretical limit for repeatedly occurring cost, like for example inspections. In short, if the cost continues for a long time the resulting present value of the cost will approach a certain limit.

In the parametric study two levels of interest rate has been used, at 3.5% and 1.5%, for the high and low estimates of the maintenance cost. For the high interest rate the total present value of the costs will become approximately 94% for a design life of 80 years and 98% if the design life is increased to 120 years. Thus an increase to the design life will only affect the present value marginally.

Conversely, for a lower interest rate the present value of a repeated cost will be go from 70% to 84% when the design life is raised from 80 to 120 years. Since the theoretical limit is more than twice as high the cost will however always be higher for the case with lower interest rate.

To summarise, the maintenance cost is not just determined by the amount of costs alone. The rate of interest is just as important to consider and also the time at which the costs occur. With a high interest rate future cost and maintenance become of much less importance. Furthermore, a longer design life of a structure may therefore not

necessarily lead to a noticeable increase in maintenance cost due to the compounded interest rate.

7 Discussion and Recommendations

After the literature study, the parametric study, results and conclusions, a lot of information about stainless steel has been obtained. This chapter aims to discuss some of the more noteworthy aspects of stainless steel as well as attempting to answer some of the more important questions about the use of stainless steel in the field of structural engineering.

This chapter includes three sections, namely; Discussion, recommendations and finally about the weaknesses of this thesis. Of course, this chapter includes reflections and observations from the authors themselves.

7.1 Discussion

This section aims at giving reflections and more in depth interpretations of the conclusions and findings within this report. Also included are the possible implications of the results and conclusions.

To make the discussion more comprehensible and accessible, it has been broken down into the following sections:

- Is stainless steel a superior option compared to carbon steel?
- An additional note about the economy of stainless steel
- About the fatigue capacity of stainless steel.
- Experience in the structural engineering industry
- When should stainless steel be considered?

Is stainless steel a superior option compared to carbon steel?

This is to a great extent one of the more central questions for this thesis. Much like any good question it demands and equally good answer. However, there is not a single short answer. With this in mind, the question has been broken down into sections, which are the following:

- *Is stainless steel superior from an economical point of view?*
- *Is stainless steel structurally superior material?*
- *Are there ethical and environmental implications of stainless steel?*

Economy

Without doubt, it is indeed possible to use stainless steel in the field of structural engineering. As a matter of fact, it has already been done on occasion. However, much hinges on the fact whether stainless steel is more economically viable than carbon steel. Unfortunately, this is the complicated question with many answers.

First and foremost, the stainless steel material itself is more expensive than that of carbon steel. Consequently, there must be some saving in material consumption, manufacturing or maintenance for stainless steel to be worthwhile from an economical point of view. Fortunately, this is the case as both material consumption can be reduced somewhat and maintenance cost is significantly lower.

Also, when considering short time investments or bridges with a relatively short life expectancy, stainless steel is likely going to be a more expensive alternative than that of carbon steel. In addition, besides being a more expensive in shorter time spans, there are no significant structural benefits of using stainless steel. Barring the fact that cross section can be made more slender due to the high strength of stainless steel.

However, most bridges that are erected in modern times have a considerable life expectancy, ranging from approximately 80-120 years. In these time frames, stainless steel is a rather promising alternative from an economical point of view. As shown in the parametric study, the maintenance cost ranges from approximately 25-80% of the initial cost for carbon steel. Whilst at the same time being insignificantly small for stainless steel, being approximately 1% of the initial cost. Consequently, for long term investments, stainless steel shows great promise of reducing the total cost of the bridge.

An additional noteworthy aspect pertaining to long service life for steel bridges is where the cost takes place in time. For carbon steel, the total cost is spread over a rather large timeframe. While stainless steel to the contrary entails most of the cost in the initial phase of the bridge. In other words, less currency is spent on maintenance whilst material cost increases. This is arguably somewhat of a benefit for stainless steel as it gives more steady cost assessments.

So far, it appears that stainless steel is a better option when considering long term investments. However, there are more aspects to consider, especially price fluctuations.

As already stated, stainless steel has a higher material cost than that of carbon steel. This is due to the alloys used in stainless steel. A noteworthy aspect of these alloys is that the raw material cost fluctuates considerably compared to carbon steel. In extreme cases, the price of stainless steel does not only vary on a daily basis, but also during different times of the day. This makes the price of stainless steel material rather precarious. When the price fluctuates, there is an inherent degree of risk and insecurity, which in turn leads to increased cost as “risk money” is added for stainless steel.

There are some measures that are implemented to circumvent the worst of the fluctuations. Especially noteworthy is the substitution of nickel with nitrogen, since nickel is both expensive and the price fluctuates.

So for, it appears that stainless steel is somewhat more expensive than it ought to be due to price fluctuations as. Still, even so stainless steel is a better alternative for long term investments.

However, although this thesis only discusses it outmost briefly, there are still people who make the decisions of which material should be used for a given bridge. These people might not be overly inclined to opt for an alternative that is more expensive today for cost saving in a future which might be far off for them. As shown in the parametric study, the time required for stainless steel to be economically beneficial is several years. It should be acknowledged that decision makers might be less disposed to repayment plan of for example 50 years.

The last important aspect of economy is what rate of interest a given contractor or company uses for future cost. If the rent is sufficiently high, the value of future money is sufficiently low that the time of repayment becomes nothing short of incongruously long. In fact, in some cases the initial cost may never be repaid no matter how long the service life. Conversely, if the interest rate is sufficiently low, stainless steel tends to be economically superior to that of carbon steel for long term investments.

To conclude the aspect of economy, stainless steel is more expensive in the initial phase of the bridge. However, in long term perspective stainless steel is in many regards a superior alternative. However, it is highly dependent on the interest rate and the initial cost of stainless steel.

Material properties

When comparing stainless steel with carbon steel from the viewpoint of material properties, there are; similarities, advantages and disadvantages alike.

The advantage of stainless steel is that there is an increased proof strength and ductility. Test data also suggest that stainless steel might have a superior fatigue strength compared to carbon steel. Test data shows that the fatigue strength sometimes is significantly higher than that of carbon steel. This is an aspect that deserves some emphasis due to its importance. The fatigue strength of stainless steel is discussed a bit later within this chapter.

One of the greater advantages of stainless steel lies in its superior corrosion resistance. If correctly implemented, the corrosion is miniscule and there is practically no upper limit on how durable stainless steel is relation to corrosion. Of course, this does not imply that stainless steel is everlasting in any sense.

There are also disadvantages to consider for stainless steel. Among other items, stainless steel has a somewhat lower Young's modulus of elasticity, about 200GPa for duplex stainless steel compared to 210GPa for carbon steel.

However, as stated in the literature study, stainless steel does not have a pronounced yield limit. Though it might sound somewhat benign and easily circumvented by implementing proof strength, the fact is that stainless steel has another structural response than that of carbon steel. As shown in the parametric study, instability and buckling is more severe for stainless steel than carbon steel. This is observation is further justified by test data, which states that stainless steel is more prone to buckling than carbon steel.

To conclude, stainless steel has a higher ultimate strength, on par with high strength carbon steel. In addition, research suggests that the fatigue strength is considerably higher. Though stainless steel also entail more austere instability and a structural response that differ somewhat to that of carbon steel. Still, from a structural point of view stainless steel shows a lot of potential, even though it is not exclusively so.

Ethical aspects

As with most technologies, they are implemented to improve or benefit mankind, albeit sometimes to a much localised degree, Of course, there are additional aspects of technology, that is however a somewhat philosophical debate that goes beyond the scope of this thesis.

However, a brief section is dedicated to discuss the ethical implications of implementing stainless steel. This also includes the environmental aspects of stainless steel.

That being said, stainless steel does not differ much from carbon steel on a larger scale. Even though the knowledge and introduction of steel has affected early human history to a considerably degree, the introduction of stainless steel will most likely not result in a major turning point of cataclysmic proportions. In short, stainless steel appears to have no direct cost of human living conditions.

However, the environmental aspect of stainless steel deserves some attention. Stainless steel does not corrode readily nor does it require any maintenance in form of protective paint coating. Protective paint is quite toxic and often entails a detrimental effect on ecosystems in the immediate vicinity. Moreover, the detrimental effect can be further enhanced if water helps spread the paint components. However, as stainless steel does not require protective coating, this issue is circumvented to the benefit of both stainless steel and the ecosystem.

Concluding statement

There are several advantages of stainless steel which makes it a promising alternative to carbon steel. To reconnect to the initial question; whether stainless steel is a superior alternative. The short answer is that sometimes stainless steel is superior. Though the conclusion is not as simple as stainless steel being superior in every aspect, instead it does point out that carbon steel is not always the optimal choice.

Stainless steel is especially promising when dealing with corrosive environments, such as marine or coastal. Moreover, the material indicates towards a lot of potential when dealing with higher stress amplitudes and fatigue loading. Which are of interest if slender cross sections and long service life is desired.

Additional about the economy of stainless steel

Another topic worth discussing pertaining to the economy of stainless steel is that stainless is most likely considerably less expensive than structural engineer imagine it to be.

There are several supporting arguments for this statement. Firstly, contractors and workshops alike have little to no experience with stainless steel. This holds true at least when Sweden is considered, although it is a valid statement for almost any given European country as well. When companies are unfamiliar with a material, they see it as a greater risk due to inexperience. As such, companies add extra cost to the material itself. In short, stainless steel is somewhat more expensive for the sole reason of inexperience within the field of structural engineering and steel workshops.

An additional reason to why stainless steel is more expensive is due to the fact that it does not draw the full benefit of mass production. To elaborate, stainless steel for construction industry is somewhat unusual. Thus, stainless steel plates for instance are produced in lower volumes compared to carbon steel plates. In other words, stainless steel beams is attributed with an additional cost due to the fact that it is not a common structural material.

Lastly, as comment from the authors of this paper, there appears to be a tendency to simply overestimate the true cost of the stainless steel. In short, engineers and mechanics tend to overestimate the price of stainless steel somewhat. To exemplify, during this master thesis, the authors did not find anyone that underestimated the price though on several occasions the price was overestimated. Though, this is only a comment and observation. There is no reliable supporting fact, study or the like. As such, this paragraph should be used with caution.

To conclude this section, there are a few reasons to why stainless steel is more expensive than necessary. These costs are not connected to extra work, more expensive material and such, but rather, due to the inexperience within the field of structural engineering. As such, it is reasonable to assume that stainless steel is likely to become cheaper if stainless steel were to be used to a greater extent.

How is the fatigue capacity of stainless steel?

The fatigue strength is especially relevant, or *critical* if you will, for road- and railway bridges. Both of which are subjected to high stress amplitudes and frequent cyclic loading during service life. Thus, the delimitating circumstance for many steel bridges is the fatigues strength. Thus, this section is dedicated to answer whether stainless steel entails better fatigue characteristics than that of carbon steel.

From the conclusions chapter we obtain the following statements:

- In the current standard, Eurocode, the fatigue strength of stainless steel is neither higher nor lower than that of carbon steel. In short, stainless steel has no additional benefits when standards are considered.

- Test data however suggests that the fatigue strength of stainless steel is as high, higher or considerably higher than that of carbon steel.

- Post weld treatment is a promising alternative to increase the fatigue strength of carbon steel. In theory, there is nothing indicating that it would not work for stainless steel as well. However, there is no test data available to support this assumption.

With this in mind, it becomes clear that stainless steel most likely does not have any detrimental effect of the overall fatigue strength. As a matter of fact, there are indications that the fatigue strength is superior to that of carbon steel. Still, it is important to keep in mind that the test data for the fatigue strength of stainless steel is scarce and dispersed.

However, to actually use the indicated improved fatigue strength of stainless steel more research has to be conducted.

As such, currently it is possible to use stainless steel with the same fatigue characteristics as that of carbon steel, meaning that the materials are on par with each other. However with the complement that stainless steel might actually be somewhat better when considering the fatigue strength of the material.

Experience in the structural engineering industry

One of the major questions for this thesis was to find out what is currently known about stainless steel in structural engineer within the field of academia. Also included, though on periphery, is what the current knowledge about the material within the structural engineering industry.

In short, it appears that it is much as one can expect; that the current standards, especially Eurocode in this instance, influence greatly on the usage of stainless steel. An example of this is that the previous Swedish standard, *Bro 2004*, required that all steel including stainless steel should have protective paint against corrosion. Of course, this made the whole point of stainless steel somewhat superfluous and the cost incongruous. To conclude, the current standards holds much sway on how stainless steel is used within the industry of structural engineering.

Unfortunately, the standards are not very well developed to incorporate stainless steel. Mostly, the current standard treats stainless steel as another type of carbon steel. Still, the authors of this thesis would like to make the case that Eurocode does not capture the behaviour of stainless steel to a sufficient degree.

To exemplify, fatigue is treated the same for stainless steel as for carbon steel. Whilst the findings in the literature study indicate that this might not be the case. Regarding the fatigue, where test data is insufficient to raise the fatigue strength of stainless steel, this is a conservative simplification.

Of course, the issue of a detailed contra simplified standard is an issue with multiple viewpoints with different priorities. A standard that is too complex to put into practise might not be very beneficial at all. As such, the authors chose to intentionally abnegate from directly recommending a more detailed standard. Instead, that the standard it revised to better capture the behaviour of stainless steel.

To conclude, the expertise within the industry is limited. Few engineers have ever utilised stainless steel in structures and the material might appear for many as unfamiliar territory. It should not be neglected that there is a certain threshold to introduce new ideas in the field of structural engineering. In addition to limited experience, the standard themselves are not sufficiently developed for stainless steel. As such, despite the fact that stainless steel appears to be superior in many situations, it might be neglected due to the aforementioned reasons.

When should stainless steel be considered

Let it first be stated that there is no given situation where stainless steel always is the optimal choice. However, there are circumstances that advocates for the use of stainless steel.

The first and probably most intuitive is when highly corrosive environments are involved. Stainless steel is also of some use down to medium corrosive environments as well. It depends a bit on the requirements and tolerances for the specific bridge or structure in question. However, when corrosion is not an issue, for instance in arid desert environments, there is no benefit from the corrosive properties of stainless steel.

Another usage of stainless steel is when slender cross sections are desired, since stainless steel possesses a high proof strength. In addition, when slender cross sections are considered, corrosion becomes more critical as a minor reduction in an already small cross section entails higher consequences. In short, stainless steel is more stable for slender cross sections.

Lastly, though it is not currently relevant, is that stainless steel given time, attention and research might include higher fatigue strength than that of carbon steel. Consequently, with better fatigue if not at least better durability, stainless steel is likely to be a better choice if long service life is of interest.

In short, stainless steel bridges probably have the most relevant area of implementation of corrosive environments and where long service life is desired. Additionally, it might also be quite relevant where service and inspection of structural members are difficult or overly expensive, or simple not desired for that matter.

7.2 Recommendations

This thesis is not the last instalment in a long line of previous research, quite the contrary as a matter of fact. Thus, there are some topics that the authors of this report would suggest for future research. To give a short overview, the following topics are recommended:

- Next step in this report: LCC, LCA and calculations
- Complementing stainless steel with corrosion resistant reinforcement
- About fatigue and load modelling
- About instability phenomena

These are only some suggestions from the authors. By no means are these necessarily the best course of action.

Next step in this report: LCC, LCA and calculations

There are several items that did not make the final cut of the thesis due to limited resources, especially a limited amount of time. So, if the authors through some lucky incident found themselves with a considerable amount of time to spend, what would be the next step?

First and foremost, this question excludes the possibility of doing a completely new study from scratch. As discussed in chapter 7.2 - *Recommendations*, both life cycle analysis (LCA) and life cycle cost (LCC) are likely to improve the results of this thesis. In addition, they are also expected to give a better understanding of how valuable stainless steel is and where it would be the most suitable to implement.

An additional topic is more hand calculations for the parametric study. Some calculations are omitted for the same reason as LCA and LCCA were omitted. As such, this leaves a blind-spot. If time allowed, it would be beneficial for this thesis if the calculations were more encompassing than what they already are.

There are additional steps that could be taken to further increase the quality and scope of this thesis. However, these were the major ones that did not fit within the time frame.

Complementing stainless steel with corrosion resistant reinforcement

As stated within this report, stainless steel bridges have a far superior durability when it comes to corrosion. Omitting the delimitating circumstances of fatigue for a moment, the stainless steel bridges could in theory remain in service far longer than is desired. Precisely how much is hard to determine as it is dependent on a variety of factors. However, a life expectancy of 100 years or more is likely to not propose much of a challenge.

However, most road bridges today are of a composite cross section, or at least with a concrete deck. The concrete always, in accordance with current standards, include reinforcement. This reinforcement however is prone to corrode after a certain time, for example via chloride ingress within the concrete.

A very interesting thought would be whether the service life could be increased if combining the durability of the stainless steel with more durable reinforcement. There are currently two very promising options to achieve this, which are;

- Stainless steel reinforcement
- Fibre Reinforced Concrete (FRC)

Both of these options are corrosion resistant. In addition, FRC also have other beneficial aspects worthy of consideration all by itself. Note however, that corrosion resistance alone is not sufficient to assure an increase of the service life of bridges, fatigue must also be considered, more on this in the next section.

Fatigue and fatigue load modelling

Fatigue damage is often a limiting factor when considering steel bridges. If to increase the service life of bridges via implementing stainless steel, fatigue becomes an even more important issue.

Currently, the test data when it comes to fatigue capacity of stainless steel is scarce. However, the little that is available indicates that stainless steel has more fatigue capacity than what is currently used.

Of course, this is a topic that simply should not be overlooked. Consequently, the authors of this thesis give their strongest recommendation that more research is to be done within this topic.

There are several promising advantages if this hypothesis of increased fatigue strength were to be confirmed. Not only would it enable better and more durable bridges, it would also entail substantial economic savings.

Instability phenomena

The last recommendation is similar to that of fatigue, though instead on the topic of instability phenomena. But contrary to the fatigue section which hints at increased capacity, this is more towards the aspect of safe and reliable structures.

The topic is instability phenomena of stainless steel, which might be different from the behaviour of carbon steel. What is currently known is that the material response of stainless steel is somewhat different than that of carbon steel. In addition, although there is only a very small amount of research on this topic, it indicates that instability might be more severe for stainless steel.

Truth be told, this topic is very uncertain, which is problematic. There is little research to justify an informed assessment of the instability of stainless steel. Consequently, the authors recommend that further research is to be done on the topic of instability, to be able to assess the capacity of stainless steel more accurately.

7.3 Weaknesses of the thesis

This subchapter is dedicated to discuss some of the known weaknesses of this report and thesis. Although none of them invalidates the already obtained results, it might still be interesting to highlight the limitation of this thesis.

Of course, it is possible to simply add "more research" to a lot of the items mentioned herein. However, the authors of this report believe that there are more relevant topics to study which are more important and in turn yield better results and impact.

First and foremost, this thesis focuses mostly on the steel beams of a given composite cross section. As such, little attention has been given to what occurs in the concrete plate or the reinforcement. There might be effects that are completely left out in the parametric study.

Also, as stated in the chapter 7.2 - *Recommendations*, LCA and LCC are not included. These might further justify or disprove the viability of implementing stainless steel in structures.

Also omitted, is the study of non-linear behaviour that is typical for concrete. However, as shown in the literature study, even stainless steel has an increased amount of non-linear behaviour compared to carbon steel. However, to fully incorporate this in the parametric study, it would require the authors to rewrite the standard substantially. In short, fully including the non-linear behaviour in the parametric study was not feasible within the given timeframe of the project.

In addition, some calculations were omitted in the parametric study. Also, not all phenomena have been taken into account. In the end there are some minor variables and items missing. However, these have been omitted since they have been deemed to have a minor or even insignificant contribution to the parametric study.

Moving on to the next topic, there is also no laboratory or full scale testing of stainless steel has been carried out within this thesis. This thesis is based on other research, all of it can be found in chapter 8 - *References*. Also, since test data is scarce, which is also reflected in the standards, it is somewhat difficult to capture the true behaviour of stainless steel.

Finally, moving to the last topic, which is the selected bridge in question and how this impacts the thesis. It should be quite clear that the second half of this thesis is based on a single bridge and a specific set of circumstances. There are circumstances and parameters that are not covered in this thesis.

8 References

Abidelah, A., Averseng, J. & Bouchaïr, A., 2008. Analysis of the Behaviour of Stainless Steel Bolted Connections. *Jounral of Constructional Steel Research*, 64(11), pp.1264-74.

Akhlaghi, F.Z., 2009. *Fatigue life assessment of welded Bridge details using structural hot spot stress method*. Master's Thesis. Göteborg, Sweden: Chalmers Reposervice Chalmers University of technology, Department of Civil and Environmental Engineering. Publication no. 104.

ArcelorMittal, 2009. *Stainless Steel in bridges and footbridges*. [Online] Available at: http://www.constructalia.com/repo/Publications/Stainless%20Bridges%20and%20Footbridges/stainlesssteelbridges_EN.pdf?page=5991 [Accessed 14 Februari 2014].

Baddoo, N.R. & Kosmac, A., 2011. *Sustainable Duplex Stainless Steel Bridges*. Ascot, United Kingdoms: Euro Inox The Steel Construction Institute.

Balasubramaniam, R., 2000. *On the Corrosion Reistance of the Delhi Iron Pillar*. Kanpur: Elsevier Science Ltd - Corrosion Science 42 pp.2103-2129. Indian Institute of Technology.

Brown, D., Helzel, M. & Pauly, T., 2012. *Stainless Steel Flat products for buildings - The grades in EN 10088-4 explained*. 2nd ed. Brussels, Belgium: Euro Inox.

CEN, 2006. *EN 1993-1-4:2006 - Eurocode 3: Supplamentary Rules for Stainless Steels*. [Standard] Brussels: European Committee for standardization (CEN).

CEN, 2009. *EN 10088-4:2009 Stainless Steels - Part 4: Technical delivery conditions for sheet/plate and strip of corrosion resisting steel for construcion purposes*. Brussels: European Committee for standardization (CEN).

Comer, A.J., 2003. *Corrosion Fatigue of a Superduplex Stainless steel Weldment*. Thesis for dregree of Doctor of Philosofy. Dublin: Dublin City University, School of Mechanical and Manufacturing Engineering: Faculty of Engineering and Computing.

ESAB, 2012. *Svetsa med ESAB duplexa rostfria stål, (Weld With ESAB duplex stainless steel. In Swedish)*. [Datasheet] Gothenburg, Sweden: ESAB Available at: www.esab.se [Accessed 10 February 2014].

Euro Inox, 2004. *Pickling amd Passivating Stainless Steel*. 1st ed.

EuroInox & Stålbyggnadsinstitutet, 2006. *Dimensionering av konstruktioner i rostfritt stål (Design of Constructions in Stainless Steel, In Swedish)*. 3rd ed. Stockholm, Sweden: Stålbyggnadsinstitutet.

European Committee for standardization, 2006. *EN 1993-1-4:2006 Eurocode 3: Supplementary rules for stainless steels*. [Standard] Brussels.

Evertsson, C.M., 1993. ISSN 1102-5867 *Fatigue of Duples Stainless Steels*. Thesis for the Master's Degree. Göteborg: Chalmers Reposervice Chalmers University of Technology, Department of Engineering Metals.

Fanica, A. et al., 2008. *Application of duplex Stainless steel for welded bridge construction in an aggressive environment*. Report. Brussels: RFCS publications European Comission: Directorate-General for Research: Research fund for coal and steel unit.

Fersini, M., Sorrentino, S. & Zilli, G., 2010. Duplex Stainless Steel for Bridges Construction: Comparison Between SAW and Laser-GMA Hybrid Welding. *Welding in the World*, 54(5-6), pp.123-33.

Finnås, A., 2012. *The use of Durable High Strength (Duplex) Stainless Steel in Bridges and Lock Gates*. Degerfors, Sweden: Outokumpu Stainless AB.

Finnås, A. & Olsson, A., 2002. Rostfria stål i bärande konstruktioner (Stainless Steels in load bearing structures, in swedish). *Stålbyggnadsinstitutets årspublikation*, 175, pp.40-45.

Groth, H.L. & Johansson, R.E., 1991. Corrosion Fatigue and Fatigue Data for Duplex Stainless Steels. *Les Editions de Physique*, October 28-30, pp.283-93.

Günther H.-P., C.R.U.K., 2008. High-Strength steel fillet welded connections. *Steel construction*, I(1), pp.77-84.

Hechler, O. & Collin, P., 2008. On the use of duplex stainless steels in bridge construction. In *Proceedings of the fourth international Conference on bridge maintenance*. Seoul, Korea, 2008. Bridge Maintenance, Safety Management, Health Monitoring and Informatics.

Horton, H.L., Jones, F.D., Oberg, E. & Ryffel, H.H., 2008. In *Machinery's Handbook*. 28th ed. New York, United States of America: Industrial Press Inc. pp.396-99.

IMOA, 2009. *Practical Guidelines for the Fabrication of Duplex Stainless steels*. 2nd ed. London: International Molybdenum Association (IMOA).

International Molybdenum Association, 2009. *Practical Guidelines for the Fabrication of Duplex Stainless steels*. 2nd ed. London: International Molybdenum Association.

Johansson, P. & Liljas, M., 2002. A new lean duplex stainless steel for construction purposes. *ACOM*, 1 February. pp.17-24.

Kostakakis, K. & Mosiello, A., 2013. *The Benefits of Post Weld Treatment for Cost Efficient and Sustainable Bridge Design*. Master Thesis. Gothenburg, Sweden: Chalmers University of Technology.

Liljas, M. & Ericsson, C., 2002. Fatigue behaviour of stainless steel welds. *ACOM*, 1 February. pp.2-16.

Lukezic, D., 2013. Single-Stage Models of Stress-Strain Curves Up to Maximum Load: Duplex Stainless Steel and High Strength Steels. *Journal of Failure Analysis and Prevention*, XIV(1), pp.87-94.

Muthupandi, V., Seshadri, S.K., Srinivasan, P.B. & Sundaresan, S., 2003. Effect of weld metal chemistry and heat input on the structure and properties of duplex stainless steel welds. *Materials Science and Engineering: A*, 358(1-2), pp.9-16.

Outokumpu, 2010. *Welding handbook*. 1st ed. Sandviken, Sweden: Outokumpu Oyj.

Outokumpu, 2013. *Duplex Stainless Steel - Data Sheet, 1008EN-GB:8*. Avesta: Centrumtryck AB.

Outokumpu, 2013. *Handbook of Stainless Steel*. Avesta, Sweden: Sandvikens Tryckeri AB.

Paulsson-Tralla, J., 2012. Samverkansbroar av stålbalkar av rostfritt stål och farbana av betong och rostfri armering: En kostnads effektiv lösning? (Composite bridges made from steel girders of stainless steel and road surface from concrete and stainless reinforcement, in Swedish). *Bygg & Teknik*, Oktober. pp.12-16.

Shin, Y.T., Shin, H.S. & Lee, H.W., 2012. Effect of Heat Input on Pitting Corrosion in Super Duplex Stainless Steel Weld Metals. *Metals and Materials International*, 18(6), pp.1037-40.

SMS, 2000. *Rostfria Stål Handbok4 (Stainless Steels Reference book 4, In Swedish)*. 6th ed. Stockholm, Sweden: Graphium Norstedts Tryckeri.

Sobrino, J.A., 2006. Stainless Steel Road Bridge in Menorca, Spain. *Engineering International*, 16(2), pp.96-100.

Säll, J. & Tiderman, A., 2013. *Maintenance-free Material in Bridge Superstructures*. Bachelor Thesis. Stockholm, Sweden: KTH.

Vélon, A., 1996. *Influence of Nitrogen on the Passivation of Austenitic Stainless Steel*. Thesis for degree of chemical engineer. Göteborg, Sweden: Chalmers Reproservice Chalmers University of Technology. Publication no. 772.

Appendix A – Results from Parametric Study

In this appendix all the results obtained from the parametric study is presented. The data is presented in both tables and a few additional diagrams. Moreover, some information pertaining to the calculation of the costs is given here as well.

In more detail, appendix A consists of the following parts:

1. Result data
2. Example of the format of the input data
3. Example of the format of the result
4. Data used for the cost estimates
5. Additional diagrams

A.1 Result data

Note that the results presented here are just the values obtained in the parametric study. For further description of the results the reader is directed to Chapter 5 - *Results* in the report.

When reading the tables, please note that the value of the parameters is given at the top of each table. A description of the parameters and corresponding values which are considered in the parametric study is given in Chapter *3.3 - About the parameters and their relevance* in the report

In more detail, for the fatigue class the values can be:

- Standard, which indicates that the fatigue strength is taken according to the current recommendations in Eurocode.
- 88MPa, which indicates that the inherently higher fatigue strength of stainless steel has been considered. This applies to mode C and D, for further information see subchapter *3.3 - About the parameters and their relevance* in the report.
- +2classes/+3classes, indicates that improved fatigue strength through post-weld treatment has been considered. For further information see subchapter *3.3 - About the parameters and their relevance* in the report.

For the fatigue assessment it is indicated which fatigue assessment method that was considered in design. The two methods which have been used are the damage equivalent method and the Palmgren-Miner method. They are indicated on the short for "Lambda" respectively "Palmgren".

Parameters			
Span length [m]	10	20	30
Steel grade	EN1.4162		
Fatigue load	Low		
Traffic [category and type]	4, local		
design life [years]	80		
fatigue class	default		
fatigue assessment	Lambda		
Results			
ULS, bending, composite	0.892	0.916	0.995
ULS, bending, I-girder	0.424	0.765	0.759
ULS, shear, composite	0.712	0.699	0.759
ULS	0.892	0.916	0.995
SLS, deflection	0.326	0.418	0.503
FLS, Damage equivalent (max)	0.971	1.001	0.994
Mode A	0.185	0.195	0.232
Mode B	0.458	0.439	0.564
Mode C	0.971	1.001	0.994
Mode D	0.888	0.900	0.959
Mode E	0.613	0.702	0.577
FLS, Palmgren-Miner (max)	0.247	0.161	0.238
Mode A	0.014	0.009	0.021
Mode B	0.000	0.000	0.013
Mode C	0.186	0.125	0.149
Mode D	0.247	0.161	0.238
Mode E	0.009	0.016	0.004
Steel amount [kg]	1823	8458	17940
Exposed steel area [m2]	36	110	200
Initial cost, low estimate	45575	211450	448500
Initial cost, high estimate	154955	718930	1524900
Maintenance cost, low estimate	298	1382	2930
Maintenance cost, high estimate	543	2520	5346
Total cost, low estimate	45873	212832	451430
Total cost, high estimate	155498	721450	1530246

Parameters			
Span length [m]	40	50	60
Steel grade	EN1.4162		
Fatigue load	Low		
Traffic [category and type]	4, local		
design life [years]	80		
fatigue class	default		
fatigue assessment	Lambda		
Results			
ULS, bending, composite	0.948	0.990	1.006
ULS, bending, I-girder	0.769	0.874	0.768
ULS, shear, composite	0.831	0.853	0.909
ULS	0.948	0.990	1.006
SLS, deflection	0.665	0.612	0.657
FLS, Damage equivalent (max)	0.995	1.010	0.941
Mode A	0.244	0.270	0.219
Mode B	0.646	0.597	0.580
Mode C	0.995	1.010	0.937
Mode D	0.975	1.010	0.941
Mode E	0.527	0.379	0.323
FLS, Palmgren-Miner (max)	0.293	0.384	0.352
Mode A	0.032	0.049	0.044
Mode B	0.038	0.033	0.037
Mode C	0.187	0.263	0.246
Mode D	0.293	0.384	0.352
Mode E	0.004	0.000	0.000
Steel amount [kg]	30000	42830	60460
Exposed steel area [m2]	306	461	616
Initial cost, low estimate	750000	1070750	1511500
Initial cost, high estimate	2550000	3640550	5139100
Maintenance cost, low estimate	4900	6996	9876
Maintenance cost, high estimate	8939	12763	18016
Total cost, low estimate	754900	1077746	1521376
Total cost, high estimate	2558939	3653313	5157116

Parameters		
Span length [m]	70	80
Steel grade	EN1.4162	
Fatigue load	Low	
Traffic [category and type]	4, local	
design life [years]	80	
fatigue class	default	
fatigue assessment	Lambda	
Results		
ULS, bending, composite	1.010	1.015
ULS, bending, I-girder	0.786	0.788
ULS, shear, composite	0.980	0.967
ULS	1.010	1.015
SLS, deflection	0.698	0.704
FLS, Damage equivalent (max)	0.799	0.692
Mode A	0.133	0.086
Mode B	0.597	0.531
Mode C	0.799	0.692
Mode D	0.798	0.688
Mode E	0.285	0.243
FLS, Palmgren-Miner (max)	0.213	0.154
Mode A	0.024	0.015
Mode B	0.054	0.039
Mode C	0.158	0.115
Mode D	0.213	0.154
Mode E	0.000	0.000
Steel amount [kg]	86670	118400
Exposed steel area [m2]	783	995
Initial cost, low estimate	2166750	2960000
Initial cost, high estimate	7366950	10064000
Maintenance cost, low estimate	14157	19340
Maintenance cost, high estimate		
Total cost, low estimate		
Total cost, high estimate		

Parameters		
Span length [m]	40	
Steel grade	S355	S460
Fatigue load	Low	
Traffic [category and type]	4, local	
design life [years]	80	
fatigue class	default	
fatigue assessment	Lambda	
Results		
ULS, bending, composite	1.000	0.988
ULS, bending, I-girder	0.739	0.727
ULS, shear, composite	0.799	0.907
ULS	1.000	0.988
SLS, deflection	0.540	0.630
FLS, Damage equivalent (max)	0.869	0.985
Mode A	0.183	0.329
Mode B	0.591	0.756
Mode C	0.869	0.985
Mode D	0.793	0.966
Mode E	0.544	0.525
Mode F	0.505	0.633
FLS, Palmgren-Miner (max)	0.125	0.285
Mode A	0.018	0.053
Mode B	0.024	0.081
Mode C	0.101	0.181
Mode D	0.125	0.285
Mode E	0.005	0.003
Steel amount [kg]	33760	27920
Exposed steel area [m2]	331	304
Initial cost, low estimate	467670	431692
Initial cost, high estimate	1412950	1329320
Maintenance cost, low estimate	353377	302666
Maintenance cost, high estimate	753487	653702
Total cost, low estimate	821047	734358
Total cost, high estimate	2166437	1983022

Parameters		
Span length [m]	40	
Steel grade	S355	S460
Fatigue load	Medium	Medium
Traffic [category and type]	2, medium	2, medium
design life [years]	100	100
fatigue class	default	
fatigue assessment	Palmgren	Palmgren
Results		
ULS, bending, composite	0.984	0.992
ULS, bending, I-girder	0.728	0.746
ULS, shear, composite	0.643	0.677
ULS	0.984	0.992
SLS, deflection	0.393	0.429
FLS, Damage equivalent (max)	1.199	1.169
Mode A	0.447	0.415
Mode B	1.024	1.035
Mode C	1.199	1.169
Mode D	1.066	1.036
Mode E	1.045	1.028
Mode F	0.728	0.819
FLS, Palmgren-Miner (max)	1.011	1.001
Mode A	0.000	0.000
Mode B	0.619	0.652
Mode C	0.773	0.733
Mode D	1.011	1.001
Mode E	0.290	0.268
Steel amount [kg]	47430	45230
Exposed steel area [m2]	355	354
Initial cost, low estimate	580370	602576
Initial cost, high estimate	1908410	2056720
Maintenance cost, low estimate	473349	456780
Maintenance cost, high estimate	1032673	1000963
Total cost, low estimate	1053719	1059356
Total cost, high estimate	2941083	3057683

Parameters			
Span length [m]	40	40	40
Steel grade	EN1.4162		
Fatigue load	Low	Medium	High
Traffic [category and type]	4, local	2, medium	1, long
design life [years]	80	100	120
fatigue class	default		
fatigue assessment	Palmgren		
Results			
ULS, bending, composite	0.994	0.982	0.997
ULS, bending, I-girder	0.760	0.737	0.762
ULS, shear, composite	0.875	0.665	0.486
ULS	0.994	0.982	0.997
SLS, deflection	0.696	0.428	0.292
FLS, Damage equivalent (max)	1.343	1.214	0.836
Mode A	0.590	0.413	0.159
Mode B	0.593	1.013	0.788
Mode C	1.343	1.214	0.836
Mode D	1.307	1.029	0.756
Mode E	0.593	1.045	0.804
Mode F	0.487	0.689	0.562
FLS, Palmgren-Miner (max)	0.827	0.974	1.201
Mode A	0.000	0.000	0.000
Mode B	0.025	0.537	0.000
Mode C	0.575	0.869	0.000
Mode D	0.827	0.974	1.201
Mode E	0.010	0.290	0.000
Steel amount [kg]	27670	46730	50490
Exposed steel area [m2]	295	352	403
Initial cost, low estimate	691750	1168250	1262250
Initial cost, high estimate	2351950	3972050	4291650
Maintenance cost, low estimate	4673	7892	8527
Maintenance cost, high estimate	9172	15490	16737
Total cost, low estimate	696423	1176142	1270777
Total cost, high estimate	2361122	3987540	4308387

Parameters		
Span length [m]	10	70
Steel grade	EN1.4162	
Fatigue load	Medium	
Traffic [category and type]	2, medium	
design life [years]	100	
fatigue class	default	
fatigue assessment	Palmgren	
Results		
ULS, bending, composite	0.710	0.974
ULS, bending, I-girder	0.427	0.738
ULS, shear, composite	0.903	0.877
ULS	0.903	0.974
SLS, deflection	0.308	0.387
FLS, Damage equivalent (max)	2.432	1.061
Mode A	2.432	0.358
Mode B	0.892	0.954
Mode C	1.470	1.061
Mode D	1.242	0.993
Mode E	1.513	0.557
Mode F	1.485	0.529
FLS, Palmgren-Miner (max)	1.004	0.984
Mode A	0.153	0.000
Mode B	0.000	0.526
Mode C	0.957	0.692
Mode D	0.977	0.984
Mode E	1.004	0.000
Steel amount [kg]	2324	120300
Exposed steel area [m2]	39	933
Initial cost, low estimate	58100	3007500
Initial cost, high estimate	197540	10225500
Maintenance cost, low estimate	392	20317
Maintenance cost, high estimate	770	39877
Total cost, low estimate	58492	3027817
Total cost, high estimate	198310	10265377

Parameters			
Span length [m]	40	40	40
Steel grade	EN1.4162		
Fatigue load	Low	Medium	High
Traffic [category and type]	4, local	2, medium	1, long
design life [years]	80	100	120
fatigue class	88MPa		
fatigue assessment	Palmgren		
Results			
ULS, bending, composite	0.994	0.964	0.970
ULS, bending, I-girder	0.760	0.750	0.740
ULS, shear, composite	0.875	0.839	0.483
ULS	0.994	0.964	0.970
SLS, deflection	0.696	0.456	0.297
FLS, Damage equivalent (max)	1.221	1.181	0.817
Mode A	0.818	0.555	0.216
Mode B	0.662	1.066	0.796
Mode C	1.221	1.181	0.817
Mode D	1.188	1.035	0.763
Mode E	0.593	1.034	0.751
Mode F	0.544	0.840	0.581
FLS, Palmgren-Miner (max)	0.593	0.969	1.209
Mode A	0.184	0.164	0.000
Mode B	0.042	0.830	1.209
Mode C	0.415	0.762	0.000
Mode D	0.593	0.969	1.209
Mode E	0.010	0.275	0.000
Steel amount [kg]	27670	42730	48260
Exposed steel area [m2]	295	349	402
Initial cost, low estimate	691750	1068250	1206500
Initial cost, high estimate	2351950	3632050	4102100
Maintenance cost, low estimate	4673	7216	8150
Maintenance cost, high estimate	9172	14164	15997
Total cost, low estimate	696423	1075466	1214650
Total cost, high estimate	2361122	3646214	4118097

Parameters		
Span length [m]	10	70
Steel grade	EN1.4162	
Fatigue load	Medium	
Traffic [category and type]	2, medium	
design life [years]	100	
fatigue class	88MPa	
fatigue assessment	Palmgren	
Results		
ULS, bending, composite	0.790	0.990
ULS, bending, I-girder	0.401	0.745
ULS, shear, composite	0.559	0.740
ULS	0.790	0.990
SLS, deflection	0.340	0.435
FLS, Damage equivalent (max)	2.484	1.023
Mode A	1.505	0.504
Mode B	0.977	0.972
Mode C	1.411	1.023
Mode D	1.250	1.013
Mode E	1.499	0.569
Mode F	1.418	0.562
FLS, Palmgren-Miner (max)	0.983	0.976
Mode A	0.244	0.195
Mode B	0.000	0.591
Mode C	0.823	0.634
Mode D	0.983	0.976
Mode E	0.955	0.000
Steel amount [kg]	2232	110800
Exposed steel area [m2]	37	914
Initial cost, low estimate	55800	2770000
Initial cost, high estimate	189720	9418000
Maintenance cost, low estimate	377	18712
Maintenance cost, high estimate	740	36728
Total cost, low estimate	56177	2788712
Total cost, high estimate	190460	9454728

Parameters		
Span length [m]	40	40
Steel grade	EN1.4162	
Fatigue load	Medium	Medium
Traffic [category and type]	2, medium	2, medium
design life [years]	100	100
fatigue class	+2 classes	+3 classes
fatigue assessment	Palmgren	
Results		
ULS, bending, composite	0.990	0.983
ULS, bending, I-girder	0.736	0.726
ULS, shear, composite	0.660	0.657
ULS	0.990	0.983
SLS, deflection	0.490	0.552
FLS, Damage equivalent (max)	1.151	1.131
Mode A	0.424	0.400
Mode B	0.879	0.820
Mode C	1.151	1.131
Mode D	1.047	1.049
Mode E	0.834	0.773
Mode F	0.667	0.623
FLS, Palmgren-Miner (max)	0.990	0.989
Mode A	0.000	0.000
Mode B	0.248	0.176
Mode C	0.712	0.673
Mode D	0.990	0.989
Mode E	0.000	0.000
Steel amount [kg]	38650	34580
Exposed steel area [m2]	337	322
Initial cost, low estimate	966250	864500
Initial cost, high estimate	3285250	2939300
Maintenance cost, low estimate	6527	5840
Maintenance cost, high estimate	12812	11463
Total cost, low estimate	972777	870340
Total cost, high estimate	3298062	2950763

Parameters			
Span length [m]	40		
Steel grade	EN1.4162		
Fatigue load	Low	Medium	High
Traffic [category and type]	4, local	2, medium	1, long
design life [years]	80	100	120
fatigue class	default		
fatigue assessment	Lambda		
Results			
ULS, bending, composite	0.9483	0.9574	0.9574
ULS, bending, I-girder	0.7693	0.7369	0.7369
ULS, shear, composite	0.8309	0.845	0.845
ULS	0.9483	0.9574	0.9574
SLS, deflection	0.6652	0.4077	0.4077
FLS, Damage equivalent (max)	0.9947	0.9976	0.9976
Mode A	0.3383	0.3576	0.3576
Mode B	0.7213	0.9976	0.9976
Mode C	0.9947	0.9963	0.9963
Mode D	0.975	0.9934	0.9934
Mode E	0.5271	0.8704	0.8704
Mode F	0.5727	0.7736	0.7736
FLS, Palmgren-Miner (max)	0.293276	0.697359	5.389938
Mode A	0.055192	0	0
Mode B	0.065413	0.497511	4.027538
Mode C	0.186847	0.381968	3.10672
Mode D	0.293276	0.697359	5.389938
Mode E	0.00351	0	0
Steel amount [kg]	30000	50740	50740
Exposed steel area [m2]	306.2	362.9	362.9
Initial cost, low estimate	750000	1268500	1268500
Initial cost, high estimate	2550000	4312900	4312900
Maintenance cost, low estimate	5066.525	8569.183	8569.183
Maintenance cost, high estimate	9944.48	16819.43	16819.43
Total cost, low estimate	755066.5	1277069	1277069
Total cost, high estimate	2559944	4329719	4329719

Parameters	Analytical	Finite element model
Span length [m]	40	40
Steel grade	EN1.4162	EN1.4162
Fatigue load	Low	Low
Traffic [category and type]	4, local	4, local
design life [years]	80	80
fatigue class	default	default
fatigue assessment	Lambda	Lambda
Results		
ULS, bending, composite	0.948	0.948
ULS, bending, I-girder	0.769	0.769
ULS, shear, composite	0.831	0.831
ULS	0.948	0.948
SLS, deflection	0.665	0.665
FLS, Damage equivalent (max)	0.990	0.718
Mode A	0.333	0.651
Mode B	0.606	0.446
Mode C	0.990	0.709
Mode D	0.970	0.718
Mode F	0.475	0.270
FLS, Palmgren-Miner (max)	0.134	0.063
Mode A	0.031	0.003
Mode B	0.027	0.003
Mode C	0.129	0.060
Mode D	0.134	0.063
Steel amount [kg]	30000	30000
Exposed steel area [m2]	306	306
Initial cost, low estimate	750000	750000
Initial cost, high estimate	2550000	2550000
Maintenance cost, low estimate	5067	5067
Maintenance cost, high estimate	9944	9944
Total cost, low estimate	755067	755067
Total cost, high estimate	2559944	2559944

A.2 Example of the format of the input data

Input data for the parametric study				
Category	Sub category	Variable	Value	Unit
Geometry	Longitudinal			
		L.span	40	m
	Lower flange			
		t.main.flange.lower.span	0.04	m
		b.main.flange.lower.span	0.55	m
	Web			
		h.main.web.end	1.3	m
		h.main.web.mid	1.03	m
		slopelength.web	4.4	m
		t.main.web.end	0.016	m
		t.main.web.mid	0.012	m
	Upper flange			
		t.main.flange.upper.end	0.02	m
		t.main.flange.upper.mid	0.03	m
		b.main.flange.upper.end	0.45	m
		b.main.flange.upper.mid	0.5	m
	Welds			
		a.weld.main.lower	0.005	m
		a.weld.main.upper	0.005	m
	Splices			
		X.splice.flange.lower	6.4	m
			15.6	m
			24.4	m
			33.6	m
			stop	
		X.splice.web	8	m
			20	m
			32	m
			stop	
		X.splice.flange.upper	9.2	m
			20	m
			30.8	m
			stop	m

A.3 Example of the format of the result

Result for the parametric study		
Sub category	Variable	Value
ULS		
	u.ULS.bending.composite.elastic.max	0,948
	u.ULS.bending.main.elastic.max	0,769
	u.ULS.shear.composite.max	0,831
SLS		
	u.SLS.deflection	0,665
FLS - Lambda		
	u.FLS.Lambda.modeA.max	0,338
	u.FLS.Lambda.modeB.max	0,721
	u.FLS.Lambda.modeC.max	0,995
	u.FLS.Lambda.modeD.max	0,975
	u.FLS.Lambda.modeE.max	0,527
	u.FLS.Lambda.modeF.max	0,573
FLS – Palmgren-Miner		
	u.FLS.PalmgrenMiner.modeA.max	0,055
	u.FLS.PalmgrenMiner.modeB.max	0,065
	u.FLS.PalmgrenMiner.modeC.max	0,187
	u.FLS.PalmgrenMiner.modeD.max	0,293
	u.FLS.PalmgrenMiner.modeE.max	0,004

A.4 Data used for the cost estimates

Here is described how the estimates of the costs are calculated. The calculations are performed in Excel and based upon basic economic models. See table A.1 for a list of both the low and high estimate of the costs which were considered in the calculations.

Furthermore, for the maintenance of the protective paint layer, the same frequency has been used for both the high and low estimate. More specifically, the maintenance of the protective layer is assumed to be required with a period of 20 years. First a minor repair should be needed for 10% of the exposed area, followed by a repair of 20% of the total area. Finally after 60 years it is assumed that the entire steel area requires renewal of the paint layer. The pattern is then repeated *ad infinitum*, so after 80 years a 10% renewal is once again applied.

All the maintenance costs are calculated as a present value through the use of the interest rate. The inspections are calculated as annuities, which is identical to the method for the present value for single costs.

Table A.1 *The values used for the estimates of the cost for the bridge alternatives*

Category	Item	Value	Unit
Initial cost			
Low cost	EN1.4162	25	SEK/kg
	S460	7.85	SEK/kg
	S355	7	SEK/kg
	Initial painting	700	SEK/m^2
High cost	EN1.4162	85	SEK/kg
	S460	40	SEK/kg
	S355	35	SEK/kg
	Initial painting	700	SEK/m^2
Maintenance			
Low cost	Partial repainting	1400	SEK/m^2
	Full repainting	1600	SEK/m^2
	Routine inspection	0.04	SEK/kg
	In-depth inspection	0.5	SEK/kg
High cost	Partial repainting	2000	SEK/m^2
	Full repainting	1700	SEK/m^2
	Routine inspection	0.04	SEK/kg
	In-depth inspection	0.5	SEK/kg
Interest rate	high rate	3.50%	
	low rate	1.50%	
Frequency, carbon			
Low frequency	Routine inspection	2	Years
	In-depth inspection	6	Years
High frequency	Routine inspection	2	Years
	In-depth inspection	6	Years
Frequency, stainless	Routine inspection	6	Years

A.5 Additional diagrams

Here is a selection of diagrams which are considered to be of interest but could not be fitted into the report.

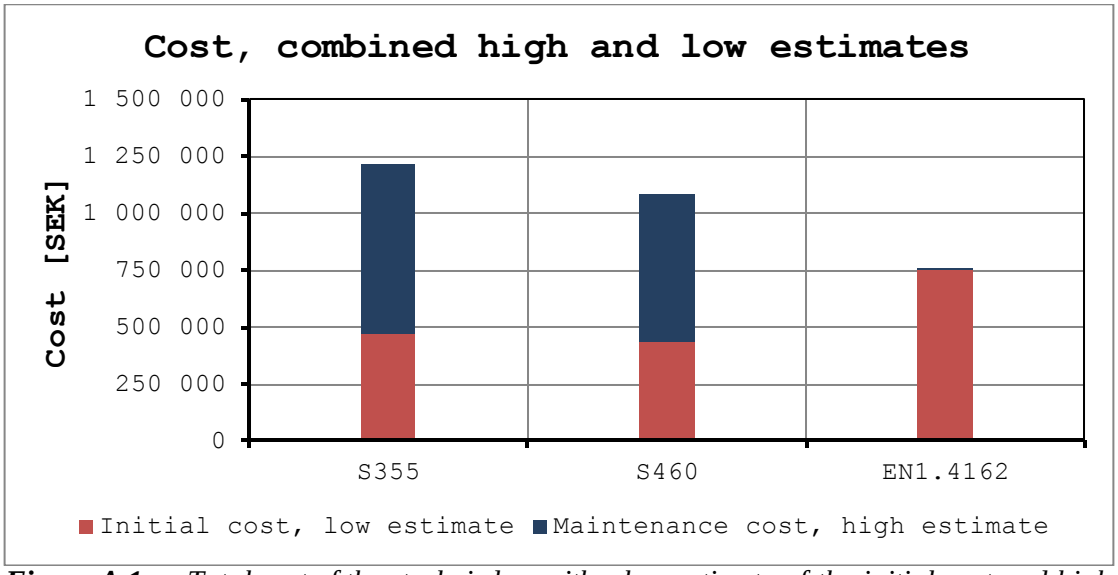

Figure A.1: *Total cost of the steel girders with a low estimate of the initial cost and high estimate of the maintenance. The design is performed with regard to the damage equivalent method for low fatigue load and 40m span*

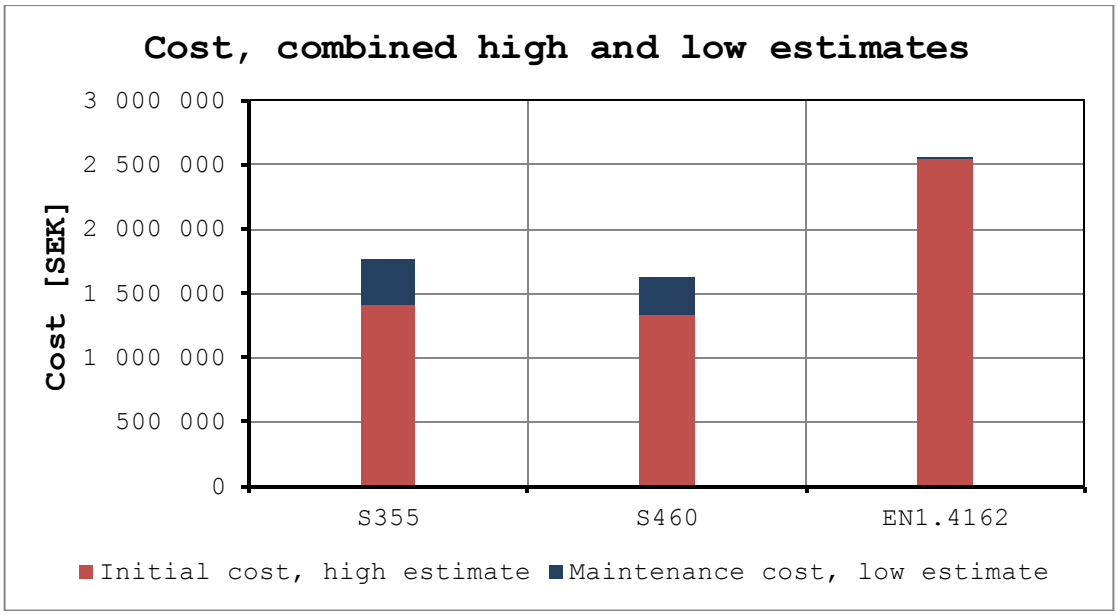

Figure A.2: *Total cost of the steel girders with a high estimate of the initial cost and low estimate of the maintenance. The design is performed with regard to the damage equivalent method for low fatigue load and 40m span*

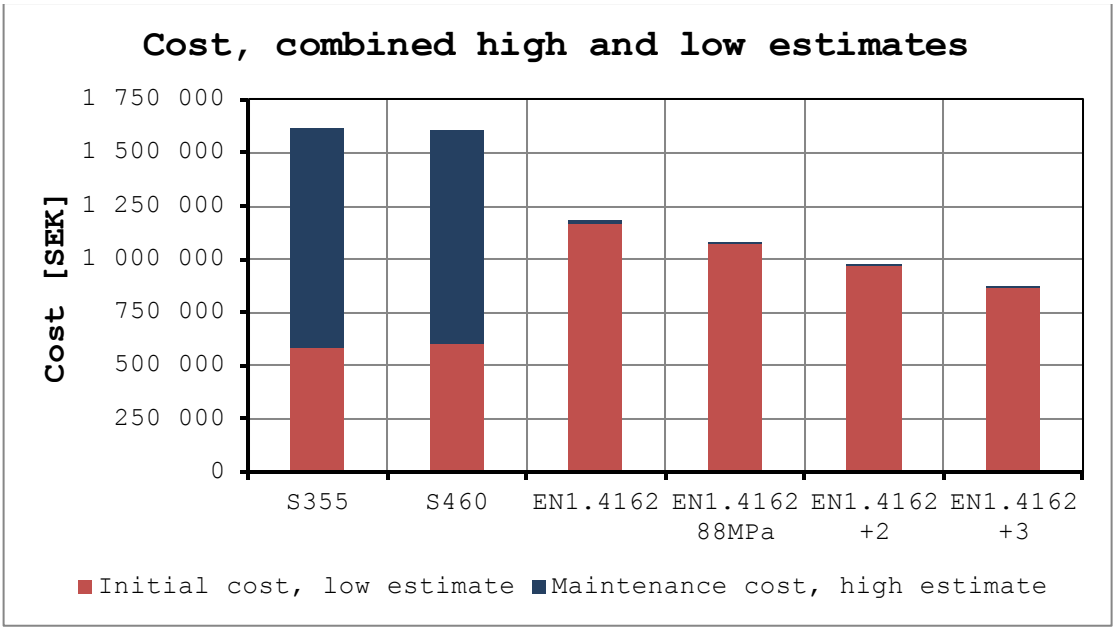

Figure A.3: *Total cost of the steel girders with a low estimate of the initial cost and high estimate of the maintenance. The design is performed with regard to the Palmgren-Miner method for medium fatigue load and 40m span*

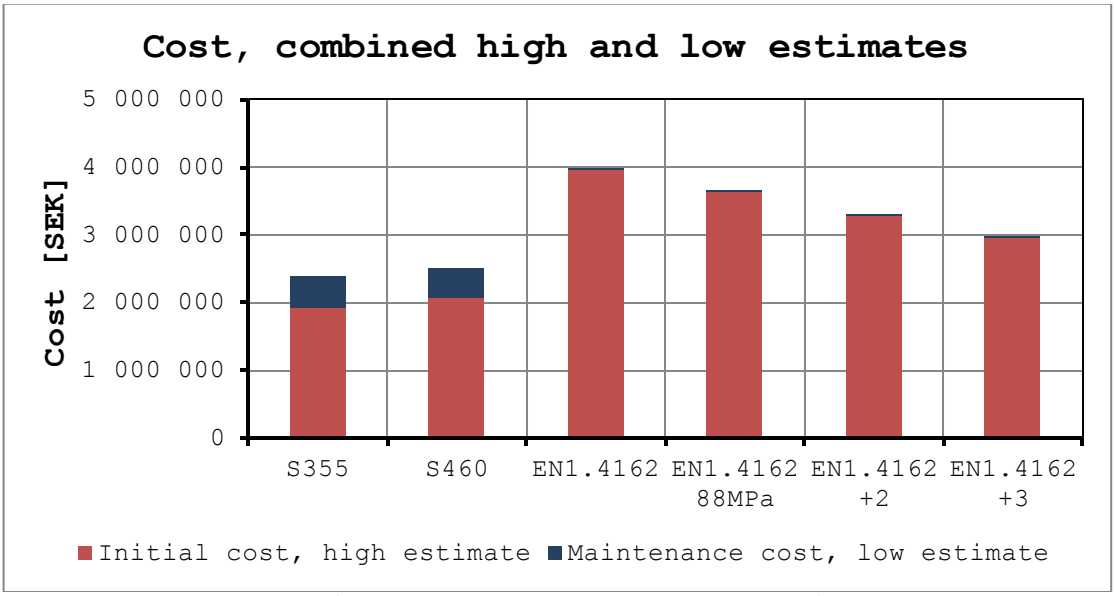

Figure A.4: *Total cost of the steel girders with a high estimate of the initial cost and low estimate of the maintenance. The design is performed with regard to the Palmgren-Miner method for medium fatigue load and 40m span*

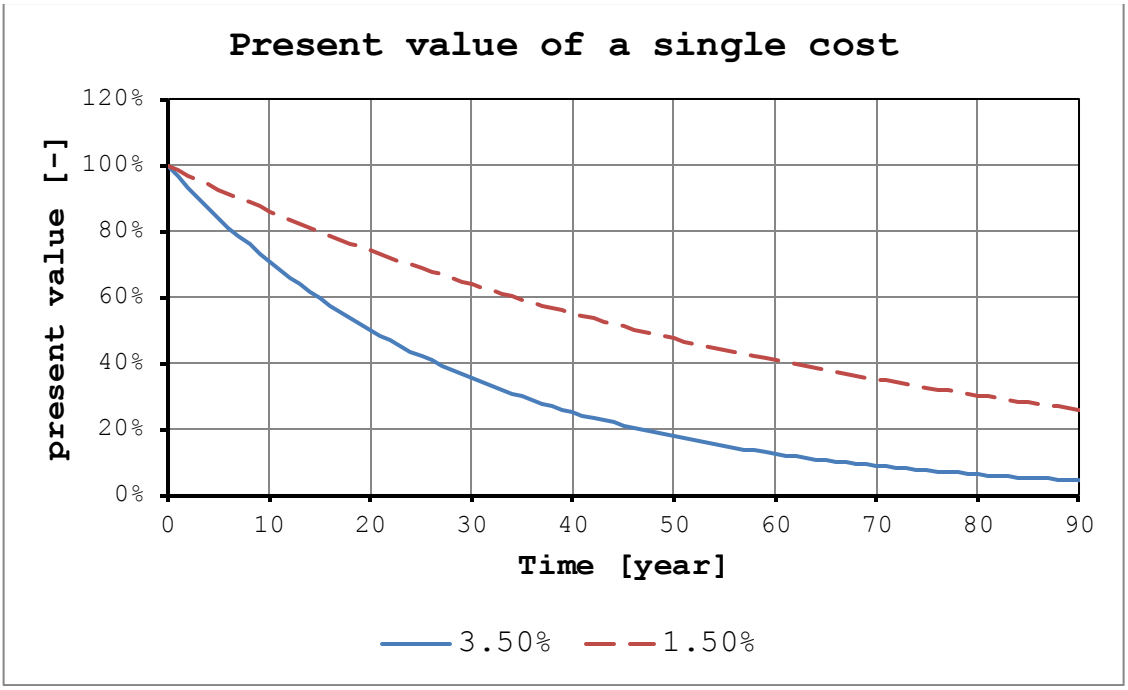

Figure A.5: *The present value of a single cost which occurs in the future.*

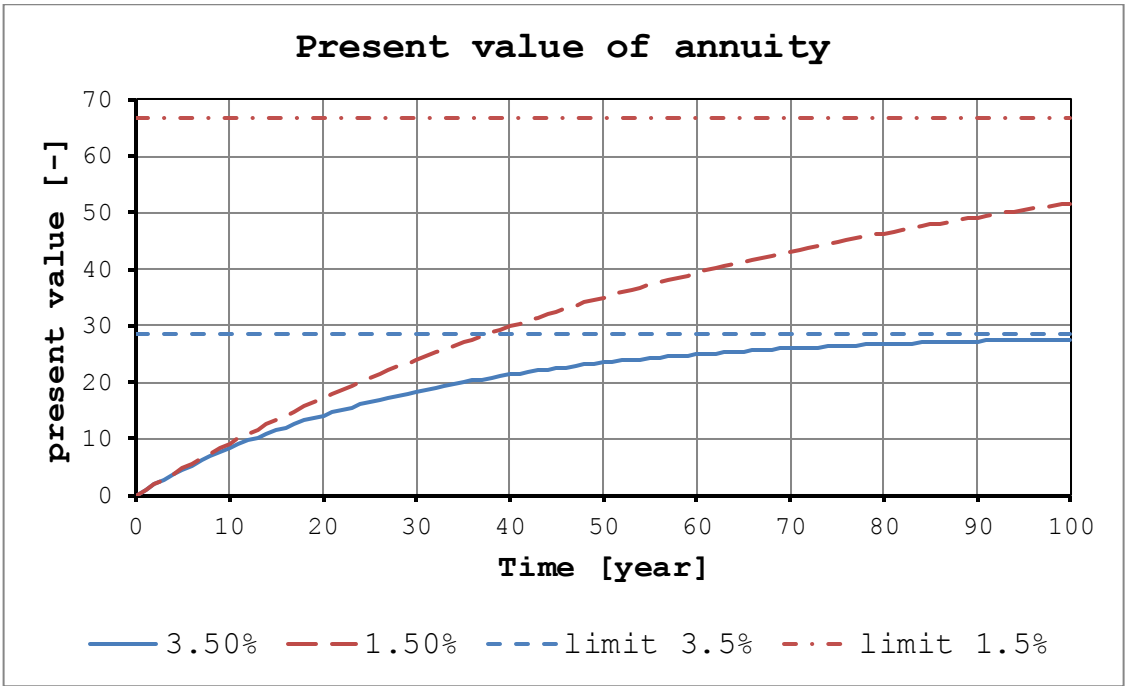

Figure A.6: *Present value of annuity. Note that there is a theoretical maximum limit for the present value in the case of fix costs and interest rate.*

Appendix B – Flow Chart for FEM Script

This appendix aims at giving some clarification of the modelling choices of the FEM model as well as some explanation of how the Python script works. Included in this script are three major sections, namely;

1. About the model and modelling choices
2. About the script
3. Flow Chart of the script

Unfortunately, the script is quite sizeable and exists in several editions, as such; it is omitted from the report. However, for anyone interested please contact the authors of the report or the department of Structural Engineering at Chalmers.

The main objective of the developed script and model is to quickly be able to assess cumulative fatigue damage. The cumulative fatigue damage is calculated with an external program, in this case, Matlab code. The routines for calculating the equivalent fatigue damage can be found in Appendix E.

B.1 About the model and modelling choices

The general idea of the script is to easily and quickly be able to assess fatigue damage over a bridge utilising the Palmgren-Miner theorem of accumulative fatigue damage using superposition of stresses. The finished model of the bridge can be found in figure b.1. A very important aspect of the bridge is that it is entirely created via a script; hence no user input in Abaqus is required.

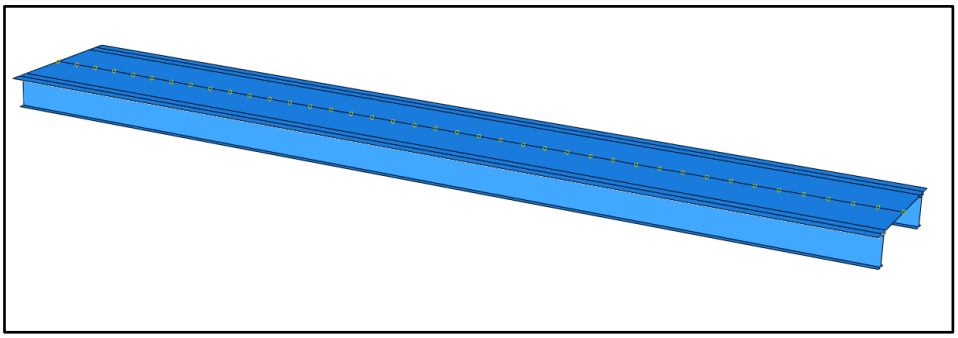

Figure B.1: *Illustration of the finished model of the bridge. The bridge is 40m long in this illustration. Though it might be hard to detect, the small dots in the middle of the plate is evenly spaced with 1m each. The plate is intended to be made out of concrete whilst the two identical beams are made of steel.*

To use superposition, it sets the condition that the model must use only elastic materials. Of course, this is not the most accurate depiction of reality, especially when considering the nonlinear properties of concrete. However, to avoid ludicrously long calculation times, elastic properties have to suffice.

About the model itself, it consists of three structural parts and a fourth special part, more on this special part shortly. An illustration of the cross section can be found in figure b.2. The two steel beams are identical and are in truth the same assembled part. Regarding the beam-part, it consists of lower flange, upper flange and web like any other beam. The point of interest is that they are independent of each other in material and dimensions. This enables greater adaptability in the model, or rather, the bridge can easily be refitted for other purposes.

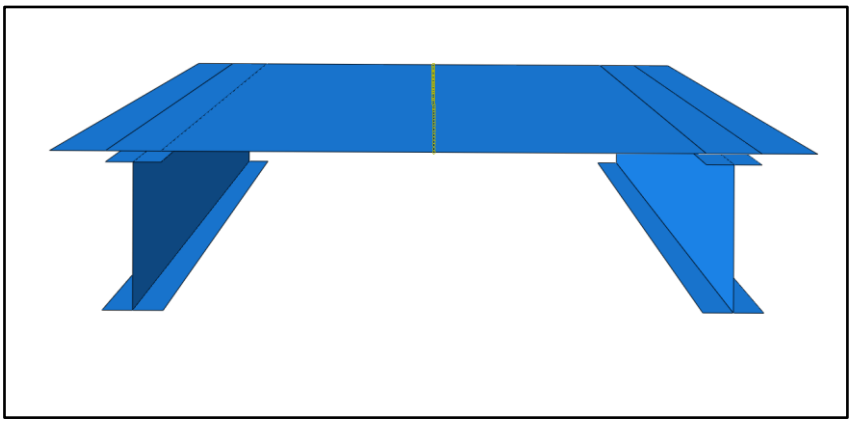

Figure B.2: *Illustration of the cross section of the bridge. The two beams are intended as steel beams and the plate as concrete. Though, since all dimensions and materials are scripted, they can be made out of any elastic material and any given dimensions or placement (with some limitations).*

When assembling the steel parts into a complete steel beam, there is some overlap in the joints. figure b.3 illustrates the problem pertaining to excessive stiffness contribution within the same area. In short, the fact that the shell thickness overlap beams the model is slightly stiffer. However, the effect of this is miniscule and can be considered negligible.

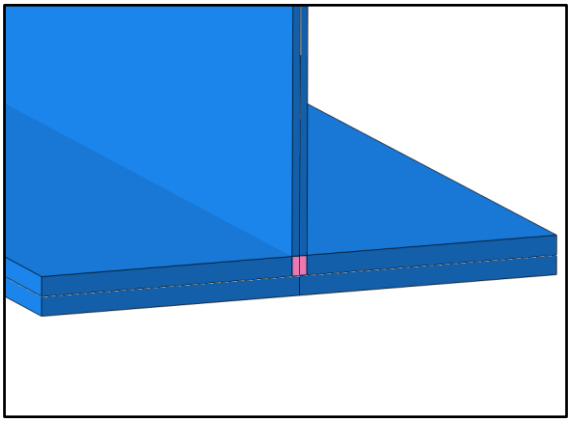

Figure B.3: *Illustration of overlap between web and flanges. The marked area shows where the model gains contribution from both flanges and web within the same space.*

An additional simplification worth mentioning is about the load itself. According to Eurocode the moving load should be modelled as pressure with given area and magnitude, notwithstanding that this also reflects reality to an amiable degree. However, the script and model in question utilises concentrated force, or *point load* if you will. Of course, concentrated force is used to simplify both model and script.

There are two reasons as to why this simplification is justifiable. The first one being that Abaqus/Brigade from the very beginning does not truly understand the concept of pressure. All pressure modelled in the FEM software is reinterpreted as many smaller concentrated forces over a given set of nodes. In other words, there is no true pressure to speak of from the beginning.

The second reason for simplifying to load as concentrated force is that it does not affect the model to any significant degree. It most definitely affects the stresses within the concrete plate. However, the concrete plate is not of particular interest for the model and is neither studied accurately nor considered as part of the results. To conclude, using concentrated load as a simplification at the cost of inaccurate stress distribution and singularities within the concrete plate is reasonable.

Of course, there are more modelling choices and simplifications. Though, a discussion of such length goes somewhat beyond the scope of this report. As such, only the most interesting simplifications are included and the rest is omitted in this version of the report.

B.2 About the script in general

With that in mind and to present the script briefly, it breaks down into a few modules. The modules are the following:

1- Input data
2- Pre-Calculations
3- Modelling Section
    a. Creating a model (object)
    b. Sketches and Parts
    c. Assembly
    d. Material
    e. Section Creation and Assignment
    f. Tie connections
    g. Partitions, for the load
    h. Step
    i. Load Application
    j. Boundary Conditions
    k. Mesh
    l. Output Request
    m. Job
4- Solver
5- Results
    a. Viewport manipulation
    b. Exporting Figures
    c. Exporting XY Data
    d. Exporting Diagrams

What follows is a short explanation of each separate part. Note that the following text mainly serves the purpose as a reference since the actual script cannot be included within this report.

Input Data

This section collects all available user input, both required and optional input. In other words, this is the only section that the user requires to interact with whilst the rest of the script runs automatically.

Included are a lot of Boolean variables that activates and deactivates features, fail safes and sections of the script.

Also worth mentioning is that the whole bridge is parameterised. Consequently, all measurements, materials, dimensions and placements can be changed via the input section. Beside the benefit of the script being adaptable to new circumstances, it is also a requirement to parameterise the bridge. Simply put, it is by far the most reliable method of obtaining pointers, variables and objects within the script.

Pre-calculations

This section of the script is somewhat larger than one might expect. It defines the classes, functions and imports all relevant Abaqus/Brigade modules. In short, a lot of programming that is relevant for the script but is not dependant on Abaqus/Brigade modules.

Modelling – Creating a model

This section creates the model. Among other items it sets the modelling space and type, as well as the name of the model. For the sake of convenience, the date of creation is appended to the name.

Modelling – Sketches and parts

Here all the sketches and parts are created. A noteworthy aspect of this section is that it is easily refitted for additional parts or less parts. This is due to the fact that it utilises object oriented programming and generalised loops and statements. A current limitation is the shape of the parts, as they cannot be of an arbitrary shape.

Here is also the first appearance of the so called *Foamer*. This is a special part that handles the load application. Or in other words, enables additional handling to include movable loads. Note however, that there are many different possibilities, besides the *Foamer*, to achieve movable loads.

Modelling – Assembly

First and foremost, it creates a very important handle for an even more important object, which is the *root assembly*. This object keeps track of almost all datum, features, load and so on.

Secondly, this section creates an instance of all steel objects. Next step is to translate and rotate all the steel parts into their intended position. Due to the fact that the model geometry is parameterised, virtually any feasible dimensions are possible without additional work. However, a limitation with the script is that only I-beams are currently supported. When the steel beam is assembled a new part is created with merged geometry on the current instances.

Lastly, the Foamer is also created and placed in a desired location, see figure b.2. Currently, the script supports an arbitrary position of the Foamer on the concrete plate. However, diagonal or transversal directions are not available. Though, it does not require much tweaking to add these features.

Modelling – Material

This section creates three elastic materials. The materials are steel, concrete and foam. The latter material is very soft, with a Young's modulus of elasticity of 10 Pa, compared to that steel of 210*109 Pa. The reason for the soft material is that Foamer should not contribute to the stiffness of the model.

Modelling – Section creation and assignment

This section of the script is relatively large. It creates all the required sections and then assigns them to their corresponding parts. A noteworthy aspect of this section is that it requires a lot of coordinates for the script to find the surfaces of which require section assignment. All coordinates points to the middle of the part surfaces.

On an additional note, the Foamer which consists of beam elements also requires a beam section orientation.

Finally, exempting the Foamer, all parts are assigned with homogenous shell sections. This is also where the thickness for each part is assigned. See Abaqus or Brigade documentation for more details.

Modelling – Tie connections

The tie connections tie certain nodes with other nodes, making a stiff connection. In this model, three specific connections are required, which are the following:

- Concrete plate ↔ Upper flange left beam
- Concrete plate ↔ Upper flange right beam
- Concrete plate ↔ Foamer

For the nodes to overlap partitions are required, see figure b.4. The partitions for all connections are created in this section as well via datum planes.

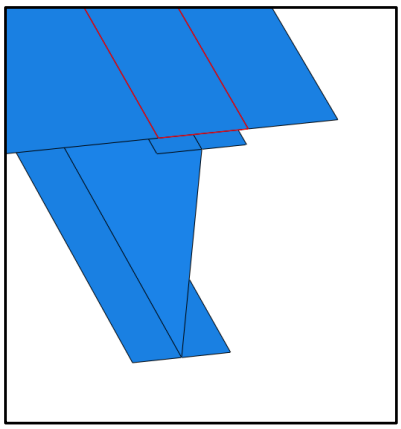

Figure B.4: *Illustration of the partitions required for the tie connections to work properly. For the keen observer, there is actually supposed to be two partitions on the top plate to better correspond to the upper flange of the beam.*

Modelling – Partitions for the load

In a very similar manner to all the other partitions, the Foamer is also divided into many segments. The reason is that Abaqus/Brigade requires the concentrated force to be applied at a given node. The only way to ensure this is via partitions. Consequently, there is a partition for each placement of the load. Incidentally, the aspect of partition is one of the reasons to why the Foamer was introduced in the first place.

Another noteworthy aspect pertaining to the Foamer is about the required input of the user. For the sake of argument, say that a secondary Foamer is to be introduced in the model. All that is required of the user is to select a start point for the partitioning process. The rest is done automatically through the script itself.

Modelling – Step

This is one of the shortest modules. It creates steps for the model. To be precise, this section creates as many steps as there are load placements. To reiterate, if the user requests 50 increments for the moving load, there will be 50 steps.

A consequence of increasing the number of steps is the increased amount of computational time for the solver. As a matter of fact, it takes approximately the same amount of time to solve each step. Consequently, doubling the amount of step just about doubles the amount of computational time for the solver.

Modelling – Load Application

This module applies the load at each increment. Not mentioned before, is that the partitioning module also creates a lot of datum and store their IDs into a list, see Python documentation about list storage. Nevertheless, the load is quite simply applied into a step and onto a given datum point via its ID.

Of course, each load is put into one step and one step only. Lest the number of concentrated forces start to accumulate as the steps increase.

Modelling – Boundary Conditions

The most noteworthy aspect of this section is the amount of coordinates. However, through the input data they are automatically calculated and do not directly require any user input per se.

The relevant geometry for the boundary conditions is divided into a few sets. Even though some geometry shares the same boundary conditions, they are still divided into groups as to better change and refit the boundary conditions to other circumstances.

Modelling – Mesh

One of the larger difficulties with the mesh is to make it of such a size that it corresponds to the partitioning. If the mesh and length of the load partitions are not evenly dividable sheared elements will start to occur, see figure b.5.

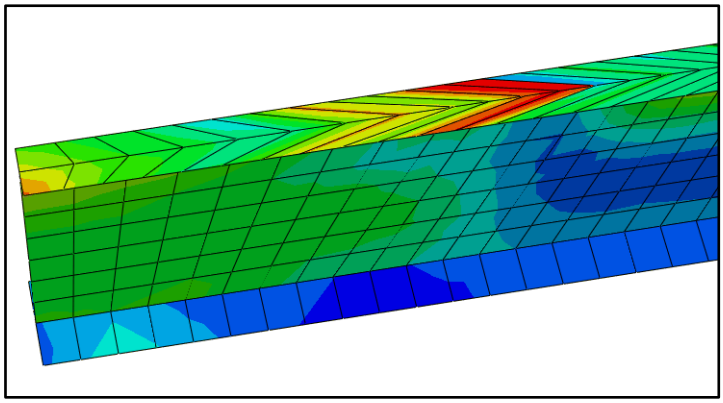

Figure B.5: *This figure highlights the issue of sheared elements. Note how they start of almost square on the left hand side and becomes increasingly sheared as the beam progresses to the right. Though it is especially prevalent in the upper flange, the web suffers from this phenomenon as well.*

The script solves this issue by changing the requested mesh size by the user to the nearest evenly dividable mesh size. To elaborate further, the script changes the mesh size to a finer mesh, if required, that fits an evenly number of elements into each partition.

Otherwise, the model is generated with a mesh consisting of freely placed quad elements with reduced integration.

Modelling – Output Request

This module creates an output request for the output database. By default, the output request contains the following:

- Stresses, included von Mises stress
- Elastic strains, plastic (which should be zero in this case), and total strain
- Displacement and rotations
- Reaction forces and stresses

Modelling – Job

This section creates a job for the solver.

Solver

The main purpose of this module is to submit the created model and problem to the solver. However, only Abaqus have scripted support for the relevant Python commands, whilst Brigade does not.

To circumvent this issue the whole module is placed within an if-statement. Thus, if the script is utilised by Brigade the submit job module is omitted and the user can manually submit the job before proceeding with the script.

Lastly, the script includes an optional fail-safe for the solver. The fail-safe consists of a timer of which the solver attempts to abort the job if the timer runs out. However, when testing this fail-safe it appears that when the procedure is scripted it does not work as intended. As such, the fail-safe is deemed to be not overly reliable.

Results – Viewport and folders

This section opens the output database. It also changes a few viewport variables, such as the default font size to a more readable one. Lastly, this section also creates a folder to store the results in.

Results – Exporting Figures, XY-data, diagrams

The script primarily exports three kinds of results, namely; figures, stress data and diagrams.

The figures are intended to give visual confirmation that the model appears to works correctly. It gives one figure for each step.

The diagrams have about the same function as the figures do, which is to give confirmation that the model works correctly. Of course, both figures and diagrams can easily be omitted from the exported results if desired.

Finally, the primary exported result is the stress data for a given path. The script cannot know in advance which path is most desired, as such, the user has to set a start point for the path. When the path is set, the script exports stress for all of the nodes within the path and for all of the steps. An example of the exported results can be found in table b.1. Note however that the actual result is exported as ASCII and does not have any table formatting. Also, there are no units in the results. Lastly, the actual results are omitted due to its daunting size. In short, the actual results would require a matrix with 500 rows and 100 columns in dimensions.

Table B.1 *Example of the exported results from the script. Note that the script, like Abaqus/Brigade in general, does not put attention to the units. As such, there are no units. Also, this is only a minor example results. The actual results are exported in ASCII formatting, not as a neat table.*

X coordinate	Step1	Step2	Step3	Step4
0	-24286,8	-34572,8	-26108,6	-10855,3
0,5	-21383,7	-32444,8	-24925,1	-10419,1
1	-10683,4	-24866,1	-20700	-9041,54
1,5	2444,83	-13462,2	-14174	-6841,92
2	10220,2	-3678,17	-8980,31	-5130,94
2,5	13752,4	6610,18	-3121,34	-3145,24
3	14377,7	16858	2454,57	-1345,25
3,5	12250,9	24427,9	8076,24	639,771

B.3 Flow Chart

Due to the large size of the script and also that there exist several versions of the script it is omitted from this appendix. However, for more information please contact the authors of this report or the department of Structural Engineering at Chalmers.

The flowchart has three types of boxes. Rounded edges, which is normal action. Diamond shape, which is signifies alternate routes. Finally triangles, which represent *try*-statements, see Python documentation for more details. Also, another simplification is the counter variable. Every time the counter is checked, it is assumed that the number is increased by one.

With this in mind, below is a flowchart that explains the basic outline of the script.

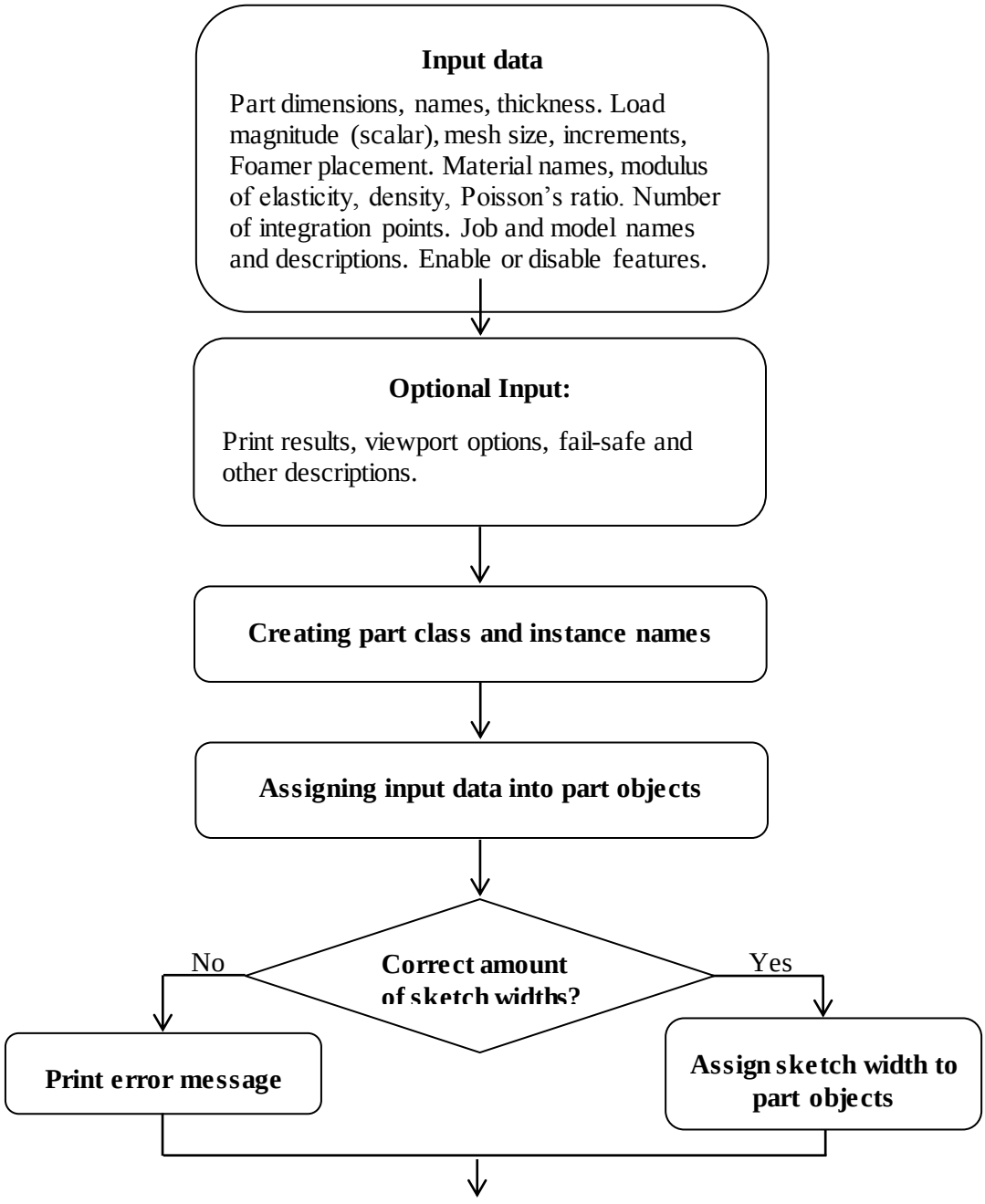

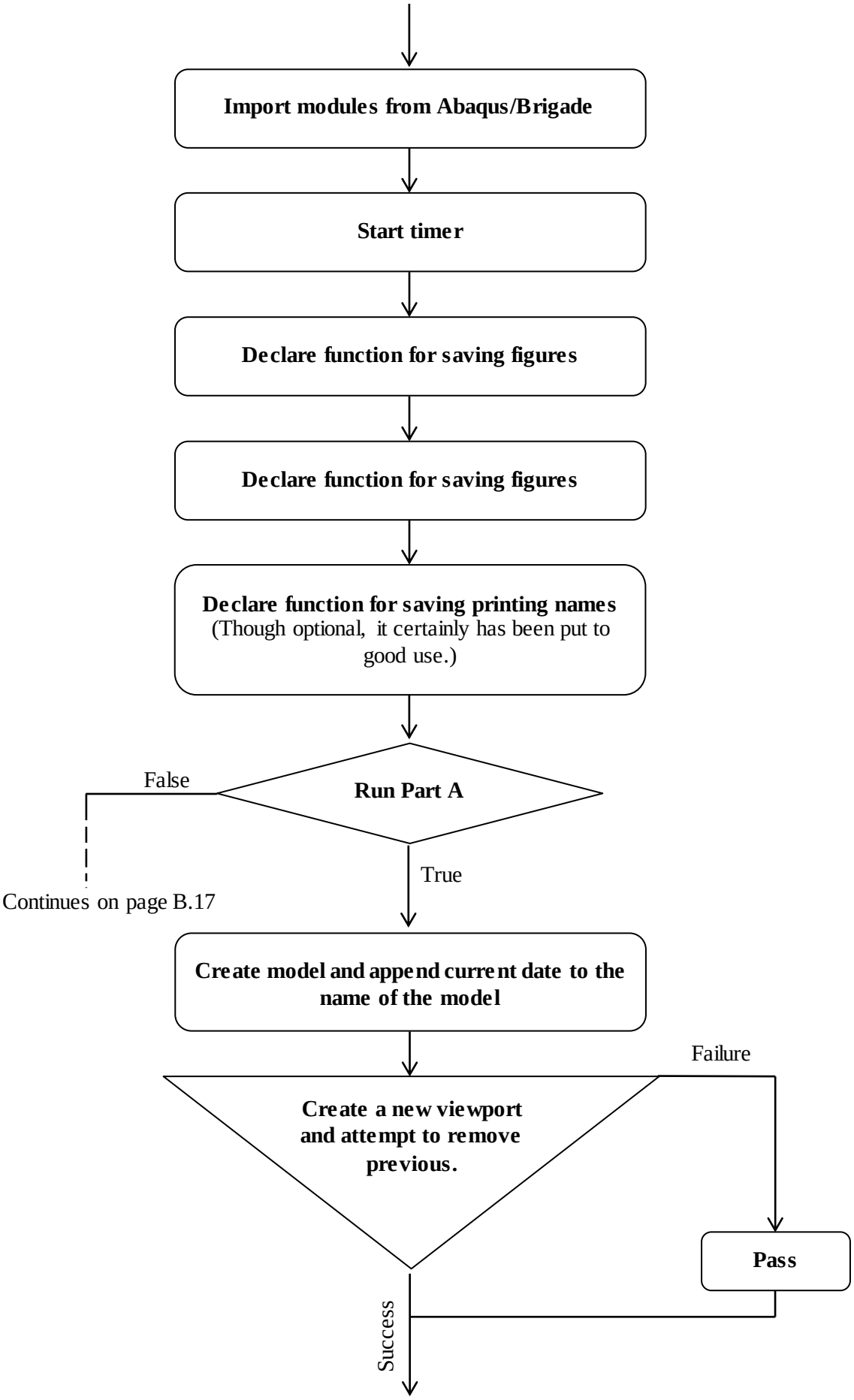
Import modules from Abaqus/Brigade
Start timer
Declare function for saving figures
Declare function for saving figures
Declare function for saving printing names
(Though optional, it certainly has been put to good use.)
Run Part A
False
Continues on page B.17
True
Create model and append current date to the name of the model
Failure
Create a new viewport and attempt to remove previous.
Pass
Success

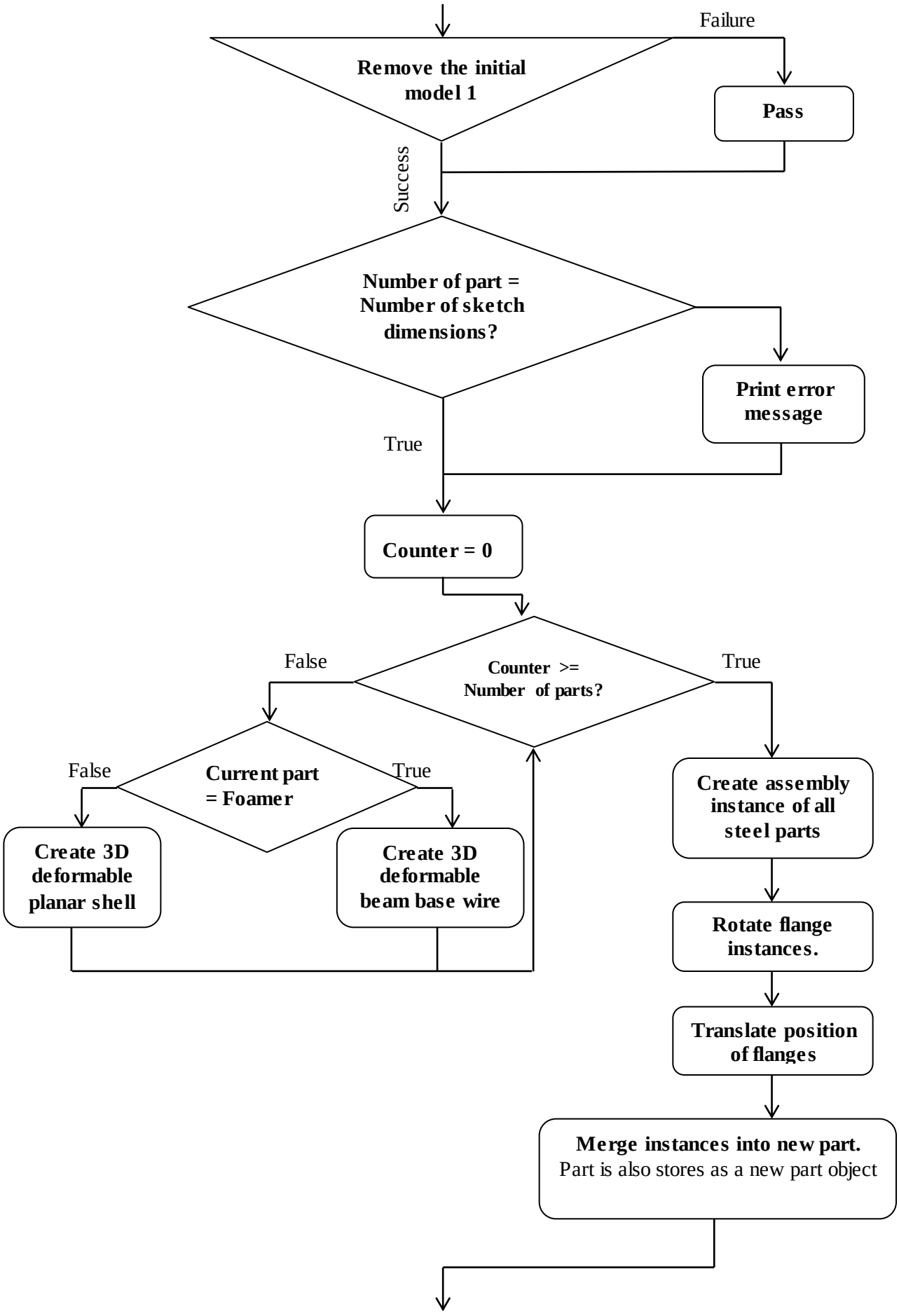
Remove the initial model 1
Failure
Pass
Success
Number of part = Number of sketch dimensions?
Print error message
True
Counter = 0
Counter >= Number of parts?
False
True
Current part = Foamer
False
True
Create 3D deformable planar shell
Create 3D deformable beam base wire
Create assembly instance of all steel parts
Rotate flange instances.
Translate position of flanges
Merge instances into new part.
Part is also stores as a new part object

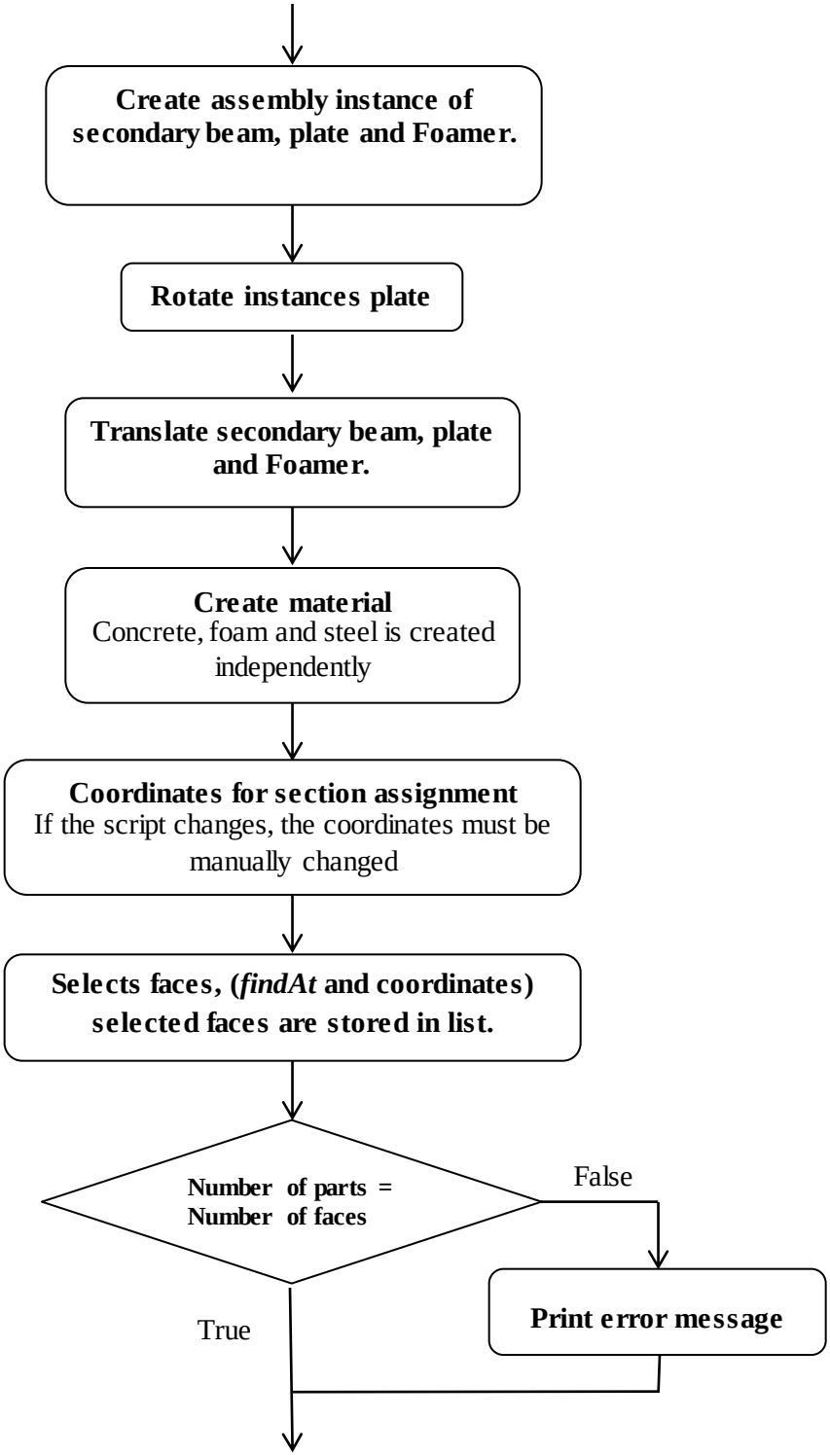
Create assembly instance of secondary beam, plate and Foamer.
Rotate instances plate
Translate secondary beam, plate and Foamer.
Create material
Concrete, foam and steel is created independently
Coordinates for section assignment
If the script changes, the coordinates must be manually changed
Selects faces, (findAt and coordinates) selected faces are stored in list.
Number of parts = Number of faces
False
Print error message
True

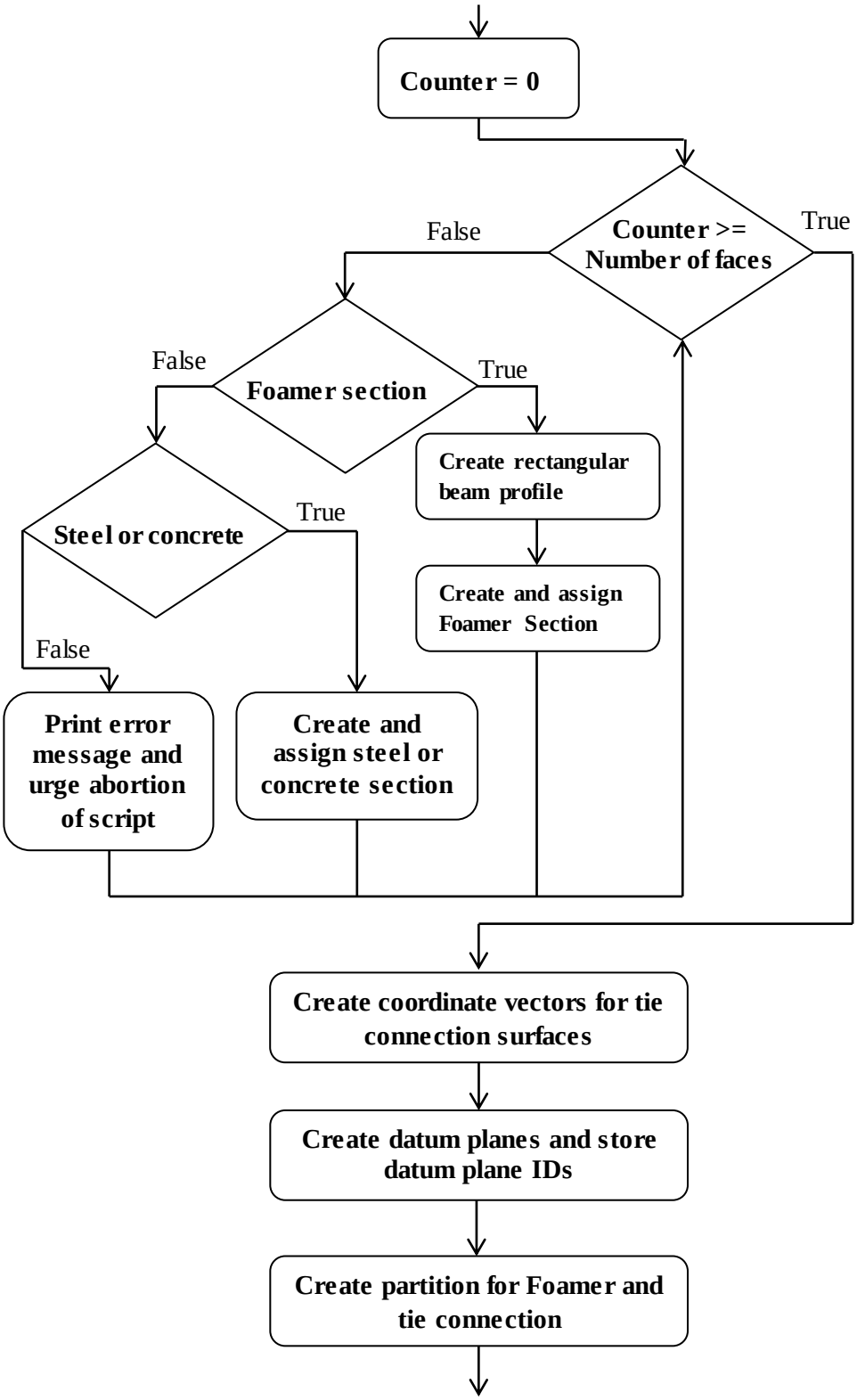
Counter = 0
Counter >= Number of faces
False
True
Foamer section
False
True
Steel or concrete
True
False
Create rectangular beam profile
Create and assign Foamer Section
Print error message and urge abortion of script
Create and assign steel or concrete section
Create coordinate vectors for tie connection surfaces
Create datum planes and store datum plane IDs
Create partition for Foamer and tie connection

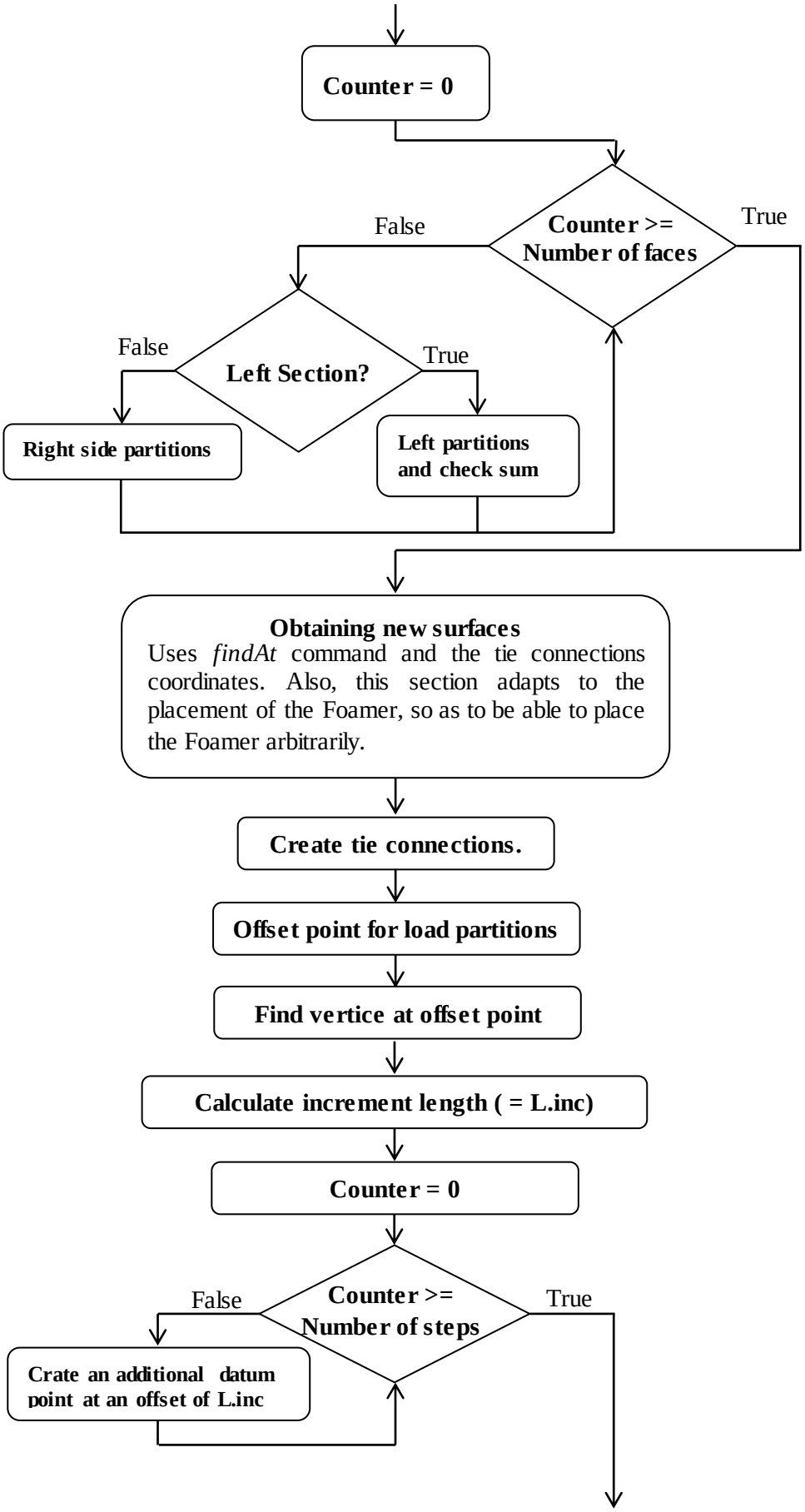
Counter = 0
Counter >= Number of faces
False
True
Left Section?
False
True
Right side partitions
Left partitions and check sum
Obtaining new surfaces
Uses findAt command and the tie connections coordinates. Also, this section adapts to the placement of the Foamer, so as to be able to place the Foamer arbitrarily.
Create tie connections.
Offset point for load partitions
Find vertice at offset point
Calculate increment length (= L.inc)
Counter = 0
Counter >= Number of steps
False
True
Crate an additional datum point at an offset of L.inc

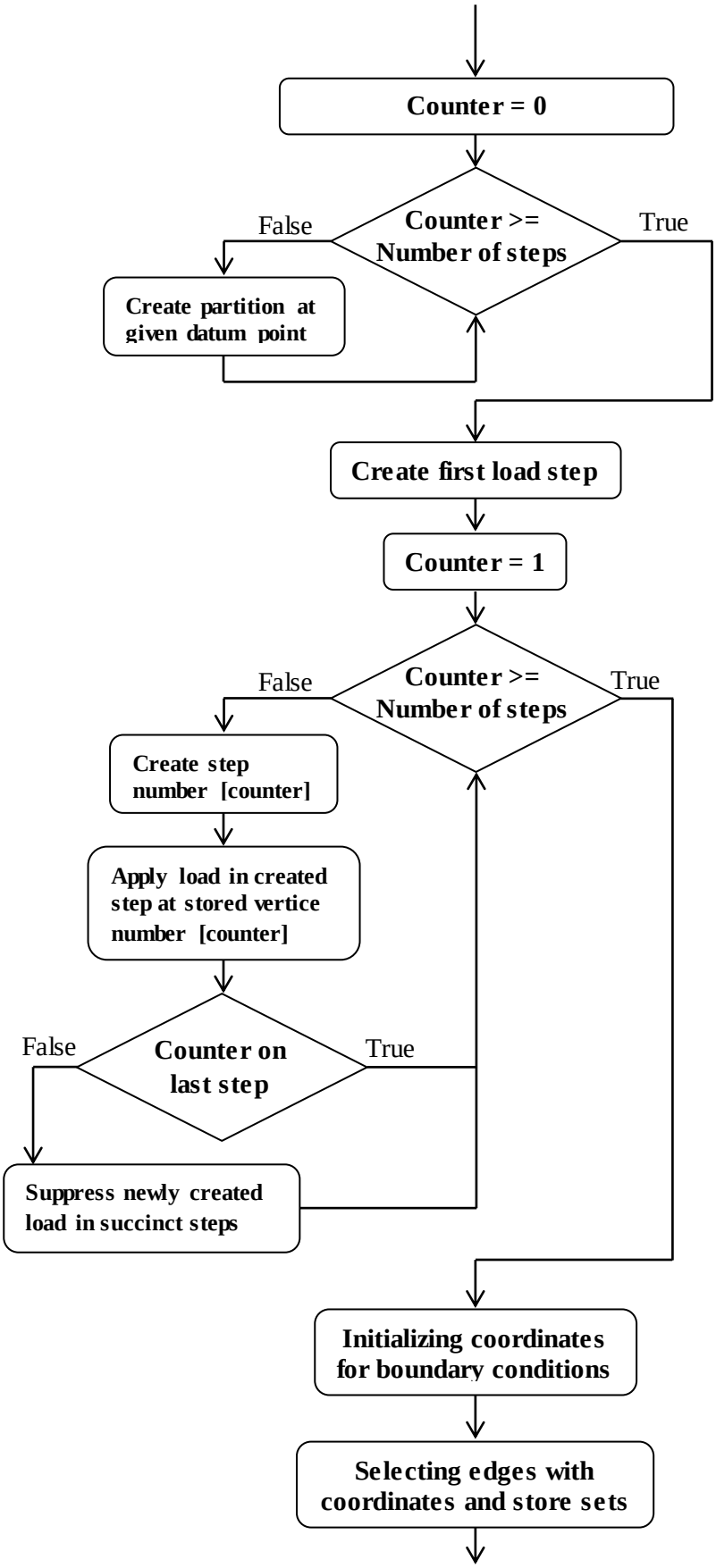
Counter = 0
Counter >= Number of steps
False
True
Create partition at given datum point
Create first load step
Counter = 1
Counter >= Number of steps
False
True
Create step number [counter]
Apply load in created step at stored vertice number [counter]
Counter on last step
False
True
Suppress newly created load in succinct steps
Initializing coordinates for boundary conditions
Selecting edges with coordinates and store sets

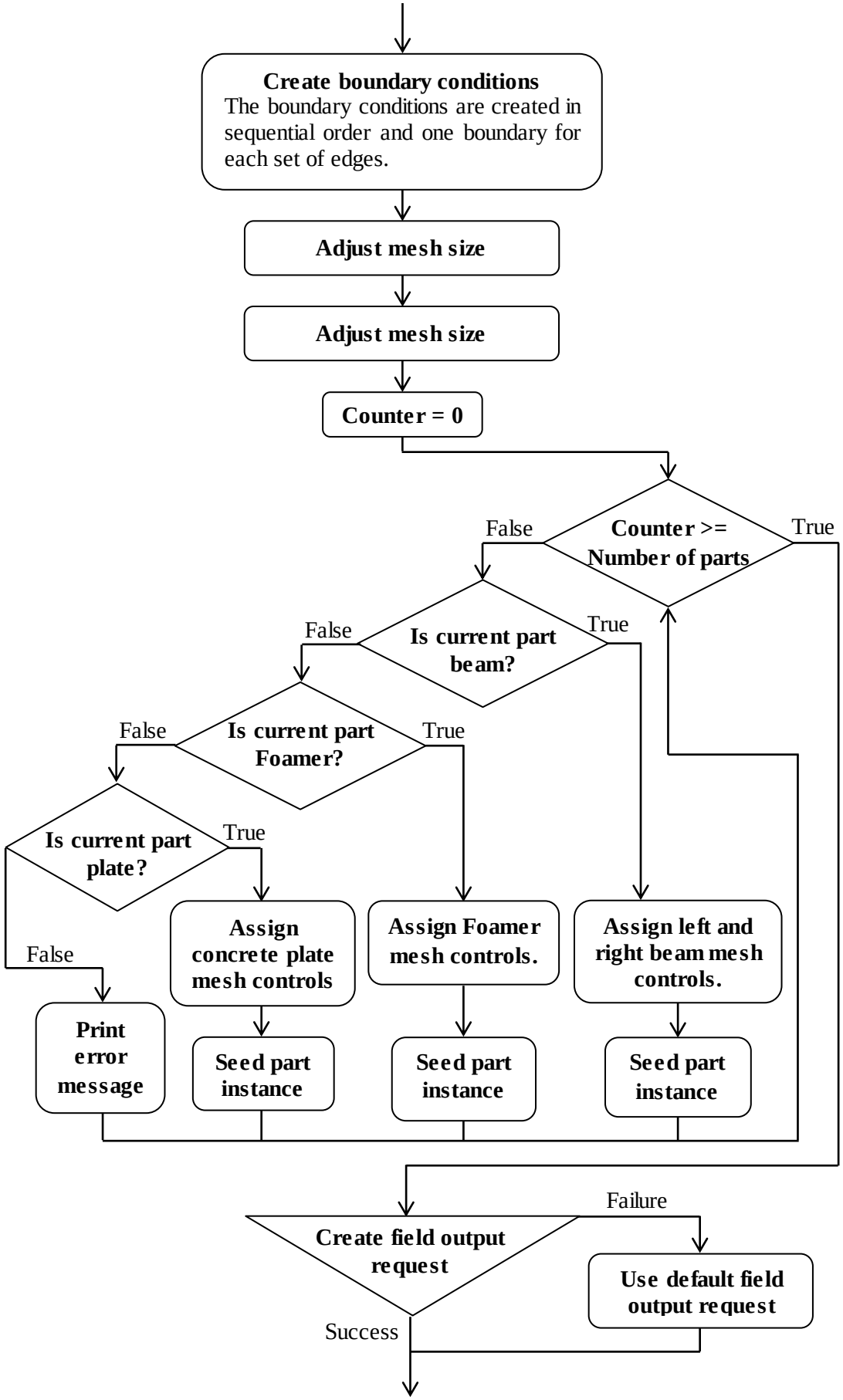
Create boundary conditions
The boundary conditions are created in sequential order and one boundary for each set of edges.
Adjust mesh size
Adjust mesh size
Counter = 0
Counter >= Number of parts
False
True
Is current part beam?
False
True
Is current part Foamer?
False
True
Is current part plate?
True
False
Assign concrete plate mesh controls
Assign Foamer mesh controls.
Assign left and right beam mesh controls.
Print error message
Seed part instance
Seed part instance
Seed part instance
Create field output request
Failure
Use default field output request
Success

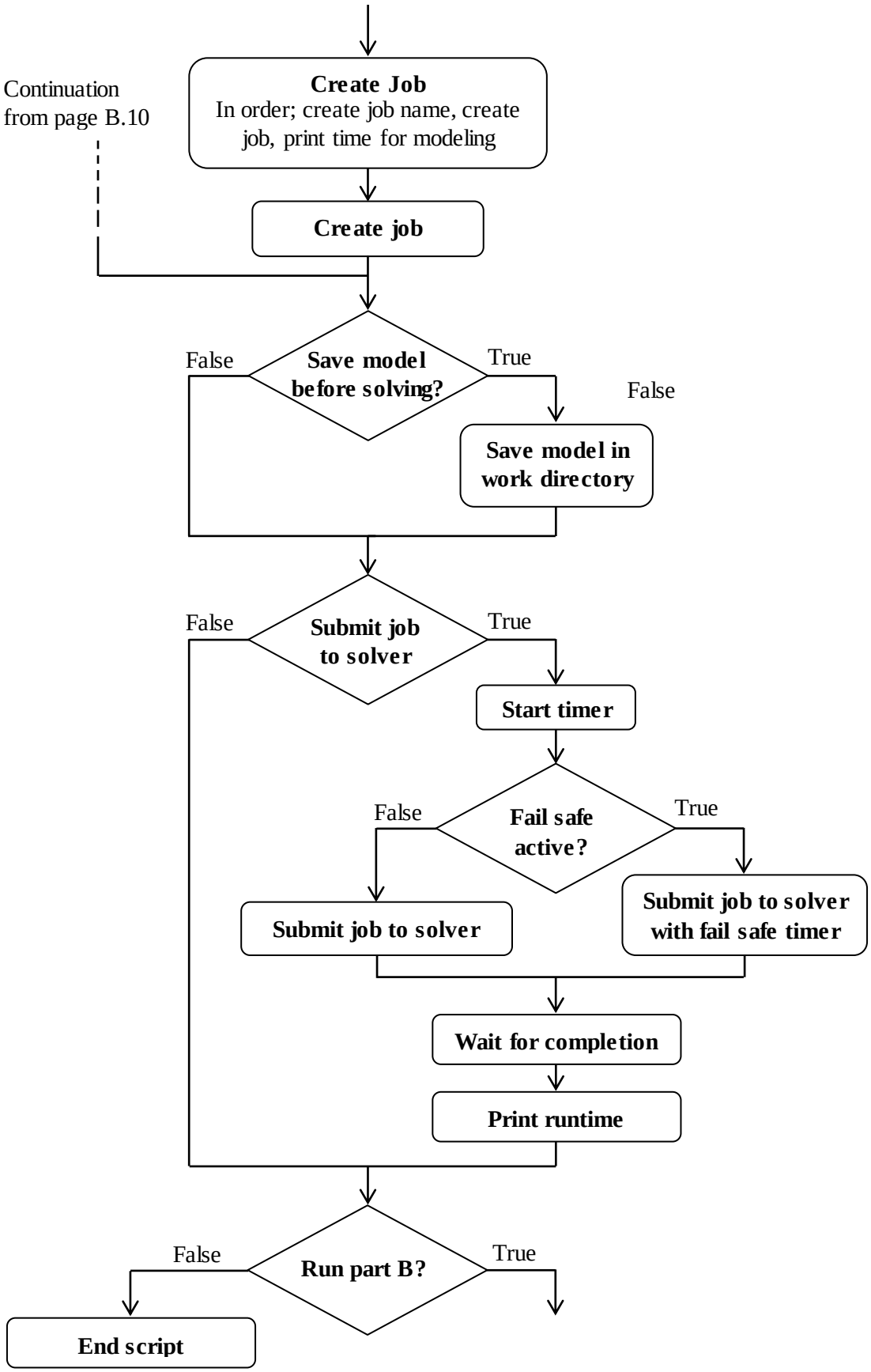
Continuation
from page B.10
Create Job
In order; create job name, create job, print time for modeling
Create job
Save model before solving?
False
True
Save model in work directory
False
Submit job to solver
False
True
Start timer
Fail safe active?
False
True
Submit job to solver
Submit job to solver with fail safe timer
Wait for completion
Print runtime
Run part B?
False
True
End script

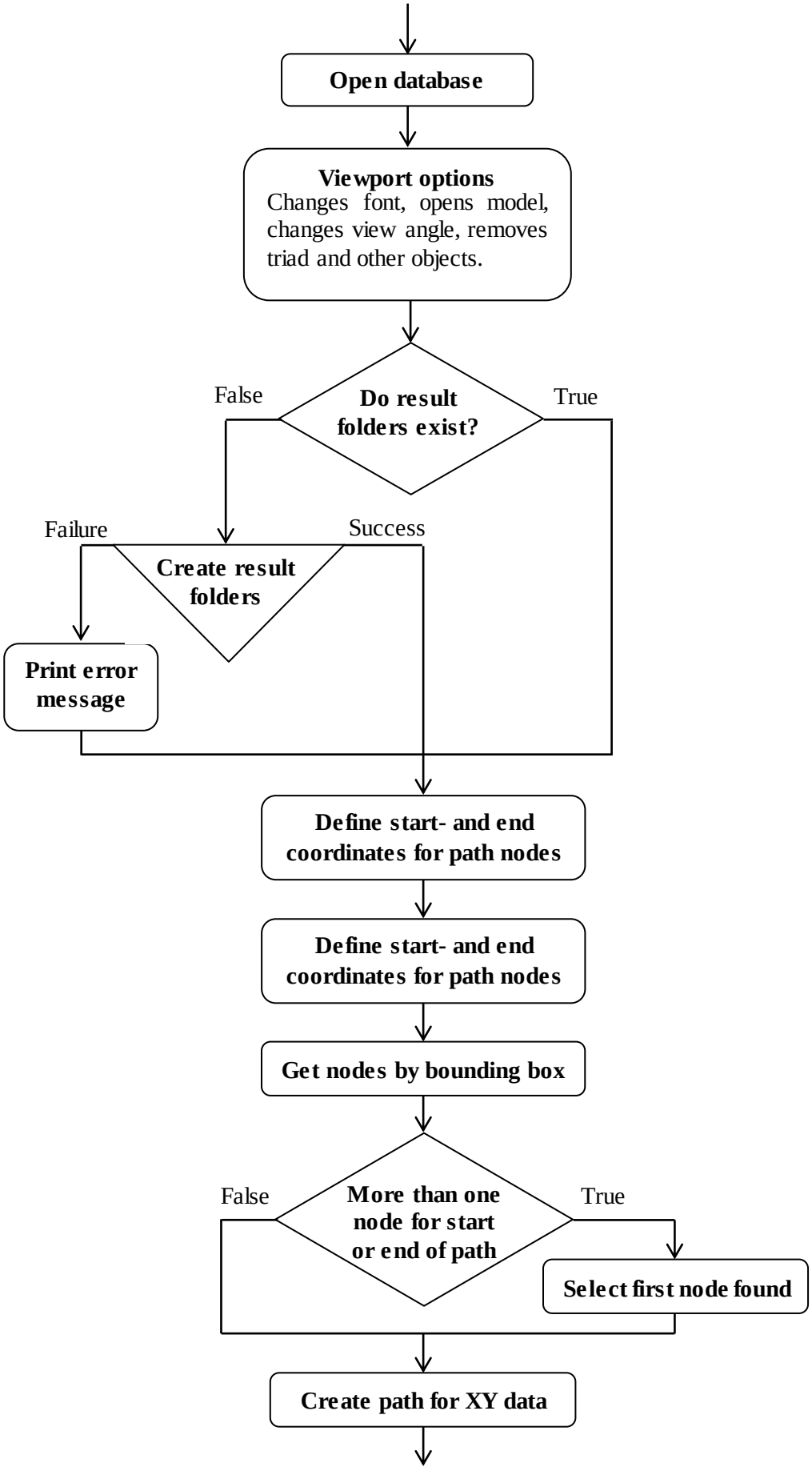
Open database
Viewport options
Changes font, opens model, changes view angle, removes triad and other objects.
Do result folders exist?
False
True
Create result folders
Failure
Success
Print error message
Define start- and end coordinates for path nodes
Define start- and end coordinates for path nodes
Get nodes by bounding box
More than one node for start or end of path
False
True
Select first node found
Create path for XY data

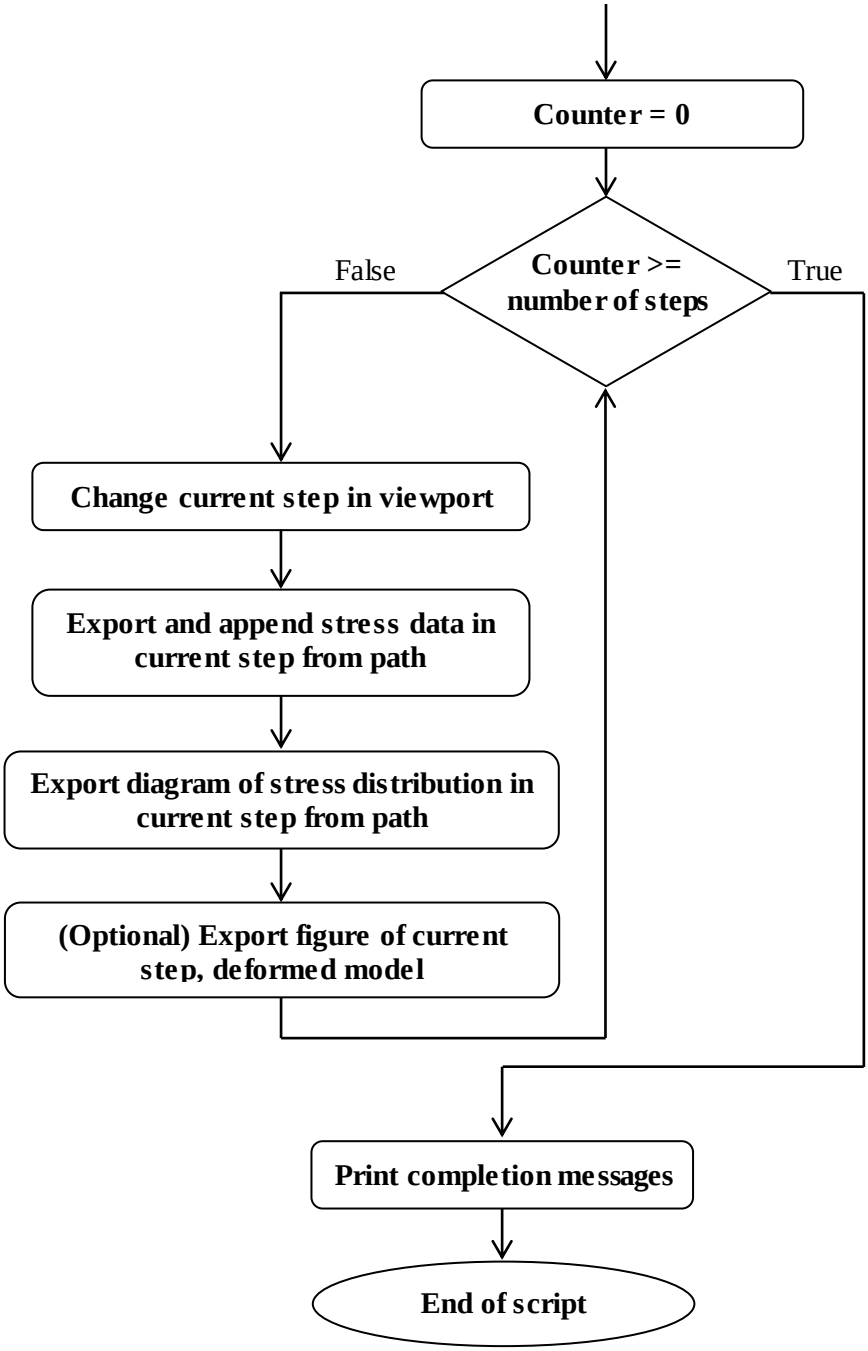
Counter = 0
Counter >= number of steps
False
True
Change current step in viewport
Export and append stress data in current step from path
Export diagram of stress distribution in current step from path
(Optional) Export figure of current step, deformed model
Print completion messages
End of script

Appendix C – Convergence Study and model validation

This appendix, as the title suggest is a convergence study. To be more precise, it is a convergence study about the Abaqus/Brigade script developed for this master thesis. Also included in this appendix, albeit as a minor part, is a brief discussion about the impact of the tie connections used in the script.

The appendix contains the following parts

1. How the study was conducted
2. Results of the study
3. Validation of the model
4. Raw data of the study
5. Hand calculations

This appendix includes mesh convergence study with regard to vertical deflection and magnitude of deflection as well as principal stress and in-plane stress. Also included is the comparison between FEM results and hand calculations. Conclusion about the study can be found at the end.

First and foremost, to give a brief overview of what the script does. The main task is to the move a load over a given bridge in increments. The script does so by modelling the bridge with shell elements in a three dimensional model space. To apply the load a given number of partitions are created, as a matter of fact, there are as many partitions as there are increments. Finally, the load is then moved forward by the means of *steps*, see Abaqus/Brigade documentation for more details, where each steps includes a single point load.

To validate the model both hand calculations and a mesh convergence study was made. Of course, there are additional aspects that have been observed in an attempt to validate the model, such as stress distribution and overall deformation behaviour.

C.1 How the study was conducted

Two categories of variables were chosen for the study, namely deflection and stress. Within these categories four primary variables were chosen, which are the following:

- Magnitude of deflection
- Vertical deflection
- Principal stress, also known as *von Mises Stress*
- In-plane stress, see illustration below.

The motivations for selecting these specific variables are that they are both relevant for the bridge, as opposed to friction of vibration, and they can be compared with hand calculations.

There is an additional reason for studying both magnitude of deflection and the vertical component of deflection. The reason might seem trivial; though it explains a lot of both the result and how the bridge deforms under load. However, before elaborating further on this topic the location where the convergence study takes place should be known. In words, the convergence study takes place in the middle of the bridge. To be more precise, in the outermost node of the lower flanges, an illustration of this can be found in figure c.7.

Returning to the topic of selecting both vertical- and magnitude of deflection, first note the location of the node and also that the steel beams have no real cross bracings. Though the concrete plate may prevent lateral bending of the beams, lateral torsional bending is never prevented, see figure c.8. As such, the node does not only deform in vertical directions, but also outwards from the bridge. This is the main reason for selecting two variables for deflection, to compare how much vertical deflection in relation to the total amount of deflection there is. Lastly, due to the aforementioned reasons the magnitude of the deflection ought to be larger than the vertical deflection alone.

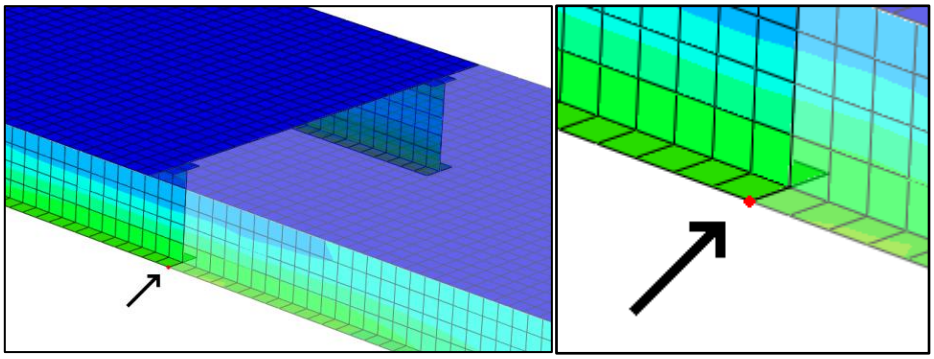

Figure C.7: *This figure shows at what point in the model the convergence study takes place. Though it cannot be seen in the figure, the point always exactly in the middle of the bridge. This is done by via partitions. The right illustration shows a close up showing that the point is always taken as the outmost node in the lower flange.*

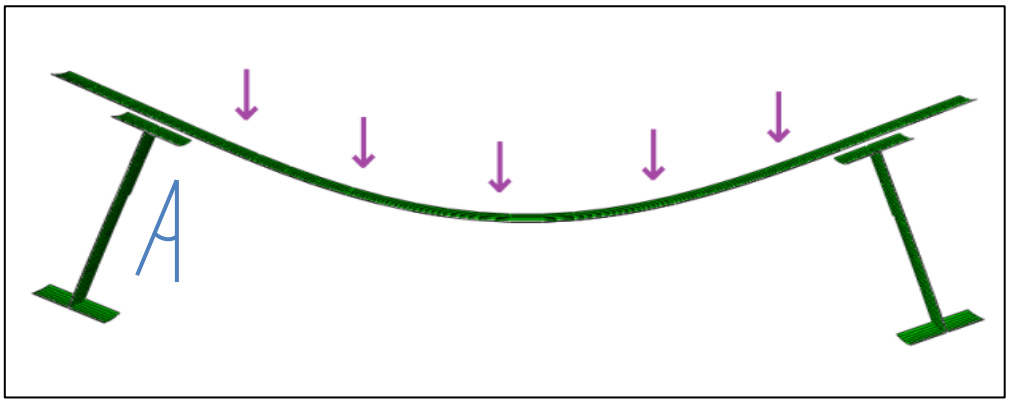

Figure C.8: *Illustration of how the model deforms in the middle of the bridge. Note the lateral torsional bending of the beams. This phenomenon is not studied in this thesis. However, it should be noted that the bending is still there.*

C.2 Results of the Convergence study

To begin, there are three types of results presented in this study; deflection, stress and computational time. The latter is however only mentioned briefly at the end. Consequently, focus lies on the first two mentioned and whether the results converge.

The first result to study is the deflection magnitude which can be found in figure c.9. As can be seen in this figure, the deflection fluctuates quite a bit, especially at the larger mesh sizes. This is however quite well explained as the tie connections cannot properly form. To be more specific, when the desired distance between two nodes are 2m and the maximum distance allowed is about 0.5 some problems are expected. Consequently, anything larger than 1m can easily be disregarded.

Also quite apparent is the large drop that occurs at a mesh size of approximately 1m. The reason for this is that the tie connections between the steel flanges and the concrete plate starts working at about 1m, or to be more precise, 0.909m. Prior to that, the concrete plate carried alone the load. Whereas afterwards, the steel beams contributes to carry the load and thus a lower deflection is obtained.

Finally, in the last segment which is marked by the rectangular box, the deflection appears to converge at a certain value. At the finer mesh sizes the variation in deflection is miniscule. In other words, the results converge and a recommendation is to use mesh sizes finer than 0.4m after studying the results.

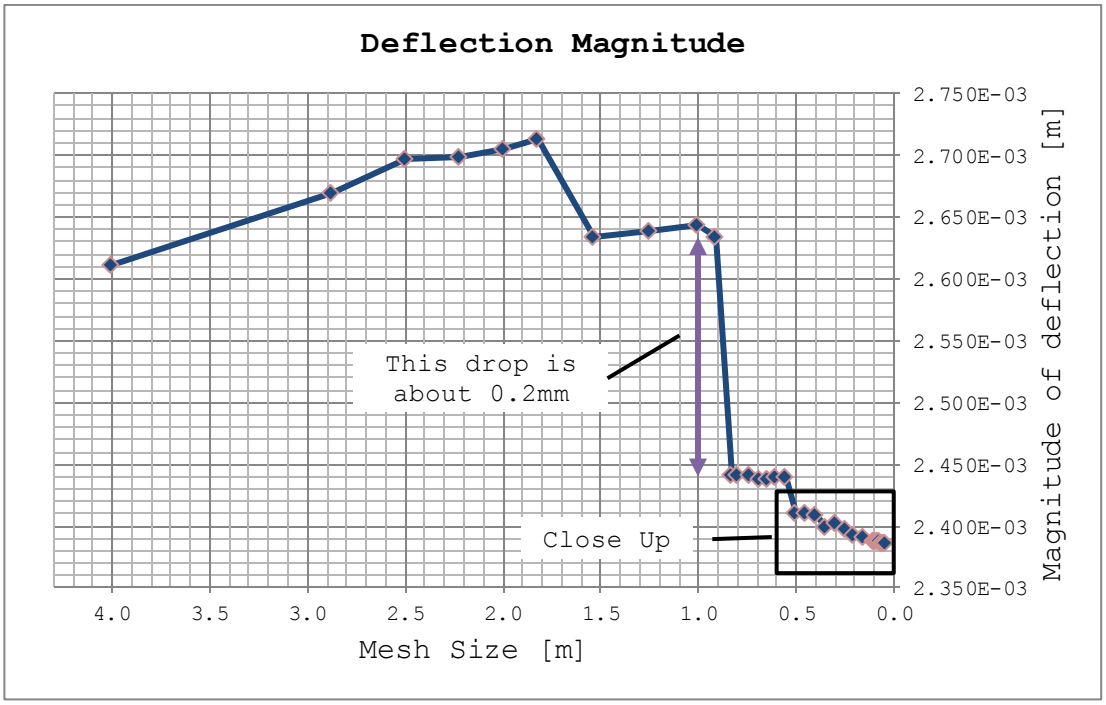

Figure C.9: *Magnitude of the deflection, which is in this instance always a positive scalar value. Pay special attention the vertical scale as the total height of the diagram represents 0.4mm. Consequently, the curve is actually to be considered quite flat.*

When looking at the close up, of the deflection magnitude, the most important aspect to notice is that the curve is rather flat. The difference between the largest value and the lowest value is approximately 2%.

Also included in the close up is a dashed line. This line represents an earlier version of the convergence study. It is included since it somewhat illustrates the problems with the tie connections. The earliest version of the convergence study entailed a non-partitioned concrete plate with regard to the plate-beam connection. However, since nodes overlapped poorly and the tie connection gave of a somewhat erratic behaviour, they were upgraded. The upgrade consisted of a partitioning of the concrete plate; an illustration of this can be seen in figure c.10.

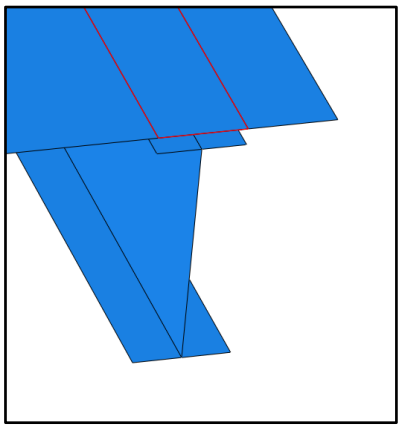

Figure C.10: *Partitions to improve the tie connections. The partition can be seen as marked above the I-beam. The partition forces some nodes to coincide on the vertical plane and more stable tie connections.*

The aforementioned improvement enhanced the overall behaviour of the model, especially at larger mesh sizes. However, as can be seen in the close up diagram, figure c.11, they ultimately only have a minor influence. Moreover, the dashed and solid curve follows the same behaviour. This fact to some extent contradicts the likelihood of the tie connections being the sole disturbance in gaining optimal convergence. Adding more support for some kind of singularity issue or poor boundary conditions.

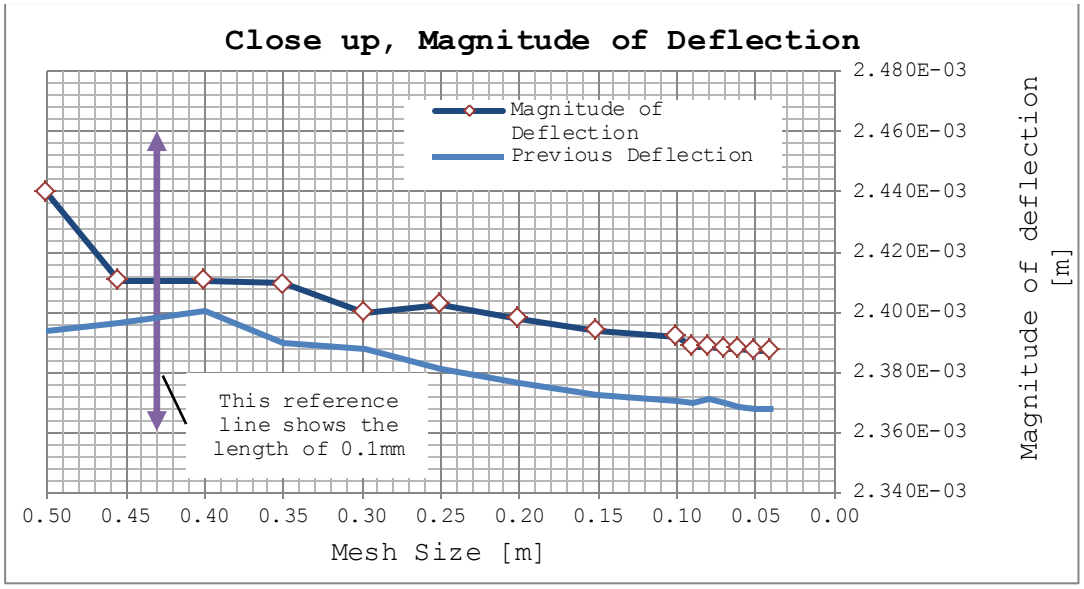

Figure C.11: *This shows a close up. The biggest point of interest is that there is almost no significant variation. Also, pay special attention the scale of the diagram as the total height represents 0.14mm. This is indeed an insignificantly small distance when discussing a 40m bridge. The dashed line represents deflection before modifications to the model.*

Moving on to the second area of study which is principal stress, see figure c.12. The first section to mention is what happens to mesh sizes larger than 1m. Here, the stress shows a rather stable behaviour, which is actually somewhat unexpected given the results from the deflections. As mentioned earlier, the tie connections between steel beams and concrete plate have some problems forming properly at excessively large meshes. However, it still appears that the principal stress is stable in this section.

Similar to the deflections, see figure c.9, the stress also makes a sudden change at a mesh size of 0.9m. This is for the very same reason as for the deflections, namely that it is at this instance where the tie connections can form properly.

The third and final section of the curve, which is marked by a rectangular box, shows quite stable behaviour. The fluctuations in this final section are less than 2%. In other words, the results appear to converge relatively quickly after a mesh size that is lower than 0.9m. In short, convergence is reached.

Also included in this convergence study is the in-plane stress in figure c.13. To clarify, the stress that is normal to the cross section of the bridge. In the Abaqus/Brigade model for this thesis it is also referred to as S11 stress.

The reason for including both types of stresses in the convergence study is for comparison. If everything is in order, the in-plane stress and the principal stress should be close to identical. Otherwise, it would be a strong indication of an erroneous model. Fortunately, both stresses exhibit a more than sufficiently similar behaviour.

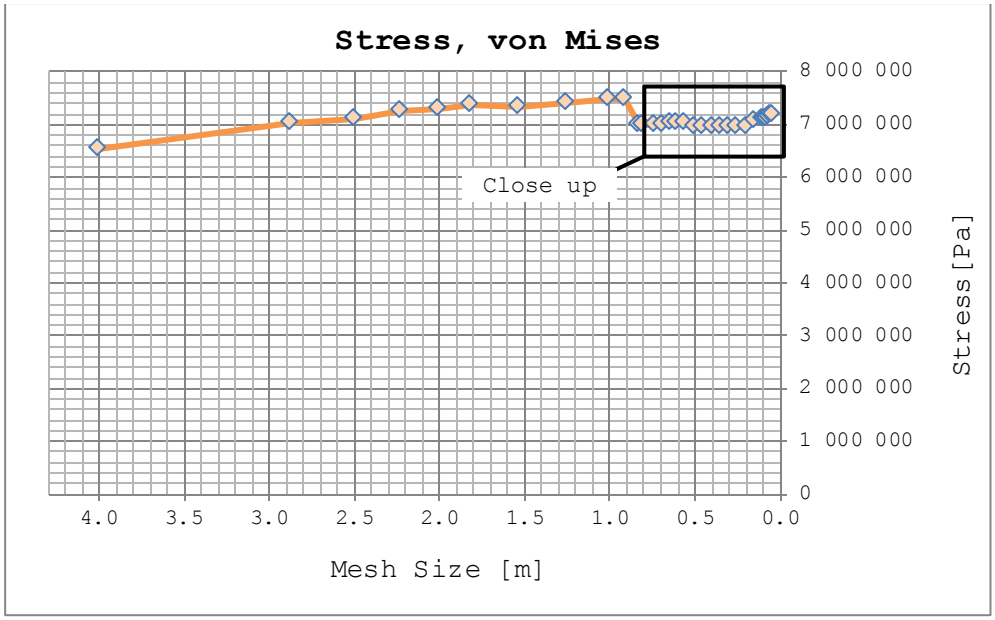

Figure C.12: *Principal stress change in relation to mesh size. Note that there is a jump at a mesh size of 0.9m. This phenomenon is due to the tie connections, which is more elaborately discussed in this appendix.*

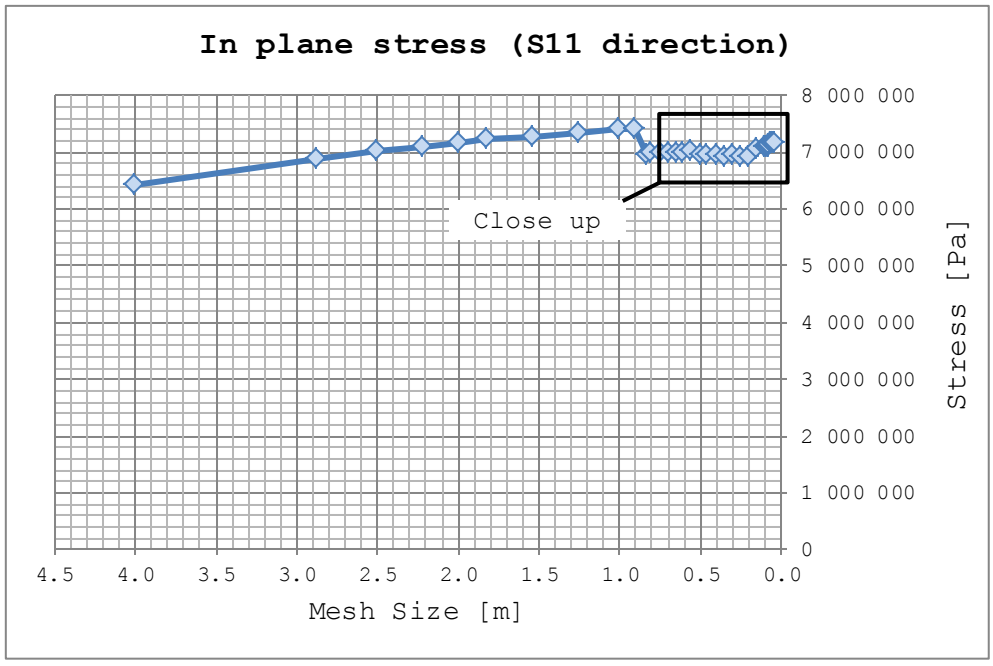

Figure C.13: *Showing the in plane stress at the node. Note that the behaviour is essentially the same as for the principal stress. Also note the same sudden change at a mesh size of 0.9m. This is once again due to the tie connections.*

The close up diagram for the stresses, figure c.14, includes both principal stress and the direct stress. Also note that there is a dashed line representing the principal stress before partitioning and improvement of the tie connections were introduced. Most noteworthy about this diagram is how well the in-plane stress corresponds to the principal stress. At the very end, they coincide close to perfectly. That the two types of stresses share the same behaviour is expected and is to be taken as a good sign.

Also note that the stress increases as the mesh size decreases. Especially the steep slope at the end is of some concern. The inclination of the slope and especially the fact that the curve does not plateau indicates that there is a less than desired level of convergence. A likely explanation is that there is a stress singularity that causes the stress not to converge. Another hypothesis is that the assembly of the beam, especially the nodes that belong to both web and flanges, gives cause for poor convergence. However, the true reason for the convergence issue is not known at this moment, though the issue itself is known.

A final point of interest is the behaviour of the dashed line in figure c.14. As already mentioned, this line represents an earlier version of the convergence study, before improved tie connections were introduced. Note that the dashed line succinctly coincides to a greater degree with the principal stress as the mesh size decreases. In other words, the smaller the mesh size the less influence the partitions have over the tie connections. Conversely, at larger mesh sizes the partitions have a greater influence, even as far as postponing model failure.

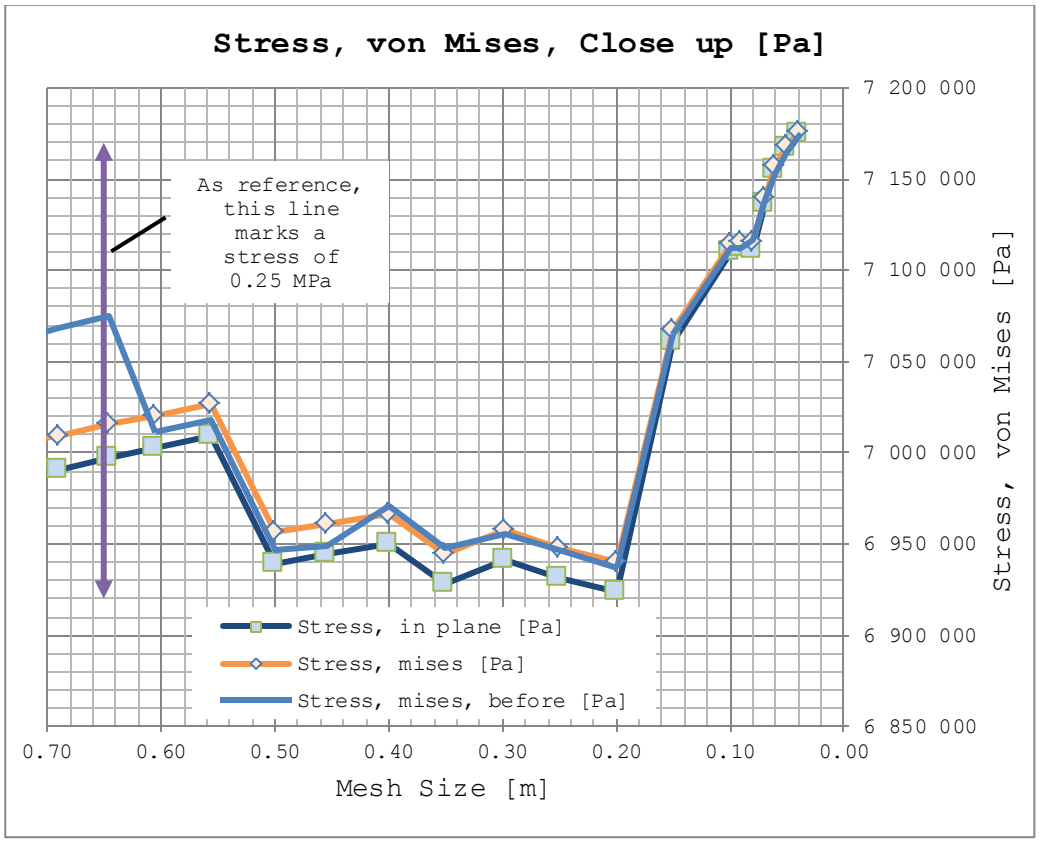

Figure C.14: *Close up of both the principal stress and the in plane stress. Once again, note the scale of the vertical axis as it might enhance the effect stress variations to some degree. The dashed line shows stress before modifications to the model, which is of some interest.*

Also worth mentioning, however briefly, is the time for solving each model. The script that creates and runs the program also records the time for each run of the script. The result is presented below in figure c.15. Of course, the whole of the convergence study was conducted on the same computer hardware. The point of interest for this figure is that the computational time is less than 20s for all meshes up to a mesh size of 0.2m. After this point, the calculation time increases exponentially, making it increasingly harder for each succinct step.

With this in mind and as a comment about the convergence study; the study was conducted with succinctly smaller mesh sizes. The mesh sizes were decreased to the point of where the available computer hardware simply was insufficient to solve the problem. In other words, the mesh size was decreased to the point of failure. Of course, the last and also unreliable results are omitted.

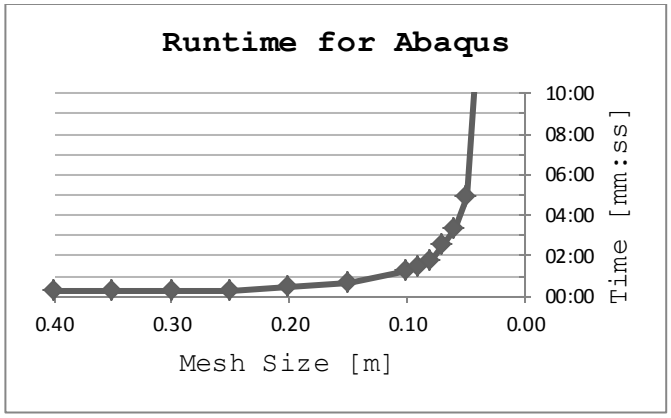

Figure C.15: *More as a point of interest compared to the other studied variables is the necessary computational time for one run of the script. Note that the modelling time itself, when scripted, is around 1 second. The rest of the time is for solving the FEM problem.*

C.3 Validation of the model

In addition to the convergence study, the FEM script and model was also validated through comparison to hand calculations. Similarly to the convergence study both stress and deflection was studied.

As indicated in the convergence study, both stress and deflection changes in the FEM model depending on the mesh size. For the validation, both maximum and minimum values for stress and deflection are taken into account. However, mesh sizes over 0.9m are omitted in total since they are unreliable, see convergence study for more details.

Direct stress FEM: $\sigma_{FEM.min} = 6.92\ Mpa$
$\sigma_{FEM.max} = 7.17\ Mpa$

Stress, Hand calculations: $\sigma_{hand} = 7.15\ Mpa$

When comparing the stresses, the FEM calculations have a difference that ranges from -1.7% to +0.3%. In other words, the values are within very reasonable limits. One might even go so far as calling it quite an excellent degree of coincidence.

Deflection FEM: $\delta_{FEM.min} = 2.32mm$
$\delta_{FEM.max} = 2.27mm$

Stress, Hand calculations: $\delta_{hand} = 2.08\ mm$

When comparing the deflections the degree of coincidence is not as good. Here the FEM calculations diverge between 8-11% of what the hand calculations indicates. Though it is not an excessively high degree divergence it is neither optimal.

C.4 Tables from the convergence study

This section displays the unprocessed data obtained from the convergence study. See prior section in this appendix for comments and discussion. In this section, there are only two tables, namely _____

Table C.2 *The values from where the concrete plate is partitioned. All values are stored directly from Abaqus/Bridage with the probe value tool. The mesh size is the actual mesh size in the model and not the input mesh size.*

Mesh size [m]	Runtime [mm:ss]	Stress, mises [Pa]	Stress, in plane [Pa]	Deflection, Magnitude [m]	Deflection, Vertical [m]
4,0000	00:15	6548110	6,4369E+06	0,00261148	-0,00247844
2,8750	00:13	7015550	6,8859E+06	0,00266889	-0,00253605
2,5000	00:13	7120010	7,0100E+06	0,00269644	-0,00256581
2,2222	00:13	7247520	7,1062E+06	0,00269849	-0,00256600
2,0000	00:13	7291440	7,1811E+06	0,00270494	-0,00257339
1,8182	00:13	7371380	7,2259E+06	0,00271267	-0,00258037
1,5385	00:13	7340480	7,2750E+06	0,00263400	-0,00250547
1,2500	00:13	7411930	7,3580E+06	0,00263931	-0,00251065
1,0000	00:13	7476430	7,4220E+06	0,00264334	-0,00251455
0,9091	00:13	7478010	7,4167E+06	0,00263468	-0,00250643
0,8333	00:13	6989060	6,9689E+06	0,00244087	-0,00232022
0,8000	00:13	6994420	6,9748E+06	0,00244115	-0,00232052
0,7407	00:17	7004500	6,9844E+06	0,00244180	-0,00232112
0,6897	00:13	7008890	6,9905E+06	0,00243840	-0,00231775
0,6452	00:17	7015310	6,9969E+06	0,00243882	-0,00231812
0,6061	00:13	7020620	7,0023E+06	0,00243916	-0,00231844
0,5556	00:13	7026980	7,0087E+06	0,00243959	-0,00231882
0,5000	00:13	6956090	6,9394E+06	0,00241022	-0,00229047
0,4545	00:15	6960990	6,9444E+06	0,00241054	-0,00229075
0,4000	00:15	6966330	6,9497E+06	0,00240950	-0,00228969
0,3509	00:15	6944230	6,9282E+06	0,00239960	-0,00228008
0,2985	00:17	6957660	6,9411E+06	0,00240259	-0,00228032
0,2500	00:19	6948230	6,9319E+06	0,00239752	-0,00227535
0,2000	00:27	6940280	6,9242E+06	0,00239356	-0,00227157
0,1504	00:38	7067720	7,0611E+06	0,00239148	-0,00228078
0,1000	01:18	7114100	7,1101E+06	0,00238864	-0,00227966
0,0901	01:28	7115650	7,1117E+06	0,00238809	-0,00227865
0,0800	01:48	7115310	7,1114E+06	0,00238771	-0,00227825
0,0699	02:31	7139160	7,1365E+06	0,00238744	-0,00227895
0,0601	03:20	7157160	7,1552E+06	0,00238713	-0,00227853
0,0500	04:56	7168020	7,1665E+06	0,00238685	-0,00227839
0,0400	12:04	7176060	7,1748E+06	0,00238677	-0,00227839
0,0200	99:99*	Computer Failure	Computer Failure	Computer Failure	Computer Failure

Table C.3 *The values from where the concrete plate is without partitions pertaining to the tie connections. All values are stored directly from Abaqus/Bridage with the probe value tool. The mesh size is the actual mesh size in the model and not the input mesh size.*

Mesh size [m]	Stress, mises[Pa]	Deflection, Magnitude [m]	Deflection, Vertical [m]
4,0000	Model Failure	Model Failure	Model Failure
2,8750	Model Failure	Model Failure	Model Failure
2,5000	Model Failure	Model Failure	Model Failure
2,2222	---	---	---
2,0000	7 138 160	0,00262310	-0,00252874
1,8182	---	---	---
1,5385	7 284 050	0,00266175	-0,00254634
1,2500	---	---	---
1,0000	7 485 840	0,00263395	-0,00250906
0,9091	7 475 780	0,00269961	-0,00253699
0,8333	6 962 610	0,00246678	-0,00231346
0,8000	6 967 280	0,00246745	-0,00231415
0,7407	7 059 120	0,00246734	-0,00233723
0,6897	7 067 890	0,00246832	-0,00233818
0,6452	7 075 240	0,00246917	-0,00233900
0,6061	7 011 300	0,00242162	-0,00229881
0,5556	7 017 450	0,00242199	-0,00229915
0,5000	6 947 130	0,00239367	-0,00227513
0,4545	6 949 150	0,00239660	-0,00228031
0,4000	6 970 820	0,00240033	-0,00228007
0,3509	6 948 030	0,00238987	-0,00226869
0,2985	6 955 800	0,00238775	-0,00226388
0,2500	6 946 330	0,00238088	-0,00225758
0,2000	6 936 910	0,00237653	-0,00225431
0,1504	7 064 790	0,00237233	-0,00226104
0,1000	7 111 740	0,00237035	-0,00226044
0,0901	7 111 790	0,00236939	-0,00225840
0,0800	7 116 310	0,00237092	-0,00226003
0,0699	7 138 760	0,00236937	-0,00225953
0,0601	7 152 880	0,00236814	-0,00225894
0,0500	7 165 190	0,00236794	-0,00225843
0,0400	7 173 170	0,00236785	-0,00225857
0,0200	Computer Failure	Computer Failure	Computer Failure

Appendix D – Matlab functions for the parametric study

The purpose of the Matlab functions which are used for the parametric study is to store and collect the data. While this task certainly could be performed by hand the functions reduces the risk of human error. In addition it lightens the work load for the parametric study.

The main function is ExcelWriter which utilise the two functions cellWriter and cellFinder to write data to Excel documents. Additionally it also utilises some of the functions for fatigue calculations which can be found in Appendix E.

The functions can be found in more detail within this appendix in the order given below:

D.1 ExcelWriter

```
function [lostVariables, nVariables] = ExcelWriter(pathDir, importInput, importResult)
%%%%%%%%%%%%%%%%%%%%%%%%%%%%%%%%%%%%%%%%%%%%%%%%%%%%%%%%%%%%%%%%%%%%%%%%%%%%%%%
% This is a function that reads Mathcad output data and writes the data to an Excel file.
%
% Input:
%
%   pathDir:      The relative or full path to the directory. The path should be given as a string
%
%   importInput:  Indicates if the input data should be imported. zero to not import and one to
%                 import.
%
%   importResult: Indicates if the default result excel file should be imported. zero to not
%                 import and one to not import. It is recommended to import the file in order to
%                 reduce the risk of keeping old data.
%
% Output:
%
%   lostVariables: Cell matrix which contains the name and value of the variables that could not be
%                  written to the Excel file.
%
%
% Description:
%
%   ExcelWriter is a function that reads Mathcad output data and writes the data to an Excel file.
%   Furthermore, the fatigue is assessed with both the damage equivalent method and Palmgren-Miner
%   method.
%   The function may require additional user input and prints the results at the end.
%
% Important note:
%
%   The directory must contain a subdirectory named 'Mathcad data' that contains .dat
%   files obtained through Mathcad. In addition the directory must contain a Excel file that is
%   named Result.xls or it should be imported.
%
%   Additionally, note that both the result and input directory are found by relative paths.
%   Therefore a revision may be needed before using the function elsewhere.
%
%
% Developed by:
% Mattias Renström
% Oskar Rydh
%
% Developed in cooperation with:
% Chalmers University of Engineering
% NCC Teknik, Gothenburg
%
% Last edited:
% 2014-06-02
%%%%%%%%%%%%%%%%%%%%%%%%%%%%%%%%%%%%%%%%%%%%%%%%%%%%%%%%%%%%%%%%%%%%%%%%%%%%%%%

% Initialisation of the list of lost variables.
lostVariables = [];

% Initialisation of counter of the number of variables that is found.
nVariables = 0;
```

```
% The Mathcad output should always be located in subfolder called 'Mathcad data'
pathData = [pathDir '\Mathcad data\'];

% The Mathcad output that is needed for the fatigue calculations should be located in
% the subfolder called 'Fatigue'
pathFatigue = [pathDir 'Fatigue\'];

% ================================================================== %
% ============ Importing Excel documents to directory ============== %
% ================================================================== %

% Creates a list of the items in the current directory
directoryList = dir([pathDir]);

fprintf(['Checked that all the paths are correct?\n'])
answer = input('[y/n]\n\n','s');
if answer != 'y'
   % stops the function
   stop
end

% Importing the Excel input file if is requested
if importInput == 1
   copyfile('..\Input\Parameters.xls',[pathDir 'Parameters.xls'])
end

% Checks if the result file exists.
resultExists = 0;
for i = 1:length(directoryList)
   if isequal(directoryList(i).name,'Result.xls')
      resultExists = 1;
   end
end

% Importing the Excel input file if is requested, after confirmation from the user.
% if the result file doesn't exist user input is automatically requested.
if resultExists == 0
   fprintf(['Result.xls file does not exist in the chosen directory\n'...
         'Do you wish to copy the default file to this directory?'])
   answer1 = input('[y/n]\n\n','s');

   if isequal(answer1,'y')
      fprintf('\nUnderstood, the file will be created.\n\n')
      copyfile('..\Results\Result default.xls',[pathDir 'Result.xls'])
   else
      fprintf('\nUnderstood, the file will not be created. Expect problems.\n\n')
   end
```

```
elseif resultExists == 1
   if importResult == 1
      fprintf('Please confirm the overwriting of the existing Result.xls\n')
      answer2 = input('Proceed? [y/n]\n\n','s');
      if isequal(answer2,'y')
         fprintf('\nUnderstood, the file will be overwritten.\n\n')
         copyfile('..\Results\Result default.xls',[pathDir 'Result.xls'])
      end
   end
end


% ================================================================== %
% ================  Importing Excel data to Matlab ================== %
% ================================================================== %


% Obtaining the names of all the sheets in the result Excel file.
[~,sheetNames] = xlsfinfo([pathDir '\Result.xls']);

% All the data in the Excel file is read and stored in a structure array. The data for each sheet is
% stored as a matrix with the sheet name as index.
for i = 1:length(sheetNames)
   % The cell containing the sheet name is transformed from a cell into a string.
   sheet = char(sheetNames(i));

   % The data in the current sheet is read and stored in a temporary matrix. Note that the matrix
   % contains cells.
   [~,DATA,~]=xlsread([pathDir '\Result.xls'],sheet);

   % Finally the data for the current sheet is stored in the Excel data matrix. The index is the
   % name of the current sheet.
   ExcelData.(sheet) = DATA;
end

% ---------- Writing some miscellaneous data ----------

% Writing the current date
currentDate = date;
cellWriter(currentDate,'Date',sheetNames,ExcelData,[pathDir '\Result.xls']);

% Writing the current directory
cellWriter(pathDir,'Folder',sheetNames,ExcelData,[pathDir '\Result.xls']);

% ================================================================== %
% ================  Calculating the fatigue life ================== %
% ================================================================== %

% In addition to the calculations performed in the Mathcad documents there
% are calculations performed in Matlab to assess the fatigue life with the
% help of the Palmgren-Miner method.

% The maximum damage is obtained through another Matlab function given the path to the
% cross-sectional data from Mathcad.
[damagePalmgrenMiner,~,modeList] = Kea_allCrackingModes(pathFatigue);
```

```
% Printing the damage for each fatigue cracking mode to the Result Excel document.
for i = 1:length(modeList)
   % Damage for the current mode is obtained from the structure array that corresponds to the
   % letter given in the list of modes. Note that modeList is a string on the format 'ABC...'.
   currentDamage = damagePalmgrenMiner.(modeList(i));

   % The name of the variable as it should be given in the Result Excel document.
   currentName = ['u.FLS.PalmgrenMiner.mode'  modeList(i) '.max'];

   % The value is written to the Result Excel document.
   cellWriter(currentDamage,currentName,sheetNames,ExcelData,[pathDir '\Result.xls']);
end

% ================================================================== %
% ================  Exporting the variable data to Excel ============= %
% ================================================================== %

% Creates a list of the items in the Mathcad data directory
itemList = dir([pathData]);

% The for loop runs for all the items in the selected subdirectory.
for i = 1:size(itemList,1);

   % Stores the name of the current directory item
   itemName = [itemList(i).name];

   % Stores the file extension and variable name for all items that are four characters or longer.
   % Note that this only works for extensions that is on the format '.***'.
   if length(itemName) > 3

      % The extension is assumed to be the four last characters in the item name
      extension = itemName([end-3:end]);

      % The variable name should then be the item name except the four last characters that should
      % be the extension.
      variableName = itemName([1:end-4]);
   else
      % if the item name is too short the extension is set to 'void'. this is done to overwrite
      % the previous value and allow the extension to be checked in the following steps.
      extension = 'void';
   end

   % The extension is checked to see if the item is a Mathcad output file. If the item is a Mathac
   % output file the variable value that it contains will first be read and then written to the
   % Excel result file.
   if extension == '.dat'

      % Counting the number of variables
      nVariables = nVariables+1;

      % The data in the Matcad output file is read and stored temporarily.
      data = importdata([pathData itemName]);

      % Initialisation and resetting of the variable that tracks the number of cells matching the
      % the name of the current variable.
      hitCount = 0;
```

```
% Finding the cell adjacent to the cell matching the searched variable name
[ hitCoord,hitSheet,hitCount ] = cellFinder(variableName,sheetNames,ExcelData);


% ---------- Exporting the data to the Excel result file ----------------------------------


% For the current variable it is checked if the data obtained from the corresponding Mathcad
% output file is a value with the format double. If it is a double the value is written to
% the cell adjacent and to the right of the matching cell in the Excel result file. Note
% that this only done if there are exactly one match.
if isa(data,'double') && hitCount == 1

   % The value of the variable is written to Excel result file.
   xlswrite([pathDir '\Result.xls'],data,hitSheet,hitCoord);


% If the format is double but the number of matches are two or higher the data will not be
% written to the Excel result file. A warning message will be printed to the user and the
% variable name is stored as a lost variable.
elseif isa(data,'double') && hitCount >= 2

   % Warning message to the user
   fprintf(['Warning: Multiple matches for the variable ' variableName '\n'])
   lostVariables = [lostVariables ; {variableName}];

   % Since the variable is not written to the Excel result file the variable is considered
   % lost and stored in the list of lost variables.
   lostVariables = [lostVariables ; {variableName}];

% If there is no matches for the variable name a warning will be printed to the user and the
% variable name is stored as a lost variable.
elseif isa(data,'double') && hitCount == 0

   % Warning message to the user
   fprintf(['Warning: No matches for the variable ' variableName '\n'])

   % Since the variable is not written to the Excel result file the variable is considered
   % lost and stored in the list of lost variables.
   lostVariables = [lostVariables ; {variableName}];


% if the data in the Mathcad output file is a structure array no data will be written.
% A warning message will be printed to the user and the variable name is stored as a lost
% variable.
elseif isa(data,'struct')

   %  Warning message to the user
   fprintf(['Warning: the Mathcad output is an structure array for ' variableName '\n'])

   % Since the variable is not written to the Excel result file the variable is considered
   % lost and stored in the list of lost variables.
   lostVariables = [lostVariables ; {variableName}];


% if the data in the Mathcad output file is neither a double or structure array no data will
```

```
      % be written. A warning message will be printed to the user and the variable name is stored
      % as a lost variable.
      else

        %  Warning message to the user
        fprintf([['Warning: Unknown format of data file for ' variableName '\n']])

        % Since the variable is not written to the Excel result file the variable is considered
        % lost and stored in the list of lost variables.
        lostVariables = [lostVariables ; {variableName}];
      end
    end
end

% Printing the results to the user.
fprintf([['Number of variables found: ' num2str(nVariables) '\n       Expected number: 13\n\n']])
fprintf([['Number of fatigue cracking modes found: ' num2str(length(modeList)) '\n']])
damagePalmgrenMiner

% the end of the function
end
```

D.2 cellFinder

```
function [hitCoord, hitSheet, hitCount] = cellFinder(variableName, sheetNames, ExcelData)
%%%%%%%%%%%%%%%%%%%%%%%%%%%%%%%%%%%%%%%%%%%%%%%%%%%%%%
% This is a function to locate cells in Excel document which corresponds to the selected input
%
% Input:
%
%   variableName:   The variable name or cell content which is should be found. Should be given as a
%               string.
%
%   sheetNames:     List of the sheet names in the Excel document.
%
%   ExcelData       The data from the Excel document. The data can be read by the 'xlsread' function
%               in Matlab.
% Output:
%
%   hitCoord:       The cell coordinates for the cell adjacent, to the right, of the cell matching
%               the given variable name. The coordinate is given with letters for the column so
%               that the coordinate can be used in Excel. The format is string, example: 'A1'
%
%   hitSheet        Returns the name of the sheet in which the matching value was found.
%
%   hitCount        Returns the number of matches that was found. However, the function can
%               currently NOT find multiple instances.
%
% Description:
%
%   This is a function to locate cells in Excel document which corresponds to the selected input.
%   Please note that the function cannot find multiple instances.
%
% Developed by:
% Mattias Renström
% Oskar Rydh
%
% Developed in cooperation with:
% Chalmers University of Engineering
% NCC Teknik, Gothenburg
%
% Last edited:
% 2014-06-02
%%%%%%%%%%%%%%%%%%%%%%%%%%%%%%%%%%%%%%%%%%%%%%%%%%%%%%

% Initialisation and resetting of the variable that tracks the number of cells matching the
% the name of the current variable.
hitCount = 0; hitCoord = []; hitSheet = [];

% The for loop runs for all the sheets in the Excel result file.
for i = 1:length(sheetNames)

  % The cell containing the sheet name is transformed from a cell into a string.
  sheet = char(sheetNames(i));

  % The Excel data that is stored in a cell matrix array is checked by the function
  % strncmp to see if each cell matches the variable name. In this case the function
  % strncmp yields a matrix containing ones (match) and zeroes (no match). the find
  % function returns the row and column of the matching cells.
```

```
    [row column] = find(strncmp(variableName,ExcelData.(sheet),length(variableName)));

    % If there are exactly one match for the variable name in the excel sheet then the
    % sheet coordinates for the cell to the right of the matching cell is stored.
    %Furthermore, the name of the current sheet where the match was found is also stored.
    if size(row,1) == 1

        % Sheet coordinate for the cell adjecent and to the right of the matching cell. Note
        % that the column index is increased by one and transformed into a letter. Currently
        % letter indexes are limited to just one character.
        hitCoord = [char(column+1+'A') num2str(row+1)];

        % The current sheet name for the match is stored
        hitSheet = char(sheetNames(i));

        % The counter for the number of matches is increased by one.
        hitCount = hitCount + 1;

    % If the number of matches are more than one a warning message will be printed. The
    % counter for the number of matches are increased by the number of matches.
    elseif size(row,1) > 1
        % Warning message is printed to the user
        fprintf([['Warning: two or more instances are found for ' variableName ...
        ' in sheet ' sheetName '\n']])

        % The counter for the number of matches are increased by the number of matches.
        hitCount = hitCount + size(row,1);
    end
end
end % End of function
```

D.3 cellWriter

```
function [hitCount] = cellWriter(inputData,cellName,sheetNames, ExcelData, filePath)
%%%%%%%%%%%%%%%%%%%%%%%%%%%%%%%%%%%%%%%%%%%%%%%%%
% This is a function which write data to a cell in a Excel document.
%
% Input:
%
1234567890123456789012345678901234567890123456789012345678901234567890123456789012345678901234
5678901234567890
%   cellName:      The variable name or cell content which is should be found. Should be given as a
%                  string. The data is written to the adjacent cell to right of the matching cell.
%
%   sheetNames:    List of the sheet names in the Excel document.
%
%   ExcelData:     The data from the Excel document. The data can be read by the 'xlsread' function
%                  in Matlab.
%
%   filePath:      The absolute or relative path to the Excel file which should be edited.
%
% Output:
%
%   hitCount       Returns the number of matches that was found. However, the function can
%                  currently NOT find multiple instances.
%
% Description:
%
%   This is a function which write data to a cell in a Excel document. Please note that the function
%   builds on the function cellFinder which cannot find multiple instances.
%
%
% Developed by:
% Mattias Renström
% Oskar Rydh
%
% Developed in cooperation with:
% Chalmers University of Engineering
% NCC Teknik, Gothenburg
%
% Last edited:
% 2014-06-02
%%%%%%%%%%%%%%%%%%%%%%%%%%%%%%%%%%%%%%%%%%%%%%%%%



% Finding the right cell with the function cellFinder
[ hitCoord,hitSheet,hitCount ] = cellFinder(cellName,sheetNames,ExcelData);

% Writes the input data to the designated cell. Note that cellFinder gives the coordinates
% for the cell adjacent to the cell that contains the chosen cellName.
xlswrite(filePath,{inputData},hitSheet,hitCoord);
```

Appendix E – Matlab functions for fatigue calculations

In this appendix all the Matlab functions pertaining to the calculation of fatigue life can be found. There are two sets of functions which are used for the analytical approach and the finite element model respectively.

The functions which are specifically intended to be used with the finite element model are Kea_allAbaqus and Kea_Abaqus. Conversely, the functions specifically intended to be used with the analytical calculations are Kea_allCrackingModes and Kea_crackingModes.

All the functions can be found in more detail within this appendix in the order given below, here is given the function name and the page number:

E.1 Kea_allAbaqus

```
function [damageMax, damage, modeList] = Kea_allCrackingModes(method, pathDir, Lspan)
%%%%%%%%%%%%%%%%%%%%%%%%%%%%%%%%%%%%%%%%%%%%%%%%%%%%%%%%%%%%%%%%%%%%%%%%%%%%%%%%
% This is a function that calculates the damage for all the fatigue cracking modes for the finite
% element model.
%
%
% Input:
%
%  method:    There are two methods to choose from, Palmgren-Miner cumulative damage and the
%             damage equivalent method. The input should be given as a string in the format
%             "PalmgrenMiner" or "Lambda".
%
%  PathDir:   The absolute or relative path to the directory which contains the stress data.
%
%  Lspan:     The span length for the bridge.
%
% Output:
%
%  damageMax: The maximum damage which is caused by the stress spectra for each
%             fatigue cracking mode.
%
%  damage:    the individual damage which is caused by the stress spectra for each fatigue
%             cracking mode.
%
% Description:
%
%  This function is used to calculate the damage for a all the fatigue cracking modes which are
%  considered in the finite element model. The input data should be placed in the directory which
%  is given in the input, the format is described in the note below.
%  The reference load which is assumed to be used in the finite element model is 1kN.
%  The load model which is used for damage equivalent method is fatigue load model 3 and a lambda
%  value of 1.029. The load model which is used for Palmgren-Miner method is fatigue load model 4
%  with traffic category 4 and local traffic.
%
% Important note:
%  The input file must have have a name on the format:
%  stressHistory.modeX_pathX_trackX_stressType.dat
%  where X should be replaced with the corresponding mode, path and track. the stress type should
%  be given as either direct, shear or mises.
%
%  Additionally, for the data in the input file the following format is required:
%  x      Step-1      Step-2      ...      [Column Header]
%  0        1E3      0.5E3       ...      [number]
%
% Developed by:
% Mattias Renström
% Oskar Rydh
%
% Developed in cooperation with:
% Chalmers University of Engineering
% NCC Teknik, Gothenburg
%
% Last edited:
% 2014-06-02
%%%%%%%%%%%%%%%%%%%%%%%%%%%%%%%%%%%%%%%%%%%%%%%%%%%%%%%%%%%%%%%%%%%%%%%%%%%%%%%%
```

```
% The method may also be chosen by a number where 1 corresponds to the damage equivalent method
and
% 2 corresponds to the Palmgren-Miner method.
if isequal(method,1)
   method = 'Lambda'
elseif isequal(method,2)
   method = 'PalmgrenMiner'
end

% List of all the implemented fatigue cracking modes. Note that mode E is omitted since the welds
% are not included in the finite element model.
modeList = 'ABCDF';

% the corresponding stresses for the modes.
stressType.A = [{'shear'},{'direct'}];
stressType.B = {'direct'};
stressType.C = {'mises'};
stressType.D = {'direct'};
stressType.F = {'mises'};

% the number of paths for each mode
numberOfPaths.A = 2;
numberOfPaths.B = 4;
numberOfPaths.C = 1;
numberOfPaths.D = 2;
numberOfPaths.F = 2;
% fatigueStrength for each mode and path
% (Except mode A which gives the strength for each stress type).
fatigueStrength.A = [100E6 112E6];
fatigueStrength.B = [70E6 70E6 93E6 93E6];
fatigueStrength.C = [80E6 80E6];
fatigueStrength.D = [80E6 80E6];
fatigueStrength.F = [112E6 112E6];

% The damage is calculated for all of the implemented fatigue cracking modes.
for i = 1:length(modeList)
   % The current fatigue cracking mode is loaded from the list
   mode = modeList(i);

   % Initiating and resetting
   modeDamageMax = [];
   modeDamage = [];

   % Collecting the stress types for the current mode
   currentStressType = stressType.(mode);

   % extracting the fatigue strength for each path or stress type
   currentFatigueStrength = fatigueStrength.(mode);

   % Calculation of the damage for the case of a single stress type
   if length(currentStressType) == 1
      % For each path
      for n = 1:numberOfPaths.(mode)
         % The damage for the current mode is calculated
         [currentDamageMax,~] =
Kea_Abaqus(mode,n,char(currentStressType),method,currentFatigueStrength(n),pathDir,Lspan);
```

```
        % Storing the data
        modeDamageMax = [modeDamageMax currentDamageMax];
      end

    % Calculation of the damage for the case of two stress types for the same fatigue cracking mode.
    elseif length(currentStressType) == 2

      % For each path
      for n = 1:numberOfPaths.(mode)
        % resetting the current damage
        currentDamage = [];

        % Runs for each stress type
        for k = 1:2
          % The damage for the current mode is calculated
          [~,currentDamage(:,k)] =
Kea_Abaqus(mode,n,char(currentStressType(k)),method,currentFatigueStrength(k),pathDir,Lspan);
        end
        % The current damage is stored for the mode
        modeDamage(:,:,n) = currentDamage;

        % Calculating the combined damage
        combinedDamage = sum(currentDamage,2);

        % Calculating the maximum damage
        currentDamageMax = max(combinedDamage);

        % Storing the data
        modeDamageMax = [modeDamageMax currentDamageMax];
      end
    end

    % Accumulating the data in the output structure matrices.
    damageMax.(mode) = max(modeDamageMax);
    damage.(mode) = modeDamage;
end

% Printing a message that the calculations are finished.
fprintf('\nfinished!\n\n')

% End of the function.
end
```

E.2 Kea_Abaqus

```
function [damageMax, damage] = Kea_Abaqus(mode, path, stressType, method, fatigueStrength,
pathDir,Lspan)
%%%%%%%%%%%%%%%%%%%%%%%%%%%%%%%%%%%%%%%%%%%%%%%%%%%%%%%%%
% This is a function that calculates the damage from a given fatigue cracking mode and stress type.
%
%
% Input:
%
%   mode:       The name of the fatigue cracking mode to be calculated.
%
%   path:       The path in the finite element model for which the fatigue life should be calculated
%               for.
%
%   stressType: The stress type which should be considered, this can be either direct, principal or
%               shear stress. The input should be given as a string in the format "direct".
%
%   method:     There are two methods to choose from, Palmgren-Miner cumulative damage and the
%               damage equivalent method.  The input should be given as a string in the format
%               "PalmgrenMiner" or "Lambda".
%
%   fatigueStrength: The nominal fatigue strength of the detail which is selected.
%
%   PathDir:    The absolute or relative path to the directory which contains the stress data.
%
%   Lspan:      The span length for the bridge.
%
% Output:
%
%   damageMax:  The maximum damage which is caused by the stress spectra.
%
%   damage:     The individual damage which is caused by the stress spectra.
%
% Description:
%
%   This function is used to calculate the damage for a stress spectra that is derived for a
%   reference load in a finite element model. The input data should be placed in the directory which
%   is given in the input, the format is described in the note below.
%   The reference load which is assumed to be used in the finite element model is 1kN.
%   The load model which is used for damage equivalent method is fatigue load model 3 and a lambda
%   value of 1.029. The load model which is used for Palmgren-Miner method is fatigue load model 4
%   with traffic category 4 and local traffic.
%
% Important note:
%
%   The input file must have have a name on the format:
%   stressHistory.modeX_pathX_trackX_stressType.dat
%   where X should be replaced with the corresponding mode, path and track.
%   the stress type should be given as either 'direct', 'shear' or 'mises'.
%
%   Additionally, for the data in the input file the following format is required:
%   x      Step-1     Step-2     ...     [Column Header]
%   0        1E3      0.5E3      ...     [number]
%
%
% Developed by:
```

```
% Mattias Renström
% Oskar Rydh
%
% Developed in cooperation with:
% Chalmers University of Engineering
% NCC Teknik, Gothenburg
%
% Last edited:
% 2014-06-02
%%%%%%%%%%%%%%%%%%%%%%%%%%%%%%%%%%%%%%%%%%%%%%%%%%%%%%%%%%%%%%%%

% ================================================================== %
% ========================== Input Data ============================ %
% ================================================================== %

% selected x-coordinates for the vehicle load. Note that the step length
% must be chosen so that the axle loads are exactly on the range when it is moved.
steplength = 0.1;

% Reference load that is used in Abaqus. it is presumed that it is 1000N.
% Caution! this should be the reference load that is put in each TRACK. note that depending on the
% number of tracks the reference load per lane is changed.
referenceLoadTrack = 1E3;

% Traffic type
rangeTraffic = 'local';

% Fatigue load model, for Palmgren-Miner fatigue load model 4 is used. For the damage equivalent
% method fatigue load model 3 is used.
fatigueLoadModel = 'FLM4';
if isequal({method},{'Lambda'})
   fatigueLoadModel = 'FLM3';
end


% Safety factors for the fatigue calculations
gammaFF = 1;
gammaMF = 1.35;

% import from Mathcad when damage equivalent method should be used.
lambda = 1.029;

% traffic category 4 and 80 year design life
loadCycles = 5E4*80;

% number of tracks that has been recorded in the finite element software.
numberOfTracks = 2;

% two wheels per axle means 2 tracks per lane.
tracksPerLane = 2;

% reference load per axle load, which is taken as the reference load per track times the number of
% tracks per lane.
referenceLoad = tracksPerLane * referenceLoadTrack;

% Calculating the number of lanes
numberOfLanes = floor((numberOfTracks-1)/tracksPerLane)+1;
```

```
% ================================================================= %
% ==================== Import Data and Loads ======================== %
% ================================================================= %

% Example of the format of input files from Abaqus/Brigade+
% stressHistory.modeC.path1.track1.mises.dat

% Import the data obtained from Abaqus for the fatigue cracking mode. Note that the first column
% is omitted when extracting the stress history, this since this column should contain the
% x-coordinates for the node in each row.
for i = 1:numberOfTracks;
   A = [pathDir 'stressHistory.mode' mode '_path' num2str(path) '_track' num2str(i) '_' stressType '.dat'];
   fprintf([['Currently processing: mode ' mode ', path ' num2str(path) ', track ' num2str(i) ', with regard
to ' stressType ' stress\n\n']])

   % A = ['ModeC.track' num2str(i) '.dat']
   % A = [pathDir 'stressHistory.modeB_path1_track' num2str(i) '_direct.dat']
   rawData = importdata(A);
   currentStressHistory = rawData.data;
   stressHistory(:,:,i) = currentStressHistory(:,2:end);
end


% ================================================================= %
% ========================== Processing data ======================== %
% ================================================================= %

% Obtaining data for the fatigue load model
[vehicleAxles,vehicleLoads,vehicleDistribution] =
Kea_fatigueLoadModel(fatigueLoadModel,rangeTraffic,referenceLoad);

% Calculating the total number of each vehicle passing during the design life of the bridge
vehicleCycles = vehicleDistribution * loadCycles;

% Location of the load in the finite element model. It is assumed that it goes from the one end of
% span to the other side in even steps.
loadCoordinates = linspace(0,Lspan,size(stressHistory,2));


% Coordinate vector for the vehicle load. The vector goes from zero to the end of the span plus
% the length of the longest vehicle. The step length is decided previously.
vehicleRange = 0:steplength:Lspan+max(max(vehicleAxles));

% ================================================================= %
% ================== Vehicle stress history ======================== %
% ================================================================= %

% Initialising the matrix that contains all the stress history for all the nodes, vehicles and lanes
vehicleStressHistory =
zeros(size(stressHistory,1),length(vehicleRange),size(vehicleAxles,1),numberOfLanes);

% In the following for-loop:

% k - the vehicles in the load model
% n - the nodes in the stress history
```

```
% i - the location of the vehicle
% j - the axle of the current vehicle
% t - the track (for the wheels, two per lane in most cases)
fprintf('\n\nProgress: %2.0f%%\n\n',1)

for t = 1:numberOfTracks

   % Initiating the stress history for the vehicles in the current track.
   currentVehicleStressHistory = zeros(size(vehicleStressHistory(:,:,:,1)));

   % The stress range spectra is obtained for each vehicle in the load model.
   for k = 1:size(vehicleAxles,1);

      % obtains the axle locations of the current vehicle.
      currentVehicleAxles = vehicleAxles(k,:);

      % removing placeholder axles at the end and then adding the first axle at position zero,
      % since it was removed in the first step.
      currentVehicleAxles(currentVehicleAxles==0) = [];
      currentVehicleAxles = [ 0 currentVehicleAxles];

      % Initialising and resetting the temporary matrix that contains the stresses for each axle in
      % the current vehicle
      axleStress = zeros(size(stressHistory,1),length(vehicleRange),length(currentVehicleAxles));


      % Calculating the axle load for each of the selected nodes in the input data.
      for n = 1:size(stressHistory,1)

         % The stress should be calculated for all the steps of the movable load. Note that this is
         % the steps used in Matlab and not the steps used in the Abaqus model.
         for i = 1:length(vehicleRange);

            % The stress should be obtained for each axle load of the vehicle.
            for j = 1:length(currentVehicleAxles)

               % The current x-coordinate for the axle load in the load model
               xstep = vehicleRange(i) - currentVehicleAxles(j);

               % The stress due to the axle load at the current node. Note that if the axle load
               % is not placed on the bridge the stress is zero. The corresponding load for the
               % specific axle is used to scale the stress to the correct value.
               axleStress(n,i,j) = vehicleLoads(k,j) *
Kea_interpolation(xstep,loadCoordinates,stressHistory(n,:,t));

               % The stress contribution from the current axle load is stored
               % for the vehicle.
               currentVehicleStressHistory(n,i,k) = currentVehicleStressHistory(n,i,k) + axleStress(n,i,j);

            end
         end
      end
   end
   tmp = t/numberOfTracks*100-1;
   fprintf('\n\nProgress: %2.0f%%\n\n',tmp)

   % Finding the number of the current lane
```

```
    lane = floor((t-1)/tracksPerLane)+1;

    % stores the stress history, all tracks in a lane is merged since a vehicle must pass the bridge
    % with the wheels synced in transversal direction.
    vehicleStressHistory(:,:,:,lane) = vehicleStressHistory(:,:,:,lane) + currentVehicleStressHistory;
end


% ================================================================= %
% ====================== Palmgren-Miner Method ==================== %
% ================================================================= %

% The damage caused by the chosen load model is calculated with Palmgren-Miner supported by the
% rainflow counting method. The damage is calculated for all the nodes in the input file, where
% each row corresponds to a node.
if isequal({method},{'PalmgrenMiner'})

    % Initiating the matrix containing the damage for each node
    damagePalmgrenMiner = zeros(size(vehicleStressHistory,1),size(vehicleStressHistory,3));

    % damage for each node
    for n = 1:size(vehicleStressHistory,1)
        % Calculating the damage for each vehicle in the load model
        for k = 1:size(vehicleStressHistory,3)
            % Current stress history for the current vehicle in the load model
            currentStressHistory = vehicleStressHistory(n,:,k);

            if isequal({stressType},{'mises'})
                stressType = 'principal';
            end

            % Calculating the damage for the current vehicle with the Palmgren-Miner method.
            damagePalmgrenMiner(n,k) =
Kea_PalmgrenMiner(currentStressHistory,stressType,fatigueStrength,vehicleCycles(k),1,gammaFF,gam
maMF);
        end
    end

    % Storing the damage and maximum damage
    damage = sum(damagePalmgrenMiner,2);
    damageMax = max(damage);
end


% ================================================================= %
% ================== Damage Equivalent Method ===================== %
% ================================================================= %

% The damage is calculated for all the nodes in the input file, where each row corresponds to one
% node.
if isequal({method},{'Lambda'})

    % Initiating the matrix containing the damage for each node
    damageLambda = zeros(size(vehicleStressHistory,1),size(vehicleStressHistory,3));

    % damage for each node
    for n = 1:size(vehicleStressHistory,1)
```

```
      for k = 1:size(vehicleStressHistory,3)
        % Current stress history for the current vehicle in the load model
        currentStressHistory = vehicleStressHistory(n,:,k);

        % Calculating the damage for the current vehicle with the Palmgren-Miner method.
        damageLambda(n,k) =
Kea_damageEquivalent(currentStressHistory,fatigueStrength,lambda,gammaFF,gammaMF);
      end
    end

    % Storing the damage and maximum damage. Here the damage is only allowed to be the maximum
for
    % each vehicle (However, note that the damage equivalent method is intended to be used with
    % fatigue load model 3, which only consists of one vehicle)
    if size(damageLambda,1) ~= 1
      damage = max(damageLambda')';
    else
      damage = damageLambda;
    end
    damageMax = max(damage);
end

% End of the function
end
```

E.3 Kea_allCrackingModes

```
function [damageMax, damage,modeList] = Kea_allCrackingModes(path)
%%%%%%%%%%%%%%%%%%%%%%%%%%%%%%%%%%%%%%%%%%%%%%%%%%%%%%%%%%%%%%%%
% This is a function that calculates the damage for all the fatigue cracking modes for the
% analytical approach.
%
% Input:
%   path:      The path to the input data. Can be given as either the absolute or relative path in
%              string format.
%
% Output:
%   damageMax:  The maximum damage which is caused by the stress spectra for each
%               fatigue cracking mode.
%   damage:     the individual damage which is caused by the stress spectra for each fatigue
%               cracking mode.
%
%   modeList:   Returns the list of the modes which is considered.
%
% Description:
%   This function is used to calculate the damage for a all the fatigue cracking modes which are
%   considered in the analytical approach. Note that the result for the damage is given as structure
%   arrays.
%
% Important note:
%   The input files must have have the extension .dat
%
% Developed by:
% Mattias Renström
% Oskar Rydh
%
% Developed in cooperation with:
% Chalmers University of Engineering
% NCC Teknik, Gothenburg
%
% Last edited:
% 2014-06-02
%%%%%%%%%%%%%%%%%%%%%%%%%%%%%%%%%%%%%%%%%%%%%%%%%%%%%%%%%%%%%%%%

% List of all the implemented fatigue cracking modes.
modeList = 'ABCDE';

% The damage is calculated for all of the implemented fatigue cracking modes.
for i = 1:length(modeList)
   % The current fatigue cracking mode is loaded from the list
   mode = modeList(i);

   % The damage for the current mode is calculated
   [currentDamageMax,currentDamage] = Kea_crackingModes(mode,path);

   % Accumulating the data in the output structure matrices.
   damageMax.(mode)  = currentDamageMax.(mode);
   damage.(mode)  = currentDamage.(mode);
end

% End of the function.
end
```

E.4 Kea_crackingModes

```
function [damageMax, damage] = Kea_crackingModes(mode, path, loadmodel)
%%%%%%%%%%%%%%%%%%%%%%%%%%%%%%%%%%%%%%%%%%%%%%%%%%%%%%%%%%%%%%%%%%%%%%%%
% This is a function that calculates the fatigue damage for a chosen fatigue cracking mode with the
% Palmgren-Miner method.
%
% Input:
%
%   mode:       The name of the fatigue cracking mode to be calculated.
%
%   path:       The path to the directory which contains the output data from the analytical
%               calculations.
%
%   loadmodel: The choice of load model. The recommended model is fatigue is fatigue load model 4
%               which is chosen by giving the string 'FLM4' as input.
%
%
% Output:
%
%   damageMax: The maximum damage for the chosen fatigue cracking mode.
%
%   damage      damage for the nodes considered in the chosen fatigue cracking mode.
%
% Description:
%
%   Calculates the fatigue damage for a chosen fatigue cracking mode with the Palmgren-Miner method.
%   Requires additional input data to be stored in the directory which is given in the input data.
%   Note that the files must have the extension '.dat'.
%
% Developed by:
% Mattias Renström
% Oskar Rydh
%
% Developed in cooperation with:
% Chalmers University of Engineering
% NCC Teknik, Gothenburg
%
% Last edited:
% 2014-06-02
%%%%%%%%%%%%%%%%%%%%%%%%%%%%%%%%%%%%%%%%%%%%%%%%%%%%%%%%%%%%%%%%%%%%%%%%

% Step length, must be chosen so that the distance between vehicle axles is always evenly dividable
% by the step length. The default of 0.1m is assumed to fit most cases.
stepLength = 0.1;

% ================================================================== %
% ============= Importing data from Mathcad calculations ============== %
% ================================================================== %

% ---------------------------- Constants ------------------------------ %

% The span length
Lspan = importdata([path 'L.span.dat']);

% Damage equivalent factor
lambda = importdata([path 'Lambda.fatigue.dat']);
```

```
% Thickness of the lower longitudinal weld
aWeldMainLower = importdata([path 'a.weld.main.lower.dat']);

% Thickness of the upper longitudinal weld
aWeldMainUpper = importdata([path 'a.weld.main.upper.dat']);

% Design life of the bridge
tDesignLife = importdata([path 't.designlife.dat']);

% Observed heavy vehicles per year
NfatigueObserved = importdata([path 'N.fatigue.observed.dat']);

% The distance or range of the traffic passing the bridge. for fatigue load model 4 this can be
% long, medium or local.
rangeTrafficRaw=importdata([path 'range.traffic.dat']);

% Constant taking into account the amount of the fatigue load that is carried by the most loaded
% main I-girder.
reductionLane1 = importdata([path 'reduction.lane1.dat']);
reductionLane2 = importdata([path 'reduction.lane2.dat']);

% Constant amplitude nominal stress fatigue strength for each cracking mode except mode C which
% is given as vectors instead of constant values.
deltaSigmaCModeA = importdata([path 'DeltaSigma.C.modeA.dat']);
deltaTauCModeA =  importdata([path 'DeltaTau.C.modeA.dat']);
deltaSigmaCModeC = importdata([path 'DeltaSigma.C.modeC.dat']);
deltaSigmaCModeD = importdata([path 'DeltaSigma.C.modeD.dat']);
deltaTauCModeE =  importdata([path 'DeltaTau.C.modeE.dat']);
deltaSigmaCModeF = importdata([path 'DeltaSigma.C.modeF.dat']);
% Safety factors for the fatigue calculations
gammaFF = importdata([path 'Gamma.F.fatigue.dat']);
gammaMF = importdata([path 'Gamma.M.fatigue.dat']);


% ---------------------------- Vectors --------------------------------- %

% Vector containing the x-coordinates for which the following vectors corresponds to.
nodeRange = importdata([path 'x.range.dat']);

% Vector containing
zRangeModeC = importdata([path 'z.range.modeC.dat']);

% Second moment of area for the composite cross-section when subjected to negative respectively
% positive bending.
IcompositeNegative = importdata([path 'I.composite.negative.dat']);
IcompositePositive=importdata([path 'I.composite.positive.dat']);

% Second moment of area for the main I-girder that is not reduced to any buckling phenomena.
ImainBeamUnreduced = importdata([path 'I.main.beam.unreduced.dat']);

% First moment of area for the main I-girder at the bottom and top of the web respectively.
SmainBeamLower = importdata([path 'S.main.beam.lower.dat']);
SmainBeamUpper = importdata([path 'S.main.beam.upper.dat']);

% First moment of area corresponding to the z-values in the range given for Mode C.
SmainBeamModeC = importdata([path 'S.main.beam.modeC.dat']);
```

```
% Thickness of the web of the main I-girder.
tMainWeb = importdata([path 't.main.web.dat']);

% Global z-coordinate for the upper and lower part of the web respectively.
zBottomMainWeb = importdata([path 'z.bottom.main.web.dat']);
zTopMainWeb = importdata([path 'z.top.main.web.dat']);

% Global z-coordinate for the upper and lower part of the web respectively.
zBottomMainFlangeLower = importdata([path 'z.bottom.main.flange.lower.dat']);
zTopMainFlangeUpper = importdata([path 'z.top.main.flange.upper.dat']);

% Global z-coordinate for the location of the neutral axis for the composite cross-section in
% negative and positive bending respectively.
zNAcompositeNegative = importdata([path 'z.NA.composite.negative.dat']);
zNAcompositePositive = importdata([path 'z.NA.composite.positive.dat']);

% Location of the splices in the lower and upper flange respectively
XspliceFlangeLower = importdata([path 'X.splice.flange.lower.dat']);
XspliceFlangeUpper = importdata([path 'X.splice.flange.upper.dat']);

% Constant amplitude nominal stress fatigue strength for cracking mode C.
deltaSigmaCModeBLower = importdata([path 'DeltaSigma.C.modeB.lower.dat']);
deltaSigmaCModeBUpper = importdata([path 'DeltaSigma.C.modeB.upper.dat']);


% ================================================================== %
% ================  Post-processing of Mathcad data ================= %
% ================================================================== %

% ---------- The local z-coordinates for the upper and lower part of the web --------- %

% The local z-coordinate for the upper and lower part of the web respectively with regard to
% negative bending of the composite cross-section. The local coordinate system starts in the neutral
% layer of the cross-section with positive direction upwards.
zNegativeWebLower = zBottomMainWeb - zNAcompositeNegative;
zNegativeWebUpper = zTopMainWeb - zNAcompositeNegative;

% The local z-coordinate for the upper and lower part of the web respectively with regard to
% positive bending of the composite cross-section. The local coordinate system starts in the neutral
% layer of the cross-section with positive direction upwards.
zPositiveWebLower = zBottomMainWeb - zNAcompositePositive;
zPositiveWebUpper = zTopMainWeb - zNAcompositePositive;

% ---------- fatigue cycles and load ---------- %

% Total number of heavy vehicles that will pass the bridge during its design service life.
loadCycles = NfatigueObserved * tDesignLife;

% Reduction of the load for each nominal lane is stored in a vector.
reductionLanes = [reductionLane1 reductionLane2];

% The traffic range is designated a as string. Note that it is difficult to export strings from
% Mathcad to Matlab in a satisfactory way.
if rangeTrafficRaw == 1
   rangeTraffic = 'long';
elseif rangeTrafficRaw == 2
```

```
    rangeTraffic = 'medium';
elseif rangeTrafficRaw == 3
    rangeTraffic = 'local';
end
% ---------- The local z-coordinates for the upper and lower part of the flanges --------- %

% The local z-coordinate for the uppermost and lowermost part of the flanges respectively with
% regard to negative bending of the composite cross-section. The local coordinate system starts in
% the neutral layer of the cross-section with positive direction upwards.
zNegativeFlangeLower = zBottomMainFlangeLower - zNAcompositeNegative;
zNegativeFlangeUpper = zTopMainFlangeUpper - zNAcompositeNegative;

% The local z-coordinate for the uppermost and lowermost part of the flanges respectively with
% regard to positive bending of the composite cross-section. The local coordinate system starts in
% the neutral layer of the cross-section with positive direction upwards.
zPositiveFlangeLower = zBottomMainFlangeLower - zNAcompositePositive;
zPositiveFlangeUpper = zTopMainFlangeUpper - zNAcompositePositive;

% ---------- z coordinates for cracking mode D ---------- %

% For mode D only the lower and upper flange is considered at the support.
zRangeModeD = [zBottomMainFlangeLower(1) zTopMainFlangeUpper(1)];


% ---------- finding the location of the splices in the flanges ---------- %

% Initialising variables
n = 1;
i = 1;
spliceFlangeLower = [];

% Running a while loop until the location of all the splices in the lower flange is found.
while i <= length(nodeRange) && n <= length(XspliceFlangeLower)

    % Checking if the current node is past the current splice in the lower flange.
    if nodeRange(i) > XspliceFlangeLower(n)
        % When the current splice is found the numbers of the nodes before and after will be
        % accumulated in a vector
        spliceFlangeLower = [spliceFlangeLower i-1 i];

        % When the current splice is found the next splice will be searched for.
        n = n + 1;
    end

    % Checking the next node in the node range for the next run
    i = i + 1;
end


% Initialising and resetting the variables
n = 1;
i = 1;
spliceFlangeUpper = [];

% Running a while loop until the location of all the splices in the upper flange is found.
while i <= length(nodeRange) && n <= length(XspliceFlangeUpper)
```

```
    % Checking if the current node is past the current splice in the upper flange.
    if nodeRange(i) > XspliceFlangeUpper(n)
        % When the current splice is found the numbers of the nodes before and after will be
        % accumulated in a vector
        spliceFlangeUpper = [spliceFlangeUpper i-1 i];

        % When the current splice is found the next splice will be searched for.
        n = n + 1;
    end

    % Checking the next node in the node range for the next run
    i = i + 1;
end

% ================================================================== %
% ========================= load model ============================= %
% ================================================================== %

% Obtaining the data for the chosen load model. The location axles and corresponding axle loads is
% obtained for all the vehicles in the load model. In addition, the distribution of the vehicles
% with regard to the amount of vehicles passing the bridge are also obtained. The reference load is
% 1N.
% Note that the rows corresponds to vehicles and that the columns corresponds to axles.
[vehicleAxles,vehicleLoads,vehicleDistribution] = Kea_fatigueLoadModel(loadmodel,rangeTraffic,1);


% From the axle positions it is possible to find the longest vehicle. The length is needed since the
% vehicle has to travel from the start of the bridge and stop when the last axle reaches the end of
% the bridge. Therefore the vehicle range starts at zero and stops at the span length plus the
% length of the longest vehicle.
vehicleRange = 0:stepLength:Lspan+max(max(vehicleAxles));

% The number of load cycles for each vehicle in the load model.
vehicleCycles = vehicleDistribution * loadCycles;

% ================================================================== %
% ==================== Fatigue Cracking Mode A ===================== %
% ================================================================== %

% Check if this is the chosen fatigue cracking mode
if mode == 'A'

% ---------------------- Palmgren-Miner ----------------------- %

% The damage caused by the chosen load model is calculated with Palmgren-Miner supported by
% the rain flow counting method.
% The damage is calculated for all the nodes along the bridge span.
for n = 1:length(nodeRange)

    % The current splice node is saved in a temporary variable.
    xSpan = nodeRange(n);

    % The stress spectra is obtained by calculating all the stresses for all the positions of the
    % vehicles in the load model as they move across the span.
    for i = 1:length(vehicleRange)

        % The current location of the vehicle is stored in a temporary variable.
```

```
    xVehicle = vehicleRange(i);

    % The shear force and bending moment is obtained for caused by each vehicle in the current
    % node is obtained for the current location of the vehicles.
    % note that shearForce and bendingMomement is column vectors where each row corresponds to a
    % vehicle in the load model.
    [shearForce,bendingMoment] = Kea_vehicleLoad(xSpan,xVehicle,vehicleAxles,vehicleLoads,Lspan);


    % Shear stress in the upper and lower part of the web of the main I-girder.
    TauLower(:,i) = shearForce * SmainBeamLower(n)/(ImainBeamUnreduced(n) * tMainWeb(n));
    TauUpper(:,i) = shearForce * SmainBeamUpper(n)/(ImainBeamUnreduced(n) * tMainWeb(n));

    % Direct stress in the lower and upper part of the the web of the main I-girder.
    % For the direct stress the calculation depends on the bending moment being positive or
    % negative. For negative bending the concrete is considered while for positive bending the
    % reinforcement is considered for the second moment of area of the composite cross-section.
    for j = 1:length(bendingMoment)
      % For negative bending the concrete is considered for the second moment of area of the
      % composite cross-section.
      if bendingMoment(j) < 0
        SigmaLower(j,i) = bendingMoment(j) * zNegativeWebLower(n) / IcompositeNegative(n);
        SigmaUpper(j,i) = bendingMoment(j) * zNegativeWebUpper(n) / IcompositeNegative(n);

      % For positive bending the reinforcement is considered for the second moment of area of
      % the composite cross-section.
      elseif bendingMoment(j) >= 0
        SigmaLower(j,i) = bendingMoment(j) * zPositiveWebLower(n) / IcompositePositive(n);
        SigmaUpper(j,i) = bendingMoment(j) * zPositiveWebUpper(n) / IcompositePositive(n);
      end
    end
  end

  % The damage is calculated for each lane
  for m = 1:length(reductionLanes)
    % The damage is stored with each row representing a vehicle in the load model in a nominal
    % lane. The first rows is for the first lane and then the vehicles are repeated for the
    % next lane until all lanes has been included.
    v = [1:5]+5*(m-1);

    % The damage for the current node is calculated for the shear stress.
    damageTauLower(v,n) =
Kea_PalmgrenMiner(TauLower,'shear',deltaTauCModeA,vehicleCycles,reductionLanes(m),gammaFF,ga
mmaMF);
    damageTauUpper(v,n) =
Kea_PalmgrenMiner(TauUpper,'shear',deltaTauCModeA,vehicleCycles,reductionLanes(m),gammaFF,ga
mmaMF);

    % The damage for the current node is calculated for the direct stress.
    damageSigmaLower(v,n) =
Kea_PalmgrenMiner(SigmaLower,'direct',deltaSigmaCModeA,vehicleCycles,reductionLanes(m),gammaF
F,gammaMF);
    damageSigmaUpper(v,n) =
Kea_PalmgrenMiner(SigmaUpper,'direct',deltaSigmaCModeA,vehicleCycles,reductionLanes(m),gammaF
F,gammaMF);
  end
end
```

```
% ---------------------------------- Damage ---------------------------------- %

% The damage from the shear stress and direct stress is simply added together.
damageLower = damageTauLower + damageSigmaLower;
damageUpper = damageTauUpper + damageSigmaUpper;

% The damage for each node is obtained when the damage caused by each vehicle is added together.
damageLowerTotal = sum(damageLower);
damageUpperTotal = sum(damageUpper);

% --------------------- Output --------------------------- %

% The highest damage between the upper and lower part is stored in a vector
damage.A = [damageLower ; damageUpper];


% The highest damage for the current fatigue cracking mode
damageMax.A = max(max([damageLowerTotal damageUpperTotal]));

% End of mode A
end

% ========================================================================= %
% ==================== Fatigue Cracking Mode B ======================== %
% ========================================================================= %

% Check if this is the chosen fatigue cracking mode
if mode == 'B'

% ---------------------- Palmgren-Miner ----------------------- %

% The damage caused by the chosen load model is calculated with Palmgren-Miner supported by
% the rain flow counting method.
% The damage is calculated for all the nodes adjacent to a splice in the lower flange. Note that
% since the splices in the upper and lower flange has different locations it is easier and more
% stable to run them separate.
for n = 1:length(spliceFlangeLower)

   % the current node of the cross-sectional resistance
   node = spliceFlangeLower(n);

   % The current node is saved in a temporary variable.
   xSpan = XspliceFlangeLower(ceil(n/2));

   % The stress spectra is obtained by calculating all the stresses for all the positions of the
   % vehicles in the load model as they move across the span.
   for i = 1:length(vehicleRange)

      % The current location of the vehicle is stored in a temporary variable.
      xVehicle = vehicleRange(i);

      % The shear force and bending moment is obtained for caused by each vehicle in the current
      % node is obtained for the current location of the vehicles.
      % note that shearForce and bendingMomement is column vectors where each row corresponds to a
      % vehicle in the load model.
      [shearForce,bendingMoment] = Kea_vehicleLoad(xSpan,xVehicle,vehicleAxles,vehicleLoads,Lspan);
```

```
    % Direct stress in the lower part of the the flange of the main I-girder.
    % For the direct stress the calculation depends on the bending moment being positive or
    % negative. For negative bending the concrete is considered while for positive bending the
    % reinforcement is considered for the second moment of area of the composite cross-section.
    for j = 1:length(bendingMoment)
      % For negative bending the concrete is considered for the second moment of area of the
      % composite cross-section.
      if bendingMoment(j) < 0
        SigmaLower(j,i) = bendingMoment(j) * zNegativeFlangeLower(node) /
IcompositeNegative(node);

      % For positive bending the reinforcement is considered for the second moment of area of
      % the composite cross-section.
      elseif bendingMoment(j) >= 0
        SigmaLower(j,i) = bendingMoment(j) * zPositiveFlangeLower(node) / IcompositePositive(node);
      end
    end
  end

  % The damage is calculated for each lane
  for m = 1:length(reductionLanes)
    % The damage is stored with each row representing a vehicle in the load model in a nominal
    % lane. The first rows is for the first lane and then the vehicles are repeated for the
    % next lane until all lanes has been included.
    v = [1:5]+5*(m-1);

    % The damage for the current node is calculated for the direct stress.
    damageSigmaLower(v,n) =
Kea_PalmgrenMiner(SigmaLower,'direct',deltaSigmaCModeBLower(node),vehicleCycles,reductionLanes
(m),gammaFF,gammaMF);
  end
end


% The damage caused by the chosen load model is calculated with Palmgren-Miner supported by
% the rain flow counting method.
% The damage is calculated for all the nodes adjacent to a splice in the upper flange. Note that
% since the splices in the upper and lower flange has different locations it is easier and more
% stable to run them separate.
for n = 1:length(spliceFlangeUpper)

  % the current node of the cross-sectional resistance
  node = spliceFlangeUpper(n);

  % The current node is saved in a temporary variable.
  xSpan = XspliceFlangeUpper(ceil(n/2));

  % The stress spectra is obtained by calculating all the stresses for all the positions of the
  % vehicles in the load model as they move across the span.
  for i = 1:length(vehicleRange)

    % The current location of the vehicle is stored in a temporary variable.
    xVehicle = vehicleRange(i);

    % The shear force and bending moment is obtained for caused by each vehicle in the current
```

```
    % node is obtained for the current location of the vehicles.
    % note that shearForce and bendingMomement is column vectors where each row corresponds to a
    % vehicle in the load model.
    [shearForce,bendingMoment] = Kea_vehicleLoad(xSpan,xVehicle,vehicleAxles,vehicleLoads,Lspan);


    % Direct stress in the upper part of the the flange of the main I-girder.
    % For the direct stress the calculation depends on the bending moment being positive or
    % negative. For negative bending the concrete is considered while for positive bending the
    % reinforcement is considered for the second moment of area of the composite cross-section.
    for j = 1:length(bendingMoment)
      % For negative bending the concrete is considered for the second moment of area of the
      % composite cross-section.
      if bendingMoment(j) < 0
        SigmaUpper(j,i) = bendingMoment(j) * zNegativeFlangeUpper(node) /
IcompositeNegative(node);

      % For positive bending the reinforcement is considered for the second moment of area of
      % the composite cross-section.
      elseif bendingMoment(j) >= 0
        SigmaUpper(j,i) = bendingMoment(j) * zPositiveFlangeUpper(node) /
IcompositePositive(node);
      end
    end
  end

  % The damage is calculated for each lane
  for m = 1:length(reductionLanes)
    % The damage is stored with each row representing a vehicle in the load model in a nominal
    % lane. The first rows is for the first lane and then the vehicles are repeated for the
    % next lane until all lanes has been included.
    v = [1:5]+5*(m-1);

    % The damage for the current node is calculated for the direct stress.
    damageSigmaUpper(v,n) =
Kea_PalmgrenMiner(SigmaUpper,'direct',deltaSigmaCModeBUpper(node),vehicleCycles,reductionLanes
(m),gammaFF,gammaMF);
  end
end

% ------------------------------- Damage -------------------------------- %

% The damage for each node is obtained when the damage caused by each vehicle is added together.
damageLowerTotal = sum(damageSigmaLower);
damageUpperTotal = sum(damageSigmaUpper);

% ---------------------- Output ---------------------------- %

% The highest damage between the upper and lower part is stored in a vector
damage.B = [damageSigmaLower damageSigmaUpper];

% The highest damage for the current fatigue cracking mode
damageMax.B = max([damageLowerTotal damageUpperTotal]);

% End of mode B
end
```

```
% ================================================================= %
% ==================== Fatigue Cracking Mode C ==================== %
% ================================================================= %

% Check if this is the chosen fatigue cracking mode
if mode == 'C'

% ---------------------- Palmgren-Miner ---------------------- %

% The damage caused by the chosen load model is calculated with Palmgren-Miner supported by
% the rain flow counting method.
% The damage is calculated at the end of the span for the height of weld of the vertical stiffener.
% This is the weld between the stiffener and the web.
for n = 1:length(zRangeModeC)

   % Current node is at the end of the span
   node = 1;

   % % the current node of the cross-sectional resistance
   zNode = zRangeModeC(n);

   % The current node is saved in a temporary variable.
   xSpan = 0;

   % The stress spectra is obtained by calculating all the stresses for all the positions of the
   % vehicles in the load model as they move across the span.
   for i = 1:length(vehicleRange)

      % The current location of the vehicle is stored in a temporary variable.
      xVehicle = vehicleRange(i);

      % The shear force and bending moment is obtained for caused by each vehicle in the current
      % node is obtained for the current location of the vehicles.
      % note that shearForce and bendingMomement is column vectors where each row corresponds to a
      % vehicle in the load model.
      [shearForce,bendingMoment] = Kea_vehicleLoad(xSpan,xVehicle,vehicleAxles,vehicleLoads,Lspan);


      % Shear stress in the upper and lower part of the web of the main I-girder.
      shearStress(:,i) = shearForce * SmainBeamModeC(n)/(ImainBeamUnreduced(node) *
tMainWeb(node));


      % Direct stress in the upper part of the the flange of the main I-girder.
      % For the direct stress the calculation depends on the bending moment being positive or
      % negative. For negative bending the concrete is considered while for positive bending the
      % reinforcement is considered for the second moment of area of the composite cross-section.
      for j = 1:length(bendingMoment)
         % For negative bending the concrete is considered for the second moment of area of the
         % composite cross-section.
         if bendingMoment(j) < 0
            zNegative = zNode - zNAcompositeNegative(node);
            directStress(j,i) = bendingMoment(j) * zNegative / IcompositeNegative(node);

         % For positive bending the reinforcement is considered for the second moment of area of
```

```
        % the composite cross-section.
        elseif bendingMoment(j) >= 0
          zPositive = zNode - zNAcompositePositive(node);
          directStress(j,i) = bendingMoment(j) * zPositive / IcompositePositive(node);
        end
      end
    end

    principalStress = (abs(directStress) / 2) + 0.5 * sqrt( directStress.^2 + 4 * shearStress.^2 );

    % The damage is calculated for each lane
    for m = 1:length(reductionLanes)
      % The damage is stored with each row representing a vehicle in the load model in a nominal
      % lane. The first rows is for the first lane and then the vehicles are repeated for the
      % next lane until all lanes has been included.
      v = [1:5]+5*(m-1);

      % The damage for the current node is calculated for the direct stress.
      damagePrincipal(v,n) =
Kea_PalmgrenMiner(principalStress,'principal',deltaSigmaCModeC,vehicleCycles,reductionLanes(m),ga
mmaFF,gammaMF);
    end
end

% ---------------------------------- Damage ---------------------------------- %

% The damage for each node is obtained when the damage caused by each vehicle is added together.
damageTotal = sum(damagePrincipal);

% ---------------------- Output ---------------------------- %

% The highest damage between the upper and lower part is stored in a vector
damage.C = [damagePrincipal];

% The highest damage for the current fatigue cracking mode
damageMax.C = max(damageTotal);

% End of part C
end

% ================================================================== %
% ==================== Fatigue Cracking Mode D ====================== %
% ================================================================== %

% Check if this is the chosen fatigue cracking mode
if mode == 'D'
% ---------------------- Palmgren-Miner ---------------------- %

% The damage caused by the chosen load model is calculated with Palmgren-Miner supported by
% the rain flow counting method.
% The damage is calculated for the weld of the vertical stiffener.
% This is the weld between the stiffener and the flange.
for n = 1:length(zRangeModeD)

  % Current node is at the end of the span
  node = 1;
```

```
  % % the current node of the cross-sectional resistance
  zNode = zRangeModeD(n);

  % The current node is saved in a temporary variable.
  xSpan = 0;

  % The stress spectra is obtained by calculating all the stresses for all the positions of the
  % vehicles in the load model as they move across the span.
  for i = 1:length(vehicleRange)

    % The current location of the vehicle is stored in a temporary variable.
    xVehicle = vehicleRange(i);

    % The shear force and bending moment is obtained for caused by each vehicle in the current
    % node is obtained for the current location of the vehicles.
    % note that shearForce and bendingMomement is column vectors where each row corresponds to a
    % vehicle in the load model.
    [shearForce,bendingMoment] = Kea_vehicleLoad(xSpan,xVehicle,vehicleAxles,vehicleLoads,Lspan);


    % Direct stress at the current z-coordinate.
    % For the direct stress the calculation depends on the bending moment being positive or
    % negative. For negative bending the concrete is considered while for positive bending the
    % reinforcement is considered for the second moment of area of the composite cross-section.
    for j = 1:length(bendingMoment)
      % For negative bending the concrete is considered for the second moment of area of the
      % composite cross-section.
      if bendingMoment(j) < 0
        zNegative = zNode - zNAcompositeNegative(node);
        directStress(j,i) = bendingMoment(j) * zNegative / IcompositeNegative(node);

      % For positive bending the reinforcement is considered for the second moment of area of
      % the composite cross-section.
      elseif bendingMoment(j) >= 0
        zPositive = zNode - zNAcompositePositive(node);
        directStress(j,i) = bendingMoment(j) * zPositive / IcompositePositive(node);
      end
    end
  end

  plot(directStress')

  % The damage is calculated for each lane
  for m = 1:length(reductionLanes)
    % The damage is stored with each row representing a vehicle in the load model in a nominal
    % lane. The first rows is for the first lane and then the vehicles are repeated for the
    % next lane until all lanes has been included.
    v = [1:5]+5*(m-1);

    % The damage for the current node is calculated for the direct stress.
    damageDirect(v,n) =
Kea_PalmgrenMiner(directStress,'direct',deltaSigmaCModeD,vehicleCycles,reductionLanes(m),gammaF
F,gammaMF);
  end
end

% ---------------------------------- Damage ---------------------------------- %
```

```
% The damage for each node is obtained when the damage caused by each vehicle is added together.
damageTotal = sum(damageDirect);

% ---------------------- Output ----------------------------- %

% The highest damage between the upper and lower part is stored in a vector
damage.D = [damageDirect];

% The highest damage for the current fatigue cracking mode
damageMax.D = max(damageTotal);


% End of mode D
end

% ========================================================================= %
% ====================  Fatigue Cracking Mode E ======================== %
% ========================================================================= %

% Check if this is the chosen fatigue cracking mode
if mode == 'E'


% ---------------------- Palmgren-Miner ----------------------- %

% The damage caused by the chosen load model is calculated with Palmgren-Miner supported by
% the rain flow counting method.
% The damage is calculated for all the nodes along the bridge span.
for n = 1:length(nodeRange)


   % The current splice node is saved in a temporary variable.
   xSpan = nodeRange(n);

   % The stress spectra is obtained by calculating all the stresses for all the positions of the
   % vehicles in the load model as they move across the span.
   for i = 1:length(vehicleRange)

      % The current location of the vehicle is stored in a temporary variable.
      xVehicle = vehicleRange(i);

      % The shear force and bending moment is obtained for caused by each vehicle in the current
      % node is obtained for the current location of the vehicles.
      % note that shearForce and bendingMomement is column vectors where each row corresponds to a
      % vehicle in the load model.
      [shearForce,bendingMoment] = Kea_vehicleLoad(xSpan,xVehicle,vehicleAxles,vehicleLoads,Lspan);


      % Shear stress in the upper and lower part of the web of the main I-girder.
      TauLower(:,i) = shearForce * SmainBeamLower(n)/(ImainBeamUnreduced(n) * 2 *
aWeldMainUpper);
      TauUpper(:,i) = shearForce * SmainBeamUpper(n)/(ImainBeamUnreduced(n) * 2 *
aWeldMainLower);

   end
```

```
    % The damage is calculated for each lane
    for m = 1:length(reductionLanes)
        % The damage is stored with each row representing a vehicle in the load model in a nominal
        % lane. The first rows is for the first lane and then the vehicles are repeated for the
        % next lane until all lanes has been included.
        v = [1:5]+5*(m-1);

        % The damage for the current node is calculated for the shear stress.
        damageTauLower(v,n) =
Kea_PalmgrenMiner(TauLower,'shear',deltaTauCModeE,vehicleCycles,reductionLanes(m),gammaFF,ga
mmaMF);
        damageTauUpper(v,n) =
Kea_PalmgrenMiner(TauUpper,'shear',deltaTauCModeE,vehicleCycles,reductionLanes(m),gammaFF,ga
mmaMF);
    end
end


% ---------------------------------- Damage ---------------------------------- %

% The damage for each node is obtained when the damage caused by each vehicle is added together.
damageLowerTotal = sum(damageTauLower);
damageUpperTotal = sum(damageTauUpper);

% ---------------------- Output ----------------------------- %

% The highest damage between the upper and lower part is stored in a vector
damage.E = [damageTauLower ; damageTauUpper];

% The highest damage for the current fatigue cracking mode
damageMax.E = max(max([damageLowerTotal ; damageUpperTotal]));

% End of mode E
end

% End of the function
end
```

E.5 Kea_fatigueLoadModel

```
function [vehicleAxles, vehicleLoads, vehicleDistribution] = Kea_fatigueLoadModel(fatigueLoadModel,
rangeTraffic, referenceLoad)
%%%%%%%%%%%%%%%%%%%%%%%%%%%%%%%%%%%%%%%%%%%%%%%%%%%%%%%%%%%%%%%%%%%%%%%%
% This is a function that returns the location and load of the axles of the vehicles in the chosen
% vehicle model.
%
% Input:
%
%   fatigueLoadModel: The choice of fatigue load model. Currently fatigue load model 3 and 4 is
%             implemented and they can be selected with the string 'FLM3' and 'FLM4'
%             respectively.
%
%   rangeTraffic:  The range of the traffic is used in fatigue load model 4 and can be selected
%             as the string 'long', 'medium' and 'local'.
%
%   referenceLoad:  The reference load which is used in the calculations. should be given in N.
%
%
% Output:
%
%   vehicleAxles:  The distance to each axle measured from the first axle. Matrix where each row
%             corresponds to a vehicle in the load model and each column corresponds to an
%             axle.
%
%   vehicleLoads:  The load for each axle in the load model. Matrix where each row corresponds to a
%             vehicle in the load model and each column corresponds to an axle.
%
%
% Description:
%   This is a function that returns the location and load of the axles of the vehicles in the chosen
%   vehicle model. In addition the distribution of vehicles within the load model is also returned.
%   Note that is easy to add additional load models if needed.
%   If additional load models are added please update the description in the input data.
%
% Developed by:
% Mattias Renström
% Oskar Rydh
%
% Developed in cooperation with:
% Chalmers University of Engineering
% NCC Teknik, Gothenburg
%
% Last edited:
% 2014-06-02
%%%%%%%%%%%%%%%%%%%%%%%%%%%%%%%%%%%%%%%%%%%%%%%%%%%%%%%%%%%%%%%%%%%%%%%%

% ================================================================== %
% ======================  Fatigue load Model 3 ======================== %
% ================================================================== %

% Fatigue load model 3
if isequal({fatigueLoadModel},{'FLM3'})
   % Values relevant values for fatigue load model 3
```

```
    % Assigning the location of the axles for each vehicle in load model 3
    % Note that the matrix has to be uniform, thus empty places has to be filled with zeroes.
    % the zeroes are automatically removed later in the calculations.
    % Each row corresponds to a vehicle.
    % Each column corresponds to an additional axle.
    % [m]
    vehicleAxles = [ 0 1.2 7.2 8.4 ];

    % Assigning the axle load of the axles for each vehicle in load model 4
    % Note that here the first axle must be included. All the axles must be placed in order that
    % corresponds to those in the Vehicle vector. Note that the matrix has to be uniform, thus
    % empty places has to be filled with zeroes.
    % Each row corresponds to a vehicle.
    % Each column corresponds to an additional axle.
    % [N]
    vehicleLoads = [ 120 120 120 120 ] * 1E3/referenceLoad;

    % Distribution of vehicles of the total amount vehicles passing the bridge
    % Currently the values for medium long distance traffic is implemented.
    % Each row corresponds to a vehicle.
    % [-]
    vehicleDistribution = [ 1 ];

end

% ================================================================== %
% ======================  Fatigue load Model 4 ======================== %
% ================================================================== %

% Fatigue load model 4
if isequal({fatigueLoadModel},{'FLM4'})
    % Values relevant values for fatigue load model 4 is given in Eurocode 1991-2: Table 4.7.


    % Assigning the location of the axles for each vehicle in load model 4
    % Note that the matrix has to be uniform, thus empty places has to be filled with zeroes.
    % the zeroes are automatically removed later in the calculations.
    % Each row corresponds to a vehicle.
    % Each column corresponds to an additional axle.
    % [m]
    vehicleAxles = [ 0  4.5 0   0    0
                     0  4.2 5.5 0    0
                     0  3.2 8.4 9.7  11.0
                     0  3.4 9.4 11.2 0
                     0  4.8 8.4 12.8 14.1  ];

    % Assigning the axle load of the axles for each vehicle in load model 4
    % Note that here the first axle must be included. All the axles must be placed in order that
    % corresponds to those in the Vehicle vector. Note that the matrix has to be uniform, thus
    % empty places has to be filled with zeroes.
    % Each row corresponds to a vehicle.
    % Each column corresponds to an additional axle.
    % [N]
    vehicleLoads = [   70  130 0   0   0
                       70  120 120 0   0
                       70  150 90  90  90
                       70  140 90  90  0
```

```
                70  130 90  80  80  ] * 1E3/referenceLoad;

    % Distribution of vehicles of the total amount vehicles passing the bridge
    % Currently the values for medium long distance traffic is implemented.
    % Each row corresponds to a vehicle.
    % [-]
    vehicleDistributionAll = [  .20 .40 .80
                                .05 .10 .05
                                .50 .30 .05
                                .15 .15 .05
                                .10 .05 .05 ];

    % The vehicle distribution is chosen with regard to the distance that the type traffic is
    % presumed to travel. This can either be long, medium or local for fatigue load model 4.
    if isequal({rangeTraffic},{'long'})
        vehicleDistribution = vehicleDistributionAll(:,1);
    elseif isequal({rangeTraffic},{'medium'})
        vehicleDistribution = vehicleDistributionAll(:,2);
    elseif isequal({rangeTraffic},{'local'})
        vehicleDistribution = vehicleDistributionAll(:,3);
    end
end

% ================================================================== %
% ========================== Placeholder ========================== %
% ================================================================== %
% Place holder for additional load models, please make a copy of the placeholder when adding
% additional load models

% "Name_of_load_model"
if isequal({fatigueLoadModel},{'Name_of_load_model'})

    % Assigning the location of the axles for each vehicle in "Name_of_load_model"
    % [m]
    vehicleAxles = [ ];

    % Assigning the axle load of the axles for each vehicle in "Name_of_load_model"
    % [N]
    vehicleLoads = [ ]/referenceLoad;

    % Distribution of vehicles of the total amount vehicles passing the bridge
    % [-]
    vehicleDistribution = [ ];
end

% ================================================================== %
% ========================== Miscellaneous ========================= %
% ================================================================== %

% Check that the vehicle distribution have a sum of 1. This is an common mistake. Some errors are
% allowed and this is only a warning message in case the error is intentional.
if sum(vehicleDistribution) < 0.99 && sum(vehicleDistribution) > 1.01
    fprintf('Warning: The distribution of vehicles does not add up to 1')
end

% End of the function
end
```

E.6 Kea_axleLoad

```
function [shearForce, bendingMoment] = Kea_axleLoad(xSpan, xLoad, axleLoad, spanLength)
%%%%%%%%%%%%%%%%%%%%%%%%%%%%%%%%%%%%%%%%%%%%%%%%%%%%%%%%%%%%%%%%%%%%%%%%%%%%%%%
% This is a function that calculates the influence line for bending moment and shear force for a
% axle load, assuming fixed supports.
%
% Input:
%
%   xSpan:     Location of the chosen section in x-direction along the span. should be given in m
%
%   xLoad:     Location of the axle load in x-direction along the span. Should be given in m
%
%   axleLoad:  The total force of the axle load. Should be given N
%
%   spanLength: The length of the span. Should be given in m.
%
%
% Output:
%
%   shearForce: The shear force in the given section caused by the axle load, given as N
%
%   bendingMoment: The bending moment in the given section caused by the axle load, given as Nm
%
%
% Description:
%
%   This is a function that calculates the influence line for bending moment and shear force for a
%   axle load, assuming fixed supports. If the load is placed outside the bridge both the shear
%   force and the bending moment will be zero.
%
% Developed by:
% Mattias Renström
% Oskar Rydh
%
% Developed in cooperation with:
% Chalmers University of Engineering
% NCC Teknik, Gothenburg
%
% Last edited:
% 2014-06-02
%%%%%%%%%%%%%%%%%%%%%%%%%%%%%%%%%%%%%%%%%%%%%%%%%%%%%%%%%%%%%%%%%%%%%%%%%%%%%%%

% The calculations is only carried out if the axle load is within the boundary of the bridge span.
% Note that the default value of zero is returned if the load is applied outside the boundary.
if 0 <= xLoad && xLoad <= spanLength
   % Location of the load measured from the the beginning and end of the span.
   a = xLoad;
   b = spanLength - xLoad;

   % Reaction forces at the beginning and end of the span.
   % Here is assumed fixed supports in both ends.
   Ra = ((axleLoad*b^2)/spanLength^2)*(1+(2*a)/spanLength);
   Rb = ((axleLoad*a^2)/spanLength^2)*(1+(2*b)/spanLength);

   % Support moment at the beginning and end of the span.
   % Here is assumed fixed supports in both ends.
```

```
    Ma = (axleLoad*a*b^2)/spanLength^2;
    Mb = (axleLoad*b*a^2)/spanLength^2;

    % Calculation of the shear force.
    if xSpan < xLoad
        shearForce = -Ra;
    elseif xSpan > xLoad
        shearForce = Rb;
    elseif xSpan == xLoad
        if Ra > Rb
            shearForce = -Ra;
        elseif Ra <= Rb
            shearForce = Rb;
        end
    end

    % Calculation of the bending moment
    if xSpan < xLoad
        bendingMoment = -Ra*xSpan + Ma;
    elseif xSpan >= xLoad
        bendingMoment = Rb*(xSpan-spanLength) + Mb;
    end

% If the load is not applied within the boundary of the bridge both the shear force and bending
% moment is set to zero.
elseif 0 <= xSpan && xSpan <= spanLength
    shearForce = 0;
    bendingMoment=0;
end
end % End of the function.
```

E.7 Kea_vehicleLoad

```
function [shearForce, bendingMoment] = Kea_vehicleLoad(xSpan, xVehicle, vehicleAxles, vehicleLoads,
spanLength)
%%%%%%%%%%%%%%%%%%%%%%%%%%%%%%%%%%%%%%%%%%%%%%%%%%%%%%%%%%%%%%%%%%%%%%%%%%%%%%%%%%%%%%%%%%%
% This is a function that calculates the influence line for bending moment and shear force for a
% vehicle, assuming fixed supports.
%
% Input:
%
%   xSpan:      Location of the chosen section in x-direction along the span. should be given in m
%
%   xVehicle:   Location of the first axle of the vehicle in x-direction along the span. Should be
%               given in m.
%
%   vehicleAxles: The distance to each axle measured from the first axle. Matrix where each row
%               corresponds to a vehicle in the load model and each column corresponds to an
%               axle.
%
%   vehicleLoads: The load for each axle in the load model. Matrix where each row corresponds to a
%               vehicle in the load model and each column corresponds to an axle.
%
%   spanLength: The length of the span. Should be given in m.
%
%
% Output:
%
%   shearForce: The shear force in the given section caused by the vehicle, given as N
%
%   bendingMoment: The bending moment in the given section caused by the vehicle, given as Nm
%
% Description:
%
%   This is a function that calculates the influence line for bending moment and shear force for a
%   vehicle. The calculation is based on the assumption of fixed supports.
%
%
% Developed by:
% Mattias Renström
% Oskar Rydh
%
% Developed in cooperation with:
% Chalmers University of Engineering
% NCC Teknik, Gothenburg
%
% Last edited:
% 2014-06-02
%%%%%%%%%%%%%%%%%%%%%%%%%%%%%%%%%%%%%%%%%%%%%%%%%%%%%%%%%%%%%%%%%%%%%%%%%%%%%%%%%%%%%%%%%

% Initiating the variables
shearForce = zeros(size(vehicleAxles,1),1);
bendingMoment = zeros(size(vehicleAxles,1),1);

% Calculating the shear force and bending moment for all the vehicles in the input data
% Each row in the axle position and axle load matrices should contain a new vehicle.
for k = 1:size(vehicleAxles,1)
```

```
    % Calculating the shear force and bending moment for all the axles of the current vehicle.
    % Each column in the axle position and axle load matrices should contain a new axle.
    for i = 1:size(vehicleAxles,2)
        % Obtaining the location of the current axle in the current vehicle
        xLoad = xVehicle - vehicleAxles(k,i);

        % Obtaining the load of the current axle in the current vehicle
        axleLoad = vehicleLoads(k,i);

        % Obtaining the shear force and the bending moment caused by the current axle in the
        % current vehicle.
        [shearForceStep,bendingMomentStep] = Kea_axleLoad(xSpan,xLoad,axleLoad,spanLength);

        % Stores and accumulates the values of the shear force and bending moment for the
        % current vehicle.
        shearForce(k) = shearForce(k) + shearForceStep;
        bendingMoment(k) = bendingMoment(k) + bendingMomentStep;
    end
end

% end of the function
end
```

E.8 Kea_interpolation

```
function [yvalue] = Kea_interpolation(xcoord,Xcoords ,Yvalues)
%%%%%%%%%%%%%%%%%%%%%%%%%%%%%%%%%%%%%%%%%%%%%%%%%%%%%%%%%%%%%%%%
% This is a function that gives an linear interpolation of a selected x-value.
%
% Input:
%
%  xcoord:    Selected x-coordinate for which the interpolated value will be given.
%
%  Xcoords:   Vector which contains the x-coordinates of the original data.
%
%  Yvalues:   Vector which contains the y-values which corresponds to the x-coordinates given
%             in the Xcoords above.
%
% Output:
%  yvalue:    The interpolated value corresponding to the selected x-coordinate. Note that if the
%             x-coordinate is taken outside the range of the Xcoords in the input, the returned
%             value will always have the value zero.
%
% Important note:
%  For the interpolation to work the x-coordinate vector must be sorted. Furthermore it is of
%  outmost importance that the x-coordinates corresponds to the given y-values.
%
%
% Developed by:
% Mattias Renström
% Oskar Rydh
%
% Developed in cooperation with:
% Chalmers University of Engineering
% NCC Teknik, Gothenburg
%
% Last edited:
% 2014-06-02
%%%%%%%%%%%%%%%%%%%%%%%%%%%%%%%%%%%%%%%%%%%%%%%%%%%%%%%%%%%%%%%%

% For the interpolation to function properly the coordinate vector has to
% be sorted. For this reason it is checked if the vector is sorted before
% the calculations are continued.
if issorted(Xcoords)

   % If the coordinate vector is sorted the first check is to control that
   % the requested x-coordinate is contained within the interval in the
   % coordinate vector.
   if (Xcoords(1) > xcoord) || (Xcoords(end) < xcoord)
      % Coordinate is outside the boundary, hence the stress is zero
      yvalue = 0;

   else
      % For a x-coordinate inside the boundary all the coordinates
      % are checked until a matching or higher coordinate is found.

      % runloop is used to check if a solution has been found. It is
      % initialised as 1 and will retain this value until a solution is
      % found. When the solution is found the value is changed to zero
      % and the loop will stop.
```

```
    runloop = 1;

    % i is used to check the coordinates in the coordinate vector. It
    % is initiated as 2 and will be increased for each iteration in the
    % while-loop.
    i = 1;

    % The while-loop runs for all nodes inside the interval as long as
    % a solution has not been found.
    while i <= length(Xcoords) && runloop;

      if Xcoords(i) == xcoord
        % If the current coordinate is an exact match with the
        % requested coordinate the y-value can be obtained directly
        % from the y-value vector.
        yvalue = Yvalues(i);

        % Since a solution is found the while-loop is stopped
        % by changing the value of runloop
        runloop = 0;

      elseif Xcoords(i) > xcoord
        % if the current coordinate exceeds the requested
        % coordinate the y-value has to be calculated by means of
        % linear interpolation.
        % In the interpolation the current and previous coordinate
        % is used since they are closest to the requested
        % coordinate.

        % Temporary variables used in the linear interpolation.
        Ya = Yvalues(i-1);
        Yb = Yvalues(i);
        xa = Xcoords(i-1);
        xb = Xcoords(i);
        yvalue = Ya + (Yb-Ya)*((xcoord - xa)/(xb-xa));

        % Since a solution is found the while-loop is stopped
        % by changing the value of runloop
        runloop = 0;

      else
        % If the current coordinate does not exceed or match
        % the requested coordinate the while loop will continue
        % to run. the next coordinate in the coordinate vector
        % is chosen by increasing i by one.
        i = i + 1;
      end
    end
  end
else
  % If the coordinate vector was not sorted the interpolation function cannot work properly.
  % Thus no y-value can be calculated and the following message is printed.
  fprintf('the vector with x-coordinates is not sorted!\n Interpolation aborted!')
end

% End of the function.
end
```

E.9 Kea_PalmgrenMiner

```
function [damage] = Kea_PalmgrenMiner(stressSpectra,stressType, fatigueStrength, loadCycles,
reductionLane, gammaFF, gammaMF)
%%%%%%%%%%%%%%%%%%%%%%%%%%%%%%%%%%%%%%%%%%%%%%%%%%%%%%%%%%%%%%%%%%%%%%%%%%%%%%%
% This is a function that calculates the fatigue damage sustained with the Palmgren-Miner method for
% a given stress spectra
%
% Input:
%
%  stressSpectra: Matrix which contains the stress spectra of the vehicle load model for a node
%              Each column contains a step in the stress spectra. Each row is a load case
%              or vehicle in the load model.
%
%  stressType:    The type of stress, should be indicated with a string
%              Acceptable stress types are: 'shear', 'direct' and 'principal'
%
%  fatigueStrength: The constant amplitude fatigue strength of the detail with regard to the
%              indicated stress type. This is either the shear or direct/principal stress.
%
%  loadCycles:   The number of load cycles for each load case or vehicle in the load model.
%
%  redutionLane:   Reduction factor taking into account how much of the the load from the lane
%              which is carried by the most loaded main I-girder (or corresponding detail which
%              is considered).
%
%  gammaFF:       The partial factor for the fatigue load.
%
%  gammaMF:       The partial factor for the fatigue strength.
%
% Output:
%
%  damage        The accumulated damage for the current detail.
%
%
% Description:
%
%  This is a function that calculates the fatigue damage sustained with the Palmgren-Miner method
%  for a given stress spectra. Several stress spectra can be calculated for several load cases or
%  vehicles in a fatigue load model.
%
%
% Developed by:
% Mattias Renström
% Oskar Rydh
%
% Developed in cooperation with:
% Chalmers University of Engineering
% NCC Teknik, Gothenburg
%
% Last edited:
% 2014-06-02
%%%%%%%%%%%%%%%%%%%%%%%%%%%%%%%%%%%%%%%%%%%%%%%%%%%%%%%%%%%%%%%%%%%%%%%%%%%%%%%

% Initialising the vector containing the damage for each load case.
damage = zeros(size(stressSpectra,1),1);
```

```
% Direct or principal stress
if isequal({stressType},{'direct'}) || isequal({stressType},{'principal'})
   % deltaSigma_C is given by the input data
   deltaSigma_C = fatigueStrength;

   % deltaSigma_D is given in Eurocode 1993-1-9: Paragraph 7.1-(2)
   deltaSigma_D = deltaSigma_C * nthroot(2/5,3);

   % deltaSigma_L is given in Eurocode 1993-1-9: Paragraph 7.1-(3)
   deltaSigma_L = deltaSigma_D * nthroot(5/100,5);

   % Applying the partial factor
   deltaSigma_C = deltaSigma_C / gammaMF;
   deltaSigma_D = deltaSigma_D / gammaMF;
   deltaSigma_L = deltaSigma_L / gammaMF;

% Shear stress
elseif isequal({stressType},{'shear'})
   % deltaTau_C is given by the input data
   deltaTau_C = fatigueStrength;

   % deltaTau_L is given in Eurocode 1993-1-9: Paragraph 7.1-(2)
   deltaTau_L = deltaTau_C * nthroot(2/100,5);

   % Applying the partial factor
   deltaTau_C = deltaTau_C / gammaMF;
   deltaTau_L = deltaTau_L / gammaMF;
end
% Calculating the damage that each load case causes. Presumably each load case corresponds to
% a vehicle in the load model.
for n = 1:size(stressSpectra,1)
   % Stress range and number of cycles for the Palmgren-Miner method is obtained from the
   % stress spectra for the current load case with help of the rain flow counting method.
   [deltaStressReference,numberOfCycles] = rainflow_borrowed(stressSpectra(n,:)');

   % the stress ranges are scaled with the reduction factor that takes into account how much of the
   % load is carried by the most loaded main I-girder. Note that the partial factor is applied.
   deltaStress_Ed = deltaStressReference * reductionLane * gammaFF;


   % The damage is calculated for each stress range obtained from the stress spectra.
   for i = 1:length(deltaStress_Ed)
      % The number of load cycles for the current load case and stress range.
      currentNumberOfCycles = loadCycles(n) * numberOfCycles(i);

      % The current number of load cycles to failure is reset to 0 each run. This leads to
      % infinite damage if the correct cycles to failure cannot be found.
      cyclesToFailure = 0;

      % Number of cycles to failure is calculated for direct or principal stresses
      if isequal({stressType},{'direct'}) || isequal({stressType},{'principal'})
         % If the stress range is higher than the constant amplitude fatigue limit the damage
         % can be calculated as follows
         if deltaStress_Ed(i) > deltaSigma_D
            cyclesToFailure = 2E6 * (deltaSigma_C/deltaStress_Ed(i))^3;

         % If the stress range is higher than the cut-off limit the damage can be calculated
```

```
        % as follows
        elseif deltaSigma_D >= deltaStress_Ed(i) && deltaStress_Ed(i) >= deltaSigma_L
            cyclesToFailure = 5E6 * (deltaSigma_D/deltaStress_Ed(i))^5;

        % if the stress range is below the cut-off limit no damage is accumulated.
        % This effectively means that the number of cycles to failure are infinite.
        % Note that if a number is divided by "inf" the result is always zero.
        elseif deltaStress_Ed(i) < deltaSigma_L
            cyclesToFailure = inf;
        end

    % Number of cycles to failure is calculated for shear stresses
    elseif isequal({stressType},{'shear'})

        % If the stress range is higher than the cut-off limit
        if deltaStress_Ed(i) >= deltaTau_L
            cyclesToFailure = 2E6 * (deltaTau_C/deltaStress_Ed(i))^5;

        % if the stress range is below the cut-off limit no damage is caused.
        % This effectively means that the number of cycles to failure are infinite.
        elseif deltaStress_Ed(i) < deltaTau_L
            cyclesToFailure = inf;
        end
    end
    % The damage for the current stress range is added to the overall damage for the load case
    damage(n) = damage(n) + currentNumberOfCycles/cyclesToFailure;

  end
end

% end of the function
end
```

E.10 Kea_damageEquivalent

```
function [damage] = Kea_damageEquivalent(stressSpectra,fatigueStrength, lambda,gammaFF,
gammaMF);
%%%%%%%%%%%%%%%%%%%%%%%%%%%%%%%%%%%%%%%%%%%%%%%%%
% This is a function that calculates the utilisation ratio with the damage equivalent method for a
% given stress spectrum.
%
% Input:
%   stressSpectra: Matrix which contains the stress spectra of the vehicle load model for a node
%              Each column contains a step in the stress spectra. Each row is a load case
%              or vehicle in the load model. Note, that a stress spectrum from a single vehicle
%              is more applicable for the damage equivalent method.
%
%   fatigueStrength: The constant amplitude fatigue strength of the detail with regard to the
%              indicated stress type. This is either the shear or direct/principal stress.
%
%   lambda:      The damage equivalent factor.
%   gammaFF:      The partial factor for the fatigue load.
%   gammaMF:      The partial factor for the fatigue strength.
%
%
% Output:
%   damage:       The damage for the current detail. In the case of a single vehicle
%              and a single stress spectrum the damage will be a scalar.
%
% Description:
%   This is a function that calculates the utilisation ratio with the damage equivalent method for a
%   given stress spectrum. Note that it is recommended to use only one vehicle for the damage
%   equivalent method.
%
%
% Developed by:
% Mattias Renström
% Oskar Rydh
%
% Developed in cooperation with:
% Chalmers University of Engineering
% NCC Teknik, Gothenburg
%
% Last edited:
% 2014-06-02
%%%%%%%%%%%%%%%%%%%%%%%%%%%%%%%%%%%%%%%%%%%%%%%%%
% Initiating the variables
damage = zeros(size(stressSpectra,1),1);

for n = 1:size(stressSpectra,1)
  % Stress range for the lambda method. This only the difference between the highest and the
  % lowest value for the stress range spectra.
  currentStressRange = max(stressSpectra(n,:))-min(stressSpectra(n,:));

  % Calculating the damage
  damage(n) = (gammaFF*currentStressRange*lambda)/(fatigueStrength/gammaMF);
end

% end of the function
end
```

E.11 Kea_damageEquivalentCombined

```
function [damage] = Kea_damageEquivalentCombined(stressSpectraShear, stressSpectraDirect,
fatigueStrengthShear, fatigueStrengthDirect, lambda, gammaFF, gammaMF);
%%%%%%%%%%%%%%%%%%%%%%%%%%%%%%%%%%%%%%%%%%%%%%%%%%%%%%%%%%%%%%%%%%%%%%%%%%%%%%%%%%%%%%%%%%%%%%%%
% This is a function that calculates the utilisation ratio with the damage equivalent method for a
% given stress spectrum where both shear and direct stress should be considered.
%
% Input:
%
%   stressSpectraShear: Matrix which contains the stress spectra for shear stress of the vehicle
%             load model for a node. Each column contains a step in the stress spectra. Each
%             row is a load case or vehicle in the load model.
%
%   stressSpectraDirect: Matrix which contains the stress spectra for direct stress of the vehicle
%             load model for a node. Each column contains a step in the stress spectra. Each
%             row is a load case or vehicle in the load model.
%
%   fatigueStrengthShear: The constant amplitude fatigue strength of the detail with regard to the
%             shear stress.
%
%   fatigueStrengthDirect: The constant amplitude fatigue strength of the detail with regard to the
%             direct stress.
%
%   lambda:       The damage equivalent factor.
%
%   gammaFF:       The partial factor for the fatigue load.
%
%   gammaMF:       The partial factor for the fatigue strength.
%
%
% Output:
%
%   damage:       The damage for the current detail. In the case of a single vehicle
%             and a single stress spectrum the damage will be a scalar.
%
%
% Description:
%
%   This is a function that calculates the utilisation ratio with the damage equivalent method for a
%   given stress spectrum where both shear and direct stress should be considered. For the standard
%   version see the Kea_damageEquivalent function instead. Note that it is recommended to use only
%   one vehicle for the damage equivalent method.
%
%
% Developed by:
% Mattias Renström
% Oskar Rydh
%
% Developed in cooperation with:
% Chalmers University of Engineering
% NCC Teknik, Gothenburg
%
% Last edited:
% 2014-06-02
%%%%%%%%%%%%%%%%%%%%%%%%%%%%%%%%%%%%%%%%%%%%%%%%%%%%%%%%%%%%%%%%%%%%%%%%%%%%%%%%%%%%%%%%%%%%%%%%
```

```
% Initiating the variables.
damageShear = zeros(size(stressSpectraShear,1),1);
damageDirect = zeros(size(stressSpectraShear,1),1);

for n = 1:size(stressSpectraShear,1)
   % Stress range for the lambda method. This only the difference between the highest and the
   % lowest value for the stress range spectra.
   currentStressRangeShear = max(stressSpectraShear(n,:))-min(stressSpectraShear(n,:));
   currentStressRangeDirect = max(stressSpectraDirect(n,:))-min(stressSpectraDirect(n,:));

   % Calculating the damage.
   damageShear(n) = (gammaFF*currentStressRangeShear*lambda)/(fatigueStrengthShear/gammaMF);
   damageDirect(n) =
(gammaFF*currentStressRangeDirect*lambda)/(fatigueStrengthDirect/gammaMF);
end

% The combined damage is calculated.
damage = damageShear.^5 + damageDirect.^3;


% end of the function
end
```

Appendix F – Calculations for parametric study

The calculations which are used in the parametric study are to a large extent performed in Mathcad. Incidentally, in this appendix all the Mathcad calculations are presented.

The main chapters and corresponding page number in the Mathcad calculations are listed below:

1 Input data

In this document all the required data for the bridge analysis is initialized and described.

Note that for most measurements the values are obtained from the technical drawing of the bridge built in Nynäshamn. See the report for further information about this bridge.

This chapter encompasses the following subchapters:

Sign conventions

The sign convention which is established here is used in all of the calculations. The conventions are the following:

- Tensile stresses are set as a positive stresses in the calculations. By the same token compressive stresses are set as negative stresses.
- Bending moment is defined according to the right-hand rule. Thus, positive moment yields tension ín the upper part of the cross-section and compression in the lower part of the cross-section.

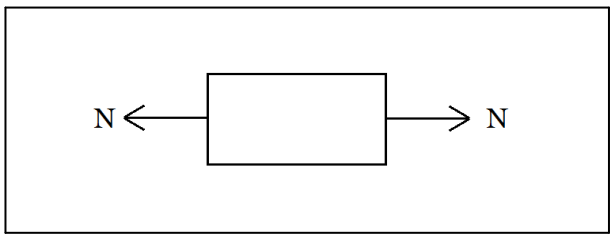

Positive direction for normal forces. Thus tension is defined as postive stress and compression is negative.

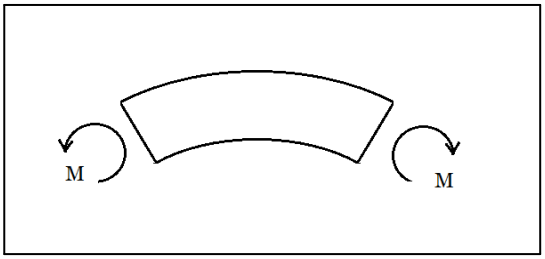

Postive moment yields tension in the upper parts of the cross-section and compression in the lower parts of the cross-section.

1.1 Geometry

All measurements and most geometrical properties of the bridge is presented in this chapter.

1.1.1 General measurements and axes

Before assigning measurement for the bridge it is needed to clarify how the origin, axes and their positive directions are defined. The global coordinate system is shown in the figure below and described in more detail for each axis in this subchapter. Note that there are local coordinate systems which are used for the z-direction for the different cross-sections.

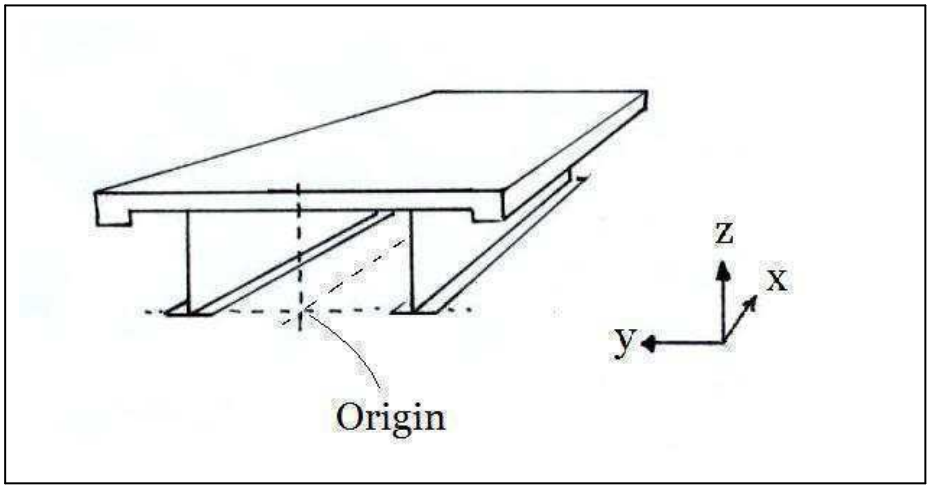

Illustration of the axes and their positive direction. In addition, the location of the origin is marked in the figure.

The general x-coordinate along the bridge span. x_{span} starts at the end of the main I-girders. The main girders starts at zero and the bridge extends in positive direction.

$$x_{span}$$

The global z-coordinate for the bridge. z_{bridge} is measured from the lowest part of the web at the support and positive direction is upward.

$$z_{bridge}$$

In addition to the global z-axis there are also local z-axis and associated z-coordinate systems. These coordinate system is used for calculations of bending resistance. The origin is set to coincide with the neutral axis of the considered cross-section.

$$z_{local}$$

The general y-coordinate for the bridge. y_{bridge} is perpendicular to the span direction and is zero in the middle of the bridge. Positive direction is according to the right-hand rule though in calculations only the positive values are used due to symmetry.

$$y_{bridge}$$

Total span length, measured for the steel girders.

$$L_{span} := 40m$$

Height of the web at the end of the span.

$$h_{main.web.end} := 1330mm$$

Height of the web at the middle of the span.

$$h_{main.web.mid} := 1030mm$$

The length of the sloped part at the bottom of the web close to the supports

$$slopelength_{web} := 4.4m$$

Distance between vertical stiffeners. According to the technical drawing there is only eight stiffeners, two in each end of the the two main I-girders. This implies that there are no intermediate stiffeners used in the bridge, and consequently the distance between stiffeners becomes the length of the span.

$$d_{stiff.vertical} := L_{span}$$

1.1.2 Dimensions of the cross-section

In this chapter all the dimensions and measurements related to the cross-section of the bridge are given.

Thickness of the longitudinal welds of the main I-girders.

$$a_{weld.main.lower} := 5mm$$

$$a_{weld.main.upper} := 5mm$$

Distance between the centres of the two main I-girders, in y-direction.

$$cc_{maingirders} := 5.4m$$

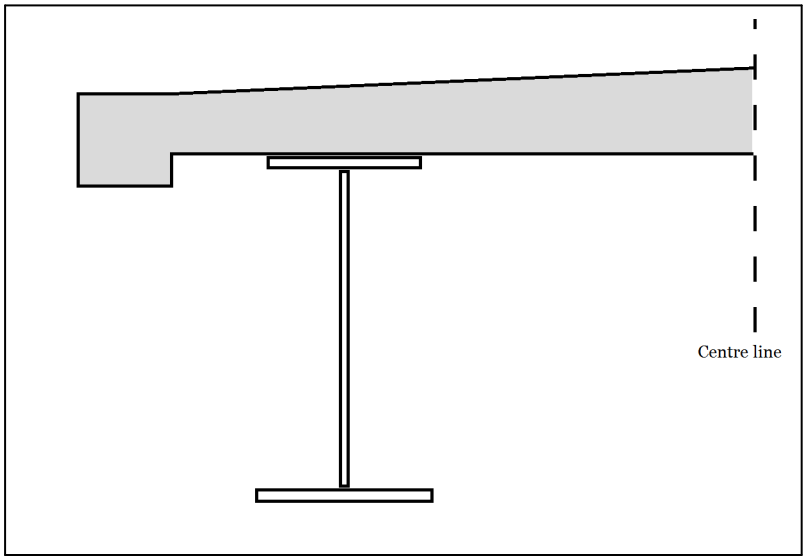

Illustration of the cross-section showing one of the two main I-girders and the concrete deck with slab and edge beam.

Distance between the centres of the oustand shear connectors. The value is obtained from the technical drawing. Note that the distance remains the same throughout the span.

$$b_{shearconnectors} := 300mm$$

Location of the splices the main I-girders

Location of the splices in the lower flange of the main I-girders.

$$X_{splice.flange.lower} := \begin{pmatrix} 6542mm \\ 15642mm \\ 24542mm \\ 33542mm \end{pmatrix}$$

Location of the splices in the web of the main I-girders.

$$X_{splice.web} := \begin{pmatrix} 7944mm \\ 20045mm \\ 32145mm \end{pmatrix}$$

Location of the splices in the upper flange of the main I-girders.

$$X_{splice.flange.upper} := \begin{pmatrix} 9220mm \\ 20062mm \\ 30904mm \end{pmatrix}$$

Dimensions of the I-girders

Thickness of the lower flange of the main I-girders. Note that the thickness of the lower flange is constant over the whole span length.

$$t_{main.flange.lower.span} := 40mm$$

Thickness of the web of the main I-girders. Note that the web is thinner in the middle of the span than at the support. This since the shear is primarily carried by the web and the shear force is greater closer to the supports.

$$t_{main.web.mid} := 12mm$$

$$t_{main.web.end} := 16mm$$

Thickness of the upper flange of the main I-girders. Note that the flange is thicker in the middle of the span than at the supports.

$$t_{main.flange.upper.mid} := 30mm$$

$$t_{main.flange.upper.end} := 20mm$$

Width of the lower flange of the main I-girders. Note that the width of the lower flange is constant over the whole span length.

$$b_{main.flange.lower.span} := 550mm$$

Width of the upper flange of the main I-girders. Note that the flange is wider in the middle of the span than at the supports.

$$b_{main.flange.upper.mid} := 500mm$$

$$b_{main.flange.upper.end} := 450mm$$

Dimensions of the concrete deck

Width of the concrete slab, exluding the edge beams

$$b_{deck.slab.span} := 6900mm$$

Width of the edge beams which are integrated into the concrete deck

$$b_{deck.beam.span} := 400mm$$

Thickness of the concrete slab at the mid-section of the bridge

$$t_{deck.slab.mid.span} := 258mm$$

Thickness of the concrete slab adjecent to the edge beam

$$t_{deck.slab.edge.span} := 170mm$$

Height of the edge beams which are integrated into the concrete deck

$$h_{deck.beam.span} := 400mm$$

Placement of reinforcement in the concrete deck

The placement of the reinforcement is simplified since the stainless steel and not the reinforced is the main focus of this analysis. Thus the reinforcement is given as three distinct layers; the upper layer in slab, the lower layer in the slab and the layer in the edge beam.

Note that the amounts of reinforcement is given for the support regions at the end of the span. Here the bending moment will result in tension in the concrete. This simplification is made since no detailed placement of the reinforcement is made and hence only the maximum contribution is of interest. To elaborate, the lower amount of reinforcement that is used in the middle of the span will be neglected in the calculations of concrete in compresion.

The consequence of this is that the deflections at the support will be slightly less than if a decreased amount of reinforcement where considered. However the consequenece of this choice is deemed negligable on the analysis of the performance of the stainless steel.

For the layers the distance from the concrete edge and the reinforcement amount is given.

Distance from the concrete edge to the centre of the upper reinforcement layer in the concrete slab.

$$d_{reinf.slab.lower} := 25mm + 20mm + \frac{16mm}{2}$$

$$d_{reinf.slab.lower} = 53 \cdot mm$$

distance from the concrete edge to the centre of the upper reinforcement layer in the concrete slab.

$$d_{reinf.slab.upper} := 30mm + 12mm + \frac{25mm}{2}$$

$$d_{reinf.slab.upper} = 54.5 \cdot mm$$

It is assumed that the reinforcement in the edge beam is placed so that the centre of gravity falls in the middle of the beam.

Steel area per meter for the lower reinforcement layer in the concrete slab. Values estimated from the technical drawing. There are 31 ϕ16 reinforcement bars over the slab width.

$$\rho_{reinf.slab.lower} := \frac{31 \cdot \left[\pi \cdot \left(\frac{16mm}{2}\right)^2\right]}{b_{deck.slab.span}}$$

$$\rho_{reinf.slab.lower} = 903.32 \cdot \frac{mm^2}{m}$$

Steel area per meter for the upper reinforcement layer in the concrete slab. Values estimated from the technical drawing.There are 69 ϕ25 reinforcement bars over the slab width.

$$\rho_{reinf.slab.upper} := \frac{69}{b_{deck.slab.span}} \cdot \left[\pi \cdot \left(\frac{25mm}{2}\right)^2\right]$$

$$\rho_{reinf.slab.upper} = 4908.74 \cdot \frac{mm^2}{m}$$

Steel area per meter for the reinforcement layer in the edge beam. Values estimated from the technical drawing. There are 8 ϕ16 reinforcement bars in the edge beam

$$\rho_{reinf.beam} := \frac{8 \cdot \left[\pi \cdot \left(\frac{16mm}{2}\right)^2\right]}{b_{deck.beam.span}}$$

$$\rho_{reinf.beam} = 4021.24 \cdot \frac{mm^2}{m}$$

1.1.3 Measurements of the carriageway

The width of the carriageway. given by Eurocode 1991-2 4.2.3-(1) as the distance between the kerbs or between the inner limits of vechicle restraint systems. Value is obtained from technical drawing.

$$w_{carriageway} := 7000mm$$

The thickness of the road surface. Measured from the technical drawing.

$$t_{roadsurface} := 10cm$$

1.2 Material properties

In this chapter all the material properties that are used in the calculations are given.

Miscellaneous

Partial factor for caclulation of cross-sectional resistance. Recommended values specific to stainless steel is given by Eurocode 1993-1-4: Paragraph 5.1-(2). However, here the values given in the Swedish Annex Chapter 12 paragrapgh 1 will be used insted.
Note that in Eurocode the values for stainless steel and carbon steel are 1.1 and 1.0 respectively.

$$\gamma_{M0.stainless} := 1.0$$

$$\gamma_{M0.carbon} := 1.0$$

Partial factor for calculation of instability phenomena. Recommended values specific to stainless steel is given by Eurocode 1993-1-4: Paragraph 5.1-(2).

$$\gamma_{M1.stainless} := 1.0$$

$$\gamma_{M1.carbon} := 1.0$$

Partial factor. Recommended values specific to stainless steel is given by Eurocode 1993-1-4: Paragraph 5.1-(2).

$$\gamma_{M2.stainless} := 1.2$$

$$\gamma_{M2.carbon} := 1.25$$

Partial factor for the concrete used for the strength of the concrete. Recomended value given by Eurocode 1992-1-1: Table 2.1N. The action is assumed to be persisitent and transient since no accidental loads are calculated.

$$\gamma_{c.concrete} := 1.5$$

Partial factor for the concrete used for the elastic modulus of the concrete in compression. Recomended value given by Eurocode 1992-1-1: paragraph 5.8.6-(3).

$$\gamma_{cE.concrete} := 1.2$$

Partial factor for the reinforcement. Recomended value given by Eurocode 1992-1-1: Table 2.1N. The action is assumed to be persisitent and transient since no accidental loads are calculated.

$$\gamma_{s.reinf} := 1.15$$

Specific weights and densities

Standard gravity

$$g = 9.81 \frac{m}{s^2}$$

Density of the reinforced concrete. Note that this value is an approximation and that the reinforcement content vary in both longitudinal and transversal directions.

$$\rho_{concrete} := 2500 \frac{kg}{m^3}$$

Density of the structural steel.

$$\rho_{steel} := 7700 \frac{kg}{m^3}$$

Density of air, used for calculation of wind load. Recommended value given by Eurocode 1991-2: Paragraph 4.5-(1)

$$\rho_{air} := 1.25 \frac{kg}{m^3}$$

Specific weight of reinforced concrete, Note that this value is an approximation.

$$\gamma_{concrete} := \rho_{concrete} \cdot g$$

$$\gamma_{concrete} = 24.52 \cdot \frac{kN}{m^3}$$

Specific weight of stainless steel

$$\gamma_{steel} := \rho_{steel} \cdot g$$

$$\gamma_{steel} = 75.51 \cdot \frac{kN}{m^3}$$

Specific weight of roadsurface material, estimated value.

$$\gamma_{roadsurface} := 23 \frac{kN}{m^3}$$

Mechanical properties of the concrete

The concrete that is used in the bridge is class C40/50, given by the technical drawing. Note that the use of other concrete classes is NOT implemented or supported.

$$\mathrm{concreteclass} := \text{"C40/50"}$$

Characteristic value of the concrete strength in compression for class C40/50. Value is obtained from Eurocode 1992-1-1: Table 3.1.

$$f_{ck.concrete} := 40\,\mathrm{MPa}$$

Characteristic value of the concrete strength in tension for class C40/50. Value is obtained in Eurocode 1992-1-1: Table 3.1.

$$f_{ctk.0.05.concrete} := 2.5\,\mathrm{MPa}$$

Characteristic value of the elastic modulus for the concrete for class C40/50. Value is obtained in Eurocode 1992-1-1: Table 3.1.

$$E_{concrete.cm} := 35\,\mathrm{GPa}$$

Mechanical properties of the reinforcement

Characteristic value of the yield strength of the reinforcement

$$f_{yk.reinf} := 600\,\mathrm{MPa}$$

Characteristic value of the elastic modulus for the reinforcement

$$E_{reinf} := 200\,\mathrm{GPa}$$

Choice of structural steel

Here the steel grade and type of steel is chosen. The steel grade has to defined since the calculations should work for different grades of both stainless steel and carbon steel.

$$\mathrm{steelgrade} := \text{"EN1.4162"}$$

Mechanical properties of the stainless structural steel

Material properties of the steel in that is used in the structure. Note that accordning to Eurocode 1994-2: Paragraph 3.3-(2) the maximum nominal yield strength that is allowed for structural steel in bridges is 460MPa.

Characteristic value of the ultimate strength of the structural steel

$$f_{uk.EN1.4162} := 690\,\mathrm{MPa}$$

Characteristic value of the yield strength of the structural steel. Eurocode 1994-2: Paragraph 3.3-(2) gives that the maximum nominal yield strength is limited to 460MPa for structural steel in bridges.

$$f_{yk.EN1.4162} := 450MPa$$

$$f_{yk.S355} := 355MPa$$

$$f_{yk.S460} := 460MPa$$

Poissons ratio for the steel

$$\nu_{steel} := 0.3$$

Elastic modulus for the structural steel ued in general calcuations. Note that for stainless steels the modulus of elasticity has a value of 200GPa compared to 210GPa for carbon steels. The recomended value for stainless duplex steel grades is taken in accordance with Eurocode 1993-1-4: paragraph 2.1.3-(1). However, note that the duplex grade EN 1.4162 is not included in the listed duplex steel grades but is assumed to have the same modulus of elasticity nontheless.

$$E_{EN1.4162} := 200GPa$$

$$E_{carbon} := 210GPa$$

Coefficient used for calculating the modulus of elasticity for stainless steel. Dependent on the steel grade and direction. Here the steel grade is EN 1.4162 and the direction is longitudinal.

$$\eta_{EN1.4162.long} := 5$$

1.3 Constants, factors and loads

In this chapter all the constans, factors and characteristic loads that are used in calculations are given.

Miscellaneous factors

Factor used in shear calculations of the structural steel. Given by Eurocode 1993-1-5: Section 5. Conservative value of 1.0 given by Eurocode 1993-1-5: Paragraph 6.2.6-(3). For steel grades up to and including S460 the recommended value is 1.2, given by Eurocode 1993-1-5: Paragraph 5.1-(2).

$$\eta_{shear} := 1.2$$

Partial factor used in the fatigue calculations. It is assumed that for all parts the the consequence of failure is high. Furthermore the safe life method is used to avoid regular inspections in addition to the risk of rapid failure. For more information about the safe life method see Eurocode 1993-1-9: Paragraph 3-(3). Recommended values are given by Eurocode 1993-1-9: Table 3.1.

$$\gamma_{M.fatigue} := 1.35$$

Partial factor used in the fatigue calculations. Recommended value is given by Eurocode 1993-2 paragraph 9.3-(1).

$$\gamma_{F.fatigue} := 1.0$$

The traffic category for the bridge. Definition of the categorys is given by Eurocode 1991-2: Table 4.5. Category 2 is chosen since it corresponds to roads and motorways with medium flow rates of lorries.

$$category_{traffic} := 2$$

For load model 4 the distribution of vehicle types depends on the distance the traffic is pressumed to travel. The traffic can be long distance, medium distance or local. In the calculation this is indicated by the string 'long', 'medium' or 'local'

$$range_{traffic} := "local"$$

The design life of the bridge, the unit is years.

$$t_{designlife} := 80years$$

Load combination factors

Partial coefficients for the load combinations in the ultimate limit state and the serviceability limit state.

In accordance with the Swedish Annex the partial factor γ_d is set to 1 in both the building phase and in the service life of the bridge. This corresponds to the most severe safety class of 3, values are given in Swedish Annex Chapter 1 paragraph 11.

$$\gamma_d := 1.0$$

Partial factor for the wind load. This is the momentary force and not for the persistent loading of wind. The recomended value of 1 can be found in both Eurocode 1990-A1: Table A2.1 and in the Swedish Annex in Chapter 7 paragraph 5. Note that no values are given for ψ_1 and ψ_2, however, for the sake of calcuations they will be given the value zero.

$$\psi_{wind.0} := 1.0$$

$$\psi_{wind.1} := 0$$

$$\psi_{wind.2} := 0$$

Partial factors for the traffic load acting on the bridge. Recomended values are given in Eurocode 1990-A1: Table A2.1. However, here the values are taken from the Swedish Annex in Chapter 7 paragrapgh 5.

$$\psi_{traffic.0} := 0.75$$

$$\psi_{traffic.1} := 0.75$$

$$\psi_{traffic.2} := 0$$

Characteristic traffic loads and factors

Reduction factor for axleloads, load model 1. Recomended value given by Eurocode 1991-2: 4.3.2-(3). However, Trafikverkets författningssamling Chpater 6, paragraph 4 contains a table with recomended values that will be used instead.

$$\alpha_{Q.model1.lane1} := 0.9$$

$$\alpha_{Q.model1.lane2} := 0.9$$

$$\alpha_{Q.model1.lane3} := 0$$

Reduction factor for distributed loads, load model 1. Recomended value given by Eurocode 1991-2: 4.3.2-(3). However, Trafikverkets författningssamling Chpater 6, paragraph 4 contains a table with recomended values that will be used instead.

$$\alpha_{q.model1.lane1} := 0.7$$

$$\alpha_{q.model1.lane2} := 1.0$$

$$\alpha_{q.model1.lane3} := 1.0$$

$$\alpha_{q.model1.remaining} := 1.0$$

Characteristic values of the loads in load model 1. Note that the load is dependent on the lane number. Values are taken from Eurocode 1991-2: 4.3.2-(6) which are applicable to bridges longer than 10m.

Axle weight, single axle

$$Q_{k.model1.lane1} := 600kN$$

$$Q_{k.model1.lane2} := 400kN$$

$$Q_{k.model1.lane3} := 200kN$$

Distributed loads

$$q_{k.model1.lane1} := 9\frac{kN}{m^2}$$

$$q_{k.model1.lane2} := 2.5\frac{kN}{m^2}$$

$$q_{k.model1.lane3} := 2.5\frac{kN}{m^2}$$

$$q_{k.model1.remaining} := 2.5\frac{kN}{m^2}$$

Characteristic fatigue loads and factors

Axle load for fatigue load model 3

$$Q_{k.fatigue} := 120kN$$

The refernce loads and corresponding cycles for fatigue calculations using the lambda-method. Values given by Eurocode 1993-2: Paragraph 9.5.2-(3).

$$Q_{fatigue.lambda.0} := 480kN$$

$$N_{fatigue.lambda.0} := \frac{0.5 \cdot 10^6}{year}$$

Windloads

The height of the traffic on the bridge which is used for calculation of wind loads. Value given by Eurocode 1991-2: Paragraph 8.3.1-(5a)

$$h_{traffic.wind} := 2000mm$$

The height of the bridge including traffic which is used for calculation of wind loads. Note that a estimation of 4m is used.

$$z_{bridge.max} := 4m$$

Terrain category for the bridge location. Explained by Eurocode 1991-2: Table 4.1. Note that terrain category 1 corresponds to lake area or similar flat areas with little vegetation and other obstacles.

$$Category_{terrain} := 1$$

Factor taking into account the strength of the wind in different directions. Recommended value given by Eurocode 1991-1-4: paragraph 8.1-(5).

$$c_{wind.direction} := 1.0$$

Factor taking into account the seasonal variation of the wind strength. Recommended value given by Eurocode 1991-1-4: paragraph 8.1-(5)

$$c_{wind.season} := 1.0$$

Basic value of the wind speed. Recommended value given by Eurocode 1991-1-4: paragraph 8.1-(5).

$$v_{wind.0} := 23\frac{m}{s}$$

Orography factor, taken as the value of 1 unless otherwise specified. Rules concerning this factor is given in Eurocode 1991-1-4: Section 4.3.3.

$$c_{orography} := 1$$

Miscellaneous self-weights

Note that for this bridge design there is no cross-bracing or intermediate vertical stiffeners.

Self-weight of the road surface material

$$g_{bridge.roadsurface} := w_{carriageway} \cdot t_{roadsurface} \cdot \gamma_{roadsurface}$$

$$g_{bridge.roadsurface} = 16.1 \cdot \frac{kN}{m}$$

Self-weight of the safety barrier. Estimated value.

$$g_{bridge.safetybarrier} := 1\frac{kN}{m}$$

Self-weight of the form work. Note that the weight of the form work on is relevant for the structure when the concrete is cast, thus it is not considered for calculations pertaining to the composite cross-section. According to the technical drawing the weight of the form work is limited to 80kg per square meter for the bridge deck area.

$$g_{bridge.formwork} := \frac{g \cdot 80kg}{m^2} \cdot \left(b_{deck.slab.span} + 2 \cdot b_{deck.beam.span}\right)$$

$$g_{bridge.formwork} = 6.04 \cdot \frac{kN}{m}$$

1.4 Fatigue strength classes

The fatigue classes of different details in the main I-girder.

Due to the scope of the thesis there are certain limitations to the fatigue assessment. No fatigue assessment is carried out for any of the concrete parts of the bridge. Furthermore, the shear studs connecting the main I-girders and the concrete slab is omitted in the fatigue assessment.

Here is presented the constant amplitude nominal stresses fatigue strength for the cracking modes in the main I-girders.

Cracking mode A1 and A2

Fatigue cracking mode A is based on detail 3 in Eurocode 1993-1-9: Table 8.2 in combination with detail 6 in Eurocode 1993-1-9: Table 8.1. The details takes into account fatigue cracking in the web at the longitudinal weld between the web and the flanges. The stress type is direct stress and shear stress respectively.

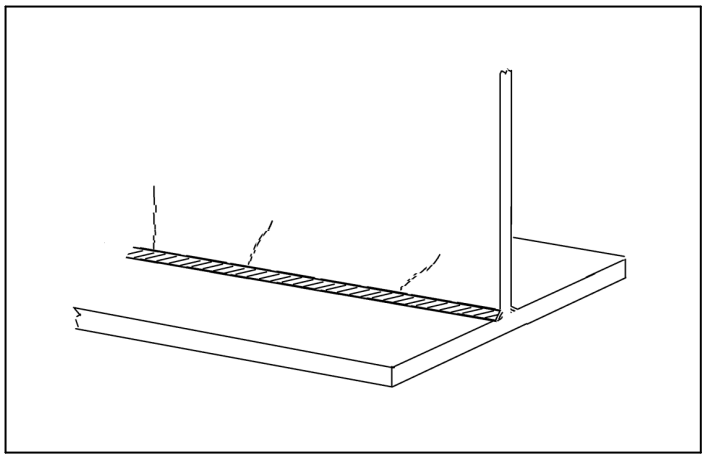

Illustration of fatigue cracking mode A

Constant amplitude nominal stresses fatigue strength for cracking mode A with regard to shear stress.

$$\Delta\tau_{C.modeA} := 100MPa$$

Constant amplitude nominal stresses fatigue strength for cracking mode A with regard to direct stress.

$$\Delta\sigma_{C.modeA} := 112MPa$$

Cracking mode B

Fatigue cracking mode B is based on detail 2 and 4 in Eurocode 1993-1-9: Table 8.3 which takes into account fatigue cracking in the flanges at the location of the splices in the flange. The stress type is direct stress.
For this mode there is size effect with regard to the thickness of the flanges. For this reason the mode has the additional index 'unreduced' appended to the name.

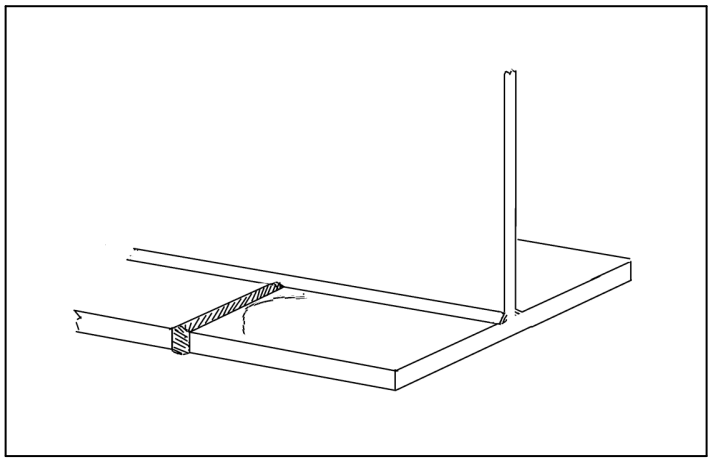

Illustration of fatigue cracking mode B

Constant amplitude nominal stresses fatigue strength for cracking mode B with regard to direct stress.

$$\Delta\sigma_{C.modeB.unreduced} := 112MPa$$

Cracking mode C

Fatigue cracking mode C is based on detail 7 in Eurocode 1993-1-9: Table 8.4 which takes into account the fatigue cracking in the web at the location of the vertical stiffeners. The stress type is principal stress.

Constant amplitude nominal stresses fatigue strength for cracking mode C with regard to principal stress.

$$\Delta\sigma_{C.modeC} := 80MPa$$

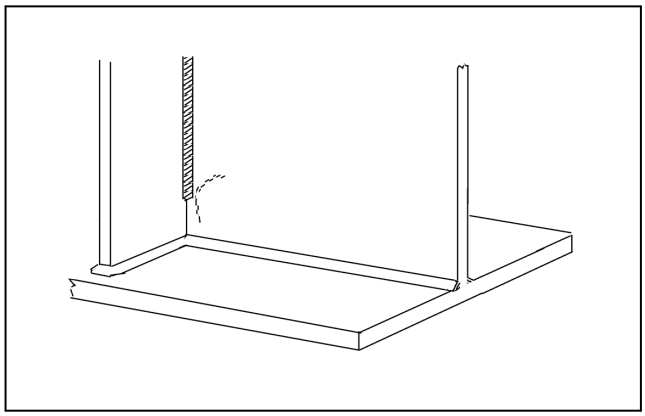

Illustration of fatigue cracking mode C

Cracking mode D

Fatigue cracking mode D is based on detail 7 in Eurocode 1993-1-9: Table 8.4 which takes into account the fatigue cracking in the flange at the location of the vertical stiffeners. The stress type is direct stress.

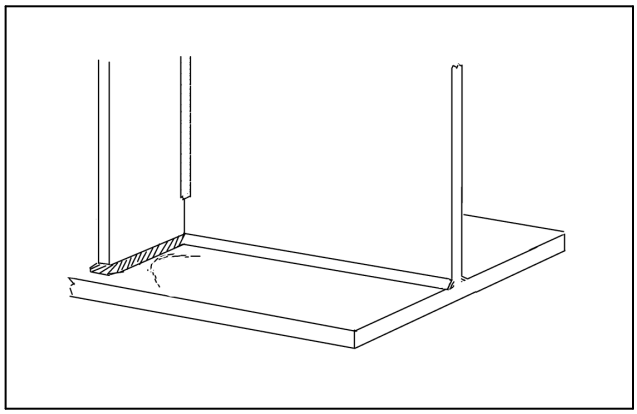

Illustration of fatigue cracking mode D

Constant amplitude nominal stresses fatigue strength for cracking mode D with regard to direct stress.

$$\Delta\sigma_{C.modeD} := 80MPa$$

Cracking mode E

Fatigue cracking mode E is based on detail 8 in Eurocode 1993-1-9: Table 8.5 which takes into account the fatigue cracking in the longitudinal weld between the web and the lower

and upper flange respectively. The stress type is shear stress.

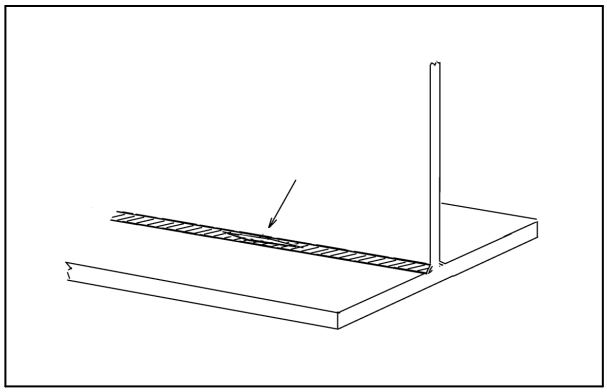

Illustration of fatigue cracking mode E

Constant amplitude nominal stresses fatigue strength for cracking mode E with regard to shear stress.

$$\Delta\tau_{C.modeE} := 80MPa$$

Cracking mode F

Fatigue cracking mode F is based on detail 2 and 4 in Eurocode 1993-1-9: Table 8.3 which takes into account fatigue cracking in the web at the location of the splices in the web. The stress type is direct stress.

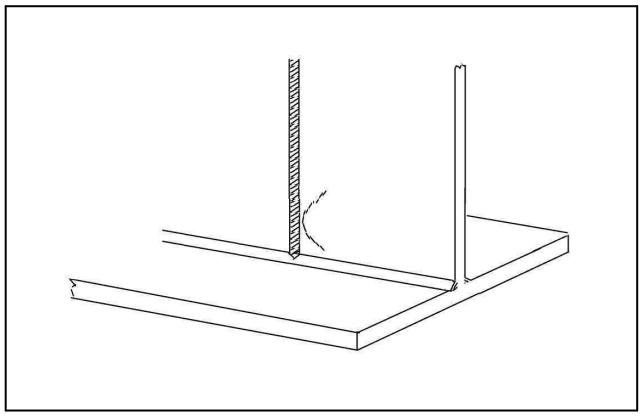

Illustration of fatigue cracking mode F

Constant amplitude nominal stresses fatigue strength for cracking mode F with regard to direct stress.

$$\Delta\sigma_{C.modeF.unreduced} := 112MPa$$

1.7 General mathcad functions

Zeros, a function which returns a matrix containing zeroes. The input is given as the number of rows and columns in the matrix. This function mimics the zeros function found in Matlab, hence

the name.
Here
A is the matrix containg zeroes. Initiated as a scalar.
B is a scalar which is utilised to transform A to a vector
C is vector which is utilised to transform A to a matrix

```
zeros(i, j) := | A ← 0
               | B ← 0
               | for tmp ∈ 1, 2.. i − 1 if i > 1
               |   A ← stack(A, B)
               | C ← A
               | for tmp ∈ 1, 2.. j − 1 if j > 1
               |   A ← augment(A, C)
               | A
```

Illustration of how the zeros function works. Note that the function could easily be addapted to create other matrices as well.

$$\text{zeros}(3,5) = \begin{pmatrix} 0 & 0 & 0 & 0 & 0 \\ 0 & 0 & 0 & 0 & 0 \\ 0 & 0 & 0 & 0 & 0 \end{pmatrix}$$

Function for obtaining a row from any matrix. The matrix has to be transposed since mathcad only allows for columns to be obtained from matrices.

$$\text{getRow}(\text{matrix}, \text{rowNumber}) := \left(\text{matrix}^{T}\right)^{\langle \text{rowNumber} \rangle^{T}}$$

Range function, primarily intended for finding maximum or minimum values over a certain range.

$$\text{range}(\text{start}, \text{stop}, \text{steps}) := \left| \begin{array}{l} \text{step} \leftarrow \dfrac{\text{stop} - \text{start}}{\text{steps} - 1} \\ \text{start}, \text{start} + \text{step} .. \quad \text{stop} \end{array} \right.$$

Range function, which creates a range for all the elements in a given vector.

```
range_vector(vector) := | n ← rows(vector)
                        | 0, 1.. n − 1 if n > 1
```

Function that is used to adjusts diagrams that plots over the length of the span for functions that depends only on x_{span}. Note that this function is exlusively used to adjust diagrams. The input is the function name and if it is a upper or lower value that should be used.

```
limit(function, A) := | for step ∈ 0m, 2m .. L_span
                      |     value ← function(step)
                      |     v_max ← max(value, v_max)
                      |     v_min ← min(value, v_min)
                      | (v_max · 1.1)  if A = 1
                      | (v_min · 1.1)  if A = 0 ∧ v_min < 0
                      | (v_min · 0.9)  if A = 0 ∧ v_min > 0
                      | 0  if A = 0 ∧ v_min = 0
```

Vectorsuper is a function that automatically creates an vector of the result of a function within a chosen range. the vector is a column vector and is intended for exportation of ranges of data.
Here
function is the name of the function to obtain the results for
start is the first input value in the vector
stop is the last input value in the vector
length is the number of elements in the vector

```
vector_super(function, start, stop, length) := | step ← (stop − start) / (length − 1)
                                               | A ← function(start)
                                               | for i ∈ start + step, start + 2step .. stc
                                               |   A ← stack(A, function(i))
                                               | A
```

Simple function that returns the input value. Used to create vectors containing x and z-coordinates that corresponds to the values of the other output variables.

```
echo(any) := any
```

Function that takes a vector and returns the values hust below and below the original ones. Used to check the plices in the main I-girder at both sides of the actual splice.

```
splitter(A, distance) := | n ← rows(A)
                         | B ← zeros(2n, 1)
                         | for i ∈ 0, 1 .. n − 1
                         |     B_(i·2), 0 ← A_i − distance
                         |     B_(i·2+1), 0 ← A_i + distance
                         | B
```

0. Parametric study

This chapter is essentially the same as chapter 1 - *Input*. The variables and constants which are defined here is also defined in chapter 1. However, this document is used in the parametric study and for this purpose some values is read from an external document. This allows for the parametric study to be automated and reduce the work load by removing some of the manual labour.

This chapter encompasses the following subchapters:

Importing the external data

Loading the sheets from the excel document which contains the input data.

$Exceldata_{Miscellaneous} :=$ ...\Parameters.xls

$Exceldata_{Geometry} :=$ ...\Parameters.xls

$Exceldata_{Fatigue} :=$ ...\Parameters.xls

$Exceldata_{Information} :=$ ...\Parameters.xls

Function that supplies the requested sheet as a matrix.

$$getSheet(name_{sheet}) := \begin{cases} Exceldata_{Geometry} & \text{if } name_{sheet} = \text{"Geometry"} \\ Exceldata_{Miscellaneous} & \text{if } name_{sheet} = \text{"Miscellaneous"} \\ Exceldata_{Fatigue} & \text{if } name_{sheet} = \text{"Fatigue"} \\ Exceldata_{Information} & \text{if } name_{sheet} = \text{"Information"} \end{cases}$$

Confirmation that the sheets exists and have the appropriate names. Note that this builds upon the fact that the excel sheet has a certain structure.

$$\text{getSheet}(\text{"Geometry"})_{5,1} = \text{"Geometry"}$$

$$\text{getSheet}(\text{"Miscellaneous"})_{5,1} = \text{"Miscellaneuos"}$$

$$\text{getSheet}(\text{"Fatigue"})_{5,1} = \text{"Fatigue"}$$

$$\text{getSheet}(\text{"Information"})_{5,1} = \text{"Information"}$$

Function that finds the row that matches the chosen varaible name. Note that there currently is no way to handle the case of two rows containing the exact same variable, please use caution. Furthermore, the excel document must have the correct structure of the columns, otherwise the correct names and rows cannot be found. Note that this could be improved to support more general structure, but as of yet it has not been implemented.
Here
sheet is the matrix containg all the data from the selected sheet. The data has the format string.
$name_{cell}$ gives the name of the current cell
$range_{rows}$ is the range of all the available rows in the current sheet
result is the variable that contains the row number for the matching row. Initiated as -1.
multi is the variable that indicates if there are multiple instances of matching rows

$$\begin{aligned}
&\text{findRow}(\text{name}, \text{sheet}) := \\
&\quad \text{name}_{\text{cell}}(\text{row}) \leftarrow \text{sheet}_{\text{row},3} \\
&\quad \text{range}_{\text{rows}} \leftarrow 0, 1 .. \ \text{rows}(\text{sheet}) - 1 \\
&\quad \text{result} \leftarrow -1 \\
&\quad \text{for} \ \ \text{row} \in \text{range}_{\text{rows}} \\
&\quad\quad \text{multi} \leftarrow 1 \ \ \text{if} \ \text{name}_{\text{cell}}(\text{row}) = \text{name} \wedge \text{result} \neq -1 \\
&\quad\quad \text{result} \leftarrow \text{row} \ \ \text{if} \ \text{name}_{\text{cell}}(\text{row}) = \text{name} \\
&\quad \text{result} \leftarrow \text{"Warning: not found"} \ \ \text{if result} = -1 \\
&\quad \text{result} \leftarrow \text{"Warning: Multiple instances"} \ \ \text{if multi} \neq 0 \\
&\quad \text{result}
\end{aligned}$$

Function which gives a matrix containing information about the given varaible name. The matrix has four rows that describes the name, value, unit and row of the given varible name. Note that the row is given for Mathcad which has origin set to zero.

$$\begin{aligned}
&\text{Info}\left(\text{name}, \text{name}_{\text{sheet}}\right) := \\
&\quad \text{sheet} \leftarrow \text{getSheet}\left(\text{name}_{\text{sheet}}\right) \\
&\quad \text{row} \leftarrow \text{findRow}(\text{name}, \text{sheet}) \\
&\quad \begin{pmatrix} \text{"Name:"} & \text{sheet}_{\text{row},3} \\ \text{"Value:"} & \text{sheet}_{\text{row},4} \\ \text{"Unit:"} & \text{sheet}_{\text{row},5} \\ \text{"Row:"} & \text{row} \end{pmatrix}
\end{aligned}$$

Function that imports the value of the chosen variable from the Excel sheet. Note that MathCad cannot handle functions with different units in the output. Hence, the unit has to be assigned manually in the input.

```
Import(name , unit , name_sheet) :=  sheet ← getSheet(name_sheet)
                                     row ← findRow(name , sheet)
                                     sheet_row , 4 · unit
```

Function that imports the value of the chosen variable from the Excel sheet. Same function as *Import* but without unit assingment.

```
Import_unitless(name , name_sheet) :=  sheet ← getSheet(name_sheet)
                                       row ← findRow(name , sheet)
                                       sheet_row , 4
```

Function that imports a range of values for the the chosen variable. The range must be stopped with the string 'stop' in the excel sheet, otherwise all data beneath the starting value will be imported. Note that MathCad cannot handle functions with different units in the output. Hence, the unit has to be assigned manually in the input.
Here
row is the current row. Initated as the matching row and increased in the while-loop.
vector is the vector that is requested. It is initialised with the first value in the range.
v is the value of the current row. Initated as 'void'.

```
Import_range(name , unit , name_sheet) :=  sheet ← getSheet(name_sheet)
                                           row ← findRow(name , sheet)
                                           row_max ← rows(sheet) − 1
                                           vector ← sheet_row , 4
                                           v ← "void"
                                           while  row < row_max ∧ v ≠ "stop"
                                               row ← row + 1
                                               v ← sheet_row , 4
                                               vector ← stack(vector , v)  if v ≠ "stop"
                                           vector · unit
```

0.1 Geometry

This chapter contains the measurements of the geometry which can be changed in the parametric study.

0.1.1 General geometry

Total span length, measured for the steel girders.

$$\text{Info}(\text{"L.span"},\text{"Geometry"}) = \begin{pmatrix} \text{"Name:"} & \text{"L.span"} \\ \text{"Value:"} & 40 \\ \text{"Unit:"} & \text{"m"} \\ \text{"Row:"} & 6 \end{pmatrix}$$

$$L_{span} := \text{Import}(\text{"L.span"}, m, \text{"Geometry"})$$

$$L_{span} = 40\,m$$

Height of the web at the end of the span.

$$\text{Info}(\text{"h.main.web.end"},\text{"Geometry"}) = \begin{pmatrix} \text{"Name:"} & \text{"h.main.web.end"} \\ \text{"Value:"} & 1.3 \\ \text{"Unit:"} & \text{"m"} \\ \text{"Row:"} & 11 \end{pmatrix}$$

$$h_{main.web.end} := \text{Import}(\text{"h.main.web.end"}, m, \text{"Geometry"})$$

$$h_{main.web.end} = 1.3\,m$$

Height of the web at the middle of the span.

$$\text{Info}(\text{"h.main.web.mid"},\text{"Geometry"}) = \begin{pmatrix} \text{"Name:"} & \text{"h.main.web.mid"} \\ \text{"Value:"} & 1.03 \\ \text{"Unit:"} & \text{"m"} \\ \text{"Row:"} & 12 \end{pmatrix}$$

$$h_{main.web.mid} := \text{Import}(\text{"h.main.web.mid"}, m, \text{"Geometry"})$$

$$h_{main.web.mid} = 1.03\,m$$

The length of the sloped part at the bottom of the web close to the supports

$$\text{Info}(\text{"slopelength.web"}, \text{"Geometry"}) = \begin{pmatrix} \text{"Name:"} & \text{"slopelength.web"} \\ \text{"Value:"} & 4.4 \\ \text{"Unit:"} & \text{"m"} \\ \text{"Row:"} & 13 \end{pmatrix}$$

$$\text{slopelength}_{\text{web}} := \text{Import}(\text{"slopelength.web"}, m, \text{"Geometry"})$$

$$\text{slopelength}_{\text{web}} = 4.4\,m$$

0.1.2 Dimensions of the cross-section

In this chapter all the dimensions and measurements related to the cross-section of the bridge are given. See chapter 1 - Input data for more information.

Thickness of the lower longitudinal weld of the main I-girders.

$$\text{Info}(\text{"a.weld.main.lower"}, \text{"Geometry"}) = \begin{pmatrix} \text{"Name:"} & \text{"a.weld.main.lower"} \\ \text{"Value:"} & 0.01 \\ \text{"Unit:"} & \text{"m"} \\ \text{"Row:"} & 22 \end{pmatrix}$$

$$a_{\text{weld.main.lower}} := \text{Import}(\text{"a.weld.main.lower"}, m, \text{"Geometry"})$$

$$a_{\text{weld.main.lower}} = 5 \cdot mm$$

Thickness of the upper longitudinal weld of the main I-girders.

$$\text{Info}(\text{"a.weld.main.upper"}, \text{"Geometry"}) = \begin{pmatrix} \text{"Name:"} & \text{"a.weld.main.upper"} \\ \text{"Value:"} & 0.01 \\ \text{"Unit:"} & \text{"m"} \\ \text{"Row:"} & 23 \end{pmatrix}$$

$$a_{\text{weld.main.upper}} := \text{Import}(\text{"a.weld.main.upper"}, m, \text{"Geometry"})$$

$$a_{\text{weld.main.upper}} = 5 \cdot mm$$

Location of the splices the main I-girders

Location of the splices in the lower flange of the main I-girders.

$$\text{Info}(\text{"X.splice.flange.lower"}, \text{"Geometry"}) = \begin{pmatrix} \text{"Name:"} & \text{"X.splice.flange.lower"} \\ \text{"Value:"} & 6.4 \\ \text{"Unit:"} & \text{"m"} \\ \text{"Row:"} & 25 \end{pmatrix}$$

$$X_{splice.flange.lower} := \text{Import}_{range}(\text{"X.splice.flange.lower"}, m, \text{"Geometry"})$$

$$X_{splice.flange.lower} = \begin{pmatrix} 6.4 \\ 15.6 \\ 24.4 \\ 33.6 \end{pmatrix} m$$

Location of the splices in the web of the main I-girders.

$$\text{Info}(\text{"X.splice.web"}, \text{"Geometry"}) = \begin{pmatrix} \text{"Name:"} & \text{"X.splice.web"} \\ \text{"Value:"} & 8 \\ \text{"Unit:"} & \text{"m"} \\ \text{"Row:"} & 30 \end{pmatrix}$$

$$X_{splice.web} := \text{Import}_{range}(\text{"X.splice.web"}, m, \text{"Geometry"})$$

$$X_{splice.web} = \begin{pmatrix} 8 \\ 20 \\ 32 \end{pmatrix} m$$

Location of the splices in the upper flange of the main I-girders.

$$\text{Info}(\text{"X.splice.flange.upper"}, \text{"Geometry"}) = \begin{pmatrix} \text{"Name:"} & \text{"X.splice.flange.upper"} \\ \text{"Value:"} & 9.2 \\ \text{"Unit:"} & \text{"m"} \\ \text{"Row:"} & 34 \end{pmatrix}$$

$$X_{splice.flange.upper} := \text{Import}_{range}(\text{"X.splice.flange.upper"}, m, \text{"Geometry"})$$

$$X_{splice.flange.upper} = \begin{pmatrix} 9.2 \\ 20 \\ 30.8 \end{pmatrix} m$$

Dimensions of the I-girders

Thickness of the lower flange of the main I-girders. Note that the thickness of the lower flange is constant over the whole span length.

$$\text{Info}(\text{"t.main.flange.lower.span"},\text{"Geometry"}) = \begin{pmatrix} \text{"Name:"} & \text{"t.main.flange.lower.span"} \\ \text{"Value:"} & 0.04 \\ \text{"Unit:"} & \text{"m"} \\ \text{"Row:"} & 8 \end{pmatrix}$$

$$t_{\text{main.flange.lower.span}} := \text{Import}(\text{"t.main.flange.lower.span"}, m, \text{"Geometry"})$$

$$t_{\text{main.flange.lower.span}} = 40 \cdot mm$$

Thickness of the web of the main I-girders at the end of the span. Note that the web is thinner in the middle of the span than at the support. This since the shear is primarily carried by the web and the shear force is greater closer to the supports.

$$\text{Info}(\text{"t.main.web.end"},\text{"Geometry"}) = \begin{pmatrix} \text{"Name:"} & \text{"t.main.web.end"} \\ \text{"Value:"} & 0.02 \\ \text{"Unit:"} & \text{"m"} \\ \text{"Row:"} & 14 \end{pmatrix}$$

$$t_{\text{main.web.end}} := \text{Import}(\text{"t.main.web.end"}, m, \text{"Geometry"})$$

$$t_{\text{main.web.end}} = 16 \cdot mm$$

Thickness of the web of the main I-girders at the middle of the span. Note that the web is thinner in the middle of the span than at the support. This since the shear is primarily carried by the web and the shear force is greater closer to the supports.

$$\text{Info}(\text{"t.main.web.mid"},\text{"Geometry"}) = \begin{pmatrix} \text{"Name:"} & \text{"t.main.web.mid"} \\ \text{"Value:"} & 0.01 \\ \text{"Unit:"} & \text{"m"} \\ \text{"Row:"} & 15 \end{pmatrix}$$

$$t_{\text{main.web.mid}} := \text{Import}(\text{"t.main.web.mid"}, m, \text{"Geometry"})$$

$$t_{\text{main.web.mid}} = 12 \cdot mm$$

Thickness of the upper flange of the main I-girders at the end of the span. Note that the flange is thicker in the middle of the span than at the supports.

$$\mathrm{Info}(\text{"t.main.flange.upper.end"},\text{"Geometry"}) = \begin{pmatrix} \text{"Name:"} & \text{"t.main.flange.upper.end"} \\ \text{"Value:"} & 0.02 \\ \text{"Unit:"} & \text{"m"} \\ \text{"Row:"} & 17 \end{pmatrix}$$

$$t_{main.flange.upper.end} := \mathrm{Import}(\text{"t.main.flange.upper.end"}, m, \text{"Geometry"})$$

$$t_{main.flange.upper.end} = 20 \cdot mm$$

Thickness of the upper flange of the main I-girders at the middle of the span. Note that the flange is thicker in the middle of the span than at the supports.

$$\mathrm{Info}(\text{"t.main.flange.upper.mid"},\text{"Geometry"}) = \begin{pmatrix} \text{"Name:"} & \text{"t.main.flange.upper.mid"} \\ \text{"Value:"} & 0.03 \\ \text{"Unit:"} & \text{"m"} \\ \text{"Row:"} & 18 \end{pmatrix}$$

$$t_{main.flange.upper.mid} := \mathrm{Import}(\text{"t.main.flange.upper.mid"}, m, \text{"Geometry"})$$

$$t_{main.flange.upper.mid} = 30 \cdot mm$$

Width of the lower flange of the main I-girders. Note that the width of the lower flange is constant over the whole span length.

$$\mathrm{Info}(\text{"b.main.flange.lower.span"},\text{"Geometry"}) = \begin{pmatrix} \text{"Name:"} & \text{"b.main.flange.lower.span"} \\ \text{"Value:"} & 0.55 \\ \text{"Unit:"} & \text{"m"} \\ \text{"Row:"} & 9 \end{pmatrix}$$

$$b_{main.flange.lower.span} := \mathrm{Import}(\text{"b.main.flange.lower.span"}, m, \text{"Geometry"})$$

$$b_{main.flange.lower.span} = 0.55\,m$$

Width of the upper flange of the main I-girders at the end of the span. Note that the flange is wider in the middle of the span than at the supports.

$$\text{Info}(\text{"b.main.flange.upper.end"}, \text{"Geometry"}) = \begin{pmatrix} \text{"Name:"} & \text{"b.main.flange.upper.end"} \\ \text{"Value:"} & 0.45 \\ \text{"Unit:"} & \text{"m"} \\ \text{"Row:"} & 19 \end{pmatrix}$$

$$b_{main.flange.upper.end} := \text{Import}(\text{"b.main.flange.upper.end"}, m, \text{"Geometry"})$$

$$b_{main.flange.upper.end} = 0.45\,m$$

Width of the upper flange of the main I-girders at the middle of the span. Note that the flange is wider in the middle of the span than at the supports.

$$\text{Info}(\text{"b.main.flange.upper.mid"}, \text{"Geometry"}) = \begin{pmatrix} \text{"Name:"} & \text{"b.main.flange.upper.mid"} \\ \text{"Value:"} & 0.5 \\ \text{"Unit:"} & \text{"m"} \\ \text{"Row:"} & 20 \end{pmatrix}$$

$$b_{main.flange.upper.mid} := \text{Import}(\text{"b.main.flange.upper.mid"}, m, \text{"Geometry"})$$

$$b_{main.flange.upper.mid} = 0.5\,m$$

0.2 Material properties

In this chapter all the material properties that are used in the calculations are given.

The steel grade that is used for the main I-girders. Currently the stainless steel grade EN1.4162 and carbon steel grades S355 and S460 is implemented.

$$\text{Info}(\text{"steelgrade"}, \text{"Miscellaneous"}) = \begin{pmatrix} \text{"Name:"} & \text{"steelgrade"} \\ \text{"Value:"} & \text{"EN1.4162"} \\ \text{"Unit:"} & \text{"-"} \\ \text{"Row:"} & 6 \end{pmatrix}$$

$$\text{steelgrade} := \text{Import}_{unitless}(\text{"steelgrade"}, \text{"Miscellaneous"})$$

$$\text{steelgrade} = \text{"EN1.4162"}$$

0.3 Constants, factors and loads

In this chapter all the constans, factors and characteristic loads that are used in calculations are given.

The traffic category for the bridge. Definition of the categorys is given by Eurocode 1991-2: Table 4.5. Values ranges from 0 to 4 where 0 is the most severe category.

$$\text{Info}(\text{"category.traffic"}, \text{"Miscellaneous"}) = \begin{pmatrix} \text{"Name:"} & \text{"category.traffic"} \\ \text{"Value:"} & 4 \\ \text{"Unit:"} & \text{"-"} \\ \text{"Row:"} & 9 \end{pmatrix}$$

$$\text{category}_{\text{traffic}} := \text{Import}_{\text{unitless}}(\text{"category.traffic"}, \text{"Miscellaneous"})$$

$$\text{category}_{\text{traffic}} = 4$$

The design life of the bridge, the unit is years.

$$\text{Info}(\text{"t.designlife"}, \text{"Miscellaneous"}) = \begin{pmatrix} \text{"Name:"} & \text{"t.designlife"} \\ \text{"Value:"} & 80 \\ \text{"Unit:"} & \text{"years"} \\ \text{"Row:"} & 10 \end{pmatrix}$$

$$t_{\text{designlife}} := \text{Import}(\text{"t.designlife"}, \text{years}, \text{"Miscellaneous"})$$

$$t_{\text{designlife}} = 80 \cdot \text{years}$$

For load model 4 the distribution of vehicle types depends on the distance the traffic is pressumed to travel. The traffic can be long distance, medium distance or local. In the calculation this is indicated by the string 'long', 'medium' or 'local'

$$\text{Info}(\text{"range.traffic"}, \text{"Miscellaneous"}) = \begin{pmatrix} \text{"Name:"} & \text{"range.traffic"} \\ \text{"Value:"} & \text{"local"} \\ \text{"Unit:"} & \text{"-"} \\ \text{"Row:"} & 11 \end{pmatrix}$$

$$\text{range}_{\text{traffic}} := \text{Import}_{\text{unitless}}(\text{"range.traffic"}, \text{"Miscellaneous"})$$

$$\text{range}_{\text{traffic}} = \text{"local"}$$

0.4 Fatigue strength classes

The fatigue classes of different details in the main I-girder.

Due to the scope of the thesis there are certain limitations to the fatigue assessment. No fatigue assessment is carried out for any of the concrete parts of the bridge. Furthermore, the shear studs connecting the main I-girders and the concrete slab is omitted in the fatigue assessment.

Here is presented the constant amplitude nominal stresses fatigue strength for the cracking modes in the main I-girders.

Caution: Mathcad cannot handle Δ, σ, τ and other greek letters in the varaiablenames in the Excel document. Due to this limitation the name of these variables has replaced greek letters with roman letters in the following manner: 'Delta', 'Sigma' and 'Tau'. Currently all greek letters are spelled with a capital first letter with no regard to the greek letter being capital or not.

Cracking mode A1 and A2

Fatigue cracking mode A is based on detail 3 in Eurocode 1993-1-9: Table 8.2 in combination with detail 6 in Eurocode 1993-1-9: Table 8.1. The details takes into account fatigue cracking in the web at the longitudinal weld between the web and the flanges. The stress type is direct stress and shear stress respectively.

Constant amplitude nominal stresses fatigue strength for cracking mode A with regard to shear stress.

$$\text{Info}(\text{"DeltaTau.C.modeA"}, \text{"Fatigue"}) = \begin{pmatrix} \text{"Name:"} & \text{"DeltaTau.C.modeA"} \\ \text{"Value:"} & 100 \\ \text{"Unit:"} & \text{"MPa"} \\ \text{"Row:"} & 6 \end{pmatrix}$$

$$\Delta\tau_{C.modeA} := \text{Import}(\text{"DeltaTau.C.modeA"}, MPa, \text{"Fatigue"})$$

$$\Delta\tau_{C.modeA} = 100 \cdot MPa$$

Constant amplitude nominal stresses fatigue strength for cracking mode A with regard to direct stress.

$$\text{Info}(\text{"DeltaSigma.C.modeA"}, \text{"Fatigue"}) = \begin{pmatrix} \text{"Name:"} & \text{"DeltaSigma.C.modeA"} \\ \text{"Value:"} & 112 \\ \text{"Unit:"} & \text{"MPa"} \\ \text{"Row:"} & 7 \end{pmatrix}$$

$$\Delta\sigma_{C.modeA} := \text{Import}(\text{"DeltaSigma.C.modeA"}, MPa, \text{"Fatigue"})$$

$$\Delta\sigma_{C.modeA} = 112 \cdot MPa$$

Cracking mode B

Fatigue cracking mode B is based on detail 2 and 4 in Eurocode 1993-1-9: Table 8.3 which takes into account fatigue cracking in the flanges at the location of the splices in the flange. The stress type is direct stress.
For this mode there is size effect with regard to the thickness of the flanges. For this reason the mode has the additional index 'unreduced' appended to the name.

Constant amplitude nominal stresses fatigue strength for cracking mode B with regard to direct stress.

$$\text{Info}(\text{"DeltaSigma.C.modeB.unreduced"}, \text{"Fatigue"}) = \begin{pmatrix} \text{"Name:"} & \text{"DeltaSigma.C.modeB.un} \\ \text{"Value:"} & 112 \\ \text{"Unit:"} & \text{"Mpa"} \\ \text{"Row:"} & 9 \end{pmatrix}$$

$$\Delta\sigma_{C.modeB.unreduced} := \text{Import}(\text{"DeltaSigma.C.modeB.unreduced"}, MPa, \text{"Fatigue"})$$

$$\Delta\sigma_{C.modeB.unreduced} = 112 \cdot MPa$$

Cracking mode C

Fatigue cracking mode C is based on detail 7 in Eurocode 1993-1-9: Table 8.4 which takes into account the fatigue cracking in the web at the location of the vertical stiffeners. The stress type is principal stress.

Constant amplitude nominal stresses fatigue strength for cracking mode C with regard to principal stress.

$$\text{Info}(\text{"DeltaSigma.C.modeC"}, \text{"Fatigue"}) = \begin{pmatrix} \text{"Name:"} & \text{"DeltaSigma.C.modeC"} \\ \text{"Value:"} & 80 \\ \text{"Unit:"} & \text{"Mpa"} \\ \text{"Row:"} & 11 \end{pmatrix}$$

$$\Delta\sigma_{C.modeC} := \text{Import}(\text{"DeltaSigma.C.modeC"}, MPa, \text{"Fatigue"})$$

$$\Delta\sigma_{C.modeC} = 80 \cdot MPa$$

Cracking mode D

Fatigue cracking mode D is based on detail 7 in Eurocode 1993-1-9: Table 8.4 which takes into account the fatigue cracking in the flange at the location of the vertical stiffeners. The stress type is direct stress.

Constant amplitude nominal stresses fatigue strength for cracking mode D with regard to direct stress.

$$\text{Info}(\text{"DeltaSigma.C.modeD"}, \text{"Fatigue"}) = \begin{pmatrix} \text{"Name:"} & \text{"DeltaSigma.C.modeD"} \\ \text{"Value:"} & 80 \\ \text{"Unit:"} & \text{"Mpa"} \\ \text{"Row:"} & 13 \end{pmatrix}$$

$$\Delta\sigma_{C.modeD} := \text{Import}(\text{"DeltaSigma.C.modeD"}, MPa, \text{"Fatigue"})$$

$$\Delta\sigma_{C.modeD} = 80 \cdot MPa$$

Cracking mode E

Fatigue cracking mode E is based on detail 8 in Eurocode 1993-1-9: Table 8.5 which takes into account the fatigue cracking in the longitudinal weld between the web and the lower and upper flange respectively. The stress type is shear stress.

Constant amplitude nominal stresses fatigue strength for cracking mode E with regard to shear stress.

$$\text{Info}(\text{"DeltaTau.C.modeE"}, \text{"Fatigue"}) = \begin{pmatrix} \text{"Name:"} & \text{"DeltaTau.C.modeE"} \\ \text{"Value:"} & 80 \\ \text{"Unit:"} & \text{"Mpa"} \\ \text{"Row:"} & 15 \end{pmatrix}$$

$$\Delta\tau_{C.modeE} := \text{Import}(\text{"DeltaTau.C.modeE"}, MPa, \text{"Fatigue"})$$

$$\Delta\tau_{C.modeE} = 80 \cdot MPa$$

Cracking mode F

Fatigue cracking mode F is based on detail 2 and 4 in Eurocode 1993-1-9: Table 8.3 which takes into account fatigue cracking in the web at the location of the splices in the web. The stress type is direct stress.

Constant amplitude nominal stresses fatigue strength for cracking mode F with regard to principal stress.

$$\text{Info}(\text{"DeltaSigma.C.modeF"}, \text{"Fatigue"}) = \begin{pmatrix} \text{"Name:"} & \text{"DeltaSigma.C.modeF"} \\ \text{"Value:"} & 112 \\ \text{"Unit:"} & \text{"Mpa"} \\ \text{"Row:"} & 17 \end{pmatrix}$$

$$\Delta\sigma_{C.modeF.unreduced} := \text{Import}(\text{"DeltaSigma.C.modeF"}, MPa, \text{"Fatigue"})$$

$$\Delta\sigma_{C.modeF.unreduced} = 112 \cdot MPa$$

2 Calculations

In this chapter all of the calculations will be performed. The calculations are performed in accordance with the rules and recomendations given Eurocode. References to the applicable sections and parts of Eurocode is given in the calcuatlions where they are used.

This chapter encompasses the following chapters:
2.1 Cross-sectional constants
2.2 Loads
2.3 Bending moment resistance
2.4 Shear resistance
2.5 Interaction between shear force and bending moment
2.6 Deflections
2.7 Fatigue assessment

2.1 Cross-sectional constants

In this document all the cross-sectional constants will be calculated and described.

This chapter encompasses the following subchapters:
2.1.1 Material properties
2.1.2 General calculations and geometrical properties
2.1.3 Nominal cross-section
2.1.4 Cross-sectional classes for the main I-girders
2.1.5 Reduction factors for parts in the main I-girders
2.1.6 Measurements for the effective composite cross-section
2.1.7 Second moment of area for the composite cross-section
2.1.8 Capacity of the main I-girders
2.1.9 Limitations to the dimensions

Simplified special case of the range function that goes over the entire span length in a desired amount of steps.

$$\mathrm{range}_{span}(steps) := \mathrm{range}\left(0m, L_{span}, steps\right)$$

2.1.1 Material properties

Here the material properties of the bridge is calculated from the data given in the chapter Input data and Parametric study.

Mechanical properties of the concrete

Design value of the concrete strength in compression. Given by Eurocode 1992-1-1: paragraph 3.1.6-(1).

$$\alpha_{concrete.compresion} := 1$$

$$f_{cd.concrete} := \frac{\alpha_{concrete.compresion} \cdot f_{ck.concrete}}{\gamma_{c.concrete}} = 26.67 \cdot MPa$$

Design value of the concrete strength in tension.Given by Eurocode 1992-1-1: paragraph 3.1.6-(2).

$$\alpha_{concrete.tension} := 1$$

$$f_{td.concrete} := \frac{\alpha_{concrete.tension} \cdot f_{ctk.0.05.concrete}}{\gamma_{c.concrete}} = 1.67 \cdot MPa$$

Design value of the elastic modulus for the concrete

$$E_{cd.concrete} := \frac{E_{concrete.cm}}{\gamma_{cE.concrete}}$$

Mechanical properties of the reinforcement

De3sign value of the yield strength of the reinforcement

$$f_{yd.reinf} := \frac{f_{yk.reinf}}{\gamma_{s.reinf}} = 521.74 \cdot MPa$$

Mechanical properties of the structural steel

Note that all of the mechanical properties of the structural steel is dependent on which grade and type of steel that is used. Thus the following parameters will take either the steel type or steel grade as an input.

The steel grade that is used for the main I-girders. Intended to be implemented in this analysis is the stainless steel grade EN 1.4162 (LDX2101) and the two carbon steel grades S355 and S460. The steel type can be either stainless steel or carbon steel. Stainless steel should be indicated with the text string "stainless" and carbon steel should be indicated with the text string "carbon"

$$steelgrade = "EN1.4162"$$

$$steeltype := \begin{cases} grade_{EN1.4162} \leftarrow "EN1.4162" \\ grade_{S355} \leftarrow "S355" \\ grade_{S460} \leftarrow "S460" \\ "stainless" \quad \text{if } steelgrade = grade_{EN1.4162} \\ "carbon" \quad \text{if } steelgrade = grade_{S355} \\ "carbon" \quad \text{if } steelgrade = grade_{S460} \end{cases}$$

$$steeltype = "stainless"$$

Characteristic value of the yield strength of the structural steel

$$steelgrade = "EN1.4162"$$

$$f_{yk.steel} := \begin{cases} grade_{EN1.4162} \leftarrow "EN1.4162" \\ grade_{S355} \leftarrow "S355" \\ grade_{S460} \leftarrow "S460" \\ f_{yk.EN1.4162} \quad \text{if } steelgrade = grade_{EN1.4162} \\ f_{yk.S355} \quad \text{if } steelgrade = grade_{S355} \\ f_{yk.S460} \quad \text{if } steelgrade = grade_{S460} \end{cases}$$

$$f_{yk.steel} = 450 \cdot MPa$$

Partial factors

Partial factor. Recommended values specific to stainless steel is given by Eurocode 1993-1-4: Paragraph 5.1-(2).

$$\text{steeltype} = \text{"stainless"}$$

$$\gamma_{M0.steel} := \begin{cases} \gamma_{M0.stainless} & \text{if steeltype} = \text{"stainless"} \\ \gamma_{M0.carbon} & \text{if steeltype} = \text{"carbon"} \end{cases}$$

$$\gamma_{M1.steel} := \begin{cases} \gamma_{M1.stainless} & \text{if steeltype} = \text{"stainless"} \\ \gamma_{M1.carbon} & \text{if steeltype} = \text{"carbon"} \end{cases}$$

$$\gamma_{M2.steel} := \begin{cases} \gamma_{M1.stainless} & \text{if steeltype} = \text{"stainless"} \\ \gamma_{M1.carbon} & \text{if steeltype} = \text{"carbon"} \end{cases}$$

Design value of the yield strength of the structural steel

$$f_{yd.steel} := \frac{f_{yk.steel}}{\gamma_{M0.steel}}$$

$$f_{yd.steel} = 450 \cdot MPa$$

Value of the elastic modulus of the structural steel to be used in global analysis.

$$\text{steeltype} = \text{"stainless"}$$

$$E_{steel} := \begin{cases} E_{EN1.4162} & \text{if steelgrade} = \text{"EN1.4162"} \\ E_{carbon} & \text{if steeltype} = \text{"carbon"} \end{cases}$$

$$E_{steel} = 200 \cdot GPa$$

Secant modulus of eleasticity at a given stress. Given by Eurocode 1993-1-4: Paragraph 4.2-(7). Only applicable for stainless steels.

$$E_{steel.secant}(\sigma_{steel}) := \begin{cases} E_s \leftarrow \dfrac{E_{steel}}{1 + 0.002 \cdot \dfrac{E_{steel}}{\sigma_{steel}} \cdot \left(\dfrac{\sigma_{steel}}{f_{yk.steel}} \right)^{n_{EN1.4162.long}}} \\ E_s \quad \text{if steeltype} = \text{"stainless"} \\ E_{steel} \quad \text{if steeltype} = \text{"carbon"} \end{cases}$$

Below is a graph displaying how the secant modulus of elasticity varies depending on the stress level in the stainless structural steel.

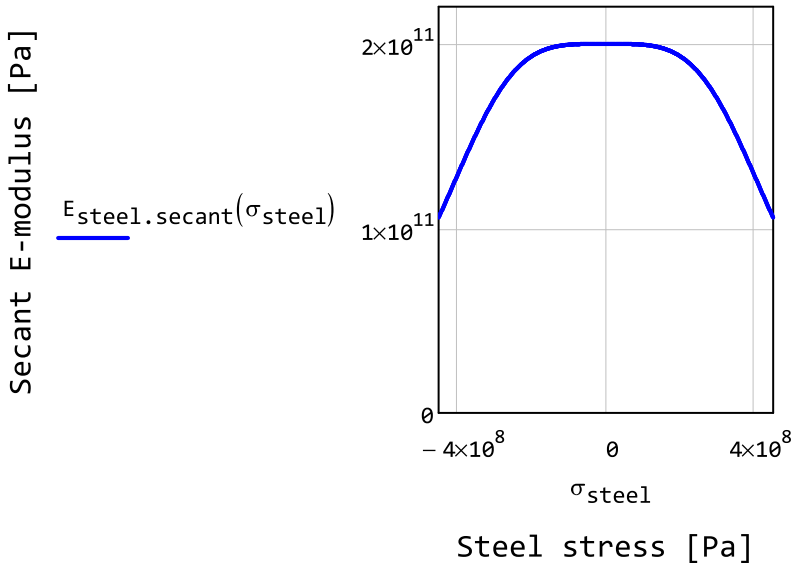

Miscellaneous material properties

Scalar that is used when transforming concrete area into equivalent steel area with regard to stiffness. The scalar is based on the design values of the elastic modulus for the structural steel and concrete respectively. No regard is taken to the stiffness contribution from the reinforcement in the concrete.

$$\alpha_{steel.concrete} := \frac{E_{cd.concrete}}{E_{steel}}$$

$$\alpha_{steel.concrete} = 0.15$$

Scalar that is used when transforming reinforcement area into equivalent steel area with regard to stiffness. The scalar is based on the design values of the elastic modulus for the structural steel and reinforcemt respectively.

$$\alpha_{steel.reinf} := \frac{E_{reinf}}{E_{steel}}$$

$$\alpha_{steel.reinf} = 1$$

Factor used for accounting the actual yield strength and modulus of elasticity in calculations. Given by Eurocode 1993-1-4: Table 5.2

$$\varepsilon_{steel} := \sqrt{\frac{235MPa}{f_{yk.steel}} \cdot \frac{E_{steel}}{210GPa}}$$

$$\varepsilon_{steel} = 0.71$$

2.1.2 General calculations and geometrical properties

Here several calculations are performed, for example are the measurements of the cross-section given as functions of the x-coordinate. Note that all the indata is still taken from the chapter Input data and Parametric study.

z-coordinates for the web

The z-coordinate for the bottom of the web of the main girders

$$z_{bottom.main.web}(x_{span}) := \begin{| l} diff \leftarrow h_{main.web.end} - h_{main.web.mid} \\ slope \leftarrow \dfrac{diff}{slopelength_{web}} \\ slope \cdot x_{span} \quad \text{if } x_{span} < slopelength_{web} \\ slope \cdot (L_{span} - x_{span}) \quad \text{if } x_{span} > L_{span} - slopelength_{we} \\ h_{main.web.end} - h_{main.web.mid} \quad \text{otherwise} \end{|}$$

The z-coordinate for the top of the web of the main girders

$$z_{top.main.web}(x_{span}) := h_{main.web.end}$$

The geometry of the web is displayed in the graph below. Note that the curvature of the bridge is neglected since it will not be considered in the calculations. Furthermore, the euler spirals that are used for the lower part of the flange is simplified into a constant change of slope instead.

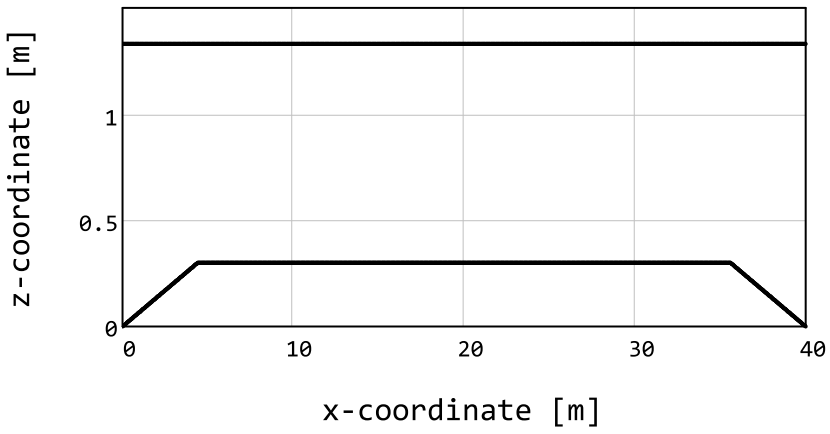

The approximate distance between section with zero-moment. Derived from the span length and assumed a uniform distributed load.

$$L_{effective} := 2\sqrt{\frac{L_{span}^{2}}{12}}$$

$$L_{effective} = 23.09\,m$$

Limit for maximum vertical deflections in the serviceability limit state.

$$\delta_{limit.SLS} := \frac{L_{span}}{400}$$

$$\delta_{limit.SLS} = 0.1\,m$$

In case a desing that implements intermidiate vertical stiffeners for the main I-girders the following assumption is checked. Note that the current calculations cannot take into account intermediate vertical stiffeners,

$$assumption_{no\_intermediate\_stiffeners} := \begin{cases} "true" & \text{if } d_{stiff.vertical} = L_{span} \\ "false" & \text{otherwise} \end{cases}$$

$$assumption_{no\_intermediate\_stiffeners} = "true"$$

Variation of the steel cross-sectional measurements along the span

The measurements that are used in the following calculations are given in Chapter 1 - *Input* or in Chapter 0 - *Parametric study*.

Thickness of the lower flange of the main I-girders

$$t_{main.flange.lower}(x_{span}) := t_{main.flange.lower.span}$$

Thickness of the web of the main I-girders

$$t_{main.web}(x_{span}) := \begin{cases} t_{main.web.end} & \text{if } x_{span} < X_{splice.web_0} \\ t_{main.web.end} & \text{if } x_{span} > X_{splice.web_2} \\ t_{main.web.mid} & \text{otherwise} \end{cases}$$

Thickness of the upper flange of the main I-girders

$$t_{main.flange.upper}(x_{span}) := \begin{cases} t_{main.flange.upper.end} & \text{if } x_{span} < X_{splice.flange.upper} \\ t_{main.flange.upper.end} & \text{if } x_{span} > X_{splice.flange.upper} \\ t_{main.flange.upper.mid} & \text{otherwise} \end{cases}$$

Height of the web of the main I-girders. Note that this is solely dependent on the z-coordinates of the upper and lower part of the web.

$$h_{main.web}(x_{span}) := z_{top.main.web}(x_{span}) - z_{bottom.main.web}(x_{span})$$

Width of the upper flange of the main I-girders

$$b_{\texttt{main.flange.upper}}(x_{\texttt{span}}) := \begin{cases} b_{\texttt{main.flange.upper.end}} & \text{if } x_{\texttt{span}} < x_{\texttt{splice.flange.upper}} \\ b_{\texttt{main.flange.upper.end}} & \text{if } x_{\texttt{span}} > x_{\texttt{splice.flange.upper}} \\ b_{\texttt{main.flange.upper.mid}} & \text{otherwise} \end{cases}$$

Width of the lower flange of the main I-girders

$$b_{\texttt{main.flange.lower}}(x_{\texttt{span}}) := b_{\texttt{main.flange.lower.span}}$$

Total height of the main I-girders

$$h_{\texttt{main.beam}}(x_{\texttt{span}}) := \begin{cases} t_{\texttt{fl}} \leftarrow t_{\texttt{main.flange.lower}}(x_{\texttt{span}}) \\ t_{\texttt{w}} \leftarrow h_{\texttt{main.web}}(x_{\texttt{span}}) \\ t_{\texttt{fu}} \leftarrow t_{\texttt{main.flange.lower}}(x_{\texttt{span}}) \\ t_{\texttt{fl}} + t_{\texttt{w}} + t_{\texttt{fu}} \end{cases}$$

Variation of the concrete cross-sectional measurements along the span

Overall width of the bridge concrete deck, including slab and the edge beams

$$b_{\texttt{deck}}(x_{\texttt{span}}) := b_{\texttt{deck.slab.span}} + 2 \cdot b_{\texttt{deck.beam.span}}$$

Width of the concrete slab, exluding the edge beams

$$b_{\texttt{deck.slab}}(x_{\texttt{span}}) := b_{\texttt{deck.slab.span}}$$

Width of the edge beams which are integrated into the concrete deck

$$b_{\texttt{deck.beam}}(x_{\texttt{span}}) := b_{\texttt{deck.beam.span}}$$

Thickness of the concrete slab at the mid-section of the bridge

$$t_{\texttt{deck.slab.mid}}(x_{\texttt{span}}) := t_{\texttt{deck.slab.mid.span}}$$

Thickness of the concrete slab adjecent to the edge beam

$$t_{\texttt{deck.slab.edge}}(x_{\texttt{span}}) := t_{\texttt{deck.slab.edge.span}}$$

Mean thickness of the concrete slab

$$t_{\texttt{deck.slab.mean}}(x_{\texttt{span}}) := \frac{t_{\texttt{deck.slab.mid}}(x_{\texttt{span}}) + t_{\texttt{deck.slab.edge}}(x_{\texttt{span}})}{2}$$

Thickness of the concrete slab
Here:
slope is the inclination of the top surface of the concrete slab in transversal direction.

$$t_{deck.slab}(x_{span}, y_{bridge}) := \left| \begin{array}{l} slope \leftarrow \left(\dfrac{t_{deck.slab.mid}(x_{span}) - t_{deck.slab.edge}(x_{span})}{\frac{b_{deck.slab}(x_{span})}{2}} \right) \\ t_{deck.slab.mid}(x_{span}) - slope \cdot y_{bridge} \end{array} \right.$$

Height of the edge beams which are integrated into the concrete deck

$$h_{deck.beam}(x_{span}) := h_{deck.beam.span}$$

Functions for calculating the second moment of area

Function for calculating the contribution to the second moment of area for a square part of a cross-section. The input for the function is the height and width of the part plus the distance from the centroid of the part to the neutral axis of the relevant cross-section.
Note that this function may also be used for reinforcement. For reinforcement the height is preferably taken as the area of the reinfocement divided by the effective width of the cross-section. Note that this diminshes the second moment of area of the bars themselves, however this contribution is small and usually completely neglected. To iterate, for reinforcement it is Steiner's theorem that dominates the formula.

$$I_{square}(height, width, distance_{NA}) := \frac{width \cdot height^3}{12} + width \cdot height \cdot distance_{NA}^2$$

Function for calculating the contribution to the second moment of area for a triangular part of a cross-section. Input data is the height, width and distance from centroid of part to the neutral axis of the cross-section.

$$I_{triangle}(height, width, distance_{NA}) := \frac{width \cdot height^3}{36} + width \cdot height \cdot distance_{NA}^2$$

Measurements of the carriageway

The width of the carriageway. given by Eurocode 1991-2 4.2.3-(1) as the distance between the kerbs or between the inner limits of vechicle restraint systems. Value is obtained from technical drawing.

$$w_{carriageway} = 7\,m$$

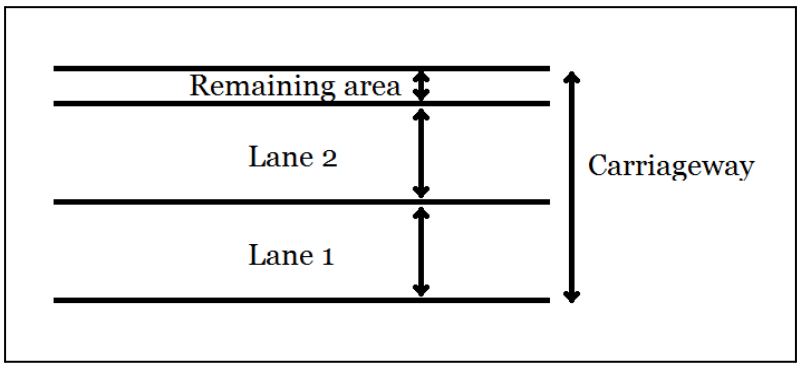

Illustration of how the notional lanes and remaining area should be assigned over the width of the carriage way.

The number of notional lanes, given by Eurocode 1991-2 Table 4.1

$$n_{lanes.notional} := \begin{cases} 1 & \text{if } w_{carriageway} < 5.4m \\ 2 & \text{if } 5.4m \le w_{carriageway} < 6m \\ \text{floor}\left(\frac{w_{carriageway}}{3m}\right) & \text{if } 6m \le w_{carriageway} \end{cases}$$

$$n_{lanes.notional} = 2$$

Width of a notional lane, given by Eurocode 1991-2 Table 4.1

$$w_{lane.notional} := \begin{cases} 3m & \text{if } w_{carriageway} < 5.4m \\ \frac{w_{carriageway}}{2} & \text{if } 5.4m \le w_{carriageway} < 6m \\ 3m & \text{if } 6m \le w_{carriageway} \end{cases}$$

$$w_{lane.notional} = 3\,m$$

Width of the remaining area, given by Eurocode 1991-2 Table 4.1

$$w_{lane.remaining} := \begin{cases} w_{carriageway} - 3m & \text{if } w_{carriageway} < 5.4m \\ 0m & \text{if } 5.4m \le w_{carriageway} < 6m \\ w_{carriageway} - 3m \cdot n_{lanes.notional} & \text{if } 6m \le w_{carriageway} \end{cases}$$

$$w_{lane.remaining} = 1\,m$$

2.1.3 Nominal cross-section

The nominal cross-section is the full composite cross-section that is not reduced due to buckling or other instability phenomena.

Cross-sectional area

Area of the upper flange of the main I-girders

$$A_{\texttt{main.flange.upper}}(x_{\texttt{span}}) := t_{\texttt{main.flange.upper}}(x_{\texttt{span}}) \cdot b_{\texttt{main.flange.upper}}(x_{\texttt{span}})$$

Area of the lower flange of the main I-girders

$$A_{\texttt{main.flange.lower}}(x_{\texttt{span}}) := t_{\texttt{main.flange.lower}}(x_{\texttt{span}}) \cdot b_{\texttt{main.flange.lower}}(x_{\texttt{span}})$$

Total area of the flanges for one of the main-I-girders

$$A_{\texttt{main.flanges}}(x_{\texttt{span}}) := A_{\texttt{main.flange.lower}}(x_{\texttt{span}}) + A_{\texttt{main.flange.upper}}(x_{\texttt{span}})$$

Area of the web of the main I-girders

$$A_{\texttt{main.web}}(x_{\texttt{span}}) := h_{\texttt{main.web}}(x_{\texttt{span}}) \cdot t_{\texttt{main.web}}(x_{\texttt{span}})$$

Area of a main girder

$$A_{\texttt{main.beam}}(x_{\texttt{span}}) := \left| \begin{array}{l} A_{\texttt{fl}} \leftarrow A_{\texttt{main.flange.lower}}(x_{\texttt{span}}) \\ A_{\texttt{w}} \leftarrow A_{\texttt{main.web}}(x_{\texttt{span}}) \\ A_{\texttt{fu}} \leftarrow A_{\texttt{main.flange.upper}}(x_{\texttt{span}}) \\ A_{\texttt{fl}} + A_{\texttt{w}} + A_{\texttt{fu}} \end{array} \right.$$

Area of half the concrete slab, which does not include the edge beams.

$$A_{\texttt{deck.slab}}(x_{\texttt{span}}) := \frac{t_{\texttt{deck.slab.mean}}(x_{\texttt{span}}) \cdot b_{\texttt{deck.slab}}(x_{\texttt{span}})}{2}$$

Area of the edge beam which is integrated into the the concrete deck

$$A_{\texttt{deck.beam}}(x_{\texttt{span}}) := h_{\texttt{deck.beam}}(x_{\texttt{span}}) \cdot b_{\texttt{deck.beam}}(x_{\texttt{span}})$$

Area of half the the concrete deck

$$A_{\texttt{deck}}(x_{\texttt{span}}) := A_{\texttt{deck.slab}}(x_{\texttt{span}}) + A_{\texttt{deck.beam}}(x_{\texttt{span}})$$

Total steel equivalent area of half the bridge cross-section. The concrete area is transformed into equivalent steel area by means of design values of the elastic modulus for the steel and concrete. Note that no regard is taken to the stiffness contribution from the reinforcement.

$$A_{\texttt{bridge.steel\_equivalent}}(x_{\texttt{span}}) := A_{\texttt{main.beam}}(x_{\texttt{span}}) + A_{\texttt{deck}}(x_{\texttt{span}}) \cdot \alpha_{\texttt{steel.concret}}$$

Surface area

The surface area of the bridge is of interest for calculation of the cost of painting the bridge. For this purpose only the estimated area of the exposed steel is of interest. Note that stainless steel does not require painting.

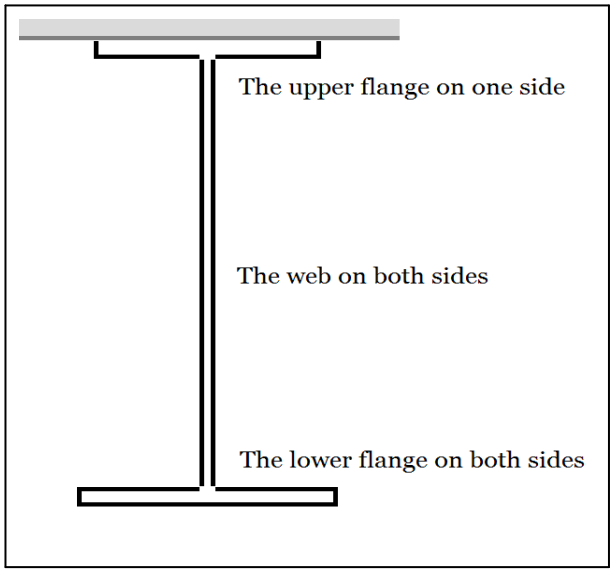

The perimeter of the main I-girder that requires painting.

The perimeter of the exposed surface of a main I-girder.

$$\text{Perimeter}_{\text{main.beam.exposed}}(x_{\text{span}}) := \left| \begin{array}{l} b_{\text{fl}} \leftarrow b_{\text{main.flange.lower}}(x_{\text{span}}) \\ h_{\text{w}} \leftarrow h_{\text{main.web}}(x_{\text{span}}) \\ b_{\text{fu}} \leftarrow b_{\text{main.flange.upper}}(x_{\text{span}}) \\ t_{\text{fl}} \leftarrow 2 \cdot t_{\text{main.flange.lower}}(x_{\text{span}}) \\ t_{\text{fu}} \leftarrow 2 \cdot t_{\text{main.flange.upper}}(x_{\text{span}}) \\ 2 \cdot b_{\text{fl}} + 2 \cdot h_{\text{w}} + b_{\text{fu}} + t_{\text{fl}} + t_{\text{fu}} \end{array} \right.$$

The total surface area of a main I-girder is calculated.

$$A_{\text{main.beam.steelsurface}} := \int_{0\text{m}}^{L_{\text{span}}} \text{Perimeter}_{\text{main.beam.exposed}}(x_{\text{span}})\, dx_{\text{span}}$$

$$A_{\text{main.beam.steelsurface}} = 153\,\text{m}^2$$

The total exposed steel area of the bridge. Note that this is only considering the main I-girders.

$$A_{\text{bridge.steelsurface}} := 2 \cdot A_{\text{main.beam.steelsurface}}$$

$$A_{\text{bridge.steelsurface}} = 307\,\text{m}^2$$

Mass of the cross-section

The mass of the cross-section is of interest when calculating the cost of the building materials. Note that only the stainless steel will be considered.

Mass of a main I-girder.

$$m_{main.beam} := \int_{0m}^{L_{span}} A_{main.beam}(x_{span}) \cdot \rho_{steel}\, dx_{span}$$

$$m_{main.beam} = 15.02 \cdot tonne$$

Total mass of the stainless steel in the bridge. Note that only the main I-girders are considered.

$$m_{bridge.steel} := 2 \cdot m_{main.beam}$$

$$m_{bridge.steel} = 30.04 \cdot tonne$$

Distance between parts

distance between the centre of the upper and lower flange of the main I-girders.

$$d_{main.flanges}(x_{span}) := \left| \begin{array}{l} t_{fl} \leftarrow t_{main.flange.lower}(x_{span}) \\ h_w \leftarrow h_{main.web}(x_{span}) \\ t_{fu} \leftarrow t_{main.flange.upper}(x_{span}) \\ t_{fl} + h_w + t_{fu} \end{array} \right.$$

Additional z-coordinates for the lower flange of the main I-girders

With regard to the z-axis; all z-coordinates is measured from the lowest part of the web at the support. positive direction is upward.

The measurement is noted with the index top, centre or bottom depending on the referrence point which is used.

z-coordinates for the lower flange of the main I-girders. Note that the top of the lower flange coincides with the bottom of the web of the main I-girders. Hence, this measurement is already defined for the web and will not be defined specially for the flange.

$$z_{bottom.main.flange.lower}(x_{span}) := z_{bottom.main.web}(x_{span}) - t_{main.flange.lower}(x_{span}$$

$$z_{centre.main.flange.lower}(x_{span}) := z_{bottom.main.web}(x_{span}) - \frac{t_{main.flange.lower}(x_{span}}{2}$$

Additional z-coordinate for the web of the main I-girders

z-coordinate for the centre of the web of the main I-girders.

$$z_{\texttt{centre.main.web}}(x_{\texttt{span}}) := \frac{z_{\texttt{top.main.web}}(x_{\texttt{span}}) + z_{\texttt{bottom.main.web}}(x_{\texttt{span}})}{2}$$

Additional z-coordinates for the upper flange of the main I-girders

z-coordinates for the upper flange of the main I-girders. Note that the bottom of the upper flange coincides with the top of the web of the main I-girders. Hence, this measurement is already defined for the web and will not be defined specially for the flange.

$$z_{\texttt{centre.main.flange.upper}}(x_{\texttt{span}}) := z_{\texttt{top.main.web}}(x_{\texttt{span}}) + \frac{t_{\texttt{main.flange.upper}}(x_{\texttt{spa}}}{2}$$

$$z_{\texttt{top.main.flange.upper}}(x_{\texttt{span}}) := z_{\texttt{top.main.web}}(x_{\texttt{span}}) + t_{\texttt{main.flange.upper}}(x_{\texttt{span}})$$

Additional z-coordinates for concrete slab and edge beam

z-coordinates for the concrete slab. Note that there are mid, edge and mean values included since the thickness of the slab varies in the transversal direction. The plate is thickest in the mid-section and varies linear towards the edge where it is thinnest. This may to a small degree affect the result if only the mean value is uesd for the calculation of second moment of area.

It is pressumed that the bottom part of the concrete slab is horizontal and coincides with the top of the upper flange of the main I-girders. Hence, this measurement is already defined for the upper flange and will not be defined specially for the concrete slab.

$$z_{\texttt{centre.deck.slab.mean}}(x_{\texttt{span}}) := z_{\texttt{top.main.flange.upper}}(x_{\texttt{span}}) + \frac{t_{\texttt{deck.slab.mean}}(x_{\texttt{span}}}{2}$$

$$z_{\texttt{top.deck.slab.mid}}(x_{\texttt{span}}) := z_{\texttt{top.main.flange.upper}}(x_{\texttt{span}}) + t_{\texttt{deck.slab.mid}}(x_{\texttt{span}})$$

$$z_{\texttt{top.deck.slab.edge}}(x_{\texttt{span}}) := z_{\texttt{top.main.flange.upper}}(x_{\texttt{span}}) + t_{\texttt{deck.slab.edge}}(x_{\texttt{spa}}$$

$$z_{\texttt{top.deck.slab.mean}}(x_{\texttt{span}}) := z_{\texttt{top.main.flange.upper}}(x_{\texttt{span}}) + t_{\texttt{deck.slab.mean}}(x_{\texttt{spa}}$$

z-coordinates for the edge beam. Note that the top of the edge beam coincides with the top of the edge part of the concrete slab. Hence, this measurement is already defined for the concrete slab and will not be defined specially for the edge beam.

$$z_{\texttt{bottom.deck.beam}}(x_{\texttt{span}}) := z_{\texttt{top.deck.slab.edge}}(x_{\texttt{span}}) - h_{\texttt{deck.beam}}(x_{\texttt{span}})$$

$$z_{\texttt{centre.deck.beam}}(x_{\texttt{span}}) := z_{\texttt{top.deck.slab.edge}}(x_{\texttt{span}}) - \frac{h_{\texttt{deck.beam}}(x_{\texttt{span}})}{2}$$

z-coordinate for the centre of the respective reinforcement layer. Note that it is assumed that the reinforcement in the edge beam is placed so that the centre falls in the middle of the beam.

$$z_{reinf.slab.lower}(x_{span}) := z_{top.main.flange.upper}(x_{span}) + d_{reinf.slab.lower}$$

$$z_{reinf.slab.upper}(x_{span}) := z_{top.deck.slab.mean}(x_{span}) - d_{reinf.slab.upper}$$

$$z_{reinf.slab.upper.uppermost}(x_{span}) := z_{top.deck.slab.mid}(x_{span}) - d_{reinf.slab.uppe}$$

$$z_{reinf.slab.upper.lowermost}(x_{span}) := z_{top.deck.slab.edge}(x_{span}) - d_{reinf.slab.upp}$$

$$z_{reinf.beam}(x_{span}) := z_{centre.deck.beam}(x_{span})$$

Height of the bridge

An average height of the bridge construction used in wind load calculations.

$$h_{bridge.wind} := \left| \begin{array}{l} z_{top}(x_{span}) \leftarrow z_{top.deck.slab.mid}(x_{span}) \\ z_{bottom}(x_{span}) \leftarrow z_{bottom.main.web}(x_{span}) \\ t_{fl}(x_{span}) \leftarrow t_{main.flange.lower}(x_{span}) \\ h_{bridge}(x_{span}) \leftarrow z_{top}(x_{span}) - z_{bottom}(x_{span}) + t_{fl}(x_{span}) \\ \dfrac{\displaystyle\int_{0m}^{L_{span}} h_{bridge}(x_{span})\, dx_{span}}{L_{span}} \end{array} \right.$$

$$h_{bridge.wind} = 1.39\,m$$

2.1.4 Cross-sectional classes for the main I-girders

For the composite cross-section it is given by Eurocode 1994-2: Paragraph 5.5.1-(1) that Eurocode 1993-1-1: Section 5.5.2 should be used to determine the cross-sectional classes. However, when the cross-section is made from stainless steel the cross-sectional classes should be taken in accordance with Eurocode 1993-1-4: Table 5.2 instead.

Note that it is only elements in compression that requires cross-sectional class. However, since the cross-section is subjected to both positive and negative moment all parts need to be classified.

The cross-section is assumed to be welded. However, no regard is taken to the thickness of the welds when determing the c-measurement of the parts. See Eurocode 1993-1-4: table 5.2 for the definition of the c-measurements.

According to Eurocode 1994-2: Paragraph 5.5.1-(3) a part that is restrained by the concrete deck may be taken as a more favourable class. This is only applicable if the performance has been proved. This is henceforth assumed to be the case for the upper flange of the main I-girders, which will be taken as class 3 for the composite section.

Cross-section class for the lower flange

The lower flange is considered as an outstand flange in compression. Classification for stainless steel is given by Eurocode 1993-1-4: Table 5.2. Classification for carbon steel is given by Eurocode 1993-1-1: Table 5.2. The limitation for cross-section class 1 is the same for stainless steel and carbon steel.
Note that Mathcad does not have any "elseif" statement, therefore a otherwise has to be used for carbon steel which is assumed when the steel grade is not stainless steel.
Here:
c is the unsupported length of the part
t is the thickness of the part
limiti is the limitation for obtaining the corresponding cross-section class.

$$\text{steeltype} = \text{"stainless"}$$

$$\text{crossclass}_{\text{main.flange.lower}}(x_{\text{span}}) := \left| \begin{array}{l} c \leftarrow \dfrac{b_{\text{main.flange.lower}}(x_{\text{span}})}{2} - t_{\text{main.web}}(x_{\text{spa}} \\ t \leftarrow t_{\text{main.flange.lower}}(x_{\text{span}}) \\ \text{steel} \leftarrow \text{steeltype} \\ \text{limit}_1 \leftarrow 9 \cdot \varepsilon_{\text{steel}} \\ \text{limit}_2 \leftarrow \left| \begin{array}{ll} 9.4 \cdot \varepsilon_{\text{steel}} & \text{if steel} = \text{"stainless"} \\ 10 \cdot \varepsilon_{\text{steel}} & \text{if steel} = \text{"carbon"} \end{array} \right. \\ \text{limit}_3 \leftarrow \left| \begin{array}{ll} 11 \cdot \varepsilon_{\text{steel}} & \text{if steel} = \text{"stainless"} \\ 14 \cdot \varepsilon_{\text{steel}} & \text{if steel} = \text{"carbon"} \end{array} \right. \\ 1 \quad \text{if } \dfrac{c}{t} \le \text{limit}_1 \\ 2 \quad \text{if } \text{limit}_1 < \dfrac{c}{t} \le \text{limit}_2 \\ 3 \quad \text{if } \text{limit}_2 < \dfrac{c}{t} \le \text{limit}_3 \\ 4 \quad \text{otherwise} \end{array} \right.$$

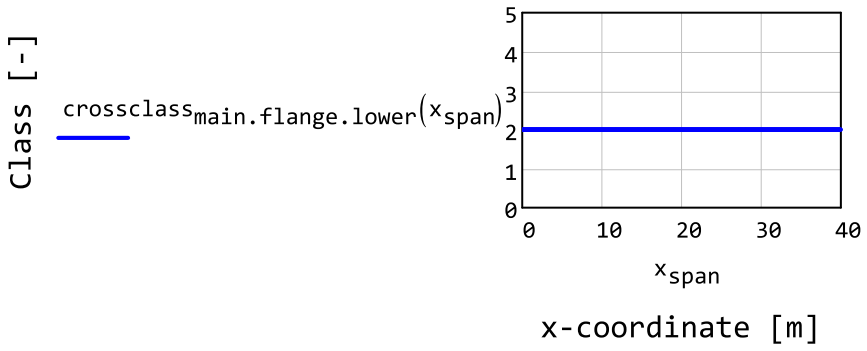

Buckling factor used for the web

Buckling factor for internal compression part with regard to ψ. Given by Eurocode 1993-1-5: table 4.1. The value of ψ is defined in said table as the smaller stress divided by the larger stress in the edges of the compression part. Note that here the larger stress is with regard to sign and a positive stress is therefore allways larger than a negative stress. Furthermore, the ψ is limited between 1 and -3.

$$k_{\sigma.internal}(\psi) := \begin{cases} 4 & \text{if } \psi > 1 \\ \frac{8.2}{1.05 + \psi} & \text{if } 1 \geq \psi > 0 \\ 7.81 - 6.29\psi + 9.78\psi^2 & \text{if } 0 \geq \psi > -1 \\ 5.98\,(1 - \psi)^2 & \text{if } -1 \geq \psi > -3 \\ \left(5.98 \times 4^2\right) & \text{if } \psi < -3 \end{cases}$$

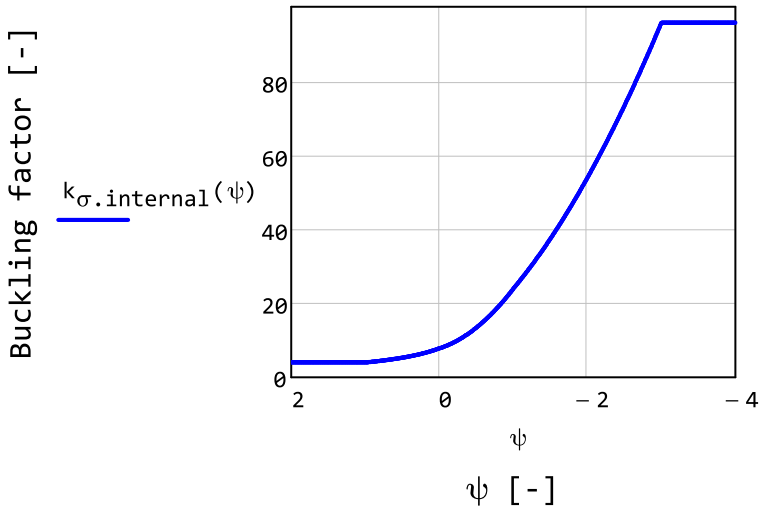

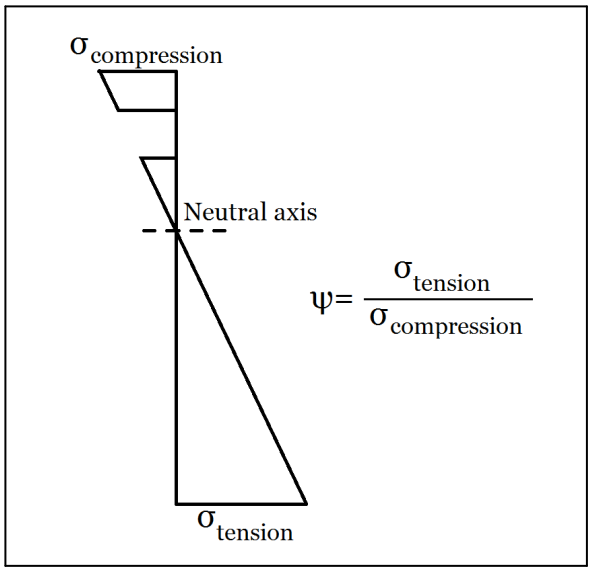

Illustration of how psi is calculated

The division between the largest compressive stress and the opposite, often tensile stress, in the web. The location of the buckle and the related compressive stress changes depending on the moment being positive and negative. therefore two formulas are given to simplfy calculations. Note that the value is negative when there are tensile stresses present in the web.

$$\psi_{web.positive}(x_{span}, z_{NA}) := \frac{z_{top.main.web}(x_{span}) - z_{NA}}{z_{bottom.main.web}(x_{span}) - z_{NA}}$$

$$\psi_{web.negative}(x_{span}, z_{NA}) := \frac{z_{NA} - z_{bottom.main.web}(x_{span})}{z_{NA} - z_{top.main.web}(x_{span})}$$

Cross-section class for the web in pure bending

Cross-sectional class for the web assuming pure bending is given purely as an indication of which cross-sectional the web is in. The web is assumed to be an internal compression part in pure bending. Classification for stainless steel is given by Eurocode 1993-1-4: Table 5.2.
Classification for carbon steel is given by Eurocode 1993-1-1: Table 5.2.
Note that Mathcad does not have any "elseif" statement, therefore a otherwise has to be used for carbon steel which is assumed when the steel grade is not stainless steel.
Here:
c is the unsupported length of the part, which is the height for the web.
t is the thickness of the part

$steeltype = "stainless"$

$$crossclass_{main.web.bending}(x_{span}) := \begin{array}{l} c \leftarrow h_{main.web}(x_{span}) \\ t \leftarrow t_{main.web}(x_{span}) \\ steel \leftarrow steeltype \\ limit_1 \leftarrow \begin{cases} 56 \cdot \varepsilon_{steel} & \text{if } steel = "stainless" \\ 72 \cdot \varepsilon_{steel} & \text{if } steel = "carbon" \end{cases} \\ limit_2 \leftarrow \begin{cases} 58.2 \cdot \varepsilon_{steel} & \text{if } steel = "stainless" \\ 83 \cdot \varepsilon_{steel} & \text{if } steel = "carbon" \end{cases} \\ limit_3 \leftarrow \begin{cases} 74.8 \cdot \varepsilon_{steel} & \text{if } steel = "stainless" \\ 124 \cdot \varepsilon_{steel} & \text{if } steel = "carbon" \end{cases} \\ 1 \quad \text{if } \frac{c}{t} \le limit_1 \\ 2 \quad \text{if } limit_1 < \frac{c}{t} \le limit_2 \\ 3 \quad \text{if } limit_2 < \frac{c}{t} \le limit_3 \\ 4 \quad \text{otherwise} \end{array}$$

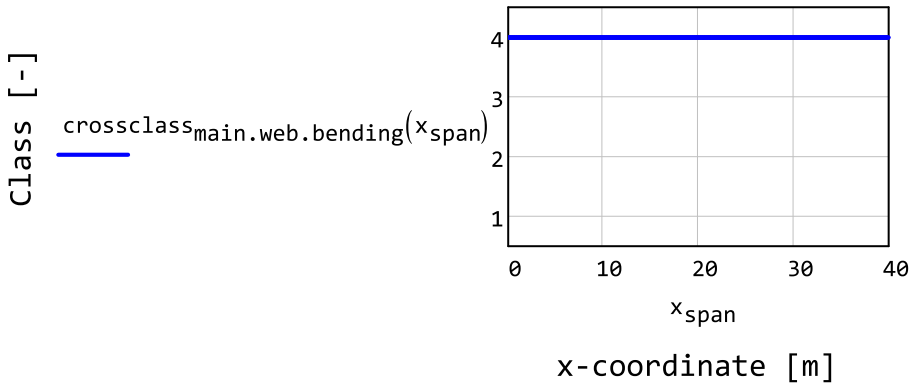

Cross-section class for the web, general

Cross-sectional class for the web given the location of the plastic neutral axis and the elastic neutral axis. The location of the plastic neutral axis in relation to the web is needed and taken into account by the α value. In a similar way the location of the elastic neutral axis is taken into account by a ψ value. The web is then assumed to be an internal compression part in both bending and compression. Classification for stainless steel is given by Eurocode 1993-1-4: Table 5.2. Classification for stainless steel is given by Eurocode 1993-1-1: Table 5.2.
Here:
c is the unsupported length of the part
t is the thickness of the part
k_σ is the buckling factor of the part

Cross-sectional class if the cross-section is made from stainless steel

$$\text{crossclass}_{\text{main.web.stainless}}(x_{span}, \alpha, \psi) := \begin{cases} c \leftarrow h_{main.web}(x_{span}) \\ t \leftarrow t_{main.web}(x_{span}) \\ k_\sigma \leftarrow k_{\sigma.internal}(\psi) \\ 1 \quad \text{if} \quad \begin{cases} \frac{c}{t} \le \frac{308 \cdot \varepsilon_{steel}}{13 \cdot \alpha - 1} & \text{if } \alpha > 0.5 \\ \frac{c}{t} \le \frac{28 \cdot \varepsilon_{steel}}{\alpha} & \text{otherwise} \end{cases} \\ 2 \quad \text{if} \quad \begin{cases} \frac{c}{t} \le \frac{320 \cdot \varepsilon_{steel}}{13 \cdot \alpha - 1} & \text{if } \alpha > 0.5 \\ \frac{c}{t} \le \frac{29.1 \cdot \varepsilon_{steel}}{\alpha} & \text{otherwise} \end{cases} \\ 3 \quad \text{if} \quad \frac{c}{t} \le 15.3 \cdot \varepsilon_{steel} \cdot \sqrt{k_\sigma} \\ 4 \quad \text{otherwise} \end{cases}$$

Cross-sectional class if the cross-section is made from carbon steel

$$\text{crossclass}_{\text{main.web.carbon}}(x_{\text{span}}, \alpha, \psi) := \left| \begin{array}{l} c \leftarrow h_{\text{main.web}}(x_{\text{span}}) \\ t \leftarrow t_{\text{main.web}}(x_{\text{span}}) \\ k_\sigma \leftarrow k_{\sigma.\text{internal}}(\psi) \\ 1 \quad \text{if} \quad \left| \begin{array}{ll} \frac{c}{t} \le \frac{396 \cdot \varepsilon_{\text{steel}}}{13 \cdot \alpha - 1} & \text{if } \alpha > 0.5 \\ \frac{c}{t} \le \frac{36 \cdot \varepsilon_{\text{steel}}}{\alpha} & \text{otherwise} \end{array} \right. \\ 2 \quad \text{if} \quad \left| \begin{array}{ll} \frac{c}{t} \le \frac{456 \cdot \varepsilon_{\text{steel}}}{13 \cdot \alpha - 1} & \text{if } \alpha > 0.5 \\ \frac{c}{t} \le \frac{41.5 \cdot \varepsilon_{\text{steel}}}{\alpha} & \text{otherwise} \end{array} \right. \\ 3 \quad \text{if} \quad \left| \begin{array}{ll} \frac{c}{t} \le \frac{42 \cdot \varepsilon_{\text{steel}}}{0.67 + 0.33 \cdot \psi} & \text{if } \psi > -1 \\ \frac{c}{t} \le 62 \cdot \varepsilon_{\text{steel}} \cdot (1 - \psi) \cdot \sqrt{-\psi} & \text{if } \psi \le -1 \end{array} \right. \\ 4 \quad \text{otherwise} \end{array} \right.$$

The cross-sectional class is taken for the appropriate material which is either stainless steel or carbon steel.

$$\text{steeltype} = \text{"stainless"}$$

$$\text{crossclass}_{\text{main.web}}(x_{\text{span}}, \alpha, \psi) := \left| \begin{array}{l} A \leftarrow \text{crossclass}_{\text{main.web.stainless}}(x_{\text{span}}, \alpha, \psi) \\ B \leftarrow \text{crossclass}_{\text{main.web.carbon}}(x_{\text{span}}, \alpha, \psi) \\ A \quad \text{if steeltype} = \text{"stainless"} \\ B \quad \text{if steeltype} = \text{"carbon"} \end{array} \right.$$

Cross-section class for the web, class 3 or 4

Reduced check of the cross-sectional class where it only is of interest if the web is in class 3 or 4.

$$\text{crossclass}_{\text{main.web.34}}(x_{\text{span}}, \psi) := \begin{bmatrix} c \leftarrow h_{\text{main.web}}(x_{\text{span}}) \\ t \leftarrow t_{\text{main.web}}(x_{\text{span}}) \\ k_\sigma \leftarrow k_{\sigma.\text{internal}}(\psi) \\ \text{limit}_s \leftarrow 15.3 \cdot \varepsilon_{\text{steel}} \cdot \sqrt{k_\sigma} \\ \text{limit}_c \leftarrow \begin{bmatrix} \frac{42 \cdot \varepsilon_{\text{steel}}}{0.67 + 0.33 \cdot \psi} & \text{if } \psi > -1 \\ \left[62 \cdot \varepsilon_{\text{steel}} \cdot (1 - \psi) \cdot \sqrt{-\psi}\right] & \text{if } \psi \le -1 \end{bmatrix} \\ 3 \quad \text{if} \begin{bmatrix} \frac{c}{t} \le \text{limit}_s & \text{if steeltype} = \text{"stainless"} \\ \frac{c}{t} \le \text{limit}_c & \text{if steeltype} = \text{"carbon"} \end{bmatrix} \\ 4 \quad \text{otherwise} \end{bmatrix}$$

Cross-section class for the upper flange

The upper flange is considered as an outstand flange in compression. Classification for stainless steel is given by Eurocode 1993-1-4: Table 5.2. Classification for carbon steel is given by Eurocode 1993-1-1: Table 5.2. The limitation for cross-section class 1 is the same for stainless steel and carbon steel.
Note that Mathcad does not have any "elseif" statement, therefore a otherwise has to be used for carbon steel which is assumed when the steel grade is not stainless steel.
Here:
c is the unsupported length of the part
t is the thickness of the part
limiti is the limitation for obtaining the corresponding cross-section class.

$$\text{steeltype} = \text{"stainless"}$$

$$\text{crossclass}_{\text{main.flange.upper}}(x_{\text{span}}) := \left| \begin{array}{l} c \leftarrow \dfrac{b_{\text{main.flange.upper}}(x_{\text{span}})}{2} - t_{\text{main.web}}(x_{\text{spa}} \\ t \leftarrow t_{\text{main.flange.upper}}(x_{\text{span}}) \\ \text{steel} \leftarrow \text{steeltype} \\ \text{limit}_1 \leftarrow 9 \cdot \varepsilon_{\text{steel}} \\ \text{limit}_2 \leftarrow \left| \begin{array}{ll} 9.4 \cdot \varepsilon_{\text{steel}} & \text{if steel} = \text{"stainless"} \\ 10 \cdot \varepsilon_{\text{steel}} & \text{if steel} = \text{"carbon"} \end{array} \right. \\ \text{limit}_3 \leftarrow \left| \begin{array}{ll} 11 \cdot \varepsilon_{\text{steel}} & \text{if steel} = \text{"stainless"} \\ 14 \cdot \varepsilon_{\text{steel}} & \text{if steel} = \text{"carbon"} \end{array} \right. \\ 1 \quad \text{if } \dfrac{c}{t} \le \text{limit}_1 \\ 2 \quad \text{if } \text{limit}_1 < \dfrac{c}{t} \le \text{limit}_2 \\ 3 \quad \text{if } \text{limit}_2 < \dfrac{c}{t} \le \text{limit}_3 \\ 4 \quad \text{otherwise} \end{array} \right.$$

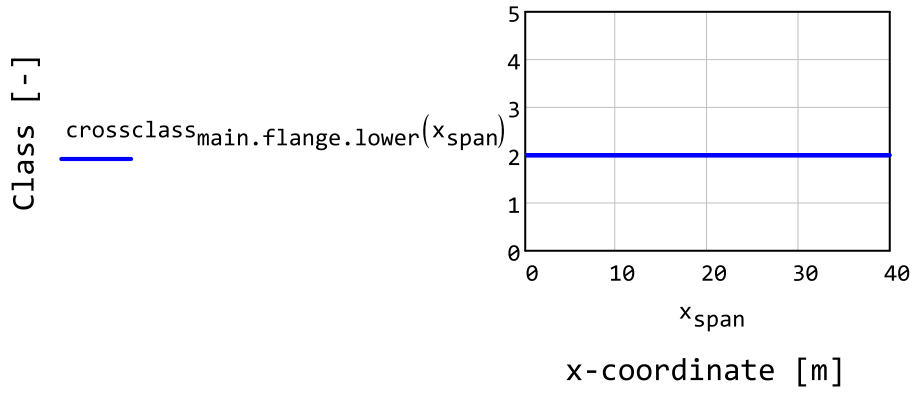

2.1.5 Reduction factors for parts in the main I-girders

The cross-section is reduced with regard to plate buckling.

Reduction factor for the lower flange when in class 4

Reduction factor due to plate buckling of the lower flange when it is in cross-section class 4. The flange is considered a welded outstand element and the reduction factor is given by Eurocode 1993-1-4: paragraph 5.2.3-(1) for stainless steel and Eurocode 1993-1-5: paragraph 4.4-(2) for carbon steel.
The buckling factor k_σ is obtained from Eurocode 1993-1-5: Table 4.2 for outstand compresion element with constant compressive stress over the element.
Note that the reduction factor is set to 1 if the flange is not in cross-section class 4. This is done so that the reduction factor may be applied in all calculations without checking the cross-section class.

Here
crossclass is the cross-sectional class of the flange
c is the unsupported width of the oustand flange
t is thickness of the outstand flange
k_σ is the buckling factor for the outstand flange. Dependent on the stress distribution
ρ is the reduction factor. The value of the reduction factor must not exceed 1.0

$$\rho_{main.flange.lower}(x_{span}) := \left| \begin{array}{l} crossclass \leftarrow crossclass_{main.flange.lower}(x_{span}) \\ c \leftarrow \dfrac{b_{main.flange.lower}(x_{span}) - t_{main.web}(x_{span})}{2} \\ t \leftarrow t_{main.flange.lower}(x_{span}) \\ k_\sigma \leftarrow 0.43 \\ \lambda_p \leftarrow \dfrac{\frac{c}{t}}{28.4 \cdot \varepsilon_{steel} \cdot \sqrt{k_\sigma}} \\ \rho \leftarrow \left| \begin{array}{ll} \dfrac{1}{\lambda_p} - \dfrac{0.242}{\lambda_p^{\,2}} & \text{if steeltype} = \text{"stainless"} \\ \dfrac{\lambda_p - 0.188}{\lambda_p^{\,2}} & \text{if steeltype} = \text{"carbon"} \end{array} \right. \\ \min(\rho, 1.0) \quad \text{if crossclass} = 4 \\ 1.0 \quad \text{otherwise} \end{array} \right.$$

Reduction factor for the web when in class 4

Reduction factor due to plate buckling of the web when it is in cross-section class 4. The web is considered a welded internal element and the reduction factor is given by Eurocode 1993-1-4: paragraph 5.2.3-(1) for stainless steel and Eurocode 1993-1-5: paragraph 4.4-(2).
Note that the reduction factor is set to 1 if the web is not in cross-section class 4. This is done so that the reduction factor may be applied in all calculations without checking the cross-section class. Furthermore, the reduction factor is dependent on the plate buckling factor which in turn depends on the stress distribution in the web. Therefore the function have the ψ as an additional input.

Assumption for carbon steel:

$\psi > -3$

$$\rho_{main.web}(x_{span},\psi) := \left|\begin{array}{l} b \leftarrow h_{main.web}(x_{span}) \\ t \leftarrow t_{main.web}(x_{span}) \\ k_\sigma \leftarrow k_{\sigma.internal}(\psi) \\ crossclass \leftarrow crossclass_{main.web.34}(x_{span},\psi) \\ \lambda_p \leftarrow \dfrac{\frac{b}{t}}{28.4\cdot\varepsilon_{steel}\cdot\sqrt{k_{\sigma.internal}(\psi)}} \\ \rho \leftarrow \left|\begin{array}{ll} \left(\dfrac{0.772}{\lambda_p}-\dfrac{0.125}{\lambda_p^{\,2}}\right) & \text{if } steeltype = "stainless" \\ \dfrac{\lambda_p - 0.055\cdot(3+\psi)}{\lambda_p} & \text{if } steeltype = "carbon" \end{array}\right. \\ \min(\rho, 1.0) \quad \text{if } crossclass = 4 \\ 1.0 \quad \text{otherwise} \end{array}\right.$$

Reduction factor for the upper flange when in class 4

Reduction factor due to plate buckling of the upper flange when it is in cross-section class 4. The flange is considered a welded outstand element and the reduction factor is given by Eurocode 1993-1-4: paragraph 5.2.3-(1) for stainless steel and Eurocode 1993-1-5: paragraph 4.4-(2) for carbon steel.
The buckling factor k_σ is obtained from Eurocode 1993-1-5: Table 4.2 for outstand compresion element with constant compressive stress over the element.
Note that the reduction factor is set to 1 if the flange is not in cross-section class 4. This is done so that the reduction factor may be applied in all calculations without checking the cross-section class.
Here
crossclass is the cross-sectional class of the flange
c is the unsupported width of the oustand flange
t is thickness of the outstand flange
k_σ is the buckling factor for the outstand flange. Dependent on the stress distribution
ρ is the reduction factor. The value of the reduction factor must not exceed 1.0

$$\rho_{main.flange.upper}(x_{span}) := \left| \begin{array}{l} crossclass \leftarrow crossclass_{main.flange.upper}(x_{span}) \\ c \leftarrow \dfrac{b_{main.flange.upper}(x_{span}) - t_{main.web}(x_{span})}{2} \\ t \leftarrow t_{main.flange.upper}(x_{span}) \\ k_\sigma \leftarrow 0.43 \\ \lambda_p \leftarrow \dfrac{\frac{c}{t}}{28.4 \cdot \varepsilon_{steel} \cdot \sqrt{k_\sigma}} \\ \rho \leftarrow \left| \begin{array}{ll} \left(\dfrac{1}{\lambda_p} - \dfrac{0.242}{\lambda_p^{\,2}}\right) & \text{if steeltype} = \text{"stainless"} \\ \dfrac{\lambda_p - 0.188}{\lambda_p^{\,2}} & \text{if steeltype} = \text{"carbon"} \end{array} \right. \\ \min(\rho, 1.0) \quad \text{if crossclass} = 4 \\ 1.0 \quad \text{otherwise} \end{array} \right.$$

2.1.6 Measurements for the effective composite cross-section

For more accurate calculations the effective width of the cross-section should be considered in both the serviceability limit state and the ultimate limit state. For composite cross-sections the effective cross-section is given by Eurocode 1994-2: Section 5.4.1.2 for both calculations in the ultimate limit state and serviceability limit state. For more detail see Eurocode 1994-2: paragraph 7.2.1-(2) and paragraph 6.1.2-(1).

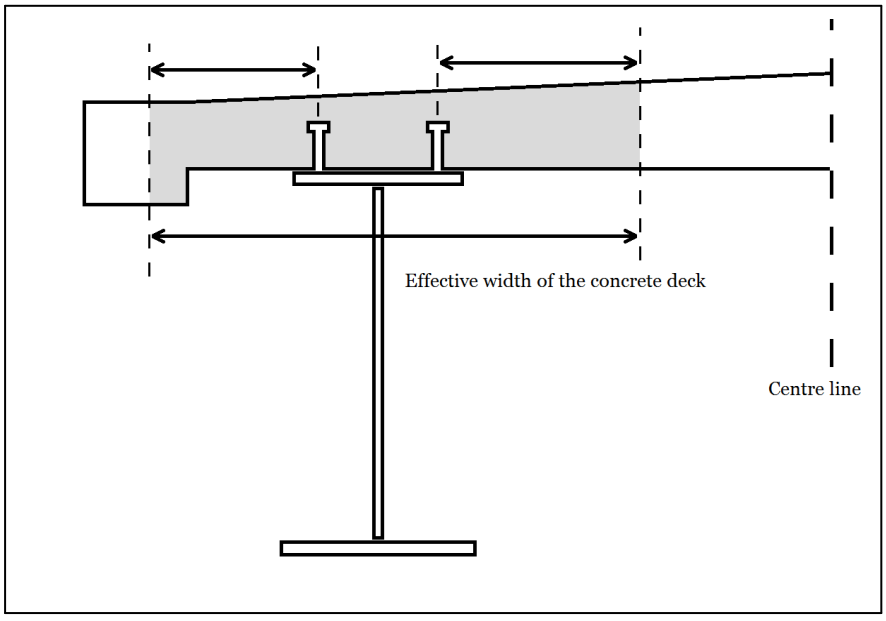

Illustration of how the effective width of the composite cross-section is measured. Note that it is assumed that the width of the main I-girders is never reduced. The effective width of the concrete is measured from the most outstand shear connectors.

Effective width of the steel

Effective width of the steel in global analysis is assumed to be unreduced. However, this should not be confused with the local buckling that is taken into account through special reduction factors for parts in cross-sectional class 4. The check is based of conservative simplification of the rules given by Eurocode 1993-1-5: Paragraph 2.2-(2) and 2.2-(3). This assumption is made to simplify the calculations since the assumption should remain true for almost any choice of bridge span.

$$\text{assumption}_{\text{steel\_unreduced}} := \begin{cases} \text{"true"} & \text{if } b_{\text{main.flange.lower}}\left(\frac{L_{\text{span}}}{2}\right) < \frac{L_{\text{span}}}{4} \\ \text{"false"} & \text{otherwise} \end{cases}$$

$$\text{assumption}_{\text{steel\_unreduced}} = \text{"true"}$$

Effective width of the concrete slab

The effective width of the concrete deck. In accordance with Eurocode 1994-2: Paragraph 5.4.1.2-(4) the effective witdh is constant over the entire span length. Since the bridge has fix supports the value of the effective width is taken at middle of the span. The effective width is given by Eurocode 1994-2: Paragraph 5.4.1.2-(5).

$$b_{\text{deck.slab.effective}} := \left| \begin{array}{l} b_0 \leftarrow \min\left(b_{\text{shearconnectors}}, b_{\text{main.flange.upper.mid}} - 50\text{mm}\right. \\ b_e \leftarrow \frac{L_{\text{effective}}}{8} \\ b_{\text{inner.limit}} \leftarrow \frac{cc_{\text{maingirders}} - b_0}{2} \\ b_{\text{outer.limit}} \leftarrow \frac{b_{\text{deck.slab}}\left(\frac{L_{\text{span}}}{2}\right) - cc_{\text{maingirders}} - b_0}{2} \\ b_{\text{inner}} \leftarrow \min\left(b_e, b_{\text{inner.limit}}\right) \\ b_{\text{outer}} \leftarrow \min\left(b_e, b_{\text{outer.limit}}\right) \\ b_{\text{inner}} + b_0 + b_{\text{outer}} \end{array} \right.$$

$$b_{\text{deck.slab.effective}} = 3.45\,\text{m}$$

Comparison with the unreduced width of the concrete slab. Note that the effective width is tied to the main I-girders, thus limiting it to half of the entire width.

$$\frac{b_{\text{deck.slab}}\left(\frac{L_{\text{span}}}{2}\right)}{2} = 3.45\,\text{m}$$

Thickness for the effective width of the concrete slab

Thickness of the slab towards the centre of the bridge for the effective width of composite cross-section.

$$t_{deck.slab.effective.inner} := \left| \begin{array}{l} b_0 \leftarrow b_{shearconnectors} \\ b_e \leftarrow \frac{L_{effective}}{8} \\ b_{inner.limit} \leftarrow \frac{cc_{maingirders} - b_0}{2} \\ b_{inner} \leftarrow \min\left(b_e, b_{inner.limit}\right) \\ y_{inner} \leftarrow b_{inner.limit} - b_{inner} \\ t_{deck.slab}\left(\frac{L_{span}}{2}, y_{inner}\right) \end{array} \right.$$

$$t_{deck.slab.effective.inner} = 0.26\,m$$

Thickness of the slab towards the edge of the bridge for the effective width of composite cross-section.

$$t_{deck.slab.effective.outer} := \left| \begin{array}{l} b_0 \leftarrow b_{shearconnectors} \\ b_e \leftarrow \frac{L_{effective}}{8} \\ b_{inner.limit} \leftarrow \frac{cc_{maingirders} - b_0}{2} \\ b_{outer.limit} \leftarrow \frac{b_{deck.slab}\left(\frac{L_{span}}{2}\right) - cc_{maingirders} - b_0}{2} \\ b_{outer} \leftarrow \min\left(b_e, b_{outer.limit}\right) \\ y_{outer} \leftarrow b_{inner.limit} + b_0 + b_{outer} \\ t_{deck.slab}\left(\frac{L_{span}}{2}, y_{outer}\right) \end{array} \right.$$

$$t_{deck.slab.effective.outer} = 0.17\,m$$

Mean thickness of the slab for the effective width of composite cross-section.

$$t_{deck.slab.effective.mean} := \left| \begin{array}{l} b_0 \leftarrow b_{shearconnectors} \\ b_e \leftarrow \frac{L_{effective}}{8} \\ b_{inner.limit} \leftarrow \frac{cc_{maingirders} - b_0}{2} \\ b_{outer.limit} \leftarrow \frac{b_{deck.slab}\left(\frac{L_{span}}{2}\right) - cc_{maingirders} - b_0}{2} \\ b_{inner} \leftarrow \min\left(b_e, b_{inner.limit}\right) \\ b_{outer} \leftarrow \min\left(b_e, b_{outer.limit}\right) \\ y_{inner} \leftarrow b_{inner.limit} - b_{inner} \\ y_{outer} \leftarrow b_{inner.limit} + b_0 + b_{outer} \\ \frac{t_{deck.slab}\left(\frac{L_{span}}{2}, y_{inner}\right) + t_{deck.slab}\left(\frac{L_{span}}{2}, y_{outer}\right)}{2} \end{array} \right.$$

$$t_{deck.slab.effective.mean} = 0.21\,m$$

Comparison with the mean thickness of the unreduced slab of the concrete deck.

$$t_{deck.slab.mean}\left(\frac{L_{span}}{2}\right) = 0.21\,m$$

Difference in thickness of the slab for the effective width of composite cross-section. Used to take into account the slope in transversal direction of the concrete slab.

$$t_{deck.slab.effective.diff} := t_{deck.slab.effective.inner} - t_{deck.slab.effective.outer}$$

$$t_{deck.slab.effective.diff} = 0.09\,m$$

Area for the effective width of the concrete slab

Effective area of the compostite cross-section

$$A_{deck.slab.effective} := b_{deck.slab.effective} \cdot t_{deck.slab.effective.mean}$$

$$A_{deck.slab.effective} = 0.74\,m^2$$

Effective area of the compostite cross-section, the lower square formed area

$$A_{deck.slab.effective.square} := b_{deck.slab.effective} \cdot t_{deck.slab.effective.outer}$$

$$A_{deck.slab.effective.square} = 0.59\,m^2$$

Effective area of the compostite cross-section, the upper triangle formed area

$$A_{deck.slab.effective.triangle} := \frac{b_{deck.slab.effective} \cdot t_{deck.slab.effective.diff}}{2}$$

$$A_{deck.slab.effective.triangle} = 0.15\,m^2$$

Comparison with the unreduced area of the concrete deck

$$A_{deck.slab}\left(\frac{L_{span}}{2}\right) = 0.74\,m^2$$

Effective width and area of the edge beam

Effective width of the edge beam of the concrete deck.

$$b_{deck.beam.effective} := \left| \begin{array}{l} b_0 \leftarrow b_{shearconnectors} \\ b_e \leftarrow \frac{L_{effective}}{8} \\ b_{min} \leftarrow \frac{b_{deck.slab}\left(\frac{L_{span}}{2}\right) - cc_{maingirders} - b_0}{2} \\ b_{max} \leftarrow \frac{b_{deck}\left(\frac{L_{span}}{2}\right) - cc_{maingirders} - b_0}{2} \\ b_e - b_{min} \quad \text{if } b_{min} < b_e < b_{max} \\ b_{deck.beam}\left(\frac{L_{span}}{2}\right) \quad \text{if } b_e > b_{max} \\ 0m^2 \quad \text{otherwise} \end{array} \right.$$

$$b_{deck.beam.effective} = 0.4\,m$$

Comparison with the unreduced width of the edge beam

$$b_{deck.beam}\left(\frac{L_{span}}{2}\right) = 0.4\,m$$

Effective area of the edge beam.

$$A_{deck.beam.effective} := b_{deck.beam.effective} \cdot h_{deck.beam}\left(\frac{L_{span}}{2}\right)$$

$$A_{deck.beam.effective} = 0.16\,m^2$$

Comparison with the unreduced area of the edge beam.

$$A_{deck.beam}\left(\frac{L_{span}}{2}\right) = 0.16\,m^2$$

Effective width and area of the concrete deck

Effective area of half of the concrete deck.

$$A_{deck.effective} := A_{deck.slab.effective} + A_{deck.beam.effective}$$

$$A_{deck.effective} = 0.9\,m^2$$

Comparison with the unreduced area of half of the concrete deck

$$A_{deck}\left(\frac{L_{span}}{2}\right) = 0.9\,m^2$$

Total steel equivalent area of half the effective composite cross-section. The concrete area is transformed into equivalent steel area by means of design values of the elastic modulus. Note that no regard is taken to the stiffness contribution from the reinforcement.

$$A_{composite.effective}(x_{span}) := A_{main.beam}(x_{span}) + A_{deck.effective} \cdot \alpha_{steel.concrete}$$

Area of the square part of the concrete slab of the effective cross-section.

$$A_{deck.slab.effective.sqr} := b_{deck.slab.effective} \cdot t_{deck.slab.effective.outer}$$

Area of the triangular part of the concrete slab of the effective cross-section.

$$A_{deck.slab.effective.tri} := \frac{b_{deck.slab.effective} \cdot t_{deck.slab.effective.diff}}{2}$$

z-coordinate for the centroid of the square part of the concrete slab of the effective cross-section.

$$z_{centre.deck.slab.effective.sqr}(x_{span}) := \left| \begin{array}{l} z \leftarrow z_{top.main.flange.upper}(x_{span}) \\ t \leftarrow \dfrac{t_{deck.slab.effective.outer}}{2} \\ z + t \end{array} \right.$$

z-coordinate for the centroid of the square part of the concrete slab of the effective cross-section. Note that for a right triangle the centroid is located one third of the height from the bottom.

$$z_{centre.deck.slab.effective.tri}(x_{span}) := \left| \begin{array}{l} z \leftarrow z_{top.main.flange.upper}(x_{span}) \\ t_0 \leftarrow t_{deck.slab.effective.outer} \\ t_1 \leftarrow \frac{t_{deck.slab.effective.diff}}{3} \\ z + t_0 + t_1 \end{array} \right.$$

Miscellaneous

height of the buckle in the web. Note that the buckle in the web occurs below respectively above the neutral axis if the moment is positive or negative. Calculation of the height of the buckle is therefore different if the cross-section is in positive or negative bending.

$$b_{buckle.negative}(x_{span}, z_{NA}) := \left| \begin{array}{l} \psi \leftarrow \psi_{web.negative}(x_{span}, z_{NA}) \\ b_{compression} \leftarrow z_{top.main.web}(x_{span}) - z_{NA} \\ b_{compression} \cdot (1 - \rho_{main.web}(x_{span}, \psi)) \end{array} \right.$$

$$b_{buckle.positive}(x_{span}, z_{NA}) := \left| \begin{array}{l} \psi \leftarrow \psi_{web.negative}(x_{span}, z_{NA}) \\ b_{compression} \leftarrow z_{NA} - z_{bottom.main.web}(x_{span}) \\ b_{compression} \cdot (1 - \rho_{main.web}(x_{span}, \psi)) \end{array} \right.$$

z-location of the of the centre of the buckle in the web. Note that the buckle in the web occurs below respectively above the neutral axis if the moment is positive or negative. Calculation of the location of the buckle is therefore different if the cross-section is in positive or negative bending.

$$z_{buckle.negative}(x_{span}, z_{NA}) := \left| \begin{array}{l} b \leftarrow b_{buckle.negative}(x_{span}, z_{NA}) \\ z_{upper} \leftarrow z_{top.main.web}(x_{span}) - 0.4 \cdot b \\ z_{lower} \leftarrow z_{NA} + 0.6 \cdot b \\ \frac{z_{lower} + z_{upper}}{2} \end{array} \right.$$

$$z_{buckle.positive}(x_{span}, z_{NA}) := \left| \begin{array}{l} b \leftarrow b_{buckle.positive}(x_{span}, z_{NA}) \\ z_{upper} \leftarrow z_{NA} - 0.6 \cdot b \\ z_{lower} \leftarrow z_{bottom.main.web}(x_{span}) + 0.4 \cdot b \\ \frac{z_{lower} + z_{upper}}{2} \end{array} \right.$$

2.1.7 Second moment of area for the composite cross-section

Calculation of the second moment of area for the composite cross section. Here is taken into account the resistance in both positive and negative bending.

Location of the neutral axis of the effective composite cross-section in negative bending

Location of the neutral axis for the effective composite cross-section subjected to negative moment. For negative moment the concrete deck is in compression, thus concrete is considered but the stiffness contribution from the reinforcement is neglected. The concrete area is transformed into equivalent steel area with regard to the difference in modulus of elasticity. Note that the concrete slab is calculated in two parts due to the variation in thickness in the transversal direction.
Since the web may buckle the calculation is performed in two steps. first the centre of the equivalent steel area is located for the cross-section without reducing for buckling of the web. Secondly the web buckle is calculated with the gravity centre that was obtained in the first step. Finally the buckle is included in the cross-section as an negative contribution and the location of the neutral axis may be calculated.
Note that the upper flange is not reduced due to buckling since it is stabilised by the concrete deck with composite action.
Here:
$\rho_{fl/fu}$ buckling reduction of the lower and upper flange respectively.
z_i is the global z-coordinate for the centre of each part
A_i is the area of each part. Here is also taken into account the stiffness difference.
z_{gc} is the centre of gravity for the equivalent steel area
b_{buckle} is the height of the buckle in the web
and
$\alpha_{steel.concrete}$ is the factor taking into account the difference in stiffness for concrete and steel
legend
0 - lower flange of the main I-girders
1 - web of the main I-girders
2 - upper flange of the main I-girders
3 - lower square of concrete slab
4 - upper triangle of concrete slab
5 - edge beam of the concrete deck
6 - buckle in the web (negative contribution)

$$z_{NA.composite.negative}(x_{span}) :=$$

$$\rho_{fl} \leftarrow \rho_{main.flange.lower}(x_{span})$$

$$\rho_{fu} \leftarrow 1$$

$$z_0 \leftarrow z_{centre.main.flange.lower}(x_{span})$$

$$z_1 \leftarrow z_{centre.main.web}(x_{span})$$

$$z_2 \leftarrow z_{centre.main.flange.upper}(x_{span})$$

$$z_3 \leftarrow z_{centre.deck.slab.effective.sqr}(x_{span})$$

$$z_4 \leftarrow z_{centre.deck.slab.effective.tri}(x_{span})$$

$$z_5 \leftarrow z_{centre.deck.beam}(x_{span})$$

$$A_0 \leftarrow A_{main.flange.lower}(x_{span}) \cdot \rho_{fl}$$

$$A_1 \leftarrow A_{main.web}(x_{span})$$

$$A_2 \leftarrow A_{main.flange.upper}(x_{span}) \cdot \rho_{fu}$$

$$A_3 \leftarrow A_{deck.slab.effective.sqr} \cdot \alpha_{steel.concrete}$$

$$A_4 \leftarrow A_{deck.slab.effective.tri} \cdot \alpha_{steel.concrete}$$

$$A_5 \leftarrow A_{deck.beam.effective} \cdot \alpha_{steel.concrete}$$

$$z_{gc} \leftarrow \frac{\sum_{i=0}^{5} (A_i \cdot z_i)}{\sum_{j=0}^{5} A_j}$$

$$b_{buckle} \leftarrow b_{buckle.negative}(x_{span}, z_{gc})$$

$$A_6 \leftarrow -(b_{buckle} \cdot t_{main.web}(x_{span}))$$

$$z_6 \leftarrow z_{buckle.negative}(x_{span}, z_{gc})$$

$$\frac{\sum_{i=0}^{6} (A_i \cdot z_i)}{\sum_{j=0}^{6} A_j}$$

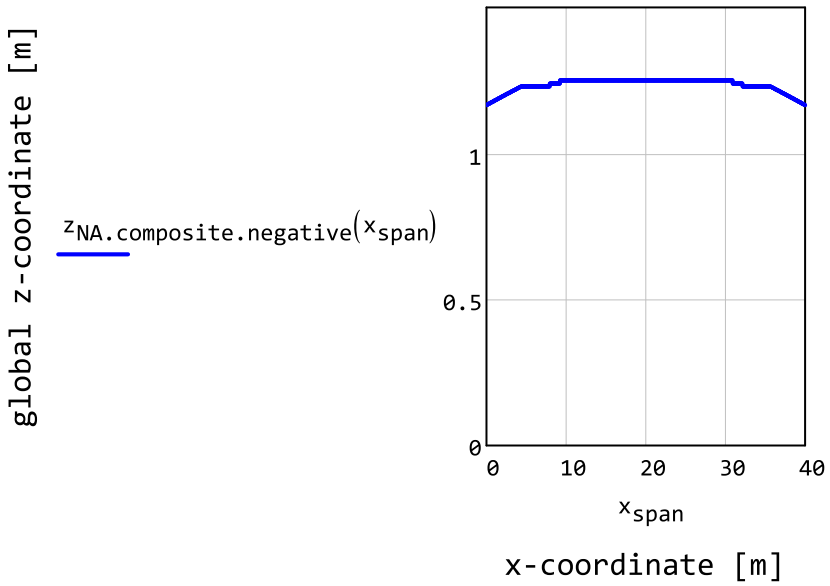

Function for obtaining the local z-coordinate for the effective composite cross-section. The local z-axis begins at the neutral axis of the cross-section, with postitive direction upwards. The input is the z-coordinate in the global coordinate system and the location in x-direction. The x-coordinate is needed due to small variations of the location of the neutral axis along the span.

$$z_{composite.negative}(x_{span}, z_{bridge}) := z_{bridge} - z_{NA.composite.negative}(x_{span})$$

Second moment of area of the effective composite cross-section in negative bending

Second moment of area for half of the effective composite cross-section subjected to negative moment. For negative moment the concrete deck is in compression, thus concrete is considered but the stiffness contribution from the reinforcement is neglected. The concrete area is transformed into equivalent steel area with regard to the difference in modulus of elasticity.
Note that the concrete slab is calculated in two parts due to the variation in thickness in the transversal direction. The triangular part has to be calculated differently due to the nature of calculations of the second moment of area.
Note that the upper flange is not reduced due to buckling since it is stabilised by the concrete deck with composite action. Furthermore, note that the web buckle is included in the cross-section as an negative contribution to the second moment of area.
Here:
z_{NA} is the z-coordinate for the equivalent steel area
$\rho_{fl/fu}$ buckling reduction of the lower and upper flange respectively
z_i is the local z-coordinate for the centroid of each part
h_i is the height of each part, z-direction
b_i is the width of each part, y-direction. Includes reductions and difference in stiffness.
and
z_{local} yields the local z-coordinates given any global z-coordinate
I_{square} is a function that yields each part's contribution to the second moment of area
$I_{triangle}$ is a function that yields the triangular part's contribution to the second moment of area
$\alpha_{steel.concrete}$ is the factor taking into account the difference in stiffness for concrete and steel

legend
0 - lower flange of the main I-girders
1 - web of the main I-girders
2 - upper flange of the main I-girders
3 - lower square of concrete slab
4 - upper triangle of concrete slab. Must be calculated separately.
5 - edge beam of the concrete deck
6 - buckle in the web (negative contribution)

$$I_{composite.negative}(x_{span}) :=$$

$z_{NA} \leftarrow z_{NA.composite.negative}(x_{span})$

$z_{local}(z_{bridge}) \leftarrow z_{composite.negative}(x_{span}, z_{bridge})$

$\rho_{fl} \leftarrow \rho_{main.flange.lower}(x_{span})$

$\rho_{fu} \leftarrow \rho_{main.flange.upper}(x_{span})$

$z_0 \leftarrow z_{local}(z_{centre.main.flange.lower}(x_{span}))$

$z_1 \leftarrow z_{local}(z_{centre.main.web}(x_{span}))$

$z_2 \leftarrow z_{local}(z_{centre.main.flange.upper}(x_{span}))$

$z_3 \leftarrow z_{local}(z_{centre.deck.slab.effective.sqr}(x_{span}))$

$z_4 \leftarrow z_{local}(z_{centre.deck.beam}(x_{span}))$

$z_5 \leftarrow z_{local}(z_{centre.deck.slab.effective.tri}(x_{span}))$

$z_6 \leftarrow z_{local}(z_{buckle.negative}(x_{span}, z_{NA}))$

$h_0 \leftarrow t_{main.flange.lower}(x_{span})$

$h_1 \leftarrow h_{main.web}(x_{span})$

$h_2 \leftarrow t_{main.flange.upper}(x_{span})$

$h_3 \leftarrow t_{deck.slab.effective.outer}$

$h_4 \leftarrow h_{deck.beam}(x_{span})$

$h_5 \leftarrow t_{deck.slab.effective.diff}$

$h_6 \leftarrow b_{buckle.negative}(x_{span}, z_{NA})$

$b_0 \leftarrow b_{main.flange.lower}(x_{span}) \cdot \rho_{fl}$

$b_1 \leftarrow t_{main.web}(x_{span})$

$b_2 \leftarrow b_{main.flange.upper}(x_{span}) \cdot \rho_{fu}$

$b_3 \leftarrow b_{deck.slab.effective} \cdot \alpha_{steel.concrete}$

$b_4 \leftarrow b_{deck.beam.effective} \cdot \alpha_{steel.concrete}$

$b_5 \leftarrow b_{deck.slab.effective} \cdot \alpha_{steel.concrete}$

$b_6 \leftarrow -t_{main.web}(x_{span})$

$$I \leftarrow \sum_{i=0}^{3} \left(I_{square}(h_i, b_i, z_i)\right) + \sum_{i=5}^{6} \left(I_{square}(h_i, b_i, z_i\right.$$

$I + I_{triangle}(h_4, b_4, z_4)$

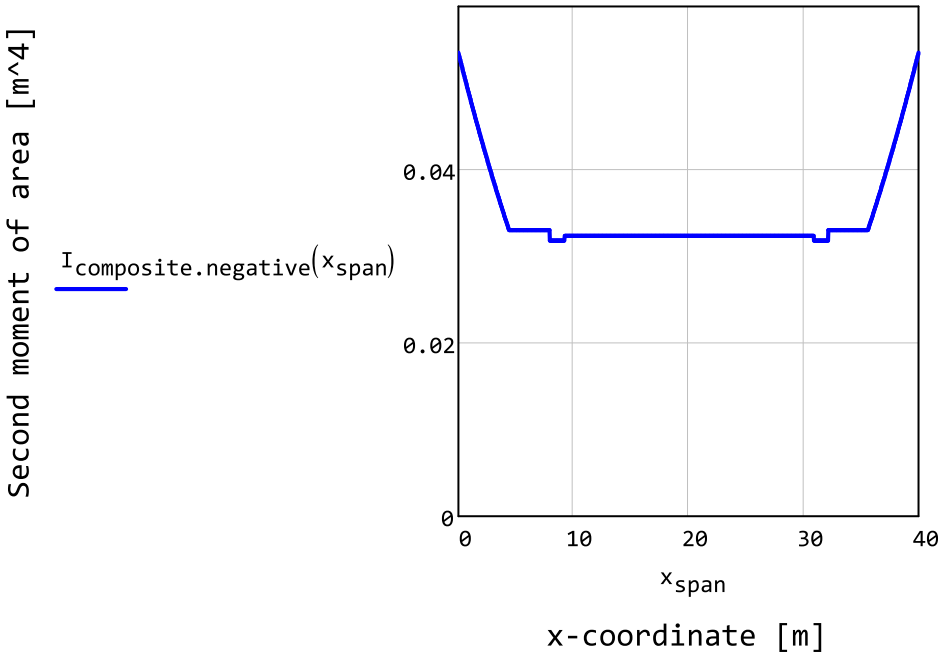

Location of the neutral axis of the effective composite cross-section in positive bending

Location of the neutral axis for the effective composite cross-section subjected to positive moment. For positive moment the concrete deck is in tension, thus the concrete is neglected. Instead the reinforcement is considered and transformed into equivalent structural steel area with regard to the difference in modulus of elasticity.
Since the web may buckle the calculation is performed in two steps. first the centre of the equivalent steel area is located for the cross-section without reducing for buckling of the web. Secondly the web buckle is calculated with the gravity centre that was obtained in the first step. Finally the buckle is included in the cross-section as an negative contribution and the location of the neutral axis may be calculated.
Note that the upper flange is not reduced due to buckling since it is stabilised by the concrete deck with composite action.
Here:
$\rho_{fl/fu}$ buckling reduction of the lower and upper flange respectively.
$\alpha_{steel.reinf}$ is the factor taking into account the difference in stiffness for reinforcement and steel
z_i is the global z-coordinate for the centre of each part
A_i is the area of each part. Here is also taken into account the stiffness difference.
z_{gc} is the centre of gravity for the equivalent steel area
b_{buckle} is the height of the buckle in the web
legend
0 - lower flange of the main I-girders
1 - web of the main I-girders
2 - upper flange of the main I-girders
3 - lower reinforcement in the slab
4 - upper reinforcement in the slab
5 - reinforcement in the edge beam
6 - buckle in the web (negative contribution)

$$z_{NA.composite.positive}(x_{span}) :=$$

$$\rho_{fl} \leftarrow \rho_{main.flange.lower}(x_{span})$$

$$\rho_{fu} \leftarrow 1$$

$$\alpha \leftarrow \alpha_{steel.reinf}$$

$$z_0 \leftarrow z_{centre.main.flange.lower}(x_{span})$$

$$z_1 \leftarrow z_{centre.main.web}(x_{span})$$

$$z_2 \leftarrow z_{centre.main.flange.upper}(x_{span})$$

$$z_3 \leftarrow z_{reinf.slab.lower}(x_{span})$$

$$z_4 \leftarrow z_{reinf.slab.upper}(x_{span})$$

$$z_5 \leftarrow z_{reinf.beam}(x_{span})$$

$$A_0 \leftarrow A_{main.flange.lower}(x_{span}) \cdot \rho_{fl}$$

$$A_1 \leftarrow A_{main.web}(x_{span})$$

$$A_2 \leftarrow A_{main.flange.upper}(x_{span}) \cdot \rho_{fu}$$

$$A_3 \leftarrow b_{deck.slab.effective} \cdot \rho_{reinf.slab.lower} \cdot \alpha$$

$$A_4 \leftarrow b_{deck.slab.effective} \cdot \rho_{reinf.slab.upper} \cdot \alpha$$

$$A_5 \leftarrow b_{deck.beam.effective} \cdot \rho_{reinf.beam} \cdot \alpha$$

$$z_{gc} \leftarrow \frac{\sum_{i=0}^{5} (A_i \cdot z_i)}{\sum_{j=0}^{5} A_j}$$

$$b_{buckle} \leftarrow b_{buckle.positive}(x_{span}, z_{gc})$$

$$A_6 \leftarrow -(b_{buckle} \cdot t_{main.web}(x_{span}))$$

$$z_6 \leftarrow z_{buckle.positive}(x_{span}, z_{gc})$$

$$\frac{\sum_{i=0}^{6} (A_i \cdot z_i)}{\sum_{j=0}^{6} A_j}$$

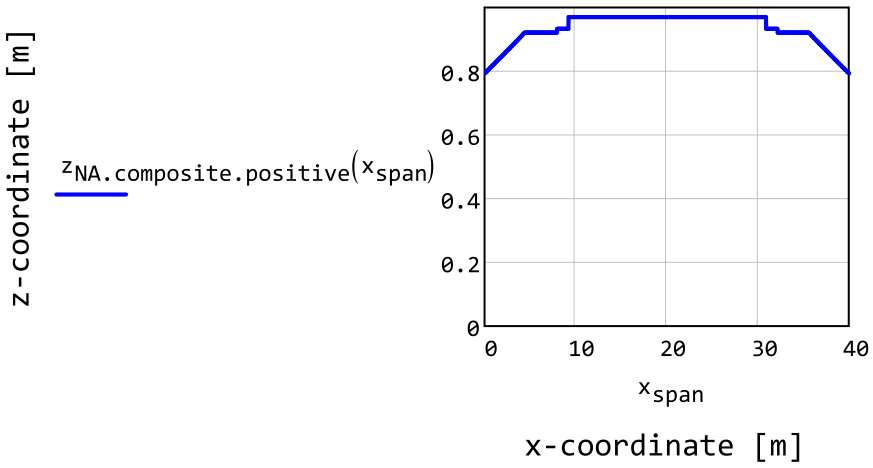

Function for obtaining the z-coordinate in the local geometry for the effective composite cross-section. The local z-axis begins at the neutral axis of the cross-section, with postitive direction upwards. The input is the z-coordinate in the global coordinate system and the location in x-direction. The x-coordinate is needed due to small variations of the location of the neutral axis along the span.

$$z_{composite.positive}(x_{span}, z_{bridge}) := z_{bridge} - z_{NA.composite.positive}(x_{span})$$

Second moment of area of the effective composite cross-section in positive bending

Second moment of area for half of the effective composite cross-section subjected to positive moment. For positive moment the concrete deck is in tension, thus the concrete is neglected. Instead the reinforcement is considered and transformed into equivalent structural steel area with regard to the difference in modulus of elasticity.
Note that the upper flange is not reduced due to buckling since it is stabilised by the concrete deck with composite action. Furthermore, note that the web buckle is included in the cross-section as an negative contribution to the second moment of area.
Here:
z_{NA} is the z-coordinate for the equivalent steel area
$\rho_{fl/fu}$ buckling reduction of the lower and upper flange respectively
z_i is the local z-coordinate for the centroid of each part
h_i is the height of each part, z-direction
b_i is the width of each part, y-direction. Includes reductions and difference in stiffness.
and
z_{local} yields the local z-coordinates given any global z-coordinate
I_{square} is a function that yields each part's contribution to the second moment of area
$I_{triangle}$ is a function that yields the triangular part's contribution to the second moment of area
$\alpha_{steel.concrete}$ is the factor taking into account the difference in stiffness for concrete and steel
legend
0 - lower flange of the main I-girders
1 - web of the main I-girders
2 - upper flange of the main I-girders
3 - lower reinforcement in the slab
4 - upper reinforcement in the slab
5 - reinforcement in the edge beam
6 - buckle in the web (negative contribution)

$$
\begin{aligned}
&I_{\texttt{composite.positive}}\left(x_{\texttt{span}}\right) := \\
&\quad z_{\texttt{NA}} \leftarrow z_{\texttt{NA.composite.positive}}\left(x_{\texttt{span}}\right) \\
&\quad z_{\texttt{local}}\left(z_{\texttt{bridge}}\right) \leftarrow z_{\texttt{composite.positive}}\left(x_{\texttt{span}}, z_{\texttt{bridge}}\right) \\
&\quad \rho_{\texttt{fl}} \leftarrow \rho_{\texttt{main.flange.lower}}\left(x_{\texttt{span}}\right) \\
&\quad \rho_{\texttt{fu}} \leftarrow \rho_{\texttt{main.flange.upper}}\left(x_{\texttt{span}}\right) \\
&\quad z_0 \leftarrow z_{\texttt{local}}\left(z_{\texttt{centre.main.flange.lower}}\left(x_{\texttt{span}}\right)\right) \\
&\quad z_1 \leftarrow z_{\texttt{local}}\left(z_{\texttt{centre.main.web}}\left(x_{\texttt{span}}\right)\right) \\
&\quad z_2 \leftarrow z_{\texttt{local}}\left(z_{\texttt{centre.main.flange.upper}}\left(x_{\texttt{span}}\right)\right) \\
&\quad z_3 \leftarrow z_{\texttt{local}}\left(z_{\texttt{reinf.slab.lower}}\left(x_{\texttt{span}}\right)\right) \\
&\quad z_4 \leftarrow z_{\texttt{local}}\left(z_{\texttt{reinf.slab.upper}}\left(x_{\texttt{span}}\right)\right) \\
&\quad z_5 \leftarrow z_{\texttt{local}}\left(z_{\texttt{reinf.beam}}\left(x_{\texttt{span}}\right)\right) \\
&\quad z_6 \leftarrow z_{\texttt{local}}\left(z_{\texttt{buckle.positive}}\left(x_{\texttt{span}}, z_{\texttt{NA}}\right)\right) \\
&\quad h_0 \leftarrow t_{\texttt{main.flange.lower}}\left(x_{\texttt{span}}\right) \\
&\quad h_1 \leftarrow h_{\texttt{main.web}}\left(x_{\texttt{span}}\right) \\
&\quad h_2 \leftarrow t_{\texttt{main.flange.upper}}\left(x_{\texttt{span}}\right) \\
&\quad h_3 \leftarrow \rho_{\texttt{reinf.slab.lower}} \cdot \alpha_{\texttt{steel.reinf}} \\
&\quad h_4 \leftarrow \rho_{\texttt{reinf.slab.upper}} \cdot \alpha_{\texttt{steel.reinf}} \\
&\quad h_5 \leftarrow \rho_{\texttt{reinf.beam}} \cdot \alpha_{\texttt{steel.reinf}} \\
&\quad h_6 \leftarrow b_{\texttt{buckle.positive}}\left(x_{\texttt{span}}, z_{\texttt{NA}}\right) \\
&\quad b_0 \leftarrow b_{\texttt{main.flange.lower}}\left(x_{\texttt{span}}\right) \cdot \rho_{\texttt{fl}} \\
&\quad b_1 \leftarrow t_{\texttt{main.web}}\left(x_{\texttt{span}}\right) \\
&\quad b_2 \leftarrow b_{\texttt{main.flange.upper}}\left(x_{\texttt{span}}\right) \cdot \rho_{\texttt{fu}} \\
&\quad b_3 \leftarrow b_{\texttt{deck.slab.effective}} \\
&\quad b_4 \leftarrow b_{\texttt{deck.slab.effective}} \\
&\quad b_5 \leftarrow b_{\texttt{deck.beam.effective}} \\
&\quad b_6 \leftarrow -t_{\texttt{main.web}}\left(x_{\texttt{span}}\right) \\
&\quad \sum_{i\,=\,0}^{6} \left(I_{\texttt{square}}\left(h_i, b_i, z_i\right)\right)
\end{aligned}
$$

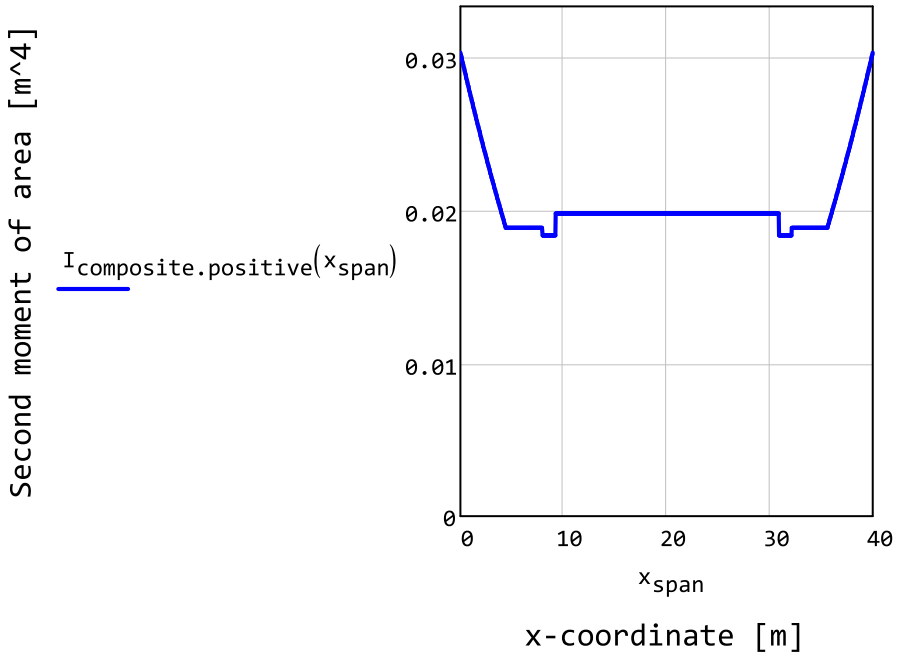

2.1.8 Capacity of the main I-girders

Bending resistance of the main I-girders with and without composite action. Here is taken into account the stabilising effect of the concrete deck on the upper flange when the composite action is considered. Additionally, the bending resistance is taken for both psoitive and negative bending when the composite action is considered. When the composite action is not considered only negative bending moment is considered.

Location of the neutral axis for the unreduced main I-girders

Location of the neutral axis for the main I-girder without consideration to any buckling phenomena. This is used for the calculation of the first moment of area for the main I-girders. The first moment of area in turn is used in fatigue calculations where it is assumed that the web or any other part of the cross-section will not buckle.

$$z_{NA.main.beam.unreduced}(x_{span}) := \left| \begin{array}{l} z_0 \leftarrow z_{centre.main.flange.lower}(x_{span}) \\ z_1 \leftarrow z_{centre.main.web}(x_{span}) \\ z_2 \leftarrow z_{centre.main.flange.upper}(x_{span}) \\ A_0 \leftarrow A_{main.flange.lower}(x_{span}) \\ A_1 \leftarrow A_{main.web}(x_{span}) \\ A_2 \leftarrow A_{main.flange.upper}(x_{span}) \\ \dfrac{\sum_{i=0}^{2} (A_i \cdot z_i)}{\sum_{j=0}^{2} A_j} \end{array} \right.$$

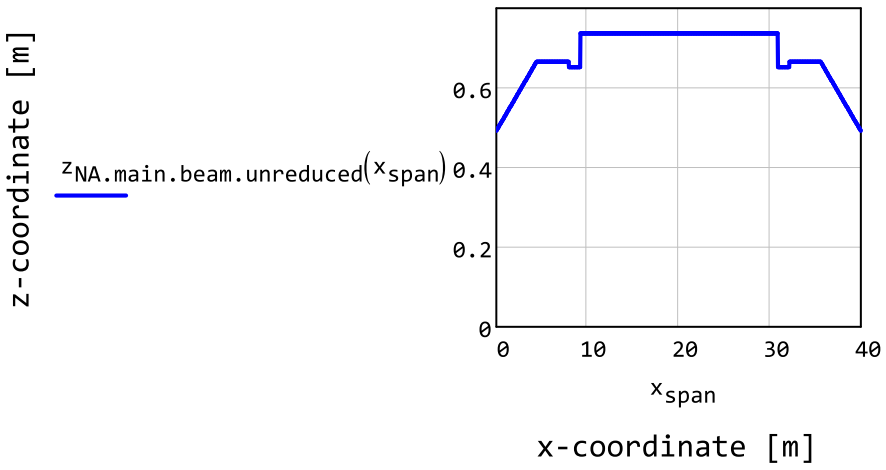

Function for obtaining the z-coordinate in the local geometry for the main I-girder. The local z-axis begins at the neutral axis of the cross-section, with postitive direction upwards. The input is the z-coordinate in the global coordinate system and the location in x-direction. The x-coordinate is needed due to small variations of the location of the neutral axis along the span.

$$z_{main.beam.unreduced}(x_{span}, z_{bridge}) := z_{bridge} - z_{NA.main.beam.unreduced}(x_{span})$$

Second moment of area for the unreduced main I-girders

Second moment of area for the unreduced main I-girders
Here:
z_{NA} is the z-coordinate for the resulting steel area
$\rho_{fl/fu}$ buckling reduction of the lower and upper flange respectively.
z_i is the local z-coordinate for the centroid of each part
h_i is the height of each part, z-direction
b_i is the width of each part, y-direction. Takes into account the reduction due to local buckling.
legend
0 - lower flange of the main I-girders
1 - web of the main I-girders
2 - upper flange of the main I-girders

$$I_{main.beam.unreduced}(x_{span}) := \left| \begin{array}{l} z_{NA} \leftarrow z_{NA.main.beam.unreduced}(x_{span}) \\ z_{local}(z_{bridge}) \leftarrow z_{main.beam.unreduced}(x_{span}, z_{bridge} \\ z_0 \leftarrow z_{local}(z_{centre.main.flange.lower}(x_{span})) \\ z_1 \leftarrow z_{local}(z_{centre.main.web}(x_{span})) \\ z_2 \leftarrow z_{local}(z_{centre.main.flange.upper}(x_{span})) \\ h_0 \leftarrow t_{main.flange.lower}(x_{span}) \\ h_1 \leftarrow h_{main.web}(x_{span}) \\ h_2 \leftarrow t_{main.flange.upper}(x_{span}) \\ b_0 \leftarrow b_{main.flange.lower}(x_{span}) \\ b_1 \leftarrow t_{main.web}(x_{span}) \\ b_2 \leftarrow b_{main.flange.upper}(x_{span}) \\ \sum_{i=0}^{2} \left(I_{square}(h_i, b_i, z_i)\right) \end{array} \right.$$

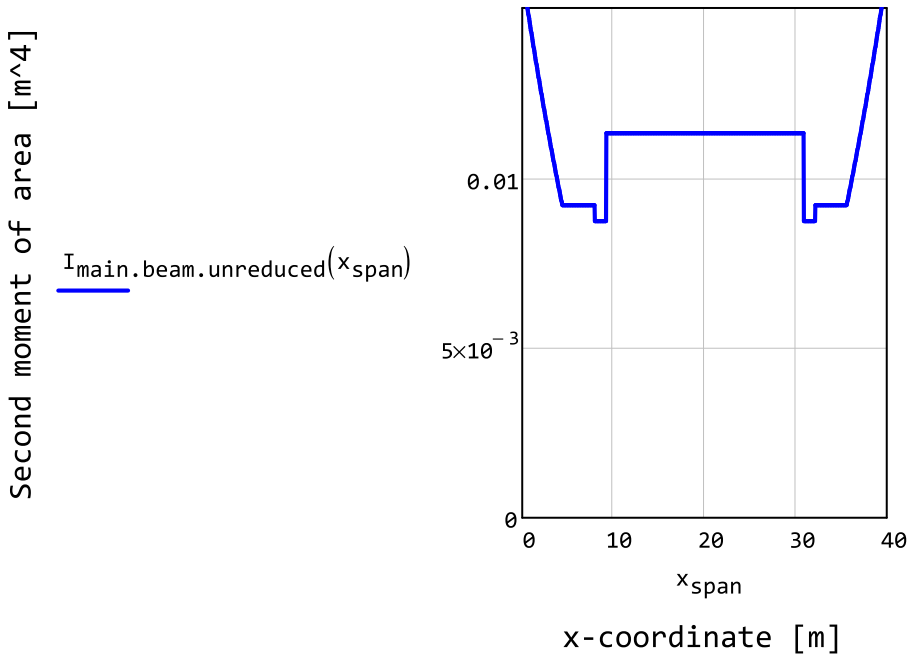

Location of the neutral axis for the main I-girders in negative bending

Location of the neutral axis for the main I-girders when subjected to negative bending. Note that only the resistance to negative bending moment is implemented for the main I-girders. Due to negative moment the web may only buckle localy in the upper part of the web, above the neutral axis.

It is posible to assume the upper flange as restrained by the concrete deck by assigning the input argument composite as the value 1. Note that the upper flange is not reduced due to buckling when it is assumed to be stabilised by the concrete deck in composite action.
Since the web may buckle the calculation is performed in two steps. first the centre of the equivalent steel area is located for the cross-section without reducing for buckling of the web. Secondly the web buckle is calculated with the gravity centre that was obtained in the first step. Finally the buckle is included in the cross-section as an negative contribution and the location of the neutral axis may be calculated.
Here:
$\rho_{fl/fu}$ buckling reduction of the lower and upper flange respectively.
z_i is the global z-coordinate for the centre of each part
A_i is the area of each part. Here is also taken into account the reduction due to local buckling.
z_{gc} is the centre of gravity for the steel area
b_{buckle} is the height of the buckle in the web
legend
0 - lower flange of the main I-girders
1 - web of the main I-girders
2 - upper flange of the main I-girders
3 - buckle in the web (negative contribution)

$$z_{NA.main.beam.neg}(x_{span}, composite) :=$$

$$\rho_{fl} \leftarrow \rho_{main.flange.lower}(x_{span})$$

$$\rho_{fu} \leftarrow 1 \quad \text{if } composite = 1$$

$$\rho_{fu} \leftarrow \rho_{main.flange.upper}(x_{span}) \quad \text{otherwise}$$

$$z_0 \leftarrow z_{centre.main.flange.lower}(x_{span})$$

$$z_1 \leftarrow z_{centre.main.web}(x_{span})$$

$$z_2 \leftarrow z_{centre.main.flange.upper}(x_{span})$$

$$A_0 \leftarrow A_{main.flange.lower}(x_{span}) \cdot \rho_{fl}$$

$$A_1 \leftarrow A_{main.web}(x_{span})$$

$$A_2 \leftarrow A_{main.flange.upper}(x_{span}) \cdot \rho_{fu}$$

$$z_{gc} \leftarrow \frac{\sum_{i=0}^{2} (A_i \cdot z_i)}{\sum_{j=0}^{2} A_j}$$

$$b_{buckle} \leftarrow b_{buckle.negative}(x_{span}, z_{gc})$$

$$A_6 \leftarrow -(b_{buckle} \cdot t_{main.web}(x_{span}))$$

$$z_6 \leftarrow z_{buckle.negative}(x_{span}, z_{gc})$$

$$\frac{\sum_{i=0}^{6} (A_i \cdot z_i)}{\sum_{j=0}^{6} A_j}$$

Note the minor difference in the location of the neutral axis between the case where the upper flange is reduced due to local buckling, compared to the case with no reduction thanks to composite action.

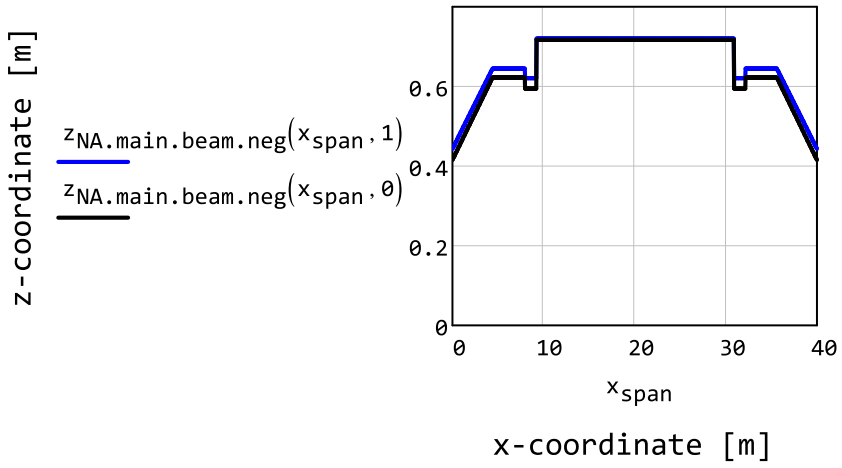

Function for obtaining the z-coordinate in the local geometry for the main I-girder. The local z-axis begins at the neutral axis of the cross-section, with postitive direction upwards. The input is the z-coordinate in the global coordinate system and the location in x-direction. The x-coordinate is needed due to small variations of the location of the neutral axis along the span.

$$z_{main.beam.neg}(x_{span}, z_{bridge}, composite) := z_{bridge} - z_{NA.main.beam.neg}(x_{span}, composit$$

Second moment of area for the main I-girders

Second moment of area for the main I-girders when subjected to negative bending. Note that only resistance to negative bending moment is implemented for the main I-girders. Due to negative moment the web may only buckle localy in the upper part of the web, above the neutral axis.
It is posible to assume the upper flange as restrained by the concrete deck by assigning the input argument composite as the value 1. Note that the upper flange is not reduced due to buckling when it is assumed to be stabilised by the concrete deck in composite action.
Furthermore, note that the web buckle is included in the cross-section as an negative contribution to the second moment of area.
Here:
z_{NA} is the z-coordinate for the resulting steel area
$\rho_{fl/fu}$ buckling reduction of the lower and upper flange respectively.
z_i is the local z-coordinate for the centroid of each part
h_i is the height of each part, z-direction
b_i is the width of each part, y-direction. Takes into account the reduction due to local buckling.
legend
0 - lower flange of the main I-girders
1 - web of the main I-girders
2 - upper flange of the main I-girders
3 - buckle in the web (negative contribution)

$$I_{main.beam.neg}(x_{span}, comp) :=$$

$z_{NA} \leftarrow z_{NA.main.beam.neg}(x_{span}, comp)$

$z_{local}(z_{bridge}) \leftarrow z_{main.beam.neg}(x_{span}, z_{bridge}, comp)$

$\rho_{fl} \leftarrow \rho_{main.flange.lower}(x_{span})$

$\rho_{fu} \leftarrow 1 \quad \text{if } comp = 1$

$\rho_{fu} \leftarrow \rho_{main.flange.upper}(x_{span}) \quad \text{otherwise}$

$z_0 \leftarrow z_{local}(z_{centre.main.flange.lower}(x_{span}))$

$z_1 \leftarrow z_{local}(z_{centre.main.web}(x_{span}))$

$z_2 \leftarrow z_{local}(z_{centre.main.flange.upper}(x_{span}))$

$z_3 \leftarrow z_{local}(z_{buckle.negative}(x_{span}, z_{NA}))$

$h_0 \leftarrow t_{main.flange.lower}(x_{span})$

$h_1 \leftarrow h_{main.web}(x_{span})$

$h_2 \leftarrow t_{main.flange.upper}(x_{span})$

$h_3 \leftarrow b_{buckle.negative}(x_{span}, z_{NA})$

$b_0 \leftarrow b_{main.flange.lower}(x_{span}) \cdot \rho_{fl}$

$b_1 \leftarrow t_{main.web}(x_{span})$

$b_2 \leftarrow b_{main.flange.upper}(x_{span}) \cdot \rho_{fu}$

$b_3 \leftarrow -t_{main.web}(x_{span})$

$$\sum_{i=0}^{3} \left(I_{square}(h_i, b_i, z_i)\right)$$

Note the minor difference second moment of area between the case where the upper flange is reduced due to local buckling compared to the case with no reduction thanks to composite action.

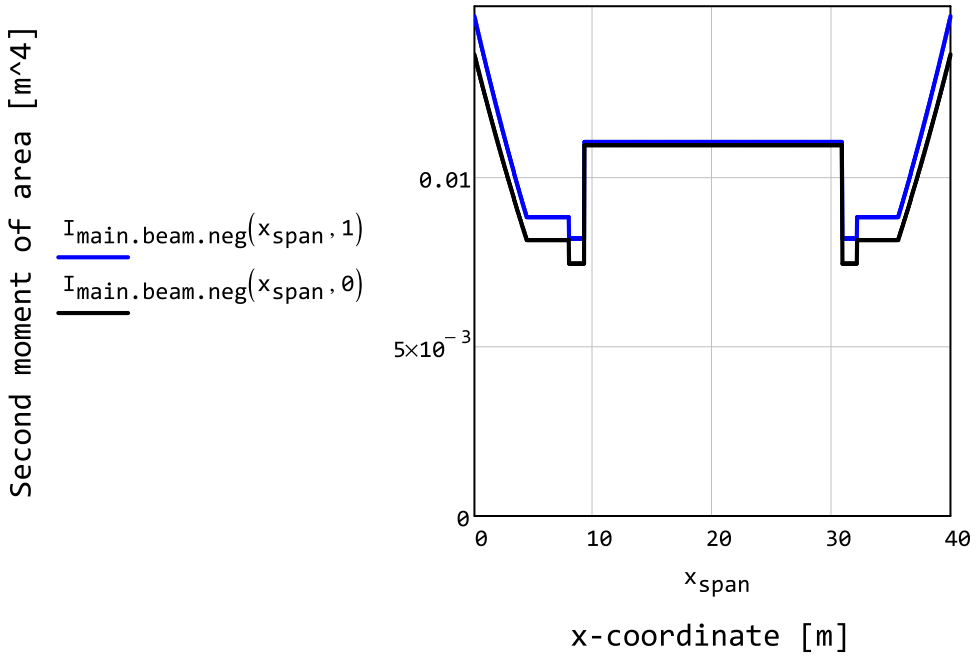

First moment of area of the main I-girders

first moment of one of the main I-girders. Note that since the first moment of area is only used in the fatigue assessment, the web will not be allowed to buckle.
Here:
z_o is the global z-coordinate for the bottom of the flange
z_{NA} is the global z-coordinate for the neutral axis of the cross-section with no regard to buckling
b_i is the width of each part, in y-direction
$h_{i.limit}$ is the maximum geometrical height of each part, in z-direction
$h_{i.max}$ is the height of each part with regard to the z-coordinate chosen. Can be negative.
h_i is the actual height of each part, in z-direction.
d_i is the distance from the centroid of each part to the neutral axis of the cross-section

$$
\begin{aligned}
&S_{main.beam}(x_{span}, z_{bridge}) := \\
&\quad z_0 \leftarrow z_{bottom.main.flange.lower}(x_{span}) \\
&\quad z_{NA} \leftarrow z_{NA.main.beam.unreduced}(x_{span}) \\
&\quad \rho_{fl} \leftarrow \rho_{main.flange.lower}(x_{span}) \\
&\quad b_0 \leftarrow b_{main.flange.lower}(x_{span}) \cdot \rho_{fl} \\
&\quad b_1 \leftarrow t_{main.web}(x_{span}) \\
&\quad b_2 \leftarrow b_{main.flange.upper}(x_{span}) \\
&\quad h_{0.limit} \leftarrow t_{main.flange.lower}(x_{span}) \\
&\quad h_{1.limit} \leftarrow h_{main.web}(x_{span}) \\
&\quad h_{2.limit} \leftarrow t_{main.flange.upper}(x_{span}) \\
&\quad h_{0.max} \leftarrow z_{bridge} - z_0 \\
&\quad h_{1.max} \leftarrow z_{bridge} - (h_{0.limit} + z_0) \\
&\quad h_{2.max} \leftarrow z_{bridge} - (h_{1.limit} + h_{0.limit} + z_0) \\
&\quad h_0 \leftarrow \begin{cases} \min(h_{0.max}, h_{0.limit}) & \text{if } h_{0.max} > 0m \\ 0m & \text{otherwise} \end{cases} \\
&\quad h_1 \leftarrow \begin{cases} \min(h_{1.max}, h_{1.limit}) & \text{if } h_{1.max} > 0m \\ 0m & \text{otherwise} \end{cases} \\
&\quad h_2 \leftarrow \begin{cases} \min(h_{2.max}, h_{2.limit}) & \text{if } h_{2.max} > 0m \\ 0m & \text{otherwise} \end{cases} \\
&\quad d_0 \leftarrow z_{NA} - \left(\frac{h_0}{2} + z_0\right) \\
&\quad d_1 \leftarrow z_{NA} - \left(\frac{h_1}{2} + h_0 + z_0\right) \\
&\quad d_2 \leftarrow z_{NA} - \left(\frac{h_2}{2} + h_1 + h_0 + z_0\right) \\
&\quad \sum_{i=0}^{2} (b_i \cdot h_i \cdot d_i)
\end{aligned}
$$

Note that the first moment of area goes to zero when the entire z.coordinate is outside the boundary of the main I-girder. In addition, the maximum value of the first moment of area should always be obtained at the location of the neutral axis.

$$S_{tmp} := S_{main.beam}\left(\frac{L_{span}}{2}, z_{NA.main.beam.unreduced}\left(\frac{L_{span}}{2}\right)\right)$$

$$S_{tmp} = 0.01 \cdot m^3$$

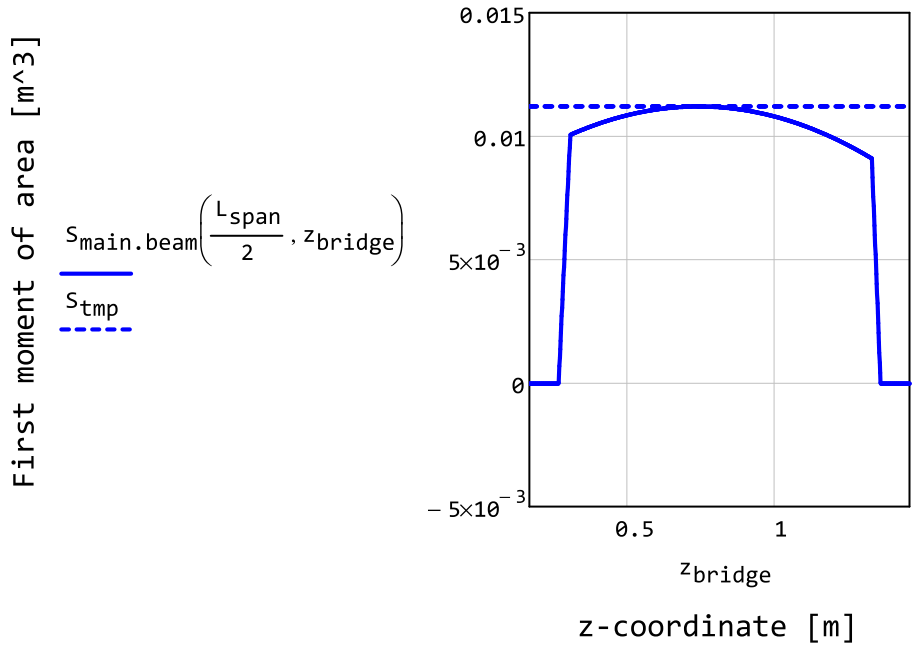

2.1.9 Limitations to the dimensions

In accordance with the guide lines pertaining to stainless steel in Eurocode 1993-1-4: paragrapgh 5.2.1-(1) the height to width ratio of the web should be limited. The ratio of web height to thickness should not exceed the value of 400. Note that web is checked both in the mid span and at the support.

$$\frac{h_{main.web.mid}}{t_{main.web.mid}} = 85.83$$

$$\frac{h_{main.web.end}}{t_{main.web.end}} = 83.13$$

The check if the height to thickness ratio is within the limits

$$\text{assumption}_{\text{web.width.thickness}} := \left\| \begin{array}{l} \text{end} \leftarrow \dfrac{h_{\text{main.web.end}}}{t_{\text{main.web.end}}} \\ \text{mid} \leftarrow \dfrac{h_{\text{main.web.mid}}}{t_{\text{main.web.mid}}} \\ \text{"true"} \quad \text{if } \max(\text{mid}, \text{end}) \leq 400 \\ \text{"false"} \quad \text{otherwise} \end{array} \right.$$

$$\text{assumption}_{\text{web.width.thickness}} = \text{"true"}$$

2.2 Loads

In this document all the loads will be calculated and described. Note that all moments acting on the composite structure are calculated assuming that one support is completely fix and the other is fix in z-direction and allow no rotation.

However, this is not the case when the casting of the concrete takes place. At casting the bridge is supposed to be simply supported since one end of the main I-girders are allowed to move. Due to this the moment distribution will differ depending on the type of load.

This chapter encompasses the following subchapters:
2.2.1 Self-weight
2.2.2 Traffic loads, load model 1
2.2.3 Fatigue loads and fatigue load model 3
2.2.4 Wind load
2.2.5 Load combinations in ultimate limit state
2.2.6 Load combinations in serviceability limit state

2.2.1 Self-weight

Here the self-weight of the cross-section of the bridge is calculated. Note that there are two different phases, the service phase and the casting phase. In the service phase the enitire structure is included, except form work. In the casting phase, which is when the concrete deck is cast, only the weight of the strucutre and form work is included.

Furthermore, note that for the sake of further calculations only half of the cross-section is considered for the bending moment and shear force. In addition, in order to be able to use analytical calculations of the moment the self-weight is taken as a constant maximum value.

Self-weight of cross-sections

Self-weight of the loadbearing structure. The self weight is given as distributed load in the x-direction along the span.

$$g_{bridge.structure}(x_{span}) := \left| \begin{array}{l} g_0 \leftarrow A_{deck}(x_{span}) \cdot \gamma_{concrete} \\ g_1 \leftarrow 2\,A_{main.beam}(x_{span}) \cdot \gamma_{steel} \\ \sum_{i=0}^{1} g_i \end{array} \right.$$

In order to be able to use analytical calculations of the moment, the self-weight is taken as a constant maximum value.

$$g_{bridge.structure.max} := \left| \begin{array}{l} X_{span} \leftarrow 0m, 1m .. L_{span} \\ \text{for } x_{step} \in X_{span} \\ \quad \left| \begin{array}{l} g_{step} \leftarrow g_{bridge.structure}(x_{step}) \\ g_{max} \leftarrow \max(g_{step}, g_{max}) \end{array} \right. \\ g_{max} \end{array} \right.$$

$$g_{bridge.structure.max} = 29.92 \cdot \frac{kN}{m}$$

Total self-weight of the bridge in the service phase

$$g_{bridge.total.composite} := \left| \begin{array}{l} g_0 \leftarrow g_{bridge.structure.max} \\ g_1 \leftarrow g_{bridge.roadsurface} \\ g_2 \leftarrow g_{bridge.safetybarrier} \\ \sum_{i=0}^{2} g_i \end{array} \right.$$

$$g_{bridge.total.composite} = 47.02 \cdot \frac{kN}{m}$$

Total self-weight of the bridge in the concrete casting phase

$$g_{bridge.total.casting} := g_{bridge.structure.max} + g_{bridge.formwork}$$

$$g_{bridge.total.casting} = 35.96 \cdot \frac{kN}{m}$$

Maximum total self-weigth of the bridge in the service phase

$$G_{bridge.total.composite} := g_{bridge.total.composite} \cdot L_{span}$$

$$G_{bridge.total.composite} = 1.88 \times 10^6 \, N$$

Maximum total self-weigth of the bridge in the service phase, for half of the cross-section

$$G_{bridge.total.casting} := g_{bridge.total.casting} \cdot L_{span}$$

$$G_{bridge.total.casting} = 1.44 \times 10^6 \, N$$

Bending moment and shear force due to self-weight

For the calculations of both shear force and bending moment it is assumed that the bridge is simply supported in both ends of the span. Note that the bending and shear is calculated for only half of the cross-section.

Shear force in the service phase, for half of the cross-section. The shear force is zero in the middle of the span and has the same value with opposite sign at the supports.

$$V_{E.self.composite}(x_{span}) := \frac{g_{bridge.total.composite}}{2} \cdot \left(x_{span} - \frac{L_{span}}{2} \right)$$

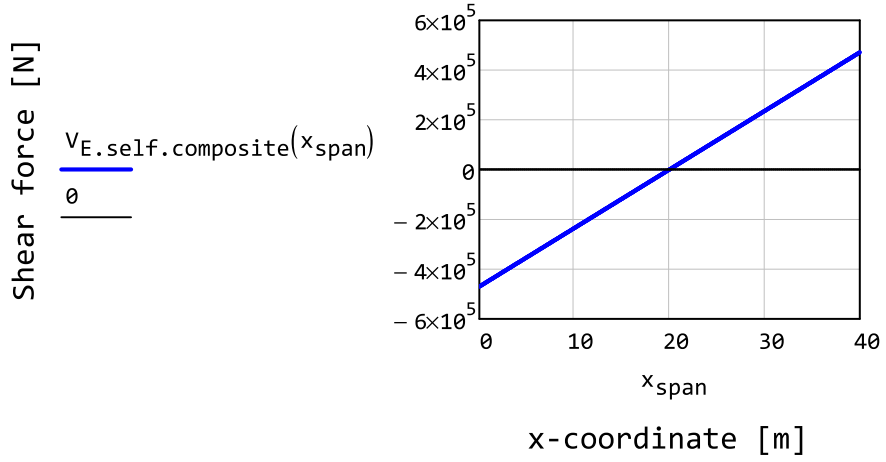

The maximum value of the shear force is obtained at the ends of the span

$$V_{E.self.composite}(0m) = -4.7 \times 10^5 \cdot N$$

$$V_{E.self.composite}(L_{span}) = 4.7 \times 10^5 \cdot N$$

Bending moment in the service phase, for half of the cross-section.

$$M_{E.self.composite}(x_{span}) := \left| g \leftarrow \frac{g_{bridge.total.composite}}{2} \right| \frac{g \cdot x_{span}^2}{2} - g \cdot \frac{L_{span}}{2} \cdot x_{span}$$

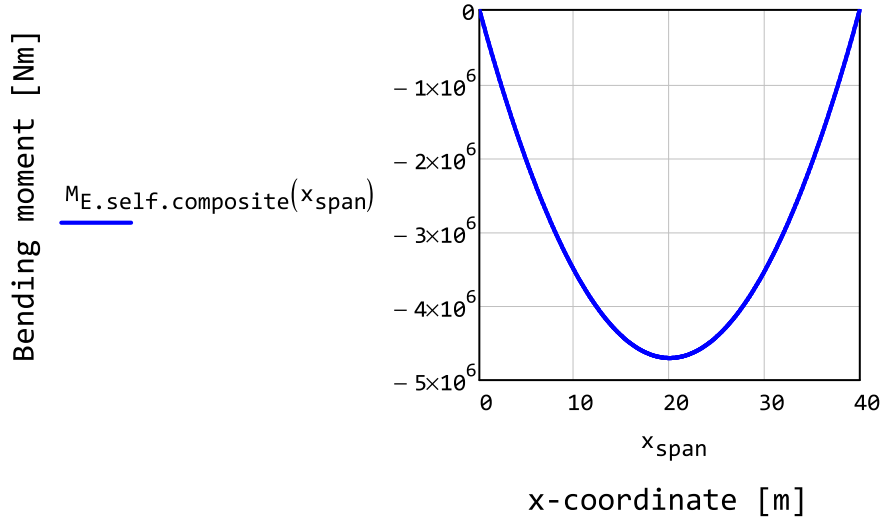

Shear force in the casting phase, for half of the cross-section. The shear force is zero in the middle of the span and has the same value with opposite sign at the supports.

$$V_{E.self.casting}(x_{span}) := \frac{g_{bridge.total.casting}}{2} \cdot \left(x_{span} - \frac{L_{span}}{2} \right)$$

The maximum value of the shear force is obtained at the ends of the span

$$V_{E.self.casting}(0m) = -3.6 \times 10^5 \cdot N$$

$$V_{E.self.casting}(L_{span}) = 3.6 \times 10^5 \cdot N$$

Bending moment in the composite phase, for half of the cross-section.

$$M_{E.self.casting}(x_{span}) := \left| \begin{array}{l} g \leftarrow \frac{g_{bridge.total.casting}}{2} \\ \frac{g \cdot x_{span}^2}{2} - g \cdot \frac{L_{span}}{2} \cdot x_{span} \end{array} \right.$$

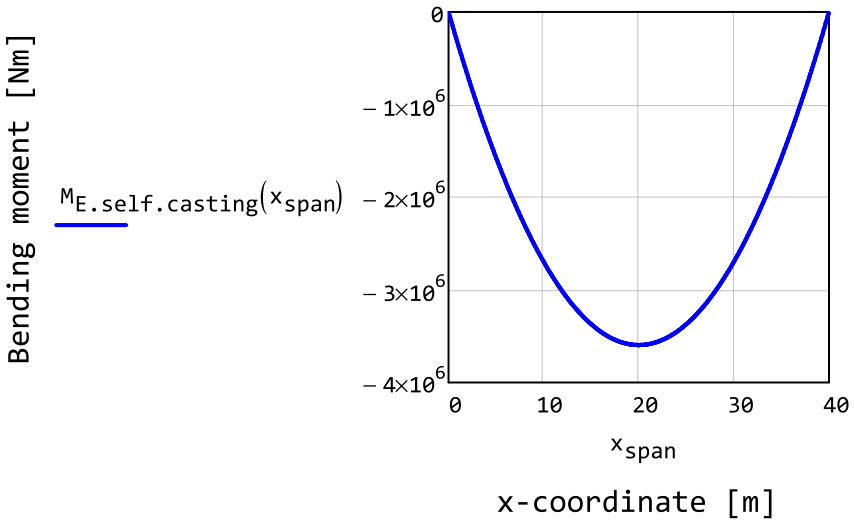

2.2.2 Traffic loads, load model 1

The load models that are used for the traffic loads can be found Eurocode 1991-2 Chapter 4. There are in total four different load models that can be applied, however only one of these will be used in this analysis. The load model to be used in this analysis is load model 1.

Load model 1 should be used for bridges that spans up to 200m. Note that load model 1 usually is on the safe side even for bridges longer than 200m.

The load should be applied so that the most adverse effect is obtained. For this reason calculations are only carried out for the most loaded main I-girder of the bridge.

Load model 1 takes into account concentrated and uniformly distributed loads. It should be used for general and local verifaction. Load model 1 can be found in Eurocode 1991-2

Load model 1 consists of two different kinds of loads. The loads are concentrated axle loads and distributed loads respectively.

Note that for the axle loads only one axle should be taken into account for each notional lane. The contact area is a square with the side of 0.40m, see the figure below. However,

for simplicity the axle loads will be treated as a point load in the calculations

Load model 1 should be applied on all the nominal lanes as well as on the remaining area.

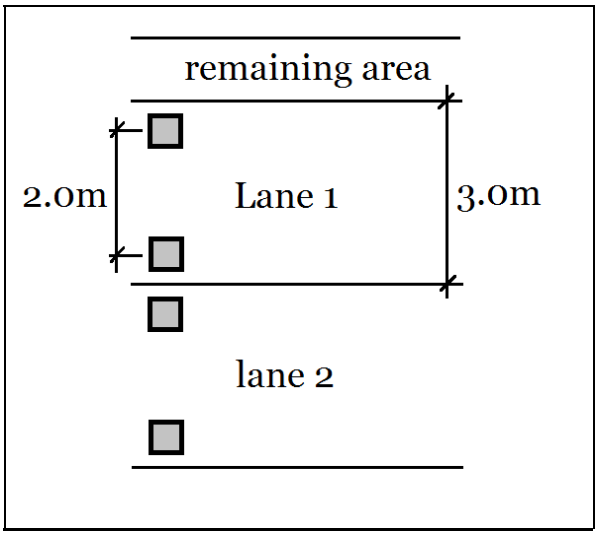

Illustration of load placement according to Eurocode

The following calculations for load model 1 builds on the assumption that there is exactly two notional lanes in the carriageway. Therefore we check that this assumption remains true.

$$\text{assumption}_{2\_notional\_lanes} := \begin{cases} \text{"true"} & \text{if } n_{lanes.notional} = 2 \\ \text{"false"} & \text{otherwise} \end{cases}$$

$$\text{assumption}_{2\_notional\_lanes} = \text{"true"}$$

Note that since the lanes does not occupy the entire carriageway the lanes will be placed asymetrically. for this reason the load is distributed according to the lane placement, see the figure below for clarity.

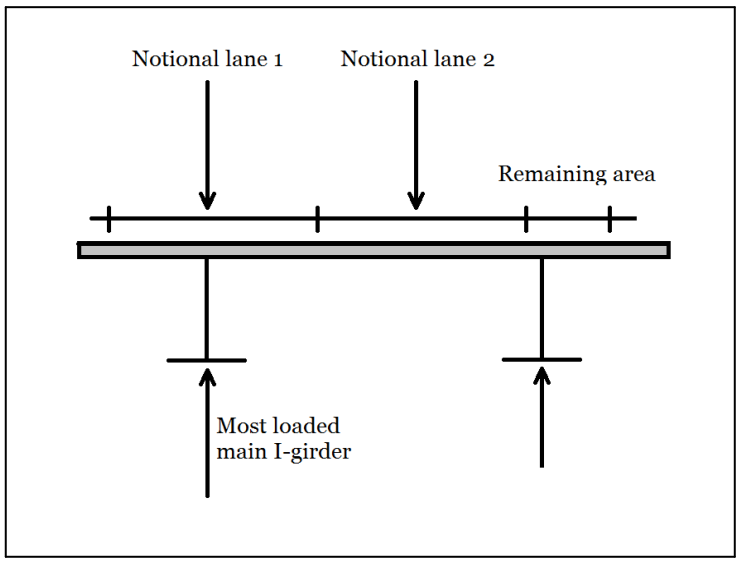

Illustration of the distribution of forces between the I-girders

For the following calculations the axle loads in transversal direction is transformed into a equivalent point load. The point load is corresponding to the load that is acting on the most loaded main girder.

$$Q_{model1.equivalent} := \left| \begin{array}{l} d_0 \leftarrow \dfrac{w_{carriageway} - w_{lane.notional} + cc_{maingirders}}{2} \\ d_1 \leftarrow \dfrac{w_{carriageway} - 3 \cdot w_{lane.notional} + cc_{maingirders}}{2} \\ M_0 \leftarrow Q_{k.model1.lane1} \cdot \alpha Q_{.model1.lane1} \cdot d_0 \\ M_1 \leftarrow Q_{k.model1.lane2} \cdot \alpha Q_{.model1.lane2} \cdot d_1 \\ \dfrac{M_0 + M_1}{cc_{maingirders}} \end{array} \right.$$

$$Q_{model1.equivalent} = 5.83 \times 10^5 \, N$$

For the following calculations the distributed loads in transversal direction is transformed into a equivalent line load. The line load is corresponding to the load that is acting on the most loaded main girder.

$$q_{model1.equivalent} := \left| \begin{array}{l} d_0 \leftarrow \dfrac{w_{carriageway} - w_{lane.notional} + cc_{maingirders}}{2} \\ d_1 \leftarrow \dfrac{w_{carriageway} - 3 \cdot w_{lane.notional} + cc_{maingirders}}{2} \\ d_2 \leftarrow \dfrac{w_{carriageway} - 5 \cdot w_{lane.notional} + cc_{maingirders}}{2} \\ q_0 \leftarrow q_{k.model1.lane1} \cdot \alpha q_{.model1.lane1} \cdot w_{lane.notional} \\ q_1 \leftarrow q_{k.model1.lane2} \cdot \alpha q_{.model1.lane2} \cdot w_{lane.notional} \\ q_2 \leftarrow q_{k.model1.remaining} \cdot \alpha q_{.model1.remaining} \cdot w_{lane.remaining} \\ \dfrac{\sum_{i=0}^{2} (q_i \cdot d_i)}{cc_{maingirders}} \end{array} \right.$$

$$q_{model1.equivalent} = 18.21 \cdot \frac{kN}{m}$$

Shear force due to axle loads

Shear force due to axle loads on the most loaded main-girder, load model 1. The second parameter, x_{load}, indicates where the load is placed along the bridge. Note that in order to obtain the maximum shear force the load should be placed at location of measurement.

$$V_{E.model1.axle}(x_{span}, x_{load}) := \begin{| a \leftarrow x_{load} \\ b \leftarrow L_{span} - x_{load} \\ R_A \leftarrow Q_{model1.equivalent} \cdot \frac{b^2}{L_{span}^2} \cdot \left(1 + \frac{2a}{L_{span}}\right) \\ R_B \leftarrow Q_{model1.equivalent} \cdot \frac{a^2}{L_{span}^2} \cdot \left(1 + \frac{2b}{L_{span}}\right) \\ -R_A \text{ if } x_{span} < x_{load} \\ R_B \text{ if } x_{span} > x_{load} \\ -R_A \text{ if } x_{span} = x_{load} \wedge R_A > R_B \\ R_B \text{ if } x_{span} = x_{load} \wedge R_A \leq R_B}$$

Maximum shear force in the span, which is obtained when the load is placed at the point of measurement

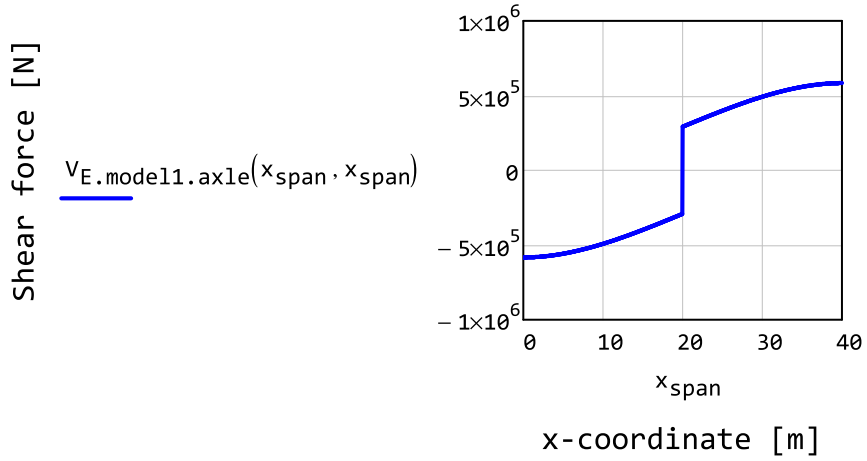

Maximimum shear force is achieved at the supports when the load is placed at the same support.

$$V_{E.model1.axle}(L_{span}, L_{span}) = 5.83 \times 10^5 \text{ N}$$

Bending moment due to axle loads

Bending moment due to axle loads on the most loaded main-girder, load model 1. The second parameter, x_{load}, indicates where the load is placed along the bridge. Note that maximum moment is obtained in the middle of the span when the load also is placed at the middle of the span.

$$M_{E.model1.axle}(x_{span}, x_{load}) := \begin{cases} a \leftarrow x_{load} \\ b \leftarrow L_{span} - x_{load} \\ Q \leftarrow Q_{model1.equivalent} \\ R_A \leftarrow Q \cdot \frac{b^2}{L_{span}^2} \cdot \left(1 + \frac{2a}{L_{span}}\right) \\ R_B \leftarrow Q \cdot \frac{a^2}{L_{span}^2} \cdot \left(1 + \frac{2b}{L_{span}}\right) \\ M_A \leftarrow Q \cdot \frac{a \cdot b^2}{L_{span}^2} \\ M_B \leftarrow Q \cdot \frac{a^2 \cdot b}{L_{span}^2} \\ -R_A \cdot x_{span} + M_A \quad \text{if } x_{span} < x_{load} \\ R_B \cdot (x_{span} - L_{span}) + M_B \quad \text{if } x_{span} \geq x_{load} \end{cases}$$

Maximum bending moment, which is obtained when the load is placed at the point of measurement

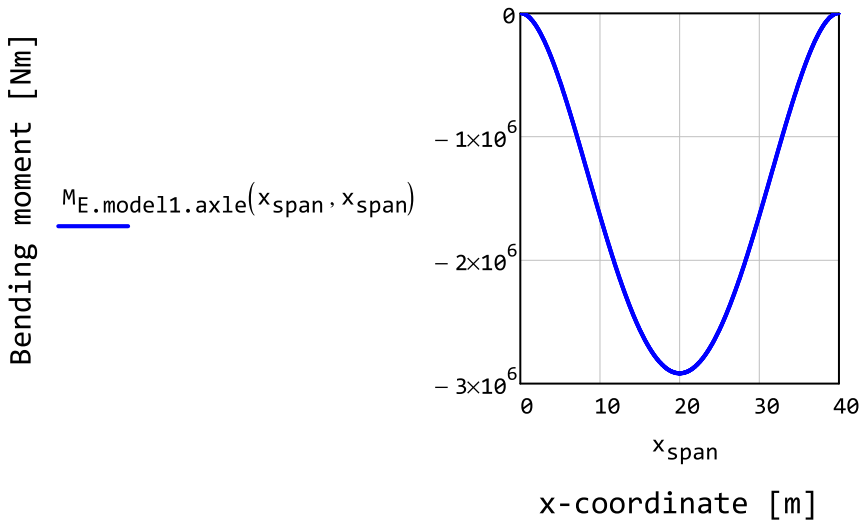

Bending moment in the middle of the span

$$M_{E.model1.axle}\left(\frac{L_{span}}{2}, \frac{L_{span}}{2}\right) = -2.92 \times 10^6 \text{ J}$$

Shear force due to distributed loads

Shear force due to distributed loads on the most loaded main-girder, load model 1. The shear force is zero in the middle of the span and has the same value with opposite sign at the supports.

$$V_{E.model1.distributed}(x_{span}) := q_{model1.equivalent} \cdot \left(x_{span} - \frac{L_{span}}{2} \right)$$

$$V_{E.model1.distributed}(L_{span}) = 3.64 \times 10^{5} \cdot N$$

Bending moment due to distributed loads

Bending moment due to axle loads on the most loaded main-girder, load model 1

$$M_{E.model1.distributed}(x_{span}) := \left| \begin{array}{l} q \leftarrow q_{model1.equivalent} \\ \frac{q \cdot x_{span}^{2}}{2} - q \cdot \frac{L_{span}}{2} \cdot x_{span} + \frac{q \cdot L_{span}^{2}}{12} \end{array} \right.$$

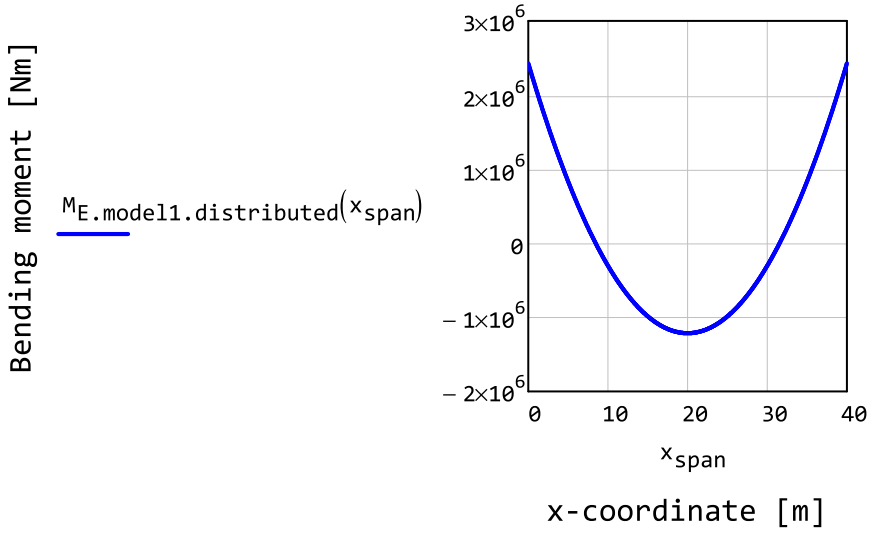

Bending moment in the middle of the span

$$M_{E.model1.distributed}\left(\frac{L_{span}}{2} \right) = -1.21 \times 10^{6} \cdot N \cdot m$$

Distribution of maximum shear force

Distribution of shear force for the most loaded main-girder, load model 1. The second parameter, x.load, indicates where the point load is placed along the bridge.

$$V_{E.model1.total}(x_{span}, x_{load}) := \left| \begin{array}{l} V_1 \leftarrow V_{E.model1.axle}(x_{span}, x_{load}) \\ V_2 \leftarrow V_{E.model1.distributed}(x_{span}) \\ V_1 + V_2 \end{array} \right.$$

Maximum shear force, obtained when the load is placed at the point of measurement

$V_{E.model1.total}(x_{span}, x_{span})$

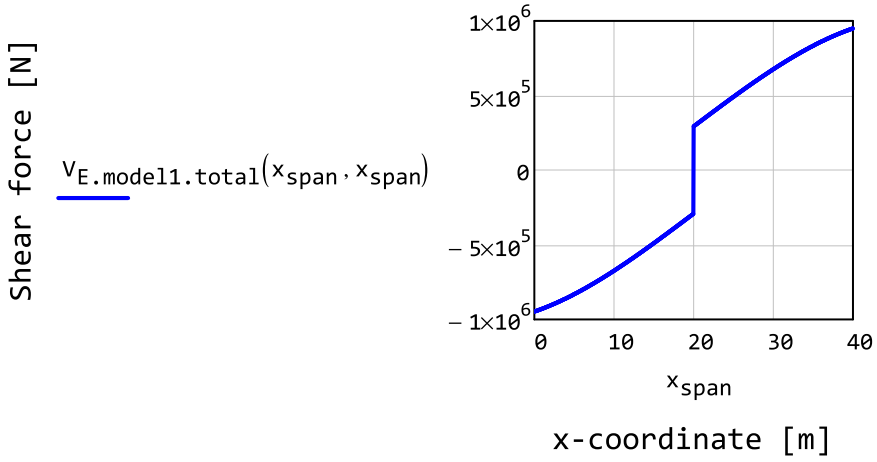

Maximimum shear force is achieved at the supports when the load is placed at the same support.

$V_{E.model1.total}(L_{span}, L_{span}) = 9.48 \times 10^5\ \mathrm{N}$

Distribution of maximum bending moment

Distribution of bending moment for the most loaded main-girder, load model 1. The second parameter, x.load, indicates where the point load is placed along the bridge.

$M_{E.model1.total}(x_{span}, x_{load}) := M_{E.model1.axle}(x_{span}, x_{load}) + M_{E.model1.distributed}(x_{s}$

Maximum bending moment, obtained when the load is placed at the point of measurement

$M_{E.model1.total}(x_{span}, x_{span})$

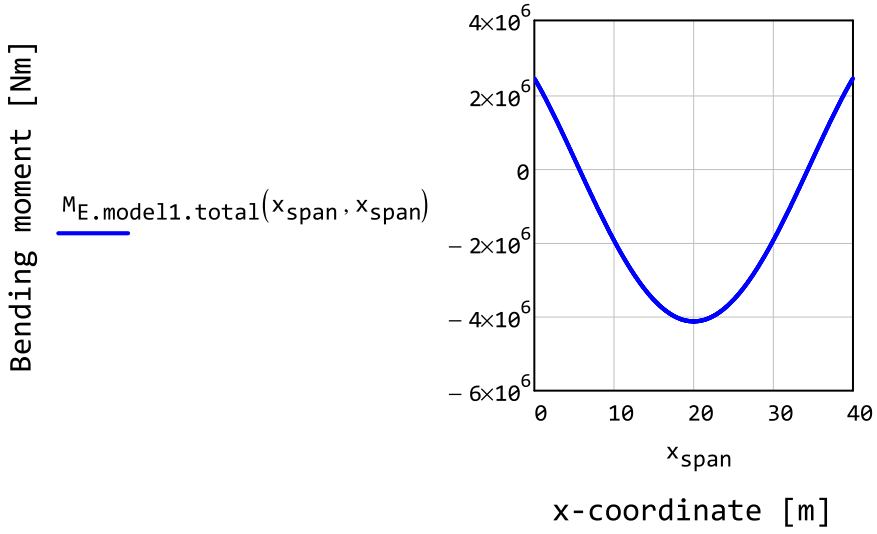

Bending moment in the middle of the span

$$M_{E.model1.total}\left(\frac{L_{span}}{2}, \frac{L_{span}}{2}\right) = -4.13 \times 10^6 \cdot N \cdot m$$

2.2.3 Fatigue loads and fatigue load model 3

The fatigue load model that is used for fatigue calculations is fatigue model 3, in accordance with Eurocode 1994-2: paragraph 6.8.2-(4) . This fatigue load model takes into account a single vehicle with four axles. Each axle load is 120kN and placed according to the figure below.

Miscellanous

The number of heavy vehicles that pass over the bridge each year per each slow lane. With heavy vehicles is here refered to vehicles with a gross weight exceeding 100kN, or approximately 10 tonnes. Recommended values depending on the traffic category is given in Eurocode 1991-2: Table 4.5. $N_{fatigue.observed}$ can depsite the name be either estimated or measured. The values given in table 4.5 is applicable for fatigue load model 3 and 4. Intermediate values are not excluded, but deemed to have little effect on the resulting fatigue life.

$$N_{fatigue.observed} := \begin{cases} \frac{2 \cdot 10^6}{year} & \text{if } category_{traffic} = 1 \\ \frac{0.5 \cdot 10^6}{year} & \text{if } category_{traffic} = 2 \\ \frac{0.125 \cdot 10^6}{year} & \text{if } category_{traffic} = 3 \\ \frac{0.05 \cdot 10^6}{year} & \text{if } category_{traffic} = 4 \end{cases}$$

$$N_{fatigue.observed} = 5 \times 10^5 \cdot \frac{1}{year}$$

For fatigue load model 3 the vehicle is defined in Eurocode 1991-2: Figure 4.8. For further detail see the Illustration below. In addition, a second vehicle is included 40m behind the primary vehicle. The second vehicle has a lower load of 30% and is only relevant for bridge spans of over 40m in length. The following vectors is used to account for both vehicles in the calculations.

$$d_{FLM3} := \begin{pmatrix} 0 \\ 1.2 \\ 7.2 \\ 8.4 \\ 40 \\ 41.2 \\ 47.2 \\ 48.4 \end{pmatrix} m \qquad load_{FLM3} := \begin{pmatrix} 1 \\ 1 \\ 1 \\ 1 \\ 0.3 \\ 0.3 \\ 0.3 \\ 0.3 \end{pmatrix}$$

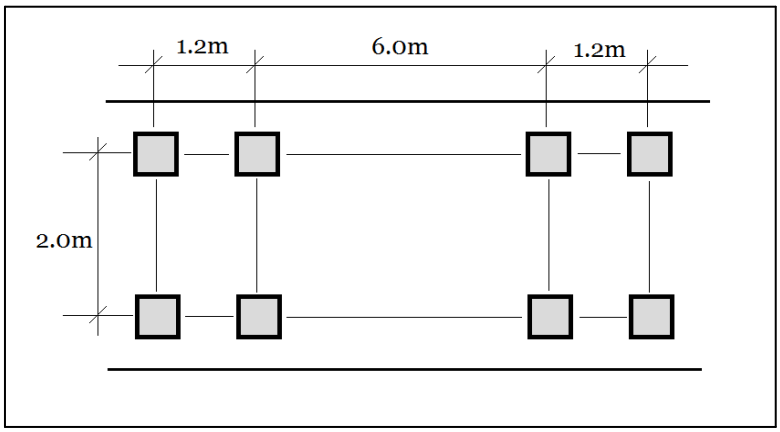

Illustration of the vehicle model in fatigue load model 3

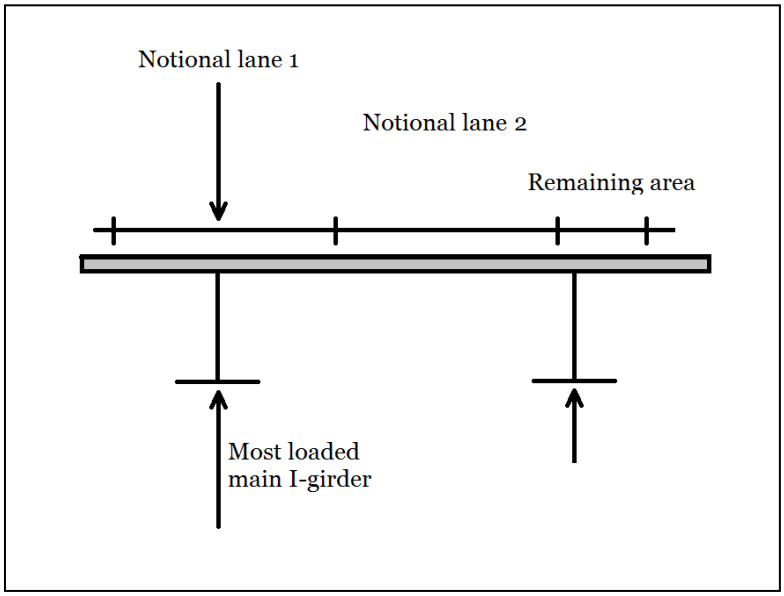

Illustration of the load distribution for the fatigue load.

For the following calculations the axle loads in transversal direction is transformed into a equivalent point load, in the exact same maner as for load model 1. The point load is corresponding to the load that is acting on the most loaded main girder. Note that load is only placed in one of the notional lanes at a time. In addition since fatigue load model 3 is only used for the damage equivalent method the load will only be calculated for lane 1.

$$\text{reduction}_{\text{lane1}} := \left| \begin{array}{l} d_0 \leftarrow \dfrac{w_{\text{carriageway}} - w_{\text{lane.notional}} + cc_{\text{maingirders}}}{2} \\ M_0 \leftarrow \alpha_{Q.\text{model1.lane1}} \cdot d_0 \\ \dfrac{M_0}{cc_{\text{maingirders}}} \end{array} \right.$$

$$reduction_{lane1} = 0.78$$

$$reduction_{lane2} := \left\| \begin{array}{l} d_0 \leftarrow \frac{w_{carriageway} - 3w_{lane.notional} + cc_{maingirders}}{2} \\ M_0 \leftarrow \alpha_{Q.model1.lane1} \cdot d_0 \\ \frac{M_0}{cc_{maingirders}} \end{array} \right.$$

$$reduction_{lane2} = 0.28$$

Equivalent point load when the axle load is placed in lane 1, the worst case.

$$Q_{fatigue.equivalent} := Q_{k.fatigue} \cdot reduction_{lane1}$$

$$Q_{fatigue.equivalent} = 94 \cdot kN$$

Shear force due to fatigue load

Shear force due to a single axle loads on the most loaded main-girder, fatigue load model 3. The second parameter x_{load} indicates where the load is placed along the bridge.

$$V_{E.fatigue.axle}(x_{span}, x_{load}) := \left\| \begin{array}{l} a \leftarrow x_{load} \\ b \leftarrow L_{span} - x_{load} \\ R_A \leftarrow Q_{fatigue.equivalent} \cdot \frac{b^2}{L_{span}^2} \cdot \left(1 + \frac{2a}{L_{span}}\right) \\ R_B \leftarrow Q_{fatigue.equivalent} \cdot \frac{a^2}{L_{span}^2} \cdot \left(1 + \frac{2b}{L_{span}}\right) \\ -R_A \quad \text{if } x_{span} < x_{load} \\ R_B \quad \text{if } x_{span} > x_{load} \\ -R_A \quad \text{if } x_{span} = x_{load} \wedge R_A > R_B \\ R_B \quad \text{if } x_{span} = x_{load} \wedge R_A \leq R_B \end{array} \right.$$

Maximum shear force in the span, which is obtained when the load is placed at the point of measurement

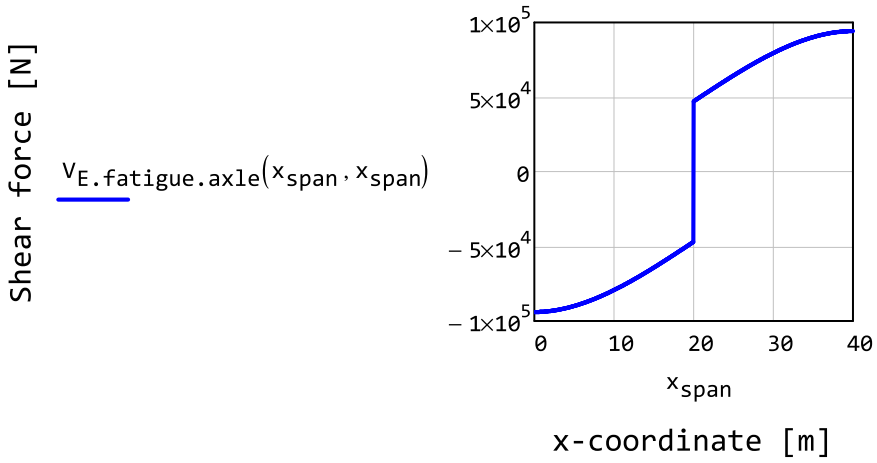

Influence line for a selected point at x=30m when the axle load moves alongs the span.

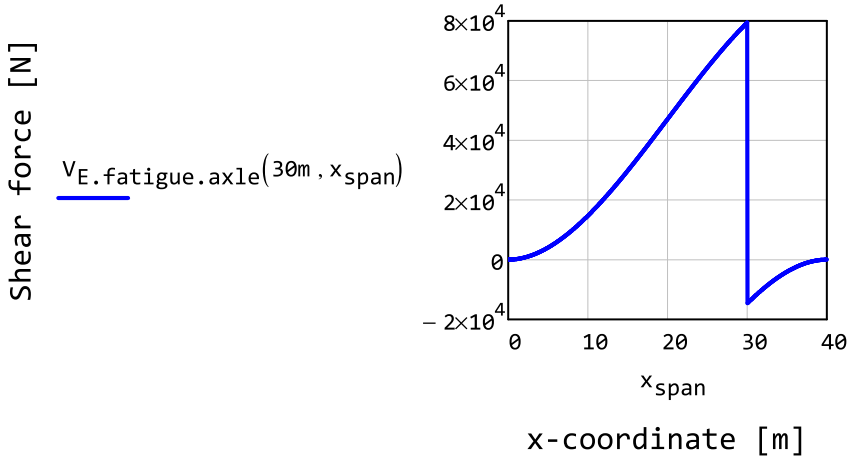

The axle loads are placed at a distance of respectively 1.2m, 7.2m and 8.4m from the first axle. Note that only the axles that are on the bridge give an contribution to the shear force. The variable $x_{vehicle}$ indicates the location of the first axle load.

Here:
V(x) is the shear force for a given placement of an axle load for the chosen section.
d is the x-coordinate of each axle load in the vehicle model
n is the last row in the vehicle model
load is the amount of axler load, either full or reduced for the second vehicle.

$$V_{E.fatigue.vehicle}(x_{span}, x_{vehicle}) := \left| \begin{array}{l} V(x_{load}) \leftarrow V_{E.fatigue.axle}(x_{span}, x_{load}) \\ d \leftarrow x_{vehicle} - d_{FLM3} \\ n \leftarrow rows(d) - 1 \\ load \leftarrow load_{FLM3} \\ \sum_{i=0}^{n} \left(\begin{array}{l} V(d_i) \cdot load_i \quad \text{if } 0 \le d_i \le L_{span} \\ 0N \quad \text{otherwise} \end{array} \right) \end{array} \right.$$

$V_{E.fatigue.vehicle}(20m, x_{span})$

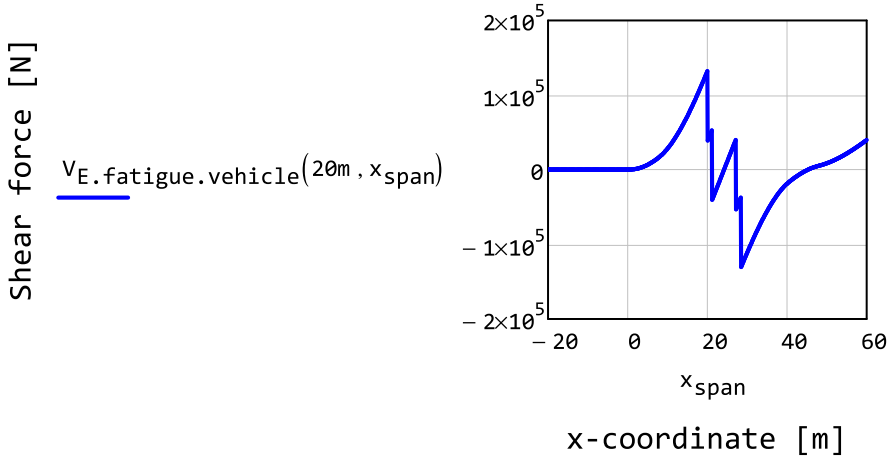

Bending moment due to fatigue load

Bending moment due to axle loads on the most loaded main-girder, load model 1. The second parameter, x.load, indicates where the load is placed along the bridge.

$$M_{E.fatigue.axle}(x_{span}, x_{load}) := \begin{cases} a \leftarrow x_{load} \\ b \leftarrow L_{span} - x_{load} \\ R_A \leftarrow Q_{fatigue.equivalent} \cdot \frac{b^2}{L_{span}^2} \cdot \left(1 + \frac{2a}{L_{span}}\right) \\ R_B \leftarrow Q_{fatigue.equivalent} \cdot \frac{a^2}{L_{span}^2} \cdot \left(1 + \frac{2b}{L_{span}}\right) \\ M_A \leftarrow Q_{fatigue.equivalent} \cdot \frac{a \cdot b^2}{L_{span}^2} \\ M_B \leftarrow Q_{fatigue.equivalent} \cdot \frac{a^2 \cdot b}{L_{span}^2} \\ -R_A \cdot x_{span} + M_A \quad \text{if } x_{span} < x_{load} \\ R_B \cdot (x_{span} - L_{span}) + M_B \quad \text{if } x_{span} \geq x_{load} \end{cases}$$

Maximum bending moment, which is obtained when the load is placed at the point of measurement

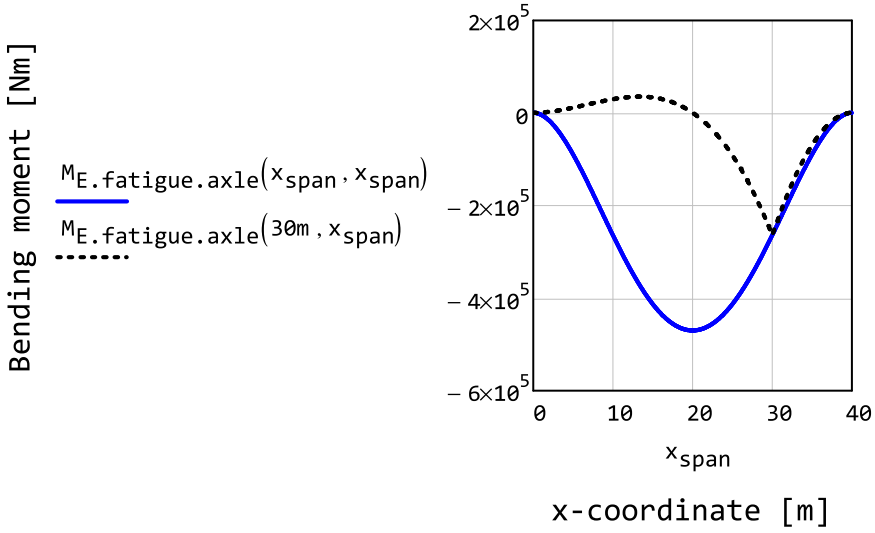

The axle loads are placed at a distance of respectively 1.2m, 7.2m and 8.4m from the first axle. Note that only the axles that are on the bridge give an contribution to the bending moment. The variable $x_{vehicle}$ indicates the location of the first axle load of the vehicle.

Here:
M*(x)* is the bending moment for a given placement of an axle load for the chosen section.
d is the x-coordinate of each axle load in the vehicle model
n is the last row in the vehicle model
load is the amount of axler load, either full or reduced

$$M_{E.fatigue.vehicle}(x_{span}, x_{vehicle}) := \left| \begin{array}{l} M(x_{load}) \leftarrow M_{E.fatigue.axle}(x_{span}, x_{load}) \\ d \leftarrow x_{vehicle} - d_{FLM3} \\ n \leftarrow rows(d) - 1 \\ load \leftarrow load_{FLM3} \\ \sum_{i=0}^{n} \left(\left| \begin{array}{ll} M(d_i) \cdot load_i & \text{if } 0 \le d_i \le L_{span} \\ 0N & \text{otherwise} \end{array} \right. \right) \end{array} \right.$$

Influence line for a selected point at a 1/4 of the span length when the vehicle moves alongs the span.

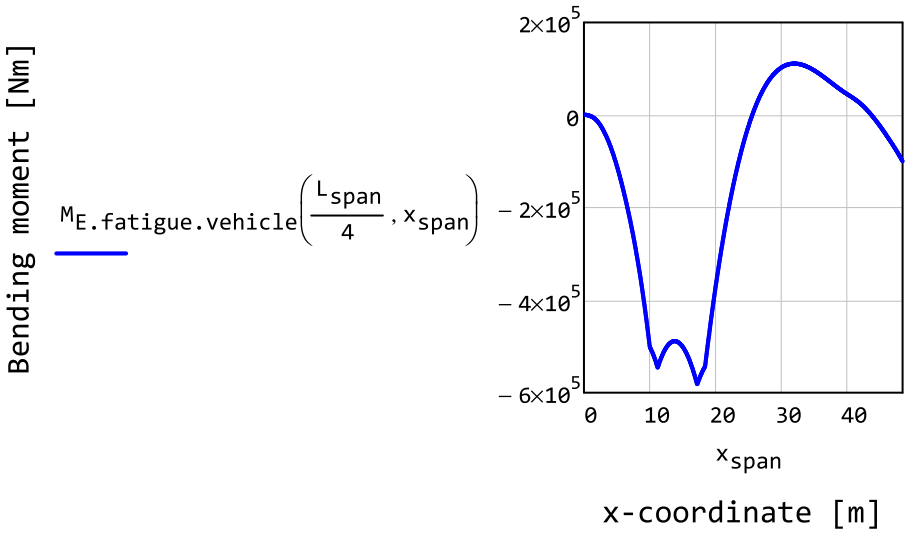

Influence line for a selected point at a 1/5 of the span length when the vehicle moves alongs the span. Note that due to the fix support the positive moment becomes more prominent closer to the support.

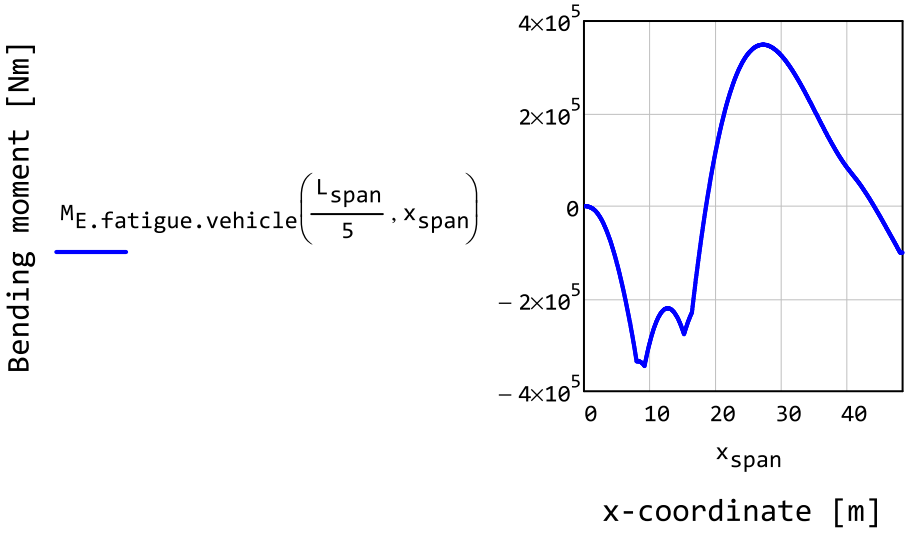

2.2.4 Wind load

Calculation of the wind load which acts on the bridge.

Height of the bridge

The height of the traffic on the bridge which is used for calculation of wind loads. Value given by Eurocode 1991-2: Paragraph 8.3.1-(5a)

$$h_{traffic.wind} = 2\,m$$

The height of the bridge including traffic which is used for calculation of wind loads

$$z_{bridge.max} = 4\,m$$

Terrain category of the bridge location. Explained by Eurocode 1991-2: Table 4.1

$$Category_{terrain} = 1$$

Roughness length corresponding to the terrain category. Given by Eurocode 1991-2: Table 4.1

$$z_{bridge.wind.0} := \begin{cases} 0.003m & \text{if } Category_{terrain} = 0 \\ 0.010m & \text{if } Category_{terrain} = 1 \\ 0.050m & \text{if } Category_{terrain} = 2 \\ 0.300m & \text{if } Category_{terrain} = 3 \\ 1.000m & \text{if } Category_{terrain} = 4 \end{cases}$$

$$z_{bridge.wind.0} = 0.01\,m$$

Minium height to be used in wind load calculations. The value is corresponding to the terrain category. Given by Eurocode 1991-2: Table 4.1

$$z_{bridge.wind.minimum} := \begin{cases} 1m & \text{if } Category_{terrain} = 0 \\ 1m & \text{if } Category_{terrain} = 1 \\ 2m & \text{if } Category_{terrain} = 2 \\ 5m & \text{if } Category_{terrain} = 3 \\ 10m & \text{if } Category_{terrain} = 4 \end{cases}$$

$$z_{bridge.wind.minimum} = 1\,m$$

The height of the bridge is not allowed to be less than the minimum value obtained from the terrain category.

$$z_{bridge.wind.max} := \max\left(z_{bridge.max}, z_{bridge.wind.minimum}\right)$$

$$z_{bridge.wind.max} = 4\,m$$

Factor taking into account the strength of the wind in different directions. Recommended

value given by Eurocode 1991-1-4: paragraph 8.1-(5).

$$c_{wind.direction} = 1$$

Factor taking into account the seasonal variation of the wind strength. Recommended value given by Eurocode 1991-1-4: paragraph 8.1-(5)

$$c_{wind.season} = 1$$

Basic value of the wind speed. Recommended value given by Eurocode 1991-1-4: paragraph 8.1-(5).

$$v_{wind.0} = 23\frac{m}{s}$$

Wind speed, used for wind load calculations. Given by Eurocode 1991-2: Expression 4.1

$$v_{wind.basic} := c_{wind.direction} \cdot c_{wind.season} \cdot v_{wind.0}$$

$$v_{wind.basic} = 23\frac{m}{s}$$

Force coefficient for horizontal wind loads perpendicular to the span direction. Recommended value given by Eurocode 1991-1-4: Figure 8.3

$$c_{fx.0} := \begin{cases} 2.4 & \text{if } \frac{b_{deck.slab.span} + 2 \cdot b_{deck.beam.span}}{z_{bridge.wind.max}} < \frac{1}{3} \\ 1.0 & \text{if } \frac{b_{deck.slab.span} + 2 \cdot b_{deck.beam.span}}{z_{bridge.wind.max}} > 5 \\ 2.5 - 0.3\frac{b_{deck.slab.span} + 2 \cdot b_{deck.beam.span}}{z_{bridge.wind.max}} & \text{otherwise} \end{cases}$$

$$c_{fx.0} = 1.92$$

Basic velocity pressure, given by Eurocode 1991-2: Expression 4.10

$$q_{wind.basic} := \frac{1}{2} \cdot \rho_{air} \cdot v_{wind.basic}^{2}$$

$$q_{wind.basic} = 330.63\,Pa$$

Orography factor, taken as the value of 1 unless otherwise specified. Rules concerning this factor is given in Eurocode 1991-1-4: Section 4.3.3.

$$c_{orography} = 1$$

Terrain roughness factor that takes into account the roughness of the terrain and the height of the structure. Given by Eurocode 1991-1-4: paragraph 4.3.2-(1)

$$c_{roughness}(z_{wind}) := 0.19 \cdot \left(\frac{z_{bridge.wind.0}}{0.05m}\right)^{0.07} \cdot \ln\left(\frac{z_{wind}}{z_{bridge.wind.0}}\right)$$

$$c_{roughness}\left(z_{bridge.wind.max}\right) = 1.02$$

mean wind velocity at a given height

$$v_{wind.mean}\left(z_{wind}\right) := c_{roughness}\left(z_{wind}\right) \cdot c_{orography} \cdot v_{wind.basic}$$

Wind turbulence intensity at a given height. Eurocode 1991-1-4: paragrapgh 4.4-(1)

$$intensity_{wind.velocity}\left(z_{wind}\right) := \frac{1}{\ln\left(\frac{z_{wind}}{z_{bridge.wind.0}}\right)}$$

Peak velocity pressure, given by Eurocode 1991-2: Expression 4.8.

$$q_{wind.peak} := \left| \begin{array}{l} c \leftarrow 1 + 7 \cdot intensity_{wind.velocity}\left(z_{bridge.wind.max}\right) \\ q_{mean} \leftarrow \frac{1}{2} \cdot \rho_{air} \cdot v_{wind.mean}\left(z_{bridge.wind.max}\right)^2 \\ c \cdot q_{mean} \end{array} \right.$$

$$q_{wind.peak} = 741.61\,Pa$$

The exposure factor. Given by Eurocode 1991-1-4: paragraph 4.5-(1)

$$c_{wind.exposure} := \frac{q_{wind.peak}}{q_{wind.basic}} = 2.24$$

Wind load factor. Given by Eurocode 1991-2: paragraph 8.3.2-(1)

$$C_{wind} := c_{wind.exposure} \cdot c_{fx.0}$$

$$C_{wind} = 4.31$$

Windload acting on the most loaded main I-girder

The equivalent distributed load that acts on the most loaded main I-girder in the composite cross-section. The horizontal wind force acting perpendicualar to the bridge span is calculated using the simplified method as described in Eurocode 1991-2: Paragraph 8.3.2-(1).
The referrence area for the wind load acting horizontal and perpendicular to the bridge span, is taken as the worst case between just the bridge and the bridge with traffic. The height of the traffic is given by Eurocode 1991-2: Figure 8.3. In more detail, the worst case senario is the case that gives the larges moment on the bridge. The rotation centre is assummed to be located at the top of the bridge. The moment is then carried by the main I-girders, thus the moment is divided by the distance between the main I-girders. Note that the height of the bridge is taken as an average, this should be an conservative simplifatication that leads to higher moment.

$$q_{wind.equivalent.composite} := \left| \begin{array}{l} h_{bridge} \leftarrow h_{bridge.wind} \\ h_{traffic} \leftarrow 2 \cdot m + h_{bridge.wind} \\ lever_{bridge} \leftarrow \frac{h_{bridge}^{2}}{2} \\ lever_{traffic} \leftarrow \left| h_{traffic} \cdot \left(\frac{h_{traffic}}{2} - h_{bridge} \right) \right| \\ lever \leftarrow \max\left(lever_{bridge}, lever_{traffic} \right) \\ moment_{wind} \leftarrow \frac{1}{2} \left(\rho_{air} \cdot v_{wind.basic}^{2} \cdot C_{wind} \cdot lever \right) \\ \frac{moment_{wind}}{cc_{maingirders}} \end{array} \right.$$

$$q_{wind.equivalent.composite} = 0.27 \cdot \frac{kN}{m}$$

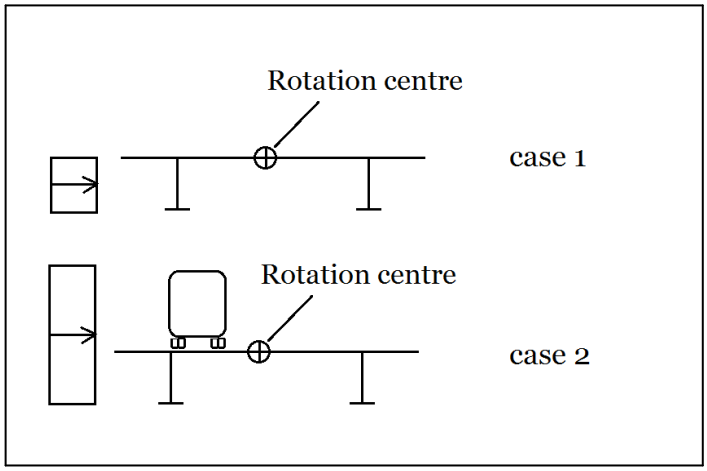

Illustration of the two cases considered for the wind load

The shear force in the most loaded main I-girder due to horisontal wind load. Since the composite cross-section is considered the shear force is calculated assuming fix supports.

$$V_{E.wind.composite}(x_{span}) := q_{wind.equivalent.composite} \cdot \left(x_{span} - \frac{L_{span}}{2} \right)$$

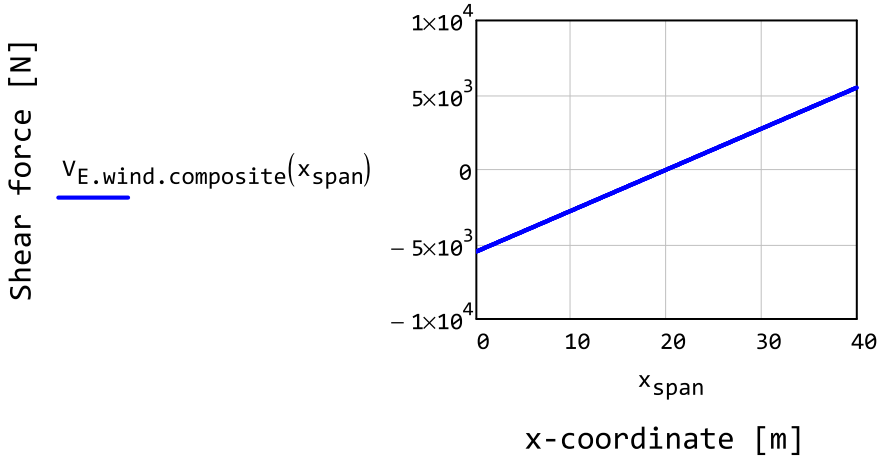

The bending moment in the most loaded main I-girder due to horisontal wind load. Since the composite cross-section is considered the bending moment is calculated assuming fix supports.

$$M_{E.wind.composite}(x_{span}) := \left| q \leftarrow q_{wind.equivalent.composite} \right| \frac{q \cdot L_{span}^{2}}{12} + \frac{q \cdot x_{span}^{2}}{2} - q \cdot \frac{L_{span}}{2} \cdot x_{span}$$

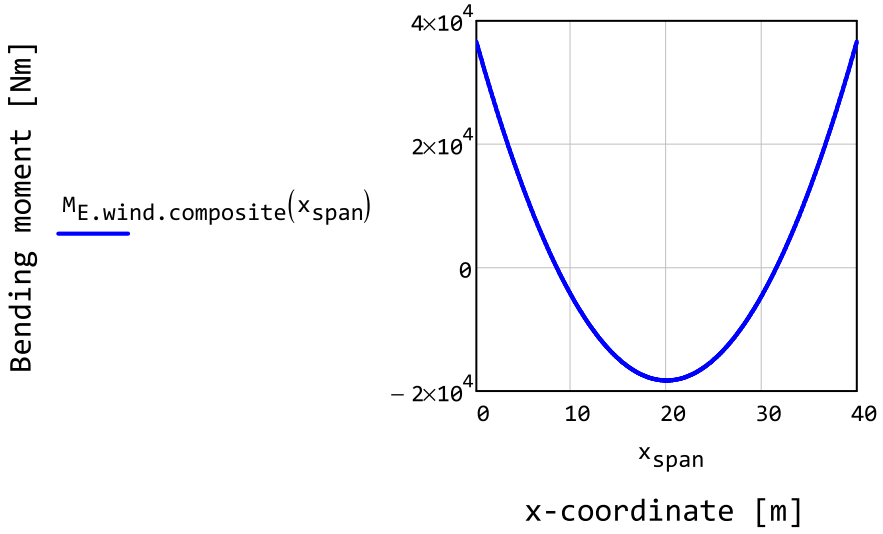

2.2.5 Load combinations in ultimate limit state

Calculations of the load combinations in the ultimate limit state.

Service phase

Distribution of minimum design bending moment in the ultimate limit state for the composite structure in the service life. The equation is given by Eurocode 1990-A1: Table A2.4(B). However note that here the equation and values are taken from the Swedish Annex Chapter 7 Table A2.4(B)S instead.
In order to obtain the maximum negative moment in each section along the span the axle load should be applied at the current section. There are two load combinations to consider which is based on equation 10.6a and 10.6b. For both load combinations the self weight is unfavourable since it always give an negative contribution.
Here
M_A is the load combination for 10.6a
M_B is the load combination for 10.6b

$$M_{Ed.ULS.imposed.negative}(x_{span}, equ) :=$$
$$tmp \leftarrow \gamma_d \cdot 1.5 \cdot \psi_{traffic.0}$$
$$M_{A_0} \leftarrow tmp \cdot M_{E.model1.total}(x_{span}, x_{span})$$
$$M_{A_1} \leftarrow \gamma_d \cdot 1.5 \cdot \psi_{wind.0} \cdot M_{E.wind.composite}(x_{span}$$
$$M_{B_0} \leftarrow \gamma_d \cdot 1.5 \cdot M_{E.model1.total}(x_{span}, x_{span})$$
$$M_{B_1} \leftarrow \gamma_d \cdot 1.5 \cdot \psi_{wind.0} \cdot M_{E.wind.composite}(x_{span}$$
$$\sum_{i=0}^{1} M_{A_i} \quad \text{if } equ = "A"$$
$$\sum_{i=0}^{1} M_{B_i} \quad \text{if } equ = "B"$$

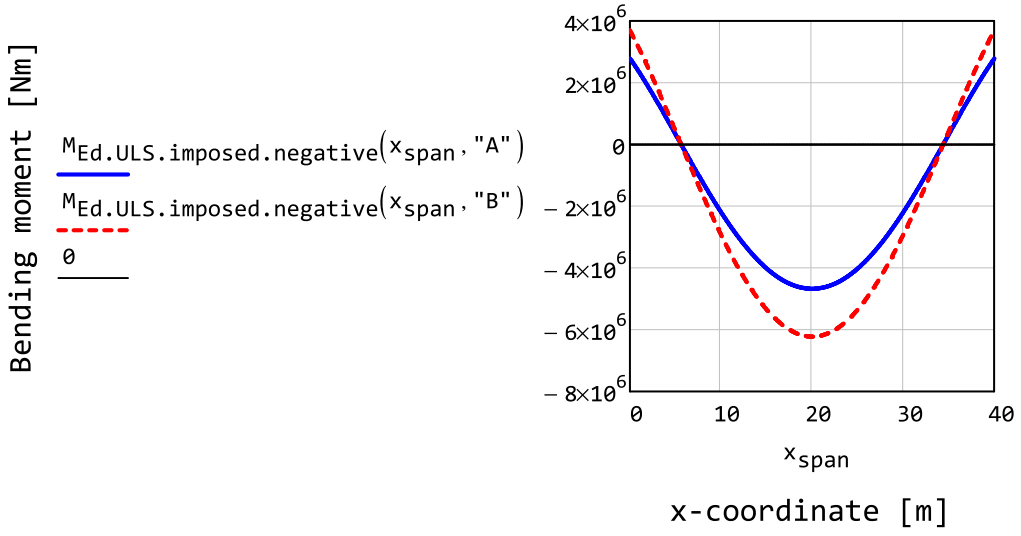

Distribution of maximum design bending moment in the ultimate limit state for the composite structure in the service life. The equation is given by Eurocode 1990-A1: Table A2.4(B). However note that here the equation and values are taken from the Swedish Annex Chapter 7 Table A2.4(B)S instead.
For the positive bending the selfweight is always favourable. Thus only equation 10.6b has to be

applied since it always will give a larger contribution from the traffic load. In order to find the maximum positive moment the load has to be moved along the span. The maximum moment should be found with relative ease.
Here
M_2 is the contribution from the traffic load
M_3 is the contribution from the wind load
M_{max} is the maxium bending moment which has been obtained
M_{step} is the bending moment for the current step
and
$range_{span}$ is a function that yields a range vector over the span length. input is number of steps.

$$M_{Ed.ULS.imposed.positive}(x_{span}) := \left| \begin{array}{l} M_2(x_{load}) \leftarrow \gamma_d \cdot 1.5 \cdot M_{E.model1.total}(x_{span}, x_{load}) \\ M_3 \leftarrow \gamma_d \cdot 1.5 \cdot \psi_{wind.0} \cdot M_{E.wind.composite}(x_{span}) \\ M(x_{load}) \leftarrow M_2(x_{load}) + M_3 \\ M_{max} \leftarrow M(0m) \\ \text{for } step \in range_{span}(50) \\ \quad \left| \begin{array}{l} M_{step} \leftarrow M(step) \\ M_{max} \leftarrow \max(M_{step}, M_{max}) \end{array} \right. \\ M_{max} \end{array} \right.$$

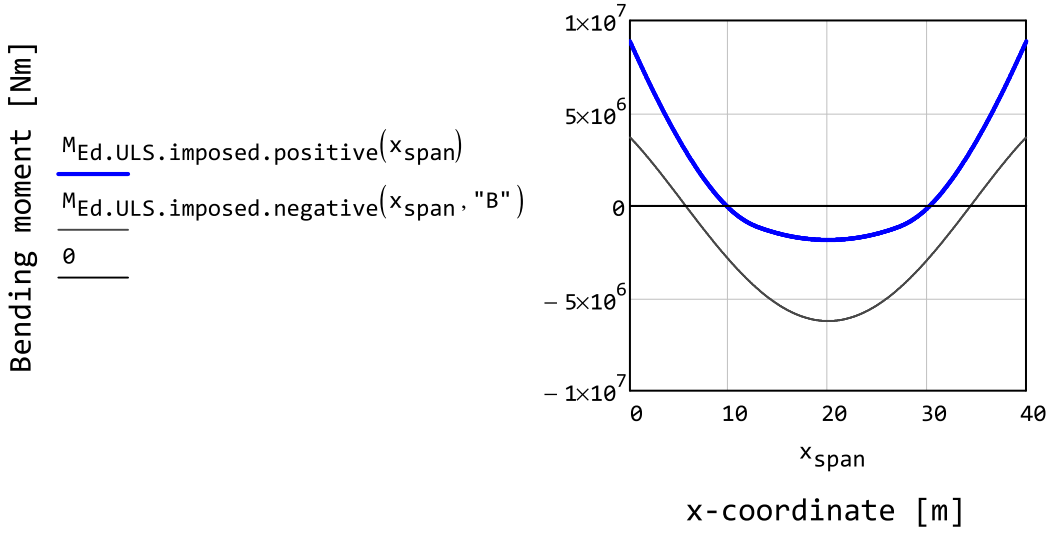

Distribution of the design bending moment due to self weight in the ultimate limit state for the composite structure in the service life. The equation is given by Eurocode 1990-A1: Table A2.4(B). However note that here the equation and values are taken from the Swedish Annex Chapter 7 Table A2.4(B)S instead.

For the positive bending the selfweight is always favourable. Thus only equation 10.6b has to be applied for positive moment since it always gives a larger contribution from the traffic load.
Here
M_A is the load combination for 10.6a, self-weight unfavourable
M_B is the load combination for 10.6b, self-weight unfavourable
M_C is the load combination 10.6b, self-weight favourable

$$M_{Ed.ULS.selfweight}(x_{span}, choice) := \begin{cases} M_A \leftarrow \gamma_d \cdot 1.35 \cdot M_{E.self.composite}(x_{span}) \\ M_B \leftarrow \gamma_d \cdot 0.89 \cdot 1.35 \cdot M_{E.self.composite}(x_{span}) \\ M_C \leftarrow 1.00 \cdot M_{E.self.composite}(x_{span}) \\ M_A \text{ if } choice = \text{"A-"} \\ M_B \text{ if } choice = \text{"B-"} \\ M_C \text{ if } choice = \text{"B+"} \end{cases}$$

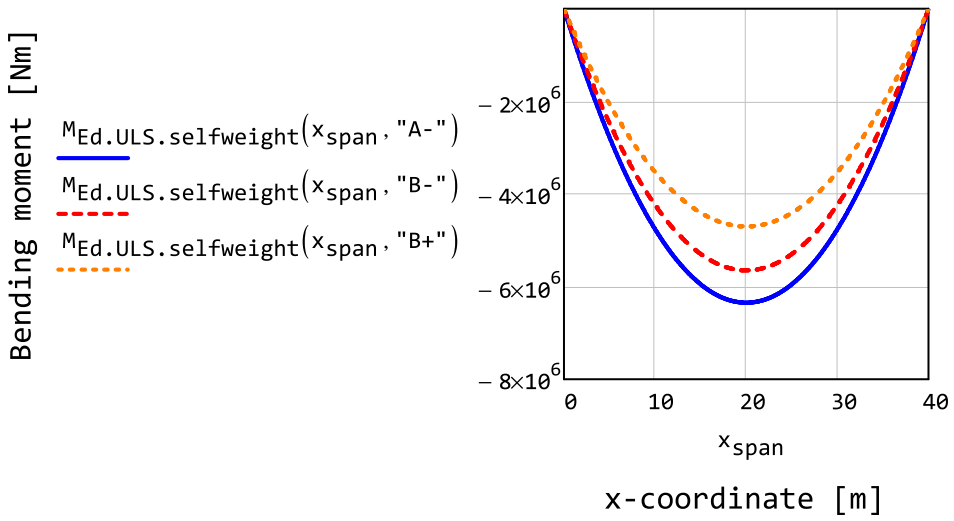

Distribution of the worst case design bending moment. This is function is used to simplify the calcualtions in the following chapters. Furthermore, only the maximum absulute value of the bending moment is of interest.
Here
M_{self} is the contribution from the self weight for respective load combination
$M_{imposed}$ is the contribution from the imposed loads for respective load combination
M is the resulting moment for respective load combination

$$M_{Ed.ULS.max}(x_{span}) := \left| \begin{array}{l} M_{self.A} \leftarrow M_{Ed.ULS.selfweight}(x_{span}, "A-") \\ M_{self.B} \leftarrow M_{Ed.ULS.selfweight}(x_{span}, "B-") \\ M_{self.C} \leftarrow M_{Ed.ULS.selfweight}(x_{span}, "B+") \\ M_{imposed.A} \leftarrow M_{Ed.ULS.imposed.negative}(x_{span}, "A") \\ M_{imposed.B} \leftarrow M_{Ed.ULS.imposed.negative}(x_{span}, "B") \\ M_{imposed.C} \leftarrow M_{Ed.ULS.imposed.positive}(x_{span}) \\ M_A \leftarrow M_{self.A} + M_{imposed.A} \\ M_B \leftarrow M_{self.B} + M_{imposed.B} \\ M_C \leftarrow M_{self.C} + M_{imposed.C} \\ \max(|M_A|, |M_B|, |M_C|) \end{array} \right.$$

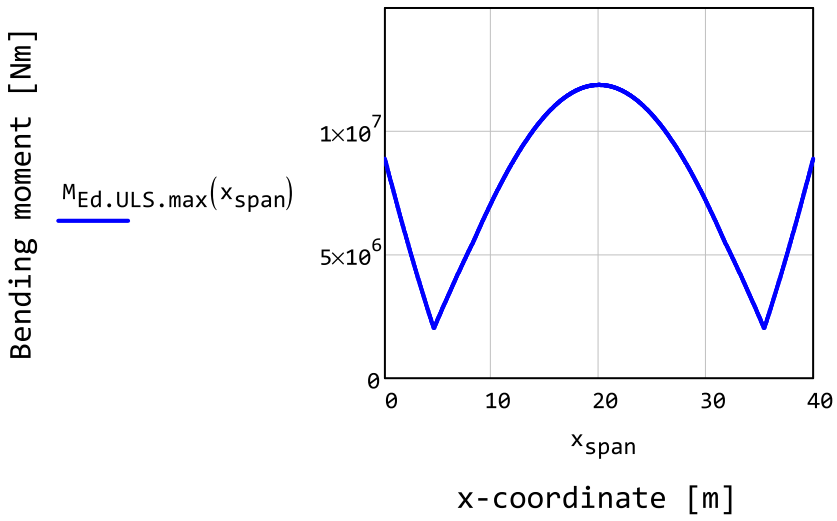

The location where the maximum value of the bending moment chages from being for positive bending moment to negative moment.

$$location := \left| \begin{array}{l} M_{previous} \leftarrow M_{Ed.ULS.max}(0m) \\ x_{step} \leftarrow \frac{L_{span}}{1000} \\ \text{while } x_{step} < L_{span} \wedge M_{previous} > M_{Ed.ULS.max}(x_{step}) \\ \quad \left| \begin{array}{l} M_{previous} \leftarrow M_{Ed.ULS.max}(x_{step}) \\ x_{step} \leftarrow x_{step} + \frac{L_{span}}{1000} \end{array} \right. \\ x_{step} \end{array} \right.$$

$$location = 4.6\,m$$

Distribution of design shear force in the ultimate limit state for the composite structure in the service life. The equation is given by Eurocode 1990-A1: Table A2.4(B). However note that here the equation and values are taken from the Swedish Annex Chapter 7 Table A2.4(B)S instead.
For the shear force only the maximum absolute value is of interest. The maximum absolute value is obtained when the load is placed directly above the current cross-section. The self-weight always contribute to a larger shear force, therfore it is always taken as unfavourable.
Here
V_A is the shear force in accordance with equation 10.6a given in Table A4.2(B)S, Swedish Annex
V_B is the shear force in accordance with equation 10.6b given in Table A4.2(B)S, Swedish Annex

$$V_{Ed.ULS.composite}(x_{span}) := \begin{vmatrix} V_{A_0} \leftarrow \gamma_d \cdot 1.35 \cdot V_{E.self.composite}(x_{span}) \\ V_{A_1} \leftarrow \gamma_d \cdot 1.5 \cdot \psi_{traffic.0} \cdot V_{E.model1.total}(x_{span}, x_{span}) \\ V_{A_2} \leftarrow \gamma_d \cdot 1.5 \cdot \psi_{wind.0} \cdot V_{E.wind.composite}(x_{span}) \\ V_{B_0} \leftarrow \gamma_d \cdot 0.89 \cdot 1.35 \cdot V_{E.self.composite}(x_{span}) \\ V_{B_1} \leftarrow \gamma_d \cdot 1.5 \cdot V_{E.model1.total}(x_{span}, x_{span}) \\ V_{B_2} \leftarrow \gamma_d \cdot 1.5 \cdot \psi_{wind.0} \cdot V_{E.wind.composite}(x_{span}) \\ V_A \leftarrow \sum_{i=0}^{2} V_{A_i} \\ V_B \leftarrow \sum_{i=0}^{2} V_{B_i} \\ \min(V_A, V_B) \quad \text{if } V_A \le 0 \\ \max(V_B, V_A) \quad \text{if } V_A > 0 \end{vmatrix}$$

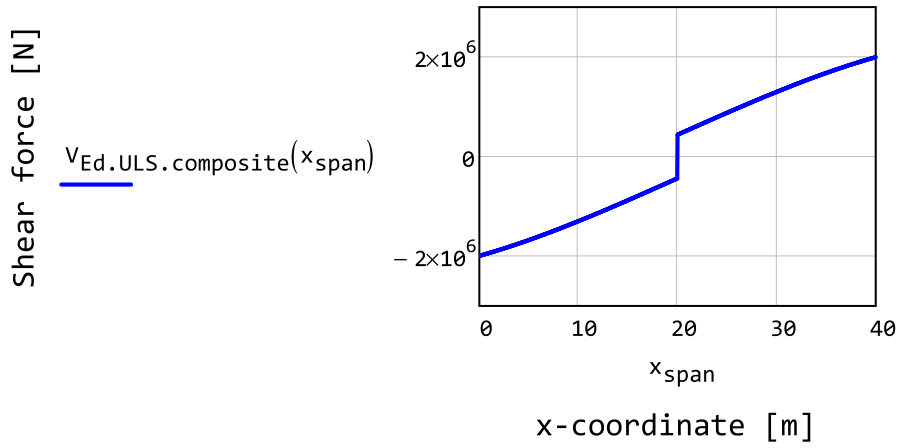

Shear force in each end of the span, note that the values should be identical but with opposite sign for a symmetric bridge.

$$V_{Ed.ULS.composite}(0m) = -1.99 \cdot MN$$

$$V_{Ed.ULS.composite}(L_{span}) = 1.99 \cdot MN$$

Casting phase

Bending moment distribution in the ultimate limit state (ULS), for the casting phase.

$$M_{Ed.ULS.casting}(x_{span}) := \gamma_d \cdot 1.35 \cdot M_{E.self.casting}(x_{span})$$

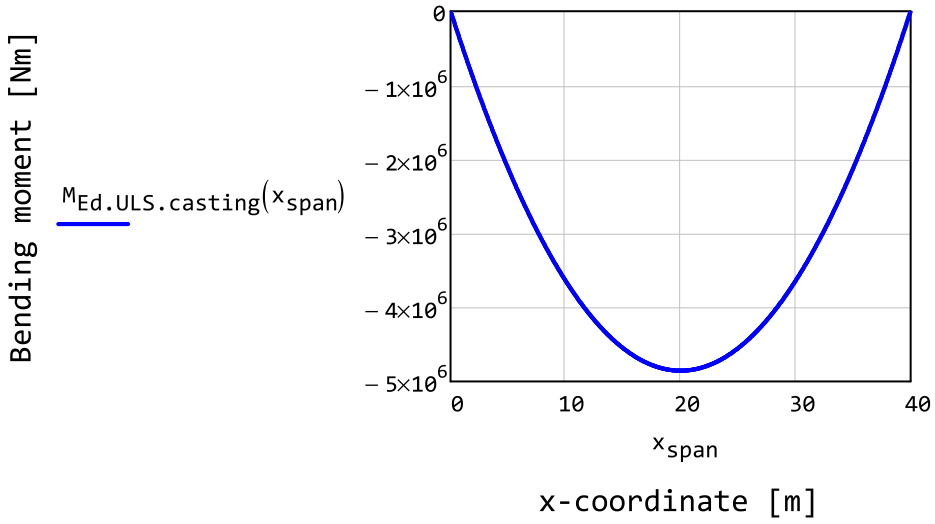

2.2.6 Load combinations in serviceability limit state

Calculation of the load combinations in the serviceablity limit state.

Service phase

Bending moment distribution in the servicability limit state (SLS), for the service phase. Note that maximum bending moment is obtained when the load is placed at the point of measurement for the traffic loads.
Currently the bending in the serviceability limit state is only used in the calculation of deflections or for calculations related to the deformation. An example of an related calculation is the calculation of stress in the main I-girder in order to determine the secant modulus of elasticity to be used in the calcuation of deflections.
For calculations of deflections the frequent load combination is recomended in Eurocode 1993-2: paragraph 7.8.1-(2). The frequent load combination is given in Eurocode 1990-A1: Table A2.6.

$$M_{Ed.SLS.composite}(x_{span}, x_{load}) := \left| \begin{array}{l} M_0 \leftarrow M_{E.self.composite}(x_{span}) \\ M_1 \leftarrow \psi_{traffic.1} \cdot M_{E.model1.total}(x_{span}, x_{load}) \\ M_2 \leftarrow \psi_{wind.2} \cdot M_{E.wind.composite}(x_{span}) \\ \sum_{i=0}^{2} M_i \end{array} \right.$$

Bending moment distribution along the bridge span, when the point load from load model 1 is placed in the middle of the span.

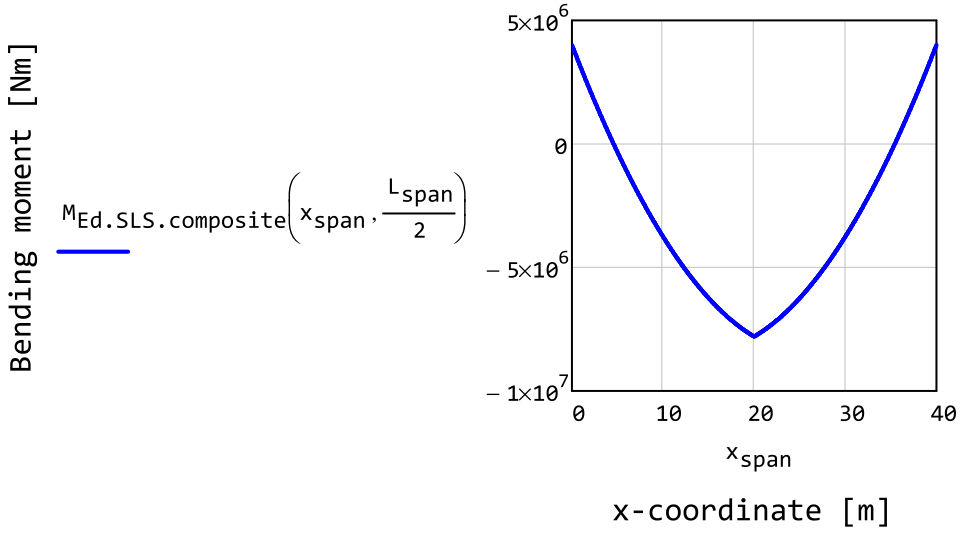

Maximum bending moment at the middle of the span is obtained when the axle load also is placed at the middle if the span.

$$M_{Ed.SLS.composite}\left(\frac{L_{span}}{2}, \frac{L_{span}}{2}\right) = -7.8 \cdot MN \cdot m$$

2.3 Bending moment resistance

In this document the bending moment resistance of the bridge is calculated.

This chapter encompasses the following subchapters:
2.3.1 Bending resistance of the composite cross-section in the ultimate limit state, elastic
2.3.2 Bending resistance of the composite cross-section in the ultimate limit state, plastic
2.3.3 Bending resistance of the main I-girders in the ultimate limit state at casting
2.3.4 Stress distribution due to bending in the serviceability limit state
2.3.5 Miscellaneous moment resistances

2.3.1 Bending resistance of the composite cross-section in the ultimate limit state, elastic analysis

For the bending resistance of the composite cross-section in the ulimate limit state the elastic resistance of the cross-section will be considered. Note that due to the precambering the main I-girders will carry more load than the concrete in the composite structure when elastic analysis is used.

Note that for stainless steel it is given by Eurocode 1993-1-4: Paragraph 5.1-(3) that global plastic analysis may not be used unless experimental results support the assumptions made in calculations. Special note is taken to the effect of strain hardening on the loads carried by the joints.

Furthermore, pressumably the upper flange of the main I-girders is in cross-section class 3 or 4. According to Eurocode 1994-2: Paragraph 5.5.1-(3) a part that is restrained by the concrete deck may be taken as a more favourable class. This is only applicable if the performance has been proved. Therefore it is henceforth assumed to be the case for the upper flange of the main I-girders, which will be taken as cross-section class 3 for the composite section.

In accordance with Eurocode 1994-2: paragraph 6.1.2.5-(1) and 6.1.2-(1) the effective cross-section is given by Eurocode 1994-2: Section 5.4.1.2.

In accordance with Eurocode 1994-2: Paragraph 6.2.1.1 all concrete in tension should be neglected.

Stress and utilisation in the composite cross-section, elastic analysis

In accordance with Eurocode 1994-2: paragraph 6.2.1.5-(2) the stress for the concrete in compression should be limited to the design cylinder compressive strength when considering the composite cross-section. Note that the effect of reinforcement is neglected for concrete in compression. Since the stress is derived for steel it must be converted into equivalent concrete stress.
The moment that is carried by the composite cross-section and the concrete is only the reduced part of the moment in the ultimate limit state. The reduced part of the moment does not consider the self-weight since it is carried only by the main I-girders. Furthermore, for the concrete it is sufficient to check only case A since this gives a larger contribution from the imposed loads.

$$\sigma_{Ed.ULS.concrete}(x_{span}) := \left| \begin{array}{l} z \leftarrow z_{composite.negative}(x_{span}, z_{top.deck.slab.mid}(x_{span})) \\ \sigma \leftarrow \left(\frac{M_{Ed.ULS.imposed.negative}(x_{span}, "A")}{I_{composite.negative}(x_{span})} \cdot z \right) \\ \sigma \cdot \alpha_{steel.concrete} \quad \text{if } \sigma < 0Pa \\ 0Pa \quad \text{otherwise} \end{array} \right.$$

Utilisation ratio. Since the concrete is only considered when in compression the utilisation will go to zero close to the supports. Note that the absolute value of the stress is used.

$$u_{ULS.bending.concrete}(x_{span}) := \frac{|\sigma_{Ed.ULS.concrete}(x_{span})|}{f_{cd.concrete}}$$

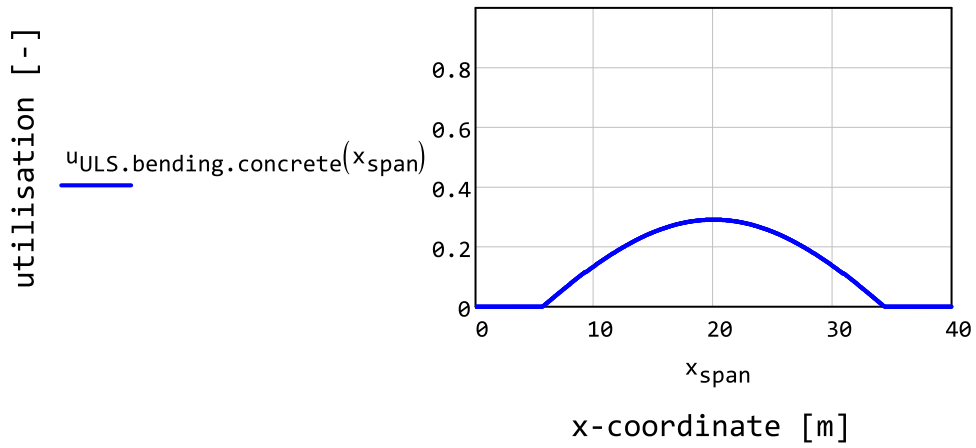

Calculation of the steel stress in the lowermost and uppermost part of the main I-girders respectively. In accordance with Eurocode 1994-2: paragraph 6.2.1.5-(2) the stress in the structural steel should be limited to the design yield strength when considering the composite cross-section.
Note that the main I-girders carry the entire self-weight. In addition, the steel is part of the compoiste cross-section and therefore the main I-girders carries part of the imposed loads as well.
For the steel section there are three relevant load combinarions in the ultimate limit state. For negative moment the self-weight is unfavourable and the imposed loads or the self-weight can be chosen to dominate. This is considered with equation 10.6a and 10.6b respectively.
On the other hand, for positive moments the self-weight is always favourable. Therefore only equation 10.6b needs to be applied since it gives the largest contribution from imposed loads.
Here:
composite indicates with the value 1 that the composite cross-section is considered
zglobal is the global z-coordinate for the considered part
zmain is the local z-coordinate with regard to bending of just the main I-girders at casting
z_{AB} is the local z-coordinate with regard to negative bending of the composite cross-section
z_C is the local z-coordinate with regard to positive bending of the composite cross-section
$\sigma_{main.A/B/C}$ is the stress with regard to respective load combination
$\sigma_{comp.A/B/C}$ is the stress with regard to respective load combination

$$\sigma_{Ed.ULS.steel}(x_{span}, part) :=$$

composite ← 1

$z_{lower} \leftarrow z_{bottom.main.flange.lower}(x_{span})$

$z_{upper} \leftarrow z_{top.main.flange.upper}(x_{span})$

$z_{global} \leftarrow z_{lower}$ if part = "lower"

$z_{global} \leftarrow z_{upper}$ if part = "upper"

$z_{main} \leftarrow z_{main.beam.neg}(x_{span}, z_{global}, composite)$

$z_{AB} \leftarrow z_{composite.negative}(x_{span}, z_{global})$

$z_C \leftarrow z_{composite.positive}(x_{span}, z_{global})$

$$\sigma_{main.A} \leftarrow \frac{M_{Ed.ULS.selfweight}(x_{span}, "A-")}{I_{main.beam.neg}(x_{span}, composite)} \cdot z_{main}$$

$$\sigma_{main.B} \leftarrow \frac{M_{Ed.ULS.selfweight}(x_{span}, "B-")}{I_{main.beam.neg}(x_{span}, composite)} \cdot z_{main}$$

$$\sigma_{main.C} \leftarrow \frac{M_{Ed.ULS.selfweight}(x_{span}, "B+")}{I_{main.beam.neg}(x_{span}, composite)} \cdot z_{main}$$

$$\sigma_{comp.A} \leftarrow \frac{M_{Ed.ULS.imposed.negative}(x_{span}, "A")}{I_{composite.negative}(x_{span})} \cdot z_{AB}$$

$$\sigma_{comp.B} \leftarrow \frac{M_{Ed.ULS.imposed.negative}(x_{span}, "B")}{I_{composite.negative}(x_{span})} \cdot z_{AB}$$

$$\sigma_{comp.C} \leftarrow \frac{M_{Ed.ULS.imposed.positive}(x_{span})}{I_{composite.positive}(x_{span})} \cdot z_C$$

$\sigma_A \leftarrow \sigma_{main.A} + \sigma_{comp.A}$

$\sigma_B \leftarrow \sigma_{main.B} + \sigma_{comp.B}$

$\sigma_C \leftarrow \sigma_{main.C} + \sigma_{comp.C}$

$\max(|\sigma_A|, |\sigma_B|, |\sigma_C|)$

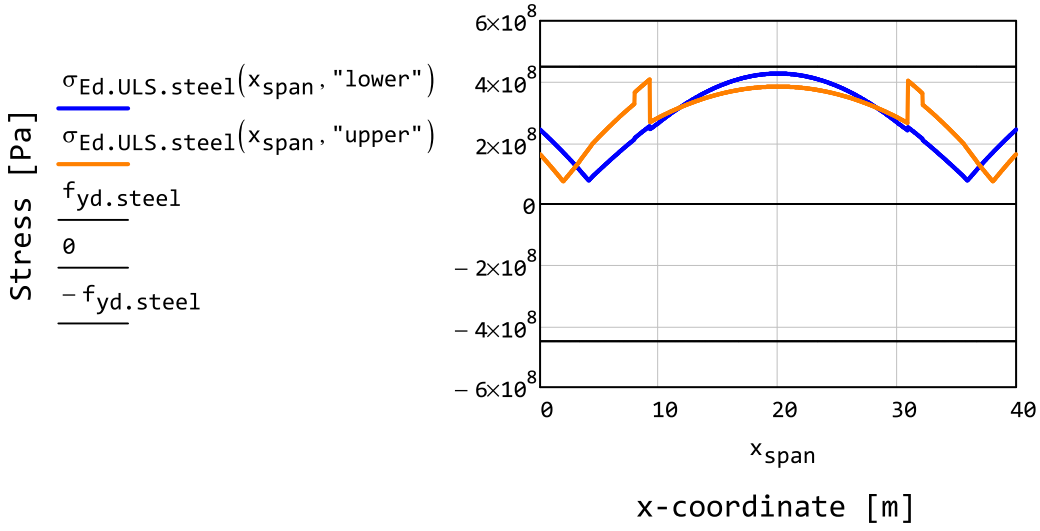

Utilisation ratio for the steel in the ultimate limit state. Here only the maximum stress is of interest, it is not of interest if it is tension or compression. The maximum stress in the steel can be found in the lower or upper flange.

$$u_{ULS.bending.steel}(x_{span}) := \left| \begin{array}{l} \sigma_{lower} \leftarrow \sigma_{Ed.ULS.steel}(x_{span}, "lower") \\ \sigma_{upper} \leftarrow \sigma_{Ed.ULS.steel}(x_{span}, "upper") \\ \dfrac{\max(\sigma_{lower}, \sigma_{upper})}{f_{yd.steel}} \end{array} \right.$$

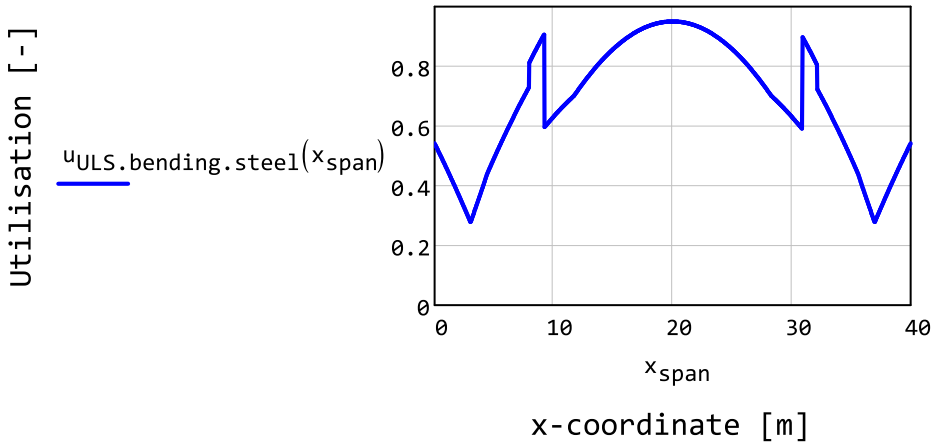

Calculation of the maximum stress in the reinforcement. In accordance with Eurocode 1994-2: paragraph 6.2.1.5-(2) the stress the reinforcement in tension should be limited to f_{sd} when considering the composite cross-section. Since the stress is derived for steel it must be converted into equivalent stress in the reinforcement.
Note that the effect of reinforcement is neglected for concrete in compression, hence that no check is performed for negative bending moment. For positive moments the self-weight is always favourable. Therefore only equation 10.6b needs to be applied since it gives the largest contribution from imposed loads.
Here:
z_{global} is the global z-coordinate for the uppermost part of the concrete deck
z^{local} is the local z-coordinate for the uppermost part of the concrete deck
σ is the stress in the concrete in the uppermost part of the concrete deck
and
$\alpha_{steel.reinf}$ is the factor transforming corresponding steel stress to concrete stress

$$\sigma_{Ed.ULS.reinf}(x_{span}) := \left| \begin{array}{l} z_{global} \leftarrow z_{reinf.slab.upper.uppermost}(x_{span}) \\ z_{local} \leftarrow z_{composite.positive}(x_{span}, z_{global}) \\ \sigma \leftarrow \dfrac{M_{Ed.ULS.imposed.positive}(x_{span})}{I_{composite.positive}(x_{span})} \cdot z_{local} \cdot \alpha_{steel.rein} \\ \sigma \quad \text{if } \sigma > 0Pa \\ 0Pa \quad \text{otherwise} \end{array} \right.$$

Utilisation ratio

$$u_{ULS.bending.reinf}(x_{span}) := \frac{\left|\sigma_{Ed.ULS.reinf}(x_{span})\right|}{f_{yd.reinf}}$$

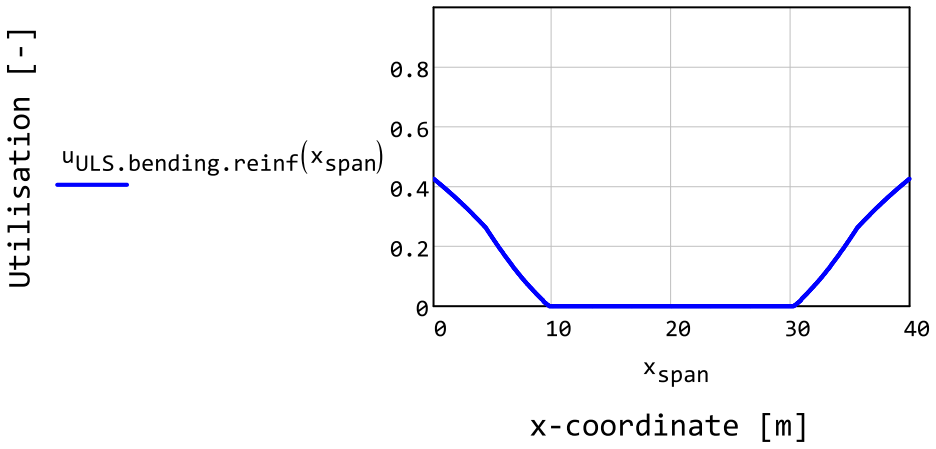

Maximum utilisation ratio

Maximum utilisation ratio in the sections along the span with regard to bending of the composite cross-section in the ultimate limit state.

$$u_{ULS.bending.composite.elastic}(x_{span}) := \left| \begin{array}{l} u_{concrete} \leftarrow u_{ULS.bending.concrete}(x_{sp} \\ u_{steel} \leftarrow u_{ULS.bending.steel}(x_{span}) \\ u_{reinf} \leftarrow u_{ULS.bending.reinf}(x_{span}) \\ \max(u_{concrete}, u_{steel}, u_{reinf}) \end{array} \right.$$

Maximum utilisation ratio with regard to bending of the composite cross-section in the ultimate limit state.

$$u_{ULS.bending.composite.elastic.max} := \left| \begin{array}{l} X_{span} \leftarrow \text{range}_{span}(100) \\ \text{for } x_{step} \in X_{span} \\ \quad \left| \begin{array}{l} u \leftarrow u_{ULS.bending.composite.elastic}(x_{step}) \\ u_{max} \leftarrow \max(u, u_{max}) \end{array} \right. \\ u_{max} \end{array} \right.$$

$$u_{ULS.bending.composite.elastic.max} = 0.95$$

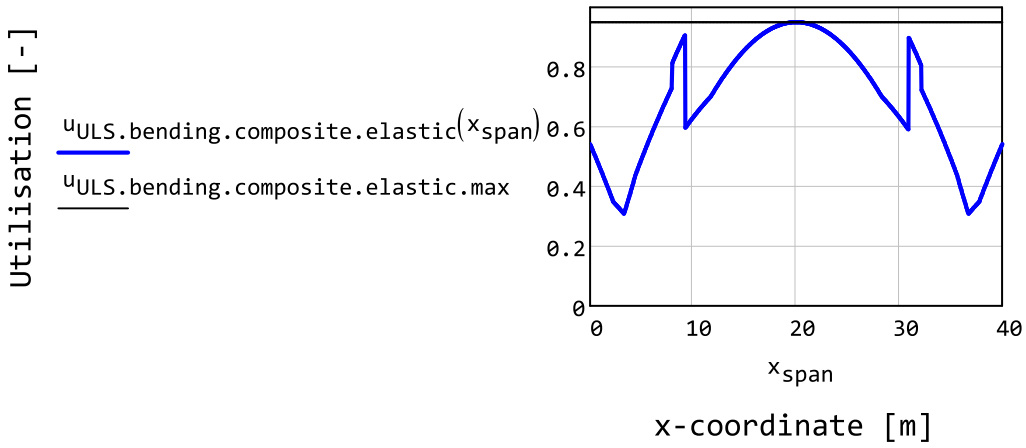

2.3.2 Bending resistance of the composite cross-section in the ultimate limit state, plastic analysis

For the bending resistance of the composite cross-section in the ulimate limit state the plastic resistance of the cross-section will be considered.

In addition, the plastic bending resistance of the flanges of the composite cross-section is of interest when calculating the combined effect of shear force and bending moment. Therefore the following calculations will be performed with an additional input that will determine if the whole cross-section or just the flanges will be considered

For stainless steel it is given by Eurocode 1993-1-4: Paragraph 5.1-(3) that global plastic analysis may not be used unless experimental results support the assumptions made in calculations. Special note is taken to the effect of strain hardening on the loads carried by the joints. However, in this analysis it is simply assumed that plastic analysis can be used for this stainless steel section. Note however, that this may not be the case and that further investigation is required.

In accordance with Eurocode 1994-2: Paragraph 6.2.1.1 all concrete in tension should be neglected.

Effective width of the steel in global analysis is assumed to be unreduced. This assumption is made to simplify the calculations since the assumption should remain true for almost any choice of bridge span.

$$assumption_{steel\_unreduced} = \text{"true"}$$

Concrete in compression, negative moment

Duplex stainless steel is used in the steel section, and since it has similar strength and mechanical properties to that of the structural carbon steel S460 the rules in Eurocode 1994-2: Paragraph 6.2.1.2-(2) will be used. According to the rules the plastic moment should be reduced by a β-value. Alternativly, when the β-factor is not applicable, the plastic analysis should be replaced with a elastic or non-linear analysis.

Eurocode 1994-2: Paragraph 6.2.1.2-(1) gives that:

- Reinforcement in compresion may be neglected.
- The effective area of the longitudinal reinforcement may be stressed to the design yield strength.
- The effective area of the structural steel may be stressed to the design yield strength in both tension and compression.
- The effective area of the concrete may be stressed to 0.85 of the design cylinder compressive strength of the concrete. The stress should be taken as constant over the area of the compressed concrete.

Calculation of the plastic neutral axis of the composite cross-section when the concrete is in compression, negative moment. Note that the neutral axis is assumed to never be in the upper triangular part of the concrete slab.
Here:
low_i is the global z-coordinate of the bottom of each part
$high_i$ is the global z-coordinate for the top of each part
centre is the global z-coordinate for the centre of all parts
F_i is the resulting force in plastic bending for each part
Equilibrium(z) is the force balance for the cross-section
and
root is a function that finds the where given function is zero.
legend
0 - the lower flange of the main I-girder
1 - the web of the main I-girder
2 - the upper flange of the main I-girder
3 - the square part of the effective concrete slab
4 - the triangular part of the effective concrete slab
5 - the effective part of the edge beam of the concrete deck

$$z_{NA.composite.plastic.neg}(x_{span}) :=$$

$$t_{tmp} \leftarrow t_{deck.slab.effective.outer}$$

$$bottom_0 \leftarrow z_{bottom.main.flange.lower}(x_{span})$$

$$bottom_1 \leftarrow z_{bottom.main.web}(x_{span})$$

$$bottom_2 \leftarrow z_{top.main.web}(x_{span})$$

$$bottom_3 \leftarrow z_{top.main.flange.upper}(x_{span})$$

$$bottom_4 \leftarrow z_{top.main.flange.upper}(x_{span}) + t_{tmp}$$

$$bottom_5 \leftarrow z_{bottom.deck.beam}(x_{span})$$

$$top_0 \leftarrow z_{bottom.main.web}(x_{span})$$

$$top_1 \leftarrow z_{top.main.web}(x_{span})$$

$$top_2 \leftarrow z_{top.main.flange.upper}(x_{span})$$

$$top_3 \leftarrow z_{top.main.flange.upper}(x_{span}) + t_{tmp}$$

$$top_4 \leftarrow top_3 + t_{deck.slab.effective.diff}$$

$$top_5 \leftarrow z_{top.deck.slab.edge}(x_{span})$$

$$centre \leftarrow \frac{top + bottom}{2}$$

$$F_0 \leftarrow f_{yd.steel} \cdot A_{main.flange.lower}(x_{span})$$

$$F_1 \leftarrow f_{yd.steel} \cdot A_{main.web}(x_{span})$$

$$F_2 \leftarrow f_{yd.steel} \cdot A_{main.flange.upper}(x_{span})$$

$$F_3 \leftarrow A_{deck.slab.effective.square} \cdot 0.85 \cdot f_{cd.concr}$$

$$F_4 \leftarrow A_{deck.slab.effective.triangle} \cdot 0.85 \cdot f_{cd.con}$$

$$F_5 \leftarrow A_{deck.beam.effective} \cdot 0.85 \cdot f_{cd.concrete}$$

$$tmp(z, i) \leftarrow \max\left[\min\left[\left(2 \cdot \frac{z - centre_i}{top_i - bottom_i}\right), 1\right], -1\right]$$

$$Equilibrium(z) \leftarrow \sum_{i=0}^{5} \left(F_i \cdot tmp(z, i)\right)$$

$$root\left(Equilibrium(z), z, bottom_0, bottom_4\right)$$

Location of the plastic neutral axis when the composite cross-section is considered.

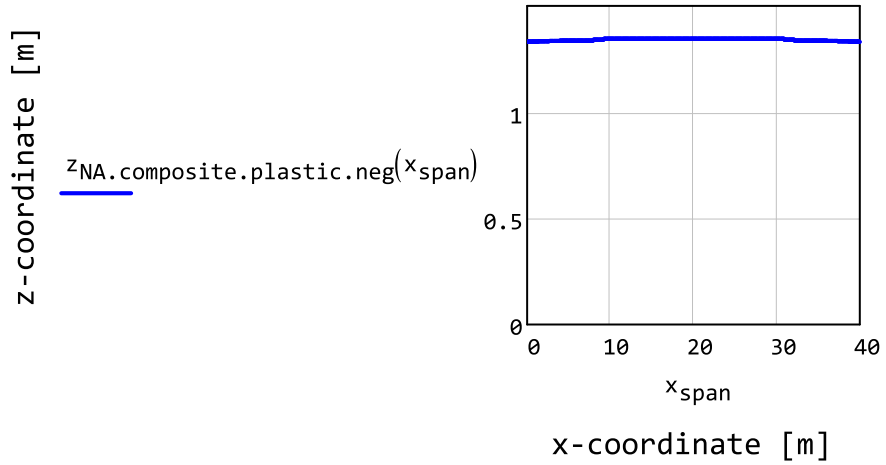

Reduction factor for the plastic moment capacity for the composite cross-section in negative bending. Given by Eurocode 1994-2: paragraph 6.2.1.2-(2).

$$\beta_{reduction}(x_{span}) := \left| \begin{array}{l} t_0 \leftarrow t_{deck.slab.effective.outer} \\ t_1 \leftarrow t_{deck.slab.effective.diff} \\ z_{uppermost} \leftarrow z_{top.main.flange.upper}(x_{span}) + t_0 + t_1 \\ x_{plastic} \leftarrow z_{uppermost} - z_{NA.composite.plastic.neg}(x_{span}) \\ h_{structure} \leftarrow z_{uppermost} - z_{bottom.main.flange.lower}(x_{span}) \\ a \leftarrow \dfrac{x_{plastic}}{h_{structure}} \\ 1 \quad \text{if } a < 0.15 \\ 1.09 - a \cdot 0.6 \quad \text{if } 0.15 \le a \le 0.4 \\ 0 \quad \text{if } a > 0.4 \end{array} \right.$$

Note that the factor should be applied only for S420 and S460, however we will also apply it to EN1.4162 since it have very similar properties to S460 carbon steel.

$$steelgrade = \text{"EN1.4162"}$$

$$\beta_{reduction.plastic}(x_{span}) := \left| \begin{array}{ll} \beta_{reduction}(x_{span}) & \text{if } steelgrade = \text{"S460"} \\ \beta_{reduction}(x_{span}) & \text{if } steelgrade = \text{"EN1.4162"} \\ 1 & \text{if } steelgrade = \text{"carbon"} \end{array} \right.$$

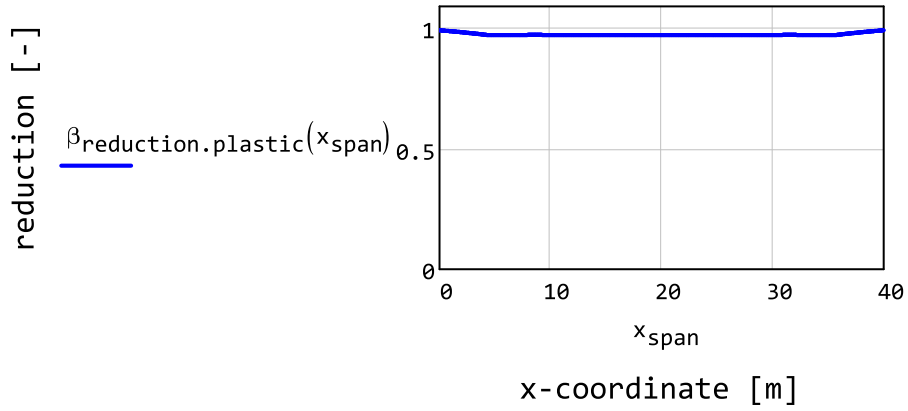

Calculation of the plastic bending capacity of the composite cross-section when the concrete is in compression, negative moment. Note that the neutral axis is assumed to never be in the upper triangular part of the concrete slab.
Furthermore, to reduce the amount of calculations the moment capacity can be obtained either for the entire cross-section or for the flanges only. To calculate the entire cross-section the second argument should be one. The resistance of the flanges is used for the interaction between shear force and bending moment.
Here:
z_{NA} is the global z-ccordinate for the plastic neutral axis
F_i is the resulting force in plastic bending for each part
d_i is the distance from the centroid of each part to the plastic neutral axis

$$M_{Rd.composite.plastic.neg}(x_{span}, A) :=$$
$$tmp \leftarrow 0.85 \cdot f_{cd.concrete}$$
$$x \leftarrow x_{span}$$
$$z_{NA} \leftarrow z_{NA.composite.plastic.neg}(x)$$
$$F_0 \leftarrow f_{yd.steel} \cdot A_{main.flange.lower}(x)$$
$$F_1 \leftarrow f_{yd.steel} \cdot A_{main.web}(x) \quad \text{if } A = 1$$
$$F_2 \leftarrow f_{yd.steel} \cdot A_{main.flange.upper}(x)$$
$$F_3 \leftarrow A_{deck.slab.effective.square} \cdot tmp$$
$$F_4 \leftarrow A_{deck.slab.effective.triangle} \cdot tmp$$
$$F_5 \leftarrow A_{deck.beam.effective} \cdot 0.85 \cdot f_{cd.concrete}$$
$$d_0 \leftarrow z_{centre.main.flange.lower}(x) - z_{NA}$$
$$d_1 \leftarrow z_{centre.main.web}(x) - z_{NA}$$
$$d_2 \leftarrow z_{centre.main.flange.upper}(x) - z_{NA}$$
$$d_3 \leftarrow z_{centre.deck.slab.effective.sqr}(x) - z_{NA}$$
$$d_4 \leftarrow z_{centre.deck.slab.effective.tri}(x) - z_{NA}$$
$$d_5 \leftarrow z_{centre.deck.beam}(x) - z_{NA}$$
$$\sum_{i=0}^{5} \left(F_i \cdot |d_i|\right) \cdot \beta_{reduction.plastic}(x)$$

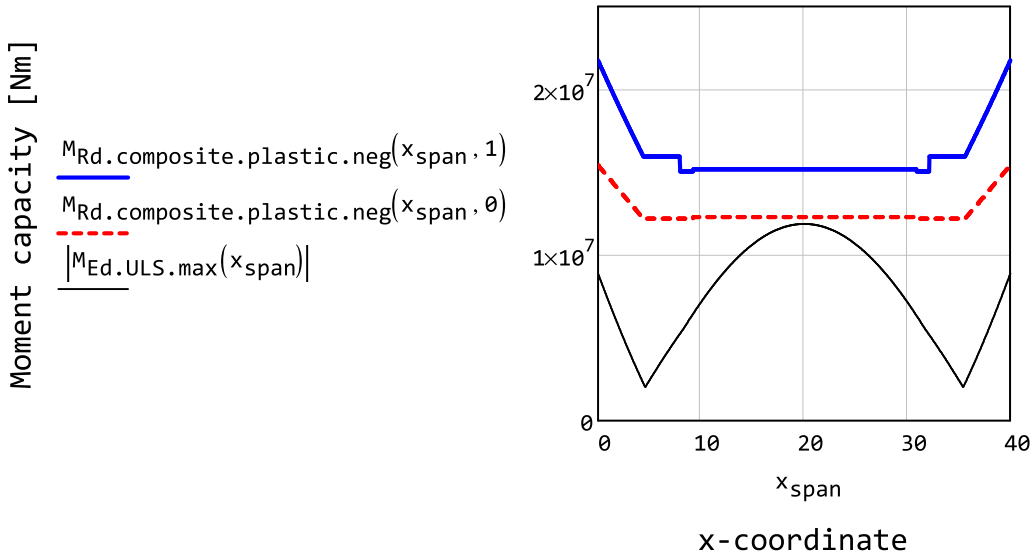

Concrete in tension, positive moment

Eurocode 1994-2: Paragraph 6.2.1.2-(1) gives that:

- The effective area of the longitudinal reinforcement may be stressed to the design yield strength.
- The effective area of the structural steel may be stressed to the design yield strength in both tension and compression.
- The effective area of the concrete may be stressed to 0.85 of the design cylinder compressive strength of the concrete. The stress should be taken as constant over the area of the compressed concrete.

Calculation of the plastic neutral axis of the composite cross-section when the concrete is tension, positive moment. Note that the reinforcement in the edge beam si simplified to be evenly distributed through out the height of the edge beam. Note that the lower reinforcement in the slab is given a height so that the calculations may be performed without dividing by zero.
Here:
low_i is the global z-coordinate of the bottom of each part
$high_i$ is the global z-coordinate for the top of each part
centre is the global z-coordinate for the centre of all parts
F_i is the resulting force in plastic bending for each part
Equilibrium(z) is the force balance for the cross-section
and
root is a function that finds the where given function is zero.

$$z_{\mathrm{NA.composite.plastic.positive}}(x_{\mathrm{span}}) :=$$

$\rho_3 \leftarrow \rho_{\mathrm{reinf.slab.lower}}$

$\rho_4 \leftarrow \rho_{\mathrm{reinf.slab.upper}}$

$\rho_5 \leftarrow \rho_{\mathrm{reinf.beam}}$

$\mathrm{bottom}_0 \leftarrow z_{\mathrm{bottom.main.flange.lower}}(x_{\mathrm{span}})$

$\mathrm{bottom}_1 \leftarrow z_{\mathrm{bottom.main.web}}(x_{\mathrm{span}})$

$\mathrm{bottom}_2 \leftarrow z_{\mathrm{top.main.web}}(x_{\mathrm{span}})$

$\mathrm{bottom}_3 \leftarrow z_{\mathrm{reinf.slab.lower}}(x_{\mathrm{span}}) - 8\mathrm{mm}$

$\mathrm{bottom}_4 \leftarrow z_{\mathrm{reinf.slab.upper.lowermost}}(x_{\mathrm{spa}}$

$\mathrm{bottom}_5 \leftarrow z_{\mathrm{bottom.deck.beam}}(x_{\mathrm{span}})$

$\mathrm{top}_0 \leftarrow z_{\mathrm{bottom.main.web}}(x_{\mathrm{span}})$

$\mathrm{top}_1 \leftarrow z_{\mathrm{top.main.web}}(x_{\mathrm{span}})$

$\mathrm{top}_2 \leftarrow z_{\mathrm{top.main.flange.upper}}(x_{\mathrm{span}})$

$\mathrm{top}_3 \leftarrow z_{\mathrm{reinf.slab.lower}}(x_{\mathrm{span}}) + 8\mathrm{mm}$

$\mathrm{top}_4 \leftarrow z_{\mathrm{reinf.slab.upper.uppermost}}(x_{\mathrm{span}})$

$\mathrm{top}_5 \leftarrow z_{\mathrm{top.deck.slab.edge}}(x_{\mathrm{span}})$

$$\mathrm{centre} \leftarrow \frac{\mathrm{top} + \mathrm{bottom}}{2}$$

$F_0 \leftarrow f_{\mathrm{yd.steel}} \cdot A_{\mathrm{main.flange.lower}}(x_{\mathrm{span}})$

$F_1 \leftarrow f_{\mathrm{yd.steel}} \cdot A_{\mathrm{main.web}}(x_{\mathrm{span}})$

$F_2 \leftarrow f_{\mathrm{yd.steel}} \cdot A_{\mathrm{main.flange.upper}}(x_{\mathrm{span}})$

$F_3 \leftarrow b_{\mathrm{deck.slab.effective}} \cdot \rho_3 \cdot f_{\mathrm{yd.reinf}}$

$F_4 \leftarrow b_{\mathrm{deck.slab.effective}} \cdot \rho_4 \cdot f_{\mathrm{yd.reinf}}$

$F_5 \leftarrow b_{\mathrm{deck.beam.effective}} \cdot \rho_5 \cdot f_{\mathrm{yd.reinf}}$

$$d(z, i) \leftarrow \max\left[\min\left[\left(2 \cdot \frac{z - \mathrm{centre}_i}{\mathrm{top}_i - \mathrm{bottom}_i}\right), 1\right], -1\right]$$

$$\mathrm{Equilibrium}(z) \leftarrow \sum_{i=0}^{5} \left(F_i \cdot d(z, i)\right)$$

$$\mathrm{root}\left(\mathrm{Equilibrium}(z), z, \mathrm{bottom}_0, \mathrm{bottom}_4\right)$$

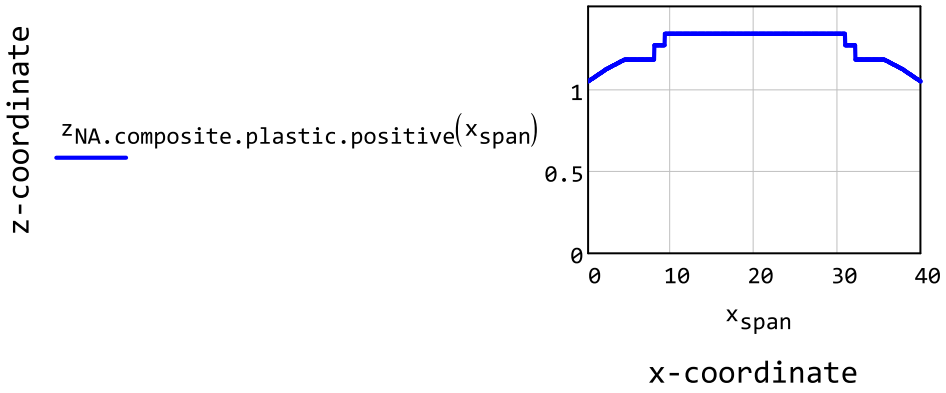

Calculation of the plastic bending capacity of the composite cross-section when the concrete is in compression, positive moment. Note that the neutral axis is assumed to never be in the upper triangular part of the concrete slab.
Furthermore, to reduce the amount of calculations the moment capacity can be obtained either for the entire cross-section or for the flanges only. To calculate the entire cross-section the second argument should be set to 1. The resistance of the flanges is used for the interaction between shear force and bending moment.
Here:
z_{NA} is the global z-ccordinate for the plastic neutral axis
F_i is the resulting force in plastic bending for each part
d_i is the distance from the centroid of each part to the plastic neutral axis

$$M_{Rd.composite.plastic.pos}(x_{span}, web) :=$$

$$\rho_3 \leftarrow \rho_{reinf.slab.lower}$$

$$\rho_4 \leftarrow \rho_{reinf.slab.upper}$$

$$\rho_5 \leftarrow \rho_{reinf.beam}$$

$$z_{NA} \leftarrow z_{NA.composite.plastic.positive}(x_{span})$$

$$F_0 \leftarrow f_{yd.steel} \cdot A_{main.flange.lower}(x_{span})$$

$$F_1 \leftarrow f_{yd.steel} \cdot A_{main.web}(x_{span}) \quad \text{if } web = 1$$

$$F_2 \leftarrow f_{yd.steel} \cdot A_{main.flange.upper}(x_{span})$$

$$F_3 \leftarrow b_{deck.slab.effective} \cdot \rho_3 \cdot f_{yd.reinf}$$

$$F_4 \leftarrow b_{deck.slab.effective} \cdot \rho_4 \cdot f_{yd.reinf}$$

$$F_5 \leftarrow b_{deck.beam.effective} \cdot \rho_5 \cdot f_{yd.reinf}$$

$$d_0 \leftarrow z_{centre.main.flange.lower}(x_{span}) - z_{NA}$$

$$d_1 \leftarrow z_{centre.main.web}(x_{span}) - z_{NA}$$

$$d_2 \leftarrow z_{centre.main.flange.upper}(x_{span}) - z_{NA}$$

$$d_3 \leftarrow z_{reinf.slab.lower}(x_{span}) - z_{NA}$$

$$d_4 \leftarrow z_{reinf.slab.upper}(x_{span}) - z_{NA}$$

$$d_5 \leftarrow z_{centre.deck.beam}(x_{span}) - z_{NA}$$

$$\sum_{i=0}^{5} \left(F_i \cdot |d_i|\right)$$

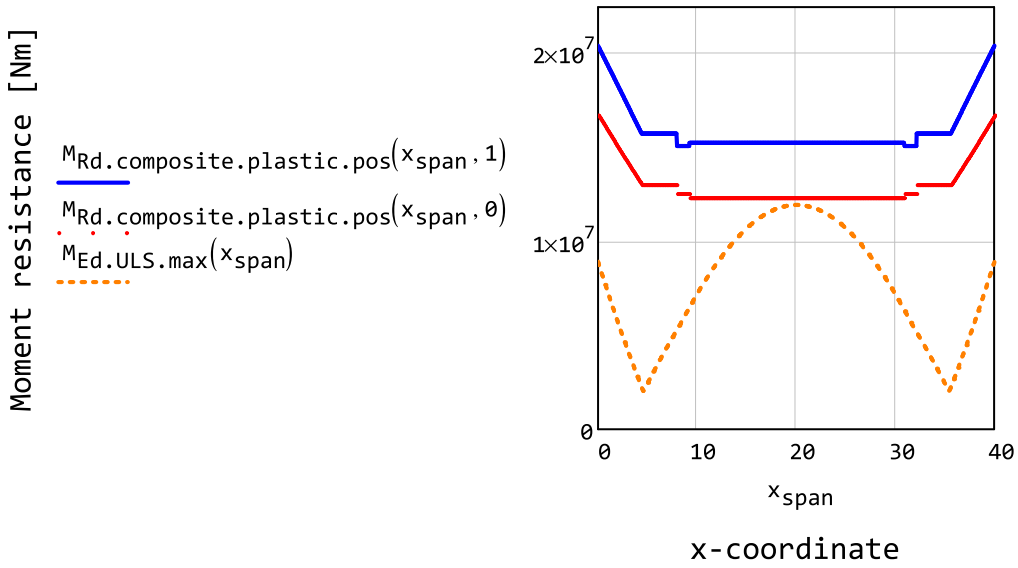

2.3.3 Bending resistance of the main I-girders in the ultimate limit state at casting

At casting of the concrete the entire self-weight of the bridge structure and fromwork is carried by the main I-girders.

According to the specific rules for stainless steel given by Eurocode 1993-1-4: paragraph 5.1-(1) the rules given in Eurocode 1993-1-1: Section 5 and 6 should be applied. However, note that there are some exceptions given in Eurocode 1993-1-4: Section 5.1 that are taken into account where applicable.

Furthermore, in accordance with Eurocode 1993-1-1: paragraph 6.2.1-(4) it is allowed to use elastic moment resistance regardless of cross-section class as long as the reduced cross-section is used for all parts in cross-section class 4.

Moment resistance of a main I-girder without composite action. Given byEurocode 1993-1-1: paragraph 6.2.5-(2)

$$M_{Rd.main.beam}(x_{span}) := \left| \begin{array}{l} composite \leftarrow 0 \\ z_{local}(z_{global}) \leftarrow z_{main.beam.neg}(x_{span}, z_{global}, composite) \\ I \leftarrow I_{main.beam.neg}(x_{span}, composite) \\ d_{lower} \leftarrow \left| z_{local}(z_{bottom.main.flange.lower}(x_{span})) \right| \\ d_{upper} \leftarrow \left| z_{local}(z_{top.main.flange.upper}(x_{span})) \right| \\ d_{maximum} \leftarrow \max(d_{lower}, d_{upper}) \\ \frac{I}{d_{maximum}} \cdot \frac{f_{yd.steel}}{\gamma_{M0.stainless}} \end{array} \right.$$

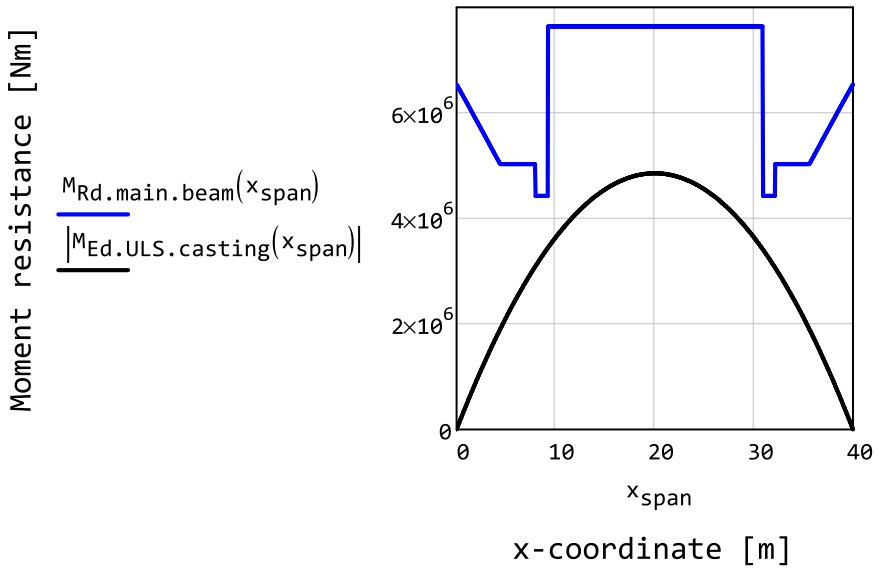

Utilisation ratio for the bending moment resistance in the ultimate limit state for the I-girder at casting. In accordance with Eurocode 1993-1-1: paragraph 6.2.5-(1).

$$u_{ULS.bending.main.elastic}(x_{span}) := \frac{|M_{Ed.ULS.casting}(x_{span})|}{M_{Rd.main.beam}(x_{span})}$$

The maximum value of the utilisation ratio is of interest.

$$u_{ULS.bending.main.elastic.max} := \left| \begin{array}{l} X_{span} \leftarrow 0m, 0.1m .. L_{span} \\ \text{for } x_{step} \in X_{span} \\ \quad \left| \begin{array}{l} u_{tmp} \leftarrow u_{ULS.bending.main.elastic}(x_{step}) \\ u_{max} \leftarrow \max(u_{tmp}, u_{max}) \end{array} \right. \\ u_{max} \end{array} \right.$$

$$u_{ULS.bending.main.elastic.max} = 0.78$$

Variation of utilisation ratio along the bridge span.

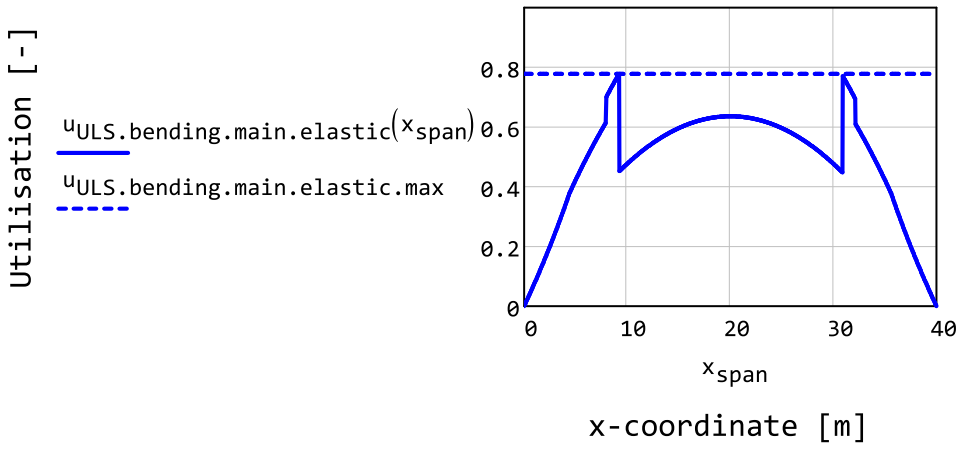

2.3.4 Stress distribution due to bending in the serviceability limit state

The stress level in the upper and lower flange of the main I-girders are of interest when calculating the secant modulus of elasticity. This stress is calculated for the nominal cross-section and the load is for the serviceablity limit state. Note that in accordance with Eurocode 1993-2: paragraph 7.8.1-(2) the frequent load combination should be used for calculations pertaining to deformations.

Note that no regard is taken to the effect of precambering of the beams and the resulting stress differences between steel and concrete. Furthermore, note that since this is a general calculation the fix value of the modulus of elsticity is used when obtaining the second moment of area for the cross-section.

It is assumed that the maximum stress is obtained in the middle of the span when the load is placed in the middle of the span. However, note that since the bridge has fix supports and concrete is neglected when in tension in accordance with Eurocode 1994-2: Paragraph 7.2.1-(5) it is possible to obtain higher stresses at the support section. Nontheless, this is deemed unlikely to occur and the effect should remain negligable.

The moment is negative in the mid span and thus the effective composite cross-section with concrete in compression is used.

The influence of tension stiffening may be neglected in the serviceability limit state in accordance with Eurocode 1994-2: paragraph 7.2.1-(7).

Stress in the lower or upper flange of the main I-girders in the serviceability limit state.
Here:
x_0 is the x-coordinate of the middle of the span
z_0 is the global z-coordinate of the centre of the flange
z is the local z-coordinate of the centre of the flange

$$\sigma_{SLS.bending.flange}(part) := \left| \begin{array}{l} x_0 \leftarrow \frac{L_{span}}{2} \\ z_0 \leftarrow z_{centre.main.flange.lower}(x_0) \quad \text{if } part = "lower" \\ z_0 \leftarrow z_{centre.main.flange.upper}(x_0) \quad \text{if } part = "upper" \\ z_{global} \leftarrow z_{composite.negative}(x_0, z_0) \\ \frac{M_{Ed.SLS.composite}(x_0, x_0)}{I_{composite.negative}(x_0)} \cdot z_{global} \end{array} \right.$$

$$\sigma_{SLS.bending.flange}("lower") = 234.83 \cdot MPa$$

$$\sigma_{SLS.bending.flange}("upper") = -22.85 \cdot MPa$$

2.3.5 Miscellaneous moment resistances

Moment resistance of the flanges of one of the main I-girders.

Plastic moment capactity of the flanges of the main I-girder, which is of interest when calculating the shear buckling resistance contribution from the flanges of the main I-girders. Note that this is a simplification since the upper and lower flange does not need to have the same area. If the flanges does not have the same area the neutral axis will not be found in the middle of the beam, this in turn affects the moment resistance.

$$M_{Rd.main.flanges}(x_{span}) := \frac{d_{main.flanges}(x_{span}) \cdot A_{main.flanges}(x_{span}) \cdot f_{yd.steel}}{2}$$

2.4 Shear resistance

In this document the shear resistance of the bridge is calculated

For the shear resistance of the bridge the main resistance is obtained from the webs of the main steel girders.

Note that in Eurocode 1994-2: paragraph 6.2.2.2-(1) it is stated that the resistance to vertical shear should take into account the contribution from the structural steel section unless the contribution from the reinforced concrete is known. The same applies for shear buckling resistance in accordance with Eurocode 1994-2: paragraph 6.2.2.3-(2). Hence that the contribution from the concrete deck will be neglected in all of the following calculations.

According to Eurocode 1993-1-1: Paragraph 6.2.6-(4) the elastic shear resistance can be calculated. However elastic shear is overly conservative and should only be used when plastic shear cannot be calculated. Since plastic shear resistanc ecan be calculated it will be used instead of elastic shear.

The shear resistance is calculated in accordance with Eurocode 1993-1-1: Section 6.2.6 and the shear buckling resistance is calculated in accordance with Eurocode 1993-1-5: Section 5. Except where replaced by the rules pertaining to stainless steel in Eurocode 1993-1-4.

Note that rigid endposts are assumed in the calculations.

This chapter encompasses the following subchapters:
2.4.1 Plastic shear resistance of the main I-girders
2.4.2 Plastic shear buckling restistance of the main I-girders
2.4.3 Resulting shear resistance of the composite cross-section in the ultimate limit state

2.4.1 Plastic shear resistance of the main I-girders

The shear capacity of the main I-girders. Since plastic design is used the shear resistance is given by Eurocode 1993-1-1: Paragraph 6.2.6-(2). the shear area to be used for the main I-girder is given by Eurocode 1993-1-1: Paragraph 6.2.6-(3). Note that it is only the web of the main I-girder which is considered in the calculation.

$$V_{Rd.main.plastic}(x_{span}) := \frac{\eta_{shear} \cdot A_{main.web}(x_{span}) \cdot \left(\frac{f_{yd.steel}}{\sqrt{3}} \right)}{\gamma_{M0.steel}}$$

2.4.2 Plastic shear buckling restistance of the main I-girders

The plastic shear buckling resistance of the main I-girders should be considered in addition to the plastic shear resistance. The smaller of the two resistances should be used when the shear buckling resistance should be considered. The shear buckling resistance is composed of the contribution from the web and the contribution from the flanges, when applicable.

Shear buckling resistance of the main I-girders, contribution from web

Calculation of the shear buckling resistance of the main I-girders is carries out in accordance with the rules and recomendations given in Eurocode 1993-1-5: Section 5 and Eurocode 1993-1-4: Section 5.6.

Shear buckling coefficient for the web panel of the main I-girders. Given by Eurocode 1993-1-5: annex A.3-(1).

$$k_{\tau.main.web}(x_{span}) := \begin{cases} 5.34 + 4\left(\frac{h_{main.web}(x_{span})}{d_{stiff.vertical}}\right)^2 & \text{if } \frac{d_{stiff.vertical}}{h_{main.web}(x_{span})} \geq 1 \\ 4.00 + 5.34\cdot\left(\frac{h_{main.web}(x_{span})}{d_{stiff.vertical}}\right)^2 & \text{if } \frac{d_{stiff.vertical}}{h_{main.web}(x_{span})} < 1 \end{cases}$$

Elastic plate buckling stress for the web of the main I-girders. Given by Eurocode 1993-1-5: paragraph A.1-(2).

$$\sigma_{E.shear.main.web}(x_{span}) := \frac{\pi^2 \cdot E_{steel} \cdot t_{main.web}(x_{span})^2}{12\cdot\left(1-\nu_{steel}{}^2\right)\cdot h_{main.web}(x_{span})^2}$$

Critical shear stress for the web of the main I-girders. Given by Eurocode 1993-1-5: paragraph 5.3-(3).

$$\tau_{critical.main.web}(x_{span}) := k_{\tau.main.web}(x_{span})\cdot\sigma_{E.shear.main.web}(x_{span})$$

Slenderness parameter for the web of the main I-girders, given by Eurocode 1993-1-5: Paragraph 5.3-(3).

$$\lambda_{slenderness.main.web}(x_{span}) := 0.76\cdot\sqrt{\frac{f_{yd.steel}}{\tau_{critical.main.web}(x_{span})}}$$

Reduction factor for the plate buckling of the web of the main I-girders. Rigid endpost is assumed for the main I-gitders at the support. Given by Eurocode 1993-1-4 Paragraph 5.6-(3) for stainless steel and Eurocode 1993-1-5: Table 5.1 for carbon steel.

For stainless steel

$$\chi_{main.web.stainless}(x_{span}) := \begin{cases} \lambda \leftarrow \lambda_{slenderness.main.web}(x_{span}) \\ \eta_{shear} \quad \text{if } \lambda \leq \frac{0.6}{\eta_{shear}} \\ 0.11 + \frac{0.64}{\lambda} - \frac{0.05}{\lambda^2} \quad \text{otherwise} \end{cases}$$

For carbon steel

$$\chi_{main.web.carbon}(x_{span}) := \left| \begin{array}{l} \lambda \leftarrow \lambda_{slenderness.main.web}(x_{span}) \\ \eta_{shear} \quad \text{if } \lambda < \frac{0.83}{\eta_{shear}} \\ \frac{0.83}{\lambda} \quad \text{if } \frac{0.83}{\eta_{shear}} \le \lambda \le 1.08 \\ \frac{1.37}{0.7 + \lambda} \quad \text{otherwise} \end{array} \right.$$

The reduction factor corresponding to the current steel type is chosen.

$$\chi_{main.web}(x_{span}) := \left| \begin{array}{l} \chi_{main.web.stainless}(x_{span}) \quad \text{if steeltype} = \text{"stainless"} \\ \chi_{main.web.carbon}(x_{span}) \quad \text{if steeltype} = \text{"carbon"} \end{array} \right.$$

Shear buckling resistance from the web is given by Eurocode 1993-1-5: Paragraph 5.2-(1).

$$V_{Rd.main.buckling.web}(x_{span}) := \frac{\chi_{main.web}(x_{span}) \cdot f_{yd.steel} \cdot A_{main.web}(x_{span})}{\sqrt{3} \cdot \gamma_{M1.steel}}$$

Shear buckling resistance of the main girders, contribution from flanges

Contribution from flanges, given by Eurocode 1993-1-5: Paragraph 5.4-(1). For the buckling of a composite section the lower flange is to be used even if the upper steel flange has less resistance, given by Eurocode 1994-2: paragraph 6.2.2.5-(1).

Note that presence of normal force is not taken into account in the current calculations, otherwise the effect is given by Eurocode 1993-1-5: Paragraph 5.4-(2). Additional exception can be found in Eurocode 1994-2: paragraph 6.2.2.5-(1)

The width of the flange on each side of the web should be limited according to Eurocode 1993-1-5: paragraph 5.4-(1).

$$b_{main.flange.buckling}(x_{span}) := \left| \begin{array}{l} b_{max} \leftarrow \left| \begin{array}{l} t_w \leftarrow t_{main.web}(x_{span}) \\ t_f \leftarrow t_{main.flange.lower}(x_{span}) \\ 15 \cdot \varepsilon_{steel} \cdot t_f \cdot 2 + t_w \end{array} \right. \\ \min\left(b_{main.flange.lower}(x_{span}), b_{max}\right) \end{array} \right.$$

Constant used for calculation of the contribution of shear resistance from the flanges. Given by Eurocode 1993-1-4: Paragraph 5.6-(4) for stainless steels and Eurocode 1993-1-5: paragraph 5.4-(1) for carbon steels.
Note that since different steel material is not implemented for the steel section the upper and lower flange has the same design yield strengt. Hence, the design yield strength is not included in the calculation. Furthermore, only the stainless steel have a limitation for the c-factor.

$$c_{shear}(x_{span}) := \begin{| a \leftarrow d_{stiff.vertical} \\ b_f \leftarrow b_{main.flange.buckling}(x_{span}) \\ t_f \leftarrow t_{main.flange.lower}(x_{span}) \\ c_s \leftarrow a \cdot \left(0.17 + \frac{3.5 \cdot b_f \cdot t_f^{\,2}}{t_{main.web}(x_{span}) \cdot h_{main.web}(x_{span})^2}\right) \\ c_c \leftarrow a \cdot \left(0.25 + \frac{1.6 \cdot b_f \cdot t_f^{\,2}}{t_{main.web}(x_{span}) \cdot h_{main.web}(x_{span})^2}\right) \\ c_c \quad \text{if steeltype} = \text{"carbon"} \\ c_s \quad \text{if } c_s \le 0.65 \cdot a \wedge \text{steeltype} = \text{"stainless"} \\ 0.65 \cdot a \quad \text{if } c_s > 0.65 \cdot a \wedge \text{steeltype} = \text{"stainless"}$$

Resulting contribution of shear resistance from the flanges of main I-girders in accordance with Eurocode 1993-1-5: paragraph 5.4-(1). Here it is assumed that the effective area of the flanges is only the steel section and not for the composite section, note that this assumption should be conservative.

$$V_{Rd.main.buckling.flange}(x_{span}) := \begin{| b \leftarrow b_{main.flange.buckling}(x_{span}) \\ t \leftarrow t_{main.flange.lower}(x_{span}) \\ M_{Ed} \leftarrow M_{Ed.ULS.max}(x_{span}) \\ M_{Rd} \leftarrow M_{Rd.main.flanges}(x_{span}) \\ V_{Rd} \leftarrow \frac{b \cdot t^2 \cdot f_{yd.steel}}{c_{shear}(x_{span}) \cdot \gamma_{M1.steel}} \cdot \left[1 - \left(\frac{M_{Ed}}{M_{Rd}}\right)^2\right] \\ V_{Rd} \quad \text{if } \frac{|M_{Ed}|}{M_{Rd}} < 1 \\ 0N \quad \text{otherwise}$$

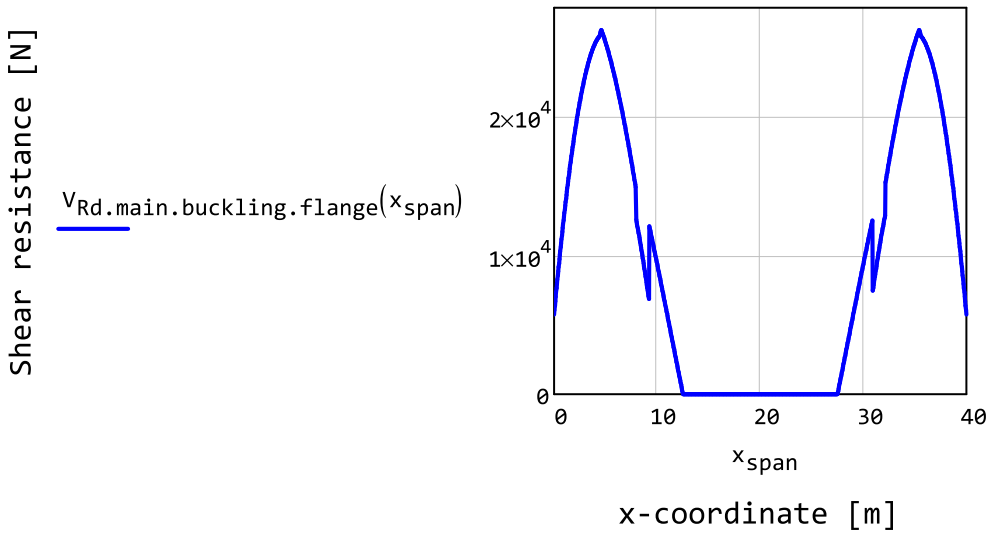

Shear buckling resistance of the main girders, resulting resistance

Shear buckling resistance of a main girder. Given by Eurocode 1993-1-5: Paragraph 5.2-(1).

$$V_{Rd.main.buckling}(x_{span}) := \left| \begin{array}{l} V_R \leftarrow \left| \begin{array}{l} V_{R.0} \leftarrow V_{Rd.main.buckling.web}(x_{span}) \\ V_{R.1} \leftarrow V_{Rd.main.buckling.flange}(x_{span}) \\ V_{R.0} + V_{R.1} \end{array} \right. \\ V_{R.max} \leftarrow \dfrac{\eta_{shear} \cdot f_{yd.steel} \cdot A_{main.web}(x_{span})}{\sqrt{3} \cdot \gamma_{M1.steel}} \\ V_R \quad \text{if } V_R < V_{R.max} \\ V_{R.max} \quad \text{otherwise} \end{array} \right.$$

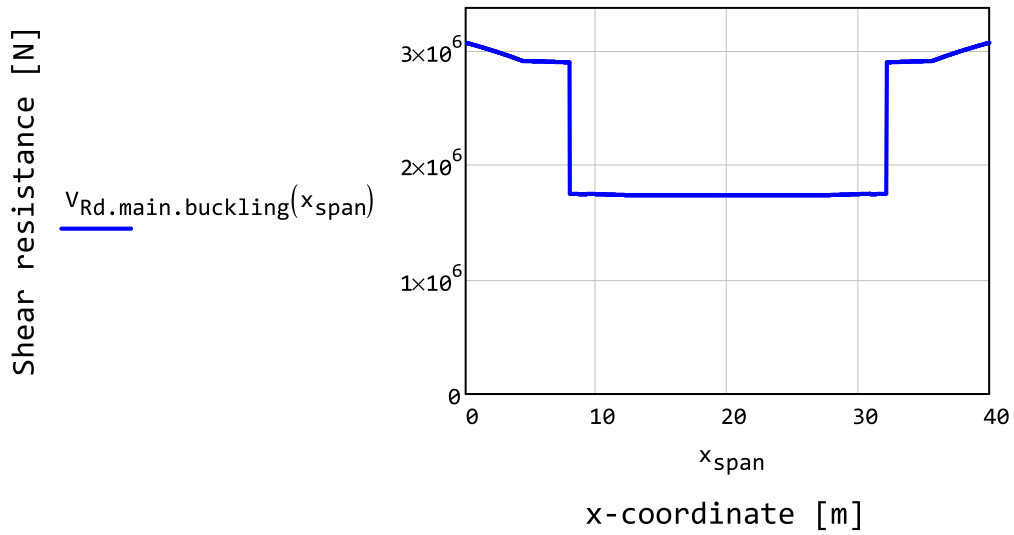

2.4.3 Resulting shear resistance of the composite cross-section in the ultimate limit state

The resulting shear resistance of the main I-girders should be taken as the lowest value of the shear resistance and the shear buckling resistance. Need for shear buckling check is given by Eurocode 1993-1-1: Paragraph 6.2.6-(6).

$$V_{Rd.main}(x_{span}) := \left| \begin{array}{l} V_{pl} \leftarrow V_{Rd.main.plastic}(x_{span}) \\ V_b \leftarrow V_{Rd.main.buckling}(x_{span}) \\ V_{pl} \quad \text{if } \dfrac{h_{main.web}(x_{span})}{t_{main.web}(x_{span})} < 72 \cdot \dfrac{\varepsilon_{steel}}{\eta_{shear}} \\ \min(V_{pl}, V_b) \quad \text{otherwise} \end{array} \right.$$

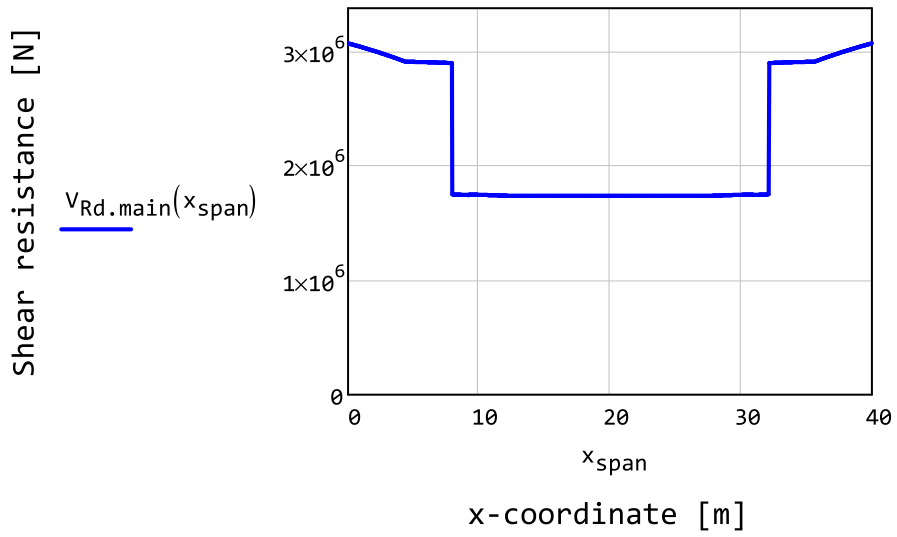

Utilisation ratios

Utilisation ratio for the shear resistance capacity in ultimate limit state. Given by, Eurocode 1993-1-1: Paragraph 6.2.6-(1)

$$u_{ULS.shear.composite}(x_{span}) := \frac{\left|V_{Ed.ULS.composite}(x_{span})\right|}{V_{Rd.main}(x_{span})}$$

The maximum value of the utilisation ratio is of interest.

$$u_{ULS.shear.composite.max} := \left| \begin{array}{l} X_{span} \leftarrow range_{span}(100) \\ \text{for } x_{step} \in X_{span} \\ \quad \left| \begin{array}{l} u_{step} \leftarrow u_{ULS.shear.composite}(x_{step}) \\ u_{max} \leftarrow \max(u_{step}, u_{max}) \end{array} \right. \\ u_{max} \end{array} \right.$$

$$u_{ULS.shear.composite.max} = 83 \cdot \%$$

Variation of utilisation along the bridge span.

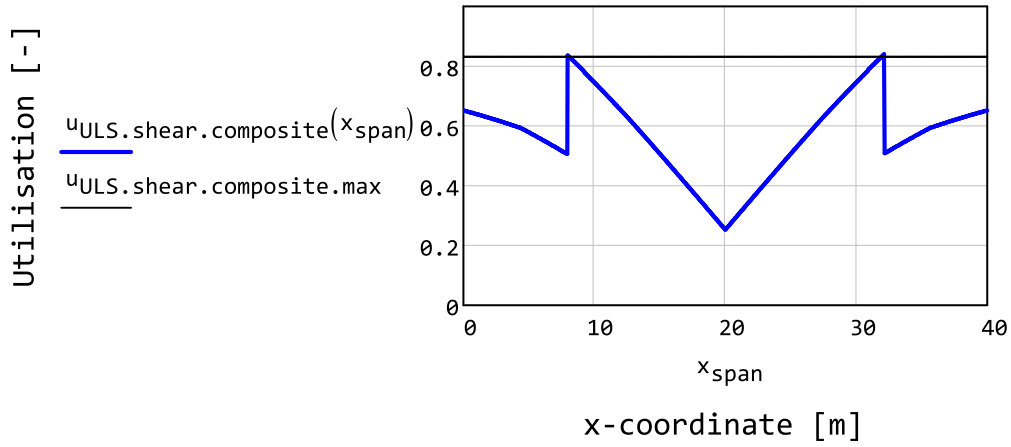

2.5 Interaction between shear and bending

The interaction between shear force and bending moment should be checked. In accordance with Eurocode 1994-2: paragraph 6.2.2.4-(1) the combined effect of shear and bending should be checked when the shear force acting on the cross-section exceeds more than half of the shear capacity of the section.

Note that the interaction is checked assuming that the cross-section is in class 3 or 4. However, note that if a better cross-section class of 1 or 2 is implemented some additional rules will apply. The additional rules are given in Eurocode 1994-2: paragraph 6.2.2.4-(2+4).

Note that currently only the composite cross-section is checked for the interaction between shear force and bending moment.

The calculations are performed with the maximum shear force and the maximum bending moment. Note that maximum shear force and maximum bening moment might not occur at the same time. However, note that this is a conservative assumption which simplifies the calculations and reduces the risk of assuming a too favourable load case.

This chapter encompasses only the following subchapter.

2.5.1 Interaction for the composite cross-section in class 3 and 4

For a composite cross-section in cross-section class 3 or 4 the rules and recomendations given in Eurocode 1993-1-5: Section 7.1 should be used, this in accordance with Eurocode 1994-2: paragraph 6.2.2.4-(3).

The plastic moment capacity of the cross section is calculated so that the correct capacity with regard to positive respectively negative bending is used. Note that here the plastic capacity should be used regardless of cross-sectional class of the composite cross-section.

$$M_{Rd.composite.plastic}(x_{span}) := \begin{cases} M_{positive} \leftarrow M_{Rd.composite.plastic.pos}(x_{span}, 1) \\ M_{negative} \leftarrow M_{Rd.composite.plastic.pos}(x_{span}, 1) \\ M_{negative} \quad \text{if } location < x_{span} < L_{span} - location \\ M_{positive} \quad \text{otherwise} \end{cases}$$

The plastic moment capacity of the flanges is calculated so that the correct capacity with regard to positive respectively negative bending is used. Note that here the plastic capacity should be used regardless of cross-sectional class of the composite cross-section.

$$M_{Rd.flanges.plastic}(x_{span}) := \begin{cases} M_{positive} \leftarrow M_{Rd.composite.plastic.pos}(x_{span}, 0) \\ M_{negative} \leftarrow M_{Rd.composite.plastic.pos}(x_{span}, 0) \\ M_{negative} \quad \text{if } location < x_{span} < L_{span} - location \\ M_{positive} \quad \text{otherwise} \end{cases}$$

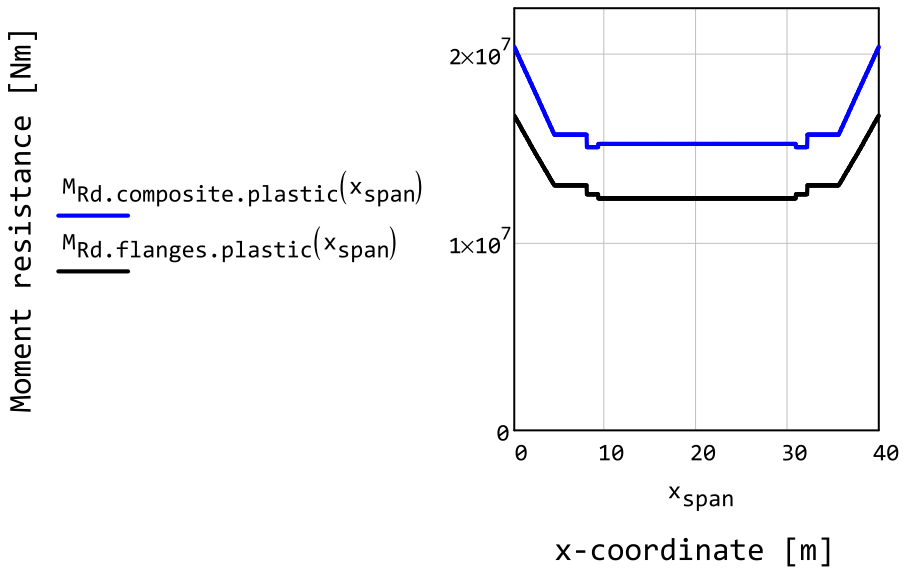

$check_{shear}$ indicates if the shear resistance of the composite cross-section is sufficient. If the utilisation of the shear resistance is keept below 50% then there is no need for an interaction check. If no check is needed the function yields the value one. If a check is needed the function yields the value zero.

$$check_{shear}(x_{span}) := \frac{\left|V_{Ed.ULS.composite}(x_{span})\right|}{V_{Rd.main}(x_{span})} < 0.5$$

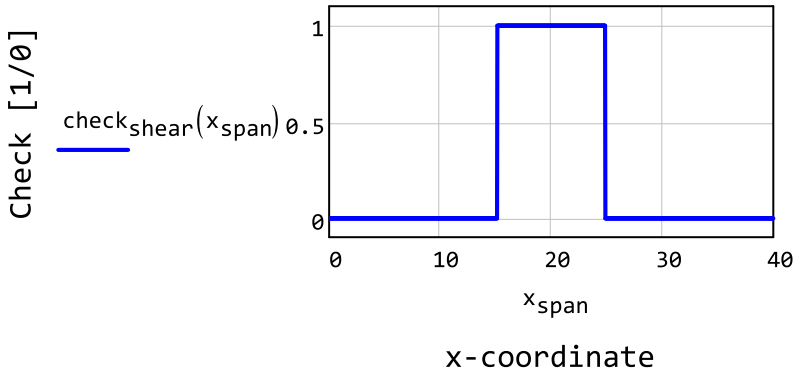

$check_{moment}$ indicates if the moment resistance of the flanges of composite cross-section is sufficient. If the bending moment for the section can be carried by the flanges alone then there is no need for an interaction check. If no check is needed the function yields the value one. If a check is needed the function yields the value zero.

$$check_{moment}(x_{span}) := M_{Rd.flanges.plastic}(x_{span}) > M_{Ed.ULS.max}(x_{span})$$

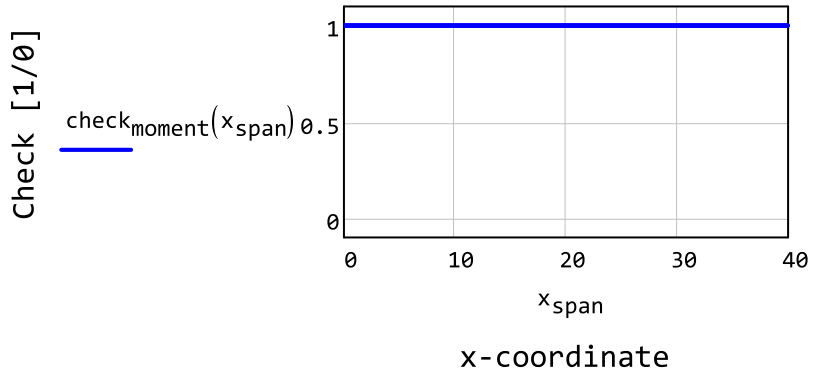

$check_{shear.moment}$ indicates if the shear or moment capacity is sufficient. If both the shear and moment resistance is insufficient then a check of the interaction is needed. If a check is needed the function yields the value zero. If no check is needed the function yields the value one.

$$check_{shear.moment}(x_{span}) := \begin{cases} 1 & \text{if } (check_{shear}(x_{span}) \vee check_{moment}(x_{span})) \\ 0 & \text{otherwise} \end{cases}$$

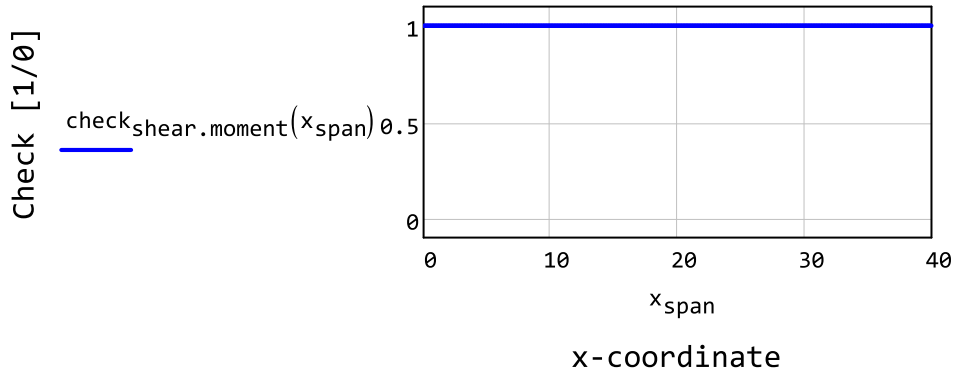

Check of the interaction between shear and moment for the composite cross-section, when applicable. The design plastic resistance of the of the effective area of the flanges should be used in accordance with Eurocode 1993-1-5: paragraph 7.1-(1). The design plastic resistance of the effective cross-section should be used in this calculation regardless of the cross-section class. Note that the cross-section class should otherwise be class 3 or 4 for this calculation to apply.
If the check is fulfilled, or not needed, the function yields the value one. If the check is needed and not fulfilled the function yields the value one.
Here:
M_{Ed} is the bending moment acting on the composite section in the ultimate limit state
V_{Ed} is the shear force acting on the composite section in the ultimate limit state
$M_{pl.Rd}$ is design plastic resistance of the effective cross-section
$M_{f.Rd}$ is the resistance of the flanges of the composite section
$V_{bw.Rd}$ is the shear buckling resistance of the web of the main I-girder
V_{Rd} is the shear buckling resistance of composite cross-section
η_1 is the ratio between bending moment and plastic resistance of the flanges
η_3 is the ratio between shear force and shear buckling resistance of the web
$check_{combined}$ is the check that is performed for interaction of shear force and bending moment and
$check_{shear.moment}$ indicates if a interaction check is needed

$$\text{check}_{\text{interaction}}(x_{\text{span}}) := \left|\begin{array}{l} M_{Ed} \leftarrow M_{Ed.ULS.max}(x_{\text{span}}) \\ V_{Ed} \leftarrow V_{Ed.ULS.composite}(x_{\text{span}}) \\ M_{pl.Rd} \leftarrow M_{Rd.composite.plastic}(x_{\text{span}}) \\ M_{f.Rd} \leftarrow M_{Rd.flanges.plastic}(x_{\text{span}}) \\ V_{bw.Rd} \leftarrow V_{Rd.main.buckling.web}(x_{\text{span}}) \\ \eta_1 \leftarrow \dfrac{|M_{Ed}|}{M_{pl.Rd}} \\ \eta_3 \leftarrow \dfrac{|V_{Ed}|}{V_{bw.Rd}} \\ \text{check}_{\text{combined}} \leftarrow \left[\eta_1 + \left(1 - \dfrac{M_{f.Rd}}{M_{pl.Rd}}\right)\cdot(2\cdot\eta_3 - 1)^2\right] \le 1.0 \\ 1 \quad \text{if } (\text{check}_{\text{combined}} \vee \text{check}_{\text{shear.moment}}(x_{\text{span}})) \\ 0 \quad \text{otherwise} \end{array}\right.$$

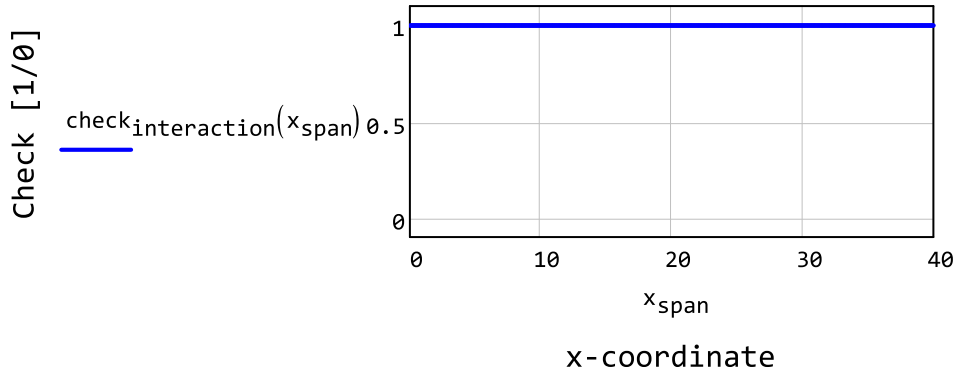

It is assumed that the resitance to shear, moment and any interaction between shear and moment is sufficient over the entire span length. This is checked for a certain amount of points along the span.

$$\text{assumption}_{\text{interaction}} := \left|\begin{array}{l} X_{\text{span}} \leftarrow \text{range}_{\text{span}}(100) \\ \text{for } x_{\text{step}} \in X_{\text{span}} \\ \quad \left|\begin{array}{l} \text{test} \leftarrow \text{check}_{\text{interaction}}(x_{\text{step}}) \\ (\text{ break }) \quad \text{if test} \neq 1 \end{array}\right. \\ \text{"true"} \quad \text{if test} = 1 \\ \text{"false"} \quad \text{otherwise} \end{array}\right.$$

$$\text{assumption}_{\text{interaction}} = \text{"true"}$$

2.6 Deflections

In this chapter the deflections of the bridge is calculated.

This chapter encompasses only the following subchapter.

2.6.1 Deflections in the serviceablity limit state

The deflection of the bridge is measured in the service phase for the composite cross-section. Note that due to precamber of the bridge there is no need to account for deflection due to self-weight. By the precambering the deflection due to self-weight is calculated and compensated for in the design so that no deflections are obtained for the unloaded bridge.

Note that both the modulus of elasticity and the second moment of inertia varies along the bridge span. However, the calculations are simplified to allow for an analytical solution with a conservative constant value is used for both the elastic modulus and second moment of area.

Modulus of elasticity

The modulus of elasticity that is used in the deflection calculation is the mean value of the secant modulus of elasticity for the upper and lower flange of the main I-girder.

Note that eventhough the stress varies along the length of the span a constant minimum value is used in the calculations. This is done in order to significantly simplify the calculations and shorten the computational requirements. The current method yields a conservative result, which should be acceptable as long as the deflection is determining the desing of the cross-section.

For calculations of deflections the frequent load combination is recomended in Eurocode 1993-2: paragraph 7.8.1-(2). Therefore the secant modulus of elasticity is derived for the stresses that is obtained for the frequent load combination.

Secant modulus of elasticity for the upper and lower flange of the main I-girder in the serviceability limit state. Calculated with the help of the stress level due to bending in the serviceablity limit state.

Secant modulus of elasticity in the upper flange in the serviceability limit state.

$$\sigma_{SLS.bending.flange}("upper") = -2.28 \times 10^{7}\ Pa$$

$$E_{deflection.flange.upper} := E_{steel.secant}\left(\sigma_{SLS.bending.flange}("upper")\right)$$

$$E_{deflection.flange.upper} = 200 \cdot GPa$$

Secant modulus of elasticity in the upper flange in the serviceability limit state.

$$\sigma_{SLS.bending.flange}("lower") = 234.83 \cdot MPa$$

$$E_{deflection.flange.lower} := E_{steel.secant}\left(\sigma_{SLS.bending.flange}("lower")\right)$$

$$E_{deflection.flange.lower} = 188 \cdot GPa$$

The modulus of elasticity that is used calculations of deflections. The modulus is taken as the mean value of the secant modulus of elasticity for the upper and lower flange of the main I-girders. Given by Eurocode 1993-1-4 paragraph 4.2-(5)

$$E_{steel.deflection} := \frac{E_{deflection.flange.lower} + E_{deflection.flange.upper}}{2}$$

$$E_{steel.deflection} = 194 \cdot GPa$$

Second moment of area

The second moment of area for the deflection calcluations of the bridge is taken as the minimal value for the nominal cross-section. The minimum value is used in order to obtain conservative value for the deflection.

$$I_{composite.min} := \left| \begin{array}{l} I_{min} \leftarrow I_{composite.nominal}(0m) \\ \text{for } x_{step} \in range_{span}(50) \\ \quad \left| \begin{array}{l} I_{negative} \leftarrow I_{composite.negative}(x_{step}) \\ I_{positive} \leftarrow I_{composite.positive}(x_{step}) \\ I_{min} \leftarrow \min(I_{negative}, I_{positive}, I_{min}) \end{array} \right. \\ I_{min} \end{array} \right.$$

$$I_{composite.min} = 0.02\,m^4$$

Contribution from load model 1

For further information about the load model 1, see chapter 2.2.2 - *Traffic loads, load model 1*

Equivalent point load for the axle loads in load model 1. The point load is corresponding to the load that is acting on the most loaded main girder. Original calculation can be found in chapter 2.2.2 - *Traffic loads, load model 1*

$$Q_{model1.equivalent} = 5.83 \times 10^5\,N$$

Equivalent line load for the distributed loads in load model 1. The line load is corresponding to the load that is acting on the most loaded main girder. Original calculation can be found in chapter 2.2.2 - *Traffic loads, load model 1*

$$q_{model1.equivalent} = 1.82 \times 10^4 \cdot \frac{N}{m}$$

Deflection due to the axle load. Note that the result can be interpreted in two ways, it can be the deflections at the middle of the span when the load is moved along the x-axis. Alternatively, it can be interpreted as the distribution of deflections when the load is stationary in the middle of the span. The furmula is valid for beams with fixed support in both ends of the span.

$$\delta_{model1.axle}(x_{span}) := \begin{cases} Q \leftarrow Q_{model1.equivalent} \\ E \leftarrow E_{steel.deflection} \\ I \leftarrow I_{composite.min} \\ \dfrac{Q \cdot x_{span}^{2} \cdot L_{span}}{48 \cdot E \cdot I} \cdot \left(3 - \dfrac{4x_{span}}{L_{span}}\right) & \text{if } x_{span} \le \dfrac{L_{span}}{2} \\ \dfrac{Q \cdot \left(L_{span} - x_{span}\right)^{2} \cdot L_{span}}{48 \cdot E \cdot I} \cdot \left[3 - \dfrac{4\left(L_{span} - x_{span}\right)}{L_{span}}\right] & \text{otherwise} \end{cases}$$

The maximum deflection is obtained at the middle of the bridge span

$$\delta_{model1.axle}\left(\frac{L_{span}}{2}\right) = 54.61 \cdot mm$$

Deflection distribution along the span due to the distributed load. The furmula is valid for beams with fixed support in both ends of the span.

$$\delta_{model1.distributed}(x_{span}) := \begin{cases} q \leftarrow q_{model1.equivalent} \\ q \cdot \left(\dfrac{x_{span}^{4}}{24} - \dfrac{L_{span}}{12} \cdot x_{span}^{3} + \dfrac{L_{span}^{2}}{24} \cdot x_{span}^{2}\right) \\ \hline E_{steel.deflection} \cdot I_{composite.min} \end{cases}$$

The maximum deflection is obtained at the middle of the bridge span

$$\delta_{model1.distributed}\left(\frac{L_{span}}{2}\right) = 34.09 \cdot mm$$

Contribution from wind loads

For further information about the wind load see chapter 2.2.4 - *Wind load*

$$\delta_{wind}(x_{span}) := \frac{q_{wind.equivalent.composite} \cdot \left(\dfrac{x_{span}^{4}}{24} - \dfrac{L_{span}}{12} \cdot x_{span}^{3} + \dfrac{L_{span}^{2}}{24} \cdot x_{span}^{2}\right.}{E_{steel.deflection} \cdot I_{composite.min}}$$

The maximum deflection is obtained at the middle of the bridge span

$$\delta_{wind}\left(\frac{L_{span}}{2}\right) = 0.51 \cdot mm$$

Check of the deflection in serviceability limit state

The deflection in the servicability limit state (SLS). For calculations of deflections the frequent load combination is recomended in Eurocode 1993-2: paragraph 7.8.1-(2). The frequent load combination which is used here is given in Eurocode 1990-A1: Table A2.6.
The deflection should be interpreted as the vertical deflection in each section along the bridge span when the axle load is placed in the middle of the span. Note that due to the precambering no regard is taken to the deflection that is caused by the self-weight.

$$\delta_{Ed.SLS}(x_{span}) := \left| \begin{array}{l} \delta_0 \leftarrow \psi_{traffic.1} \cdot \delta_{model1.distributed}(x_{span}) \\ \delta_1 \leftarrow \psi_{traffic.1} \cdot \delta_{model1.axle}(x_{span}) \\ \delta_2 \leftarrow \psi_{wind.2} \cdot \delta_{wind}(x_{span}) \\ \sum_{i=0}^{2} \delta_i \end{array} \right.$$

Maximum deflection is obtained in the middle of the span.

$$\delta_{Ed.SLS}\left(\frac{L_{span}}{2}\right) = 66.53 \cdot mm$$

Limit for maximum vertical deflections in the serviceability limit state. The limit is linearly proportionate to the span length.

$$\delta_{limit.SLS} = 100 \cdot mm$$

Utilisation ratio for the deflection. Note that maximum deflection is obtained in the middle of the span.

$$u_{SLS.deflection} := \frac{\delta_{Ed.SLS}\left(\frac{L_{span}}{2}\right)}{\delta_{limit.SLS}}$$

$$u_{SLS.deflection} = 67 \cdot \%$$

2.7 Fatigue

In this chapter the fatigue life of the bridge is calculated with the damage equivalent factor method. Note that only the main I-girders are considered for the fatigue life. Thus the fatigue life of the reinforced conrete or the shear studs connecting the I-girders and the concrete deck are not considered in the calculations.

Furthermore, note that the fatigue life is also assessed with the damage cumulative Palmgren-Miner method in complementary Matlab calculations.

This chapter encompasses the following subchapters:
2.8.1 Calculation of the damage equivalence factor, Lambda
2.8.2 Fatigue cracking modes and fatigue strength
2.8.3 Stress range for the fatigue calculations
2.8.4 Fatigue life according to damage equivalent method

2.8.1 Calculation of the damage equivalence factor, Lambda

Calculation of the damage equivalence factor which also is known as the lambda factor.

Lambda factor 1

Lambda factor 1 takes into account the damage effect of traffic.

The factor depends on the critical influence area or line, whichever is applicable. The critical length to consider is the span length. For further information see Eurocode 1993-2: Paragraph 9.5.2-(2). The value is given by Eurocode 1993-2: Table 9.5 for the graph corresponding to midspans.

$$\lambda_{fatigue.1} := \begin{cases} 2.55 & \text{if } L_{span} < 10m \\ 2.55 - 0.7 \cdot \frac{L_{span} - 10m}{70m} & \text{if } 10m \le L_{span} \le 80m \\ 1.85 & \text{otherwise} \end{cases}$$

$$\lambda_{fatigue.1} = 2.25$$

Lambda factor 2

Lambda factor 2 takes into account the traffic volume on the bridge.

Axle load and mix vehicle distribution for fatigue load model 4. Given by Eurocode 1991-2: Table 4.7.

$$axleload_{fatigue.model4} := \begin{pmatrix} 70 & 130 & 0 & 0 & 0 \\ 70 & 120 & 120 & 0 & 0 \\ 70 & 150 & 90 & 90 & 90 \\ 70 & 140 & 90 & 90 & 0 \\ 70 & 130 & 90 & 80 & 80 \end{pmatrix} kN$$

$$\text{frequency}_{\text{fatigue.model4}} := \left| \begin{array}{l} \text{tmp} \leftarrow \begin{pmatrix} 20 & 40 & 80 \\ 5 & 10 & 5 \\ 50 & 30 & 5 \\ 15 & 15 & 5 \\ 10 & 5 & 5 \end{pmatrix} \% \\ \text{tmp}^{\langle 0 \rangle} \quad \text{if } \text{range}_{\text{traffic}} = \text{"long"} \\ \text{tmp}^{\langle 1 \rangle} \quad \text{if } \text{range}_{\text{traffic}} = \text{"medium"} \\ \text{tmp}^{\langle 2 \rangle} \quad \text{if } \text{range}_{\text{traffic}} = \text{"local"} \end{array} \right.$$

Average gross weight of the lorries in the slow lane, given by Eurocode 1993-2: Paragraph 9.5.2-(3). Here the traffic is taken according to fatigue load model 4 given in Eurocode 1991-2: Table 4.7.

$$Q_{\text{fatigue.m1}} := \left| \begin{array}{l} n \leftarrow \text{cols}\left(\text{axleload}_{\text{fatigue.model4}}\right) - 1 \\ k \leftarrow \text{rows}\left(\text{axleload}_{\text{fatigue.model4}}\right) - 1 \\ Q_{\text{vehicles}} \leftarrow \sum_{i=0}^{n} \text{axleload}_{\text{fatigue.model4}}^{\langle i \rangle} \\ \left[\frac{\sum_{i=0}^{4} \left[\text{frequency}_{\text{fatigue.model4}_i} \cdot \left(Q_{\text{vehicles}_i} \right)^5 \right]}{\sum_{j=0}^{4} \text{frequency}_{\text{fatigue.model4}_j}} \right]^{\frac{1}{5}} \end{array} \right.$$

$$Q_{\text{fatigue.m1}} = 316.69 \cdot \text{kN}$$

Factor taking into account the traffic volume on the bridge. Given by Eurocode 1993-2: Paragraph 9.5.2-(3).

$$\lambda_{\text{fatigue.2}} := \frac{Q_{\text{fatigue.m1}}}{Q_{\text{fatigue.lambda.0}}} \cdot \left(\frac{N_{\text{fatigue.observed}}}{N_{\text{fatigue.lambda.0}}} \right)^{\frac{1}{5}}$$

$$\lambda_{\text{fatigue.2}} = 0.66$$

Lambda factor 3

Lambda factor 3 takes into account the design life of the bridge. Given by Eurocode 1993-2: Paragraph 9.5.2-(5). Note that the design life of the bridge is given in years, and that the reference life span is 100 years.

$$\lambda_{fatigue.3} := \left(\frac{t_{designlife}}{100 \cdot years}\right)^{\frac{1}{5}}$$

$$\lambda_{fatigue.3} = 0.96$$

Lambda factor 4

Lambda factor 4 takes into account the load that is acting on the other lanes. Given by Eurocode 1993-2: Paragraph 9.5.2-(6). Here is taken into account the fact that the bridge has a lane in each direction. It is assumed that the trafic in both directions is identical, leading to the simplification of the original formula.

$$assumption_{2\_notional\_lanes} = "true"$$

$$\lambda_{fatigue.4} := (1 + 1)^{\frac{1}{5}}$$

$$\lambda_{fatigue.4} = 1.15$$

Limitation of the lambda factor

Limiting factor for the maximum value of the damage equvivalence factor lambda. Given by Eurocode 1993-2: Paragraph 9.5.2-(7). The value is given by Eurocode 1993-2: Table 9.5 for the graph corresponding to midspans.

$$\lambda_{fatigue.max} := \begin{cases} 2.50 & \text{if } L_{span} < 10m \\ 2.50 - 0.5 \cdot \frac{L_{span} - 10m}{15m} & \text{if } 10m \le L_{span} \le 25m \\ 2.00 & \text{otherwise} \end{cases}$$

$$\lambda_{fatigue.max} = 2$$

Resulting damage equvivalence factor

The damage equvivalence factor used in fatigue calculations is given in Eurocode 1993-2: Section 9.5.2. It is applicable to bridges with a span of up to 80m.

The value of the damage equvivalence factor before limiting the value

$$\lambda_{fatigue.1} \cdot \lambda_{fatigue.2} \cdot \lambda_{fatigue.3} \cdot \lambda_{fatigue.4} = 1.63$$

Check that the assumption about span length is fulfilled

$$assumption_{span\_length\_less\_than\_80m} := \begin{cases} "true" & \text{if } L_{span} \le 80m \\ "false" & \text{otherwise} \end{cases}$$

$$assumption_{span\_length\_less\_than\_80m} = "true"$$

The value of the damage equvivalence factor. The value of the factor should not exceed 2.

$$\lambda_{fatigue} := \left| \begin{array}{l} \lambda \leftarrow \lambda_{fatigue.1} \cdot \lambda_{fatigue.2} \cdot \lambda_{fatigue.3} \cdot \lambda_{fatigue.4} \\ \min\left(\lambda, \lambda_{fatigue.max}\right) \end{array} \right.$$

$$\lambda_{fatigue} = 1.63$$

2.8.2 Fatigue cracking modes and fatigue strength

The constant amplitude nominal stresses fatigue strength for the cracking modes in the main I-girders. Note that the cracking modes and values of the fatigue strength is defined in chapter 1.4 - fatigue strength and chapter 0.4 - fatigue strength.

Cracking mode A1 and A2

Constant amplitude nominal stresses fatigue strength for cracking mode A with regard to shear stress.

$$\Delta\tau_{C.modeA} = 100 \cdot MPa$$

Constant amplitude nominal stresses fatigue strength for cracking mode A with regard to direct stress.

$$\Delta\sigma_{C.modeA} = 112 \cdot MPa$$

Cracking mode B

The unreduced fatigue strength for fatigue cracking mode B

$$\Delta\sigma_{C.modeB.unreduced} = 112 \cdot MPa$$

Factor taking into account the size effect, the sice effect is only considered for thickness above 25mm. Given by Eurocode 1993-1-9: Table 8.3.

$$k_{size.lower}\left(x_{span}\right) := \min\left(\frac{25mm}{t_{main.flange.lower}\left(x_{span}\right)}, 1\right)$$

$$k_{size.upper}\left(x_{span}\right) := \min\left(\frac{25mm}{t_{main.flange.upper}\left(x_{span}\right)}, 1\right)$$

The reduced capacity for cracking mode B. Given by Eurocode 1993-1-9: Paragraph 7.2.2-(1).

$$\Delta\sigma_{C.modeB.lower}\left(x_{span}\right) := \left| \begin{array}{l} \Delta\sigma \leftarrow \Delta\sigma_{C.modeB.unreduced} \\ \Delta\sigma \cdot k_{size.lower}\left(x_{span}\right) \end{array} \right.$$

$$\Delta\sigma_{C.modeB.upper}\left(x_{span}\right) := \left| \begin{array}{l} \Delta\sigma \leftarrow \Delta\sigma_{C.modeB.unreduced} \\ \Delta\sigma \cdot k_{size.upper}\left(x_{span}\right) \end{array} \right.$$

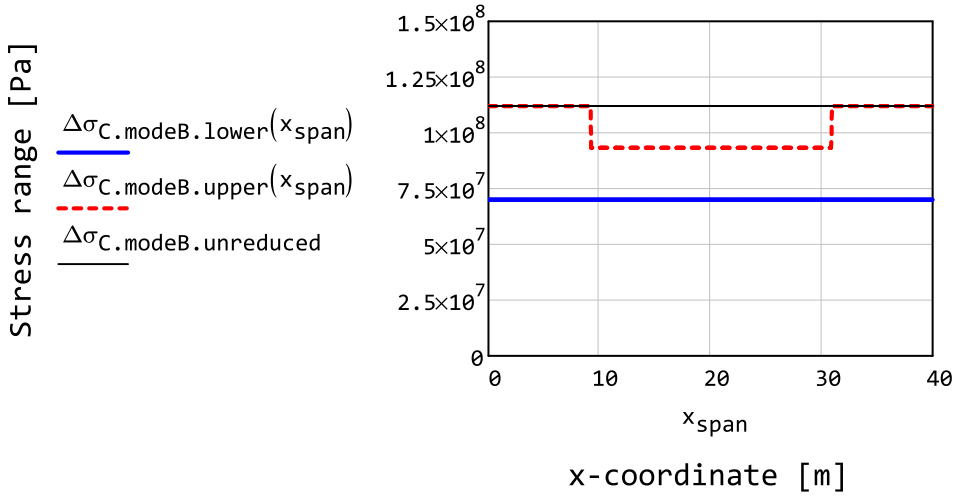

Cracking mode C

Constant amplitude nominal stresses fatigue strength for cracking mode C with regard to principal stress.

$$\Delta\sigma_{C.modeC} = 80 \cdot MPa$$

Cracking mode D

Constant amplitude nominal stresses fatigue strength for cracking mode D with regard to direct stress.

$$\Delta\sigma_{C.modeD} = 80 \cdot MPa$$

Cracking mode E

Constant amplitude nominal stresses fatigue strength for cracking mode E with regard to shear stress.

$$\Delta\tau_{C.modeE} = 80 \cdot MPa$$

Cracking mode F

The unreduced fatigue strength for fatigue cracking mode F

$$\Delta\sigma_{C.modeF.unreduced} = 112 \cdot MPa$$

Factor taking into account the size effect, the sice effect is only considered for thickness above 25mm. Given by Eurocode 1993-1-9: Table 8.3.

$$k_{size.web}(x_{span}) := \min\left(\frac{25mm}{t_{main.web}(x_{span})}, 1\right)$$

The reduced capacity for cracking mode B. Given by Eurocode 1993-1-9: Paragraph 7.2.2-(1).

$$\Delta\sigma_{C.modeF}(x_{span}) := \left| \begin{array}{l} \Delta\sigma \leftarrow \Delta\sigma_{C.modeF.unreduced} \\ \Delta\sigma \cdot k_{size.web}(x_{span}) \end{array} \right.$$

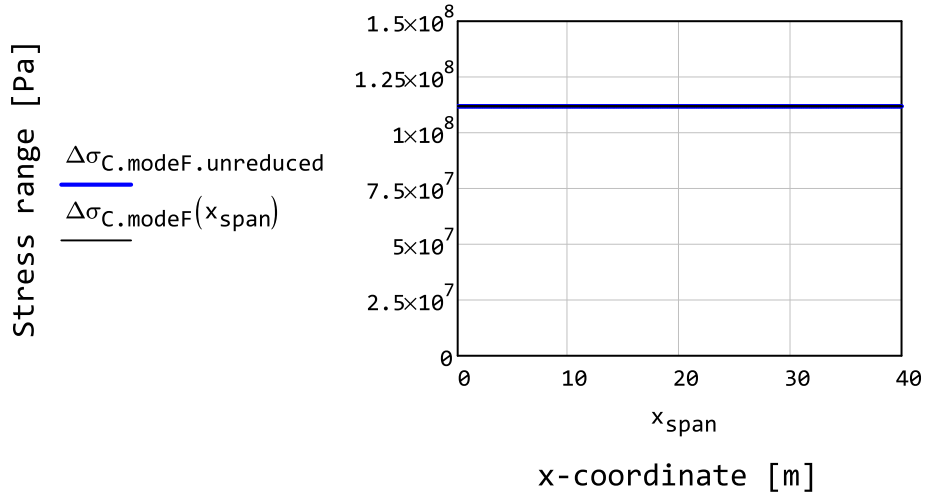

2.8.3 Stress range for the fatigue calculations

It is assumed that the direct stress is given by the effective cross-section in SLS while the shear force is carried only by the main I-girders. In accordance with Eurocode 1994-2: paragraph 1.5.2.12 the flexural stiffness, e.i. EI, the concrete should be neglected in tension and only the reinforcement should be considered.

The largest positive bending for the fatigue load in a given section.

$$M_{E.fatigue.positive}(x_{span}) := \left| \begin{array}{l} x_{vehicle} \leftarrow 0m, 1m .. L_{span} + 8.4m \\ \text{for } x_{step} \in x_{vehicle} \\ \quad M_{max} \leftarrow \max(M_{E.fatigue.vehicle}(x_{span}, x_{step}), M_{ma} \\ M_{max} \end{array} \right.$$

The largest negative bending for the fatigue load in a given section.

$$M_{E.fatigue.negative}(x_{span}) := \left| \begin{array}{l} x_{vehicle} \leftarrow 0m, 1m .. L_{span} + 8.4m \\ \text{for } x_{step} \in x_{vehicle} \\ \quad M_{min} \leftarrow \min(M_{E.fatigue.vehicle}(x_{span}, x_{step}), M_{mi} \\ M_{min} \end{array} \right.$$

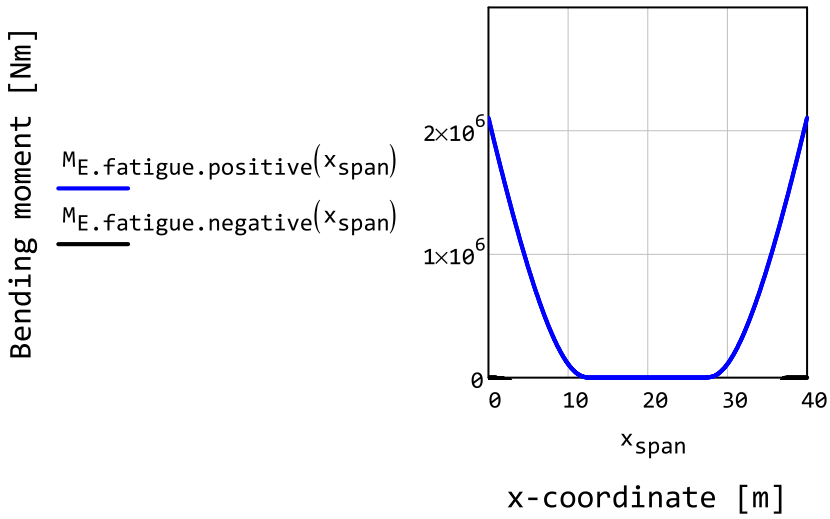

The stress range is taken as the difference between the highest and lowest value of the shear force as the vehicle load travels along the span.

$$\Delta V_{E.fatigue}(x_{span}) := \left| \begin{array}{l} x_{vehicle} \leftarrow 0m, 1m .. \ L_{span} + 8.4m \\ \text{for } x_{step} \in x_{vehicle} \\ \quad \left| \begin{array}{l} M_{max} \leftarrow \max\left(V_{E.fatigue.vehicle}(x_{span}, x_{step}), M_{max}\right) \\ M_{min} \leftarrow \min\left(V_{E.fatigue.vehicle}(x_{span}, x_{step}), M_{min}\right) \end{array} \right. \\ M_{max} - M_{min} \end{array} \right.$$

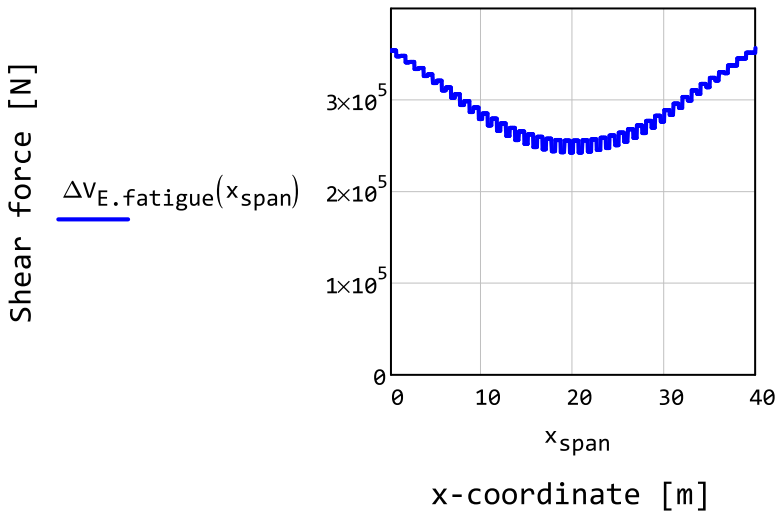

Cracking mode A

Cracking mode A takes into regard the effect of both the shear and the direct stress in the web close to the longitudinal weld.

The shear stress in the lower part of the web

$$\Delta\tau_{fatigue.modeA.lower}(x_{span}) := \left| \begin{array}{l} z \leftarrow z_{bottom.main.web}(x_{span}) \\ \dfrac{\Delta V_{E.fatigue}(x_{span}) \cdot S_{main.beam}(x_{span}, z)}{I_{main.beam.unreduced}(x_{span}) \cdot t_{main.web}(x_{span})} \end{array} \right.$$

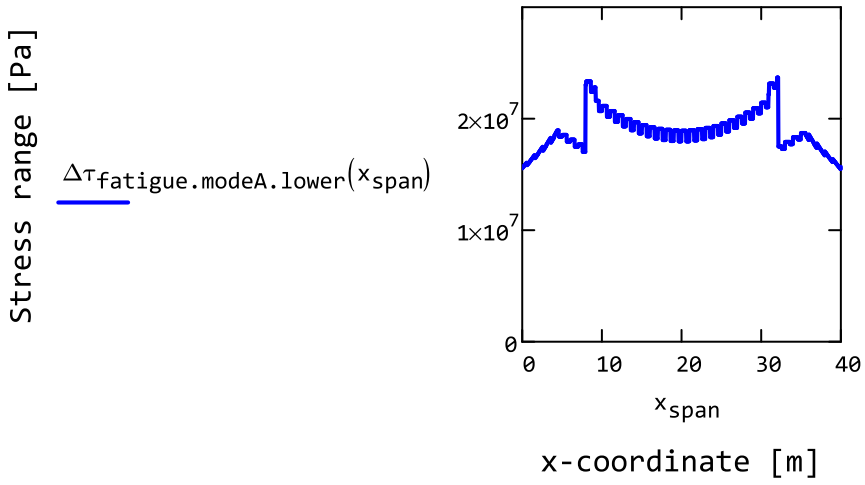

The shear stress in the upper part of the web

$$\Delta\tau_{\texttt{fatigue.modeA.upper}}(x_{span}) := \left| z \leftarrow z_{\texttt{top.main.web}}(x_{span}) \right| \frac{\Delta V_{\texttt{E.fatigue}}(x_{span}) \cdot S_{\texttt{main.beam}}(x_{span}, z)}{I_{\texttt{main.beam.unreduced}}(x_{span}) \cdot t_{\texttt{main.web}}(x_{span})}$$

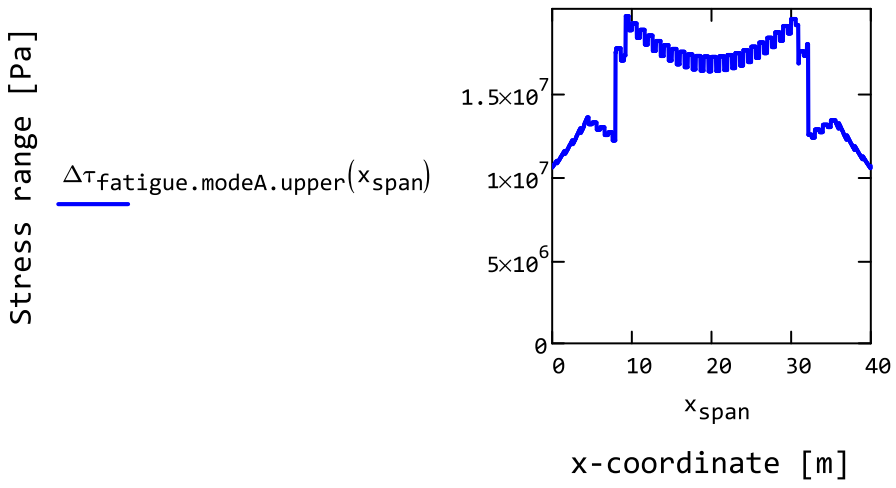

The direct stress in the lower part of the web

$$\Delta\sigma_{\texttt{fatigue.modeA.lower}}(x_{span}) := \left| \begin{array}{l} z_{global} \leftarrow z_{\texttt{bottom.main.web}}(x_{span}) \\ z_{negative} \leftarrow z_{\texttt{composite.negative}}(x_{span}, z_{global}) \\ z_{positive} \leftarrow z_{\texttt{composite.positive}}(x_{span}, z_{global}) \\ \sigma_{negative} \leftarrow \frac{M_{\texttt{E.fatigue.negative}}(x_{span})}{I_{\texttt{composite.negative}}(x_{span})} \cdot z_{negative} \\ \sigma_{positive} \leftarrow \frac{M_{\texttt{E.fatigue.positive}}(x_{span})}{I_{\texttt{composite.positive}}(x_{span})} \cdot z_{positive} \\ |\sigma_{positive}| + |\sigma_{negative}| \end{array} \right.$$

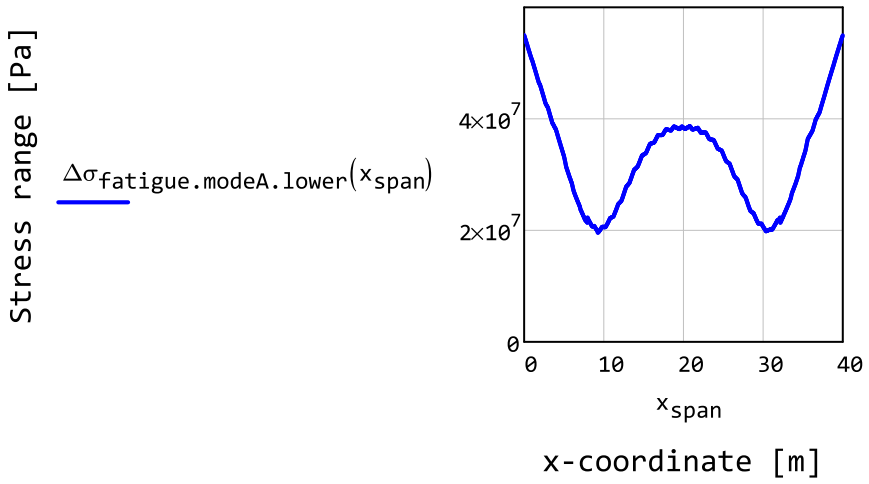

The direct stress in the upper part of the web

$$\Delta\sigma_{\text{fatigue.modeA.upper}}(x_{\text{span}}) := \left| \begin{array}{l} z_{\text{global}} \leftarrow z_{\text{top.main.web}}(x_{\text{span}}) \\ z_{\text{negative}} \leftarrow z_{\text{composite.negative}}(x_{\text{span}}, z_{\text{global}}) \\ z_{\text{positive}} \leftarrow z_{\text{composite.positive}}(x_{\text{span}}, z_{\text{global}}) \\ \sigma_{\text{negative}} \leftarrow \dfrac{M_{\text{E.fatigue.negative}}(x_{\text{span}})}{I_{\text{composite.negative}}(x_{\text{span}})} \cdot z_{\text{negative}} \\ \sigma_{\text{positive}} \leftarrow \dfrac{M_{\text{E.fatigue.positive}}(x_{\text{span}})}{I_{\text{composite.positive}}(x_{\text{span}})} \cdot z_{\text{positive}} \\ |\sigma_{\text{negative}}| + |\sigma_{\text{positive}}| \end{array} \right.$$

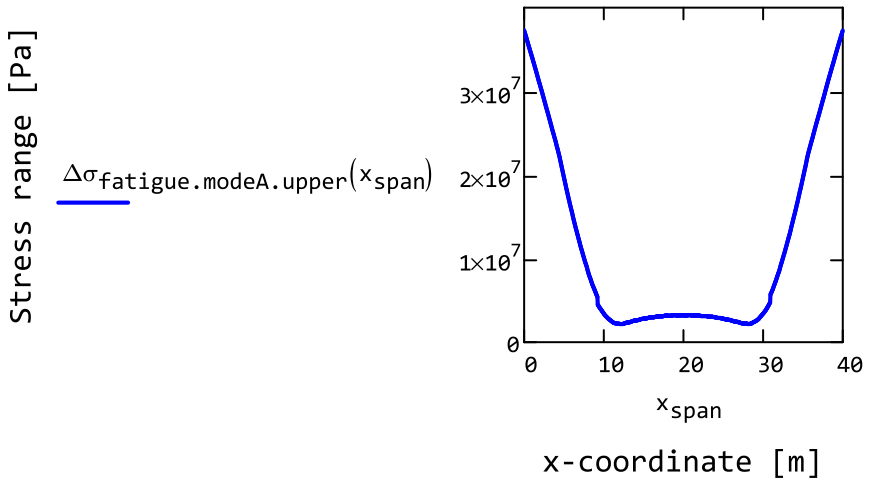

Cracking mode B

Cracking mode B takes into regard the effect of direct stress in the flanges at the splices.

The direct stress in the lower flange at the location of the splices.

$$\Delta\sigma_{fatigue.modeB.lower} := \left| \begin{array}{l} X_{splice} \leftarrow splitter\left(X_{splice.flange.lower}, 10mm\right) \\ \text{for } i \in 0, 1 .. \ rows\left(X_{splice}\right) - 1 \\ \quad \left| \begin{array}{l} z_{global} \leftarrow z_{bottom.main.flange.lower}\left(X_{splice_i}\right) \\ z_{negative} \leftarrow z_{composite.negative}\left(X_{splice_i}, z_{global}\right) \\ z_{positive} \leftarrow z_{composite.positive}\left(X_{splice_i}, z_{global}\right) \\ \sigma_{negative} \leftarrow \dfrac{M_{E.fatigue.negative}\left(X_{splice_i}\right)}{I_{composite.negative}\left(X_{splice_i}\right)} \cdot z_{negative} \\ \sigma_{positive} \leftarrow \dfrac{M_{E.fatigue.positive}\left(X_{splice_i}\right)}{I_{composite.positive}\left(X_{splice_i}\right)} \cdot z_{positive} \\ \Delta\sigma_i \leftarrow \left|\sigma_{negative}\right| + \left|\sigma_{positive}\right| \end{array} \right. \\ \Delta\sigma \end{array} \right.$$

$$\Delta\sigma_{fatigue.modeB.lower} = \begin{pmatrix} 2.79 \times 10^7 \\ 2.79 \times 10^7 \\ 3.63 \times 10^7 \\ 3.64 \times 10^7 \\ 3.61 \times 10^7 \\ 3.6 \times 10^7 \\ 2.81 \times 10^7 \\ 2.82 \times 10^7 \end{pmatrix} Pa$$

The direct stress in the upper flange at the location of the splices.

$$\Delta\sigma_{fatigue.modeB.upper} := \left| \begin{array}{l} X_{splice} \leftarrow splitter\left(X_{splice.flange.upper}, 10mm\right) \\ \text{for } i \in 0, 1 .. \ rows\left(X_{splice}\right) - 1 \\ \quad \left| \begin{array}{l} z_{global} \leftarrow z_{top.main.flange.upper}\left(X_{splice_i}\right) \\ z_{negative} \leftarrow z_{composite.negative}\left(X_{splice_i}, z_{global}\right) \\ z_{positive} \leftarrow z_{composite.positive}\left(X_{splice_i}, z_{global}\right) \\ \sigma_{negative} \leftarrow \dfrac{M_{E.fatigue.negative}\left(X_{splice_i}\right)}{I_{composite.negative}\left(X_{splice_i}\right)} \cdot z_{negative} \\ \sigma_{positive} \leftarrow \dfrac{M_{E.fatigue.positive}\left(X_{splice_i}\right)}{I_{composite.positive}\left(X_{splice_i}\right)} \cdot z_{positive} \\ \Delta\sigma_i \leftarrow \left|\sigma_{negative}\right| + \left|\sigma_{positive}\right| \end{array} \right. \\ \Delta\sigma \end{array} \right.$$

$$\Delta\sigma_{fatigue.modeB.upper} = \begin{pmatrix} 5.92 \times 10^6 \\ 5.87 \times 10^6 \\ 4.42 \times 10^6 \\ 4.42 \times 10^6 \\ 5.31 \times 10^6 \\ 5.34 \times 10^6 \end{pmatrix} Pa$$

Cracking mode C

Cracking mode C takes into regard the effect of principal stress in the web at the location of the vertical stiffeners. Note that the stiffeners is not welded the lower most and upper most 50mm of the web,

It is assumed that there is only vertical stiffeners at the supports and that the stress is equal in both ends of the span.

$$assumption_{no\_intermediate\_stiffeners} = "true"$$

The range of the z-coordinates of interest is limited by the web and decreased by 50mm at the top and bottom, since this part is not welded.

$$z_{min.modeC} := z_{bottom.main.web}(0m) + 50mm$$

$$z_{min.modeC} = 0.05\,m$$

$$z_{max.modeC} := z_{top.main.web}(0m) - 50mm$$

$$z_{max.modeC} = 1.28\,m$$

Direct stress in the web at the support.

$$\Delta\sigma_{\text{fatigue.modeC.direct}}(z_{\text{bridge}}) := \left| \begin{array}{l} x_{\text{stiff}} \leftarrow 0\text{m} \\ z_{\text{negative}} \leftarrow z_{\text{composite.negative}}(x_{\text{stiff}}, z_{\text{bridge}}) \\ z_{\text{positive}} \leftarrow z_{\text{composite.positive}}(x_{\text{stiff}}, z_{\text{bridge}}) \\ \sigma_{\text{negative}} \leftarrow \dfrac{M_{\text{E.fatigue.negative}}(x_{\text{stiff}})}{I_{\text{composite.negative}}(x_{\text{stiff}})} \cdot z_{\text{negati}} \\ \sigma_{\text{positive}} \leftarrow \dfrac{M_{\text{E.fatigue.positive}}(x_{\text{stiff}})}{I_{\text{composite.positive}}(x_{\text{stiff}})} \cdot z_{\text{positi}} \\ |\sigma_{\text{positive}}| + |\sigma_{\text{negative}}| \end{array} \right.$$

Shear stress in the web at the support.

$$\Delta\tau_{\text{fatigue.modeC.shear}}(z_{\text{bridge}}) := \left| \begin{array}{l} x_{\text{stiff}} \leftarrow 0\text{m} \\ \dfrac{\Delta V_{\text{E.fatigue}}(x_{\text{stiff}}) \cdot S_{\text{main.beam}}(x_{\text{stiff}}, z_{\text{bridge}})}{I_{\text{main.beam.unreduced}}(x_{\text{stiff}}) \cdot t_{\text{main.web}}(x_{\text{stiff}})} \end{array} \right.$$

Principal stress in the web at the support.

$$\Delta\sigma_{\text{fatigue.modeC.principal}}(z_{\text{bridge}}) := \left| \begin{array}{l} \Delta\sigma \leftarrow \Delta\sigma_{\text{fatigue.modeC.direct}}(z_{\text{bridge}}) \\ \Delta\tau \leftarrow \Delta\tau_{\text{fatigue.modeC.shear}}(z_{\text{bridge}}) \\ \dfrac{\Delta\sigma}{2} + \sqrt{\left(\dfrac{\Delta\sigma}{2}\right)^2 + \Delta\tau^2} \end{array} \right.$$

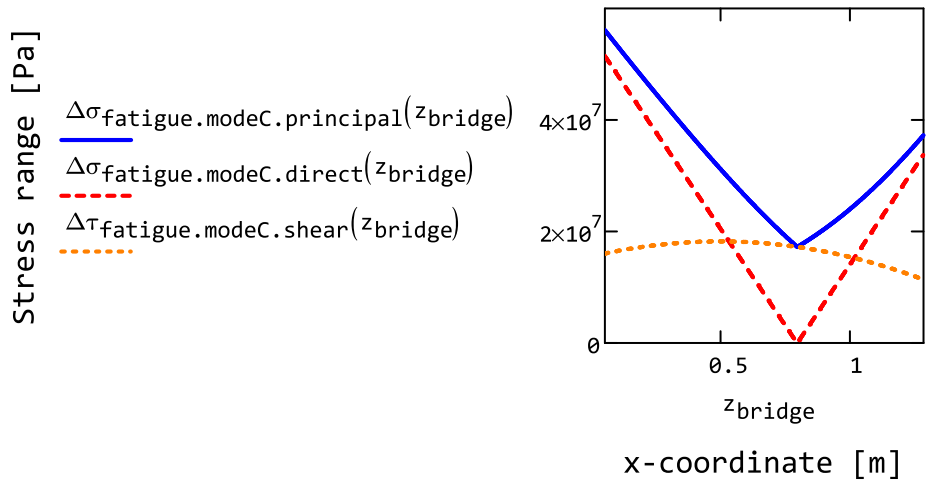

Cracking mode D

Cracking mode C takes into regard the effect of direct stress in the flange at the location of the vertical stiffeners. It is assumed that there is only vertical stiffeners at the supports and that the stress is equal in both ends of the span.

$$\mathrm{assumption}_{\mathrm{no\_intermediate\_stiffeners}} = \text{"true"}$$

The direct stress in the lower and upper flange at the location of the vertical stiffener. Note that the direct stress is checked at the level of the upper and lower part of the web. This since the weld in which the fatigue crack originates is located at this height.

$$\Delta\sigma_{\mathrm{fatigue.modeD}} := \left| \begin{array}{l} x_{\mathrm{stiff}} \leftarrow 0\,\mathrm{m} \\ z_{\mathrm{global}_0} \leftarrow z_{\mathrm{top.main.web}}\left(x_{\mathrm{stiff}}\right) \\ z_{\mathrm{global}_1} \leftarrow z_{\mathrm{bottom.main.web}}\left(x_{\mathrm{stiff}}\right) \\ \text{for } i \in 0,1 \\ \quad \left| \begin{array}{l} z_{\mathrm{negative}} \leftarrow z_{\mathrm{composite.negative}}\left(x_{\mathrm{stiff}}, z_{\mathrm{global}_i}\right) \\ z_{\mathrm{positive}} \leftarrow z_{\mathrm{composite.positive}}\left(x_{\mathrm{stiff}}, z_{\mathrm{global}_i}\right) \\ \sigma_{\mathrm{negative}} \leftarrow \dfrac{M_{\mathrm{E.fatigue.negative}}\left(x_{\mathrm{stiff}}\right)}{I_{\mathrm{composite.negative}}\left(x_{\mathrm{stiff}}\right)} \cdot z_{\mathrm{negative}} \\ \sigma_{\mathrm{positive}} \leftarrow \dfrac{M_{\mathrm{E.fatigue.positive}}\left(x_{\mathrm{stiff}}\right)}{I_{\mathrm{composite.positive}}\left(x_{\mathrm{stiff}}\right)} \cdot z_{\mathrm{positive}} \\ \Delta\sigma_i \leftarrow \left|\sigma_{\mathrm{negative}}\right| + \left|\sigma_{\mathrm{positive}}\right| \end{array} \right. \\ \Delta\sigma \end{array} \right.$$

$$\Delta\sigma_{\mathrm{fatigue.modeD}} = \begin{pmatrix} 3.73 \times 10^7 \\ 5.5 \times 10^7 \end{pmatrix} \mathrm{Pa}$$

Cracking mode E

Cracking mode E takes into regard shear stress in the longitudinal welds. In accordance with Eurocode 1993-1-9: paragraph 5-(6) the shear stress is taken as the following.

Shear stress in the lower weld of the main I-girder

$$\Delta\tau_{\mathrm{fatigue.modeE.lower}}\left(x_{\mathrm{span}}\right) := \left| \begin{array}{l} z_0 \leftarrow z_{\mathrm{bottom.main.web}}\left(x_{\mathrm{span}}\right) \\ \dfrac{\Delta V_{\mathrm{E.fatigue}}\left(x_{\mathrm{span}}\right) \cdot S_{\mathrm{main.beam}}\left(x_{\mathrm{span}}, z_0\right)}{I_{\mathrm{main.beam.unreduced}}\left(x_{\mathrm{span}}\right) \cdot 2a_{\mathrm{weld.main.lower}}} \end{array} \right.$$

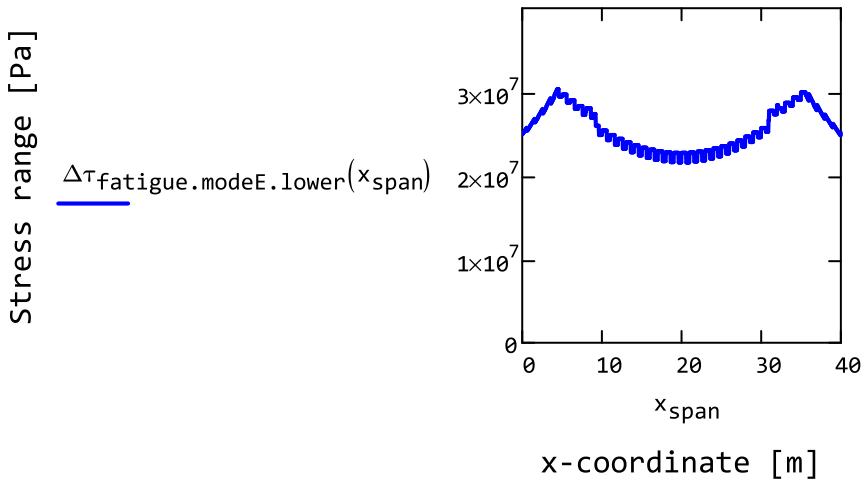

Shear stress in the upper weld of the main I-girder

$$\Delta\tau_{fatigue.modeE.upper}(x_{span}) := \left| \begin{array}{l} z_0 \leftarrow z_{top.main.web}(x_{span}) \\ \dfrac{\Delta V_{E.fatigue}(x_{span}) \cdot S_{main.beam}(x_{span}, z_0)}{I_{main.beam.unreduced}(x_{span}) \cdot 2a_{weld.main.upper}} \end{array} \right.$$

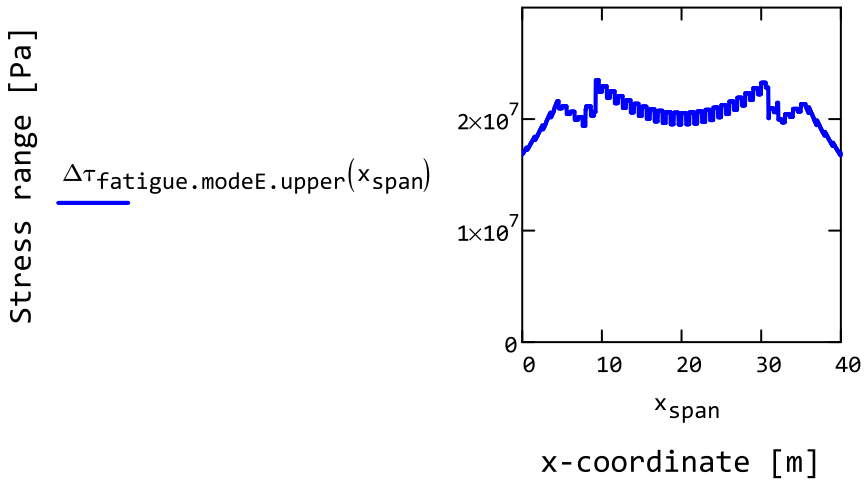

Cracking mode F

Direct stress in the web at the location of the splices in the web.

$$\Delta\sigma_{fatigue.modeF}(z_{bridge}) := \left| \begin{array}{l} X_{splice} \leftarrow splitter(X_{splice.web}, 10mm) \\ \text{for } i \in 0, 1 .. \ rows(X_{splice}) - 1 \\ \quad z_{negative} \leftarrow z_{composite.negative}(X_{splice_i}, z_{bridge}) \\ \quad z_{positive} \leftarrow z_{composite.positive}(X_{splice_i}, z_{bridge}) \\ \quad \sigma_{negative} \leftarrow \frac{M_{E.fatigue.negative}(X_{splice_i})}{I_{composite.negative}(X_{splice_i})} \cdot z_{negativ} \\ \quad \sigma_{positive} \leftarrow \frac{M_{E.fatigue.positive}(X_{splice_i})}{I_{composite.positive}(X_{splice_i})} \cdot z_{positiv} \\ \quad \Delta\sigma_i \leftarrow |\sigma_{negative}| + |\sigma_{positive}| \\ \Delta\sigma \end{array} \right.$$

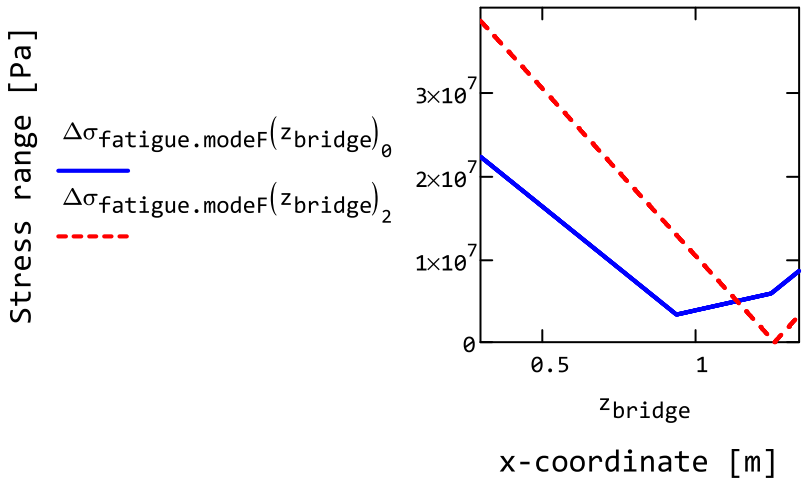

2.8.4 Fatigue life according to damage equivalent method

The utilisation of the fatigue life in is calculated with the following manner for the damage equivalent method. Note that in Eurocode 1993-1-9: P 6.2-(1) the partial factor may be added for the stress under the assumption of linear behaviour. However, if non-linear behaviour is used the partial factor should presumably be applied directly to the load.

Fatigue crack mode A

Cracking mode A takes into regard the effect of both the shear and the direct stress in the web close to the longitudinal weld. This crack mode can take place both at the top and bottom of the web. Hence that two sets of checks are performed.

The utilization ratio in the lower part. calculated in accordance with Eurocode 1993-1-9: paragraph 8-(3) and Eurocode 1993-1-9: paragraph 6.3-(1).

$$u_{FLS.Lambda.modeA.lower}(x_{span}) := \left| \begin{array}{l} \Delta\sigma_{E.2} \leftarrow \Delta\sigma_{fatigue.modeA.lower}(x_{span}) \cdot \lambda_{fatigu} \\ \Delta\tau_{E.2} \leftarrow \Delta\tau_{fatigue.modeA.lower}(x_{span}) \cdot \lambda_{fatigu} \\ \left[\frac{\gamma_{F.fatigue} \cdot \Delta\sigma_{E.2}}{\left(\frac{\Delta\sigma_{C.modeA}}{\gamma_{M.fatigue}}\right)}\right]^3 + \left[\frac{\gamma_{F.fatigue} \cdot \Delta\tau_{E.2}}{\left(\frac{\Delta\tau_{C.modeA}}{\gamma_{M.fatigue}}\right)}\right]^5 \end{array} \right.$$

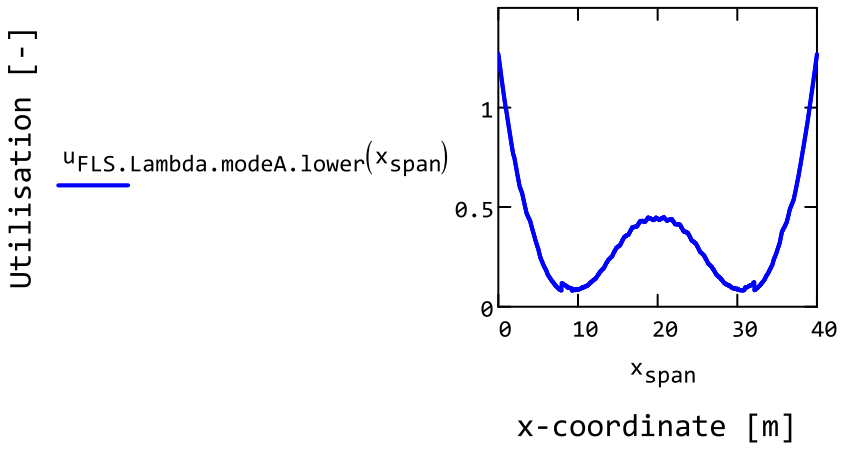

The utilization ratio in the upper part. calculated in accordance with Eurocode 1993-1-9: P 8-(3).

$$u_{FLS.Lambda.modeA.upper}(x_{span}) := \left| \begin{array}{l} \Delta\sigma_{E.2} \leftarrow \Delta\sigma_{fatigue.modeA.upper}(x_{span}) \cdot \lambda_{fatigu} \\ \Delta\tau_{E.2} \leftarrow \Delta\tau_{fatigue.modeA.upper}(x_{span}) \cdot \lambda_{fatigu} \\ \left[\frac{\gamma_{F.fatigue} \cdot \Delta\sigma_{E.2}}{\left(\frac{\Delta\sigma_{C.modeA}}{\gamma_{M.fatigue}}\right)}\right]^3 + \left[\frac{\gamma_{F.fatigue} \cdot \Delta\tau_{E.2}}{\left(\frac{\Delta\tau_{C.modeA}}{\gamma_{M.fatigue}}\right)}\right]^5 \end{array} \right.$$

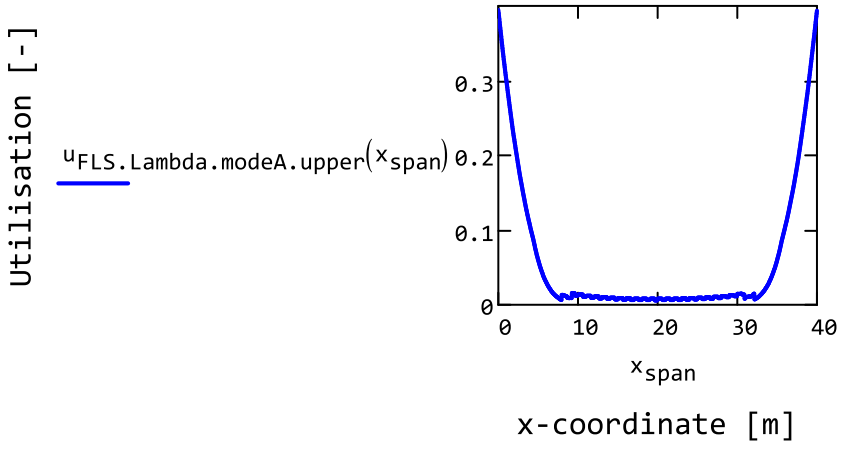

The maximum value of the utilization ratio for fatigue crack mode A

$$u_{FLS.Lambda.modeA.max} := \left| \begin{array}{l} X_{span} \leftarrow 0m, 0.1m .. \ L_{span} \\ \text{for } x_{step} \in X_{span} \\ \quad \left| \begin{array}{l} u_{upper} \leftarrow u_{FLS.Lambda.modeA.lower}(x_{step}) \\ u_{lower} \leftarrow u_{FLS.Lambda.modeA.upper}(x_{step}) \\ u_{max} \leftarrow \max(u_{max}, u_{upper}, u_{lower}) \end{array} \right. \\ u_{max} \end{array} \right.$$

$$u_{FLS.Lambda.modeA.max} = 1.27$$

Fatigue crack mode B

The utilization ratio for the fatigue life for fatigue crack mode B. The check is performed in the flanges at the location of the splices. Calculated in accordance with Eurocode 1993-1-9: P 8-(2).

For the lower flange

$$u_{FLS.Lambda.modeB.lower} := \left| \begin{array}{l} i \leftarrow 0 \\ \text{for } x_{splice} \in splitter(X_{splice.flange.lower}, 10mm) \\ \quad \left| \begin{array}{l} u_i \leftarrow \dfrac{\gamma_{F.fatigue} \cdot \Delta\sigma_{fatigue.modeB.lower_i} \cdot \lambda_{fatigu}}{\left(\dfrac{\Delta\sigma_{C.modeB.lower}(x_{splice})}{\gamma_{M.fatigue}} \right)} \\ i \leftarrow i + 1 \end{array} \right. \\ u \end{array} \right.$$

For the upper flange

$$u_{FLS.Lambda.modeB.upper} := \left| \begin{array}{l} i \leftarrow 0 \\ \text{for } x_{splice} \in splitter(X_{splice.flange.upper}, 10mm) \\ \quad \left| \begin{array}{l} u_i \leftarrow \dfrac{\gamma_{F.fatigue} \cdot \Delta\sigma_{fatigue.modeB.upper_i} \cdot \lambda_{fatigue}}{\left(\dfrac{\Delta\sigma_{C.modeB.upper}(x_{splice})}{\gamma_{M.fatigue}} \right)} \\ i \leftarrow i + 1 \end{array} \right. \\ u \end{array} \right.$$

The result

$$u_{FLS.Lambda.modeB.upper} = \begin{pmatrix} 0.12 \\ 0.12 \\ 0.1 \\ 0.1 \\ 0.13 \\ 0.13 \end{pmatrix} \qquad u_{FLS.Lambda.modeB.lower} = \begin{pmatrix} 0.88 \\ 0.88 \\ 1.14 \\ 1.14 \\ 1.13 \\ 1.13 \\ 0.88 \\ 0.89 \end{pmatrix}$$

The maximum value of the utilization ratio for fatigue crack mode B

$$u_{FLS.Lambda.modeB.max} := \max\left(u_{FLS.Lambda.modeB.lower}, u_{FLS.Lambda.modeB.upper}\right)$$

$$u_{FLS.Lambda.modeB.max} = 1.14$$

Fatigue crack mode C

The utilization ratio for the fatigue life for fatigue crack mode C. The check is performed at the end of the span along the web height, except the lower and upper most 50mm. calculated in accordance with Eurocode 1993-1-9: P 8-(2). It is assumed that the fatigue life is the same in both ends of the span, hence that only one end is tested.

$$u_{FLS.Lambda.modeC}\left(z_{bridge}\right) := \frac{\gamma_{F.fatigue} \cdot \Delta\sigma_{fatigue.modeC.principal}\left(z_{bridge}\right) \cdot \lambda_{fatigue}}{\left(\frac{\Delta\sigma_{C.modeC}}{\gamma_{M.fatigue}}\right)}$$

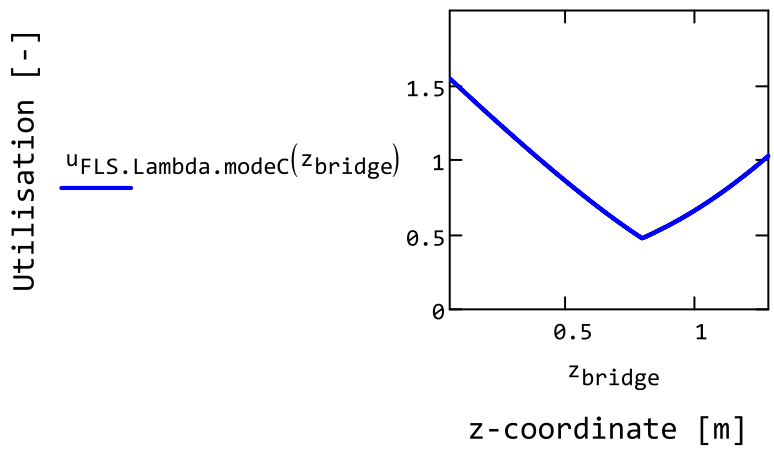

The maximum value of the utilization ratio for fatigue crack mode C

$$u_{FLS.Lambda.modeC.max} := \left| \begin{array}{l} Z_{web} \leftarrow z_{min.modeC}, z_{min.modeC} + 0.01m .. \ z_{max.modeC} \\ \text{for } \ z_{step} \in Z_{web} \\ \quad \left| \begin{array}{l} u_{step} \leftarrow u_{FLS.Lambda.modeC}(z_{step}) \\ u_{max} \leftarrow \max(u_{max}, u_{step}) \end{array} \right. \\ u_{max} \end{array} \right.$$

$$u_{FLS.Lambda.modeC.max} = 1.55$$

Fatigue crack mode D

The utilization ratio for the fatigue life for fatigue crack mode D. The check is performed in the flange at the end of the spans. calculated in accordance with Eurocode 1993-1-9: P 8-(2). It is assumed that the fatigue life is the same in both ends of the span, hence that only one end is tested.

$$u_{FLS.Lambda.modeD} := \frac{\gamma_{F.fatigue} \cdot \Delta\sigma_{fatigue.modeD} \cdot \lambda_{fatigue}}{\left(\frac{\Delta\sigma_{C.modeD}}{\gamma_{M.fatigue}} \right)}$$

$$u_{FLS.Lambda.modeD} = \begin{pmatrix} 1.03 \\ 1.51 \end{pmatrix}$$

The maximum value of the utilization ratio for fatigue crack mode D

$$u_{FLS.Lambda.modeD.max} := \max(u_{FLS.Lambda.modeD})$$

$$u_{FLS.Lambda.modeD.max} = 1.51$$

Fatigue crack mode E

The utilization ratio for the fatigue life for fatigue crack mode E. The check is performed in the longitudinal welds of the main I-girder with regard to the shear force in said welds. This fatigue crack mode can take place both at the top and bottom weld. Hence that two sets of checks are performed. The utilization ratio in the lower part. calculated in accordance with Eurocode 1993-1-9: P 8-(2).

$$u_{FLS.Lambda.modeE.lower}(x_{span}) := \frac{\gamma_{F.fatigue} \cdot \Delta\tau_{fatigue.modeE.lower}(x_{span}) \cdot \lambda_{fatigue}}{\frac{\Delta\tau_{C.modeE}}{\gamma_{M.fatigue}}}$$

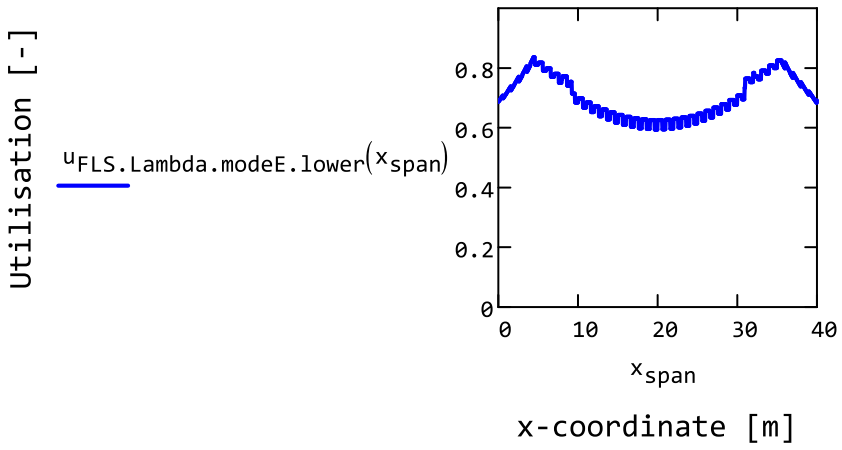

The utilization ratio in the upper part. calculated in accordance with Eurocode 1993-1-9: P 8-(3).

$$u_{FLS.Lambda.modeE.upper}(x_{span}) := \frac{\gamma_{F.fatigue} \cdot \Delta\tau_{fatigue.modeE.upper}(x_{span}) \cdot \lambda_{fatigue}}{\frac{\Delta\tau_{C.modeE}}{\gamma_{M.fatigue}}}$$

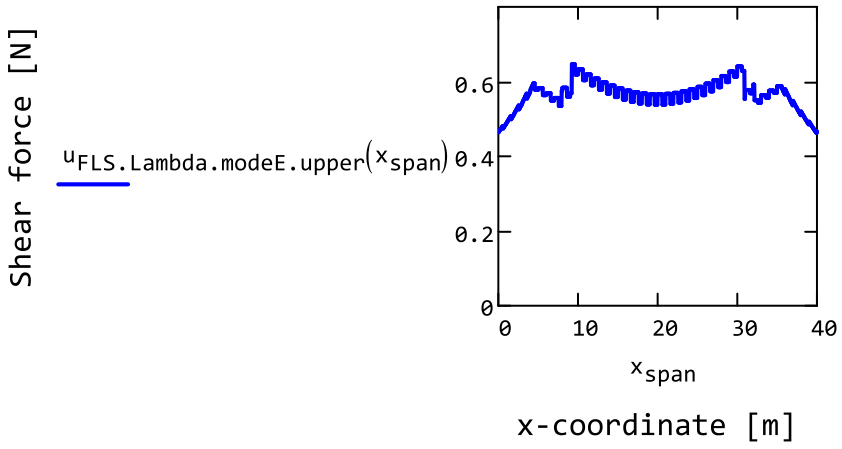

The maximum value of the utilization ratio for fatigue crack mode E

$u_{FLS.Lambda.modeE.max} :=$

$x_{span} \leftarrow 0m, 0.1m .. L_{span}$

for $x_{step} \in x_{span}$

$u_{upper} \leftarrow u_{FLS.Lambda.modeE.lower}(x_{step})$

$u_{lower} \leftarrow u_{FLS.Lambda.modeE.upper}(x_{step})$

$u_{max} \leftarrow \max(u_{max}, u_{upper}, u_{lower})$

u_{max}

$u_{FLS.Lambda.modeE.max} = 0.84$

Fatigue crack mode F

The utilization ratio for the fatigue life for fatigue crack mode F. The check is performed in the web at the location of the splices in the web. The stress which is checked is the direct stress, calculated in accordance with Eurocode 1993-1-9: P 8-(2).

$$u_{FLS.Lambda.modeF}(z_{bridge}) := \left| \begin{array}{l} i \leftarrow 0 \\ \Delta\sigma \leftarrow \Delta\sigma_{fatigue.modeF}(z_{bridge}) \\ \text{for } x_{splice} \in \text{splitter}(X_{splice.web}, 10mm) \\ \quad \left| u_i \leftarrow \dfrac{\gamma_{F.fatigue} \cdot \Delta\sigma_i \cdot \lambda_{fatigue}}{\left(\dfrac{\Delta\sigma_{C.modeF}(x_{splice})}{\gamma_{M.fatigue}}\right)} \right. \\ \quad \left| i \leftarrow i + 1 \right. \\ u \end{array} \right.$$

The maximum value of the utilization ratio for fatigue cracking mode F

$$u_{FLS.Lambda.modeF.max} := \left| \begin{array}{l} X_{splice} \leftarrow \text{splitter}(X_{splice.web}, 10mm) \\ \text{for } i \in 0, 1 .. \text{rows}(X_{splice}) - 1 \\ \quad \left| z_{start} \leftarrow z_{bottom.main.web}(X_{splice_i}) \right. \\ \quad \left| z_{stop} \leftarrow z_{top.main.web}(X_{splice_i}) \right. \\ \quad \left| z_{range} \leftarrow \text{range}(z_{start}, z_{stop}, 25) \right. \\ \quad \text{for } z_{step} \in z_{range} \\ \quad\quad \left| u_{step} \leftarrow u_{FLS.Lambda.modeF}(z_{step}) \right. \\ \quad\quad \left| u_{max} \leftarrow \max(u_{step}, u_{max}) \right. \\ u_{max} \end{array} \right.$$

$$u_{FLS.Lambda.modeF.max} = 0.76$$

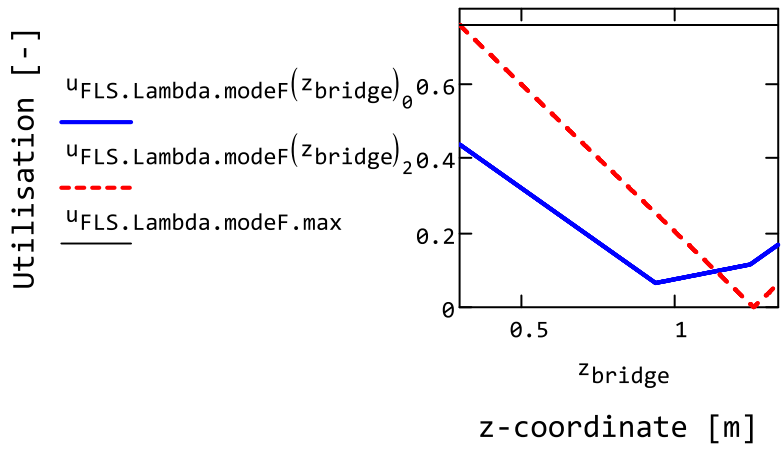

3 Results

In this document the results from the bridge analysis is presented and selected data is exported.

This chapter encompasses the following subchpaters:
3.1 Bending moment resistance
3.2 Shear resistance
3.3 Deflection
3.4 Fatigue life
3.5 Check of assumptions
3.6 General bridge data
3.7 Data needed for fatigue calculation of the bridge
    3.7.1 Constants
    3.7.2 Data along the span
    3.7.3 Other data ranges

Exporting data

To aid the export of data to other programs. Examples of programs which can be of interest is Matlab, Octave and Excel.

The current path to the result directory

$$directory_{result} = "..\Results\Test\ run\"$$

Absolute or relative path to the result folder

$$path := directory_{result}$$

Name of the subfolder

$$folder_{Excel} := "Mathcad\ data\"$$

$$folder_{fatigue} := "Fatigue\"$$

File extension

$$extension := ".dat"$$

function for obtaining the path.fatigue from the varaible name

$$path_{fatigue}(variablename) := concat(path, folder_{fatigue}, variablename, extension)$$

$$path_{Excel}(variablename) := concat(path, folder_{Excel}, variablename, extension)$$

Format for the exportation of varaibles. Note that the output may NOT contain any units, just the numerical value. Howver, the output can be a scalar, vector or matrix. In the case of too long variable names the value of the variable can be stored in temporary variable 'tmp'.

$$WRITEPRN(path_{fatigue}("variablename")) := \frac{variablename}{unit}$$

3.1 Bending moment resistance

Elastic utilisation for the composite cross-section

The utilisation ratio for bending capacity for the composite cross-section with regard to elastic analysis.

$$u_{ULS.bending.composite.elastic.max} = 95 \cdot \%$$

The value is saved to a file that will contain the numerical value of the selected varaible, all units should be SI-units or similar base unit. Note that the file should have the same name as the variable plus the extension .dat.

$$tmp := u_{ULS.bending.composite.elastic.max}$$

$$WRITEPRN\left(path_{Excel}\left("u.ULS.bending.composite.elastic.max"\right)\right) := tmp$$

Elastic utilisation for the main I-girders at casting

The utilisation ratio for bending capacity for the main I-girders at casting.

$$u_{ULS.bending.main.elastic.max} = 78 \cdot \%$$

The value is saved to a file that will contain the numerical value of the selected varaible. Note that the file should have the same name as the variable.

$$WRITEPRN\left(path_{Excel}\left("u.ULS.bending.main.elastic.max"\right)\right) := u_{ULS.bending.main.elastic.m}$$

3.2 Shear resistance

Utilisation of the capacity in the lower flange of the I-girder with regard to bending in ULS. For the nominal cross-section.

$$u_{ULS.shear.composite.max} = 83 \cdot \%$$

The value is saved to a file that will contain the numerical value of the selected varaible. Note that the file should have the same name as the variable.

$$WRITEPRN\left(path_{Excel}\left("u.ULS.shear.composite.max"\right)\right) := u_{ULS.shear.composite.max}$$

3.3 Deflection

Ratio between the maximum deflection in the middle of the span and the limit to the maximum deflection.

$$u_{SLS.deflection} = 67 \cdot \%$$

The value is saved to a file that will contain the numerical value of the selected varaible. Note that the file should have the same name as the variable.

$$\text{WRITEPRN}\left(\text{path}_{\text{Excel}}\left(\text{"u.SLS.deflection"}\right)\right) := u_{\text{SLS.deflection}}$$

3.4 Fatigue life

Fatigue cracking mode A

Utilisation of the fatigue life with regard to cracking mode A.

$$u_{\text{FLS.Lambda.modeA.max}} = 127 \cdot \%$$

The value is saved to a file that will contain the numerical value of the selected varaible. Note that the file should have the same name as the variable.

$$\text{WRITEPRN}\left(\text{path}_{\text{Excel}}\left(\text{"u.FLS.Lambda.modeA.max"}\right)\right) := u_{\text{FLS.Lambda.modeA.max}}$$

Fatigue cracking mode B

Utilisation of the fatigue life with regard to cracking mode B.

$$u_{\text{FLS.Lambda.modeB.max}} = 114 \cdot \%$$

The value is saved to a file that will contain the numerical value of the selected varaible. Note that the file should have the same name as the variable.

$$\text{WRITEPRN}\left(\text{path}_{\text{Excel}}\left(\text{"u.FLS.Lambda.modeB.max"}\right)\right) := u_{\text{FLS.Lambda.modeB.max}}$$

Fatigue cracking mode C

Utilisation of the fatigue life with regard to cracking mode C.

$$u_{\text{FLS.Lambda.modeC.max}} = 155 \cdot \%$$

The value is saved to a file that will contain the numerical value of the selected varaible. Note that the file should have the same name as the variable.

$$\text{WRITEPRN}\left(\text{path}_{\text{Excel}}\left(\text{"u.FLS.Lambda.modeC.max"}\right)\right) := u_{\text{FLS.Lambda.modeC.max}}$$

Fatigue cracking mode D

Utilisation of the fatigue life with regard to cracking mode D.

$$u_{\text{FLS.Lambda.modeD.max}} = 151 \cdot \%$$

The value is saved to a file that will contain the numerical value of the selected varaible. Note that the file should have the same name as the variable.

$$\text{WRITEPRN}\left(\text{path}_{\text{Excel}}\left(\text{"u.FLS.Lambda.modeD.max"}\right)\right) := u_{\text{FLS.Lambda.modeD.max}}$$

Fatigue cracking mode E

Utilisation of the fatigue life with regard to cracking mode E.

$$u_{FLS.Lambda.modeE.max} = 84 \cdot \%$$

The value is saved to a file that will contain the numerical value of the selected varaible. Note that the file should have the same name as the variable.

$$WRITEPRN\left(path_{Excel}\left("u.FLS.Lambda.modeE.max"\right)\right) := u_{FLS.Lambda.modeE.max}$$

Fatigue cracking mode F

Utilisation of the fatigue life with regard to cracking mode F.

$$u_{FLS.Lambda.modeF.max} = 76 \cdot \%$$

The value is saved to a file that will contain the numerical value of the selected varaible. Note that the file should have the same name as the variable.

$$WRITEPRN\left(path_{Excel}\left("u.FLS.Lambda.modeF.max"\right)\right) := u_{FLS.Lambda.modeF.max}$$

3.5 Check of assumptions

The checks and assumptions are currently not printed as output files. However, observe that the assumptions should be checked manually before accepting the results.

Check that there are no intermediate stiffeners in the main I-girders. Some of the calculations are based on this assumption and thus it must be fulfilled.

$$assumption_{no\_intermediate\_stiffeners} = "true"$$

Check if the interaction between shear and moment in the composite cross-section in the ultimate limit state is whitin the permitted limits.

$$assumption_{interaction} = "true"$$

Check that the height to width ratio for the web is not exceeded.

$$assumption_{web.width.thickness} = "true"$$

Check that the steel area is not reduced for the effective cross-section

$$assumption_{steel\_unreduced} = "true"$$

Check that there are exactly two notional lanes.

$$assumption_{2\_notional\_lanes} = "true"$$

Check that the web's height to thickness ratio is not exceeded.

$$assumption_{web.width.thickness} = "true"$$

3.6 General bridge data

Steel amount in the bridge

The mass of the stainless steel in the bridge.

$$m_{bridge.steel} = 30041\,kg$$

The value is saved to a file that will contain the numerical value of the selected varaible, all units should be SI-units or similar base unit. Note that the file should have the same name as the variable plus the extension .dat.

$$WRITEPRN\left(path_{Excel}("m.bridge.steel")\right) := \frac{m_{bridge.steel}}{kg}$$

Exposed steel area

The exposed area of steel in the bridge. This is of interest if the bridge would be painted or need regular maintence.

$$A_{bridge.steelsurface} = 307\,m^2$$

The value is saved to a file that will contain the numerical value of the selected varaible, all units should be SI-units or similar base unit. Note that the file should have the same name as the variable plus the extension .dat.

$$WRITEPRN\left(path_{Excel}("A.bridge.steelsurface")\right) := \frac{A_{bridge.steelsurface}}{m^2}$$

3.7 Data needed for fatigue calculation of the bridge

The cross-sectional properties and a few constants is needed when performing fatigue assessment of the bridge in external programs. Currently the external fatigue assessment is carried out with Matlab and the data is collected in a subfolder with the name 'Fatigue'. Note that ranges cannot be used to export data, therefore vectors will be used instead.

Supporting functions

A specialised function for creating a vector that contains a value for each 0.5m of the span.

$$vector_{span}(function) := \left| \begin{array}{l} n_{span} \leftarrow \frac{L_{span}}{0.5m} + 1 \\ vector_{super}\left(function, 0m, L_{span}, n_{span}\right) \end{array} \right.$$

A specialised function for creating a vector that contains a value for the z-coordinates for fatigue cracking mode C at the end of the span.

$$vector_{modeC}(function) := \left| \begin{array}{l} n_{span} \leftarrow 25 \\ vector_{super}\left(function, z_{min.modeC}, z_{max.modeC}, n_{span}\right) \end{array} \right.$$

A specialised function for creating a vector that contains the values for the given z-coordinates for fatigue cracking mode F at the location of the splices in the web.

$$\text{vector}_{\text{modeF}}(x_{\text{span}}) := \left| \begin{array}{l} z_{\text{start}} \leftarrow z_{\text{bottom.main.web}}(x_{\text{span}}) \\ z_{\text{stop}} \leftarrow z_{\text{top.main.web}}(x_{\text{span}}) \\ \text{vector}_{\text{super}}(\text{echo}, z_{\text{start}}, z_{\text{stop}}, 50) \end{array} \right.$$

A specialised function for creating a matrix that contains the values for the given z-coordinates for fatigue cracking mode F at the location of the splices in the web.

$$\text{matrix}_{\text{modeF}} := \left| \begin{array}{l} \text{range}_x \leftarrow \text{range}_{\text{vector}}(X_{\text{splice.web}}) \\ \text{range}_y \leftarrow \text{range}_{\text{vector}}(\text{vector}_{\text{modeF}}(0\text{m})) \\ \text{for } n \in \text{range}_x \\ \quad \text{for } i \in \text{range}_y \\ \quad\quad \left| \begin{array}{l} x_{\text{step}} \leftarrow X_{\text{splice.web}_n} \\ z_{\text{step}} \leftarrow \text{vector}_{\text{modeF}}(x_{\text{step}})_i \\ S_{i,n} \leftarrow S_{\text{main.beam}}(x_{\text{step}}, z_{\text{step}}) \end{array} \right. \\ S \end{array} \right.$$

A specialised function for creating a vector that contains the values for the given z-coordinates for fatigue cracking mode F at the location of the splices in the web.

$$z_{\text{range.modeF}} := \left| \begin{array}{l} \text{range}_x \leftarrow \text{range}_{\text{vector}}(X_{\text{splice.web}}) \\ \text{range}_y \leftarrow \text{range}_{\text{vector}}(\text{vector}_{\text{modeF}}(0\text{m})) \\ \text{for } n \in \text{range}_x \\ \quad \text{for } i \in \text{range}_y \\ \quad\quad \left| \begin{array}{l} x_{\text{step}} \leftarrow X_{\text{splice.web}_n} \\ z_{\text{step}} \leftarrow \text{vector}_{\text{modeF}}(x_{\text{step}})_i \\ z_{\text{range}_{i,n}} \leftarrow \text{echo}(z_{\text{step}}) \end{array} \right. \\ z_{\text{range}} \end{array} \right.$$

3.7.1 Constants

The span length

$$L_{\text{span}} = 40\,\text{m}$$

$$\text{WRITEPRN}(\text{path}_{\text{fatigue}}(\text{"L.span"})) := \frac{L_{\text{span}}}{\text{m}}$$

Design life of the bridge

$$t_{designlife} = 80 \cdot years$$

$$WRITEPRN(path_{fatigue}("t.designlife")) := \frac{t_{designlife}}{years}$$

Observed heavy vehicles per year.

$$N_{fatigue.observed} = 5 \times 10^5 \cdot \frac{1}{year}$$

$$WRITEPRN(path_{fatigue}("N.fatigue.observed")) := N_{fatigue.observed} \cdot year$$

The distance or range of the traffic passing the bridge. for fatigue load model 4 this can be long, medium or local. To aid compatibilty between Mathcad and Matlab the range is designated as 1,2 or 3. Here 1 is "long", 2 is "medium" and 3 is "local".

$$range_{traffic} = "local"$$

$$range_{traffic.number} := \begin{cases} 1 & \text{if } range_{traffic} = "long" \\ 2 & \text{if } range_{traffic} = "medium" \\ 3 & \text{if } range_{traffic} = "local" \end{cases}$$

$$range_{traffic.number} = 3$$

$$WRITEPRN(path_{fatigue}("range.traffic")) := range_{traffic.number}$$

Damage equivalent factor. Note that while Mathcad can save the file using the greek letter λ matlab cannot read it easily. Thus it is saved with the letter λ spelled as 'Lambda', note that in this study there is currently no destinction made between upper and lower case greek letters when saved or loaded from external sources. Note that the factor is also written to the Excel file.

$$\lambda_{fatigue} = 2$$

$$WRITEPRN(path_{fatigue}("Lambda.fatigue")) := \lambda_{fatigue}$$

$$WRITEPRN(path_{Excel}("lambda.fatigue")) := \lambda_{fatigue}$$

Thickness of the longitudinal welds.

$$a_{weld.main.lower} = 5 \cdot mm$$

$$a_{weld.main.upper} = 5 \cdot mm$$

$$WRITEPRN(path_{fatigue}("a.weld.main.lower")) := \frac{a_{weld.main.lower}}{m}$$

$$WRITEPRN(path_{fatigue}("a.weld.main.upper")) := \frac{a_{weld.main.upper}}{m}$$

Load reduction factor, takes into account how much of the fatigue vehicle load is carried by the most loaded main I-girder.

$$\mathrm{WRITEPRN}\left(\mathrm{path}_{\mathrm{fatigue}}(\text{"reduction.lane1"})\right) := \mathrm{reduction}_{\mathrm{lane1}}$$

$$\mathrm{WRITEPRN}\left(\mathrm{path}_{\mathrm{fatigue}}(\text{"reduction.lane2"})\right) := \mathrm{reduction}_{\mathrm{lane2}}$$

Constant amplitude nominal stress fatigue strength for each cracking mode. Note that the fatigue strength for node B varies along the length of the span and therefore is given in the next subchapter.

$$\mathrm{WRITEPRN}\left(\mathrm{path}_{\mathrm{fatigue}}(\text{"DeltaSigma.C.modeA"})\right) := \frac{\Delta\sigma_{\mathrm{C.modeA}}}{\mathrm{Pa}}$$

$$\mathrm{WRITEPRN}\left(\mathrm{path}_{\mathrm{fatigue}}(\text{"DeltaTau.C.modeA"})\right) := \frac{\Delta\tau_{\mathrm{C.modeA}}}{\mathrm{Pa}}$$

$$\mathrm{WRITEPRN}\left(\mathrm{path}_{\mathrm{fatigue}}(\text{"DeltaSigma.C.modeC"})\right) := \frac{\Delta\sigma_{\mathrm{C.modeC}}}{\mathrm{Pa}}$$

$$\mathrm{WRITEPRN}\left(\mathrm{path}_{\mathrm{fatigue}}(\text{"DeltaSigma.C.modeD"})\right) := \frac{\Delta\sigma_{\mathrm{C.modeD}}}{\mathrm{Pa}}$$

$$\mathrm{WRITEPRN}\left(\mathrm{path}_{\mathrm{fatigue}}(\text{"DeltaTau.C.modeE"})\right) := \frac{\Delta\tau_{\mathrm{C.modeE}}}{\mathrm{Pa}}$$

$$\mathrm{WRITEPRN}\left(\mathrm{path}_{\mathrm{fatigue}}(\text{"DeltaSigma.C.modeF"})\right) := \frac{\Delta\sigma_{\mathrm{C.modeF}}(0\mathrm{m})}{\mathrm{Pa}}$$

Partial factors for the fatigue calculations

$$\mathrm{WRITEPRN}\left(\mathrm{path}_{\mathrm{fatigue}}(\text{"Gamma.F.fatigue"})\right) := \gamma_{\mathrm{F.fatigue}}$$

$$\mathrm{WRITEPRN}\left(\mathrm{path}_{\mathrm{fatigue}}(\text{"Gamma.M.fatigue"})\right) := \gamma_{\mathrm{M.fatigue}}$$

3.7.2 Data along the span

Most of the data given here is created using $vector_{span}$ that creates a vector with the result in evenly spaced sections.

x-coordinates

x-coordinates for vectors that contains data for the whole length of the span.

$$\mathrm{WRITEPRN}\left(\mathrm{path}_{\mathrm{fatigue}}(\text{"x.range"})\right) := \frac{\mathrm{vector}_{\mathrm{span}}(\mathrm{echo})}{\mathrm{m}}$$

x-coordinates for splices in the lower flange, web and upperflange of the main I-girders.

$$\mathtt{WRITEPRN}\left(\mathtt{path}_{\mathtt{fatigue}}(\mathtt{"X.splice.flange.lower"})\right) := \frac{\mathtt{X}_{\mathtt{splice.flange.lower}}}{\mathtt{m}}$$

$$\mathtt{WRITEPRN}\left(\mathtt{path}_{\mathtt{fatigue}}(\mathtt{"X.splice.web"})\right) := \frac{\mathtt{X}_{\mathtt{splice.web}}}{\mathtt{m}}$$

$$\mathtt{WRITEPRN}\left(\mathtt{path}_{\mathtt{fatigue}}(\mathtt{"X.splice.flange.upper"})\right) := \frac{\mathtt{X}_{\mathtt{splice.flange.upper}}}{\mathtt{m}}$$

z-coordinates

Global z-coordinates for the lower and upper part of the web.

$$\mathtt{WRITEPRN}\left(\mathtt{path}_{\mathtt{fatigue}}(\mathtt{"z.bottom.main.web"})\right) := \frac{\mathtt{vector}_{\mathtt{span}}\left(\mathtt{z}_{\mathtt{bottom.main.web}}\right)}{\mathtt{m}}$$

$$\mathtt{WRITEPRN}\left(\mathtt{path}_{\mathtt{fatigue}}(\mathtt{"z.top.main.web"})\right) := \frac{\mathtt{vector}_{\mathtt{span}}\left(\mathtt{z}_{\mathtt{top.main.web}}\right)}{\mathtt{m}}$$

Global z-coordinates for the lowermost part of the flanges of the main I-girder.

$$\mathtt{tmp} := \frac{\mathtt{vector}_{\mathtt{span}}\left(\mathtt{z}_{\mathtt{bottom.main.flange.lower}}\right)}{\mathtt{m}}$$

$$\mathtt{WRITEPRN}\left(\mathtt{path}_{\mathtt{fatigue}}(\mathtt{"z.bottom.main.flange.lower"})\right) := \mathtt{tmp}$$

Global z-coordinates for the uppermost part of the flanges of the main I-girder.

$$\mathtt{tmp} := \frac{\mathtt{vector}_{\mathtt{span}}\left(\mathtt{z}_{\mathtt{top.main.flange.upper}}\right)}{\mathtt{m}}$$

$$\mathtt{WRITEPRN}\left(\mathtt{path}_{\mathtt{fatigue}}(\mathtt{"z.top.main.flange.upper"})\right) := \mathtt{tmp}$$

Global z-coordinate for the neutral layer in negative and positive bending of the composite cross-section.

$$\mathtt{WRITEPRN}\left(\mathtt{path}_{\mathtt{fatigue}}(\mathtt{"z.NA.composite.negative"})\right) := \frac{\mathtt{vector}_{\mathtt{span}}\left(\mathtt{z}_{\mathtt{NA.composite.negativ}}\right.}{\mathtt{m}}$$

$$\mathtt{WRITEPRN}\left(\mathtt{path}_{\mathtt{fatigue}}(\mathtt{"z.NA.composite.positive"})\right) := \frac{\mathtt{vector}_{\mathtt{span}}\left(\mathtt{z}_{\mathtt{NA.composite.positiv}}\right.}{\mathtt{m}}$$

Fatigue strength

Constant amplitude nominal stress fatigue strength for fatigue cracking mode C in the lower and upper flange respectively. Since the fatigue strength depends on the thickness of the flanges the fatigue strength may vary along the span.

$$\mathrm{WRITEPRN}\left(\mathrm{path}_{\mathrm{fatigue}}\left(\text{"DeltaSigma.C.modeB.lower"}\right)\right) := \frac{\mathrm{vector}_{\mathrm{span}}\left(\Delta\sigma_{\mathrm{C.modeB.lower}}\right.}{\mathrm{Pa}}$$

$$\mathrm{WRITEPRN}\left(\mathrm{path}_{\mathrm{fatigue}}\left(\text{"DeltaSigma.C.modeB.upper"}\right)\right) := \frac{\mathrm{vector}_{\mathrm{span}}\left(\Delta\sigma_{\mathrm{C.modeB.upper}}\right.}{\mathrm{Pa}}$$

Measurements

Thickness of the web of the main I-girder.

$$\mathrm{WRITEPRN}\left(\mathrm{path}_{\mathrm{fatigue}}\left(\text{"t.main.web"}\right)\right) := \frac{\mathrm{vector}_{\mathrm{span}}\left(t_{\mathrm{main.web}}\right)}{\mathrm{m}}$$

Second moment of area

Second moment of area for the composite cross-section for negative moments

$$\mathrm{WRITEPRN}\left(\mathrm{path}_{\mathrm{fatigue}}\left(\text{"I.composite.negative"}\right)\right) := \frac{\mathrm{vector}_{\mathrm{span}}\left(I_{\mathrm{composite.negative}}\right.}{\mathrm{m}^4}$$

Second moment of area for the composite cross-section for positive moments

$$\mathrm{WRITEPRN}\left(\mathrm{path}_{\mathrm{fatigue}}\left(\text{"I.composite.positive"}\right)\right) := \frac{\mathrm{vector}_{\mathrm{span}}\left(I_{\mathrm{composite.positive}}\right.}{\mathrm{m}^4}$$

Second moment of area for the unreduced main I-girder.

$$\mathrm{WRITEPRN}\left(\mathrm{path}_{\mathrm{fatigue}}\left(\text{"I.main.beam.unreduced"}\right)\right) := \frac{\mathrm{vector}_{\mathrm{span}}\left(I_{\mathrm{main.beam.unreduc}}\right.}{\mathrm{m}^4}$$

First moment of area

First moment of area for the lower flange of the unreduced main I-girder.

$$S_{\mathrm{main.beam.lower}}\left(x_{\mathrm{span}}\right) := S_{\mathrm{main.beam}}\left(x_{\mathrm{span}}, z_{\mathrm{bottom.main.web}}\left(x_{\mathrm{span}}\right)\right)$$

$$\mathrm{WRITEPRN}\left(\mathrm{path}_{\mathrm{fatigue}}\left(\text{"S.main.beam.lower"}\right)\right) := \frac{\mathrm{vector}_{\mathrm{span}}\left(S_{\mathrm{main.beam.lower}}\right)}{\mathrm{m}^3}$$

First moment of area for the upper flange of the unreduced main I-girder.

$$S_{\mathrm{main.beam.upper}}\left(x_{\mathrm{span}}\right) := S_{\mathrm{main.beam}}\left(x_{\mathrm{span}}, z_{\mathrm{top.main.web}}\left(x_{\mathrm{span}}\right)\right)$$

$$\mathrm{WRITEPRN}\left(\mathrm{path}_{\mathrm{fatigue}}\left(\text{"S.main.beam.upper"}\right)\right) := \frac{\mathrm{vector}_{\mathrm{span}}\left(S_{\mathrm{main.beam.upper}}\right)}{\mathrm{m}^3}$$

3.7.3 Other data ranges

Some miscellaneous data ranges used in the external fatigue calculations.

z-coordinates

z-coordinates that corresponds to the data taken in the web at the end of the span.

$$\mathrm{WRITEPRN}\left(\mathrm{path}_{\mathrm{fatigue}}(\text{"z.range.modeC"})\right) := \frac{\mathrm{vector}_{\mathrm{modeC}}(\mathrm{echo})}{\mathrm{m}}$$

z-coordinates that corresponds to the data taken in the web at the location at the location of the splices in the web.

$$\mathrm{WRITEPRN}\left(\mathrm{path}_{\mathrm{fatigue}}(\text{"z.range.modeF"})\right) := \frac{\mathrm{z}_{\mathrm{range.modeF}}}{\mathrm{m}}$$

First moment of area

First moment of area for selected z-coordinates in the web of the unreduced main I-girder at the end of the span.

$$\mathrm{S}_{\mathrm{main.beam.modeC}}\left(\mathrm{z}_{\mathrm{bridge}}\right) := \mathrm{S}_{\mathrm{main.beam}}\left(0\mathrm{m}, \mathrm{z}_{\mathrm{bridge}}\right)$$

$$\mathrm{WRITEPRN}\left(\mathrm{path}_{\mathrm{fatigue}}(\text{"S.main.beam.modeC"})\right) := \frac{\mathrm{vector}_{\mathrm{modeC}}\left(\mathrm{S}_{\mathrm{main.beam.modeC}}\right)}{\mathrm{m}^3}$$

First moment of area for selected z-coordinates in the web of the unreduced main I-girder at the location of the splices in the web.

$$\mathrm{WRITEPRN}\left(\mathrm{path}_{\mathrm{fatigue}}(\text{"S.main.beam.modeF"})\right) := \frac{\mathrm{matrix}_{\mathrm{modeF}}}{\mathrm{m}^3}$$